Mathematical Problems in Engineering

Advances in Modelling, Analysis, and Design of Delayed Systems

Special Issue Editor in Chief: Libor Pekař
Guest Editors: Radek Matušů and Renming Yang

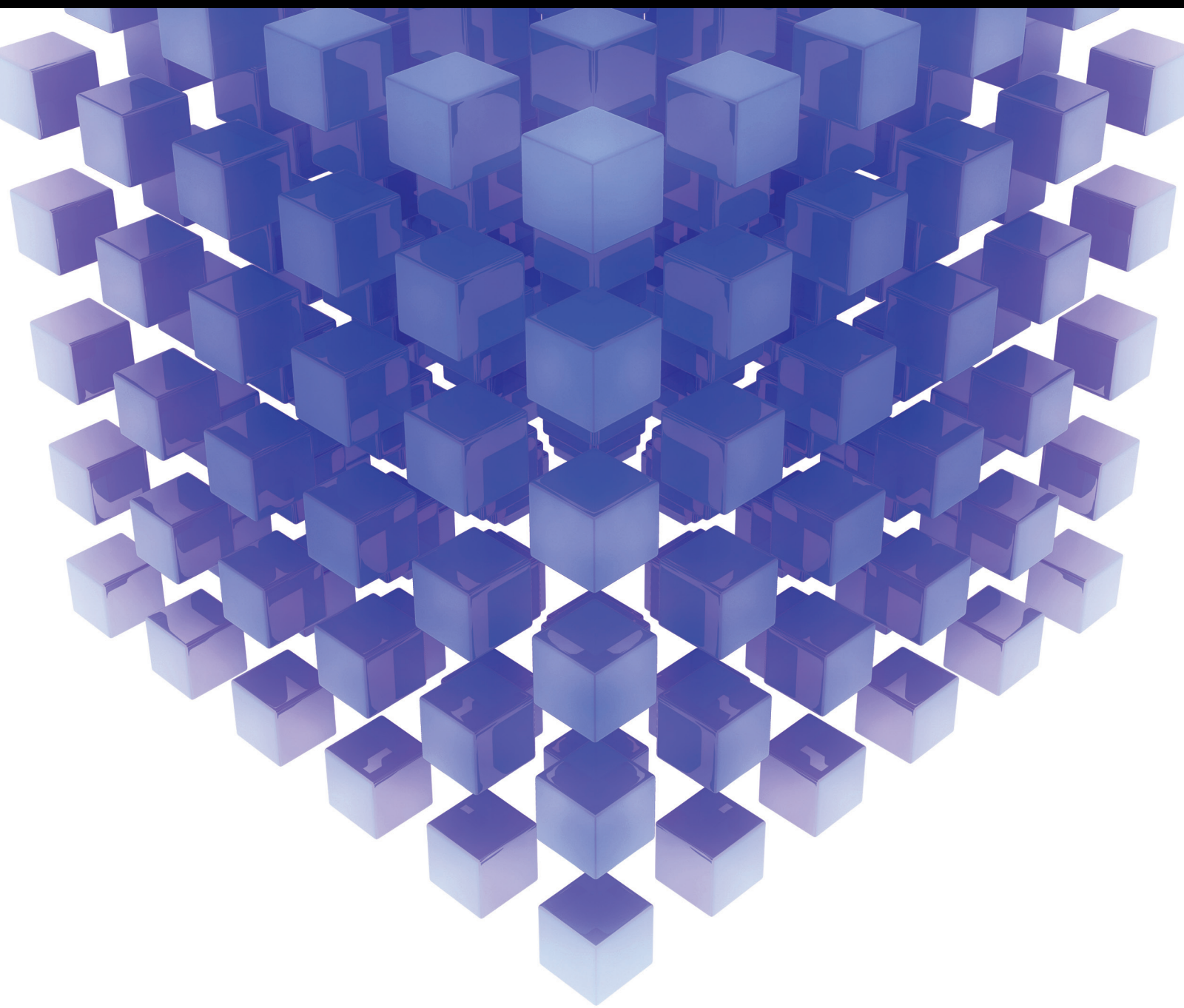

Advances in Modelling, Analysis, and Design of Delayed Systems

Mathematical Problems in Engineering

Advances in Modelling, Analysis, and Design of Delayed Systems

Special Issue Editor in Chief: Libor Pekař
Guest Editors: Radek Matušů and Renming Yang

Editorial Board

Contents

Hindawi
Mathematical Problems in Engineering
Volume 2018, Article ID 5078027, 4 pages
https://doi.org/10.1155/2018/5078027

Editorial

Advances in Modelling, Analysis, and Design of Delayed Systems

Libor Pekař,[1] **Radek Matušů**,[1] **and Renming Yang**[2]

[1]*Faculty of Applied Informatics, Tomas Bata University in Zlín, nám. T. G. Masaryka 5555, 76001 Zlín, Czech Republic*
[2]*School of Information Science and Electrical Engineering, Shandong Jiaotong University, Jinan 250357, China*

Correspondence should be addressed to Libor Pekař; pekar@fai.utb.cz

Received 29 April 2018; Accepted 29 April 2018; Published 29 May 2018

In feedback control systems, delay as a generic part of many processes, including industrial [1], communication [2], economical [3], traffic [4], automotive technology [5], and biological [6] ones, is a phenomenon which unambiguously deteriorates the quality of a control performance. Delay has inter alia a decisive impact on control system stability, and the studying of this influence is not usually mathematically simple. Modern control theory has been dealing with this problem since its nascence; the well-known Smith predictor [7] has celebrated six decades of being known and applied a year ago.

Modern and advanced control theory is confronted with higher and higher requirements on quality and performance of control systems in industry as well as in everyday reality [8]. It is well known that control of such processes often represents a very complex problem and they are hardly controllable by conventional control methods. Many related problems are unsolved and many questions remain unanswered. The aim of this special issue has been to highlight the most significant recent developments on the topics of Time Delay Systems (TDSs), their modelling and identification, stability analysis, various control strategies, and interesting academic and real-life applications.

The attractiveness of the special issue has been proved by the number of 58 submitted manuscripts collected by the editors from the authors from Argentina, Chile, China, Czech Republic, Iran, Malaysia, Mexico, Pakistan, Republic of Korea, Saudi Arabia, Sweden, Taiwan, Tunisia, Vietnam, United Kingdom, and USA (i.e., 16 countries in total). The acceptance rate has been only of 29%; that is, 17 papers have been eventually published, which indicates a high level of the review process concerning the technical quality and originality of the works.

Regarding the content and subject manner of the special issue, the broad scope of topics has been covered. Namely, in five papers, spectral and stability analysis is made, or stability conditions and criteria are developed. Asymptotic or H_2 stabilization, observer or filter design, and adaptive or robust control of TDSs using linear matrix inequalities (LMIs) tools and Lyapunov theory are addressed in four papers. Two papers are devoted to automotive technology problems; namely, optimal control of a car suspension system and improved car-following model that include the influence of strong wind are investigated. A single paper deals with associative memories for memristive neural networks with deviating argument; it is worth noting here that five papers use or incorporate neural networks. The following delay-related tasks are also represented by a single paper in the special issue: PID control design, digital predictive control design, feedback carbon emission reduction, the stationary probability density functions of an oscillator, and the passivity of delayed neural networks. A concise characterization of all papers included in the special issue follows.

In the paper titled "Delay-Dependent Stability Analysis of TS Fuzzy Switched Time-delay Systems" by N. Aoun et al., a new approach to deal with the problem of stability under arbitrary switching of continuous-time switched TDSs represented by Takagi-Sugeno (TS) fuzzy models [9] is proposed. A specific state space representation, called arrow form matrix, is used first. Then, sufficient asymptotic stability conditions are obtained through the application of Borne and Gentina practical stability criterion [10] and by constructing a

pseudo-overvaluing system. The eventual stability criteria are algebraic and easy to use and permit avoiding the problem of existence of a common Lyapunov-Krasovskii functional.

Stability characteristics of Delay-Differential Equations (DDEs) with multiple time-periodic delays are proposed by G. Jin et al. in the paper titled "A Method for Stability Analysis of Periodic Delay-Differential Equations with Multiple Time-Periodic Delays". Stability charts are produced here for two typical examples of time-periodic DDEs about milling chatter, including the variable-spindle speed milling system with one time-periodic delay [11] and variable-pitch cutter milling system with multiple delays [12]. The proposed method further provides a generalized algorithm, which possesses a good capability to predict the stability lobes for milling operations with variable-pitch cutter or variable-spindle speed.

F.-D. Li et al. deal with the stability analysis of genetic regulatory networks with interval time-varying delays in the paper titled "Stability Analysis of Delayed Genetic Regulatory Networks via a Relaxed Double Integral Inequality". Firstly, the Wiringter-type double integral inequality (WTDII) [13] is established to estimate the double integral term appearing in the derivative of Lyapunov-Krasovskii functional with a triple integral term. Then, by applying the WTDII to the stability analysis of a delayed genetic regulatory network, together with the usage of the information of regulatory functions, several delay-range- and delay-rate-dependent (or delay-rate-independent) criteria are derived in terms of linear matrix inequalities.

In the paper titled "New Stability Criterion for Takagi-Sugeno Fuzzy Cohen-Grossberg Neural Networks with Probabilistic Time-Varying Delays" by X. Wang et al., a new global asymptotic stability criterion is derived, in which the diffusion item can play its role. Owing to deleting the boundedness conditions on amplification functions, the main result is novelty to some extent. The positive definite form of p powers for Lyapunov-Krasovskii functional, which is different from those of existing literature [14], is another novel contribution of this method.

The existence of stability switches and Hopf bifurcations for the scalar DDE of the form $\ddot{x}(t) + a\dot{x}(t-\tau) + bx(t) = 0$ with complex (not real in general) coefficients is studied in the paper titled "Stability Switches and Hopf Bifurcations in a Second-Order Complex Delay Equation" by M. Roales and F. Rodríguez, by means of results published in [15].

In the paper titled "Observer Design for Delayed Markovian Jump Systems with Output State Saturation" by G. Wang and B. Feng, the observer design problem of continuous-time delayed Markovian jump systems with output state saturation [16] is considered. The probability distributions of two states are described in the observer design by exploiting the Bernoulli variable. Sufficient conditions for the designed observe with three kinds of output saturations are provided with LMI forms.

In the paper titled "Delayed Trilateral Teleoperation of a Mobile Robot" by D. Santiago et al., the stability of nonlinear, varying-time, and delayed system represented by a trilateral teleoperation system of a mobile robot is analyzed. The stability analysis is based on Lyapunov-Krasovskii theory where a functional is proposed and analyzed to get conditions for the control parameters (for three PD controllers under a position master/slave velocity strategy [17]) that assure a stable behavior, keeping the synchronism errors bounded. In the paper, a practical verification of the theoretical result is given to the reader as well.

The neural network and disturbance observer are designed to tackle the uncertainties and external disturbance for a class of nonlinear TDSs with output prescribed performance constraint in the work "Adaptive Constrained Control for Uncertain Nonlinear Time-delay System with Application to Unmanned Helicopter" by R. Li et al. In addition, prescribed performance function is constructed for the output prescribed performance constrained problem. Then the robust controller is designed via the adaptive backstepping method, and the stability analysis is considered by using Lyapunov-Krasovskii functionals [18]. The proposed method is eventually employed into the unmanned helicopter system with time delay aerodynamic uncertainty [19].

H.-J. Yu et al. focus on the generalized H_2 filtering of static neural networks with a time-varying delay in their paper "Improved Generalized H_2 Filtering for Static Neural Networks with Time-Varying Delay via Free-Matrix-Based Integral Inequality". A full-order filter such that the filtering error system is globally asymptotically stable with guaranteed H_2 performance index is designed. An improved delay-dependent condition for the generalized H_2 filtering problem is established in terms of LMIs, by constructing an augmented Lyapunov-Krasovskii functional and applying the free-matrix-based integral inequality [20] to estimate its derivative.

In the paper titled "An Improved Car-following Model Accounting for Impact of Strong Wind" by D. Liu et al., an enhanced car-following model based on the full velocity difference model is developed in order to investigate the effect of strong wind on dynamics of traffic flow. Wind force, lift force, and side force are considered in the model. Stability condition of the improved model is derived, and numerical analysis is made to explore the effect of strong wind on spatial-time evolution of a small perturbation. Moreover, the effect of strong wind to the stability of traffic flow and car driving safety in strong wind by comparing the lateral force under different wind speeds are studied. The fuel consumption of a vehicle in strong wind condition is explored as well.

The determination of coordinate values of articulated geometry for a double-wishbone independent suspension with two unequal length arms based on structural limitations and constraint equations of alignment parameters is presented in the paper titled "An Improved Genetic Algorithm to Optimize Spatial Locations for Double-Wishbone Type Suspension System with Time Delay" by Q. Li et al. The sensitivities of front wheel alignment parameters are analyzed using the space analytic geometry method with insight module in ADAMS software [21]. The multiobjective optimization functions are designed to calculate the coordinate values of hardpoints with front suspension since the effect of time delay because wheelbase can be easily obtained by vehicle speed. The kinematic and compliance characteristics

are investigated using genetic algorithm solutions [22] in the simulation environment. Experimental results are also provided to the reader.

J.-E. Zhang in his paper "Analysis and Design of Associative Memories for Memristive Neural Networks with Deviating Argument" investigates associative memories for memristive neural networks with deviating argument [23]. Firstly, the existence and uniqueness of solution for memristive neural networks with deviating argument are discussed. A derivation of sufficient conditions for this class of neural networks to possess invariant manifolds follows, and a global exponential stability criterion is presented. Next, analysis and design of autoassociative memories and heteroassociative memories for memristive neural networks with deviating argument are formulated, respectively.

In the paper titled "Proportional Retarded Controller to Stabilize Underactuated Systems with Measurement Delays: Furuta Pendulum Case Study" by T. Ortega-Montiel et al., the design and tuning of a simple feedback strategy with delay to stabilize a class of underactuated mechanical systems with dead-time are presented. A linear time-invariant model with time delay of fourth order represented by the Furuta pendulum [24] (that is a standard two-degree-of-freedom benchmark example from the class of underactuated mechanical systems) and a proportional retarded controller are considered. A step forward to obtain a better understanding of the effect of output delays and related phenomena in mechatronic systems is presented in the paper, making possible designing resilient control laws under the presence of uncertain time delays in measurements. The configuration under study includes an inherent output delay due to wireless communication used to transmit measurements of the pendulum angular position. The approach offers a constructive design and a procedure based on a combination of root-loci and Mikhailov methods [25] for the analysis of stability. An experimental comparison with a standard linear state feedback control law is also presented.

A combination of identification and discrete-time control procedures aimed at precise control of systems with any time-delay value is presented by S. Talaš and V. Bobál in the paper titled "Predictive Control Adapting to Fractional Values of Time Delay". Suggested strategy allows the predictive controller to adapt its parameters to a value of the time delay identified during the control process. The system flexibility resides in the ability to work precisely even with time-delay values that are not integer multiples of the sampling period. The authors prove by example that the designed approach represents a very precise method to control systems with both static and variable cases of time delay.

A nice study from the field of environmental engineering is presented in the paper titled "The Feedback Mechanism of Carbon Emission Reduction in Power Industry of Delayed Systems" by X. Yu et al. The paper proposes a carbon market feedback mechanism to power market, comprehensively considering the influence of generation structure, carbon intension, and technological progress on carbon emission reduction in power industry, and builds a potential model based on dynamic system. It is shown by operation system results that the increasing trend of carbon emission can be controlled effectively; however, it is always with a lag. Moreover, sensitivity analysis results show that carbon emission reduction of at most 32% and 60% can be realized by adjusting power structure and improving technological level, respectively.

In the paper titled "Response of Duffing Oscillator with Time Delay Subjected To Combined Harmonic And Random Excitations" by D. N. Hao and N. D. Anh, the stationary probability density functions of the Duffing oscillator with time delay [26] subjected to combined harmonic and white noise excitation are investigated by the method of stochastic averaging and equivalent linearization. The paper shows that the displacement and the velocity with time delay in the Duffing oscillator can be computed approximately in non-time delay terms. The transformation based on the fundamental matrix of the degenerate Duffing system is used here. Then, the stochastic system with time delay is transformed into the corresponding stochastic non-time delay equation in Ito sense. The approximate stationary probability density function of the original system can be found by combining the stochastic averaging method, the equivalent linearization method, and the technique of auxiliary function [27]. The response of Duffing oscillator is also investigated in the paper.

Several conditions for passive performance, based on appropriate Lyapunov-Krasovskii functionals and some inequalities, are established via LMIs in the paper titled "Passivity of Memristive BAM Neural Networks with Probabilistic and Mixed Time-varying Delays" by W. Wang et al. More precisely, the passivity problem of memristive bidirectional associate memory neural networks with probabilistic and mixed time-varying delays (including the leakage and distributed delays) is solved by applying random variables with Bernoulli distribution [28].

Acknowledgments

We appreciate the authors for their contributions to this special issue. Special thanks go also to the reviewers for their valuable feedback, which helps improve the quality of the submitted papers. We would like to express our gratitude to the European Regional Development Fund and to the Ministry of Education, Youth and Sports of the Czech Republic that financially supported the editors' work under Project CEBIA-Tech Instrumentation no. CZ.1.05/2.1.00/19.0376 and under the National Sustain-ability Programme Project no. LO1303 (MSMT-7778/2014), respectively.

Libor Pekař
Radek Matušů
Renming Yang

References

[1] N. Olgac, U. Zalluhoglu, and A. S. Kammer, "On blade/casing rub problems in turbomachinery: An efficient delayed differential equation approach," *Journal of Sound and Vibration*, vol. 333, no. 24, pp. 6662–6675, 2014.

[2] Q.-L. Han, Y. Liu, and F. Yang, "Optimal communication network-based Hinf quantized control with packet dropouts

for a class of discrete-time neural networks with distributed time delay," *IEEE Transactions on Neural Networks and Learning Systems*, vol. 27, pp. 426–434, 2016.

[3] M. Ellis and P. D. Christofides, "Economic model predictive control of nonlinear time-delay systems: Closed-loop stability and delay compensation," *AIChE Journal*, vol. 61, no. 12, pp. 4152–4165, 2015.

[4] G. Orosz, R. E. Wilson, and G. Stépán, "Traffic jams: dynamics and control," *Philosophical Transactions of the Royal Society A: Mathematical, Physical & Engineering Sciences*, vol. 368, no. 1928, pp. 4455–4479, 2010.

[5] W. Cao, Z. Liu, Y. Chang, and A. Szumanowski, "Direct Yaw-Moment Control of All-Wheel-Independent-Drive Electric Vehicles with Network-Induced Delays through Parameter-Dependent Fuzzy SMC Approach," *Mathematical Problems in Engineering*, vol. 2017, Article ID 5170492, 2017.

[6] O. Diekmann, P. Getto, and Y. Nakata, "On the characteristic equation $\lambda = \alpha_1 + (\alpha_2 + \alpha_3\lambda)e^{-\lambda}$ and its use in the context of a cell population model," *Journal of Mathematical Biology*, vol. 72, no. 4, pp. 877–908, 2016.

[7] O. J. Smith, "Closer control of loops with dead time," *Chemistry Engineering Progress*, vol. 53, no. 5, pp. 217–219, 1957.

[8] M. Huba, "Performance measures, performance limits and optimal PI control for the IPDT plant," *Journal of Process Control*, vol. 23, no. 4, pp. 500–515, 2013.

[9] T. Takagi and M. Sugeno, "Fuzzy identification of systems and its applications to modeling and control," *IEEE Transactions on Systems, Man, and Cybernetics*, vol. 15, no. 1, pp. 116–132, 1985.

[10] P. Borne, J. C. Gentina, and F. Laurent, "Sur la stabilité des systems échantillonnés non linéaires," *Revue Francaise dAutomatique Informatique Recherche Operationnelle*, vol. 2, pp. 96–105, 1972.

[11] S. Seguy, T. Insperger, L. Arnaud, G. Dessein, and G. Peigné, "On the stability of high-speed milling with spindle speed variation," *The International Journal of Advanced Manufacturing Technology*, vol. 48, no. 9-12, pp. 883–895, 2010.

[12] G. Jin, Q. Zhang, S. Hao, and Q. Xie, "Stability prediction of milling process with variable pitch cutter," *Mathematical Problems in Engineering*, vol. 2013, Article ID 932013, 2013.

[13] M. Park, O. Kwon, J. H. Park, S. Lee, and E. Cha, "Stability of time-delay systems via Wirtinger-based double integral inequality," *Automatica*, vol. 55, pp. 204–208, 2015.

[14] Q. Zhu, C. Huang, and X. Yang, "Exponential stability for stochastic jumping BAM neural networks with time-varying and distributed delays," *Nonlinear Analysis: Hybrid Systems*, vol. 5, no. 1, pp. 52–77, 2011.

[15] J. Li, L. Zhang, and Z. Wang, "Two effective stability criteria for linear time-delay systems with complex coefficients," *Journal of Systems Science & Complexity*, vol. 24, no. 5, pp. 835–849, 2011.

[16] W. Li and Z. Wu, "Output tracking of stochastic high-order nonlinear systems with Markovian switching," *Institute of Electrical and Electronics Engineers Transactions on Automatic Control*, vol. 58, no. 6, pp. 1585–1590, 2013.

[17] A. Ghorbanian, S. M. Rezaei, A. R. Khoogar, M. Zareinejad, and K. Baghestan, "A novel control framework for nonlinear time-delayed Dual-master/single-slave teleoperation," *ISA Transactions®*, vol. 52, no. 2, pp. 268–277, 2013.

[18] B. Niu and J. Zhao, "Tracking control for output-constrained nonlinear switched systems with a barrier Lyapunov function," *International Journal of Systems Science*, vol. 44, no. 5, pp. 978–985, 2013.

[19] R. Li, M. Chen, Q. Wu, and J. Liu, "Robust adaptive tracking control for unmanned helicopter with constraints," *International Journal of Advanced Robotic Systems*, vol. 14, no. 3, 2017.

[20] H.-B. Zeng, Y. He, M. Wu, and J. She, "Free-matrix-based integral inequality for stability analysis of systems with time-varying delay," *Institute of Electrical and Electronics Engineers Transactions on Automatic Control*, vol. 60, no. 10, pp. 2768–2772, 2015.

[21] S. Hasagasioglu, K. Kilicaslan, O. Atabay, and A. Güney, "Vehicle dynamics analysis of a heavy-duty commercial vehicle by using multibody simulation methods," *The International Journal of Advanced Manufacturing Technology*, vol. 60, no. 5-8, pp. 825–839, 2012.

[22] A. Konak, D. W. Coit, and A. E. Smith, "Multi-objective optimization using genetic algorithms: a tutorial," *Reliability Engineering & System Safety*, vol. 91, no. 9, pp. 992–1007, 2006.

[23] L. Wan and A. Wu, "Stabilization control of generalized type neural networks with piecewise constant argument," *Journal of Nonlinear Sciences and Applications. JNSA*, vol. 9, no. 6, pp. 3580–3599, 2016.

[24] K. Åström and K. Furuta, "Swinging Up a Pendulum by Energy Control ," *IFAC Proceedings Volumes*, vol. 29, no. 1, pp. 1919–1924, 1996.

[25] A. Mikhailov, "Method of harmonic analysis in control theory," *Avtomatika i Telemekhanika*, vol. 3, no. 1, pp. 27–81, 1938.

[26] C. S. Feng and R. Liu, "Response of Duffing system with delayed feedback control under bounded noise excitation," *Archive of Applied Mechanics*, pp. 1–9, 2012.

[27] N. D. Anh, V. L. Zakovorotny, and D. N. Hao, "Response analysis of Van der Pol oscillator subjected to harmonic and random excitations," *Probabilistic Engineering Mechanics*, vol. 37, pp. 51–59, 2014.

[28] G. Nagamani and S. Ramasamy, "Stochastic dissipativity and passivity analysis for discrete-time neural networks with probabilistic time-varying delays in the leakage term," *Applied Mathematics and Computation*, vol. 289, pp. 237–257, 2016.

Hindawi
Mathematical Problems in Engineering
Volume 2018, Article ID 6416375, 6 pages
https://doi.org/10.1155/2018/6416375

Research Article

Predictive Control Adapting to Fractional Values of Time Delay

Stanislav Talaš and Vladimír Bobál

Department of Process Control, Faculty of Applied Informatics, Tomas Bata University in Zlín, Zlín, Czech Republic

Correspondence should be addressed to Stanislav Talaš; talas.stanislav@gmail.com

Received 29 June 2017; Accepted 18 March 2018; Published 22 April 2018

Academic Editor: Renming Yang

A combination of identification and control procedures is presented which is aimed at precise control of systems with any value of time delay. Suggested strategy allows the predictive controller to adapt its parameters to a value of the time delay identified during the control process. The system flexibility resides in the ability to work precisely even with time-delay values that are not integer multiples of the sampling period. Overall, the designed approach presents a more precise method to control systems with both static and variable cases of time delay.

1. Introduction

Time delay is an accompanying effect for a large number of controlled processes not only in industrial areas. Control design for such cases requires an unconventional approach due to its negative impact on stability in traditional control systems. While applying control techniques in discrete form it is necessary to take into account the fact that time delay can be under these circumstances expressed only as an integer multiple of the sampling period. As a result of this limitation, the control precision is comparatively reduced. This article aims to overcome this drawback.

A number of methods is being used to identify the time-delay value in practice; an overview of several was studied in [1]. Among often used concepts there is a comparison of estimates of system outputs for a range of possible time-delay values [2], or also an application of the least square method often combined with identification of all remaining system parameters [3]. Contrary to methods attempting to determine both parameters and time delay, for example, [4, 5], the approach described in this article is focused exclusively on the value of time delay with an assumption that the remaining system parameters are known and constant.

Considering the area of discrete control methods, if we want to perform online measurements of varying time-delay, we need to take into account all changes that may happen between values quantified to individual sampling periods. This problem is still largely studied resulting in number of scientific articles with varying areas of focus. An approach similar to the method described in the article by using specific system parameters and output estimation was taken by [6]. An application of specific mathematical models to specific input signals and performing identification procedure in order to determine individual system parameters were suggested. The control issue of applying model predictive controller to handle time delay was explored in [7] among many others. The mentioned research compared performance of the model-based predictive control (MPC) in state-space system with variable time delay to PI (proportional integrating) controller and Smith predictor, proving efficiency of the predictive approach.

Several procedures exist that are able to control systems with time delay; the most significant are based on principles of the Smith predictor and model based predictive control [8]. Despite their number, only a minority of controllers are sufficiently robust in relation to the value of time delay [9]. Therefore, it is usually suitable to accompany the system control algorithm with an identification method.

The aim of this paper was to explore the option of adapting the control algorithm for cases, when a system changes its time-delay value. Both the concept of time-delay identification and controller adaptation technique were realized in simulations. The first section is focused on connecting individual elements of the control structure. The following

subchapter analyses the applied method for identification of the time-delay value. The next part investigates specific modifications of the predictive controller in order to incorporate the possibility of controlling a system with time-delay value that is not an exact multiple of the sampling period. Resulting performance of the described control structure is analyzed in the subsequent chapter, followed by final evaluation.

2. Methods

The suggested control structure contains a combination of an identification procedure and a control mechanism. Individual sections are realized and connected in the simulation environment MATLAB with the extension Simulink. The connection is designed in such a way that measured values of control input and system output are processed by the time-delay identifying algorithm, first. Consequently, the identification result is provided to the controller, which modifies its own parameters based on acquired data and performs system inputs.

The solution also utilizes MPC principle, where, in contrast to conventional control, the controller output is realized by minimizing proper (usually quadratic) objective function. It is realized as a closed-loop control system. MPC can be realized as system based on input-output process model, as well as state-space theory. In case of this publication the MPC method is based on input-output system model; therefore it utilizes external input-output signals.

2.1. Time-Delay Identification. The foundation of the identification procedure is a method capable of determining an arbitrary value of time delay during the control procedure [10]. This strategy is based on a reversed mechanism of a system behaviour prediction. Therefore, instead of determining system outputs from known parameters, the parameter is deduced from measured outputs. This approach works, provided that the dynamical properties are known and the single unknown value is time delay.

An area of input and output data is reserved for a precise determination of time delay. Based on initial conditions in the section and the series of input signals related to a value of time delay, an estimation of possible system outputs is calculated. As a result, a set of system outputs for possible values of time delay is obtained. Furthermore, individual calculated sequences of outputs are compared with the actual measured one. Comparison of these results enables determining the area of the most probable time-delay value. In addition, the modified Z-transform is applied to derive a new variant of the original system parameters for further precision increase. The new version has several times smaller sampling period and its parameters are applied to perform an estimation of system outputs with time delay of a fractional value.

Figure 1 illustrates a comparison between the measured output signal and possible outputs depending on time delay. The red line follows the development of the real system output, blue lines are estimated from the output for four different integer values of time delay and green lines fill the area of possible outputs from estimates computed with fractional time-delay values. The area with increased accuracy

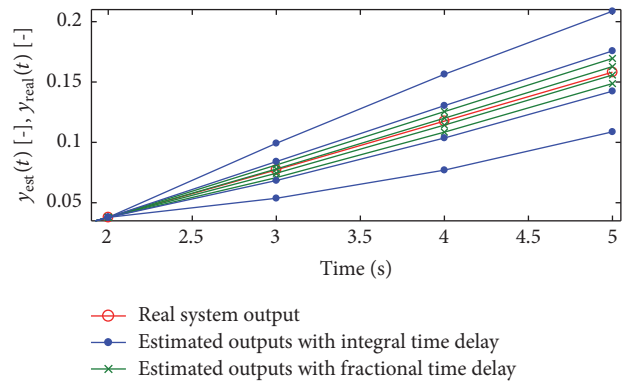

Figure 1: Output estimation for various values of time-delay: integral, fractional, and real.

may be determined from the comparison between the integer estimates and the real output first. Therefore, the number of necessary calculations can be significantly decreased and, therefore, even a wide interval of possible time-delay values does not have a major influence on computation demands. The number of estimated outputs can be lowered even further by performing computations for only selected values of time delay as each estimate-comparison operation provides a more accurate information about the real value of time delay in an optimizing search for the minimal deviation.

The comparison between individual calculated output estimates $\widehat{y}_d$ and the measured data y_{real} is realized by computing a qualitative criterion of integrated square error (ISE). Its noncontinuous version is expressed by the following equation.

$$\text{ISE}_d = \sum_{i=1}^{n} \left[y_{\text{real}}(i) - \widehat{y}_d(i) \right]^2. \tag{1}$$

The most probable value of the time delay is deduced from the sequence with the smallest calculated error. In order to increase the precision for cases with a varying value of time delay, it is possible to incorporate a directional forgetting, which decreases the significance of data measured in more distant areas. As a result, newer measurements have a greater impact.

This identification method enables us to determine the size of time delay directly during the control procedure. Another benefit of this technique is the option to set the amount of studied data. A larger measured area provides more precise results in the presence of disturbance; on the other hand, smaller area may identify a change in the time delay faster.

2.2. Predictive Control Principle. The model based predictive control is a control approach using a mathematical description of the controlled system to estimate its future behaviour. Based on the estimation, an optimal sequence of control inputs is calculated by an optimization algorithm [11, 12]. The optimality of the desired state is expressed in an objective function with the general form as follows.

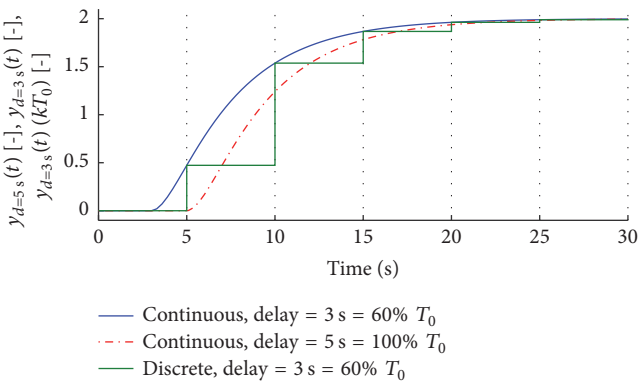

FIGURE 2: System transfer with delay outside of sampling period expressed in discrete area.

$$J = \sum_{i=N_1}^{N_2} \delta(i) \left[\hat{y}(k+i) - w(k+i)\right]^2 + \sum_{i=1}^{N_u} \lambda(i) \left[\Delta u(k+i-1)\right]^2, \quad (2)$$

Variables δ and λ represent weighting parameters determining the balance between the smallest control error and the slowest change in control input. The area of optimization is determined by horizons N_1, N_2, and N_u which set the number of sampling steps involved in calculations. The goal of optimization is to find a series of input signal differences Δu that lead to the smallest value of J.

Only the first value of the optimized series is applied as $\Delta u(k)$ and the entire procedure is repeated in the following sampling step; this is called receding horizon strategy.

The applied controller was based on the traditional design of the generalized predictive controller (GPC). This method is popular due to its versatility. The controlled system dynamics are represented by a transfer function as a base for the future output estimation. The benefit lies in its principle that it uses only a small number of values in order to reconstruct the entire step function or any output shape with knowledge of the input signal [13–16].

2.3. Modification of the Predictive Control Procedure. The control procedure is based on the above described GPC controller, in which sections of system model and future output predictions are modified.

A system described in the discrete area has the time-delay parameter represented by the power of variable z^{-d}. The value of d can assume only integral values, and, therefore, it is necessary to describe such system with modified Z-transform, which can express system dynamic outside of the original sampling area.

Figure 2 displays how a system can be described in discrete area with such a time delay that is not an integer multiple of its sampling period. The mathematical description starts in a model without time delay, from which the system state in the fraction of sampling period given by the length of time delay is deduced. The value of system response with the given length of time delay then represents the state achieved in the moment of sampling. As the source for determining the controller parameters is used a system with time-delay value rounded down and the remaining parameters were obtained from the modified Z-transformation.

Based on parameters received by modified Z-transform, it is necessary to deduce new values of matrices applied in the predictive control. During the estimation of future outputs based on a system expressed as a division of polynomials, where the order of numerator is nb and the order of denominator is na, the prediction of the output variable is given by the following equation:

$$\hat{y}(k+1) = \sum_{i=1}^{na+1} a_i y(k+1-i) + \sum_{i=1}^{nb} b_i \Delta u(k-d-i). \quad (3)$$

With the prediction of length of N sampling steps and with integral part of delay of size d, individual elements are divided according to their affiliation to the following vectors:

$$u = \begin{bmatrix} \Delta u(k) \\ \Delta u(k+1) \\ \vdots \\ \Delta u(k+N-1) \end{bmatrix},$$

$$u_1 = \begin{bmatrix} \Delta u(k-1) \\ \Delta u(k-2) \\ \vdots \\ \Delta u(k-nb) \end{bmatrix}, \quad (4)$$

$$y_1 = \begin{bmatrix} \hat{y}(k+d) \\ \hat{y}(k+d-1) \\ \vdots \\ \hat{y}(k+d-na) \end{bmatrix}.$$

And the result is a matrix form interpreted as

$$\hat{\mathbf{y}} = \mathbf{G}\mathbf{u} + \mathbf{H}\mathbf{u}_1 + \mathbf{S}\mathbf{y}_1. \quad (5)$$

Considering the fact that the system obtained by the modified Z-transformation contains a nonzero element b_0, it is required to fill additional parameters to matrices $\mathbf{G}$ and $\mathbf{H}$.

In the presence of the time delay, it is necessary to estimate future system outputs to determine the entire vector y_1. The equation for calculating these values (3) is another section that has to be altered based on system model. Besides the obvious change in existing parameters, the variable b_0 needs to be added.

Figure 3 shows the layout of the control scheme. The control input signal u originating from the predictive controller and the output signal y measured in the controlled system are recorded in every sampling step by the time-delay identification algorithm. The newly recoded data is added to the set of known values and the identification procedure

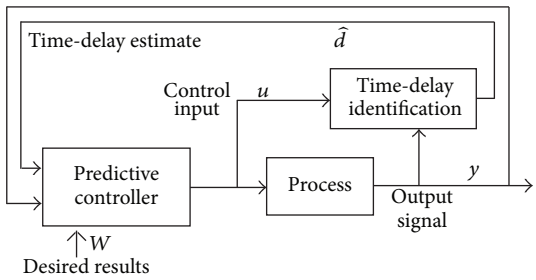

Figure 3: Adaptive control scheme.

performs a new estimate $\hat{d}$ of the time delay between the control input and the output signal. The result is consequently provided back to the predictive controller, which modifies its internal parameters accordingly. The whole procedure is ideally performed as a part of controller computations to ensure a fast response to sudden changes in time delay.

The result of the above-mentioned operations is a form of predictive control, which is able to adapt to a different dynamic caused by fractional value of time delay, while maintaining the original sampling period.

3. Results

The design functionality was verified in the simulation environment MATLAB with the Simulink extension. The system used for simulation was selected for its simple dynamics. The main goal was to demonstrate the ability of the controller to adapt itself to varying conditions of time delay.

$$G(s) = \frac{2}{4s^2 + 5s + 1}. \tag{6}$$

In the discrete version with the sampling period of 2 s,

$$G\left(z^{-1}\right) = \frac{0.4728z^{-1} + 0.2076z^{-2}}{1 - 0.7419z^{-1} + 0.08208z^{-2}}. \tag{7}$$

The development of the time-delay value was selected in such form to involve both fluent changes and sudden steps. The reference trajectory was set with respect to the fact that the method of time-delay identification needs to measure varying changes to properly determine the system state.

The predictive controller GPC had its weighting parameters set to focus more on the precision of the output signal in ratio of 1 : 2.

Figure 4 contains results of individual approaches aiming to provide information about the development of time-delay value represented by the black dotted line. The first signal uses the method proposed in the article identifying the delay with the accuracy on tenths of a second. The algorithm is able to closely follow the real value with the exception in the interval from 220 s to 240 s where the output signal remains constant. Therefore, the delay cannot be determined and maintains the last known value of 3.8 sampling period.

The second signal is a result of time-delay identification with accuracy to integers. The control precision is decreased in critical areas, where the real system time delay is distant from integral value, for example, from the time of 250 s up to the 300 s.

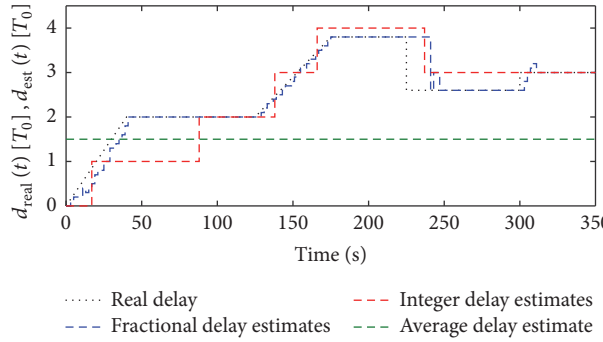

Figure 4: Time-delay estimates for the adaptive control.

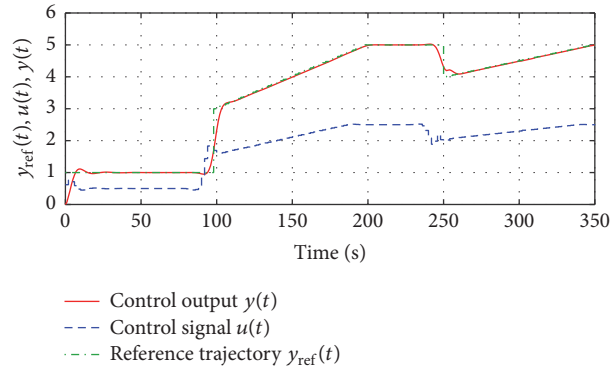

Figure 5: System control adapting to a varying time delay.

The third signal is a constant value of time delay over the entire control process selected experimentally to avoid risks of instability in areas with large differences from the estimate, for example, at the start of the process and from 175 s to 225 s.

Figure 5 demonstrates how with the changing value of time delay the control input u is also adapting in order to reach the reference trajectory y_{ref}. The controller obtains the estimated time-delay value from the identification algorithm and, based on this value, it changes parameters in control matrices, which are used in calculation of the control input. Therefore, the controller is able to adapt to a change of time delay in the form of fluent change in area 125 s to 175 s, as well as during step changes at 300 s. The relation between the identification and the control works as a mutually complementary mechanism. Change in the control input is eventually followed by a response in the output signal. The time difference in this relation is measured by the identification algorithm which provides the controller with proper data. The less precise the initial estimate of the controller is, the more significant the control input is required leading to a greater accuracy in the time-delay estimation and in the overall control as a result.

The amount of contribution of the designed identification method is demonstrated on Figures 6 and 7, where a certain level of control functionality has been limited.

Figure 6 shows the variant in which the control system is adapting to the time delay, which is being identified with accuracy of integers. The control precision has decreased in

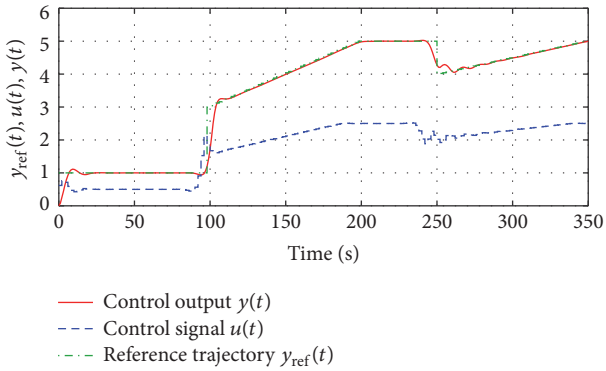

Figure 6: System control with time delay identified with accuracy of integers.

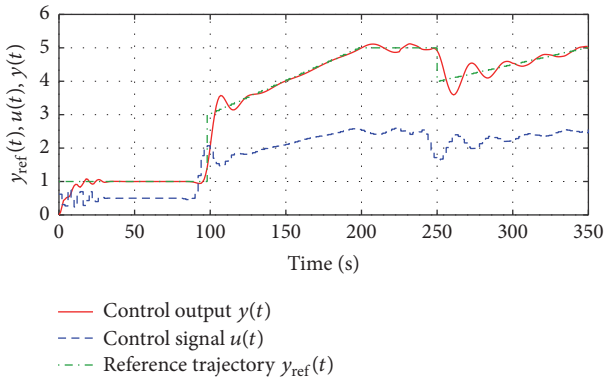

Figure 7: System control with constant estimated value of time delay.

Table 1: Comparison of the quality for various versions of time-delay identification.

Time-delay estimation	ISE criterion value
Constant delay $1.5 \cdot T_0$	16.2638
Identification of integral time delay	13.1859
Identification of fractional time delay	7.7763

critical areas, where the real system time delay is distant from integral value, for example, around 250 s.

Figure 7 illustrates the situation when the estimated time delay is represented by a constant value. The precision is heavily affected by the current distance between the real value and the constant. The negative effects are mainly visible at times of step response, but during the fluent change it is easier for the controller to adapt.

From Table 1 it is apparent that the designed combination of identification and control provides a significant improvement in the quality of systems that change the value of time delay during the control procedure.

4. Conclusion

The article describes new procedures for adaptive control of systems with variable time delay. The control structure is based on mutually cooperating algorithms fulfilling the function of time-delay identification on one hand and system output regulation on the other.

Time-delay identification is performed based on the knowledge of dynamical parameters of the controlled system, when the section of data measured in the past is compared to estimation of output development for a range of possible time-delay values. The accuracy of this approach is expanded by incorporating system model parameters with decreased sampling period and therefore it is able to operate with a greater accuracy than just individual lengths of the original sampling period.

The control procedure is founded on the traditional concept of GPC, which is extended with a function to predict behaviour of the system, where the time delay is a fractional multiple of the sampling time. Parameters, defining the system dynamic, are altered by modified Z-transform, which provides information about the system state outside of the original sampling area. Prediction matrices and output estimation are changed based on these parameters, in order to provide output predictions for systems with fractional time delay.

Functionality of the design was verified by simulations. The time-delay identification mechanism has managed to determine the size of the real time delay with a great accuracy and quickly react to its changes. The control algorithm with matrices modifiable by system model with a fractional time delay has succeeded to adequately adapt to varying conditions. The overall combination of these methods creates a chance of precise control mainly for systems with risk of unpredictable variations in the time-delay value during the control procedure.

Despite the presented functionality the described approach contains several possible directions of further improvement. One of them is the robustness of the identification procedure that would decrease its sensitivity to inaccuracies in estimated system parameters. Another option could be incorporating an identification of system parameters that were to this point considered known and constant.

Conflicts of Interest

The authors declare that there are no conflicts of interest regarding the publication of this paper.

Acknowledgments

This work was supported by Internal Grant Agency of Tomas Bata University under Project no. IGA/FAI/2017/009.

References

[1] J.-P. Richard, "Time-delay systems: an overview of some recent advances and open problems," *Automatica*, vol. 39, no. 10, pp. 1667–1694, 2003.

[2] S. V. Drakunov, W. Perruquetti, J.-P. Richard, and L. Belkoura, "Delay identification in time-delay systems using variable structure observers," *Annual Reviews in Control*, vol. 30, no. 2, pp. 143–158, 2006.

[3] A. Elnaggar, G. A. Dumont, and A.-L. Elshafei, "Recursive estimation for system of unknown delay," in *Proceedings of the 28th IEEE Conference on Decision and Control. Part 2 (of 3)*, pp. 1809-1810, December 1989.

[4] R. B. C. Lima and P. R. Barros, "Identifiaction of time-delay systems: a state-space realization approach," in *Proceedings of the 9th IFAC Symposium on Advnced Control of Chemical Processes ADCHEM*, pp. 254–259, 2015.

[5] A. Atitallah, S. Bedoui, and K. Abderrahim, "An Optimal Two Stage Identification Algorithm for Discrete Hammerstein Time Delay Systems," *IFAC-PapersOnLine*, vol. 49, no. 10, pp. 19–24, 2016.

[6] C. Shah, "On the modelling of time-varying delays," Tech. Rep., AM University, Texas, 2004.

[7] S. Himpe and V. Theunynck, *Design and advanced control of a process with variable time delay*, University of Ghent, 2006.

[8] J. E. Normey-Rico and E. F. Camacho, "Control of Dead-Time Processes," *IEEE Control Systems Magazine*, vol. 28, no. 5, pp. 136-137, 2008.

[9] E. Normey-Rico and E. F. Camacho, "Dead-time compensators: a survey," *Control Engineering Practice*, vol. 16, no. 4, pp. 407–428, 2008.

[10] S. Talaš, V. Bobál, A. Krhovják, and L. Rušar, "Discrete method for estimation of time-delay outside of sampling period," in *Proceedings of the 30th European Conference on Modelling and Simulation, ECMS 2016*, pp. 287–292, deu, June 2016.

[11] D. W. Clarke, C. Mohtadi, and P. S. Tuffs, "Generalized predictive control-Part I. the basic algorithm," *Automatica*, vol. 23, no. 2, pp. 137–148, 1987.

[12] D. W. Clarke, C. Mohtadi, and P. S. Tuffs, "Generalized Predictive Control-Part II Extensions and interpretations," *Automatica*, vol. 23, no. 2, pp. 149–160, 1987.

[13] J. M. Maciejowski, *Predictive Control with Constraints*, Prentice Hall, London, UK, 2002.

[14] J. A. Rossiter, *Model Based Predictive Control: a Practical Approach*, CRC Press, 2003.

[15] E. F. Camacho and C. Bordons, "Nonlinear model predictive control: an introductory review," in *Assessment and future directions of nonlinear model predictive control*, vol. 358 of *Lect. Notes Control Inf. Sci.*, pp. 1–16, Springer, Berlin, 2007.

[16] V. Bobal, M. Kubalcik, P. Dostal, and J. Matejicek, "Adaptive predictive control of time-delay systems," *Computers & Mathematics with Applications. An International Journal*, vol. 66, no. 2, pp. 165–176, 2013.

Hindawi
Mathematical Problems in Engineering
Volume 2018, Article ID 5830160, 25 pages
https://doi.org/10.1155/2018/5830160

Research Article

Passivity of Memristive BAM Neural Networks with Probabilistic and Mixed Time-Varying Delays

Weiping Wang[1,2], **Meiqi Wang**[1,2], **Xiong Luo**[1,2], **Lixiang Li**[3] and **Wenbing Zhao**[4]

[1] *School of Computer and Communication Engineering, University of Science and Technology Beijing, Beijing 100083, China*
[2] *Beijing Key Laboratory of Knowledge Engineering for Materials Science, Beijing 100083, China*
[3] *Information Security Center, State Key Laboratory of Networking and Switching Technology, Beijing University of Posts and Telecommunications, Beijing 100876, China*
[4] *Department of Electrical Engineering and Computer Science, Cleveland State University, Cleveland, OH 44115, USA*

Correspondence should be addressed to Weiping Wang; shiya666888@126.com and Xiong Luo; xluo@ustb.edu.cn

Received 20 June 2017; Revised 17 November 2017; Accepted 21 January 2018; Published 1 April 2018

Academic Editor: Renming Yang

This paper is concerned with the passivity problem of memristive bidirectional associative memory neural networks (MBAMNNs) with probabilistic and mixed time-varying delays. By applying random variables with Bernoulli distribution, the information of probability time-varying delays is taken into account. Furthermore, we consider the probability distribution of the variation and the extent of the delays; therefore, the results derived are less conservative than in the existing papers. In particular, the leakage delays as well as distributed delays are all taken into consideration. Based on appropriate Lyapunov-Krasovskii functionals (LKFs) and some useful inequalities, several conditions for passive performance are established in linear matrix inequalities (LMIs). Finally, numerical examples are given to demonstrate the feasibility of the presented theories, and the results reveal that the probabilistic and mixed time-varying delays have an unstable influence on the system and should not be ignored.

1. Introduction

Bidirectional associative memory neural networks (BAMNNs) are a class of two-layer neural systems, which were first introduced by Kosko in 1987. The neurons in the first layer are connected to another layer, and in the same layer, the neurons are not interconnected [1–3]. Owing to their special structure, BAMNNs have displayed many good features in various areas such as signal processing, image processing, and optimization problems [4–6]. In 2015, the stability of inertial BAMNNs with time-varying delay via impulsive control was discussed in [7]. Zhang et al. considered the exponential stability of BAMNNs with time-varying delays in [8]. Wang et al. addressed the global asymptotic stability of impulsive fractional-order BAMNNs with time delay in [9].

Memristor, a combination of a resistor and memory, has received increasing attention in many fields [10–13]. By applying the nonvolatile feature of the memristor, researchers were able to develop MBAMNN models. Because of the pinched hysteresis effects, MBAMNNs have a memory function, which can be used to imitate the human brain [14, 15]. In 2015, nonfragile synchronization of MBAMNNs with random feedback gain fluctuations was investigated in [16]. Based on functional differential inclusions, Jiang et al. obtained the dynamic behaviors for MBAMNNs with time-varying delays in [17].

Moreover, passivity is a special case of a broader theory of dissipativity, which plays a significant role in the stability analysis of dynamical systems, nonlinear control, and other areas. The main innate character of passivity theory is that the passive characteristics can make the system internally stable [18–20]. In recent years, many researchers have proposed passivity analysis for memristive neural networks (MNNs). Liu and Xu investigated the passivity analysis of MNNs with different state-dependent memductance functions and mixed time-varying delays in [21]. In 2016, the passivity of MBAMNNs with uncertain delays and different memductance was investigated in [22]. Nevertheless, there are

few people to study the passivity of MBAMNNs, which encourages our idea.

In the human brain, the transmission of information in neurons is often accompanied by a time delay, so time delay is inevitable in the neural networks, which is the origin of oscillation, divergence, and so forth [23–33]. Sometimes, the value of delay may be very large, but the probability of such delay is very small. Therefore, we use the probability distribution of time delay in the interval to reflect an actual situation better. Furthermore, it is clearer to describe the probabilistic time-varying delays through introducing random variables with Bernoulli distribution. In recent years, some researchers have discussed the probabilistic time-varying delays in the neural networks [34, 35]. In 2016, Pradeep et al. investigated the robust stability analysis of stochastic neural networks with probabilistic time-varying delays in [36]. Li et al. considered passivity analysis of memristive neural networks with probabilistic time-varying delays in [37]. Hence, it is of great importance to research the passivity of MBAMNNs with probabilistic time-varying delays.

In addition, there also exist two types of time-varying delays named leakage delays (or forgetting delays) and distributed time delays. The research of leakage time delay can be traced back to the early 90s of the last century; researchers found out that, due to the delay in switching time or signal transmission, there is a time delay in the negative feedback term of the network system; this delay is named leakage time delay. As is well known, leakage delays exist in many real systems such as population dynamics and neural networks [38, 39]. Moreover, leakage delay also has a significant influence on the dynamics of neural networks because it has been shown that such kind of time delay in the leakage term has a tendency to destabilize a system. Under the influence of leakage and additive time-varying delays, robust passivity analysis for neural networks was addressed in [40]. In 2016, the robust stability analysis for discrete-time neural networks with leakage delays was studied in [41].

On the other hand, due to the presence of multiple parallel paths with a variety of neuronal synapses' lengths and sizes, there is a spatial width of the network, and then there may exist either a distribution of the transmission voltage in these parallel paths or a distribution of transmission delays over a period of time. Hence, the distribution delay is used to describe this phenomenon [42, 43]. In 2015, Du et al. investigated the passivity of neural networks with discrete and distributed time-varying delays in [44]. In 2016, Yang et al. considered finite-time stabilization of uncertain neural networks with distributed time-varying delays in [45]. However, to the best of our knowledge, there are few results on the passivity of MBAMNNs with probabilistic, leakage, and distributed time-varying delays. Thus, it is significant to study the passivity of MBAMNNs with these time-varying delays.

Motivated by the main points discussed above, the contribution of this paper lies in three aspects.

(1) This is the first attempt to discuss the passivity analysis of MBAMNNs with probabilistic and mixed time-varying delays. In particular, the leakage delays as well as distributed delays are all taken into consideration.

(2) The LKFs that we designed include double and triple integral terms, and by applying some helpful inequalities, the passivity analysis of MBAMNNs becomes less conservative than the existing results [19, 21].

(3) After using MATLAB LMI control toolbox, all the derived results are expressed in LMIs, and a feasible solution can be easily obtained.

The rest of the paper is structured as follows. In Section 2, we introduce the model of the MBAMNNs with probabilistic time-varying delays. In Section 3, the main results on passivity analysis of MBAMNNs with probabilistic and mixed time-varying delays are derived. In Section 4, some numerical simulations are provided to demonstrate the feasibility of our results. In Section 5, the conclusion is shown.

2. Model Description and Preliminaries

In this paper, we propose the MBAMNN with probabilistic time-varying delays as follows:

$$\begin{aligned}
\dot{x}_i(t) &= -C_i x_i(t) + \sum_{j=1}^{m} a_{ji}\left(x_i(t)\right) f_j\left(y_j(t)\right) \\
&\quad + \sum_{j=1}^{m} b_{ji}\left(x_i(t)\right) f_j\left(y_j(t-\tau(t))\right) + u_i(t), \\
\dot{y}_j(t) &= -D_j y_j(t) + \sum_{i=1}^{n} e_{ij}\left(y_j(t)\right) g_i\left(x_i(t)\right) \\
&\quad + \sum_{i=1}^{n} h_{ij}\left(y_j(t)\right) g_i\left(x_i(t-d(t))\right) + v_j(t), \\
&\qquad i = 1,\ldots,n,\ \ j = 1,\ldots,m,
\end{aligned} \tag{1}$$

or it can be rewritten as follows:

$$\begin{aligned}
\dot{x}(t) &= -Cx(t) + A\left(x(t)\right) f\left(y(t)\right) \\
&\quad + B\left(x(t)\right) f\left(y(t-\tau(t))\right) + u(t), \\
\dot{y}(t) &= -Dy(t) + E\left(y(t)\right) g\left(x(t)\right) \\
&\quad + H\left(y(t)\right) g\left(x(t-d(t))\right) + v(t),
\end{aligned} \tag{2}$$

where $x_i(t)$ and $y_j(t)$ denote the state variables related to the ith and jth neurons. $A(x(t)) = (a_{ji}(x_i(t)))_{m\times n}$ and $E(y(t)) = (e_{ij}(y_j(t)))_{n\times m}$ are the connection weight matrices, $f_j(\cdot)$ and $g_i(\cdot)$ are the activation functions, and $B(x(t)) = (b_{ji}(x_i(t)))_{m\times n}$ and $H(y(t)) = (h_{ij}(y_j(t)))_{n\times m}$ are the delayed connection weight matrices. The self-feedback connection weights C_i and D_j are positive diagonal matrices. $u_i(t)$ and $v_j(t)$ represent the continuous external inputs; the nonnegative continuous variables $\tau(t)$ and $d(t)$ correspond to the time-varying delays.

Assumption 1. The functions $f_j(t)$ $(j = 1, 2, \ldots, m)$ and $g_i(t)$ $(i = 1, 2, \ldots, n)$ are bounded and continuous and satisfy the conditions as follows:

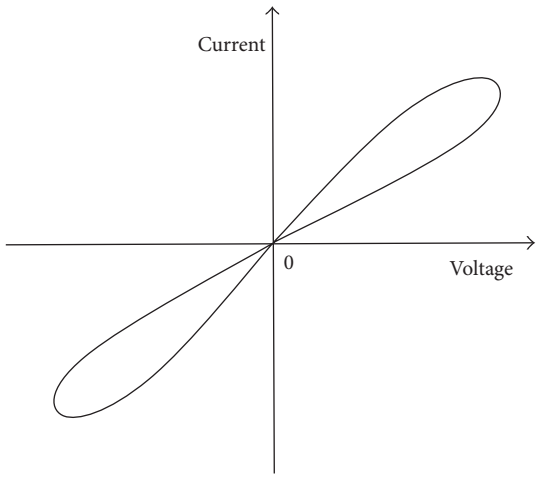

Figure 1: The typical current-voltage characteristic of a memristor.

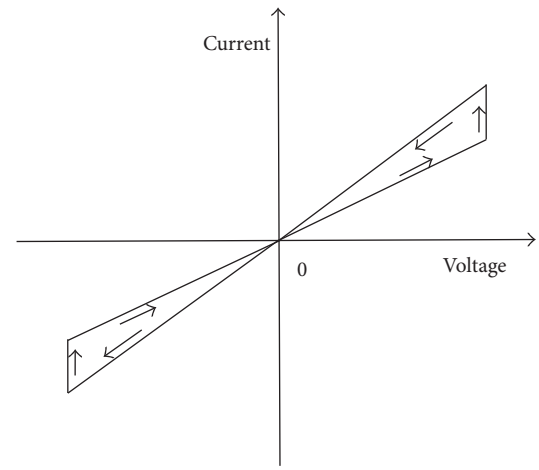

Figure 2: The characteristic of a piecewise linear charge-controlled memristor.

$$\begin{aligned} \varsigma_j^- &\le \frac{f_j(b) - f_j(a)}{b-a} \le \varsigma_j^+, \\ \sigma_i^- &\le \frac{g_i(b) - g_i(a)}{b-a} \le \sigma_i^+, \end{aligned} \tag{3}$$

with $\varsigma^- = \mathrm{diag}(\varsigma_1^-, \varsigma_2^-, \ldots, \varsigma_m^-)$, $\varsigma^+ = \mathrm{diag}(\varsigma_1^+, \varsigma_2^+, \ldots, \varsigma_m^+)$, $\sigma^- = \mathrm{diag}(\sigma_1^-, \sigma_2^-, \ldots, \sigma_n^-)$, and $\sigma^+ = \mathrm{diag}(\sigma_1^+, \sigma_2^+, \ldots, \sigma_n^+)$, $a, b \in R$, $a \ne b$.

Based on the current-voltage characteristic and the feature of memristor, the memristive connection weights $a_{ji}(x_i(t))$, $b_{ji}(x_i(t))$, $e_{ij}(y_j(t))$, and $h_{ji}(x_i(t))$ will change with time. Then, we let

$$\begin{aligned} a_{ji}(x_i(t)) &= \begin{cases} \widehat{a}_{ji}, & |x_i(t)| > \Theta_i, \\ \check{a}_{ji}, & |x_i(t)| \le \Theta_i, \end{cases} \\ b_{ji}(x_i(t)) &= \begin{cases} \widehat{b}_{ji}, & |x_i(t)| > \Theta_i, \\ \check{b}_{ji}, & |x_i(t)| \le \Theta_i, \end{cases} \\ e_{ij}(y_j(t)) &= \begin{cases} \widehat{e}_{ij}, & |y_j(t)| > \Psi_j, \\ \check{e}_{ij}, & |y_j(t)| \le \Psi_j, \end{cases} \\ h_{ij}(y_j(t)) &= \begin{cases} \widehat{f}_{ij}, & |y_j(t)| > \Psi_j, \\ \check{f}_{ij}, & |y_j(t)| \le \Psi_j, \end{cases} \end{aligned} \tag{4}$$

in which a_{ji}, b_{ji}, e_{ij}, and h_{ij} are constants and the switching jumps $\Theta_i > 0$, $\Psi_j > 0$.

Based on Figures 1 and 2, it is clear that $a_{ji}(x_i(t))$, $b_{ji}(x_i(t))$, $e_{ij}(y_j(t))$, and $h_{ij}(y_j(t))$ are piecewise continuous functions; the solutions of the systems are indicated in Filippov's sense and the interval is represented by $[\cdot, \cdot]$. Set

$$\begin{aligned} \overline{a}_{ji} &= \max\left\{\widehat{a}_{ji}, \check{a}_{ji}\right\}, \\ \underline{a}_{ji} &= \min\left\{\widehat{a}_{ji}, \check{a}_{ji}\right\}, \\ \overline{b}_{ji} &= \max\left\{\widehat{b}_{ji}, \check{b}_{ji}\right\}, \\ \underline{b}_{ji} &= \min\left\{\widehat{b}_{ji}, \check{b}_{ji}\right\}, \\ \overline{e}_{ij} &= \max\left\{\widehat{e}_{ij}, \check{e}_{ij}\right\}, \\ \underline{e}_{ij} &= \min\left\{\widehat{e}_{ij}, \check{e}_{ij}\right\}, \\ \overline{h}_{ij} &= \max\left\{\widehat{h}_{ij}, \check{h}_{ij}\right\}, \\ \underline{h}_{ij} &= \min\left\{\widehat{h}_{ij}, \check{h}_{ij}\right\}, \end{aligned} \tag{5}$$

for $i = 1, 2, \ldots, n$, $j = 1, 2, \ldots, m$. $\mathrm{co}[\overline{r}, \underline{r}]$ indicates the convex closure of $[\overline{r}, \underline{r}]$. Obviously, the set-valued maps are defined as

$$\begin{aligned} \mathrm{co}\left[a_{ji}(x_i(t))\right] &= \begin{cases} \widehat{a}_{ji}, & |x_i(t)| > \Theta_i, \\ \left[\underline{a}_{ji}, \overline{a}_{ji}\right], & |x_i(t)| = \Theta_i, \\ \check{a}_{ji}, & |x_i(t)| < \Theta_i, \end{cases} \\ \mathrm{co}\left[b_{ji}(x_i(t))\right] &= \begin{cases} \widehat{b}_{ji}, & |x_i(t)| > \Theta_i, \\ \left[\underline{b}_{ji}, \overline{b}_{ji}\right], & |x_i(t)| = \Theta_i, \\ \check{b}_{ji}, & |x_i(t)| < \Theta_i, \end{cases} \\ \mathrm{co}\left[e_{ij}(y_j(t))\right] &= \begin{cases} \widehat{e}_{ij}, & |y_j(t)| > \Psi_j, \\ \left[\underline{e}_{ij}, \overline{e}_{ij}\right], & |y_j(t)| = \Psi_j, \\ \check{e}_{ij}, & |y_j(t)| < \Psi_j, \end{cases} \end{aligned}$$

$$\operatorname{co}\left[h_{ij}\left(y_j(t)\right)\right]=\begin{cases}\widehat{h}_{ij}, & \left|y_j(t)\right|>\Psi_j,\\ \left[\underline{h}_{ij},\overline{h}_{ij}\right], & \left|y_j(t)\right|=\Psi_j,\\ \check{h}_{ij}, & \left|y_j(t)\right|<\Psi_j.\end{cases}\tag{6}$$

As a matter of convenience, we make the following assumptions.

Assumption 2. We define the probability distribution of time delays $\tau(t)$ and $d(t)$ as follows:

$$\begin{aligned}\operatorname{Prob}\{\tau(t)\in[0,\tau_1]\}&=\mu_0,\\ \operatorname{Prob}\{\tau(t)\in[\tau_1,\tau_2]\}&=1-\mu_0,\\ \operatorname{Prob}\{d(t)\in[0,d_1]\}&=\omega_0,\\ \operatorname{Prob}\{d(t)\in[d_1,d_2]\}&=1-\omega_0,\end{aligned}\tag{7}$$

where $0\le\mu_0\le1$ and $0\le\omega_0\le1$ are constants.

Thus, the random variables $\mu(t)$ and $\omega(t)$ can be defined as

$$\begin{aligned}\mu(t)&=\begin{cases}1, & \tau(t)\in[0,\tau_1],\\ 0, & \tau(t)\in[\tau_1,\tau_2],\end{cases}\\ \omega(t)&=\begin{cases}1, & d(t)\in[0,d_1],\\ 0, & d(t)\in[d_1,d_2].\end{cases}\end{aligned}\tag{8}$$

Then, it can be derived that $\mu(t)$ and $\omega(t)$ are Bernoulli distributed sequences with

$$\begin{aligned}\operatorname{Prob}\{\mu(t)=1\}&=\mu_0,\\ \operatorname{Prob}\{\mu(t)=0\}&=1-\mu_0,\\ \operatorname{Prob}\{\omega(t)=1\}&=\omega_0,\\ \operatorname{Prob}\{\omega(t)=0\}&=1-\omega_0.\end{aligned}\tag{9}$$

According to Assumption 2, it is easy to see that

$$\begin{aligned}\mathbb{E}\{\mu(t)-\mu_0\}&=0,\\ \mathbb{E}\left\{\left(\mu(t)-\mu_0\right)^2\right\}&=\mu_0\left(1-\mu_0\right),\\ \mathbb{E}\{\omega(t)-\omega_0\}&=0,\\ \mathbb{E}\left\{\left(\omega(t)-\omega_0\right)^2\right\}&=\omega_0\left(1-\omega_0\right).\end{aligned}\tag{10}$$

Now, time-varying delays $\tau_1(t)$, $\tau_2(t)$, $d_1(t)$, and $d_2(t)$ are introduced as

$$\begin{aligned}\tau(t)&=\begin{cases}\tau_1(t), & \tau(t)\in[0,\tau_1],\\ \tau_2(t), & \tau(t)\in[\tau_1,\tau_2],\end{cases}\\ d(t)&=\begin{cases}d_1(t), & d(t)\in[0,d_1],\\ d_2(t), & d(t)\in[d_1,d_2].\end{cases}\end{aligned}\tag{11}$$

Assumption 3. Here, constants τ_1, τ_2, d_1, d_2, μ_1, μ_2, ω_1, and ω_2 exist, such that

$$\begin{aligned}0\le\tau_1(t)\le\tau_1,\\ \dot{\tau}_1(t)\le\mu_1,\\ 0\le\tau_2(t)\le\tau_2,\\ \dot{\tau}_2(t)\le\mu_2,\\ 0\le d_1(t)\le d_1,\\ \dot{d}_1(t)\le\omega_1,\\ 0\le d_2(t)\le d_2,\\ \dot{d}_2(t)\le\omega_2.\end{aligned}\tag{12}$$

Assumption 4. The leakage delays $\delta(t)$ and $\rho(t)$ and distributed delays $\alpha(t)$ and $\beta(t)$ satisfy

$$\begin{aligned}0\le\delta(t)\le\delta,\\ \dot{\delta}(t)\le\delta_0,\\ 0\le\rho(t)\le\rho,\\ \dot{\rho}(t)\le\rho_0,\\ 0\le\alpha(t)\le\alpha,\\ 0\le\beta(t)\le\beta.\end{aligned}\tag{13}$$

By employing the theories of set-valued maps, differential inclusions, stochastic variables μ_0, ω_0, and new functions $\tau_1(t)$, $\tau_2(t)$, $d_1(t)$, and $d_2(t)$, system (1) becomes

$$\begin{aligned}&\dot{x}_i(t)\\ &\in -C_i x_i(t)+\sum_{j=1}^{m}\operatorname{co}\left[a_{ji}\left(x_i(t)\right)\right]f_j\left(y_j(t)\right)\\ &\quad+\mu(t)\sum_{j=1}^{m}\operatorname{co}\left[b_{ji}\left(x_i(t)\right)\right]f_j\left(y_j\left(t-\tau_1(t)\right)\right)\\ &\quad+\left(1-\mu(t)\right)\sum_{j=1}^{m}\operatorname{co}\left[b_{ji}\left(x_i(t)\right)\right]f_j\left(y_j\left(t-\tau_2(t)\right)\right)\\ &\quad+u_i(t),\\ &\dot{y}_j(t)\\ &\in -D_j y_j(t)+\sum_{i=1}^{n}\operatorname{co}\left[e_{ij}\left(y_j(t)\right)\right]g_i\left(x_i(t)\right)\\ &\quad+\omega(t)\sum_{i=1}^{n}\operatorname{co}\left[h_{ij}\left(y_j(t)\right)\right]g_i\left(x_i\left(t-d_1(t)\right)\right)\\ &\quad+\left(1-\omega(t)\right)\sum_{i=1}^{n}\operatorname{co}\left[h_{ij}\left(y_j(t)\right)\right]g_i\left(x_i\left(t-d_2(t)\right)\right)\\ &\quad+v_j(t).\end{aligned}\tag{14}$$

Or it can be rewritten as follows:

$$\begin{aligned}\dot{x}(t) &= -Cx(t) + A(x(t))\, f(y(t)) \\ &\quad + \mu(t)\, B(x(t))\, f(y(t-\tau_1(t))) \\ &\quad + (1-\mu(t))\, B(x(t))\, f(y(t-\tau_2(t))) \\ &\quad + u(t), \\ \dot{y}(t) &= -Dy(t) + E(y(t))\, g(x(t)) \\ &\quad + \omega(t)\, H(y(t))\, g(x(t-d_1(t))) \\ &\quad + (1-\omega(t))\, H(y(t))\, g(x(t-d_2(t))) \\ &\quad + v(t);\end{aligned} \tag{15}$$

equivalently,

$$\begin{aligned}\dot{x}(t) &= -Cx(t) + A(x(t))\, f(y(t)) + \mu_0 B(x(t)) \\ &\quad \cdot f(y(t-\tau_1(t))) + (1-\mu_0)\, B(x(t)) \\ &\quad \cdot f(y(t-\tau_2(t))) + (\mu(t)-\mu_0)\, B(x(t)) \\ &\quad \cdot (f(y(t-\tau_1(t))) - f(y(t-\tau_2(t)))) + u(t), \\ \dot{y}(t) &= -Dy(t) + E(y(t))\, g(x(t)) + \omega_0 H(y(t)) \\ &\quad \cdot g(x(t-d_1(t))) + (1-\omega_0)\, H(y(t)) \\ &\quad \cdot g(x(t-d_2(t))) + (\omega(t)-\omega_0)\, H(y(t)) \\ &\quad \cdot (g(x(t-d_1(t))) - g(x(t-d_2(t)))) + v(t).\end{aligned} \tag{16}$$

Definition 5. System (15) is called passive if there exists a scalar $\gamma > 0$ such that

$$\begin{aligned}&2\int_0^{t_z} \begin{bmatrix} f^T(y(s)) & g^T(x(s)) \end{bmatrix} \begin{bmatrix} u(s) \\ v(s) \end{bmatrix} ds \\ &\quad \geq -\gamma \int_0^{t_z} \begin{bmatrix} u^T(s) & v^T(s) \end{bmatrix} \begin{bmatrix} u(s) \\ v(s) \end{bmatrix} ds,\end{aligned} \tag{17}$$

for all solutions of (15) with $x(0) = 0$ and $y(0) = 0$ and for all $t_z \geq 0$.

Remark 6. Passivity analysis originates from circuit theory and it uses the input-output description method based on energy to design and analyze a system. The physical meaning of passivity is reflected in Definition 5 where the energy growth of the system is always less than or equal to the total energy of the external inputs; this means that the passive system is always accompanied by the loss of energy. In fact, the storage function of the passive system can be used as a Lyapunov function under certain conditions. Thus, both Lyapunov stability theory and passivity theory can be used to research the stability of the system.

Lemma 7. *For any scalars $p_2 > p_1 > 0$, matrix $R \in \Re^{n\times n}$, $R = R^T > 0$, and vector function $\omega : [p_1, p_2] \mapsto R^n$, the inequalities hold as follows:*

$$\begin{aligned}&(p_2 - p_1)\int_{p_1}^{p_2} \omega^T(s) R\omega(s)\, ds \\ &\quad \geq \left(\int_{p_1}^{p_2} \omega(s)\, ds\right)^T R \left(\int_{p_1}^{p_2} \omega(s)\, ds\right),\end{aligned} \tag{18}$$

$$\begin{aligned}&\frac{(p_2 - p_1)^2}{2}\int_{p_1}^{p_2}\int_{t+\theta}^{t} \omega^T(s) R\omega(s)\, ds\, d\theta \\ &\quad \geq \left(\int_{p_1}^{p_2}\int_{t+\theta}^{t} \omega(s)\, ds\right)^T R \left(\int_{p_1}^{p_2}\int_{t+\theta}^{t} \omega(s)\, ds\right).\end{aligned} \tag{19}$$

3. Main Results

For derivation convenience, we denote

$$\begin{aligned}A &= \max\left\{\left|\underline{a}_{ji}\right|, \left|\overline{a}_{ji}\right|\right\}, \\ B &= \max\left\{\left|\underline{b}_{ji}\right|, \left|\overline{b}_{ji}\right|\right\}, \\ E &= \max\left\{\left|\underline{e}_{ij}\right|, \left|\overline{e}_{ij}\right|\right\}, \\ H &= \max\left\{\left|\underline{h}_{ij}\right|, \left|\overline{h}_{ij}\right|\right\}.\end{aligned} \tag{20}$$

Theorem 8. *Under Assumptions 1–3, system (16) is passive, if there exist any appropriately dimensional matrices M_m ($m = 1, 2, \ldots, 4$), W_w ($w = 1, 2, \ldots, 6$), a scalar $\gamma > 0$, and symmetric positive definite matrices R_i ($i = 1, 2$), Q_j ($j = 3, 4, \ldots, 6$), O_o ($o = 3, 4, \ldots, 6$), P_k ($k = 2, 3, 6, 7$), Z_l ($l = 1, 2, \ldots, 4$), and N_n ($n = 1, 2$), such that the following LMIs hold:*

$$\begin{aligned}\Omega_{i,j} &= \left(\Omega_{i,j}\right)_{14\times 14} < 0, \\ \Phi_{i,j} &= \left(\Phi_{i,j}\right)_{14\times 14} < 0,\end{aligned} \tag{21}$$

where

$$\begin{aligned}\Omega_{1,1} &= -R_1 C - C^T R_1 + Q_3 + Q_4 - P_2 - 2Z_1 - 2Z_2 \\ &\quad - M_1 C - C^T M_1 - 2\varsigma^- W_1 \varsigma^+, \\ \Omega_{1,4} &= P_2, \\ \Omega_{1,6} &= -M_1 - M_2 C, \\ \Omega_{1,7} &= R_1 A + M_1 A + W_1(\varsigma^- + \varsigma^+), \\ \Omega_{1,8} &= \mu_0(R_1 + M_1) B, \\ \Omega_{1,9} &= (1-\mu_0)(M_1 + R_1) B, \\ \Omega_{1,12} &= \frac{2}{\tau_1} Z_1,\end{aligned}$$

$$\Omega_{1,13} = \frac{2}{\tau_2 - \tau_1} Z_2,$$
$$\Omega_{1,14} = R_1 + M_1,$$
$$\Omega_{2,2} = -\left(1 - \mu_1\right) Q_3 - 2\varsigma^- W_2 \varsigma^+,$$
$$\Omega_{2,8} = -\left(1 - \mu_1\right) Q_3 + W_2 \left(\varsigma^- + \varsigma^+\right),$$
$$\Omega_{3,3} = -\left(1 - \mu_2\right) Q_5 - 2\varsigma^- W_3 \varsigma^+,$$
$$\Omega_{3,9} = -\left(1 - \mu_2\right) Q_5 + W_3 \left(\varsigma^- + \varsigma^+\right),$$
$$\Omega_{4,4} = Q_5 + Q_6 - Q_4 - P_2 - P_3,$$
$$\Omega_{4,5} = P_3,$$
$$\Omega_{4,10} = Q_5 + Q_6 - Q_4,$$
$$\Omega_{5,5} = -Q_6 - P_3,$$
$$\Omega_{5,11} = -Q_6,$$
$$\Omega_{6,6} = \tau_1^2 P_2 + \left(\tau_2 - \tau_1\right)^2 P_3 + \frac{\tau_1^2}{2} Z_1 + \frac{\tau_2^2 - \tau_1^2}{2} Z_2 - 2M_2,$$
$$\Omega_{6,7} = M_2 A,$$
$$\Omega_{6,8} = \mu_0 M_2 B,$$
$$\Omega_{6,9} = \left(1 - \mu_0\right) M_2 B,$$
$$\Omega_{6,14} = M_2,$$
$$\Omega_{7,7} = -2W_1,$$
$$\Omega_{7,14} = -I,$$
$$\Omega_{8,8} = -\left(1 - \mu_1\right) Q_3 - 2W_2,$$
$$\Omega_{9,9} = -\left(1 - \mu_2\right) Q_5 - 2W_3,$$
$$\Omega_{10,10} = Q_5 + Q_6 - Q_4,$$
$$\Omega_{11,11} = -Q_6,$$
$$\Omega_{12,12} = -\frac{2}{\tau_1^2} Z_1,$$
$$\Omega_{13,13} = -\frac{2}{\left(\tau_2 - \tau_1\right)^2} Z_2,$$
$$\Omega_{14,14} = -\gamma I, \tag{22}$$

$$\Phi_{1,1} = -R_2 D - D^T R_2 + O_3 + O_4 - P_6 - 2Z_3 - 2Z_4 - M_3 D - D^T M_3 - 2\sigma^- W_4 \sigma^+,$$
$$\Phi_{1,4} = P_6,$$
$$\Phi_{1,6} = -M_3 - M_4 D,$$
$$\Phi_{1,7} = R_2 E + M_3 E + W_4 \left(\sigma^- + \sigma^+\right),$$
$$\Phi_{1,8} = \omega_0 \left(R_2 + M_3\right) H,$$
$$\Phi_{1,9} = \left(1 - \omega_0\right) \left(M_3 + R_2\right) H,$$
$$\Phi_{1,12} = \frac{2}{d_1} Z_3,$$
$$\Phi_{1,13} = \frac{2}{d_2 - d_1} Z_4,$$
$$\Phi_{1,14} = R_2 + M_3,$$
$$\Phi_{2,2} = -\left(1 - \omega_1\right) O_3 - 2\sigma^- W_5 \sigma^+,$$
$$\Phi_{2,8} = -\left(1 - \omega_1\right) O_3 + W_5 \left(\sigma^- + \sigma^+\right),$$
$$\Phi_{3,3} = -\left(1 - \omega_2\right) O_5 - 2\sigma^- W_6 \sigma^+,$$
$$\Phi_{3,9} = -\left(1 - \omega_2\right) O_5 + W_6 \left(\sigma^- + \sigma^+\right),$$
$$\Phi_{4,4} = O_5 + O_6 - O_4 - P_6 - P_7,$$
$$\Phi_{4,5} = P_7,$$
$$\Phi_{4,10} = O_5 + O_6 - O_4,$$
$$\Phi_{5,5} = -O_6 - P_7,$$
$$\Phi_{5,11} = -O_6,$$
$$\Phi_{6,6} = d_1^2 P_6 + \left(d_2 - d_1\right)^2 P_7 + \frac{d_1^2}{2} Z_3 + \frac{d_2^2 - d_1^2}{2} Z_4 - 2M_4,$$
$$\Phi_{6,7} = M_4 E,$$
$$\Phi_{6,8} = \omega_0 M_4 H,$$
$$\Phi_{6,9} = \left(1 - \omega_0\right) M_4 H,$$
$$\Phi_{6,14} = M_4,$$
$$\Phi_{7,7} = -2W_4,$$
$$\Phi_{7,14} = -I,$$
$$\Phi_{8,8} = -\left(1 - \omega_1\right) O_3 - 2W_5,$$
$$\Phi_{9,9} = -\left(1 - \omega_2\right) O_5 - 2W_6,$$
$$\Phi_{10,10} = O_5 + O_6 - O_4,$$
$$\Phi_{11,11} = -O_6,$$
$$\Phi_{12,12} = -\frac{2}{d_1^2} Z_3,$$
$$\Phi_{13,13} = -\frac{2}{\left(d_2 - d_1\right)^2} Z_4,$$
$$\Phi_{14,14} = -\gamma I. \tag{23}$$

Proof. Consider the following LKF candidate:

$$V(t) = \sum_{i=1}^{8} V_i(t), \tag{24}$$

where

$$\begin{aligned}
V_1(t) &= x^T(t) R_1 x(t),\\
V_2(t) &= y^T(t) R_2 y(t),\\
V_3(t) &= \int_{t-\tau_1(t)}^{t} \begin{bmatrix} x(s) \\ f(y(s)) \end{bmatrix}^T Q_3 \begin{bmatrix} x(s) \\ f(y(s)) \end{bmatrix} ds\\
&\quad + \int_{t-\tau_1}^{t} \begin{bmatrix} x(s) \\ f(y(s)) \end{bmatrix}^T Q_4 \begin{bmatrix} x(s) \\ f(y(s)) \end{bmatrix} ds\\
&\quad + \int_{t-\tau_2(t)}^{t-\tau_1} \begin{bmatrix} x(s) \\ f(y(s)) \end{bmatrix}^T Q_5 \begin{bmatrix} x(s) \\ f(y(s)) \end{bmatrix} ds\\
&\quad + \int_{t-\tau_2}^{t-\tau_1} \begin{bmatrix} x(s) \\ f(y(s)) \end{bmatrix}^T Q_6 \begin{bmatrix} x(s) \\ f(y(s)) \end{bmatrix} ds,\\
V_4(t) &= \int_{t-d_1(t)}^{t} \begin{bmatrix} y(s) \\ g(x(s)) \end{bmatrix}^T O_3 \begin{bmatrix} y(s) \\ g(x(s)) \end{bmatrix} ds\\
&\quad + \int_{t-d_1}^{t} \begin{bmatrix} y(s) \\ g(x(s)) \end{bmatrix}^T O_4 \begin{bmatrix} y(s) \\ g(x(s)) \end{bmatrix} ds\\
&\quad + \int_{t-d_2(t)}^{t-d_1} \begin{bmatrix} y(s) \\ g(x(s)) \end{bmatrix}^T O_5 \begin{bmatrix} y(s) \\ g(x(s)) \end{bmatrix} ds\\
&\quad + \int_{t-d_2}^{t-d_1} \begin{bmatrix} y(s) \\ g(x(s)) \end{bmatrix}^T O_6 \begin{bmatrix} y(s) \\ g(x(s)) \end{bmatrix} ds,\\
V_5(t) &= \tau_1 \int_{-\tau_1}^{0} \int_{t+\theta}^{t} \dot{x}^T(s) P_2 \dot{x}(s)\, ds\, d\theta\\
&\quad + (\tau_2 - \tau_1) \int_{-\tau_2}^{-\tau_1} \int_{t+\theta}^{t} \dot{x}^T(s) P_3 \dot{x}(s)\, ds\, d\theta,\\
V_6(t) &= d_1 \int_{-d_1}^{0} \int_{t+\theta}^{t} \dot{y}^T(s) P_6 \dot{y}(s)\, ds\, d\theta\\
&\quad + (d_2 - d_1) \int_{-d_2}^{-d_1} \int_{t+\theta}^{t} \dot{y}^T(s) P_7 \dot{y}(s)\, ds\, d\theta,\\
V_7(t) &= \int_{-\tau_1}^{0} \int_{\theta}^{0} \int_{t+\lambda}^{t} \dot{x}^T(s) Z_1 \dot{x}(s)\, ds\, d\lambda\, d\theta\\
&\quad + \int_{-\tau_2}^{-\tau_1} \int_{\theta}^{0} \int_{t+\lambda}^{t} \dot{x}^T(s) Z_2 \dot{x}(s)\, ds\, d\lambda\, d\theta,\\
V_8(t) &= \int_{-d_1}^{0} \int_{\theta}^{0} \int_{t+\lambda}^{t} \dot{y}^T(s) Z_3 \dot{y}(s)\, ds\, d\lambda\, d\theta\\
&\quad + \int_{-d_2}^{-d_1} \int_{\theta}^{0} \int_{t+\lambda}^{t} \dot{y}^T(s) Z_4 \dot{y}(s)\, ds\, d\lambda\, d\theta.
\end{aligned} \tag{25}$$

Then, we define the infinitesimal generator $\mathscr{L}$ of $V(t)$ as

$$\mathscr{L}V(t) = \lim_{\Delta \to 0^+} \frac{1}{\Delta} \left\{ \mathbb{E}\left(\frac{V(t+\Delta)}{t} \right) - V(t) \right\}. \tag{26}$$

Taking the mathematical expectation of $V(t)$, we get

$$\begin{aligned}
\mathbb{E}\{\mathscr{L}V_1(t)\} &= \mathbb{E}\{2x^T(t) R_1 (-Cx(t) + A(x(t))\\
&\quad \cdot f(y(t)) + \mu_0 B(x(t)) f(y(t - \tau_1(t)))\\
&\quad + (1 - \mu_0) B(x(t)) f(y(t - \tau_2(t))) + (\mu(t) - \mu_0)\\
&\quad \cdot B(x(t)) (f(y(t - \tau_1(t))) - f(y(t - \tau_2(t))))\\
&\quad + u(t))\} \le \mathbb{E}\{2x^T(t) R_1 (-Cx(t) + Af(y(t))\\
&\quad + \mu_0 Bf(y(t - \tau_1(t))) + (1 - \mu_0)\\
&\quad \cdot Bf(y(t - \tau_2(t))) + u(t))\},\\
\mathbb{E}\{\mathscr{L}V_2(t)\} &= \mathbb{E}\{2y^T(t) R_2 (-Dy(t) + E(y(t))\\
&\quad \cdot g(x(t)) + \omega_0 H(y(t)) g(x(t - d_1(t)))\\
&\quad + (1 - \omega_0) H(y(t)) g(x(t - d_2(t)))) + (\omega(t)\\
&\quad - \omega_0) H(y(t)) (g(x(t - d_1(t)))\\
&\quad - g(x(t - d_2(t)))) + \nu(t)\} \le \mathbb{E}\{2y^T(t)\\
&\quad \cdot R_2 (-Dy(t) + Eg(x(t)) + \omega_0 Hg(x(t - d_1(t)))\\
&\quad + (1 - \omega_0) Hg(x(t - d_2(t))) + \nu(t))\}.
\end{aligned} \tag{27}$$

According to Assumption 3, we obtain

$$\begin{aligned}
\mathbb{E}\{\mathscr{L}V_3(t)\} &\le \mathbb{E}\left\{ x^T(t) (Q_3 + Q_4) x(t) - (1 - \mu_1) \right.\\
&\quad \cdot \begin{bmatrix} x(t - \tau_1(t)) \\ f(y(t - \tau_1(t))) \end{bmatrix}^T Q_3 \begin{bmatrix} x(t - \tau_1(t)) \\ f(y(t - \tau_1(t))) \end{bmatrix}\\
&\quad + \begin{bmatrix} x(t - \tau_1) \\ f(y(t - \tau_1)) \end{bmatrix}^T (Q_5 + Q_6 - Q_4)\\
&\quad \cdot \begin{bmatrix} x(t - \tau_1) \\ f(y(t - \tau_1)) \end{bmatrix} - (1 - \mu_2) \begin{bmatrix} x(t - \tau_2(t)) \\ f(y(t - \tau_2(t))) \end{bmatrix}^T\\
&\quad \cdot Q_5 \begin{bmatrix} x(t - \tau_2(t)) \\ f(y(t - \tau_2(t))) \end{bmatrix} - \begin{bmatrix} x(t - \tau_2) \\ f(y(t - \tau_2)) \end{bmatrix}^T\\
&\quad \left. \cdot Q_6 \begin{bmatrix} x(t - \tau_2) \\ f(y(t - \tau_2)) \end{bmatrix} \right\},
\end{aligned}$$

$$\begin{aligned}\mathbb{E}\{\mathscr{L}V_4(t)\} \le \mathbb{E}\Bigg\{ & y^T(t)(O_3+O_4)y(t) - (1-\omega_1)\\ & \cdot \begin{bmatrix} y(t-d_1(t)) \\ g(x(t-d_1(t))) \end{bmatrix}^T O_3 \begin{bmatrix} y(t-d_1(t)) \\ g(x(t-d_1(t))) \end{bmatrix}\\ & + \begin{bmatrix} y(t-d_1) \\ g(x(t-d_1)) \end{bmatrix}^T (O_5+O_6-O_4)\\ & \cdot \begin{bmatrix} y(t-d_1) \\ g(x(t-d_1)) \end{bmatrix} - (1-\omega_2)\begin{bmatrix} y(t-d_2(t)) \\ g(x(t-d_2(t))) \end{bmatrix}^T\\ & \cdot O_5 \begin{bmatrix} y(t-d_2(t)) \\ g(x(t-d_2(t))) \end{bmatrix} - \begin{bmatrix} y(t-\tau_2) \\ g(x(t-\tau_2)) \end{bmatrix}^T\\ & \cdot O_6 \begin{bmatrix} y(t-\tau_2) \\ g(x(t-\tau_2)) \end{bmatrix}\Bigg\}. \end{aligned} \tag{28}$$

It is obvious that

$$\begin{aligned}\mathbb{E}\{\mathscr{L}V_5(t)\} = \mathbb{E}\Big\{ & \dot{x}^T(t)\left[\tau_1^2 P_2 + (\tau_2-\tau_1)^2 P_3\right]\dot{x}(t)\\ & - \tau_1 \int_{t-\tau_1}^{t} \dot{x}^T(s) P_2 \dot{x}(s)\,ds\\ & - (\tau_2-\tau_1)\int_{t-\tau_2}^{t-\tau_1} \dot{x}^T(s) P_3 \dot{x}(s)\,ds\Big\},\\ \mathbb{E}\{\mathscr{L}V_6(t)\} = \mathbb{E}\Big\{ & \dot{y}^T(t)\left[d_1^2 P_6 + (d_2-d_1)^2 P_7\right]\dot{y}(t)\\ & - d_1 \int_{t-d_1}^{t} \dot{y}^T(s) P_6 \dot{y}(s)\,ds\\ & - (d_2-d_1)\int_{t-d_2}^{t-d_1} \dot{y}^T(s) P_7 \dot{y}(s)\,ds\Big\}. \end{aligned} \tag{29}$$

Using Lemma 7, we have

$$\begin{aligned} & - \tau_1 \int_{t-\tau_1}^{t} \dot{x}^T(s) P_2 \dot{x}(s)\,ds \le -\left(\int_{t-\tau_1}^{t} \dot{x}(s)\,ds\right)^T\\ & \cdot P_2 \left(\int_{t-\tau_1}^{t} \dot{x}(s)\,ds\right) = -\left[x(t)-x(t-\tau_1)\right]^T\\ & \cdot P_2 \left[x(t)-x(t-\tau_1)\right],\\ & - (\tau_2-\tau_1)\int_{t-\tau_2}^{t-\tau_1} \dot{x}^T(s) P_3 \dot{x}(s)\,ds\\ & \le -\left(\int_{t-\tau_2}^{t-\tau_1} \dot{x}(s)\,ds\right)^T P_3 \left(\int_{t-\tau_2}^{t-\tau_1} \dot{x}(s)\,ds\right)\\ & = -\left[x(t-\tau_1)-x(t-\tau_2)\right]^T\\ & \cdot P_3 \left[x(t-\tau_1)-x(t-\tau_2)\right]. \end{aligned} \tag{30}$$

Similarly,

$$\begin{aligned} & - d_1 \int_{t-d_1}^{t} \dot{y}^T(s) P_6 \dot{y}(s)\,ds \le -\left(\int_{t-d_1}^{t} \dot{y}(s)\,ds\right)^T\\ & \cdot P_6 \left(\int_{t-d_1}^{t} \dot{y}(s)\,ds\right) = -\left[y(t)-y(t-d_1)\right]^T\\ & \cdot P_6 \left[y(t)-y(t-d_1)\right], \end{aligned} \tag{31}$$

$$\begin{aligned} & - (d_2-d_1)\int_{t-d_2}^{t-d_1} \dot{y}^T(s) P_7 \dot{y}(s)\,ds\\ & \le -\left(\int_{t-d_2}^{t-d_1} \dot{y}(s)\,ds\right)^T P_7 \left(\int_{t-d_2}^{t-d_1} \dot{y}(s)\,ds\right)\\ & = -\left[y(t-d_1)-y(t-d_2)\right]^T\\ & \cdot P_7 \left[y(t-d_1)-y(t-d_2)\right]. \end{aligned} \tag{32}$$

Moreover, we obtain

$$\begin{aligned}\mathbb{E}\{\mathscr{L}V_7(t)\} = \mathbb{E}\Big\{ & \dot{x}^T(t)\left(\frac{\tau_1^2}{2}Z_1 + \frac{\tau_2^2-\tau_1^2}{2}Z_2\right)\dot{x}(t)\\ & - \int_{-\tau_1}^{0}\int_{t+\theta}^{t} \dot{x}^T(s) Z_1 \dot{x}(s)\,ds\,d\theta\\ & - \int_{-\tau_2}^{-\tau_1}\int_{t+\theta}^{t} \dot{x}^T(s) Z_2 \dot{x}(s)\,ds\,d\theta\Big\},\\ \mathbb{E}\{\mathscr{L}V_8(t)\} = \mathbb{E}\Big\{ & \dot{y}^T(t)\left(\frac{d_1^2}{2}Z_3 + \frac{d_2^2-d_1^2}{2}Z_4\right)\dot{y}(t)\\ & - \int_{-d_1}^{0}\int_{t+\theta}^{t} \dot{y}^T(s) Z_3 \dot{y}(s)\,ds\,d\theta\\ & - \int_{-d_2}^{-d_1}\int_{t+\theta}^{t} \dot{y}^T(s) Z_4 \dot{y}(s)\,ds\,d\theta\Big\}. \end{aligned} \tag{33}$$

Using (18), we have

$$\begin{aligned} & - \int_{-\tau_1}^{0}\int_{t+\theta}^{t} \dot{x}^T(s) Z_1 \dot{x}(s)\,ds\,d\theta\\ & \le -\frac{2}{\tau_1^2}\left(\int_{-\tau_1}^{0}\int_{t+\theta}^{t} \dot{x}(s)\,ds\,d\theta\right)^T\\ & \cdot Z_1 \left(\int_{-\tau_1}^{0}\int_{t+\theta}^{t} \dot{x}(s)\,ds\,d\theta\right) = -2x^T(t) Z_1 x(t)\\ & + \frac{4}{\tau_1} x^T(t) Z_1 \left(\int_{t-\tau_1}^{t} x(s)\,ds\right)\\ & - \frac{2}{\tau_1^2}\left(\int_{t-\tau_1}^{t} x(s)\,ds\right)^T Z_1 \left(\int_{t-\tau_1}^{t} x(s)\,ds\right), \end{aligned}$$

$$
\begin{aligned}
&-\int_{-\tau_2}^{-\tau_1}\int_{t+\theta}^{t}\dot{x}^T(s)Z_2\dot{x}(s)\,ds\,d\theta\\
&\le -\frac{2}{(\tau_2-\tau_1)^2}\left(\int_{-\tau_2}^{-\tau_1}\int_{t+\theta}^{t}\dot{x}(s)\,ds\,d\theta\right)^T\\
&\times Z_2\left(\int_{-\tau_2}^{-\tau_1}\int_{t+\theta}^{t}\dot{x}(s)\,ds\,d\theta\right)=-2x^T(t)Z_2x(t)\\
&+\frac{4}{\tau_2-\tau_1}x^T(t)Z_2\left(\int_{t-\tau_2}^{t-\tau_1}x(s)\,ds\right)\\
&-\frac{2}{(\tau_2-\tau_1)^2}\left(\int_{t-\tau_2}^{t-\tau_1}x(s)\,ds\right)^T Z_2\left(\int_{t-\tau_2}^{t-\tau_1}x(s)\,ds\right).
\end{aligned}
\tag{34}
$$

Similarly,

$$
\begin{aligned}
&-\int_{-d_1}^{0}\int_{t+\theta}^{t}\dot{y}^T(s)Z_3\dot{y}(s)\,ds\,d\theta\\
&\le -\frac{2}{d_1^2}\left(\int_{-d_1}^{0}\int_{t+\theta}^{t}\dot{y}(s)\,ds\,d\theta\right)^T\\
&\cdot Z_3\left(\int_{-d_1}^{0}\int_{t+\theta}^{t}\dot{y}(s)\,ds\,d\theta\right)=-2y^T(t)Z_3y(t)\\
&+\frac{4}{d_1}y^T(t)Z_3\left(\int_{t-d_1}^{t}y(s)\,ds\right)\\
&-\frac{2}{d_1^2}\left(\int_{t-d_1}^{t}y(s)\,ds\right)^T Z_3\left(\int_{t-d_1}^{t}y(s)\,ds\right),\\
&-\int_{-d_2}^{-d_1}\int_{t+\theta}^{t}y^T(s)Z_4y(s)\,ds\,d\theta\\
&\le -\frac{2}{(d_2-d_1)^2}\left(\int_{-d_2}^{-d_1}\int_{t+\theta}^{t}y(s)\,ds\,d\theta\right)^T\\
&\times Z_4\left(\int_{-d_2}^{-d_1}\int_{t+\theta}^{t}y(s)\,ds\,d\theta\right)=-2y^T(t)Z_4y(t)\\
&+\frac{4}{d_2-d_1}y^T(t)Z_4\left(\int_{t-d_2}^{t-d_1}y(s)\,ds\right)\\
&-\frac{2}{(d_2-d_1)^2}\left(\int_{t-d_2}^{t-d_1}y(s)\,ds\right)^T\\
&\cdot Z_4\left(\int_{t-d_2}^{t-d_1}y(s)\,ds\right).
\end{aligned}
\tag{35}
\tag{36}
$$

To derive a less conservative criterion, we add the following inequations with any matrices M_1, M_2, M_3, and M_4 of appropriate dimensions:

$$
\begin{aligned}
0\le{}&2\left(x^T(t)M_1+\dot{x}^T(t)M_2\right)\left[-\dot{x}-Cx(t)\right.\\
&+Af(y(t))+\mu_0Bf(y(t-\tau_1(t)))\\
&\left.+(1-\mu_0)Bf(y(t-\tau_2(t)))+u(t)\right],\\
0\le{}&2\left(y^T(t)M_3+\dot{y}^T(t)M_4\right)\left[-\dot{y}-Dy(t)\right.\\
&+Eg(x(t))+\omega_0Hg(x(t-d_1(t)))\\
&\left.+(1-\omega_0)Hg(x(t-d_2(t)))+v(t)\right].
\end{aligned}
\tag{37}
$$

Based on Assumption 1 [20], we have

$$
\begin{aligned}
&\varsigma^-x(t)-f(y(t))\le 0,\\
&f(y(t))-\varsigma^+x(t)\le 0,\\
&\sigma^-y(t)-g(x(t))\le 0,\\
&g(x(t))-\sigma^+y(t)\le 0,
\end{aligned}
\tag{38}
$$

and there exist positive diagonal matrices $W_i > 0$ ($i = 1, 2, \ldots, 8$); the following inequalities hold:

$$
\begin{aligned}
0\le{}&2\left[\varsigma^-x(t)-f(y(t))\right]^T W_1\left[f(y(t))-\varsigma^+x(t)\right]\\
\le{}&-2f^T(y(t))W_1f(y(t))\\
&+2x^T(t)W_1(\varsigma^-+\varsigma^+)f(y(t))\\
&-2x^T(t)\varsigma^-W_1\varsigma^+x(t).
\end{aligned}
\tag{39}
$$

Similarly,

$$
\begin{aligned}
0\le{}&-2f^T(y(t-\tau_1))W_2f(y(t-\tau_1))\\
&+2x(t)^T(t-\tau_1)W_2(\varsigma^-+\varsigma^+)f(y(t-\tau_1))\\
&-2x^T(t-\tau_1)\varsigma^-W_2\varsigma^+x(t-\tau_1),\\
0\le{}&-2f^T(y(t-\tau_2))W_3f(y(t-\tau_2))\\
&+2x^T(t-\tau_2)W_3(\varsigma^-+\varsigma^+)f(y(t-\tau_2))\\
&-2x^T(t-\tau_2)\varsigma^-W_3\varsigma^+x(t-\tau_2),\\
0\le{}&2\left[\sigma^-y(t)-g(x(t))\right]^T W_4\left[g(x(t))-\sigma^+y(t)\right]\\
\le{}&-2g^T(x(t))W_4g(x(t))\\
&+2y^T(t)W_4(\sigma^-+\sigma^+)g(x(t))\\
&-2y^T(t)\sigma^-W_4\sigma^+y(t),\\
0\le{}&-2g^T(x(t-d_1))W_5g(x(t-d_1))\\
&+2y(t)^T(t-d_1)W_5(\sigma^-+\sigma^+)g(x(t-d_1))\\
&-2y^T(t-d_1)\sigma^-W_5\sigma^+y(t-d_1),\\
0\le{}&-2g^T(x(t-d_2))W_6g(x(t-d_2))\\
&+2y^T(t-d_2)W_6(\sigma^-+\sigma^+)g(x(t-d_2))\\
&-2y^T(t-d_2)\sigma^-W_6\sigma^+y(t-d_2).
\end{aligned}
\tag{40}
$$

Define

$$\begin{aligned}\xi(t) = &\Big\{x^T(t) \quad x^T(t-\tau_1(t)) \quad x^T(t-\tau_2(t))\\ &x^T(t-\tau_1) \quad x^T(t-\tau_2) \quad \dot{x}(t) \quad f^T(y(t))\\ &f^T(y(t-\tau_1(t))) \quad f^T(y(t-\tau_2(t))) \quad f^T(y(t-\tau_1))\\ &f^T(y(t-\tau_2)) \quad \int_{t-\tau_1}^{t} x^T(s)\,ds \quad \int_{t-\tau_2}^{t-\tau_1} x^T(s)\,ds \quad u^T(t)\Big\},\\ \zeta(t) = &\Big\{y^T(t) \quad y^T(t-d_1(t)) \quad y^T(t-d_2(t))\\ &y^T(t-d_1) \quad y^T(t-d_2) \quad \dot{y}(t) \quad g^T(x(t)) \quad g^T(x(t-d_1(t)))\\ &g^T(x(t-d_2(t))) \quad g^T(x(t-d_1)) \quad g^T(x(t-d_2))\\ &\int_{t-d_1}^{t} y^T(s)\,ds \quad \int_{t-d_2}^{t-d_1} y^T(s)\,ds \quad v^T(t)\Big\}.\end{aligned} \tag{41}$$

Combining (23), (27)–(37), and (40), we have

$$\begin{aligned}&\mathbb{E}\left\{\mathscr{L}V(t) - 2\begin{bmatrix}f^T(y(s)) & g^T(x(s))\end{bmatrix}\begin{bmatrix}u(s)\\ v(s)\end{bmatrix}\right.\\ &\left.-\gamma\begin{bmatrix}u^T(t) & v^T(t)\end{bmatrix}\begin{bmatrix}u(t)\\ v(t)\end{bmatrix}ds\right\} \le \mathbb{E}\left\{\xi^T(t)\,\Omega\xi(t)\right.\\ &\left.+\zeta^T(t)\,\Phi\zeta(t)\right\}.\end{aligned} \tag{42}$$

Thus, we conclude that if (42) holds, then

$$\begin{aligned}&\mathbb{E}\left\{\mathscr{L}V(t) - 2\begin{bmatrix}f^T(y(s)) & g^T(x(s))\end{bmatrix}\begin{bmatrix}u(s)\\ v(s)\end{bmatrix}\right.\\ &\left.-\gamma\begin{bmatrix}u^T(t) & v^T(t)\end{bmatrix}\begin{bmatrix}u(t)\\ v(t)\end{bmatrix}ds\right\} \le 0.\end{aligned} \tag{43}$$

By integrating (43) about t from 0 to t_z, we get

$$\begin{aligned}&2\mathbb{E}\int_0^{t_z}\begin{bmatrix}f^T(y(s)) & g^T(x(s))\end{bmatrix}\begin{bmatrix}u(s)\\ v(s)\end{bmatrix}ds\\ &\ge \mathbb{E}V(t) - \mathbb{E}V(0)\\ &\quad-\gamma\mathbb{E}\int_0^{t_z}\begin{bmatrix}u^T(s) & v^T(s)\end{bmatrix}\begin{bmatrix}u(s)\\ v(s)\end{bmatrix}ds\\ &\ge -\gamma\mathbb{E}\int_0^{t_z}\begin{bmatrix}u^T(s) & v^T(s)\end{bmatrix}\begin{bmatrix}u(s)\\ v(s)\end{bmatrix}ds.\end{aligned} \tag{44}$$

Therefore, from Definition 5, we know that the MBAMNN is passive. This completes the proof. □

Considering the MBAMNN with leakage, probabilistic, and distributed time-varying delays, then model (1) becomes

$$\begin{aligned}\dot{x}_i(t) = &-C_i x_i(t-\delta(t)) + \sum_{j=1}^{m} a_{ji}(x_i(t))\,f_j(y_j(t))\\ &+\sum_{j=1}^{m} b_{ji}(x_i(t))\,f_j(y_j(t-\tau(t)))\\ &+\sum_{j=1}^{m} k_{ji}(x_i(t))\int_{t-\alpha(t)}^{t} f_j(y_j(s))\,ds\\ &+u_i(t),\\ \dot{y}_j(t) = &-D_j y_j(t-\rho(t)) + \sum_{i=1}^{n} e_{ij}(y_j(t))\,g_i(x_i(t))\\ &+\sum_{i=1}^{n} h_{ij}(y_j(t))\,g_i(x_i(t-d(t)))\\ &+\sum_{i=1}^{n} l_{ij}(y_j(t))\int_{t-\beta(t)}^{t} g_i(x_i(s))\,ds\\ &+v_j(t),\end{aligned} \tag{45}$$

where the nonnegative continuous variables $\delta(t)$, $\rho(t)$ and $\alpha(t)$, $\beta(t)$ correspond to the leakage and distributed time-varying delays and $K(x(t)) = (k_{ji}(x_i(t)))_{m\times n}$ and $L(x(t)) = (l_{ij}(y_j(t)))_{n\times m}$ are the delayed connection weight matrix functions. Then, we let

$$\begin{aligned}k_{ji}(x_i(t)) &= \begin{cases}\widehat{b}_{ji}, & |x_i(t)| > \Theta_i,\\ \check{b}_{ji}, & |x_i(t)| \le \Theta_i,\end{cases}\\ l_{ij}(y_j(t)) &= \begin{cases}\widehat{f}_{ij}, & |y_j(t)| > \Psi_j,\\ \check{f}_{ij}, & |y_j(t)| \le \Psi_j,\end{cases}\end{aligned} \tag{46}$$

in which k_{ji} and l_{ij} are known constants and $k_{ji}(x_i(t))$ and $l_{ij}(y_j(t))$ are piecewise continuous functions; we set

$$\begin{aligned}\overline{k}_{ji} &= \max\left\{\widehat{k}_{ji}, \check{k}_{ji}\right\},\\ \underline{k}_{ji} &= \min\left\{\widehat{k}_{ji}, \check{k}_{ji}\right\},\\ \overline{l}_{ij} &= \max\left\{\widehat{l}_{ij}, \check{l}_{ij}\right\},\\ \underline{l}_{ij} &= \min\left\{\widehat{l}_{ij}, \check{l}_{ij}\right\}.\end{aligned} \tag{47}$$

Then, the set-valued maps are defined as

$$\begin{aligned}\mathrm{co}\left[k_{ji}(x_i(t))\right] &= \begin{cases}\widehat{k}_{ji}, & |x_i(t)| > \Theta_i,\\ \left[\underline{k}_{ji}, \overline{k}_{ji}\right], & |x_i(t)| = \Theta_i,\\ \check{k}_{ji}, & |x_i(t)| < \Theta_i,\end{cases}\\ \mathrm{co}\left[l_{ij}(y_j(t))\right] &= \begin{cases}\widehat{l}_{ij}, & |y_j(t)| > \Psi_j,\\ \left[\underline{l}_{ij}, \overline{l}_{ij}\right], & |y_j(t)| = \Psi_j,\\ \check{l}_{ij}, & |y_j(t)| < \Psi_j.\end{cases}\end{aligned} \tag{48}$$

By applying the theories of set-valued maps, differential inclusions, stochastic variables, and new functions, system (44) becomes

$$\begin{aligned}
&\dot{x}_i(t)\\
&\in -C_i x_i(t-\delta(t)) + \sum_{j=1}^{m} \mathrm{co}\left[a_{ji}(x_i(t))\right] f_j\left(y_j(t)\right)\\
&\quad + \mu(t) \sum_{j=1}^{m} \mathrm{co}\left[b_{ji}(x_i(t))\right] f_j\left(y_j(t-\tau_1(t))\right)\\
&\quad + (1-\mu(t)) \sum_{j=1}^{m} \mathrm{co}\left[b_{ji}(x_i(t))\right] f_j\left(y_j(t-\tau_2(t))\right)\\
&\quad + \sum_{j=1}^{m} \mathrm{co}\left[k_{ji}(x_i(t))\right] \int_{t-\alpha(t)}^{t} f(y(s))\,ds + u_i(t),\\
&\dot{y}_j(t)\\
&\in -D_j y_j(t-\rho(t)) + \sum_{i=1}^{n} \mathrm{co}\left[e_{ij}\left(y_j(t)\right)\right] g_i(x_i(t))\\
&\quad + \omega(t) \sum_{i=1}^{n} \mathrm{co}\left[h_{ij}\left(y_j(t)\right)\right] g_i(x_i(t-d_1(t)))\\
&\quad + (1-\omega(t)) \sum_{i=1}^{n} \mathrm{co}\left[h_{ij}\left(y_j(t)\right)\right] g_i(x_i(t-d_2(t)))\\
&\quad + \sum_{i=1}^{n} \mathrm{co}\left[l_{ij}\left(y_j(t)\right)\right] \int_{t-\beta(t)}^{t} g(x(s))\,ds + v_j(t);
\end{aligned} \tag{49}$$

equivalently,

$$\begin{aligned}
&\dot{x}(t)\\
&= -Cx(t-\delta(t)) + A(x(t))\, f(y(t))\\
&\quad + \mu_0 B(x(t))\, f(y(t-\tau_1(t)))\\
&\quad + (1-\mu_0) B(x(t))\, f(y(t-\tau_2(t)))\\
&\quad + (\mu(t)-\mu_0)\\
&\quad \times B(x(t)) \left(f(y(t-\tau_1(t))) - f(y(t-\tau_2(t)))\right)\\
&\quad + K(x(t)) \int_{t-\alpha(t)}^{t} f(y(s))\,ds + u(t),\\
&\dot{y}(t)\\
&= -Dy(t-\rho(t)) + E(y(t))\, g(x(t))\\
&\quad + \omega_0 H(y(t))\, g(x(t-d_1(t)))\\
&\quad + (1-\omega_0) H(y(t))\, g(x(t-d_2(t)))\\
&\quad + (\omega(t)-\omega_0)\\
&\quad \times H(y(t)) \left(g(x(t-d_1(t))) - g(x(t-d_2(t)))\right)\\
&\quad + L(y(t)) \int_{t-\beta(t)}^{t} g(x(s))\,ds + v(t).
\end{aligned} \tag{50}$$

For presentation convenience, we denote

$$\begin{aligned}
K &= \max\left\{\left|\underline{k}_{ji}\right|, \left|\overline{k}_{ji}\right|\right\},\\
L &= \max\left\{\left|\underline{l}_{ij}\right|, \left|\overline{l}_{ij}\right|\right\}.
\end{aligned} \tag{51}$$

Theorem 9. *Under Assumptions 1–4, system (50) is passive, if there exist any appropriately dimensional matrices M_m ($m = 1,2,\ldots,4$), W_w ($w = 1,2,\ldots,6$), a scalar $\gamma > 0$, and symmetric positive definite matrices R_i ($i = 1,2$), Q_j ($j = 1,2,\ldots,6$), O_o ($o = 1,2,\ldots,6$), P_k ($k = 1,2,\ldots,8$), Z_l ($l = 1,2,\ldots,4$), and N_n ($n = 1,2$), such that*

$$\begin{aligned}
\Omega_{i,j} &= \left(\Omega_{i,j}\right)_{18\times 18} < 0,\\
\Phi_{i,j} &= \left(\Phi_{i,j}\right)_{18\times 18} < 0,
\end{aligned} \tag{52}$$

where

$$\begin{aligned}
\Omega_{1,1} &= -R_1C - C^T R_1 + Q_1 + Q_2 + Q_3 + Q_4 + \delta^2 P_4\\
&\quad - P_1 - P_2 - 2Z_1 - 2Z_2 - 2\varsigma^- W_1 \varsigma^+,\\
\Omega_{1,2} &= -M_1C + (1-\delta_0)^2 P_1,\\
\Omega_{1,6} &= P_2,\\
\Omega_{1,8} &= -M_1,\\
\Omega_{1,9} &= R_1A + M_1A + W_1(\varsigma^- + \varsigma^+),\\
\Omega_{1,10} &= \mu_0(R_1 + M_1)B,\\
\Omega_{1,11} &= (1-\mu_0)(M_1 + R_1)B,\\
\Omega_{1,14} &= C^T R_1 C,\\
\Omega_{1,15} &= \frac{2}{\tau_1} Z_1,\\
\Omega_{1,16} &= \frac{2}{\tau_2 - \tau_1} Z_2,\\
\Omega_{1,17} &= M_1K + R_1K,\\
\Omega_{1,18} &= R_1 + M_1,\\
\Omega_{2,2} &= -(1-\delta_0) Q_1 - (1-\delta_0)^2 P_1,\\
\Omega_{2,8} &= -M_2C,\\
\Omega_{3,3} &= -Q_2,\\
\Omega_{4,4} &= -(1-\mu_1) Q_3 - 2\varsigma^- W_2 \varsigma^+,\\
\Omega_{4,10} &= -(1-\mu_1) Q_3 + W_2(\varsigma^- + \varsigma^+),\\
\Omega_{5,5} &= -(1-\mu_2) Q_5 - 2\varsigma^- W_3 \varsigma^+,
\end{aligned}$$

$$
\begin{aligned}
\Omega_{5,11} &= -\left(1-\mu_2\right)Q_5 + W_3\left(\varsigma^- + \varsigma^+\right),\\
\Omega_{6,6} &= Q_5 + Q_6 - Q_4 - P_2 - P_3,\\
\Omega_{6,7} &= P_3,\\
\Omega_{6,12} &= Q_5 + Q_6 - Q_4,\\
\Omega_{7,7} &= -Q_6 - P_3,\\
\Omega_{7,13} &= -Q_6,\\
\Omega_{8,8} &= \delta^2 P_1 + \tau_1^2 P_2 + \left(\tau_2 - \tau_1\right)^2 P_3 + \frac{\tau_1^2}{2} Z_1\\
&\quad + \frac{\tau_2^2 - \tau_1^2}{2} Z_2 - 2M_2,\\
\Omega_{8,9} &= M_2 A,\\
\Omega_{8,10} &= \mu_0 M_2 B,\\
\Omega_{8,11} &= \left(1-\mu_0\right) M_2 B,\\
\Omega_{8,17} &= M_2 K,\\
\Omega_{8,18} &= M_2,\\
\Omega_{9,9} &= -2W_1 + \alpha^2 N_1,\\
\Omega_{9,14} &= -C^T R_1 A,\\
\Omega_{9,18} &= -I,\\
\Omega_{10,10} &= -\left(1-\mu_1\right)Q_3 - 2W_2,\\
\Omega_{10,14} &= -\mu_0 C^T R_1 B,\\
\Omega_{11,11} &= -\left(1-\mu_2\right)Q_5 - 2W_3,\\
\Omega_{11,14} &= -\left(1-\mu_0\right)C^T R_1 B,\\
\Omega_{12,12} &= Q_5 + Q_6 - Q_4,\\
\Omega_{13,13} &= -Q_6,\\
\Omega_{14,14} &= -P_4,\\
\Omega_{14,17} &= -C^T R_1 K,\\
\Omega_{14,18} &= -C^T R_1,\\
\Omega_{15,15} &= -\frac{2}{\tau_1^2} Z_1,\\
\Omega_{16,16} &= -\frac{2}{\left(\tau_2 - \tau_1\right)^2} Z_2,\\
\Omega_{17,17} &= -N_1,\\
\Omega_{18,18} &= -\gamma I,
\end{aligned}
\tag{53}
$$

$$
\begin{aligned}
\Phi_{1,1} &= -R_2 C - C^T R_2 + O_1 + O_2 + O_3 + O_4 + \rho^2 P_8\\
&\quad - P_5 - P_6 - 2Z_3 - 2Z_4 - 2\sigma^- W_4 \sigma^+,\\
\Phi_{1,2} &= -M_3 C + \left(1-\rho_0\right)^2 P_5,\\
\Phi_{1,6} &= P_6,\\
\Phi_{1,8} &= -M_3,\\
\Phi_{1,9} &= R_2 A + M_3 A + W_4\left(\sigma^- + \sigma^+\right),\\
\Phi_{1,10} &= \omega_0\left(R_2 + M_3\right)B,\\
\Phi_{1,11} &= \left(1-\omega_0\right)\left(M_3 + R_2\right)B,\\
\Phi_{1,14} &= C^T R_2 C,\\
\Phi_{1,15} &= \frac{2}{d_1} Z_3,\\
\Phi_{1,16} &= \frac{2}{d_2 - d_1} Z_4,\\
\Phi_{1,17} &= M_3 K + R_2 K,\\
\Phi_{1,18} &= R_2 + M_3,\\
\Phi_{2,2} &= -\left(1-\rho_0\right)O_1 - \left(1-\rho_0\right)^2 P_5,\\
\Phi_{2,8} &= -M_4 C,\\
\Phi_{3,3} &= -O_2,\\
\Phi_{4,4} &= -\left(1-\omega_1\right)O_3 - 2\sigma^- W_5 \sigma^+,\\
\Phi_{4,10} &= -\left(1-\omega_1\right)O_3 + W_5\left(\sigma^- + \sigma^+\right),\\
\Phi_{5,5} &= -\left(1-\omega_2\right)O_5 - 2\sigma^- W_6 \sigma^+,\\
\Phi_{5,11} &= -\left(1-\omega_2\right)O_5 + W_6\left(\sigma^- + \sigma^+\right),\\
\Phi_{6,6} &= O_5 + O_6 - O_4 - P_6 - P_7,\\
\Phi_{6,7} &= P_7,\\
\Phi_{6,12} &= O_5 + O_6 - O_4,\\
\Phi_{7,7} &= -O_6 - P_7,\\
\Phi_{7,13} &= -O_6,\\
\Phi_{8,8} &= \rho^2 P_5 + d_1^2 P_6 + \left(d_2 - d_1\right)^2 P_7 + \frac{d_1^2}{2} Z_3\\
&\quad + \frac{d_2^2 - d_1^2}{2} Z_4 - 2M_4,\\
\Phi_{8,9} &= M_4 A,\\
\Phi_{8,10} &= \omega_0 M_4 B,\\
\Phi_{8,11} &= \left(1-\omega_0\right)M_4 B,\\
\Phi_{8,17} &= M_4 K,\\
\Phi_{8,18} &= M_4,\\
\Phi_{9,9} &= -2W_4 + \alpha^2 N_2,\\
\Phi_{9,14} &= -C^T R_2 A,
\end{aligned}
$$

$$\begin{aligned}
\Phi_{9,18} &= -I,\\
\Phi_{10,10} &= -\left(1-\omega_1\right)O_3 - 2W_5,\\
\Phi_{10,14} &= -\omega_0 C^T R_2 B,\\
\Phi_{11,11} &= -\left(1-\omega_2\right)O_5 - 2W_6,\\
\Phi_{11,14} &= -\left(1-\omega_0\right)C^T R_2 B,\\
\Phi_{12,12} &= O_5 + O_6 - O_4,\\
\Phi_{13,13} &= -O_6,\\
\Phi_{14,14} &= -P_8,\\
\Phi_{14,17} &= -D^T R_2 L,\\
\Phi_{14,18} &= -C^T R_2,\\
\Phi_{15,15} &= -\frac{2}{d_1^2}Z_3,\\
\Phi_{16,16} &= -\frac{2}{\left(d_2-d_1\right)^2}Z_4,\\
\Phi_{17,17} &= -N_2,\\
\Phi_{18,18} &= -\gamma I.
\end{aligned} \tag{54}$$

Proof. Consider LKF candidate as follows:

$$V(t) = \sum_{i=1}^{10} V_i(t), \tag{55}$$

where

$$\begin{aligned}
V_1(t) &= \left(x(t) - C\int_{t-\delta(t)}^{t} x(s)\,ds\right)^T\\
&\quad \cdot R_1\left(x(t) - C\int_{t-\delta(t)}^{t} x(s)\,ds\right),\\
V_2(t) &= \left(y(t) - D\int_{t-\rho(t)}^{t} y(s)\,ds\right)^T\\
&\quad \cdot R_2\left(y(t) - D\int_{t-\rho(t)}^{t} y(s)\,ds\right),\\
V_3(t) &= \int_{t-\delta(t)}^{t} x^T(s)\,Q_1 x(s)\,ds\\
&\quad + \int_{t-\delta}^{t} x^T(s)\,Q_2 x(s)\,ds\\
&\quad + \int_{t-\tau_1(t)}^{t} \begin{bmatrix} x(s)\\ f(y(s))\end{bmatrix}^T Q_3 \begin{bmatrix} x(s)\\ f(y(s))\end{bmatrix} ds\\
&\quad + \int_{t-\tau_1}^{t} \begin{bmatrix} x(s)\\ f(y(s))\end{bmatrix}^T Q_4 \begin{bmatrix} x(s)\\ f(y(s))\end{bmatrix} ds\\
&\quad + \int_{t-\tau_2(t)}^{t-\tau_1} \begin{bmatrix} x(s)\\ f(y(s))\end{bmatrix}^T Q_5 \begin{bmatrix} x(s)\\ f(y(s))\end{bmatrix} ds\\
&\quad + \int_{t-\tau_2}^{t-\tau_1} \begin{bmatrix} x(s)\\ f(y(s))\end{bmatrix}^T Q_6 \begin{bmatrix} x(s)\\ f(y(s))\end{bmatrix} ds,\\
V_4(t) &= \int_{t-\rho(t)}^{t} y^T(s)\,O_1 y(s)\,ds\\
&\quad + \int_{t-\rho}^{t} y^T(s)\,O_2 y(s)\,ds\\
&\quad + \int_{t-d_1(t)}^{t} \begin{bmatrix} y(s)\\ g(x(s))\end{bmatrix}^T O_3 \begin{bmatrix} y(s)\\ g(x(s))\end{bmatrix} ds\\
&\quad + \int_{t-d_1}^{t} \begin{bmatrix} y(s)\\ g(x(s))\end{bmatrix}^T O_4 \begin{bmatrix} y(s)\\ g(x(s))\end{bmatrix} ds\\
&\quad + \int_{t-d_2(t)}^{t-d_1} \begin{bmatrix} y(s)\\ g(x(s))\end{bmatrix}^T O_5 \begin{bmatrix} y(s)\\ g(x(s))\end{bmatrix} ds\\
&\quad + \int_{t-d_2}^{t-d_1} \begin{bmatrix} y(s)\\ g(x(s))\end{bmatrix}^T O_6 \begin{bmatrix} y(s)\\ g(x(s))\end{bmatrix} ds,\\
V_5(t) &= \delta\int_{-\delta}^{0}\int_{t+\theta}^{t} \dot{x}^T(s)\,P_1\dot{x}(s)\,ds\,d\theta\\
&\quad + \tau_1\int_{-\tau_1}^{0}\int_{t+\theta}^{t} \dot{x}^T(s)\,P_2\dot{x}(s)\,ds\,d\theta + \left(\tau_2-\tau_1\right)\\
&\quad \cdot \int_{-\tau_2}^{-\tau_1}\int_{t+\theta}^{t} \dot{x}^T(s)\,P_3\dot{x}(s)\,ds\,d\theta\\
&\quad + \delta\int_{-\delta}^{0}\int_{t+\theta}^{t} x^T(s)\,P_4 x(s)\,ds\,d\theta,\\
V_6(t) &= \rho\int_{-\rho}^{0}\int_{t+\theta}^{t} \dot{y}^T(s)\,P_5\dot{y}(s)\,ds\,d\theta\\
&\quad + d_1\int_{-d_1}^{0}\int_{t+\theta}^{t} \dot{y}^T(s)\,P_6\dot{y}(s)\,ds\,d\theta + \left(d_2-d_1\right)\\
&\quad \cdot \int_{-d_2}^{-d_1}\int_{t+\theta}^{t} \dot{y}^T(s)\,P_7\dot{y}(s)\,ds\,d\theta\\
&\quad + \rho\int_{-\delta}^{0}\int_{t+\theta}^{t} y^T(s)\,P_8 y(s)\,ds\,d\theta,\\
V_7(t) &= \int_{-\tau_1}^{0}\int_{\theta}^{0}\int_{t+\lambda}^{t} \dot{x}^T(s)\,Z_1\dot{x}(s)\,ds\,d\lambda\,d\theta\\
&\quad + \int_{-\tau_2}^{-\tau_1}\int_{\theta}^{0}\int_{t+\lambda}^{t} \dot{x}^T(s)\,Z_2\dot{x}(s)\,ds\,d\lambda\,d\theta,\\
V_8(t) &= \int_{-d_1}^{0}\int_{\theta}^{0}\int_{t+\lambda}^{t} \dot{y}^T(s)\,Z_3\dot{y}(s)\,ds\,d\lambda\,d\theta\\
&\quad + \int_{-d_2}^{-d_1}\int_{\theta}^{0}\int_{t+\lambda}^{t} \dot{y}^T(s)\,Z_4\dot{y}(s)\,ds\,d\lambda\,d\theta,
\end{aligned}$$

$$V_9(t) = \alpha \int_{-\alpha}^{0} \int_{t+\theta}^{t} f^T(y(s)) N_1 f(y(s))\, ds\, d\theta,$$
$$V_{10}(t) = \beta \int_{-\beta}^{0} \int_{t+\theta}^{t} g^T(x(s)) N_2 g(x(s))\, ds\, d\theta. \tag{56}$$

Then, we define the infinitesimal generator $\mathscr{L}$ of $V(t)$ as

$$\mathscr{L}V(t) = \lim_{\Delta \to 0^+} \frac{1}{\Delta} \left\{ \mathbb{E}\left(\frac{V(t+\Delta)}{t} \right) - V(t) \right\}. \tag{57}$$

Taking the mathematical expectation of $V(t)$, we get

$$\begin{aligned}
\mathbb{E}\{\mathscr{L}V_1(t)\} &= \mathbb{E}\left\{ 2\left(x(t) - C\int_{t-\delta(t)}^{t} x(s)\, ds \right)^T R_1 \right. \\
&\times \left(-Cx(t) + A(x(t)) f(y(t)) + \mu_0 B(x(t)) \right. \\
&\times f(y(t-\tau_1(t))) + (1-\mu_0) B(x(t)) \\
&\cdot f(y(t-\tau_2(t))) + (\mu(t)-\mu_0) B(x(t)) \\
&\cdot (f(y(t-\tau_1(t))) - f(y(t-\tau_2(t)))) + K(x(t)) \\
&\left.\left. \cdot \int_{t-\alpha(t)}^{t} f(y(s))\, ds + u(t) \right) \right\} \le \mathbb{E}\left\{ 2\left(x(t) \right.\right. \\
&- C\int_{t-\delta(t)}^{t} x(s)\, ds \Big)^T R_1 \times \left(-Cx(t) + Af(y(t)) \right. \\
&+ \mu_0 Bf(y(t-\tau_1(t))) + (1-\mu_0) \\
&\cdot Bf(y(t-\tau_2(t))) + K\int_{t-\alpha(t)}^{t} f(y(s))\, ds \\
&\left.\left. + u(t) \right) \right\}, \qquad (58)
\end{aligned}$$

$$\begin{aligned}
\mathbb{E}\{\mathscr{L}V_2(t)\} &= \mathbb{E}\left\{ 2\left(y(t) - D\int_{t-\rho(t)}^{t} y(s)\, ds \right)^T R_2 \right. \\
&\times \left(-Dy(t) + E(y(t)) g(x(t)) + \omega_0 H(y(t)) \right. \\
&\times g(x(t-d_1(t))) + (1-\omega_0) H(y(t)) \\
&\cdot g(x(t-d_2(t))) + (\omega(t)-\omega_0) H(y(t)) \\
&\cdot (g(x(t-d_1(t))) - g(x(t-d_2(t)))) + L(y(t)) \\
&\left.\left. \cdot \int_{t-\beta(t)}^{t} g(x(s))\, ds + v(t) \right) \right\} \le \mathbb{E}\left\{ 2\left(y(t) \right.\right. \\
&- D\int_{t-\rho(t)}^{t} y(s)\, ds \Big)^T R_2 \times \left(-Dy(t) + Eg(x(t)) \right. \\
&+ \omega_0 Hg(x(t-d_1(t))) + (1-\omega_0) \\
&\left.\left. \cdot Hg(x(t-d_2(t))) + L\int_{t-\beta(t)}^{t} g(x(s))\, ds + v(t) \right) \right\}.
\end{aligned}$$

According to Assumptions 3 and 4, we get

$$\begin{aligned}
\mathbb{E}\{\mathscr{L}V_3(t)\} &= \mathbb{E}\left\{ x^T(t)(Q_1+Q_2+Q_3+Q_4)x(t) \right. \\
&- (1-\delta_0) x^T(t-\delta(t)) Q_1 x(t-\delta(t)) \\
&- x^T(t-\delta) Q_2 x(t-\delta) - (1-\mu_1) \\
&\cdot \begin{bmatrix} x(t-\tau_1(t)) \\ f(y(t-\tau_1(t))) \end{bmatrix}^T Q_3 \begin{bmatrix} x(t-\tau_1(t)) \\ f(y(t-\tau_1(t))) \end{bmatrix} \\
&- (1-\mu_2) \begin{bmatrix} x(t-\tau_2(t)) \\ f(y(t-\tau_2(t))) \end{bmatrix}^T \\
&\cdot Q_5 \begin{bmatrix} x(t-\tau_2(t)) \\ f(y(t-\tau_2(t))) \end{bmatrix} + \begin{bmatrix} x(t-\tau_1) \\ f(y(t-\tau_1)) \end{bmatrix}^T \\
&\cdot (Q_5+Q_6-Q_4) \begin{bmatrix} x(t-\tau_1) \\ f(y(t-\tau_1)) \end{bmatrix} \\
&\left. + \begin{bmatrix} x(t-\tau_2) \\ f(y(t-\tau_2)) \end{bmatrix}^T Q_6 \begin{bmatrix} x(t-\tau_2) \\ f(y(t-\tau_2)) \end{bmatrix} \right\}, \qquad (59) \\
\mathbb{E}\{\mathscr{L}V_4(t)\} &= \mathbb{E}\left\{ y^T(t)(O_1+O_2+O_3+O_4)y(t) \right. \\
&- (1-\rho_0) y^T(t-\rho(t)) O_1 y(t-\rho(t)) \\
&- y^T(t-\rho) O_2 y(t-\rho) - (1-\omega_1) \\
&\cdot \begin{bmatrix} y(t-d_1(t)) \\ g(x(t-d_1(t))) \end{bmatrix}^T O_3 \begin{bmatrix} y(t-d_1(t)) \\ g(x(t-d_1(t))) \end{bmatrix} \\
&- (1-\omega_2) \begin{bmatrix} x(t-d_2(t)) \\ g(x(t-d_2(t))) \end{bmatrix}^T \\
&\cdot O_5 \begin{bmatrix} y(t-d_2(t)) \\ g(x(t-d_2(t))) \end{bmatrix} + \begin{bmatrix} x(t-d_1) \\ g(x(t-d_1)) \end{bmatrix}^T \\
&\cdot (O_5+O_6-O_4) \begin{bmatrix} y(t-d_1) \\ g(x(t-d_1)) \end{bmatrix} \\
&\left. + \begin{bmatrix} y(t-d_2) \\ g(x(t-d_2)) \end{bmatrix}^T O_6 \begin{bmatrix} y(t-d_2) \\ g(x(t-d_2)) \end{bmatrix} \right\}.
\end{aligned}$$

It is obvious that

$$\begin{aligned}
&\mathbb{E}\{\mathscr{L}V_5(t)\} \\
&= \mathbb{E}\left\{ \dot{x}^T(t) \left[\delta^2 P_1 + \tau_1^2 P_2 + (\tau_2-\tau_1)^2 P_3 \right] \dot{x}(t) \right. \\
&+ \delta^2 x^T(t) P_4 x(t) - \delta \int_{t-\delta}^{t} \dot{x}^T(s) P_1 \dot{x}(s)\, ds
\end{aligned}$$

$$
\begin{aligned}
&- \tau_1 \int_{t-\tau_1}^{t} \dot{x}^T(s) P_2 \dot{x}(s)\, ds \\
&- (\tau_2 - \tau_1) \int_{t-\tau_2}^{t-\tau_1} \dot{x}^T(s) P_3 \dot{x}(s)\, ds \\
&- \delta \int_{t-\delta}^{t} x^T(s) P_4 x(s)\, ds \Big\}, \\
&\mathbb{E}\{\mathscr{L}V_6(t)\} \\
&= \mathbb{E}\Big\{ \dot{y}^T(t) \left[\rho^2 P_5 + d_1^2 P_6 + (d_2 - d_1)^2 P_7\right] \dot{y}(t) \\
&+ \rho^2 y^T(t) P_8 y(t) - \rho \int_{t-\rho}^{t} \dot{y}^T(s) P_5 \dot{y}(s)\, ds \\
&- d_1 \int_{t-d_1}^{t} \dot{y}^T(s) P_6 \dot{y}(s)\, ds \\
&- (d_2 - d_1) \int_{t-d_2}^{t-d_1} \dot{y}^T(s) P_7 \dot{y}(s)\, ds \\
&- \rho \int_{t-\rho}^{t} y^T(s) P_8 y(s)\, ds \Big\}.
\end{aligned} \tag{60}
$$

Using Lemma 7, we have

$$
\begin{aligned}
&- \delta \int_{t-\delta}^{t} \dot{x}^T(s) P_1 \dot{x}(s)\, ds \\
&\le - \left(\int_{t-\delta(t)}^{t} \dot{x}(s)\, ds \right)^T P_1 \left(\int_{t-\delta(t)}^{t} \dot{x}(s)\, ds \right) \\
&= - \left[x(t) - (1 - \delta_0) x(t-\delta) \right]^T P_1 \\
&\quad \times \left[x(t) - (1 - \delta_0) x(t-\delta) \right], \\
&- \delta \int_{t-\delta}^{t} x^T(s) P_4 x(s)\, ds \\
&\le - \left(\int_{t-\delta(t)}^{t} x(s)\, ds \right)^T P_4 \left(\int_{t-\delta(t)}^{t} x(s)\, ds \right).
\end{aligned} \tag{61}
$$

Similarly, we have

$$
\begin{aligned}
&- \rho \int_{t-\rho}^{t} \dot{y}^T(s) P_4 \dot{y}(s)\, ds \\
&\le - \left(\int_{t-\rho(t)}^{t} \dot{y}(s)\, ds \right)^T P_4 \left(\int_{t-\rho(t)}^{t} \dot{y}(s)\, ds \right) \\
&= - \left[y(t) - (1 - \rho_0) y(t-\rho) \right]^T P_4 \\
&\quad \times \left[y(t) - (1 - \rho_0) y(t-\rho) \right], \\
&- \rho \int_{t-\rho}^{t} y^T(s) P_8 y(s)\, ds \\
&\le - \left(\int_{t-\rho(t)}^{t} y(s)\, ds \right)^T P_8 \left(\int_{t-\rho(t)}^{t} y(s)\, ds \right).
\end{aligned} \tag{62}
$$

Then, the same as (32)–(35), we can obtain $\mathbb{E}\{\mathscr{L}V_7(t)\}$ and $\mathbb{E}\{\mathscr{L}V_8(t)\}$.

Moreover,

$$
\begin{aligned}
\mathbb{E}\{\mathscr{L}V_9(t)\} &= \mathbb{E}\Big\{ \alpha^2 f^T(y(t)) N_1 f(y(t)) \\
&\quad - \alpha \int_{t-\alpha}^{t} f^T(y(s)) N_1 f(y(s))\, ds \Big\},
\end{aligned} \tag{63}
$$

$$
\begin{aligned}
\mathbb{E}\{\mathscr{L}V_{10}(t)\} &= \mathbb{E}\Big\{ \beta^2 g^T(x(t)) N_2 g(x(t)) \\
&\quad - \beta \int_{t-\beta}^{t} g^T(x(s)) N_2 g(x(s))\, ds \Big\}.
\end{aligned} \tag{64}
$$

Also, we get

$$
\begin{aligned}
&- \alpha \int_{t-\alpha}^{t} f^T(y(s)) N_1 f(y(s))\, ds \\
&\le - \left(\int_{t-\alpha(t)}^{t} f(y(s))\, ds \right)^T N_1 \left(\int_{t-\alpha(t)}^{t} f(y(s))\, ds \right), \\
&- \beta \int_{t-\beta}^{t} g^T(x(s)) N_2 g(x(s))\, ds \\
&\le - \left(\int_{t-\beta(t)}^{t} g(x(s))\, ds \right)^T N_2 \left(\int_{t-\beta(t)}^{t} g(x(s))\, ds \right).
\end{aligned} \tag{65}
$$

Now, we add the following inequations with any matrices M_1, M_2, M_3, and M_4 of appropriate dimensions to derive a less conservative criterion:

$$
\begin{aligned}
0 \le\ & 2 \left(x^T(t) M_1 + \dot{x}^T(t) M_2 \right) \Big[-\dot{x} - Cx(t - \delta(t)) \\
&+ Af(y(t)) + \mu_0 Bf(y(t - \tau_1(t))) \\
&+ (1 - \mu_0) Bf(y(t - \tau_2(t))) \\
&+ K \int_{t-\alpha(t)}^{t} f(y(s))\, ds + u(t) \Big], \\
0 \le\ & 2 \left(y^T(t) M_3 + \dot{y}^T(t) M_4 \right) \Big[-\dot{y} - Dy(t - \rho(t)) \\
&+ Eg(x(t)) + \omega_0 Hg(x(t - d_1(t))) \\
&+ (1 - \omega_0) Hg(x(t - d_2(t))) \\
&+ L \int_{t-\beta(t)}^{t} g(x(s))\, ds + v(t) \Big].
\end{aligned} \tag{66}
$$

Define

$$
\begin{aligned}
\xi(t) = \Big\{ & x^T(t) \quad x^T(t - \delta(t)) \quad x^T(t - \delta) \quad x^T(t - \tau_1(t)) \\
& x^T(t - \tau_2(t)) \quad x^T(t - \tau_1) \quad x^T(t - \tau_2) \quad \dot{x}(t)
\end{aligned}
$$

$$
\begin{aligned}
&f^T(y(t)) \quad f^T(y(t-\tau_1(t))) \quad f^T(y(t-\tau_2(t)))\\
&f^T(y(t-\tau_1)) \quad f^T(y(t-\tau_2)) \quad \int_{t-\delta(t)}^{t} x^T(s)\,ds\\
&\int_{t-\tau_1}^{t} x^T(s)\,ds \quad \int_{t-\tau_2}^{t-\tau_1} x^T(s)\,ds \quad \int_{t-\alpha(t)}^{t} f^T(y(s))\,ds \quad u^T(t)\Big\},\\
\zeta(t) = &\Big\{y^T(t) \quad y^T(t-\rho(t)) \quad y^T(t-\rho) \quad y^T(t-d_1(t))\\
&y^T(t-d_2(t)) \quad y^T(t-d_1) \quad y^T(t-d_2) \quad \dot{y}(t)\\
&g^T(x(t)) \quad g^T(x(t-d_1(t))) \quad g^T(x(t-d_2(t)))\\
&g^T(x(t-d_1)) \quad g^T(x(t-d_2)) \quad \int_{t-\rho(t)}^{t} y^T(s)\,ds\\
&\int_{t-d_1}^{t} y^T(s)\,ds \quad \int_{t-d_2}^{t-d_1} y^T(s)\,ds \quad \int_{t-\beta(t)}^{t} g^T(x(s))\,ds \quad v^T(t)\Big\}.
\end{aligned}
\tag{67}
$$

Combining (40) and (58)–(66), we have

$$
\begin{aligned}
&\mathbb{E}\left\{\mathscr{L}V(t) - 2\begin{bmatrix} f^T(y(s)) & g^T(x(s))\end{bmatrix}\begin{bmatrix} u(s)\\ v(s)\end{bmatrix}\right.\\
&\left.-\gamma\begin{bmatrix} u^T(t) & v^T(t)\end{bmatrix}\begin{bmatrix} u(t)\\ v(t)\end{bmatrix}ds\right\} \le \mathbb{E}\left\{\xi^T(t)\,\Omega\xi(t)\right.\\
&\left.+\zeta^T(t)\,\Phi\zeta(t)\right\}.
\end{aligned}
\tag{68}
$$

Thus, we conclude that if (68) holds, then

$$
\begin{aligned}
&\mathbb{E}\left\{\mathscr{L}V(t) - 2\begin{bmatrix} f^T(y(s)) & g^T(x(s))\end{bmatrix}\begin{bmatrix} u(s)\\ v(s)\end{bmatrix}\right.\\
&\left.-\gamma\begin{bmatrix} u^T(t) & v^T(t)\end{bmatrix}\begin{bmatrix} u(t)\\ v(t)\end{bmatrix}ds\right\} \le 0.
\end{aligned}
\tag{69}
$$

By integrating (69) about t from 0 to t_z, we have

$$
\begin{aligned}
&2\mathbb{E}\int_0^{t_z}\begin{bmatrix} f^T(y(s)) & g^T(x(s))\end{bmatrix}\begin{bmatrix} u(s)\\ v(s)\end{bmatrix}ds\\
&\ge \mathbb{E}V(t) - \mathbb{E}V(0)\\
&\quad -\gamma\mathbb{E}\int_0^{t_z}\begin{bmatrix} u^T(s) & v^T(s)\end{bmatrix}\begin{bmatrix} u(s)\\ v(s)\end{bmatrix}ds\\
&\ge -\gamma\mathbb{E}\int_0^{t_z}\begin{bmatrix} u^T(s) & v^T(s)\end{bmatrix}\begin{bmatrix} u(s)\\ v(s)\end{bmatrix}ds.
\end{aligned}
\tag{70}
$$

Therefore, from Definition 5, we know that the MBAMNN is passive. This completes the proof. □

Remark 10. In this paper, model (50) contains the leakage, probabilistic, and distributed time-varying delays. In particular, we treat some of these delays as a special case of some existing results.

Remark 11. In the corollary, we define leakage delays δ and ρ as constant delays. According to the preceding conditions, we consider the MBAMNN in the following:

$$
\begin{aligned}
&\dot{x}(t)\\
&= -Cx(t-\delta) + A(x(t))\,f(y(t))\\
&\quad + \mu_0 B(x(t))\,f(y(t-\tau_1(t)))\\
&\quad + (1-\mu_0)\,B(x(t))\,f(y(t-\tau_2(t)))\\
&\quad + (\mu(t)-\mu_0)\\
&\quad \times B(x(t))\,(f(y(t-\tau_1(t))) - f(y(t-\tau_2(t))))\\
&\quad + u(t),\\
&\dot{y}(t)\\
&= -Dy(t-\rho) + E(y(t))\,g(x(t))\\
&\quad + \omega_0 H(y(t))\,g(x(t-d_1(t)))\\
&\quad + (1-\omega_0)\,H(y(t))\,g(x(t-d_2(t)))\\
&\quad + (\omega(t)-\omega_0)\\
&\quad \times H(y(t))\,(g(x(t-d_1(t))) - g(x(t-d_2(t))))\\
&\quad + v(t).
\end{aligned}
\tag{71}
$$

Corollary 12. *When Assumptions 1–3 hold, system (71) is passive, if there exist any appropriately dimensional matrices M_m ($m = 1,2,\ldots,4$), W_w ($w = 1,2,\ldots,6$), a scalar $\gamma > 0$, and symmetric positive definite matrices R_i ($i = 1,2$), Q_j ($j = 2,\ldots,6$), O_o ($o = 2,\ldots,6$), P_k ($k = 1,2,\ldots,8$), and Z_l ($l = 1,2,\ldots,4$), such that*

$$
\begin{aligned}
\Omega_{i,j} &= \left(\Omega_{i,j}\right)_{17\times 17} < 0,\\
\Phi_{i,j} &= \left(\Phi_{i,j}\right)_{17\times 17} < 0,
\end{aligned}
\tag{72}
$$

where

$$
\begin{aligned}
\Omega_{1,1} &= -R_1C - C^TR_1 + Q_2 + Q_3 + Q_4 + \delta^2P_4 - P_1\\
&\quad - P_2 - 2Z_1 - 2Z_2 - 2\varsigma^-W_1\varsigma^+,\\
\Omega_{1,2} &= P_1 - M_1C,\\
\Omega_{1,5} &= P_2,\\
\Omega_{1,7} &= -M_1,\\
\Omega_{1,8} &= R_1A + M_1A + W_1(\varsigma^- + \varsigma^+),\\
\Omega_{1,9} &= \mu_0(R_1 + M_1)B,\\
\Omega_{1,10} &= (1-\mu_0)(M_1 + R_1)B,\\
\Omega_{1,13} &= C^TR_1C,\\
\Omega_{1,14} &= \frac{2}{\tau_1}Z_1,
\end{aligned}
$$

$$\Omega_{1,15} = \frac{2}{\tau_2 - \tau_1} Z_2,$$
$$\Omega_{1,16} = M_1 K,$$
$$\Omega_{1,17} = R_1 + M_1,$$
$$\Omega_{2,2} = -Q_2 - P_1,$$
$$\Omega_{2,7} = -M_2 C,$$
$$\Omega_{3,3} = -\left(1 - \mu_1\right) Q_3 - 2\varsigma^- W_2 \varsigma^+,$$
$$\Omega_{3,9} = -\left(1 - \mu_1\right) Q_3 + W_2 \left(\varsigma^- + \varsigma^+\right),$$
$$\Omega_{4,4} = -\left(1 - \mu_2\right) Q_5 - 2\varsigma^- W_3 \varsigma^+,$$
$$\Omega_{4,10} = -\left(1 - \mu_2\right) Q_5 + W_3 \left(\varsigma^- + \varsigma^+\right),$$
$$\Omega_{5,5} = Q_5 + Q_6 - Q_4 - P_2 - P_3,$$
$$\Omega_{5,6} = P_3,$$
$$\Omega_{5,11} = Q_5 + Q_6 - Q_4,$$
$$\Omega_{6,6} = -Q_6 - P_3,$$
$$\Omega_{6,12} = -Q_6,$$
$$\Omega_{7,7} = \delta^2 P_1 + \tau_1^2 P_2 + \left(\tau_2 - \tau_1\right)^2 P_3 + \frac{\tau_1^2}{2} Z_1 + \frac{\tau_2^2 - \tau_1^2}{2} Z_2 - 2M_2,$$
$$\Omega_{7,8} = M_2 A,$$
$$\Omega_{7,9} = \mu_0 M_2 B,$$
$$\Omega_{7,10} = \left(1 - \mu_0\right) M_2 B,$$
$$\Omega_{7,16} = M_2 K,$$
$$\Omega_{7,17} = M_2,$$
$$\Omega_{8,8} = -2W_1 + \alpha^2 N_1,$$
$$\Omega_{8,13} = -C^T R_1 A,$$
$$\Omega_{8,17} = -I,$$
$$\Omega_{9,9} = -\left(1 - \mu_1\right) Q_3 - 2W_2,$$
$$\Omega_{9,13} = -\mu_0 C^T R_1 B,$$
$$\Omega_{10,10} = -\left(1 - \mu_2\right) Q_5 - 2W_3,$$
$$\Omega_{10,13} = -\left(1 - \mu_0\right) C^T R_1 B,$$
$$\Omega_{11,11} = Q_5 + Q_6 - Q_4,$$
$$\Omega_{12,12} = -Q_6,$$
$$\Omega_{13,13} = -P_4,$$
$$\Omega_{13,17} = -C^T R_1,$$
$$\Omega_{14,14} = -\frac{2}{\tau_1^2} Z_1,$$
$$\Omega_{15,15} = -\frac{2}{\left(\tau_2 - \tau_1\right)^2} Z_2,$$
$$\Omega_{16,16} = -N_1,$$
$$\Omega_{17,17} = -\gamma I,$$

(73)

$$\Phi_{1,1} = -R_2 C - C^T R_2 + O_2 + O_3 + O_4 + \rho^2 P_8 - P_5 - P_6 - 2Z_3 - 2Z_4 - 2\sigma^- W_4 \sigma^+,$$
$$\Phi_{1,2} = P_5 - M_3 D,$$
$$\Phi_{1,5} = P_6,$$
$$\Phi_{1,7} = -M_3,$$
$$\Phi_{1,8} = R_2 A + M_3 A + W_4 \left(\sigma^- + \sigma^+\right),$$
$$\Phi_{1,9} = \omega_0 \left(R_2 + M_3\right) B,$$
$$\Phi_{1,10} = \left(1 - \omega_0\right) \left(M_3 + R_2\right) B,$$
$$\Phi_{1,13} = C^T R_2 C,$$
$$\Phi_{1,14} = \frac{2}{d_1} Z_3,$$
$$\Phi_{1,15} = \frac{2}{d_2 - d_1} Z_4,$$
$$\Phi_{1,16} = M_3 K,$$
$$\Phi_{1,17} = R_2 + M_3,$$
$$\Phi_{2,2} = -O_2 - P_5,$$
$$\Phi_{2,7} = -M_4 C,$$
$$\Phi_{3,3} = -\left(1 - \omega_1\right) O_3 - 2\sigma^- W_5 \sigma^+,$$
$$\Phi_{3,9} = -\left(1 - \omega_1\right) O_3 + W_5 \left(\sigma^- + \sigma^+\right),$$
$$\Phi_{4,4} = -\left(1 - \omega_2\right) O_5 - 2\sigma^- W_6 \sigma^+,$$
$$\Phi_{4,10} = -\left(1 - \omega_2\right) O_5 + W_6 \left(\sigma^- + \sigma^+\right),$$
$$\Phi_{5,5} = O_5 + O_6 - O_4 - P_6 - P_7,$$
$$\Phi_{5,6} = P_7,$$
$$\Phi_{5,11} = O_5 + O_6 - O_4,$$
$$\Phi_{6,6} = -O_6 - P_7,$$
$$\Phi_{6,12} = -O_6,$$
$$\Phi_{7,7} = \rho^2 P_5 + d_1^2 P_6 + \left(d_2 - d_1\right)^2 P_7 + \frac{d_1^2}{2} Z_3 + \frac{d_2^2 - d_1^2}{2} Z_4 - 2M_4,$$

$$\begin{aligned}
\Phi_{7,8} &= M_4 A,\\
\Phi_{7,9} &= \omega_0 M_4 B,\\
\Phi_{7,10} &= (1-\omega_0) M_4 B,\\
\Phi_{7,16} &= M_4 K,\\
\Phi_{7,17} &= M_4,\\
\Phi_{8,8} &= -2W_4 + \alpha^2 N_2,\\
\Phi_{8,13} &= -C^T R_2 A,\\
\Phi_{8,17} &= -I,\\
\Phi_{9,9} &= -(1-\omega_1) O_3 - 2W_5,\\
\Phi_{9,13} &= -\omega_0 C^T R_2 B,\\
\Phi_{10,10} &= -(1-\omega_2) O_5 - 2W_6,\\
\Phi_{10,13} &= -(1-\omega_0) C^T R_2 B,\\
\Phi_{11,11} &= O_5 + O_6 - O_4,\\
\Phi_{12,12} &= -O_6,\\
\Phi_{13,13} &= -P_8,\\
\Phi_{13,17} &= -C^T R_2,\\
\Phi_{14,14} &= -\frac{2}{d_1^2} Z_3,\\
\Phi_{15,15} &= -\frac{2}{(d_2-d_1)^2} Z_4,\\
\Phi_{16,16} &= -N_2,\\
\Phi_{17,17} &= -\gamma I.
\end{aligned} \tag{74}$$

Remark 13. In numerical simulations, we use the models of MBAMNNs with mixed time-varying delays; the models that we used are novel. In the existing papers, we can see that the most of the papers are about passivity analysis of memristive single-layer neural networks and there are few results about MBAMNNs [17–19]. MBAMNNs are a class of two-layer systems which can realize heteroassociation memory and autoassociation memory; hence, the MBAMNNs can be able to imitate the human brain better, and the limitation of traditional neural networks can be broken. The LKFs that we designed include double and triple integral terms, and using some effective methods, we can obtain several conditions about MBAMNNs with leakage, probabilistic, and distributed time-varying delays. Hence, our research results are less conservative than the existing ones in the models and the treatment methods [19, 21]. In particular, these delays are all taken into consideration separately. Thus, our paper not only improves the models but also considers a variety of time-varying delays [18–21].

4. Numerical Simulation

In this section, we provide several numerical examples to illustrate the usefulness of our stability results.

Example 1. We consider a 2-dimensional MBAMNN of (16) with the parameters as follows:

$$a_{11}(x_1(t)) = \begin{cases} 0.3, & |x_1(t)| > \Phi_1,\\ 0.7, & |x_1(t)| \le \Phi_1, \end{cases}$$

$$a_{12}(x_1(t)) = \begin{cases} 0.4, & |x_1(t)| > \Phi_1,\\ 0.5, & |x_1(t)| \le \Phi_1, \end{cases}$$

$$a_{21}(x_2(t)) = \begin{cases} -0.5, & |x_2(t)| > \Phi_2,\\ -0.6, & |x_2(t)| \le \Phi_2, \end{cases}$$

$$a_{22}(x_2(t)) = \begin{cases} -0.76, & |x_2(t)| > \Phi_2,\\ -0.7, & |x_2(t)| \le \Phi_2, \end{cases}$$

$$b_{11}(x_1(t)) = \begin{cases} 0.33, & |x_1(t)| > \Phi_1,\\ 0.3, & |x_1(t)| \le \Phi_1, \end{cases}$$

$$b_{12}(x_1(t)) = \begin{cases} 0.25, & |x_1(t)| > \Phi_1,\\ 0.2, & |x_1(t)| \le \Phi_1, \end{cases}$$

$$b_{21}(x_2(t)) = \begin{cases} 0.6, & |x_2(t)| > \Phi_2,\\ 0.56, & |x_2(t)| \le \Phi_2, \end{cases}$$

$$b_{22}(x_2(t)) = \begin{cases} 0.63, & |x_2(t)| > \Phi_2,\\ 0.6, & |x_2(t)| \le \Phi_2, \end{cases}$$

$$e_{11}(y_1(t)) = \begin{cases} 1.3, & |y_1(t)| > \Psi_1,\\ 0.4, & |y_1(t)| \le \Psi_1, \end{cases}$$

$$e_{12}(y_1(t)) = \begin{cases} 1.28, & |y_1(t)| > \Psi_1,\\ 0.38, & |y_1(t)| \le \Psi_1, \end{cases}$$

$$e_{21}(y_2(t)) = \begin{cases} -1.05, & |y_2(t)| > \Psi_2,\\ -1.1, & |y_2(t)| \le \Psi_2, \end{cases}$$

$$e_{22}(y_2(t)) = \begin{cases} -0.88, & |y_2(t)| > \Psi_2,\\ -0.8, & |y_2(t)| \le \Psi_2, \end{cases}$$

$$h_{11}(y_1(t)) = \begin{cases} 0.38, & |y_1(t)| > \Psi_1,\\ 0.4, & |y_1(t)| \le \Psi_1, \end{cases}$$

$$h_{12}(y_1(t)) = \begin{cases} 0.25, & |y_1(t)| > \Psi_1, \\ 0.2, & |y_1(t)| \le \Psi_1, \end{cases}$$

$$h_{21}(y_2(t)) = \begin{cases} 0.5, & |y_2(t)| > \Psi_2, \\ 0.87, & |y_2(t)| \le \Psi_2, \end{cases}$$

$$h_{22}(y_2(t)) = \begin{cases} 0.38, & |y_2(t)| > \Psi_2, \\ -0.5, & |y_2(t)| \le \Psi_2. \end{cases} \tag{75}$$

Here, we take the activation functions as $f_i(s) = g_i(s) = \tanh(s)$, $i = 1, 2$. Then, let $\tau_1 = 0.5$, $\tau_2 = 0.6$, $\mu_1 = 0.3$, $\mu_2 = 0.5$, $\mu_0 = 0.4$, $d_1 = 1.5$, $d_2 = 2$, $\omega_1 = 0.6$, $\omega_2 = 0.8$, and $\omega_0 = 0.3$. Probabilistic time-varying delays $\tau_1(t) = 0.7 + 0.2\sin(t)$, $\tau_2(t) = 0.65 + 0.6\cos(0.5t)$, $d_1(t) = 0.4 + 0.4\sin(t)$, and $d_2(t) = 0.3 + 0.3\cos(t)$. According to Assumption 1, we verify that $\varsigma^- = \sigma^- = 0$, and $\varsigma^+ = \sigma^+ = 1$. Then, there exist the matrices as follows:

$$C = \begin{bmatrix} 1.52 & 0 \\ 0 & 1.33 \end{bmatrix},$$

$$D = \begin{bmatrix} 1.21 & 0 \\ 0 & 1.76 \end{bmatrix},$$

$$A = \begin{bmatrix} 0.7 & 0.5 \\ -0.6 & -0.76 \end{bmatrix},$$

$$B = \begin{bmatrix} 0.33 & 0.25 \\ 0.6 & 0.63 \end{bmatrix}, \tag{76}$$

$$E = \begin{bmatrix} 1.3 & 1.28 \\ -1.1 & -0.88 \end{bmatrix},$$

$$H = \begin{bmatrix} 0.4 & 0.25 \\ 0.87 & -0.5 \end{bmatrix}.$$

Figure 3 shows the state trajectories of system (16); it is actually unstable. By solving the LMIs (21), we get the following feasible solutions:

$$R_1 = \begin{bmatrix} 10.3478 & 2.3731 \\ 2.3731 & 9.8579 \end{bmatrix},$$

$$Q_3 = \begin{bmatrix} 3.1634 & 0.6423 \\ 0.6423 & 3.7317 \end{bmatrix},$$

$$Q_4 = \begin{bmatrix} 7.1504 & 1.4750 \\ 1.4750 & 8.3565 \end{bmatrix},$$

$$Q_5 = \begin{bmatrix} 4.0425 & 1.1230 \\ 1.1230 & 4.5925 \end{bmatrix},$$

$$Q_6 = \begin{bmatrix} 1.9672 & 0.2093 \\ 0.2093 & 2.3559 \end{bmatrix},$$

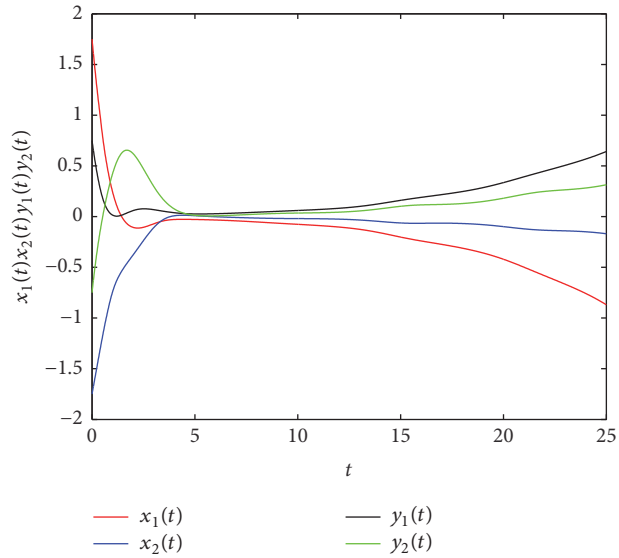

Figure 3: State trajectories of system (16).

$$P_2 = \begin{bmatrix} 4.3159 & 0.1023 \\ 0.1023 & 4.0132 \end{bmatrix},$$

$$P_3 = \begin{bmatrix} 4.7189 & -0.0015 \\ -0.0015 & 4.6924 \end{bmatrix},$$

$$Z_1 = \begin{bmatrix} 0.3110 & 0.0541 \\ 0.0541 & 0.3985 \end{bmatrix},$$

$$Z_2 = \begin{bmatrix} 0.0457 & -0.0004 \\ -0.0004 & 0.0450 \end{bmatrix},$$

$$R_2 = \begin{bmatrix} 14.0110 & 3.7932 \\ 3.7932 & 14.2218 \end{bmatrix},$$

$$O_3 = \begin{bmatrix} 3.6595 & 0.9958 \\ 0.9958 & 4.4985 \end{bmatrix},$$

$$O_4 = \begin{bmatrix} 8.0128 & 2.0885 \\ 2.0885 & 9.9776 \end{bmatrix},$$

$$O_5 = \begin{bmatrix} 5.3912 & 2.2361 \\ 2.2361 & 6.2646 \end{bmatrix},$$

$$O_6 = \begin{bmatrix} 1.6776 & -0.0893 \\ -0.0893 & 2.3607 \end{bmatrix},$$

$$P_6 = \begin{bmatrix} 7.4849 & 0.1076 \\ 0.1076 & 7.7770 \end{bmatrix},$$

$$P_7 = \begin{bmatrix} 8.7529 & -0.0353 \\ -0.0353 & 8.8750 \end{bmatrix},$$

$$Z_3 = \begin{bmatrix} 0.3312 & -0.0060 \\ -0.0060 & 0.4389 \end{bmatrix},$$

$$Z_4 = \begin{bmatrix} 0.2262 & 0.0004 \\ 0.0004 & 0.2189 \end{bmatrix},$$

$$M_1 = \begin{bmatrix} 1.7488 & 0.1600 \\ 0.1600 & 1.7944 \end{bmatrix},$$

$$M_2 = \begin{bmatrix} 4.3667 & 0.4139 \\ 0.4139 & 4.0400 \end{bmatrix},$$

$$W_1 = \begin{bmatrix} 5.4082 & 3.0213 \\ 3.0213 & 6.4308 \end{bmatrix},$$

$$W_2 = \begin{bmatrix} 3.5446 & 0.5053 \\ 0.5053 & 3.7780 \end{bmatrix},$$

$$W_3 = \begin{bmatrix} 3.5391 & 0.8050 \\ 0.8050 & 3.7611 \end{bmatrix},$$

$$M_3 = \begin{bmatrix} 2.0055 & 0.2579 \\ 0.2579 & 2.2772 \end{bmatrix},$$

$$M_4 = \begin{bmatrix} 8.1716 & 1.6020 \\ 1.6020 & 7.4034 \end{bmatrix},$$

$$W_4 = \begin{bmatrix} 7.9401 & 4.1641 \\ 4.1641 & 9.2674 \end{bmatrix},$$

$$W_5 = \begin{bmatrix} 5.0707 & 1.2361 \\ 1.2361 & 5.9315 \end{bmatrix},$$

$$W_6 = \begin{bmatrix} 5.3825 & 2.0405 \\ 2.0405 & 6.1309 \end{bmatrix},$$

$$\gamma = 20.4722. \tag{77}$$

Using the feasible solution, we obtain the state trajectories which are described in Figure 4, and we can see that both $x(t)$ and $y(t)$ are converging to the zero point; therefore, the proved MBAMNN is internally stable. Thus, it is globally passive.

Example 2. Consider a 2-dimensional MBAMNN of (50) with the parameters as follows.

Here, we take the activation functions as $f_i(s) = g_i(s) = \tanh(s)$, $i = 1, 2$. Then, let $\delta = 0.2$, $\delta_0 = 0.2$, $\tau_1 = 0.6$, $\tau_2 = 1$, $\mu_1 = 0.3$, $\mu_2 = 0.5$, $\mu_0 = 0.4$, $\alpha = 0.1$, $\rho = 0.18$, $\rho_0 = 0.15$, $d_1 = 1.5$, $d_2 = 2$, $\omega_1 = 0.6$, $\omega_2 = 0.8$, $\omega_0 = 0.3$, and $\beta = 0.2$. Leakage time-varying delays $\delta(t) = 0.5 + 0.3\sin(t)$ and $\rho(t) = 0.4 + 0.5\cos(t)$; probabilistic time-varying delays $\tau_1(t) = 0.4 + 0.3\sin(t)$, $\tau_2(t) = 0.5 + 0.5\cos(0.5t)$, $d_1(t) = 0.3 + 0.3\sin(t)$, and $d_2(t) = 0.1 + 0.5\cos(t)$; distributed

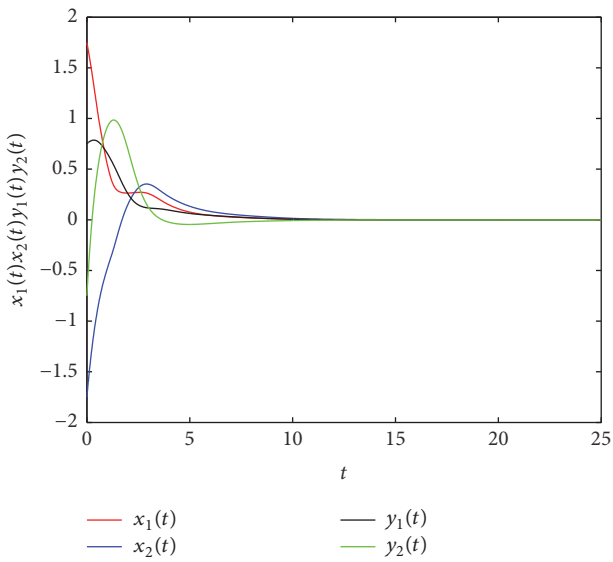

Figure 4: State trajectories of system (16).

time-varying delays $\alpha(t) = \beta(t) = 0.5 + 0.5\cos(t)$. After changing parameters, there exist the matrices

$$C = \begin{bmatrix} 1.52 & 0 \\ 0 & 1.33 \end{bmatrix},$$

$$D = \begin{bmatrix} 1.21 & 0 \\ 0 & 1.76 \end{bmatrix},$$

$$A = \begin{bmatrix} 0.3 & 0.4 \\ -0.6 & -0.76 \end{bmatrix},$$

$$B = \begin{bmatrix} 0.33 & 0.25 \\ 0.6 & 0.63 \end{bmatrix},$$

$$E = \begin{bmatrix} 1.3 & 1.28 \\ -1.1 & -0.88 \end{bmatrix},$$

$$H = \begin{bmatrix} 0.4 & 0.25 \\ 0.87 & -0.5 \end{bmatrix},$$

$$K = \begin{bmatrix} 0.12 & 0 \\ 0 & -0.1 \end{bmatrix},$$

$$L = \begin{bmatrix} -0.1 & 0 \\ 0 & -0.06 \end{bmatrix}. \tag{78}$$

From the state trajectories which are depicted in Figure 5, we find that system (50) is actually unstable. By solving the LMIs (52), we have the following feasible solutions:

$$R_1 = \begin{bmatrix} 7.0452 & 2.9361 \\ 2.9361 & 11.6063 \end{bmatrix},$$

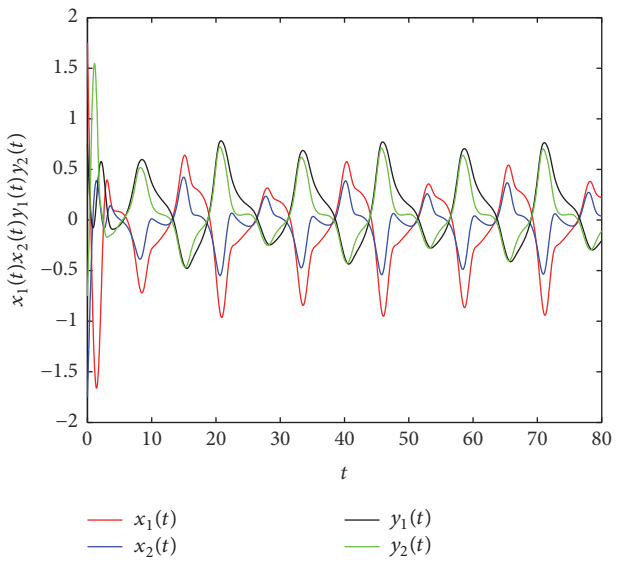

Figure 5: State trajectories of system (50).

$$Q_1 = \begin{bmatrix} 6.5971 & -1.6049 \\ -1.6049 & 9.2078 \end{bmatrix},$$

$$Q_2 = \begin{bmatrix} 0.5551 & 0.4601 \\ 0.4601 & 3.5493 \end{bmatrix},$$

$$Q_3 = \begin{bmatrix} 1.7184 & 1.0171 \\ 1.0171 & 5.9298 \end{bmatrix},$$

$$Q_4 = \begin{bmatrix} 3.5521 & 2.1946 \\ 2.1946 & 13.1443 \end{bmatrix},$$

$$Q_5 = \begin{bmatrix} 2.6799 & 1.5175 \\ 1.5175 & 7.6941 \end{bmatrix},$$

$$Q_6 = \begin{bmatrix} 0.5770 & 0.4402 \\ 0.4402 & 3.5446 \end{bmatrix},$$

$$P_1 = \begin{bmatrix} 5.6725 & -11.6662 \\ -11.6662 & 76.6622 \end{bmatrix},$$

$$P_2 = \begin{bmatrix} 0.0858 & 0.0272 \\ 0.0272 & 1.0798 \end{bmatrix},$$

$$P_3 = \begin{bmatrix} 0.1919 & 0.0517 \\ 0.0517 & 2.2235 \end{bmatrix},$$

$$P_4 = \begin{bmatrix} 478.9177 & 72.1940 \\ 72.1940 & 122.7031 \end{bmatrix},$$

$$Z_1 = \begin{bmatrix} 0.0835 & 0.0516 \\ 0.0516 & 0.6378 \end{bmatrix},$$

$$Z_2 = \begin{bmatrix} 0.1446 & -0.0612 \\ -0.0612 & 1.8780 \end{bmatrix},$$

$$M_1 = \begin{bmatrix} 1.1710 & 1.1366 \\ 1.1366 & 2.7731 \end{bmatrix},$$

$$M_2 = \begin{bmatrix} 0.5725 & 0.0760 \\ 0.0760 & 5.8435 \end{bmatrix},$$

$$W_1 = \begin{bmatrix} 2.9231 & 3.9208 \\ 3.9208 & 15.5396 \end{bmatrix},$$

$$W_2 = \begin{bmatrix} 2.5516 & 1.3400 \\ 1.3400 & 8.4107 \end{bmatrix},$$

$$W_3 = \begin{bmatrix} 2.7557 & 1.4738 \\ 1.4738 & 7.8878 \end{bmatrix},$$

$$N_1 = \begin{bmatrix} 20.6455 & 0.1674 \\ 0.1674 & 25.5954 \end{bmatrix},$$

$$R_2 = \begin{bmatrix} 22.1627 & 10.5483 \\ 10.5483 & 21.6007 \end{bmatrix},$$

$$O_1 = \begin{bmatrix} 29.6665 & -0.0928 \\ -0.0928 & 17.2449 \end{bmatrix},$$

$$O_2 = \begin{bmatrix} 2.1311 & 0.8588 \\ 0.8588 & 3.0198 \end{bmatrix},$$

$$O_3 = \begin{bmatrix} 6.9160 & 1.2013 \\ 1.2013 & 7.3828 \end{bmatrix},$$

$$O_4 = \begin{bmatrix} 20.7004 & 2.6570 \\ 2.6570 & 20.3705 \end{bmatrix},$$

$$O_5 = \begin{bmatrix} 17.4326 & 1.3252 \\ 1.3252 & 15.6910 \end{bmatrix},$$

$$O_6 = \begin{bmatrix} 2.1603 & 0.8746 \\ 0.8746 & 3.0879 \end{bmatrix},$$

$$P_5 = \begin{bmatrix} 77.8766 & -12.7230 \\ -12.7230 & 176.5013 \end{bmatrix},$$

$$P_6 = \begin{bmatrix} 0.1260 & 0.0457 \\ 0.0457 & 0.1924 \end{bmatrix},$$

$$P_7 = \begin{bmatrix} 0.8705 & 0.3558 \\ 0.3558 & 1.3869 \end{bmatrix},$$

$$P_8 = \begin{bmatrix} 860.5842 & 235.3961 \\ 235.3961 & 447.6840 \end{bmatrix},$$

$$Z_3 = \begin{bmatrix} 0.2328 & 0.0901 \\ 0.0901 & 0.3687 \end{bmatrix},$$

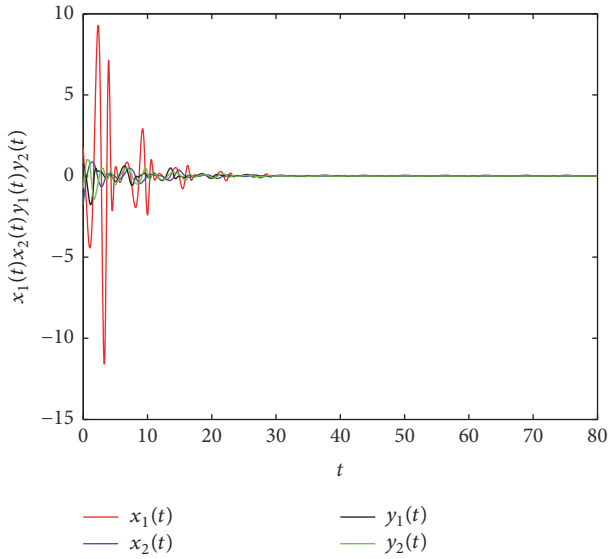

Figure 6: State trajectories of system (50).

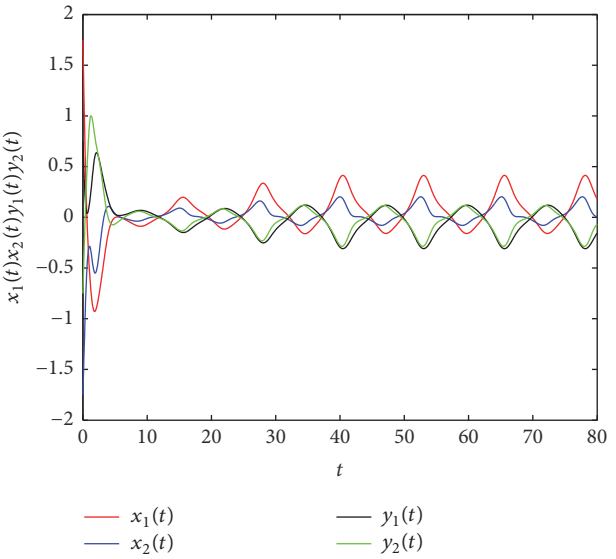

Figure 7: State trajectories of system (71).

$$Z_4 = \begin{bmatrix} 0.3230 & 0.1292 \\ 0.1292 & 0.5292 \end{bmatrix},$$

$$M_3 = \begin{bmatrix} 5.2095 & 2.3987 \\ 2.3987 & 3.2962 \end{bmatrix},$$

$$M_4 = \begin{bmatrix} 5.1434 & 1.3833 \\ 1.3833 & 8.8319 \end{bmatrix},$$

$$W_4 = \begin{bmatrix} 25.3297 & 14.2601 \\ 14.2601 & 34.2731 \end{bmatrix},$$

$$W_5 = \begin{bmatrix} 5.9791 & 1.1879 \\ 1.1879 & 6.6651 \end{bmatrix},$$

$$W_6 = \begin{bmatrix} 7.1161 & 0.6066 \\ 0.6066 & 6.5388 \end{bmatrix},$$

$$N_2 = \begin{bmatrix} 40.5252 & 2.2784 \\ 2.2784 & 38.2262 \end{bmatrix},$$

$$\gamma = 50.2752. \tag{79}$$

Using the feasible solution, we obtain the state trajectories in Figure 6, and we find that both $x(t)$ and $y(t)$ are converging to the zero point; thus, the proved MBAMNN is internally stable. Therefore, it is globally passive.

Example 3. Consider a 2-dimensional MBAMNN of (71) with the parameters as follows.

Here, we take the activation functions as $f_i(s) = g_i(s) = \tanh(s)$, $i = 1, 2$. And let $\delta = 0.3$, $\tau_1 = 0.2$, $\tau_2 = 0.3$, $\mu_1 = 0.3$, $\mu_2 = 0.4$, $\mu_0 = 0.4$, $d_1 = 1.3$, $d_2 = 1.5$, $\omega_1 = 0.6$, $\omega_2 = 0.8$, and $\omega_0 = 0.25$. Probabilistic time-varying delays $\tau_1(t) = 0.6 + 0.4\sin(t)$, $\tau_2(t) = 0.8 + 0.5\cos(0.5t)$, $d_1(t) = 0.5 + 0.3\sin(t)$, and $d_2(t) = 0.6 + 0.5\cos(t)$. After changing parameters, there exist the matrices

$$C = \begin{bmatrix} 1.52 & 0 \\ 0 & 1.33 \end{bmatrix},$$

$$D = \begin{bmatrix} 1.21 & 0 \\ 0 & 1.76 \end{bmatrix},$$

$$A = \begin{bmatrix} 0.7 & 0.5 \\ -0.6 & -0.76 \end{bmatrix},$$

$$B = \begin{bmatrix} 0.33 & 0.25 \\ 0.6 & 0.63 \end{bmatrix},$$

$$E = \begin{bmatrix} 1.3 & 1.28 \\ -1.1 & -0.88 \end{bmatrix},$$

$$H = \begin{bmatrix} 0.4 & 0.25 \\ 0.87 & -0.5 \end{bmatrix}. \tag{80}$$

Figure 7 shows the state trajectories of system (71); it is actually unstable. By solving the LMIs in Corollary 12, we obtain the following feasible solutions:

$$R_1 = \begin{bmatrix} 59.3283 & 30.3806 \\ 30.3806 & 56.1253 \end{bmatrix},$$

$$Q_2 = \begin{bmatrix} 11.2692 & 4.8104 \\ 4.8104 & 13.1800 \end{bmatrix},$$

$$Q_3 = \begin{bmatrix} 14.8695 & 8.8717 \\ 8.8717 & 14.8525 \end{bmatrix},$$

$$Q_4 = \begin{bmatrix} 29.6331 & 17.8695 \\ 17.8695 & 30.7251 \end{bmatrix},$$

$$Q_5 = \begin{bmatrix} 21.2565 & 12.7666 \\ 12.7666 & 19.9407 \end{bmatrix},$$

$$Q_6 = \begin{bmatrix} 5.4645 & 3.2592 \\ 3.2592 & 6.9941 \end{bmatrix},$$

$$P_1 = \begin{bmatrix} 36.1361 & 6.0248 \\ 6.0248 & 31.4429 \end{bmatrix},$$

$$P_2 = \begin{bmatrix} 25.8085 & 3.8441 \\ 3.8441 & 27.0796 \end{bmatrix},$$

$$P_3 = \begin{bmatrix} 33.1166 & 1.3714 \\ 1.3714 & 34.0596 \end{bmatrix},$$

$$P_4 = \begin{bmatrix} 296.1210 & 93.8823 \\ 93.8823 & 252.4336 \end{bmatrix},$$

$$Z_1 = \begin{bmatrix} 0.1137 & 0.0919 \\ 0.0919 & 0.1535 \end{bmatrix},$$

$$Z_2 = \begin{bmatrix} 0.7613 & -0.1194 \\ -0.1194 & 0.7099 \end{bmatrix},$$

$$M_1 = \begin{bmatrix} 8.3925 & 0.6621 \\ 0.6621 & 10.4709 \end{bmatrix},$$

$$M_2 = \begin{bmatrix} 12.4316 & 0.3775 \\ 0.3775 & 13.7920 \end{bmatrix},$$

$$W_1 = \begin{bmatrix} 27.1266 & 17.2502 \\ 17.2502 & 33.8015 \end{bmatrix},$$

$$W_2 = \begin{bmatrix} 19.6366 & 10.3508 \\ 10.3508 & 19.7140 \end{bmatrix},$$

$$W_3 = \begin{bmatrix} 23.9080 & 13.1438 \\ 13.1438 & 22.5256 \end{bmatrix},$$

$$R_2 = \begin{bmatrix} 25.5707 & 20.3266 \\ 20.3266 & 41.5693 \end{bmatrix},$$

$$O_2 = \begin{bmatrix} 15.1779 & 4.9012 \\ 4.9012 & 43.6250 \end{bmatrix},$$

$$O_3 = \begin{bmatrix} 13.7722 & 0.9440 \\ 0.9440 & 8.8489 \end{bmatrix},$$

$$M_4 = \begin{bmatrix} 17.9661 & 1.5273 \\ 1.5273 & 15.4807 \end{bmatrix},$$

$$W_4 = \begin{bmatrix} 55.1410 & 44.6653 \\ 44.6653 & 57.6623 \end{bmatrix},$$

$$O_6 = \begin{bmatrix} 4.9903 & 1.5755 \\ 1.5755 & 3.5372 \end{bmatrix},$$

$$P_5 = \begin{bmatrix} 104.0967 & 34.3385 \\ 34.3385 & 87.8965 \end{bmatrix},$$

$$P_6 = \begin{bmatrix} 0.8159 & 0.3667 \\ 0.3667 & 0.4678 \end{bmatrix},$$

$$P_7 = \begin{bmatrix} 24.1326 & 8.8218 \\ 8.8218 & 15.3127 \end{bmatrix},$$

$$P_8 = \begin{bmatrix} 220.2420 & 251.8009 \\ 251.8009 & 686.0176 \end{bmatrix},$$

$$Z_3 = \begin{bmatrix} 2.2774 & 1.0053 \\ 1.0053 & 1.2605 \end{bmatrix},$$

$$Z_4 = \begin{bmatrix} 38.7115 & 4.7302 \\ 4.7302 & 32.7023 \end{bmatrix},$$

$$M_3 = \begin{bmatrix} 2.8959 & 0.6752 \\ 0.6752 & 8.0316 \end{bmatrix},$$

$$W_5 = \begin{bmatrix} 12.3093 & 1.3710 \\ 1.3710 & 8.1296 \end{bmatrix},$$

$$W_6 = \begin{bmatrix} 15.9416 & -1.5426 \\ -1.5426 & 9.4538 \end{bmatrix},$$

$$O_4 = \begin{bmatrix} 46.4425 & -1.9760 \\ -1.9760 & 28.1517 \end{bmatrix},$$

$$O_5 = \begin{bmatrix} 38.9043 & -4.3696 \\ -4.3696 & 22.8177 \end{bmatrix},$$

$$\gamma = 183.3912. \tag{81}$$

Using the feasible solution, we obtain the state trajectories in Figure 8, and we can see that both $x(t)$ and $y(t)$ are converging to the zero point; therefore, the proved MBAMNN is internally stable. Thus, it is globally passive.

5. Conclusion

We have studied the passivity problem of MBAMNNs with probabilistic and mixed time-varying delays in this paper. By introducing random variables with Bernoulli distribution, using some useful inequalities, and constructing appropriate

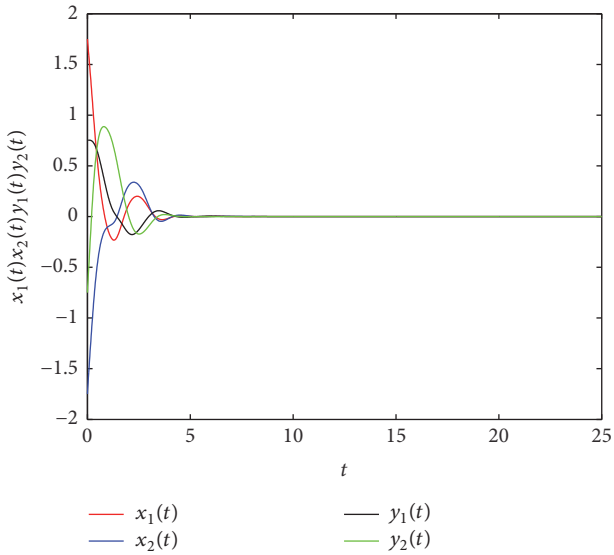

FIGURE 8: State trajectories of system (71).

LKFs, we have got new delay-dependent conditions in LMIs, which ensure the passivity criteria. Future work will focus on the passivity analysis of MBAMNNs with different types of time delays.

Conflicts of Interest

The authors declare that there are no conflicts of interest regarding the publication of this paper.

Authors' Contributions

Weiping Wang and Xiong Luo contributed equally to this work.

Acknowledgments

This work was supported by the National Key Research and Development Program of China under Grant 2017YFB0702300, the State Scholarship Fund of China Scholarship Council (CSC), the National Natural Science Foundation of China under Grants 61603032 and 61174103, the Fundamental Research Funds for the Central Universities under Grant 06500025, the National Key Technologies R&D Program of China under Grant 2015BAK38B01, and the University of Science and Technology Beijing-National Taipei University of Technology Joint Research Program under Grant TW201705.

References

[1] B. Wang, J. Jian, and M. Jiang, "Global stability in Lagrange sense for BAM-type Cohen-Grossberg neural networks with time-varying delays," *Systems Science & Control Engineering*, vol. 3, no. 1, pp. 1–7, 2015.

[2] Y. Song, M. Han, and J. Wei, "Stability and Hopf bifurcation analysis on a simplified BAM neural network with delays," *Physica D: Nonlinear Phenomena*, vol. 200, no. 3-4, pp. 185–204, 2005.

[3] Y. K. Li, L. Yang, and W. Q. Wu, "Anti-periodic solution for impulsive BAM neural networks with time-varying leakage delays on time scales," *Neurocomputing*, vol. 149, pp. 536–545, 2015.

[4] M. Yu, W. Wang, X. Luo, L. Liu, and M. Yuan, "Exponential antisynchronization control of stochastic memristive neural networks with mixed time-varying delays based on novel delay-dependent or delay-independent adaptive controller," *Mathematical Problems in Engineering*, vol. 2017, Article ID 8314757, pp. 1–16, 2017.

[5] J. D. Cao and Y. Wan, "Matrix measure strategies for stability and synchronization of inertial BAM neural network with time delays," *Neural Networks*, vol. 53, pp. 165–172, 2014.

[6] Z. Cai and L. Huang, "Functional differential inclusions and dynamic behaviors for memristor-based BAM neural networks with time-varying delays," *Communications in Nonlinear Science & Numerical Simulation*, vol. 19, no. 5, pp. 1279–1300, 2014.

[7] J. Qi, C. Li, and T. Huang, "Stability of inertial BAM neural network with time-varying delay via impulsive control," *Neurocomputing*, vol. 161, pp. 162–167, 2015.

[8] L. Zhang, S. P. University, and S. O. Science, ""Exponential stability of BAM neural network with time-varying delays," *Journal of Baoshan University*, vol. 31, no. 1, article 385, 396 pages, 2016.

[9] F. Wang, Y. Yang, X. Xu, and L. Li, "Global asymptotic stability of impulsive fractional-order BAM neural networks with time delay," *Neural Computing & Applications*, vol. 30, no. 2, pp. 1–8, 2017.

[10] R. Zhang, D. Zeng, S. Zhong, and Y. Yu, "Event-triggered sampling control for stability and stabilization of memristive neural networks with communication delays," *Applied Mathematics and Computation*, vol. 310, pp. 57–74, 2017.

[11] X. Wang, C. Li, T. Huang, and S. Duan, "Global exponential stability of a class of memristive neural networks with time-varying delays," *Neural Computing and Applications*, vol. 24, no. 7-8, pp. 1707–1715, 2014.

[12] Z. Guo, J. Wang, and Z. Yan, "Global exponential synchronization of two memristor-based recurrent neural networks with time delays via static or dynamic coupling," *Systems Man & Cybernetics Systems IEEE Transactions*, vol. 45, no. 2, 2014.

[13] W. Wang, L. Li, H. Peng, J. Kurths, J. Xiao, and Y. Yang, "Anti-synchronization control of memristive neural networks with multiple proportional delays," *Neural Processing Letters*, vol. 43, no. 1, pp. 269–283, 2016.

[14] K. Mathiyalagan, J. H. Park, and R. Sakthivel, "Synchronization for delayed memristive BAM neural networks using impulsive control with random nonlinearities," *Applied Mathematics and Computation*, vol. 259, pp. 967–979, 2015.

[15] R. Sakthivel, R. Anbuvithya, K. Mathiyalagan, Y.-K. Ma, and P. Prakash, "Reliable anti-synchronization conditions for BAM memristive neural networks with different memductance functions," *Applied Mathematics and Computation*, vol. 275, pp. 213–228, 2016.

[16] R. Anbuvithya, K. Mathiyalagan, R. Sakthivel, and P. Prakash, "Non-fragile synchronization of memristive BAM networks with random feedback gain fluctuations," *Communications in Nonlinear Science and Numerical Simulation*, vol. 29, no. 1-3, pp. 427–440, 2015.

[17] M. Jiang, S. Wang, J. Mei, and Y. Shen, "Finite-time synchronization control of a class of memristor-based recurrent neural networks," *Neural Networks*, vol. 63, pp. 133–140, 2015.

[18] Z. Meng and Z. Xiang, "Passivity analysis of memristor-based recurrent neural networks with mixed time-varying delays," *Neurocomputing*, vol. 165, pp. 270–279, 2015.

[19] H. Li, H. Gao, and P. Shi, "New passivity analysis for neural networks with discrete and distributed delays," *IEEE Transactions on Neural Networks and Learning Systems*, vol. 21, no. 11, pp. 1842–1847, 2010.

[20] M. Syed Ali, R. Saravanakumar, and J. Cao, "New passivity criteria for memristor-based neutral-type stochastic BAM neural networks with mixed time-varying delays," *Neurocomputing*, vol. 171, pp. 1533–1547, 2016.

[21] J. Liu and R. Xu, "Passivity analysis and state estimation for a class of memristor-based neural networks with multiple proportional delays," *Advances in Difference Equations*, vol. 2017, article 34, 2017.

[22] R. Anbuvithya, K. Mathiyalagan, R. Sakthivel, and P. Prakash, "Passivity of memristor-based BAM neural networks with different memductance and uncertain delays," *Cognitive Neurodynamics*, vol. 10, no. 4, pp. 339–351, 2016.

[23] R. Zhang, D. Zeng, and S. Zhong, "Novel master-slave synchronization criteria of chaotic Lur'e systems with time delays using sampled-data control," *Journal of The Franklin Institute*, vol. 354, no. 12, pp. 4930–4954, 2017.

[24] H. Wu, X. Zhang, R. Li, and R. Yao, "Adaptive anti-synchronization and H∞ anti-synchronization for memristive neural networks with mixed time delays and reaction-diffusion terms," *Neurocomputing*, vol. 168, pp. 726–740, 2015.

[25] D. Zeng, R. Zhang, Y. Liu, and S. Zhong, "Sampled-data synchronization of chaotic Lur'e systems via input-delay-dependent-free-matrix zero equality approach," *Applied Mathematics and Computation*, vol. 315, pp. 34–46, 2017.

[26] S. Ding and Z. Wang, "Stochastic exponential synchronization control of memristive neural networks with multiple time-varying delays," *Neurocomputing*, vol. 162, pp. 16–25, 2015.

[27] R. Zhang, D. Zeng, S. Zhong, and K. Shi, "Memory feedback PID control for exponential synchronisation of chaotic Lur'e systems," *International Journal of Systems Science*, vol. 48, no. 12, pp. 2473–2484, 2017.

[28] A. Abdurahman, H. Jiang, and Z. Teng, "Finite-time synchronization for memristor-based neural networks with time-varying delays," *Neural Networks*, vol. 69, pp. 20–28, 2015.

[29] A. Chandrasekar, R. Rakkiyappan, J. Cao, and S. Lakshmanan, "Synchronization of memristor-based recurrent neural networks with two delay components based on second-order reciprocally convex approach," *Neural Networks*, vol. 57, pp. 79–93, 2014.

[30] W. Wang, L. Li, H. Peng et al., "Anti-synchronization of coupled memristive neutral-type neural networks with mixed time-varying delays via randomly occurring control," *Nonlinear Dynamics*, vol. 83, no. 4, pp. 2143–2155, 2016.

[31] D. Zeng, R. Zhang, S. Zhong, J. Wang, and K. Shi, "Sampled-data synchronization control for Markovian delayed complex dynamical networks via a novel convex optimization method," *Neurocomputing*, vol. 266, pp. 606–618, 2017.

[32] X. Luo, J. Deng, J. Liu, W. Wang, X. Ban, and J. Wang, "A quantized kernel least mean square scheme with entropy-guided learning for intelligent data analysis," *China Communications*, vol. 14, no. 7, pp. 127–136, 2017.

[33] X. Luo, J. Deng, W. Wang, J.-H. Wang, and W. Zhao, "A quantized kernel learning algorithm using a minimum kernel risk-sensitive loss criterion and bilateral gradient technique," *Entropy*, vol. 19, no. 7, article 365, 2017.

[34] R. Cheng and M. Peng, "Adaptive synchronization for complex networks with probabilistic time-varying delays," *Journal of The Franklin Institute*, vol. 353, no. 18, pp. 5099–5120, 2016.

[35] G. Nagamani and S. Ramasamy, "Stochastic dissipativity and passivity analysis for discrete-time neural networks with probabilistic time-varying delays in the leakage term," *Applied Mathematics and Computation*, vol. 289, pp. 237–257, 2016.

[36] C. Pradeep, A. Chandrasekar, R. Murugesu, and R. Rakkiyappan, "Robust stability analysis of stochastic neural networks with Markovian jumping parameters and probabilistic time-varying delays," *Complexity*, vol. 21, no. 5, pp. 59–72, 2016.

[37] R. Li, J. Cao, and Z. Tu, "Passivity analysis of memristive neural networks with probabilistic time-varying delays," *Neurocomputing*, vol. 191, pp. 249–262, 2016.

[38] A. Chandrasekar, R. Rakkiyappan, and X. Li, "Effects of bounded and unbounded leakage time-varying delays in memristor-based recurrent neural networks with different memductance functions," *Neurocomputing*, vol. 202, pp. 67–83, 2016.

[39] G. Nagamani and S. Ramasamy, "Dissipativity and passivity analysis for discrete-time T-S fuzzy stochastic neural networks with leakage time-varying delays based on Abel lemma approach," *Journal of The Franklin Institute*, vol. 353, no. 14, pp. 3313–3342, 2016.

[40] R. Samidurai and R. Manivannan, "Robust passivity analysis for stochastic impulsive neural networks with leakage and additive time-varying delay components," *Applied Mathematics and Computation*, vol. 268, Article ID 21387, pp. 743–762, 2015.

[41] L. J. Banu and P. Balasubramaniam, "Robust stability analysis for discrete-time neural networks with time-varying leakage delays and random parameter uncertainties," *Neurocomputing*, vol. 179, pp. 126–134, 2016.

[42] Y. Tang, R. Qiu, J.-a. Fang, Q. Miao, and M. Xia, "Adaptive lag synchronization in unknown stochastic chaotic neural networks with discrete and distributed time-varying delays," *Physics Letters A*, vol. 372, no. 24, pp. 4425–4433, 2008.

[43] M. Fattahi and A. Afshar, "Distributed consensus of multi-agent systems with fault in transmission of control input and time-varying delays," *Neurocomputing*, vol. 189, pp. 11–24, 2016.

[44] Y. Du, S. Zhong, J. Xu, and N. Zhou, "Delay-dependent exponential passivity of uncertain cellular neural networks with discrete and distributed time-varying delays," *ISA Transactions*, vol. 56, pp. 1–7, 2015.

[45] S. Yang, C. Li, and T. Huang, "Finite-time stabilization of uncertain neural networks with distributed time-varying delays," *Neural Computing and Applications*, vol. 28, supplement 1, pp. 1155–1163, 2016.

Hindawi
Mathematical Problems in Engineering
Volume 2018, Article ID 6583908, 8 pages
https://doi.org/10.1155/2018/6583908

Research Article

An Improved Genetic Algorithm to Optimize Spatial Locations for Double-Wishbone Type Suspension System with Time Delay

Qiang Li[1,2] **Xiaoli Yu**[3] **and Jian Wu**[1,2]

[1]*School of Mechanical & Automotive Engineering, Zhejiang University of Science and Technology, Hangzhou 310023, China*
[2]*Provincial Key Laboratory of Food Logistics Equipment & Technology, Zhejiang University of Science and Technology, Hangzhou 310023, China*
[3]*Power Machinery & Vehicular Engineering Institute, Zhejiang University, Hangzhou 310013, China*

Correspondence should be addressed to Qiang Li; liqiang1353@163.com

Received 17 June 2017; Accepted 10 October 2017; Published 20 February 2018

Academic Editor: Radek Matušů

By taking account of double-wishbone independent suspension with two unequal-length arms, the coordinate values of articulated geometry are based on structural limitations and constraint equations of alignment parameters. The sensitivities of front wheel alignment parameters are analyzed using the space analytic geometry method with insight module in ADAMS® software. The multiobjective optimization functions are designed to calculate the coordinate values of hardpoints with front suspension since the effect of time delay due to wheelbase can be easily obtained by vehicle speed. The K&C characteristics have been investigated using GA solutions in the simulation environment. The camber angle decreases from 1.152° to 1.05° and toe-in angle reduces from 1.036° to 0.944°. The simulation results demonstrate that the suggested optimization method is able to satisfy the suspension motion to enhance ride comfort. Experimental results, obtained by K&C test bench, also indicate that the optimized suspension can track the desired trajectory while keeping the vehicle performance in various road conditions.

1. Introduction

Modern automotive engineers have paid more and more attention to the suspension system almost as soon as they were always concerned about automotive performance parts and accessories more than power and acceleration [1, 2]. To correspond with the increased demand for suspension system, various optimization methods have penetrated into the practical application over the last two decades [3–7]. The purpose of suspension with flexibly connecting the wheels to the vehicle frame is to provide good handling and harshness with steering stability to ensure the passengers comfort while maximizing the friction between the tires and road surface.

The suspension guides respective up-and-down wheel motions by actuating two wishbone-shaped control arms comprising six mounting positions and corresponding joints. There are three joints in individualistic control arm. The two joints link with the vehicle frame and the other joint connects with the wheel hub.

The coil springs and dampers (shock absorbers) are oriented along the bell crank through the pushrods or pullrods in view of the nonlinear time delay system. The spring and damper apparatus convert up-and-down wheel motions to back-and-forth movements that capture the lagged characteristics of road excitations.

Since the double-wishbone suspension as an important chassis part can rapidly deviate from its desired path, especially the widely used unequal length of upper and lower control arm (long short arm, LSA), the kingpin inclination, small delays, or lags can lead to deteriorating the real-time vehicle performance. The optimal solution of suspension parameters can be tuned to meet the scope of tread in alignment within acceptable limit levels. As a result, because of adjusting spatial locations in the unequal-length double-wishbone suspensions, the understeering/oversteering dynamics behaviors that express "pushing" or "loose" phenomenon of a vehicle vary widely with changes in various operating conditions. From sixteenth-century wagons to nowadays Formula one, a

wide range of studies that coordinates optimization method and nonlinear time delay system to enhance the ride and handling characteristics has been introduced.

Tak et al. [8] develop the kinematic static sensitivity equations to meet some prescribed performance targets during the whole optimization procedure. Suh et al. [9] conduct the influences of the change of rear suspension geometry to investigate the handling performances of a large-sized bus. Park et al. [10] discuss the ADAMS full vehicle model in driving condition based on the on-board measurements and transformation matrix. Kim et al. [11] examine effect on hands-free stability of steering and suspension design variables to prove their correlations with ADAMS/Car simulation methods. The numerical simulation models and optimal solution procedures have high degree of complexity. The sensitivity analysis has not been explicitly defined with high correlativity with suspension parameters. The shortcoming of traditional optimization algorithm has only one directional preset track.

The research results have also shown that several Genetic Algorithm (GA) control strategies [12–15] are extensively investigated in the development of linkage kinematics with optimal configuration in many commercial software programs, such as ADAMS and Visual C++. Mitchell et al. evaluate the impact of multiple independent metrics with the assistance of a user selectable weighting use of GA. Yan et al. [16] study GA-optimized fuzzy controller by means of MATLAB-ADAMS union simulation. The GA gives the best performances on each optimized circuit to fasten design processes and narrows and chooses the best one from alternate optimal solutions.

The paper is organized as follows. Section 2 defines novel design method of the double-wishbone type suspension. The quasi-static suspension models are evaluated using ADAMS. The sensitivity analyses are examined with several hardpoints. The binary string with certain design valuables considered as a chromosome is determined in Section 3.1 The comparison of dynamic wheel alignments with computation suspension and steering model and actual best bench are obtained in Section 3.4. Finally, we conclude that the validation of optimization method and procedure are presented to meet prescribed performance targets in Section 4.

2. Modelling and Static Analysis

2.1. Background for Suspension Model. The double-wishbone type suspension, known as an A-arm construction, is widely used for front *n* and rear axles with separate type steering trapezium, especially in mainstream larger cars and racing cars. The double-wishbone type suspension can easily modify the interaction between the tire and the road surface to achieve the improved maximum friction. The double-wishbone type suspension has proven itself as one of the effective mechanics that enhances the ride and handling ability to steer, brake, and accelerate. Meanwhile, it has advantages in the fact that it has contributed to elimination or minimization of lateral load transfer distribution for the sake of more consistent road feeling.

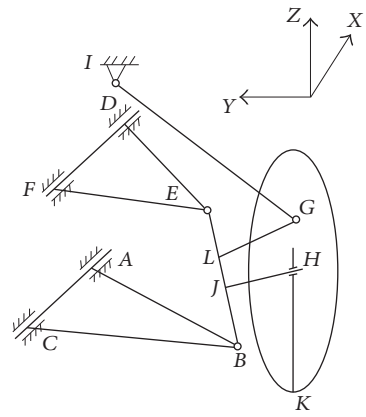

Figure 1: Schematic diagram of a front-right LSA suspension system and steering mechanism.

It is essential to design the hardpoint positions at the beginning stage through the Cartesian (absolute) coordinates in order to establish a unified standard for different work groups. The optimal method of rear hardpoint positions can be easily calculated by less constraint equations without considering the length of tie rod. The camber at steering knuckle position is designed to ensure symmetry and Ackermann geometry status during steering. Also it is a very different task for chassis assignment of checking movement interventions.

2.2. Structure of LSA Suspension. For the double-wishbone type suspension, tie rod is the line connecting two points of spherical joints *G* and *I* (rack and pinion type steering system); triangle DEF and ABC are composed of upper and lower control arm, which revolve about the *DF* axis and *AC* axis, respectively. *E* and *B* indicate upper and lower spherical joints to the steering knuckle, separately. The axes *GL* and *EB* separately represent the steering knuckle arm and steering axis inclination (SAI), also called kingpin inclination (KPI). The axis *JH* expresses the wheel linkage with kingpin. The *K* point can simplify to be regarded as contact point of wheel tread. As an example, a double-wishbone type front suspension system, as illustrated in Figure 1, is a combination of steering mechanism four degrees of freedom (DOF). Thus, constraint equations can be expressed before and after moving using initial points as rigid body motion.

The constrain equations of vertical relationships can be deduced by

$$\begin{aligned}(x_H - x_J)(x_K - x_H) + (y_H - y_J)(y_K - y_H)\\ + (z_H - z_J)(z_K - z_H) = 0.\end{aligned} \tag{1}$$

After LSA suspension moving, the new orientation of the ball joints (denoted by x', y', z') can be denoted based on the new location of SAI.

The constraint equations of constant distances can be written as

$$\begin{aligned}\Delta x, y, z = (x, y, z) - \left(x', y', z'\right),\\ l = \sqrt{(\Delta x)^2 + (\Delta y)^2 + (\Delta z)^2}.\end{aligned} \tag{2}$$

Table 1: Original design variables of hardpoint positions in front suspension system (mm).

Axis	*O*	*A*	*B*	*C*	*D*	*E*	*F*	*G*	*H*
x	0	−146.6	−10.2	126.3	−146.6	126.3	7.8	−70.0	0
y	0	196.2	571.2	196.2	261.5	555.2	261.5	571.2	622
z	0	−134.3	−129.3	−134.3	75.7	99.5	75.7	−100	0

The new locations of upper spherical joints connecting the steering knuckle can be expressed by

$$\begin{aligned} l_{EB} &= l'_{EB}, \\ l_{EF} &= l'_{EF}, \\ l_{ED} &= l'_{ED}. \end{aligned} \tag{3}$$

Similarly, the new positions G and H can be provided by

$$\begin{aligned} l_{EG} &= l'_{EG}, \\ l_{IG} &= l'_{IG}, \\ l_{BG} &= l'_{BG}, \\ l_{EH} &= l'_{EH}, \\ l_{BH} &= l'_{BH} \\ l_{GH} &= l'_{GH}. \end{aligned} \tag{4}$$

Constraint equations are solved for the corresponding locations of the lower and upper control arms using MATLAB.

To describe the three-dimensional kinematic model for suspension characteristics and wheel movements, the original hardpoint positions in the front-right LSA suspension system are listed in Table 1.

2.3. Dynamic Responses. The front LSA suspension is modelled using ADAMS as a multibody simulation tool [17]. The suspension consists of a Panhard bar to withstand the tire principal lateral force, an upper control arm, and a lower control arm which are subject to decomposing longitudinal driving, braking, and vertical forces. The steering system comprises a steering wheel, a steering column, pitman arm, rack, and pinion gearbox, as indicated in Figure 2. The distribution coefficient of the total weight can be optimized by adjusting mount positions and spring perches of control arms.

To compare the effects of different coordinate values of hardpoints, the dynamic responses of the LSA suspension are developed to evaluate the relationship between ride comfort and handling for specifying spring stiffness and damper rate under road load conditions. The dynamics ADAMS model that is integrated with steering system and suspension system expressed as boundary conditions are developed to compare the performances of current designs.

In static analysis, the wheel travel of LSA suspension is updated with a range from −30 mm to 30 mm to reflect

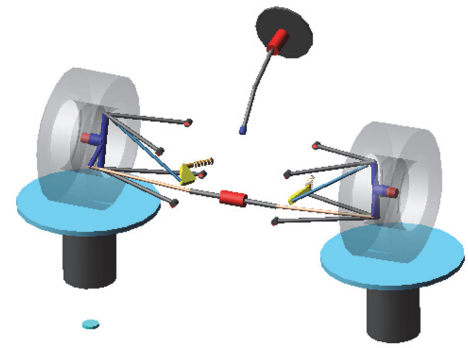

Figure 2: Simulation model of front suspension system and steering mechanism.

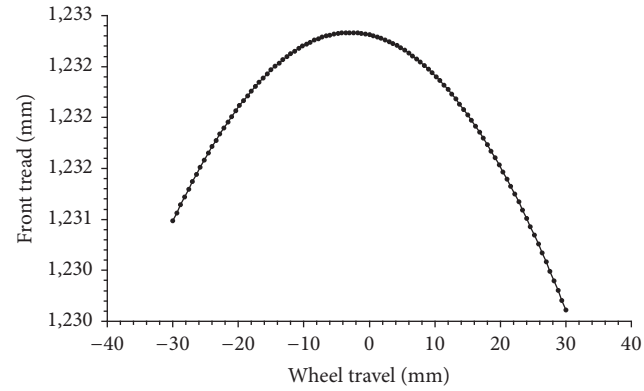

Figure 3: Variations of wheel travel related to front tire tread.

the changes of tread curve, as illustrated in Figure 3. Wheel travel measures use the following convention: positive values indicate compression motion, whereas negative displacement represents extension process. The simulation results reveal significant effect of wheel travel on tire tread. The larger the wheel travel along with up or down direction varies, the higher the change rate the tire tread generates is. The proposed positions of tie rod joint and length of steering pitman arm as important structural parameters distinguish the front suspension from the rear one considering spatial constraints and attribute constraints.

2.4. Sensitivity Analysis. The INSIGHT module from ADAMS finds the parameter sensitivity analyses that minimize the effects of road excitation or other disturbances upon the tires movement while satisfying the constraints on the double-wishbone type suspension geometry constraints. The suspension compliances are specified by variance functions that aim to describe the influence of the

Table 2: Sensitivity analysis of design variables, %.

Hardpoints	Toe	Camber	SAI	Caster
$y_A(x_1)$	−1.07	0.01	0.02	0
$z_A(x_2)$	−3.42	17.7	13.5	−1.16
$y_C(x_3)$	−1.08	0.01	0.01	0.01
$z_C(x_4)$	−2.96	17.41	13.65	0.68
$y_D(x_5)$	−0.26	−1.56	−1.61	0.42
$z_D(x_6)$	−0.68	−16.51	−16.84	1.01
$y_F(x_7)$	−0.22	−1.52	−1.61	−0.37
$z_F(x_8)$	−0.28	−16.1	−17.07	−1.97
$y_G(x_9)$	−1.32	−0.01	0	0
$z_G(x_{10})$	8.26	−7.6	0.15	0.15

coordinates of hardpoints during operations. The wheel geometry parameters that affect the steerability of the vehicle are camber, caster, SAI, and toe.

The sensitivity results of wheel geometry parameters can be calculated as the steering effort and steering wheel returnability produced by the tires to predict the behaviors of vehicle as shown in Table 2. The negative caster angles can reduce the steering effort but weaken the steering wheel returnability. Smaller SAI angles can be favourable to steering effort but deteriorate the steering wheel returnability as well. For that purpose, optimal approaches of design parameters changes used to require trade-offs to retain mutual balance. The sensitivity characteristics of different wheel alignment parameters are strongly correlated with hardpoint positions of control arms in the suspension system.

In Table 2, the different contributing levels of each hardpoint position have been revealed to their effects on the variations of wheel alignments. The SAI angle is mainly dependent on the vertical locations of A, C, Z, and F points; the toe angle depends on the vertical locations of A, C, and G points. The vertical locations of A, E, and F points as the design important parameters have a significant effect on camber angle on steering response. The data analysis of Table 2 allows us to explore potential of optimization of the locations of critical hardpoints with multiobjective function and geometry constraints.

3. Optimization and Simulation

3.1. GA Optimization Method. Genetic Algorithms as optimization techniques using powerful and global search methods imitate the processes present in natural evolution based on Darwinian's survival of the best fitness theory [18–21]. Three coral and repeating stages mainly consist of selection, crossover, and mutation. Therefore, the biological individuals contained in design variables as a population can be converted into one long informative string. It is a convenient way to regard binary segments encoding the optimal parameters as a chromosome. The convergence of population members is checked and updated at each time step after the evaluation of fitness. The fitness functions are considered within 4% for all population members to guide next steps towards optimal design solutions. The best member of the current population

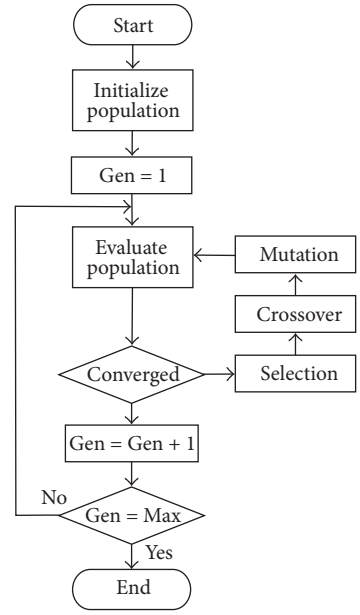

Figure 4: Flow chart of GA optimization process.

is alive and gains higher probability of reproduction, which will form a new offspring. It is the best solution that improves individual genetic characteristics generation until the optimal fitness set is obtained.

In the selection part, multiple population members are chosen at random conditions to produce the best one based on their fitness functions. The hypothetical individuals with higher fitness are reproduced by processes of crossover and mutation to generate the new offspring. Repetition of the processes brings about evolutionary population that strengthens their fitness function. After selecting one out of three members, the process repeats until the number of selected members matches the population size. Then the mating mechanism manipulates the genomes of the parent based on crossover stage. Firstly, the two selected members create two members of the new population. Then, two members are added to create the next generation under a defined crossover limit. Since the crossover operation, the algorithm of mutation allows for the possibility that some alternatives of the available population in the initial randomly can be represented within a mutation limit set. The mutation rate uses 1% in the GA arithmetic process as shown in Figure 4.

The procedure of the generic multiobjective GA is given as follows.

Step 1. Generate a random initialized population.

Step 2. For each objective Gen, Gen $= 1, 2, \ldots, k$, generate a random number and weight for each objective.

Step 3. Evaluate the fitness of the solution in the sorted population and calculate the selection probability of each solution.

Table 3: Comparison between original and optimized parameters of the LSA suspension, mm.

Design variables	y_A	z_A	y_C	z_C	y_D	z_D	y_F	z_F	y_G	z_G
Original	196.2	−134.3	196.2	−134.3	261.5	75.7	261.5	75.7	574.2	−80
Optimized	205.2	129.3	205.2	129.3	260.5	74.7	260.5	74.7	575.2	−75

Step 4. Select parents using the selection probabilities in Step 3.

Step 5. Apply the crossover on the selected parent pairs to create new offspring.

Step 6. Mutate the offspring created in Step 5 with a prespecified mutation rate and put all the offspring into the new population.

Step 7. If the stopping condition (Gen = Max) is not satisfied, set Gen = Gen + 1 and go to Step 3. Otherwise, end the procedure.

3.2. GA Optimizing Suspension Model. The aim is to find the optimal coordinates of hardpoints which are the key locations to influence on suspension characteristics according to their relative orientations. The design procedure accomplishes a suitable compromise between resolution accuracy and computational speed. In order to investigate the effect of geometry changes on suspension displacement limited to its free travel, the vertical and lateral direction of five hardpoints (A, C, D, F, and G) are selected as optimization variables and encoded into a binary string with fixed length.

The length of whole chromosome string has eight bits in GA optimization solution process because eight bits correspond to each value of parameter, y_A, z_A, y_C, z_C, y_D, z_D, y_F, z_F, y_G, and z_G, respectively.

For example, S_1 represents 00100100 which means the corresponding decimal values given as

$$y_A = X_{y_A\min} + \frac{d_{y_A}}{2^8 - 1}\left(X_{y_A\min} - X_{y_A\max}\right), \tag{5}$$

where $X_{y_A\min}$ and $X_{y_A\max}$ are the limit range for the coordinates of hardpoint y_A and d_{y_A} represents the binary value for S_1.

The aim of the optimization work is to minimize the sum of dynamic changes of wheel alignments. The design variations of hardpoint positions could be performed for geometry constrains and multiobjective optimizations.

After the preceding analysis, a GA optimization program is compiled and verified via implementation of virtual simulations. The block diagram representation of the GA operation process is given in Figure 5 with the aim of reaching minimum error. To correspond with the actual demand for the variation ranges in the wheel alignments and LAS suspension system, the corresponding original and optimized values of hardpoint positions are shown in Table 3.

3.3. Performance Analysis with Time Delay. When the constraints in multiobjective optimizations are activated, the

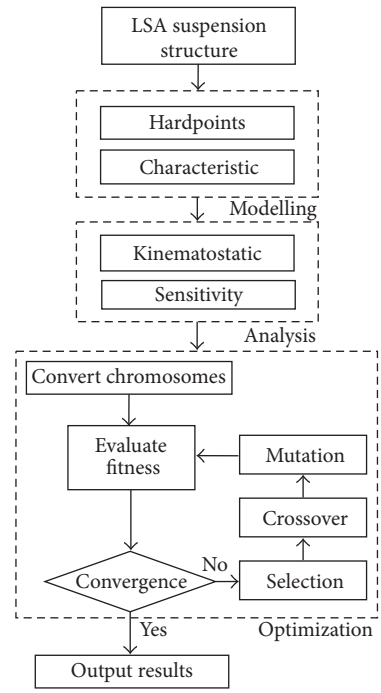

Figure 5: Block diagram of GA optimization program.

suspension system parameters, such as spring constant and damping coefficient, need to reconsider the effect of time delay on dynamic behavior due to the distance of front and rear axles (wheelbase) and different velocity.

The dynamic behavior can be correctly simulated by taking into account the value of time delay caused by the road excitations at the front and rear axles

$$q_f(t) = q_r(t + \tau), \tag{6}$$

where $q_f(t)$ and $q_r(t)$ are displacement excitations at front and rear axles, respectively, and τ means time delay, which can be calculated as follows:

$$\tau = \frac{(a + b)}{v}, \tag{7}$$

where a and b are the distance of mass center from front and rear axle, separately, and v represents vehicle speed.

The parameters of vehicle are summarized in Table 4.

The white noise disturbance that generates normally distributed random numbers, such as a sequence, feeds the input of nonlinear time delay model with the following set of parameters: noise power (the road roughness coefficient) $P = 256 \times 10^{-6}$ and sample time $T_e = 0.01$ s.

For the value of time delay, corresponding velocity of vehicle is computed by (7). $v_h = 80$ km/h indicates $\tau_1 =$

Table 4: Specification of the selected suspension system.

m_s kg	m_u kg	k_s N/m	k_t N/m	C_s N s/m	a m	b m
240	36	16000	160000	1400	1.2	1.3

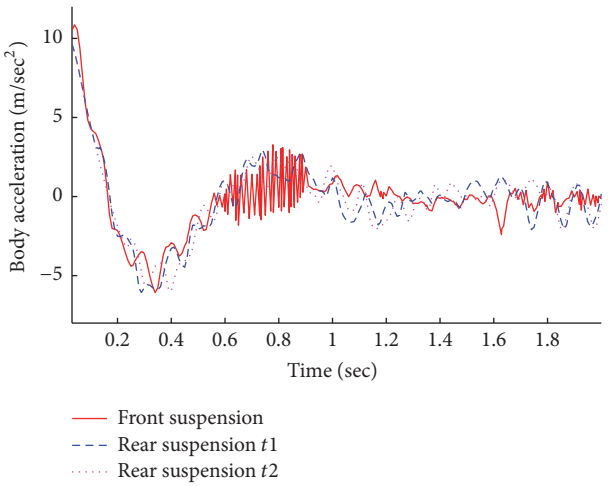

Figure 6: Time history of the body acceleration with different values of time delay.

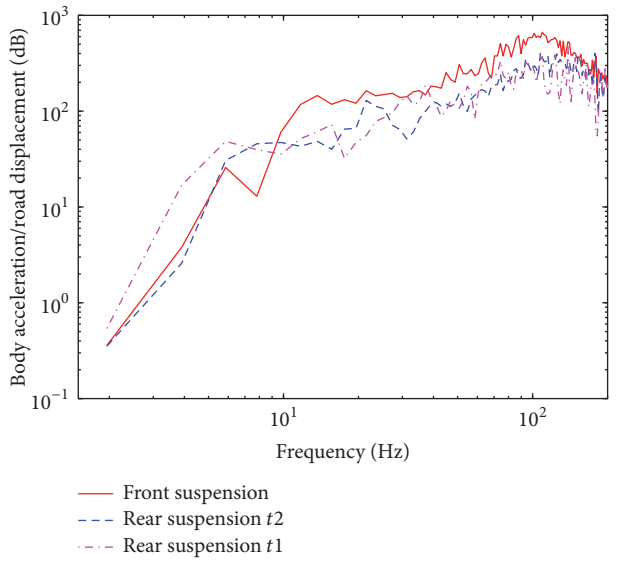

Figure 7: Frequency responses road displacement to body vertical acceleration.

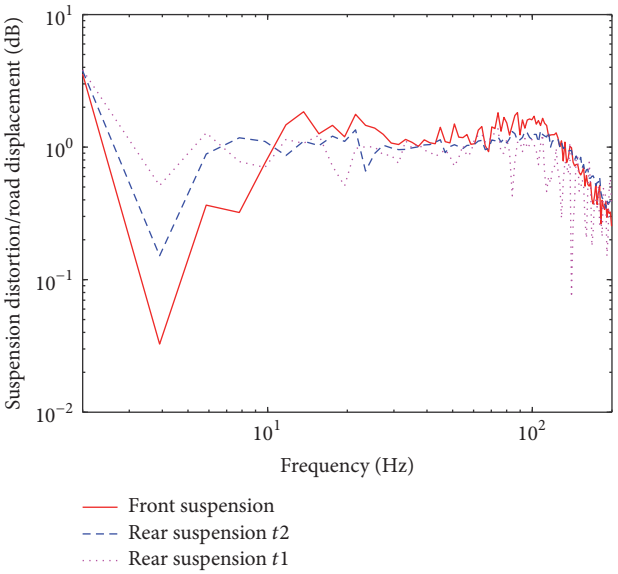

Figure 8: Frequency responses road displacement to suspension distortion.

0.1125 s and $v_l = 40$ km/h means $\tau_2 = 0.225$ s. The effects of different time delay are shown in Figure 6. The time delay is not a constant but varies with the vehicle speed and the road roughness coefficient. The variation of frequency characteristic is activated to diminish time delay that is followed by increasing vehicle speed. It is obvious that vehicle body acceleration increases with time delay, which deteriorates ride comfort of the driver.

The frequency response analyses from the road displacement to the body vertical acceleration and suspension distortion are obtained by high vehicle speed and low vehicle speed as in Figures 7 and 8.

At low frequency, suspension provides a satisfied damping of the body vertical acceleration, but a bad filter of mid and high frequencies. On the other hand, a high time delay ensures a good filtering but a badly damped body vertical acceleration.

3.4. Simulation and Experiment. To correspond with the kinematics simulation analysis, the double-wishbone type suspension is designed with understeer characteristics. The simulation and experimental curves are illustrated in comparison with original and optimization toe and camber of the front suspension travel in Figures 9 and 10.

The camber angle decreases from 1.152° to 1.05° and toe-in angle reduces from 1.036° to 0.944°. The nonlinear suspension system with different values of time delay is investigated by numerical simulation. The travel displacements from −30 mm to 30 mm are utilized on front-right suspension. In Figure 9, it has been proved that the typical toe-out characteristics with a negative camber angle are beneficial to maintain the track path. The toe angle has a tendency with relatively small variation, which improves the steering response and road feeling at different suspension travels. As shown in Figure 10, the comparison with camber angle of original and optimization coordinates is obtained with the tire bouncing from the lowest position to the highest position. The two curves of camber angle are fitted well except for two ends of the suspension travel. The negative

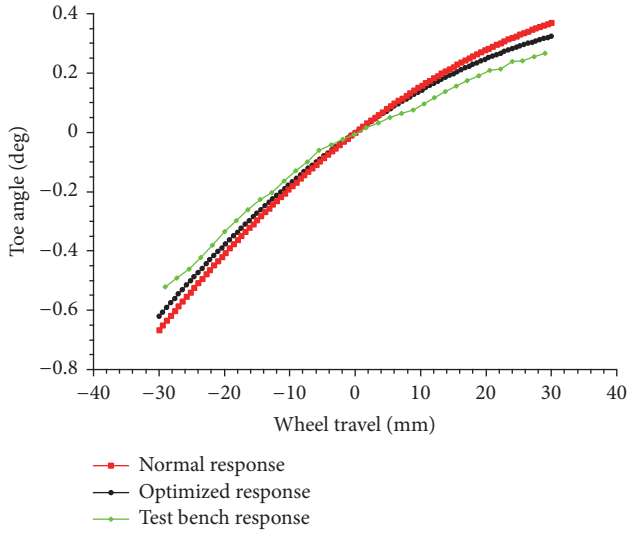

Figure 9: Block diagram of GA operation on LSA suspension and steering mechanism.

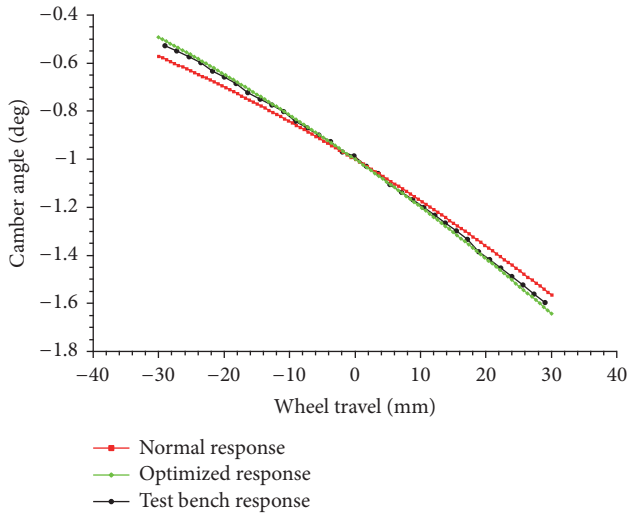

Figure 10: Block diagram of GA operation on LSA suspension and steering mechanism.

camber angle is the biggest contributor to keeping the vehicle on its straight-line path. At the compression and extension processes of suspension motion, the curves clearly indicate the hysteresis characteristic model of suspension with the optimization coordinates of hardpoint. Also there are more desirable characteristics for vehicle driving steerability than before.

The kinematics and compliance (K&C) facility is constructed with optical autocollimator sensors that are used to measure the toe and camber angle, amplifiers, and data acquisition systems to record the values in the whole test course. The test bench mainly consists of six hydraulic actuators to generate longitudinal, lateral, and vertical forces on two wheels with one axle, as shown in Figure 11. Because of the compliance steer forces, elastic bushing elements and

Figure 11: Kinematics and compliance test bench.

motions between the tire and road surface in the simulation are different from the real test bench. The influence of wheel travels on front suspension is taken into account which is essential for performing the experiment of actual working situations. The similarity of both simulation and testing curves is in very good agreement with the extremes of wheel.

4. Conclusions

By using multibody simulation tool, the double-wishbone type suspension (LSA) system has been built up for measuring values of the geometry and kinematic qualities. The sensitivity analysis process has been derived from a nonlinear computer model in order to optimize the principal design variables of main hardpoints. Consequently, the suspension model was simulated under certain driving conditions with optimized values and different values of time delay. The GA optimal solutions have been tested and modification of coefficients was repeated for the elastic elements, such as the spring stiffness and damper. It is necessary that the computer model and prototype have been obtained to validate effectiveness of the proposed method. The simulation and computational procedure can be applied to design an optimization problem of any other kind of suspension systems.

Conflicts of Interest

The authors declare that there are no conflicts of interest regarding the publication of this manuscript.

Acknowledgments

This research work was supported by International Science & Technology Cooperation Program of China (2013DFA31920), the National Key Research and Development Program of China (2017YFD0401304), and the National Natural Science Foundation of China (Grant no. 51476143).

References

[1] M. Heidari and H. Homaei, "Design a PID controller for suspension system by back propagation neural network," *Journal of Engineering*, vol. 2013, Article ID 421543, pp. 1–9, 2013.

[2] C. Tan, R. Xu, Z. Wang, L. Si, and X. Liu, "An improved genetic fuzzy logic control method to reduce the enlargement of coal floor deformation in shearer memory cutting process," *Computational Intelligence and Neuroscience*, vol. 2016, Article ID 3973627, pp. 1–14, 2016.

[3] D. Özcan, Ü. Sönmez, and L. Güvenç, "Optimisation of the nonlinear suspension characteristics of a light commercial vehicle," *International Journal of Vehicular Technology*, vol. 2013, Article ID 562424, pp. 1–16, 2013.

[4] A. Seifi, R. Hassannejad, and M. A. Hamed, "Use of nonlinear asymmetrical shock absorbers in multi-objective optimization of the suspension system in a variety of road excitations," *Proceedings of the Institution of Mechanical Engineers, Part K: Journal of Multi-body Dynamics*, vol. 231, no. 2, pp. 372–387, 2017.

[5] V. Savsani, V. Patel, B. Gadhvi, and M. Tawhid, "Pareto optimization of a half car passive suspension model using a novel multiobjective heat transfer search algorithm," *Modelling and Simulation in Engineering*, vol. 2017, Article ID 2034907, pp. 1–17, 2017.

[6] V. Mehta, M. Patel, Y. Gandhi, and B. Gadhvi, "An experimental approach of estimating speed bump profile to optimizing the suspension parameters using TLBO," *Journal of Advances in Vehicle Engineering*, vol. 2, no. 2, pp. 65–74, 2016.

[7] A. Jamali, H. Shams, and M. Fasihozaman, "Pareto multi-objective optimum design of vehicle-suspension system under random road excitations," *Proceedings of the Institution of Mechanical Engineers, Part K: Journal of Multi-body Dynamics*, vol. 228, no. 3, pp. 282–293, 2014.

[8] T. Tak, S. Chung, and H. Chun, "An optimal design software for vehicle suspension systems," SAE Technical Papers 2000-01-1618, 2000.

[9] K.-H. Suh, Y.-K. Lee, and H.-M. Jeong, "A study on the handling performances of a large-sized bus with the change of rear suspension geometry," SAE Technical Papers 2002-01-3071, 2002.

[10] J. Park, J. Yi, and D. Lee, "Investigation into suspension dynamic compliance characteristics using direct measurement and simulation," SAE Technical Papers 2004-01-1065, 2004.

[11] H.-S. Kim, W.-J. Do, J.-S. Shim, and S.-R. Choi, "The stability analysis of steering and suspension parameters on hands free motion," SAE Technical Papers 2002-01-0620, 2002.

[12] S. A. Mitchell, S. Smith, A. Damiano, J. Durgavich, and R. MacCracken, "Use of genetic algorithms with multiple metrics aimed at the optimization of automotive suspension systems," SAE Technical Papers 2004-01-3520, 2004.

[13] K. Deb, A. Pratap, S. Agarwal, and T. Meyarivan, "A fast and elitist multiobjective genetic algorithm: NSGA-II," *IEEE Transactions on Evolutionary Computation*, vol. 6, no. 2, pp. 182–197, 2002.

[14] B. Gadhvi, V. Savsani, and V. Patel, "Multi-objective optimization of vehicle passive suspension system using NSGA-II, SPEA2 and PESA-II," *Procedia Technology*, vol. 23, pp. 361–368, 2016.

[15] A. C. Mitra, G. J. Desai, S. R. Patwardhan, P. H. Shirke, W. M. H. Kurne, and N. Banerjee, "Optimization of passive vehicle suspension system by genetic algorithm," *Procedia Engineering*, vol. 144, pp. 1158–1166, 2016.

[16] J. Yan, Z. Yin, X. Guo, and C. Fu, "Fuzzy control of semi-active air suspension for cab based on genetic algorithms," SAE Technical Papers 2008-01-2681, 2008.

[17] S. Hasagasioglu, K. Kilicaslan, O. Atabay, and A. Güney, "Vehicle dynamics analysis of a heavy-duty commercial vehicle by using multibody simulation methods," *The International Journal of Advanced Manufacturing Technology*, vol. 60, no. 5-8, pp. 825–839, 2012.

[18] K. Abdullah, W. C. David, and E. S. Alice, "Multi-objective optimization using genetic algorithms: a tutorial," *Reliability Engineering & System Safety*, vol. 91, no. 9, pp. 992–1007, 2006.

[19] N. Srinivas and K. Deb, "Multiobjective optimization using non-dominated sorting in genetic algorithms," *Evolutionary Computation*, vol. 2, no. 3, pp. 221–248, 1995.

[20] R. Darvishi, M. N. Esfahany, and R. Bagheri, "Numerical study on increasing PVC suspension polymerization productivity by using PSO optimization algorithm," *International Journal of Plastics Technology*, vol. 20, no. 2, pp. 219–230, 2016.

[21] J. Wu, Z. Luo, Y. Zhang, and N. Zhang, "An interval uncertain optimization method for vehicle suspensions using Chebyshev metamodels," *Applied Mathematical Modelling*, vol. 38, no. 15-16, pp. 3706–3723, 2014.

Hindawi
Mathematical Problems in Engineering
Volume 2018, Article ID 8410360, 11 pages
https://doi.org/10.1155/2018/8410360

Research Article

Adaptive Constrained Control for Uncertain Nonlinear Time-Delay System with Application to Unmanned Helicopter

Rong Li[1], **Qingxian Wu**[1], **Qingyun Yang**[2] and **Hui Ye**[3]

[1]*College of Automation Engineering, Nanjing University of Aeronautics and Astronautics, Nanjing 210016, China*
[2]*School of Mechanical and Electrical Engineering, Zaozhuang University, Zaozhuang 277160, China*
[3]*School of Electronics and Information, Jiangsu University of Science and Technology, Zhenjiang 212003, China*

Correspondence should be addressed to Qingxian Wu; wuqingxian@nuaa.edu.cn

Received 30 June 2017; Revised 16 September 2017; Accepted 26 September 2017; Published 13 February 2018

Academic Editor: Libor Pekař

This paper investigates a class of nonlinear time-delayed systems with output prescribed performance constraint. The neural network and DOB (disturbance observer) are designed to tackle the uncertainties and external disturbance, and prescribed performance function is constructed for the output prescribed performance constrained problem. Then the robust controller is designed by using adaptive backstepping method, and the stability analysis is considered by using Lyapunov-Krasovskii. Furthermore, the proposed method is employed into the unmanned helicopter system with time-delay aerodynamic uncertainty. Finally, the simulation results illustrate that the proposed robust prescribed performance control system achieved a good control performance.

1. Introduction

Time-delay systems have drawn considerable attention in the past decade [1, 2]. The adaptive backstepping technology was employed into the uncertain nonlinear time-delay system in [3]. The dynamic surface method was presented for the nonlinear time-delay system in [4]. In [5], the nonlinear stochastic system with time delay was studied. The finite-time control method was proposed for a class of time-delay systems in [6, 7]. In the previous studies on time-delay system, the uncertain nonlinear systems consisting of both constraint and external disturbances were not considered. In this paper, we will study a class of uncertain nonlinear time-delay systems subject to constraint.

It is well known that the uncertainty and external disturbance have an effect on the tracking performance of closed systems. Neural network is popular for its ability to cope with uncertainty [8]. In [9], the neural network was introduced into a class of nonlinear systems with unknown coefficient matrices. Combining RBFNN (radial basis function neural network) and disturbance observer, fault tolerant control method was presented to deal with input saturated system with actuator faults in [10]. Moreover, the disturbance observer is a valid method to deal with external disturbance [11]. In [12], the disturbance observer was proposed for permanent-magnet synchronous motor drivers. In [13], the sliding mode disturbance observer was presented to deal with mismatched disturbance. In [14], the disturbance observer was employed into a transport aircraft control system subject to continuous heavy cargo airdrop. In this paper, the neural network and disturbance observer will be utilized to tackle uncertainties, time delay, and external disturbance.

Another challenging problem in controller design lies in the constrained condition of the nonlinear systems [15]. The existence of constraint condition may degrade the performance or cause the instability of the closed control systems [16]. Using the Barrier Lyapunov function and adaptive backstepping technology, a robust constrained controller for a class of nonlinear strict systems was presented in

[17]. In [18], the Barrier Lyapunov function was employed into the switched systems subject to output constraints. In [19], the Barrier Lyapunov function and high-gain observer were introduced to deal with the constrained trajectory tracking problem of the marine surface vessel. Additionally, prescribed performance is another method to cope with output constraints, by defining the appropriate prescribed performance. In [20], the prescribed performance-based feedback linearization method was proposed to deal with output tracking error constraints for the MIMO (multiple-input multiple-output) nonlinear systems. In [21], the prescribed performance and adaptive fuzzy logic were employed into the nonlinear adaptive controller design. To the best of the authors' knowledge, there is still no research about uncertain nonlinear time-delay system considering uncertainties, external disturbance, and output constraints. Thus, in this paper, we will present a prescribed performance-based adaptive constrained control method for the time-delay nonlinear systems.

Nowadays, the unmanned helicopter system has received an increasing attention, and there is an amount of studies about the flight control approaches [22, 23]. In [24], chattering-free sliding mode was proposed for the miniature helicopter system. To solve the tracking problem with nonlinearity, the model predictive control method for unmanned helicopters was presented in [25]. In [26], a trajectory tracking control method was proposed for unmanned helicopter system with constraint conditions. However, with the increasing demands for real time and accuracy, the aerodynamic disturbance caused by transmission delay for unmanned helicopter control system cannot be ignored. In this paper, we will apply the prescribed performance-based robust adaptive control approach for the uncertain unmanned helicopter systems with external disturbance, time delay, and output constraints.

This paper is organized as follows. In Section 2, problem statement and preliminaries of time-delay system and prescribed performance are introduced. Section 3 presents the entire adaptive controller design and stability analysis. In Section 4, the prescribed performance-based control method is employed into the unmanned helicopter system. Finally, simulation and conclusion are given in Sections 5 and 6, respectively.

2. Problem Statement and Preliminaries

In this subsection, we will review some preliminary knowledge about nonlinear time-delay system, prescribed performance, and neural network, which are necessary in the following controller design. Firstly, consider a class of uncertain MIMO nonlinear time-delay systems in the form of

$$\begin{aligned}
\dot{x}_i(t) &= f_i\left(\overline{x}_i(t)\right) + g_i\left(\overline{x}_i(t)\right) x_{i+1}(t) + h_i\left(\overline{x}_i\left(t-\tau_i\right)\right) \\
&\quad + \Delta f_i\left(\overline{x}_i(t)\right) + d_i(t), \quad 1 \le i \le n-1 \\
\dot{x}_n(t) &= f_n\left(\overline{x}_n(t)\right) + g_n\left(\overline{x}_n(t)\right) u(t) + h_n\left(\overline{x}_n\left(t-\tau_n\right)\right) \\
&\quad + \Delta f_n\left(\overline{x}_n(t)\right) + d_n(t) \\
y(t) &= x_1(t),
\end{aligned} \tag{1}$$

where $x_i(t) \in R^m$, $i = 1, 2, \ldots, n$, are the system state vectors which are assumed to be measurable, $\overline{x}_i(t) = [x_1^T(t), x_2^T(t), \ldots, x_i^T(t)]^T \in R^{m\cdot i}$, $y \in R^m$ is the output vector, and $u(t) \in R^m$ is the control input vector. $f_i(\overline{x}_i(t)) \in R^m$, $i = 1, 2, \ldots, n$, are the known smooth nonlinear function, $g_i(\overline{x}_i) \in R^{m\times m}$, $i = 1, 2, \ldots, n$, represent the known control coefficient matrices, and $h_i(\overline{x}_i(t-\tau_i)) \in R^{m\times m}$, $i = 1, 2, \ldots, n$, indicate the known time-delay functions. $\Delta f_i(\overline{x}_i(t)) \in R^m$, $i = 1, 2, \ldots, n$, denote the unknown nonlinear functions which contain both parametric and nonparametric uncertainties. $\tau_i \in R$, $i = 1, 2, \ldots, n$, stand for constant unknown time delays. $d_i(t) \in R^m$, $i = 1, 2, \ldots, n$, mean the unknown external disturbance. In this paper, we impose the following assumptions and lemmas.

Assumption 1 (see [5]). The ideal tracking signals $y_r(t)$ and their derivatives $\dot{y}_r(t)$ are known and continuous.

Assumption 2 (see [11]). The external disturbance $d_i(t)$ means the slow varying signal, while it is restricted in the bound of $\|\dot{d}_i(t)\| \le \overline{d}_i$, $\overline{d}_i > 0$.

Assumption 3 (see [10]). For $i = 1, \ldots, n$, the known continuous function $g_i(\overline{x}_i(t))$ satisfies $g_i(\overline{x}_i(t)) \ne 0$.

Lemma 4 (see [9]). *Consider a class of nonlinear systems $\dot{x} = f(x)$. For any initial conditions $x(0) \in R^n$, if there exists a C^1 continuous and positive definite Lyapunov function satisfying $\varpi_1(x) \le V(x) \le \varpi_2(x)$, $\varpi_i(\|x\|) : R^n \to R$, $i = 1, 2$, mean the K class functions, such that $\dot{V} \le -c_1 V(x) + c_2$, $c_1 > 0$, $c_2 > 0$, then one can conclude that the solution $x(t)$ is uniformly bounded.*

Lemma 5 (see [3]). *For $v > 0$, if there exists one set Z defined by $Z := \{z \mid |z| \le 0.8814v\}$, then one can conclude that, for any $z \notin Z$, the inequality $1 - 2\tanh^2(z/v) < 0$ is satisfied.*

Lemma 6 (see [10]). *For any continuous function $f(z)$, there exists a valid linear neural network to approximate it by choosing enough nodes on the compact set $z \in N_z$. The basic function can be selected as Gaussian function $s_i(z) = e^{-\|z-\mu_i\|^2/c_i}$, where $c_i > 0$ is the width of function and $\mu_i \in R$ represent the center of function. The neural network approximator consists of the weight estimate vector $\widehat{W}(z)$ and Gaussian function $S(z) = [s_1(z), \ldots, s_n(z)]^T$, which can be written as $f_p(z) = \widehat{W}^T(z)S(z) + \varepsilon$. Assume that $W^*(z)$ means the optimal approximating weight, such that*

$$W^*(z) := \arg\min_{\widehat{W}\in R^n} \left\{ \sup_{z\in\Omega_z} \left\| f(z) - f_p(z) \right\| \right\}. \tag{2}$$

In addition, the optimal approximator of continuous function $f(z)$ can be written as

$$f(z) = W^{*T}(z) S(z) + \varepsilon^*, \tag{3}$$

where ε^* indicates the optimal approximate error.

3. Controller Design and Stability Analysis

In this section, the objective is to propose a robust prescribed performance control law for uncertain nonlinear systems such that the closed-loop errors converge to a small neighborhood of the origin.

3.1. Prescribed Performance Controller Design

Step 1. Define the tracking errors $\tilde{z}_1(t) \in R^m$ and $z_2(t) \in R^m$ as follows:

$$\begin{aligned} \tilde{z}_1(t) &= x_1(t) - y_d(t) \\ z_2(t) &= x_2(t) - x_2^*(t), \end{aligned} \tag{4}$$

where $y_d(t) \in R^m$ is the ideal tracking signal and $x_2^*(t) \in R^m$ is the immediate control. The output error transformation can be defined in the form of [18]

$$\begin{aligned} z_{1j}(t) &= Q^{-1}\left(\frac{\tilde{z}_{1j}(t)}{\rho_j(t)}, \overline{\alpha}_j(t), \underline{\alpha}_j(t)\right) \\ &= \frac{1}{2}\ln\frac{\underline{\alpha}_j + \left(\tilde{z}_{1j}(t)/\rho_j(t)\right)}{\overline{\alpha}_j - \left(\tilde{z}_{1j}(t)/\rho_j(t)\right)}, \quad j = 1, \ldots, m, \end{aligned} \tag{5}$$

where $\overline{\alpha}_j$ and $\underline{\alpha}_j$ are the positive constants and $\rho_j(t)$ indicates the performance function, which can be chosen as [26]

$$\rho_j(t) = \left(\rho_{j0} - \rho_{j\infty}\right) e^{-lt} + \rho_{j\infty}. \tag{6}$$

The constant $\rho_{j\infty} > 0$ is the maximum amplitude of the tracking error at the steady state. The decreasing rate $e^{-l_j t}$ of $\rho_j(t)$ represents the desired convergence speed of the tracking error. Therefore, the appropriate choice of the performance function $\rho_j(t)$ and the design constant imposes bounds on the system output trajectory.

Define $f_1 = [f_{11}, \ldots, f_{1m}]^T \in R^m$ and $g_1 = [g_{11}^T, \ldots, g_{1m}^T]^T \in R^{m\times m}$. Thus, the time derivative of $z_{1j}(t)$ becomes

$$\begin{aligned} \dot{z}_{1j}(t) &= \frac{\partial z_{1j}(t)}{\partial\left(\tilde{z}_{1j}(t)/\rho_j(t)\right)}\frac{1}{\rho_j(t)}\dot{\tilde{z}}_{1j}(t) - \frac{\partial z_{1j}(t)}{\partial\left(\tilde{z}_{1j}(t)/\rho_j(t)\right)}\frac{\tilde{z}_{1j}(t)}{\rho_j^2(t)}\dot{\rho}_j(t) \\ &= \frac{1}{2}\frac{\overline{\alpha}_j + \underline{\alpha}_j}{\left(\underline{\alpha}_j + \left(\tilde{z}_{1j}(t)/\rho_j(t)\right)\right)\left(\overline{\alpha}_j - \left(\tilde{z}_{1j}(t)/\rho_j(t)\right)\right)}\left(\frac{1}{\rho_j(t)}\dot{\tilde{z}}_{1j}(t) - \frac{\tilde{z}_{1j}(t)}{\rho_j^2(t)}\dot{\rho}_j(t)\right) \\ &= \frac{1}{2}\frac{\overline{\alpha}_j + \underline{\alpha}_j}{\left(\underline{\alpha}_j + \left(\tilde{z}_{1j}(t)/\rho_j(t)\right)\right)\left(\overline{\alpha}_j - \left(\tilde{z}_{1j}(t)/\rho_j(t)\right)\right)} \\ &\quad \cdot\left(-\frac{\tilde{z}_{1j}(t)}{\rho_j^2(t)}\dot{\rho}_j(t) + \frac{f_{1j}(x_1(t)) + g_{1j}(x_1(t))x_2(t) + h_{1j}(x_1(t-\tau_1)) + \Delta f_{1j}(x_1(t)) + d_{1j}(t) - \dot{y}_{dj}(t)}{\rho_j(t)}\right) \end{aligned} \tag{7}$$

In order to simplify the analysis, we define M_{1j} and N_{1j} as follows:

$$\begin{aligned} &M_{1j}(t) \\ &= \frac{\overline{\alpha}_j + \underline{\alpha}_j}{2\rho_j\left(\underline{\alpha}_j + \left(\tilde{z}_{1j}(t)/\rho_j(t)\right)\right)\left(\overline{\alpha}_j - \left(\tilde{z}_{1j}(t)/\rho_j(t)\right)\right)} \\ &> 0. \\ &N_{1j}(t) \\ &= \frac{\overline{\alpha}_j + \underline{\alpha}_j}{2\rho_j^2(t)\left(\underline{\alpha}_j + \left(\tilde{z}_{1j}(t)/\rho_j(t)\right)\right)\left(\overline{\alpha}_j - \left(\tilde{z}_{1j}(t)/\rho_j(t)\right)\right)} \\ &\cdot \tilde{z}_{1j}(t)\dot{\rho}_j(t) \end{aligned} \tag{8}$$

Furthermore, we can define $M_1(t) = \mathrm{diag}\{M_{11}(t), \ldots, M_{1m}(t)\}$ and $N_1(t) = [N_{11}(t), \ldots, N_{1m}(t)]^T$, then we have

$$\begin{aligned} \dot{z}_1(t) &= M_1(t)\dot{\tilde{z}}_1(t) - N_1(t) = M_1(t)\left(f_1(x_1(t))\right. \\ &\quad + g_1(x_1(t))x_2(t) - \dot{y}_d(t) + \Delta f_1(x_1(t)) \\ &\quad \left. + h_1(x_1(t-\tau_1)) + d_1(t)\right) - N_1(t). \end{aligned} \tag{9}$$

Since $\Delta f_1(x_1(t))$ is unknown, using the RBFNN to approximate it, we obtain

$$M_1(t)\Delta f_1(x_1(t)) + \gamma_1(t) = \eta_1^{-1} W_1^{*T} S_1 + \varepsilon_1^*, \tag{10}$$

where $\gamma_1(t) = [\gamma_{1,1}(t), \ldots, \gamma_{1,m}(t)]^T$, and

$$\gamma_{1,j}(t) = \frac{16}{\tilde{z}_{1j}(t)}\tanh^2\left(\frac{\tilde{z}_{1j}(t)}{v_1}\right)h_{1j}^2(x_1(t)), \quad j = 1, \ldots, m. \tag{11}$$

Substituting (10) into (1) results in

$$\begin{aligned}\dot{x}_1(t) &= f_1(x_1(t)) + g_1(x_1(t))x_2(t)\\ &\quad + h_1(x_1(t-\tau_1)) - M_1^{-1}(t)\gamma_1(t)\\ &\quad + \eta_1^{-1}M_1^{-1}(t)W_1^{*T}S_1 + \chi_1(t).\end{aligned} \tag{12}$$

Invoking (4), (9), and (10), the time derivative of $z_1(t)$ can be rewritten as

$$\begin{aligned}\dot{z}_1(t) &= M_1(t)\\ &\quad \cdot \left(f_1(x_1(t)) + g_1(x_1(t))z_2(t) + g_1(x_1(t))x_2^*(t)\right.\\ &\quad \left. + h_1(x_1(t-\tau_1)) - \dot{y}_d(t)\right) - \gamma_1(t) + \eta_1^{-1}W_1^{*T}S_1\\ &\quad + M_1(t)\chi_1(t) - N_1(t).\end{aligned} \tag{13}$$

Construct updating law of the RBFNN

$$\dot{\widehat{W}}_1 = \Gamma_1\left(\eta_1^{-1}z_1(t)S_1 - \sigma_1\Gamma_1^{-1}\widehat{W}_1\right), \tag{14}$$

where $\sigma_1 > 0$ is a design parameter. Furthermore, the DOB can be chosen as

$$\begin{aligned}\widehat{\chi}_1(t) &= w_1(t) + \eta_1 x_1(t)\\ \dot{w}_1(t) &= -\eta_1 w_1(t) - \eta_1\left(f_1(x_1(t)) + g_1(x_1(t))x_2(t)\right.\\ &\quad \left. + \eta_1^{-1}\widehat{W}_1^T S_1 + \eta_1 x_1(t)\right) + M_1^T(t)z_1(t).\end{aligned} \tag{15}$$

According to (15), we obtain

$$\dot{\widetilde{\chi}}_1(t) = \eta_1\widetilde{\chi}_1(t) + M_1^T(t)z_1(t) + \widetilde{W}_1^T S_1. \tag{16}$$

According to the neural network updating law (14) and DOB (15), the immediate control is chosen

$$\begin{aligned}x_2^*(t) &= g_1^{-1}(x_1(t))\left(-M_1^{-1}(t)K_1 z_1(t) - f_1(x_1(t))\right.\\ &\quad + \dot{y}_d(t) + M_1^{-1}(t)N_1(t) - M_1^{-1}(t)\gamma_1(t)\\ &\quad \left. - \eta_1^{-1}\widehat{W}_1^T S_1 - \widehat{\chi}_1(t)\right),\end{aligned} \tag{17}$$

where $M_1(t) = \mathrm{diag}\{M_{11}(t), \ldots, M_{1m}(t)\}$. $\dot{y}_d(t)$ is the time derivative of reference trajectory, and $K_1 \in R^{m\times m}$ is the constant positive definite matrices. $\widehat{W}_1$ is the estimated values of W_1^*, $\widetilde{W}_1$ represents the estimated error, and $\widetilde{W}_1 = W_1^* - \widehat{W}_1$. Substituting (17) into (13), the time derivative of $z_1(t)$ becomes

$$\begin{aligned}\dot{z}_1(t) &= -K_1 z_1(t) + M_1(t)g_1(x_1(t))z_2(t) - \gamma(t)\\ &\quad + M_1(t)h_1(x_1(t-\tau_1)) + \eta_1^{-1}\widetilde{W}_1^T S_1\\ &\quad + M_1(t)\widetilde{\chi}_1(t).\end{aligned} \tag{18}$$

Choose the Lyapunov-Krasovskii functional candidate as

$$\begin{aligned}V_1 &= \frac{z_1^T(t)z_1(t)}{2} + \int_{t-\tau_1}^{t} P_1(x_1(\tau))\,d\tau\\ &\quad + tr\left(\widetilde{W}_1^T\Gamma_1^{-1}\widetilde{W}_1\right) + \frac{1}{2}\widetilde{\chi}_1^T(t)\widetilde{\chi}_1(t),\end{aligned} \tag{19}$$

where the positive function $P_1(x_1(t))$ can be designed as follows:

$$P_1(x_1(t)) = \frac{h_1^T(x_1(t))h_1(x_1(t))}{2}. \tag{20}$$

Then the time derivative of V_1 is

$$\begin{aligned}\dot{V}_1 &= z_1^T(t)\left(-K_1 z_1(t) + M_1(t)g_1(x_1(t))z_2(t)\right.\\ &\quad + M_1(t)h_1(x_1(t-\tau_1)) - \gamma_1(t) + \eta_1^{-1}\widetilde{W}_1^T S_1\\ &\quad \left. + M_1(t)\chi_1(t)\right) + P_1(x_1(t)) - P_1(x_1(t-\tau_1))\\ &\quad - tr\left(\widetilde{W}_1^T\Gamma_1^{-1}\dot{\widehat{W}}_1\right) - \widetilde{\chi}_1^T(t)\dot{\widehat{\chi}}_1(t) + \widetilde{\chi}_1^T(t)\dot{\chi}_1(t)\\ &= -z_1^T(t)K_1 z_1(t) + z_1^T(t)\widetilde{W}_1^T S_1 + z_1^T(t)\\ &\quad \cdot h_1(x_1(t-\tau_1)) - z_1^T(t)\gamma_1(t) + z_1^T(t)M_1(t)\\ &\quad \cdot g_1(x_1(t))z_2(t) + \eta_1^{-1}z_1^T(t)\widetilde{W}_1^T S_1 + z_1^T(t)M_1(t)\\ &\quad \cdot \widetilde{\chi}_1(t) + P_1(x_1(t)) - P_1(x_1(t-\tau_1))\\ &\quad - tr\left(\widetilde{W}_1^T\Gamma_1^{-1}\dot{\widehat{W}}_1\right) - \widetilde{\chi}_1^T(t)\dot{\widehat{\chi}}_1(t) + \widetilde{\chi}_1^T(t)\dot{\chi}_1(t).\end{aligned} \tag{21}$$

Substituting (14) into (21), we obtain

$$\begin{aligned}\dot{V}_1 &= -z_1^T(t)K_1 z_1(t) + z_1^T(t)\widetilde{W}_1^T S_1\\ &\quad + z_1^T(t)h_1(x_1(t-\tau_1))\\ &\quad + z_1^T(t)M_1(t)g_1(x_1(t))z_2(t) - z_1^T(t)\gamma_1(t)\\ &\quad + z_1^T(t)M_1(t)\widetilde{\chi}_1 + P_1(x_1(t))\\ &\quad - P_1(x_1(t-\tau_1)) + \sigma_1 tr\left(\widetilde{W}_1^T\Gamma_1^{-1}\widehat{W}_1\right)\\ &\quad - \widetilde{\chi}_1^T(t)\dot{\widehat{\chi}}_1(t) + \widetilde{\chi}_1^T(t)\dot{\chi}_1(t).\end{aligned} \tag{22}$$

Substituting (16) into (22) yields

$$\begin{aligned}\dot{V}_1 &= -z_1^T(t)K_1 z_1(t) + z_1^T(t)\widetilde{W}_1^T S_1\\ &\quad + z_1^T(t)h_1(x_1(t-\tau_1)) - z_1^T(t)\gamma_1(t)\\ &\quad + z_1^T(t)M_1(t)g_1(x_1(t))z_2(t) + P_1(x_1(t))\\ &\quad - P_1(x_1(t-\tau_1)) + \sigma_1 tr\left(\widetilde{W}_1^T\Gamma_1^{-1}\widehat{W}_1\right)\\ &\quad - \eta_1\widetilde{\chi}_1^T(t)\widetilde{\chi}_1(t) - \widetilde{\chi}_1^T(t)\widetilde{W}_1^T S_1 + \widetilde{\chi}_1^T(t)\dot{\chi}_1(t).\end{aligned} \tag{23}$$

Step i. Define the error variables $z_i(t) \in R^m$ and $z_{i+1}(t) \in R^m$

$$\begin{aligned}z_i(t) &= x_i(t) - x_i^*(t)\\ z_{i+1}(t) &= x_{i+1}(t) - x_{i+1}^*(t),\end{aligned} \tag{24}$$

where $x_i^*(t)$ is a virtual control law. Combining (1) and (24) and differentiating $z_i(t)$ with respect to time, we have

$$\begin{aligned}\dot{z}_i(t) &= f_i(\overline{x}_i(t)) + g_i(\overline{x}_i(t))x_{i+1}(t) + h_i(\overline{x}_i(t-\tau_i))\\ &\quad + \Delta f_i(\overline{x}_i(t)) + d_i(t) - \dot{x}_i^*(t).\end{aligned} \tag{25}$$

Since $\Delta f_i(\overline{x}_i(t))$ is unknown, we use RBFNN to approximate uncertain function. $\widehat{W}_i$ indicates the estimate of W_i^*, and ε_i^* is the approximate error. $\widetilde{W}_i$ represents the estimated error, which is defined as $\widetilde{W}_i = W_i^* - \widehat{W}_i$. Define the variable $\chi_i(t) = \varepsilon_i^* + d_i(t)$.

$$\Delta f_i\left(\overline{x}_i\left(t\right)\right) + \gamma_i\left(t\right) = \eta_i^{-1} W_i^{*T} S_i + \varepsilon_i^*, \tag{26}$$

where $\gamma_i(t) = [\gamma_{i,1}(t), \ldots, \gamma_{i,m}(t)]^T$, and

$$\gamma_{i,j}\left(t\right) = \frac{16}{z_{ij}\left(t\right)} \tanh^2\left(\frac{z_{ij}\left(t\right)}{\nu_i}\right) h_{ij}^2\left(\overline{x}_i\left(t\right)\right), \quad j = 1, \ldots, m. \tag{27}$$

Substituting (26) into (1) yields

$$\begin{aligned}\dot{x}_i\left(t\right) = {} & f_i\left(\overline{x}_i\left(t\right)\right) + g_i\left(\overline{x}_i\left(t\right)\right) x_{i+1}\left(t\right) \\ & + h_i\left(\overline{x}_i\left(t-\tau_i\right)\right) - \gamma_i\left(t\right) + \eta_i^{-1} W_i^{*T} S_i + \chi_i\left(t\right).\end{aligned} \tag{28}$$

Moreover, substituting (26) into (25), we have

$$\begin{aligned}\dot{z}_i\left(t\right) = {} & f_i\left(\overline{x}_i\left(t\right)\right) + g_i\left(\overline{x}_i\left(t\right)\right) x_{i+1}\left(t\right) \\ & + h_i\left(\overline{x}_i\left(t-\tau_i\right)\right) - \gamma_i\left(t\right) + \eta_i^{-1} W_i^{*T} S_i + \chi_i\left(t\right) \\ & - \dot{x}_i^*\left(t\right).\end{aligned} \tag{29}$$

Construct updating law of the RBFNN

$$\dot{\widehat{W}}_i = \Gamma_i\left(\eta_1^{-1} z_i\left(t\right) S_i - \sigma_i \Gamma_i^{-1} \widehat{W}_i\right), \tag{30}$$

where $\sigma_i > 0$ is a design parameter. Furthermore, the DOB can be chosen as

$$\begin{aligned}\widehat{\chi}_i\left(t\right) &= w_i\left(t\right) + \eta_i x_i\left(t\right) \\ \dot{w}_i\left(t\right) &= -\eta_i w_i\left(t\right) - \eta_i\left(f_i\left(\overline{x}_i\left(t\right)\right) + g_i\left(\overline{x}_i\left(t\right)\right) x_{i+1}\right. \\ &\quad \left. + \eta_i^{-1} \widehat{W}_i^T S_i + \eta_i x_i\left(t\right)\right) + z_i\left(t\right).\end{aligned} \tag{31}$$

According to (31), we obtain

$$\dot{\widehat{\chi}}_i\left(t\right) = \eta_i \widetilde{\chi}_i\left(t\right) + z_i\left(t\right) + \widetilde{W}_i^T S_i. \tag{32}$$

Hence, the virtual control law $x_{i+1}^*(t)$ is proposed as

$$\begin{aligned}x_{i+1}^*\left(t\right) = {} & g_i^{-1}\left(\overline{x}_i\left(t\right)\right)\left(-K_i z_i\left(t\right)\right. \\ & - g_{i-1}^T\left(\overline{x}_{i-1}\left(t\right)\right) z_{i-1}\left(t\right) - f_i\left(\overline{x}_i\left(t\right)\right) + \dot{x}_i^*\left(t\right) \\ & \left. - \eta_i^{-1} \widehat{W}_i^T S_i - \widehat{\chi}_i\left(t\right)\right).\end{aligned} \tag{33}$$

Choose the Lyapunov-Krasovskii functional candidate as

$$\begin{aligned}V_i = {} & \frac{1}{2} z_i^T\left(t\right) z_i\left(t\right) + \int_{t-\tau_i}^{t} P_i\left(\overline{x}_i\left(\tau\right)\right) d\tau \\ & + tr\left(\widetilde{W}_i^T \Gamma_i^{-1} \widetilde{W}_i\right) + \frac{1}{2} \widetilde{\chi}_i^T\left(t\right) \widetilde{\chi}_i\left(t\right),\end{aligned} \tag{34}$$

where the positive function $P_i(\overline{x}_i(\tau))$ is given in the form of

$$P_i\left(\overline{x}_i\left(\tau\right)\right) = \frac{1}{2} h_i^T\left(\overline{x}_i\left(\tau\right)\right) h_i\left(\overline{x}_i\left(\tau\right)\right). \tag{35}$$

Similar to Step 1, the time derivative of $\dot{V}_i$ can be rewritten as

$$\begin{aligned}\dot{V}_i = {} & -z_i^T\left(t\right) K_i z_i\left(t\right) + z_i^T\left(t\right) g_i\left(\overline{x}_i\left(t\right)\right) z_{i+1}\left(t\right) \\ & - z_i^T\left(t\right) g_{i-1}^T\left(\overline{x}_{i-1}\left(t\right)\right) z_{i-1}\left(t\right) - z_i^T\left(t\right) \gamma_i\left(t\right) \\ & + z_i^T\left(t\right) h_i\left(\overline{x}_i\left(t-\tau_i\right)\right) + P_i\left(\overline{x}_i\left(t\right)\right) \\ & - P_i\left(\overline{x}_i\left(t-\tau_i\right)\right) + \sigma_i tr\left(\widetilde{W}_i^T \Gamma_i^{-1} \widehat{W}_i\right) \\ & - \eta_i \widetilde{\chi}_i^T\left(t\right) \widetilde{\chi}_i\left(t\right) - \widetilde{\chi}_i^T\left(t\right) \widetilde{W}_i^T S_i + \widetilde{\chi}_i^T\left(t\right) \dot{\chi}_i\left(t\right).\end{aligned} \tag{36}$$

Step n. Define the error variable $z_n(t) \in R^m$:

$$z_n\left(t\right) = x_n\left(t\right) - x_n^*\left(t\right) \tag{37}$$

Invoking (1) and (37), differentiating $z_n(t)$ with respect to time yields

$$\begin{aligned}\dot{z}_n\left(t\right) = {} & f_n\left(\overline{x}_n\left(t\right)\right) + g_n\left(\overline{x}_n\left(t\right)\right) u\left(t\right) + h_n\left(\overline{x}_n\left(t-\tau\right)\right) \\ & + \Delta f_n\left(\overline{x}_n\left(t\right)\right) - \dot{x}_n^*\left(t\right).\end{aligned} \tag{38}$$

Since $\Delta f_n(\overline{x}_n(t))$ is unknown, the RBFNN is used to approximate $\Delta f_n(\overline{x}_n(t))$. $\widehat{W}_n$ indicates the estimate of W_n^*, and ε_n^* is the approximate error. $\widetilde{W}_n$ represents the estimated error, which is defined as $\widetilde{W}_n = W_n^* - \widehat{W}_n$. Define the variable $\chi_n = \varepsilon_n^* + d_n(t)$.

$$\Delta f_n\left(\overline{x}_n\left(t\right)\right) + \gamma_n\left(t\right) = \eta_n^{-1} W_n^{*T} S_n + \varepsilon_n^*, \tag{39}$$

where $\gamma_n(t) = [\gamma_{n,1}(t), \ldots, \gamma_{n,m}(t)]^T$, and

$$\gamma_{n,j}\left(t\right) = \frac{16}{z_{nj}\left(t\right)} \tanh^2\left(\frac{z_{nj}\left(t\right)}{\nu_n}\right) h_{nj}^2\left(\overline{x}_n\left(t\right)\right), \quad j = 1, \ldots, m. \tag{40}$$

Substituting (39) into (1) yields

$$\begin{aligned}\dot{x}_n\left(t\right) = {} & f_n\left(\overline{x}_n\left(t\right)\right) + g_n\left(\overline{x}_n\left(t\right)\right) u\left(t\right) \\ & + h_n\left(\overline{x}_n\left(t-\tau_n\right)\right) - \gamma_n\left(t\right) + \eta_n^{-1} W_n^{*T} S_n \\ & + \chi_n\left(t\right).\end{aligned} \tag{41}$$

Invoking (38) and (39), one obtains

$$\begin{aligned}\dot{z}_n\left(t\right) = {} & f_n\left(\overline{x}_n\left(t\right)\right) + g_n\left(\overline{x}_n\left(t\right)\right) u\left(t\right) \\ & + h_n\left(\overline{x}_n\left(t-\tau_n\right)\right) - \gamma_n\left(t\right) + \eta_n^{-1} W_n^{*T} S_n \\ & + \chi_n\left(t\right) - \dot{x}_n^*\left(t\right).\end{aligned} \tag{42}$$

Construct updating law of the RBFNN

$$\dot{\widehat{W}}_n\left(t\right) = \Gamma_n\left(\eta_n^{-1} z_n\left(t\right) S_n - \sigma_n \Gamma_n^{-1} \widehat{W}_n\left(t\right)\right), \tag{43}$$

where $\sigma_n \in R$, $\sigma_n > 0$, is a design parameter. Furthermore, the DOB can be chosen as

$$\begin{aligned}\widehat{\chi}_n(t) &= w_n(t) + \eta_n x_n(t)\\ \dot{w}_n(t) &= -\eta_n w_n(t) - \eta_n\left(f_n(\overline{x}_n(t)) + g_n(\overline{x}_n(t))u(t)\right.\\ &\quad \left. + \eta_n^{-1}\widehat{W}_n^T S_n + \eta_n x_n(t)\right) + z_n(t).\end{aligned} \tag{44}$$

According to (44), we obtain

$$\dot{\widehat{\chi}}_n(t) = \eta_n\widetilde{\chi}_n(t) + z_n(t) + \widetilde{W}_n^T S_n. \tag{45}$$

Therefore, design the control law $u(t)$ as

$$\begin{aligned}u(t) = g_n^{-1}(\overline{x}_n(t))\big(&-K_n z_n(t)\\ &- g_{n-1}^T(\overline{x}_{n-1}(t))z_{n-1}(t) - f_n(\overline{x}_n(t)) + \dot{x}_n^*(t)\\ &- \eta_n^{-1}\widehat{W}_n^T S_n - \widehat{\chi}_n(t)\big),\end{aligned} \tag{46}$$

where $K_n \in R^{m\times m}$, $K_n > 0$ is design matrix. Choose the Lyapunov-Krasovskii functional candidate as

$$\begin{aligned}V_n = \frac{1}{2}z_n^T(t)z_n(t) + \int_{t-\tau_n}^{t} P_n(\overline{x}_n(\tau))d\tau\\ + tr\left(\widetilde{W}_n^T\Gamma_n^{-1}\widetilde{W}_n\right) + \frac{1}{2}\widetilde{\chi}_n^T(t)\widetilde{\chi}_n(t)\end{aligned} \tag{47}$$

and the positive function $P_n(\overline{x}_n(\tau))$ can be designed as follows:

$$P_n(\overline{x}_n(\tau)) = \frac{1}{2}h_n^T(\overline{x}_n(\tau))h_n(\overline{x}_n(\tau)). \tag{48}$$

According to the derivatives in Step 1 and Step i, we have

$$\begin{aligned}\dot{V}_n = &-z_n^T(t)K_n z_n(t) - z_n^T(t)g_{n-1}^T(\overline{x}_{n-1}(t))z_{n-1}(t)\\ &+ z_n^T(t)h_n(\overline{x}_n(t-\tau_n)) - z_n^T(t)\gamma_n(t)\\ &+ P_n(\overline{x}_n(t)) - P_n(\overline{x}_n(t-\tau_n))\\ &- \sigma_n tr\left(\widetilde{W}_n^T\Gamma_n^{-1}\widehat{W}_n\right) - \eta_n\widetilde{\chi}_n^T(t)\widetilde{\chi}_n(t)\\ &- \widetilde{\chi}_n^T(t)\widetilde{W}_n^T S_n + \widetilde{\chi}_n^T(t)\dot{\chi}_n(t).\end{aligned} \tag{49}$$

From the above inductive design procedure, moreover, we can conclude the following theorem.

3.2. Stability Analysis

Theorem 7. *Considering the system dynamics described by (1), under the adaptive neural updated laws (14), (30), and (43), the disturbance observers (15), (31), and (45), and the prescribed performance-based control laws (17), (33), and (46), we can conclude that the trajectories of the closed-loop system are semiglobally uniformly bounded, while the tracking error $\widetilde{z}_1(t)$ converges to a compact set Q_z asymptotically, where C and κ are defined in (50).*

$$\begin{aligned}\kappa = \min&\left\{\left(\lambda_{\min}(K_i) - \frac{\vartheta_{\xi i}+1}{2}\right),\right.\\ &\left.\left(\eta_i - \frac{1}{2\vartheta_{\xi i}} - \frac{\delta_S\varphi_i}{2} - \frac{\pi_i}{2}\right), \frac{\sigma_i}{2}\right\}\\ C = &\sum_{i=1}^{n}\frac{\sigma_i}{2}\lambda_{\min}\left(\Gamma_i^{-1}\right)\left\|W_i^*\right\|^2 + \sum_{i=1}^{n}\frac{1}{2\pi_i}\left\|\dot{\chi}_i(t)\right\|^2,\end{aligned} \tag{50}$$

where Q_z can be made as small as desired by appropriately choosing design parameters. $\lambda_{\min}$ represents the minimum eigenvalue of the matrix. $\lambda_{\min}$ represents the minimum eigenvalue of the matrix.

Proof. For analytical purposes, define the total Lyapunov function

$$V_\Xi = \sum_{i=1}^{n} V_i, \tag{51}$$

where definition of V_i can be referred to (19), (34), and (47). According to (23), (36), and (49), we obtain

$$\begin{aligned}\dot{V}_\Xi = &-\sum_{i=1}^{n} z_i^T(t)K_i z_i(t) - \sum_{i=1}^{n}\eta_i\widetilde{\chi}_i^T(t)\widetilde{\chi}_i(t)\\ &+ \sum_{i=1}^{n} z_i^T(t)h_i(\overline{x}_i(t-\tau_i)) + \sum_{i=1}^{n} z_i^T(t)\widetilde{\chi}_i(t)\\ &- \sum_{i=1}^{n} z_i^T(t)\gamma_i(t) - \sum_{i=1}^{n}\widetilde{\chi}_i^T(t)\widetilde{W}_i^T S_i\\ &+ \sum_{i=1}^{n}\widetilde{\chi}_i^T(t)\dot{\chi}_i(t)\\ &+ \sum_{i=1}^{n}\left(P_i(\overline{x}_i(t)) - P_i(\overline{x}_i(t-\tau_i))\right)\\ &- \sum_{i=1}^{n}\sigma_i tr\left(\widetilde{W}_i^T\Gamma_i^{-1}\widehat{W}_i\right).\end{aligned} \tag{52}$$

Considering the fact that

$$\begin{aligned}&z_i^T(t)h_i(\overline{x}_i(t-\tau_i))\\ &\le \frac{1}{2}z_i^T(t)z_i(t) + \frac{1}{2}h_i^T(\overline{x}_i(t-\tau_i))h_i(\overline{x}_i(t-\tau_i))\end{aligned} \tag{53}$$

and $P_i(\overline{x}_i(t-\tau_i)) = (1/2)h_i^T(\overline{x}_i(t-\tau_i))h_i(\overline{x}_i(t-\tau_i))$, we have

$$\begin{aligned}\dot{V}_\Xi \le & -\sum_{i=1}^{n} z_i^T(t) K_i z_i(t) - \sum_{i=1}^{n} \eta_i \widetilde{\chi}_i^T(t) \widetilde{\chi}_i(t) \\ & + \sum_{i=1}^{n} z_i^T(t) \widetilde{\chi}_i(t) - \sum_{i=1}^{n} z_i^T(t) \gamma_i(t) \\ & - \sum_{i=1}^{n} \widetilde{\chi}_i^T(t) \widetilde{W}_i^T S_i + \sum_{i=1}^{n} \widetilde{\chi}_i^T(t) \dot{\chi}_i(t) \\ & + \frac{1}{2}\sum_{i=1}^{n} z_i^T(t) z_i(t) + \sum_{i=1}^{n} P_i(\overline{x}_i(t)) \\ & - \sum_{i=1}^{n} \sigma_i tr\left(\widetilde{W}_i^T \Gamma_i^{-1} \widehat{W}_i\right).\end{aligned} \tag{54}$$

Then we have the following results:

$$\begin{aligned}\dot{V}_\Xi \le & -\sum_{i=1}^{n} z_i^T(t)\left(K_i - \frac{1}{2} I^{m\times m}\right) z_i(t) \\ & - \sum_{i=1}^{n} \eta_i \widetilde{\chi}_i^T(t) \widetilde{\chi}_i(t) + \sum_{i=1}^{n} z_i^T(t) \widetilde{\chi}_i(t) \\ & - \sum_{i=1}^{n} z_i^T(t) \gamma_i(t) - \sum_{i=1}^{n} \widetilde{\chi}_i^T(t) \widetilde{W}_i^T S_i \\ & + \sum_{i=1}^{n} \widetilde{\chi}_i^T(t) \dot{\chi}_i(t) + \sum_{i=1}^{n} P_i(\overline{x}_i(t)) \\ & - \sum_{i=1}^{n} \sigma_i tr\left(\widetilde{W}_i^T \Gamma_i^{-1} \widehat{W}_i\right).\end{aligned} \tag{55}$$

In addition, it is clear that there exists $\|S_i\| \le \delta_{Si}$, $\delta_{Si} > 0$; we have the following facts:

$$\begin{aligned}\sigma_i tr\left(\widetilde{W}_i^T \Gamma_i^{-1} \widehat{W}_i\right) \le & -\frac{\sigma_i}{2} tr\left(\widetilde{W}_i^T \Gamma_i^{-1} \widetilde{W}_i\right) \\ & + \frac{\sigma_i}{2} tr\left(W_i^{*T} \Gamma_i^{-1} W_i^*\right) \\ z_i^T(t) \widetilde{\chi}_i(t) \le & \frac{\vartheta_{\xi i}}{2} z_i^T(t) z_i(t) + \frac{1}{2\vartheta_{\xi i}} \left\|\widetilde{\chi}_i(t)\right\|^2 \\ \widetilde{\chi}_i^T(t) \widetilde{W}_i^T S_i \le & \frac{\delta_{Si}\varphi_i}{2} \left\|\widetilde{\chi}_i(t)\right\|^2 + \frac{\delta_{Si}}{2\varphi_i} \left\|\widetilde{W}_i\right\|^2 \\ \widetilde{\chi}_i^T(t) \dot{\chi}_i(t) \le & \frac{\pi_i}{2} \left\|\widetilde{\chi}_i(t)\right\|^2 + \frac{1}{2\pi_i} \left\|\dot{\chi}_i(t)\right\|^2,\end{aligned} \tag{56}$$

where $\vartheta_{\xi i} > 0$ and $\varphi_i > 0$ are the constants, and then we have

$$\begin{aligned}\dot{V}_\Xi \le & -\sum_{i=1}^{n}\left(\lambda_{\min}(K_i) - \frac{\vartheta_{\xi i} + 1}{2}\right)\left\|z_i(t)\right\| - \sum_{i=1}^{n}\left(\eta_i \right. \\ & \left. - \frac{1}{2\vartheta_{\xi i}} - \frac{\delta_{Si}\varphi_i}{2} - \frac{\pi_i}{2}\right)\left\|\widetilde{\chi}_i(t)\right\| \\ & - \sum_{i=1}^{n} \frac{\sigma_i}{2} tr\left(\widetilde{W}_i^T \Gamma_i^{-1} \widetilde{W}_i\right) + \frac{1}{2} \\ & \cdot \sum_{i=1}^{n}\sum_{j=1}^{m}\left(1 - 16\tanh^2\left(\frac{z_{ij}(t)}{\nu_i}\right)\right) h_{ij}^T(\overline{x}_i(t)) \\ & \cdot h_{ij}(\overline{x}_i(t)) + \sum_{i=1}^{n} \frac{\sigma_i}{2} tr\left(W_i^{*T} \Gamma_i^{-1} W_i^*\right) \\ & + \sum_{i=1}^{n} \frac{1}{2\pi_i} \left\|\dot{\chi}_i(t)\right\|.\end{aligned} \tag{57}$$

Invoking Lemma 5, we obtain

$$\dot{V}_\Xi \le -\kappa V_\Xi + C. \tag{58}$$

$\kappa > 0, C > 0$ are defined in (50). Therefore, according to Lemma 4, we can conclude that the solution of the closed-loop system remains within a compact subset. □

4. Application to Unmanned Helicopter System

In this section, we will apply the proposed robust adaptive control strategy to solve the problem of attitude tracking for a class of uncertain unmanned helicopter systems.

The unmanned helicopters rigid-body dynamics consist of two parts, attitude angular dynamics and flapping dynamics. The unsteady aerodynamics bring out the time-delay nonlinear uncertainty; thus in this section we consider the attitude control for attitude control subject to time delay. Firstly, the attitude angular and angular velocity dynamics can be described as [26]

$$\begin{aligned}\dot{\Theta}(t) &= R(\Theta(t))\Omega(t) \\ I\dot{\Omega}(t) &= -\Omega(t) \times (I\Omega(t)) + \overline{A}(t) v_c(t) \\ &\quad + h(\Theta(t), \Omega(t)) + \overline{B}(t) \\ &\quad + \Delta_\Omega(\Theta(t), \Omega(t)) + d_\Omega(t),\end{aligned} \tag{59}$$

where $\Theta = [\psi, \theta, \phi]^T \in R^3$ indicates the attitude angle and $\Omega = [p, q, r]^T \in R^3$ represents the attitude angle velocity. $d_\Omega(t) \in R^3$ stands for the disturbance, and $\Delta_\Omega \in R^3$ stands for the uncertainties; $h(\Theta(t), \Omega(t)) \in R^3$ means the unknown

nonlinear block of time delay. $v_c = [a, b, T_T]^T \in R^3$, $R(\Theta(t))$ denotes

$$R(\Theta(t)) = \begin{bmatrix} 1 & \sin\phi(t)\tan\theta(t) & \cos\phi(t)\tan\theta(t) \\ 0 & \cos\phi(t) & -\sin\phi(t) \\ 0 & \dfrac{\sin\phi(t)}{\cos\theta(t)} & \dfrac{\cos\phi(t)}{\cos\theta(t)} \end{bmatrix}. \tag{60}$$

$\overline{A}$ and $\overline{B}$ denote

$$\overline{A} = \begin{bmatrix} -G_R & -z_R T_R + K_\beta & z_T \\ -z_R T_R + K_\beta & G_R & 0 \\ y_R T_R & x_R T_R & -x_T \end{bmatrix}$$

$$\overline{B} = \begin{bmatrix} -y_R T_R \\ x_R T_R \\ -G_R \end{bmatrix} \tag{61}$$

$$G_R = C^R |T_R|^{1.5} + D^R.$$

In the unmanned helicopter attitude control loop, the main rotor thrusts T_R are fixed. $[x_R, y_R, z_R]^T \in R^3$ indicates the location of the main rotor relative to the center of gravity; $[x_T, y_T, z_T]^T \in R^3$ indicates the location of the tail rotor relative to the center of gravity. $K_\beta \in R$ means the stiffness of the rotor hub. C^R and D^R are constants, which are associated with the antitorque. The control design procedure can be presented as follows.

Step 1. Define the attitude angle tracking errors in the form of $\widetilde{z}_\psi(t) = \psi(t) - \psi_r(t)$, $\widetilde{z}_\theta(t) = \theta(t) - \theta_r(t)$, $\widetilde{z}_\phi(t) = \phi(t) - \phi_r(t)$, and $\widetilde{z}_\Theta(t) = [\widetilde{z}_\psi(t), \widetilde{z}_\theta(t), \widetilde{z}_\phi(t)]^T$, where $\psi_r(t)$, $\theta_r(t)$, and $\phi_r(t)$ are the reference trajectories and $\Theta_r = [\psi_r(t), \theta_r(t), \phi_r(t)]^T$. Then the time derivative of $\widetilde{z}_\Theta(t)$ is achieved as

$$\dot{\widetilde{z}}_\Theta = R(\Theta(t))\Omega(t) - \dot{\Theta}_r(t). \tag{62}$$

According to the analysis in the previous section, the prescribed performance function is chosen as

$$z_{\Theta_j}(t) = \frac{1}{2}\ln\left[\frac{\left(\underline{\alpha}_j + \widetilde{z}_{\Theta_j}(t)/\rho_j(t)\right)}{\left(\overline{\alpha}_j - \widetilde{z}_{\Theta_j}(t)/\rho_j(t)\right)}\right], \quad j = 1, \ldots, 3, \tag{63}$$

and the definition of $\rho_j(t)$ can be referred to in (6). Choose the virtual control signal as

$$\Omega^*(t) = R^{-1}(\Theta(t)) \cdot \left(-M_\Theta^{-1}(t) K_\Theta z_\Theta(t) + \dot{\Theta}_r(t) + M_\Theta^{-1}(t) N_\Theta(t)\right). \tag{64}$$

Choose the Lyapunov function:

$$V_\Theta = \frac{z_\Theta^T(t) z_\Theta(t)}{2}. \tag{65}$$

Step 2. Define the tracking errors $z_p(t) = p(t) - p_r^*(t)$, $z_q(t) = q(t) - q_r^*(t)$, $z_r(t) = r(t) - r_r^*(t)$, and $\Omega^*(t) = [p_r^*(t), q_r^*(t), r_r^*(t)]^T$. Using the neural network to compensate the uncertainties and time-delay terms, such that $\Delta_\Omega(\Theta(t), \Omega(t)) + \gamma_\Omega(t) = \eta_\Omega^{-1} W_\Omega^{*T} S_\Omega + \varepsilon_\Omega^*$, assume that ε_Ω^* is the optimal approximate error, and define $\chi_\Omega(t) = \varepsilon_\Omega^* + d_\Omega(t)$. Design the neural updated law as

$$\dot{\widehat{W}}_\Omega(t) = \Gamma_\Omega\left(z_\Omega(t) S_\Omega(\Theta(t), \Omega(t)) - \sigma_\Omega \Gamma_\Omega^{-1} \widehat{W}_\Omega(t)\right). \tag{66}$$

The DOB can be constructed in the form of

$$\begin{aligned} \widehat{\chi}_\Omega(t) &= w_\Omega(t) + \eta_\Omega \Omega(t) \\ \dot{w}_\Omega(t) &= -\eta_\Omega w_\Omega(t) - \eta_\Omega\left(-\Omega(t) \times (I\Omega(t)) + \overline{A}(t) v_c(t) + \overline{B}(t) + \eta_\Omega^{-1} \widehat{W}_\Omega^T S_\Omega + \eta_\Omega \Omega(t)\right) \\ &\quad + z_\Omega(t). \end{aligned} \tag{67}$$

Based on the above design, the adaptive control law is achieved as

$$v_c(t) = \overline{A}^{-1}(t)\left(-K_\Omega z_\Omega(t) - R^T(\Theta) z_\Theta(t) + \dot{\Omega}^*(t) + \Omega(t) \times (I\Omega(t)) - \overline{B}(t) - \eta_\Omega^{-1} \widehat{W}_\Omega^T S_\Omega - \widehat{\chi}_\Omega(t)\right). \tag{68}$$

Choose the Lyapunov function:

$$V_\Omega = \frac{1}{2}\Omega^T(t)\Omega(t) + \int_{t-\tau}^{t} P\left(\Theta(t_\tau), \Omega(t_\tau)\right) dt_\tau + tr\left(\widetilde{W}_\Omega^T \Gamma_\Omega^{-1} \widetilde{W}_\Omega\right) + \frac{1}{2}\widetilde{\chi}_\Omega^T(t)\widetilde{\chi}_\Omega(t). \tag{69}$$

Similar to Theorem 7, we can conclude the following theorem.

Theorem 8. *For the unmanned helicopter system (59), combining the DOB (67) and neural network update law (66), the control procedure can be achieved as (64) and (68); thus the closed-loop signals are bounded, and the output trajectories are satisfying the prescribed performance conditions.*

For Theorem 8, the detailed proof can be referred to in Theorem 7 in the previous section.

5. Simulation Results

In this section, the numerical simulation about unmanned helicopter system is utilized for illustrating the effectiveness of the previous control method in this paper. Consider the unmanned helicopter system with the following parameters (Table 1) [24, 26].

Now let us look at the design of adaptive controller design, the DOB design parameters are chosen as $\eta_\Omega = 6$. The neural update law has been given by 70, and its parameters are chosen as $\Gamma_\Omega = 0.1 \cdot \mathrm{diag}\{1, 1, 1, 1, 1, 1, 1\}$, $\sigma_\Omega = 10$, $\mu = [-3, -2, -1, 0, 1, 2, 3]$, and $c_\Omega = [1, 1, 1, 1, 1, 2, 3]$, and the controller design parameters are chosen as $K_\Theta = \{5, 5, 5\}$ and

Table 1: Helicopter parameters.

Symbol	Unit	Number
I	kg·m^2	diag (0.18, 0.34, 0.28)
m	kg	8.2
g	m/sec^2	9.81
x_T	m	−0.91
z_T	m	−0.08
z_R	m	−0.235
x_R	m	0
y_R	m	0
z_R	m	0
K_β	N·m/rad	52
C^R	m/$\sqrt{\text{N}}$	0.004452
D^R	N · m	0.6304

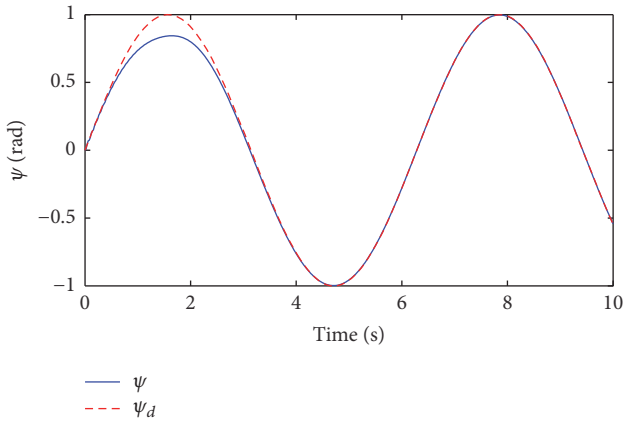

Figure 1: Yaw angle.

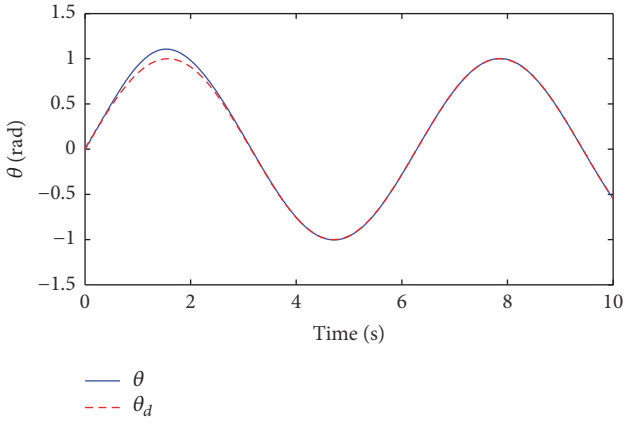

Figure 2: Pitch angle.

$K_\Omega = \{10, 10, 10\}$. The simulation environment is built under Matlab, and the simulation step is chosen as $\tau = 0.02$. The initial conditions are chosen as follows: $\psi(0) = 1$ rad, $\psi(0) = 0$ rad, and $\psi(0) = 0$ rad. The time-delay block is chosen in the form of $h(\Theta(t), \Omega(t)) = \Omega(t-\tau)^2 + \sin(0.1 \cdot \Omega(t-3\tau))$. The external disturbance is chosen as $d_\Omega(t) = 2 \cdot \sin(2 \cdot t + 0.6)$.

From the curves in Figures 1–3, it can be seen that the tracking trajectories soon reach the target trajectories, and

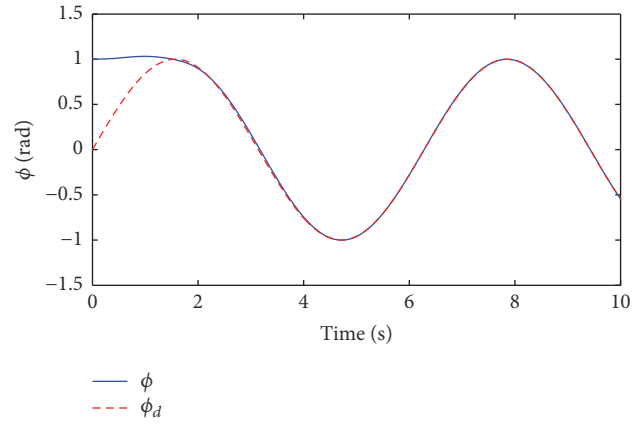

Figure 3: Roll angle.

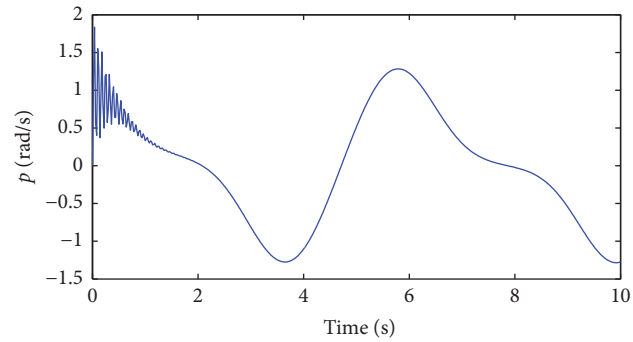

Figure 4: Yaw angular velocity.

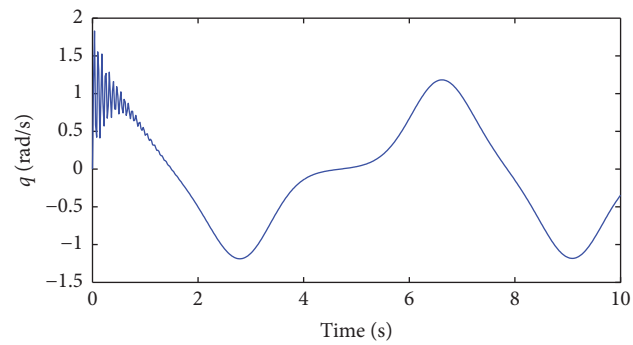

Figure 5: Pitch angular velocity.

the tracking errors are bounded in the appointed region. Figures 4–6 show the attitude angular velocities. Figures 7–9 show the control input signals. From the numerical simulation, we can conclude that the proposed control approach is valid for a class of uncertain unmanned helicopter systems with unsteady aerodynamics. Furthermore, it can be illustrated that the closed-loop system output signals are asymptotically tracking the ideal trajectories, and they are restricted in the region of output constraints.

6. Conclusion

In this paper, an adaptive prescribed performance control procedure has been proposed for a class of nonlinear time-delay systems with uncertainties, external disturbances, and

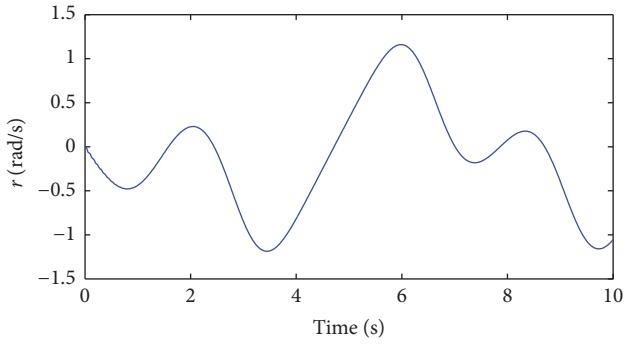

Figure 6: Roll angular velocity.

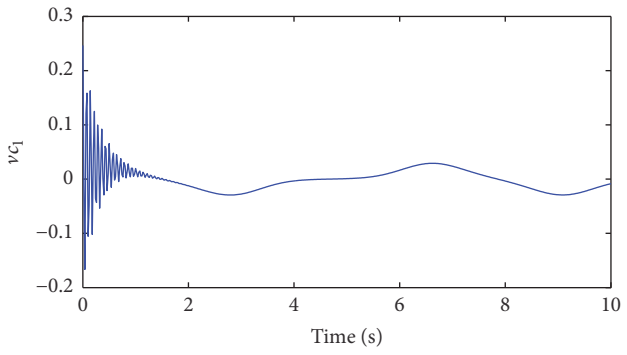

Figure 7: Control input signal $v_{c1}(t)$.

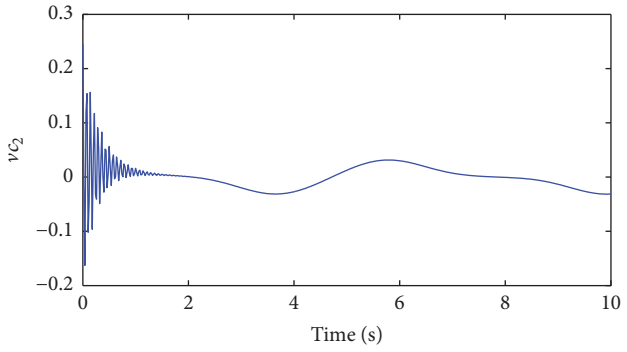

Figure 8: Control input signal $v_{c2}(t)$.

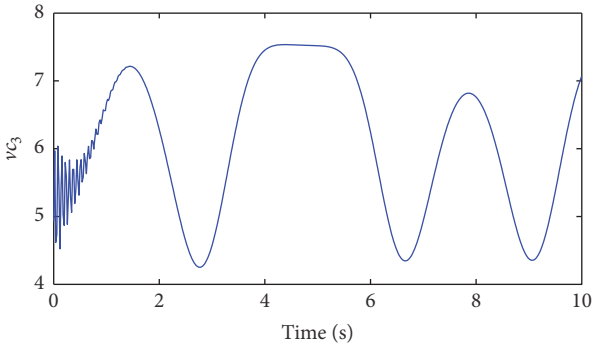

Figure 9: Control input signal $v_{c3}(t)$.

output constraints. Additionally, the robust controller has been applied to unmanned helicopter systems with unsteady aerodynamics. At last, the simulation illustrates that the proposed control approach is valid for the uncertain constrained time-delay system.

Conflicts of Interest

The authors declare that there are no conflicts of interest regarding the publication of this paper.

Acknowledgments

This article was supported by the National Natural Science Foundation of China (nos. 61573184, 61374212), the Fundamental Research Funds for the Central Universities (no. NE2016101), and the Aeronautical Science Foundation of China (no. 20165752049).

References

[1] P. Shi, E.-K. Boukas, and R. K. Agarwal, "Control of Markovian jump discrete-time systems with norm bounded uncertainty and unknown delay," *Institute of Electrical and Electronics Engineers Transactions on Automatic Control*, vol. 44, no. 11, pp. 2139–2144, 1999.

[2] J. Zhou, C. Wen, and W. Wang, "Adaptive backstepping control of uncertain systems with unknown input time-delay," *Automatica*, vol. 45, no. 6, pp. 1415–1422, 2009.

[3] S. S. Ge, F. Hong, and T. H. Lee, "Adaptive neural network control of nonlinear systems with unknown time delays," *Institute of Electrical and Electronics Engineers Transactions on Automatic Control*, vol. 48, no. 11, pp. 2004–2010, 2003.

[4] S. Tong, Y. Li, G. Feng, and T. Li, "Observer-based adaptive fuzzy backstepping dynamic surface control for a class of nonlinear systems with unknown time delays," *IET Control Theory & Applications*, vol. 5, no. 12, pp. 1426–1438, 2011.

[5] Q. Zhou, P. Shi, S. Xu, and H. Li, "Observer-based adaptive neural network control for nonlinear stochastic systems with time delay," *IEEE Transactions on Neural Networks and Learning Systems*, vol. 24, no. 1, pp. 71–80, 2013.

[6] R. Yang and Y. Wang, "Finite-time stability analysis and H control for a class of nonlinear time-delay Hamiltonian systems," *Automatica*, vol. 49, no. 2, pp. 390–401, 2013.

[7] R. Yang and Y. Wang, "Finite-time stability and stabilization of a class of nonlinear time-delay systems," *SIAM Journal on Control and Optimization*, vol. 50, no. 5, pp. 3113–3131, 2012.

[8] M. Chen and G. Tao, "Adaptive Fault-Tolerant Control of Uncertain Nonlinear Large-Scale Systems With Unknown Dead Zone," *IEEE Transactions on Cybernetics*, vol. 46, no. 8, pp. 1851–1862, 2016.

[9] M. Chen, S. S. Ge, and B. V. E. How, "Robust adaptive neural network control for a class of uncertain MIMO nonlinear systems with input nonlinearities," *IEEE Transactions on Neural Networks and Learning Systems*, vol. 21, no. 5, pp. 796–812, 2010.

[10] M. Chen, P. Shi, and C. C. Lim, "Adaptive neural fault-tolerant control of a 3-dof model helicopter system," *IEEE Transactions on Systems, Man, and Cybernetics: Systems*, vol. 46, no. 2, pp. 260–270, 2015.

[11] M. Chen, P. Shi, and C.-C. Lim, "Robust constrained control for MIMO nonlinear systems based on disturbance observer," *Institute of Electrical and Electronics Engineers Transactions on Automatic Control*, vol. 60, no. 12, pp. 3281–3286, 2015.

[12] J. Yang, W.-H. Chen, S. Li, L. Guo, and Y. Yan, "Disturbance/Uncertainty Estimation and Attenuation Techniques in PMSM Drives - A Survey," *IEEE Transactions on Industrial Electronics*, vol. 64, no. 4, pp. 3273–3285, 2017.

[13] J. Zhang, X. Liu, Y. Xia, Z. Zuo, and Y. Wang, "Disturbance Observer-Based Integral Sliding-Mode Control for Systems with Mismatched Disturbances," *IEEE Transactions on Industrial Electronics*, vol. 63, no. 11, pp. 7040–7048, 2016.

[14] B. Xu, "Disturbance observer-based dynamic surface control of transport aircraft with continuous heavy cargo airdrop," *IEEE Transactions on Systems, Man, and Cybernetics: Systems*, 2016.

[15] M. Chen, "Constrained control allocation for overactuated aircraft using a neurodynamic model," *IEEE Transactions on Systems, Man, and Cybernetics: Systems*, vol. 46, no. 12, pp. 1630–1641, 2016.

[16] R. Li, M. Chen, and Q. Wu, "Adaptive neural tracking control for uncertain nonlinear systems with input and output constraints using disturbance observer," *Neurocomputing*, vol. 235, pp. 27–37, 2017.

[17] B. Niu and J. Zhao, "Tracking control for output-constrained nonlinear switched systems with a barrier Lyapunov function," *International Journal of Systems Science*, vol. 44, no. 5, pp. 978–985, 2013.

[18] Y.-J. Liu and S. Tong, "Barrier Lyapunov Functions-based adaptive control for a class of nonlinear pure-feedback systems with full state constraints," *Automatica*, vol. 64, pp. 70–75, 2016.

[19] W. He, Z. Yin, and C. Sun, "Adaptive Neural Network Control of a Marine Vessel With Constraints Using the Asymmetric Barrier Lyapunov Function," *IEEE Transactions on Cybernetics*, 2016.

[20] C. P. Bechlioulis and G. A. Rovithakis, "Robust adaptive control of feedback linearizable MIMO nonlinear systems with prescribed performance," *Institute of Electrical and Electronics Engineers Transactions on Automatic Control*, vol. 53, no. 9, pp. 2090–2099, 2008.

[21] S. Tong, S. Sui, and Y. Li, "Fuzzy adaptive output feedback control of MIMO nonlinear systems with partial tracking errors constrained," *IEEE Transactions on Fuzzy Systems*, 2014.

[22] K. Peng, G. Cai, B. M. Chen, M. Dong, K. Y. Lum, and T. H. Lee, "Design and implementation of an autonomous flight control law for a UAV helicopter," *Automatica*, vol. 45, no. 10, pp. 2333–2338, 2009.

[23] G. W. Cai, B. M. Chen, X. Dong, and T. H. Lee, "Design and implementation of a robust and nonlinear flight control system for an unmanned helicopter," *Mechatronics*, vol. 21, no. 5, pp. 803–820, 2011.

[24] J. Fu, W.-H. Chen, and Q.-X. Wu, "Chattering-free sliding mode control with unidirectional auxiliary surfaces for miniature helicopters," *International Journal of Intelligent Computing and Cybernetics*, vol. 5, no. 3, pp. 421–438, 2012.

[25] C. Liu, W.-H. Chen, and J. Andrews, "Model predictive control for autonomous helicopters with computational delay," in *Proceedings of the UKACC International Conference on CONTROL 2010*, pp. 656–661, UK, September 2010.

[26] R. Li, M. Chen, Q. Wu, and J. Liu, "Robust adaptive tracking control for unmanned helicopter with constraints," *International Journal of Advanced Robotic Systems*, vol. 14, no. 3, 2017.

Hindawi
Mathematical Problems in Engineering
Volume 2018, Article ID 5147565, 9 pages
https://doi.org/10.1155/2018/5147565

Research Article

Improved Generalized H_2 Filtering for Static Neural Networks with Time-Varying Delay via Free-Matrix-Based Integral Inequality

Hui-Jun Yu,[1,2] Yong He,[3,4] and Min Wu[3,4]

[1]*School of Information Science and Engineering, Central South University, Changsha, Hunan 410083, China*
[2]*School of Electrical and Information Engineering, Hunan University of Technology, Zhuzhou 412007, China*
[3]*School of Automation, China University of Geosciences, Wuhan 430074, China*
[4]*Hubei Key Laboratory of Advanced Control and Intelligent Automation for Complex Systems, Wuhan 430074, China*

Correspondence should be addressed to Yong He; heyong08@cug.edu.cn

Received 18 July 2017; Revised 16 December 2017; Accepted 2 January 2018; Published 30 January 2018

Academic Editor: Renming Yang

This paper focuses on the generalized H_2 filtering of static neural networks with a time-varying delay. The aim of this problem is to design a full-order filter such that the filtering error system is globally asymptotically stable with guaranteed H_2 performance index. By constructing an augmented Lyapunov-Krasovskii functional and applying the free-matrix-based integral inequality to estimate its derivative, an improved delay-dependent condition for the generalized H_2 filtering problem is established in terms of LMIs. Finally, a numerical example is presented to show the effectiveness of the proposed method.

1. Introduction

During the past few decades, neural network (NN), which models the way a biological brain solving problems, has been successfully applied to various engineering fields, such as pattern recognition and vehicle control [1]. Because of its powerful features in learning ability, data processing, function approximation, and adaptiveness, it has gained increasing attention and become a hot topic for scholars [2], while, due to the finite information processing speed, time delays inevitably occur in many NNs and possibly lead to poor performances and complex dynamical behaviors [3]. Thus, extensive researches have been addressed for NNs with time-varying delays.

It is well known that, by choosing the external states of neurons or the internal states of neurons as basic variables, a neural network can be usually classified as a static neural network or a local field neural network [4]. Although these two types of neural network can be equivalent under some assumptions, in many applications, these assumptions cannot always be satisfied. A unified model which combines these two systems together has been constructed recently [5].

Since NNs usually are some highly interconnected networks with a great deal of neurons, it may be very hard or even impossible to acquire all neurons state information completely [6]. However, in some practical applications, to achieve some desired objectives, it is needed to know the neurons state information or estimate it in advance [7]. And the design of filter, which aims to estimate the states of a system via its output measurement, provides a method for the above problems. Consequently, it is of great practical interest to study the filtering problems of NNs with time-varying delays.

For NNs with time-varying delays, the filtering problem was firstly investigated in [8]; both H_∞ and generalized H_2 filter were obtained by solving a set of LMIs. Since then, much effort has been made and many results have been reported on this issue. In [9], the delay-dependent H_2 filter of the Luenberger form was derived for delayed switched Hopfield NNs. Considering that there is only one gain matrix in the Luenberger-type filter to be determined, which may introduce some restrictions to certain extent, [10] further studied the H_2 filtering problem of delayed static NNs based on an Arcak-type filter. Since it contains two gain matrices,

the Arcak-type filter is regarded as an extension of the Luenberger-type filter. In addition, another generalized H_2 full-order filter was designed for a class of delayed stochastic NNs in [11], in which three gain matrices were involved.

On the other hand, with the rapid development of the Lyapunov-Krasovskii functional (LKF) theory, plenty of techniques developed for delay systems have been applied to the filter design of delayed NNs, in order to reduce the conservatism of the derived conditions. The condition with less conservatism means it can provide larger feasible regions such that the filtering error system is globally asymptotically stable with an optimal performance index. It has been well recognized that constructing a suitable LKF and effectively estimating its derivative are two key points to reduce the conservatism. In early years, the simple LKFs combined with the Jensen inequality is considered to be the most popular method for the filtering problems of delayed NNs [8]. In order to consider more information about time delays, some triple integral terms were introduced into the LKF in [10]. In [12], the delay-decomposition idea was used to derive the delay-dependent condition such that the filtering error system is globally asymptotically stable with a guaranteed H_∞ performance. Based on the works of [13], less conservative filtering design results were obtained via the free-weighting matrix approach [14]. And by introducing a additional zero equation into the negative-definite conditions of LKFs' derivative, [15] derived a suitable H_∞ filter for the static NNs with mixed time-varying delays. Very recently, [16] achieved the less conservative generalized H_2 performance state estimation via an augmented LKF, Wirtinger integral inequality, and the auxiliary function-based integral inequality.

Although research on the filtering problem of delayed NNs is in progress, due to its importance, approaches or results on this topic are lacking compared with the stability analysis. For instance, some new proposed techniques, which can effectively reduce the conservatism of the derived stability criteria, have not been applied to the filtering problem of delayed NNs, to mention a few, the free-matrix-based integral inequality [17], the relaxed integral inequality [18], and the generalized free-weighting-matrix approach [19].

Due to this consideration, this paper further studies the filtering problem of NNs with a time-varying delay. The main purpose of this paper is to develop a less conservative approach for the generalized H_2 filter design. To tackle this problem, a more general Arcak-type filter is adopted firstly. Then, by employing the LKF theory and using the free-matrix-based integral inequality, some other bounding inequalities and the free-weighting matrix approach, new delay-dependent condition is derived to guarantee the asymptotic stability of the filtering error system of delayed static NNs with guaranteed H_2 performance index. Finally, a numerical example is provided to illustrate the effectiveness of our proposed method.

Notations. Throughout this paper, the notations are standard. $\mathscr{R}^n$ is the set of all $n \times n$ real matrices; $P > 0$ (≥ 0) means that P is a real symmetric and positive-definite (semi-positive-definite) matrix; diag$\{\cdots\}$ denotes a block-diagonal matrix; I and 0 represent the identity matrix and the zero-matrix, respectively; the symmetric term in a symmetric matrix is denoted by $*$; and Sym$\{X\} = X + X^T$.

2. Preliminaries

Consider the following delayed static NN with external disturbance:

$$\begin{aligned} \dot{x}(t) &= -Ax(t) + f(Wx(t - d(t)) + J) + B_1\omega(t), \\ y(t) &= Cx(t) + Dx(t - d(t)) + B_2\omega(t), \\ z(t) &= Hx(t), \\ x(t) &= \phi(t), \quad t \in [-h, 0], \end{aligned} \tag{1}$$

where $x(t) = [x_1(t), x_2(t), \ldots, x_n(t)]^T \in \mathscr{R}^n$ is the neuron state vector, $f(x(t)) = [f_1(x_1(t)), f_2(x_2(t)), \ldots, f_n(x_n(t))]^T$ is the neural activation functions, $\omega(t)$ is the external disturbance belonging to $L_2[0, \infty)$, $y(t) \in \mathscr{R}^p$ is the network output, $z(t)$ is the linear combination of states to be estimated, $J = [J_1, J_2, \ldots, J_n]^T$ is an exogenous input vector, A, W, B_1, B_2, C, D, and H are known real matrices with appropriate dimensions, $\phi(t)$ is the initial function, and $d(t)$ is time-varying delay satisfying:

$$\begin{aligned} 0 \leq d(t) \leq h, \\ \dot{d}(t) \leq \mu, \end{aligned} \tag{2}$$

where h and μ are known scalars.

Assumption 1. For each $i = 1, 2, \ldots, n$, there exist real scalars $l_i > 0$ such that the continuous activation function $f_i(\cdot)$ satisfies

$$0 \leq \frac{f_i(a) - f_i(b)}{a - b} \leq l_i, \quad a \neq b \in \mathscr{R}. \tag{3}$$

A full-order Arcak-type filter for the delayed static NN (1) is constructed as

$$\begin{aligned} \dot{\hat{x}}(t) &= -A\hat{x}(t) \\ &\quad + f\left(W\hat{x}(t - d(t)) + J + K_1\left(y(t) - \hat{y}(t)\right)\right) \\ &\quad + K_2\left(y(t) - \hat{y}(t)\right), \\ \hat{y}(t) &= C\hat{x}(t) + D\hat{x}(t - d(t)), \\ \hat{z}(t) &= H\hat{x}(t), \\ \hat{x}(t) &= 0, \quad t \in [-h, 0], \end{aligned} \tag{4}$$

where $\hat{x}(t) = [\hat{x}_1(t), \hat{x}_2(t), \ldots, \hat{x}_n(t)]^T \in \mathscr{R}^n$ and matrices K_1, K_2 are the gains of the filter to be determined.

Define the error signals as $e(t) = x(t) - \hat{x}(t)$ and $z_e(t) = z(t) - \hat{z}(t)$. Then, the filtering error system is expressed as follows:

$$\begin{aligned} \dot{e}(t) &= -\left(A + K_2C\right)e(t) - K_2De(t - d(t)) + g(t) \\ &\quad + \left(B_1 - K_2B_2\right)\omega(t), \\ z_e(t) &= He(t), \end{aligned} \tag{5}$$

where $g(t) = f(Wx(t-d(t))+J) - f(W\hat{x}(t-d(t))+J + K_1(y(t)-\hat{y}(t)))$.

This paper aims to present a less conservative approach for the H_2 filtering problem of delayed static NN (1). Toward this problem, the following definition is indispensable.

Definition 2. For given $\gamma > 0$, the H_2 filtering problem is said to be solved if a suitable full-order filter (4) can be found such that

(1) the filtering error system (5) with $\omega(t) = 0$ is globally asymptotically stable;

(2) the H_2 performance $\|z_e(t)\|_\infty \le \gamma\|\omega(t)\|_2$ is guaranteed under zero initial conditions for all nonzero $\omega(t) \in \mathscr{L}_2[0,\infty)$, where $\|z_e(t)\|_\infty = \sup_t \sqrt{z_e^T(t)z_e(t)}$ and $\|\omega(t)\|_2 = \sqrt{\int_0^\infty \omega^T(t)\omega(t)dt}$.

Before proceeding, we present the following lemmas, which will be used in the sequel.

Lemma 3 (free-matrix-based integral inequality [17]). *Let ω be a differentiable signal in $[\alpha,\beta] \to \mathscr{R}^n$; for positive definite matrices $R \in \mathscr{R}^{n\times n}$, $X, Z \in \mathscr{R}^{3n\times 3n}$, and any matrices $Y \in \mathscr{R}^{3n\times 3n}$, $M, N \in \mathscr{R}^{3n\times n}$ satisfying*

$$\begin{bmatrix} X & Y & M \\ * & Z & N \\ * & * & R \end{bmatrix} \ge 0 \tag{6}$$

the following inequality holds:

$$-\int_\beta^\alpha \dot{\omega}^T(s) R\dot{\omega}(s)\,ds \le \varpi^T \widehat{\Omega}\varpi, \tag{7}$$

where

$$\begin{aligned} \widehat{\Omega} &= (\alpha-\beta)\left(X + \frac{1}{3}Z\right) + \mathrm{Sym}\{MG_1 + NG_2\}, \\ G_1 &= [I, -I, O], \\ G_2 &= [-I, -I, 2I], \\ \varpi &= \left[\omega^T(\alpha), \omega^T(\beta), \frac{1}{\alpha-\beta}\int_\beta^\alpha \omega^T(s)\,ds\right]^T. \end{aligned} \tag{8}$$

Lemma 4 (Jensen's inequality [20]). *Let ω be a differentiable signal in $[\alpha,\beta] \to \mathscr{R}^n$; for positive definite matric $R \in \mathscr{R}^n$, the following inequalities hold:*

$$\begin{aligned} &\frac{(\alpha-\beta)^2}{2}\int_\beta^\alpha\int_s^\alpha \omega^T(s) R\omega(s)\,ds\,d\theta \\ &\ge \left(\int_\beta^\alpha\int_s^\alpha \omega(s)\,ds\,d\theta\right)^T R\left(\int_\beta^\alpha\int_s^\alpha \omega(s)\,ds\,d\theta\right). \end{aligned} \tag{9}$$

3. Main Result

In this section, by employing an augmented LKF and using the free-matrix-based integral inequality to estimate its derivative, an improved delay-dependent condition is derived such that the filtering error system (5) is globally asymptotically stable with guaranteed generalized H_2 performance indexes.

Theorem 5. *For given scalars h and μ, the H_2 filtering problem of NN (1) with time-varying delay satisfying (2) is solved with $\gamma_{\min}$ if there exist positive definite matrices $P = \begin{bmatrix} P_1 & P_2 \\ * & P_3 \end{bmatrix} \in \mathscr{R}^{2n}$, $Q_1, Q_2, R, Z \in \mathscr{R}^n$, positive definite diagonal matrices $\Lambda = \mathrm{diag}\{\lambda_1, \lambda_2, \ldots, \lambda_n\} \in \mathscr{R}^n$, symmetric matrices $X_1, X_3, Y_1, Y_3, Z_1, Z_3 \in \mathscr{R}^{3n}$, and any matrices $X_2, Y_2, Z_2 \in \mathscr{R}^{3n}$, $M_1, M_2, N_1, N_2, G_1, G_2 \in \mathscr{R}^{3n\times n}$, $T \in \mathscr{R}^n$, $V_1, V_2 \in \mathscr{R}^{n\times p}$, satisfying the following LMIs:*

$$\begin{bmatrix} X_1 & X_2 & M_1 \\ * & X_3 & M_2 \\ * & * & R \end{bmatrix} \ge 0, \tag{10}$$

$$\begin{bmatrix} Y_1 & Y_2 & N_1 \\ * & Y_3 & N_2 \\ * & * & R \end{bmatrix} \ge 0, \tag{11}$$

$$\begin{bmatrix} Z_1 & Z_2 & G_1 \\ * & Z_3 & G_2 \\ * & * & Z \end{bmatrix} \ge 0, \tag{12}$$

$$\begin{bmatrix} P_1 & P_2 & H^T \\ * & P_3 & O \\ * & * & \gamma^2 I \end{bmatrix} \ge 0, \tag{13}$$

$$\begin{aligned} \Gamma(0) &< 0, \\ \Gamma(h) &< 0, \end{aligned} \tag{14}$$

where

$$\begin{aligned} \Gamma(d(t)) &= \Phi_1(d(t)) + \Phi_2 + \Phi_3(d(t)) + \Phi_4(d(t)) \\ &\quad + \Omega, \\ \Phi_1(d(t)) &= \mathrm{Sym}\left\{\Pi_1^T P \Pi_2\right\}, \\ \Phi_2 &= e_1^T(Q_1+Q_2)e_1 - (1-\mu)e_2^T Q_1 e_2 - e_3^T Q_2 e_3, \\ \Phi_3(d(t)) &= he_7^T Re_7 + d(t)\Pi_3^T\left(X_1 + \frac{1}{3}X_3\right)\Pi_3 + (h \\ &\quad - d(t))\Pi_4^T\left(Y_1 + \frac{1}{3}Y_3\right)\Pi_4 + \mathrm{Sym}\left\{\Pi_3^T M\Pi_5\right. \\ &\quad \left. + \Pi_4^T N\Pi_6\right\}, \\ \Phi_4(d(t)) &= \frac{h^2}{2}e_7^T Ze_7 - 2(e_1-e_4)^T Z(e_1-e_4) \\ &\quad - 2(e_2-e_5)^T Z(e_2-e_5) + h(h-d(t))\Pi_3^T\left(Z_1\right. \\ &\quad \left. + \frac{1}{3}Z_3\right)\Pi_3 + (h-d(t))\,\mathrm{Sym}\left\{\Pi_3^T G\Pi_5\right\}, \end{aligned}$$

$$\begin{aligned}
\Omega &= \mathrm{Sym}\left\{e_6^T\Lambda\left(LWe_2 - e_6\right)\right.\\
&\quad - e_6^T V_1\left(Ce_1 + De_2 + B_2e_8\right) + \left(e_1 + e_7\right)^T\\
&\quad \cdot T\left(e_7 + Ae_1 - e_6 - B_1e_8\right) + \left(e_1 + e_7\right)^T\\
&\quad \left.\cdot V_2\left(Ce_1 + De_2 + B_2e_8\right)\right\},\\
\Pi_1 &= \left[e_1^T, d(t)\,e_4^T + (h - d(t))\,e_5^T\right]^T,\\
\Pi_2 &= \left[e_7^T, e_1^T - e_3^T\right]^T,\\
\Pi_3 &= \left[e_1^T, e_2^T, e_4^T\right]^T,\\
\Pi_4 &= \left[e_2^T, e_3^T, e_5^T\right]^T,\\
\Pi_5 &= \left[e_1^T - e_2^T, -e_1^T - e_2^T + 2e_4^T\right]^T,\\
\Pi_6 &= \left[e_2^T - e_3^T, -e_2^T - e_3^T + 2e_5^T\right]^T,\\
M &= \left[M_1, M_2\right],\\
N &= \left[N_1, N_2\right],\\
G &= \left[G_1, G_2\right],\\
e_i &= \left[0_{n\times(i-1)n}, I_n, 0_{n\times(7-i)n}, 0_{n\times p}\right], \quad (i = 1, 2, \ldots, 7),\\
e_8 &= \left[0_{p\times 7n}, I_p\right],\\
L &= \mathrm{diag}\left\{l_1, l_2, \ldots, l_n\right\},\\
\xi(t) &= \left[e^T(t), e^T(t - d(t)), e^T(t - h), \int_{t-d(t)}^{t}\frac{e^T(s)}{d(t)}ds,\right.\\
&\quad \left.\int_{t-h}^{t-d(t)}\frac{e^T(s)}{h - d(t)}ds, g^T(t), \dot{e}^T(t), \omega^T(t)\right]^T
\end{aligned} \tag{15}$$

and the gain matrices K_1, K_2 of the filter of (4) can be designed as

$$\begin{aligned}
K_1 &= (\Lambda L)^{-1} V_1,\\
K_2 &= T^{-1}V_2.
\end{aligned} \tag{16}$$

Proof. Let us construct a new augmented LKF candidate as

$$V\left(e_t\right) = \sum_{i=1}^{4} V_i\left(e_t\right), \tag{17}$$

where

$$\begin{aligned}
V_1\left(e_t\right) &= \begin{bmatrix} x(t) \\ \int_{t-h}^{t} e(s)\,ds \end{bmatrix}^T P \begin{bmatrix} x(t) \\ \int_{t-h}^{t} e(s)\,ds \end{bmatrix},\\
V_2\left(e_t\right) &= \int_{t-d(t)}^{t} e^T(s)\,Q_1 e(s)\,ds\\
&\quad + \int_{t-h}^{t} e^T(s)\,Q_2 e(s)\,ds,\\
V_3\left(e_t\right) &= \int_{-h}^{0}\int_{t+\theta}^{t} \dot{e}^T(s)\,R\dot{e}(s)\,ds\,d\theta,\\
V_4\left(e_t\right) &= \int_{-h}^{0}\int_{\theta}^{t}\int_{t+u}^{t} \dot{e}^T(s)\,Z\dot{e}(s)\,ds\,du\,d\theta.
\end{aligned} \tag{18}$$

Taking the derivative of $V_1(e_t)$ along the filtering error system (5) yields

$$\begin{aligned}
\dot{V}_1\left(e_t\right) &= 2\begin{bmatrix} x(t) \\ \int_{t-h}^{t} e(s)\,ds \end{bmatrix}^T P \begin{bmatrix} \dot{x}(t) \\ e(t) - e(t-h) \end{bmatrix}\\
&= \xi^T(t)\,\Phi_1(d(t))\,\xi(t).
\end{aligned} \tag{19}$$

By the time derivative of $V_2(e_t)$, we get

$$\begin{aligned}
\dot{V}_2\left(e_t\right) &= e^T(t)\left(Q_1 + Q_2\right)e(t)\\
&\quad - \left(1 - \dot{d}(t)\right)e^T(t - d(t))\,Q_1 e(t - d(t))\\
&\quad - e^T(t - h)\,Q_2 e(t - h) = \xi^T(t)\,\Phi_2\xi(t).
\end{aligned} \tag{20}$$

Calculating the derivative of $V_3(e_t)$, we have

$$\begin{aligned}
\dot{V}_3\left(e_t\right) &= h\dot{e}^T(t)\,R\dot{e}(t) - \int_{t-d(t)}^{t}\dot{e}^T(s)\,R\dot{e}(s)\,ds\\
&\quad - \int_{t-h}^{t-d(t)}\dot{e}^T(s)\,R\dot{e}(s)\,ds.
\end{aligned} \tag{21}$$

Then by applying Lemma 3 to estimate the above R-dependent integral term, if LMIs (10) and (11) hold, one has

$$\begin{aligned}
&-\int_{t-d(t)}^{t}\dot{e}^T(s)\,R\dot{e}(s)\,ds\\
&\quad \le d(t)\,\chi_1^T\left(X_1 + \frac{1}{3}X_3\right)\chi_1\\
&\qquad + \mathrm{Sym}\left\{\chi_1^T M_1\chi_2 + \chi_1^T M_2\chi_3\right\},
\end{aligned} \tag{22}$$

$$\begin{aligned}
&-\int_{t-h}^{t-d(t)}\dot{e}^T(s)\,R\dot{e}(s)\,ds\\
&\quad \le (h - d(t))\,\chi_4^T\left(Y_1 + \frac{1}{3}Y_3\right)\chi_4\\
&\qquad + \mathrm{Sym}\left\{\chi_4^T N_1\chi_5 + \chi_4^T N_2\chi_6\right\},
\end{aligned} \tag{23}$$

where

$$\begin{aligned}
\chi_1 &= \left[e^T(t), e^T(t - d(t)), \frac{1}{d(t)}\int_{t-d(t)}^{t} e^T(s)\,ds\right]^T,\\
\chi_2 &= e(t) - e(t - d(t)),
\end{aligned}$$

$$\chi_3 = -e(t) - e(t-d(t)) + \frac{2}{d(t)}\int_{t-d(t)}^{t} e(s)\,ds,$$

$$\chi_4 = \left[e^T(t-d(t)), e^T(t-h), \frac{1}{h-d(t)} \cdot \int_{t-h}^{t-d(t)} e^T(s)\,ds\right]^T,$$

$$\chi_5 = e(t-d(t)) - e(t-h),$$

$$\chi_6 = -e(t-d(t)) - e(t-h) + \frac{2}{h-d(t)} \cdot \int_{t-h}^{t-d(t)} e(s)\,ds. \tag{24}$$

Combining (21) with (23), it is clear that

$$\dot{V}_3(e_t) \le \xi^T(t)\,\Phi_3(d(t))\,\xi(t). \tag{25}$$

Finally, the derivative of $V_4(e_t)$ can be obtained as

$$\begin{aligned}\dot{V}_4(e_t) &= \frac{h^2}{2}\dot{e}^T(t)\,Z\dot{e}(t) - \int_{t-h}^{t}\int_{\theta}^{t}\dot{e}^T(s)\,Z\dot{e}(s)\,ds\,d\theta \\ &= \frac{h^2}{2}\dot{e}^T(t)\,Z\dot{e}(t) \\ &\quad - \int_{t-d(t)}^{t}\int_{\theta}^{t}\dot{e}^T(s)\,Z\dot{e}(s)\,ds\,d\theta \\ &\quad - \int_{t-h}^{t-d(t)}\int_{\theta}^{t-d(t)}\dot{e}^T(s)\,Z\dot{e}(s)\,ds\,d\theta \\ &\quad - (h-d(t))\int_{t-d(t)}^{t}\dot{e}^T(s)\,Z\dot{e}(s)\,ds.\end{aligned} \tag{26}$$

For the first double integral term in $\dot{V}_4(e_t)$, we can do the following treatment based on Lemma 4:

$$\begin{aligned}&-\int_{t-d(t)}^{t}\int_{\theta}^{t}\dot{e}^T(s)\,Z\dot{e}(s)\,ds\,d\theta \\ &\le -\frac{2}{d^2(t)}\left(\int_{t-d(t)}^{t}\int_{\theta}^{t}\dot{e}(s)\,ds\,d\theta\right)^T \\ &\quad\cdot Z\left(\int_{t-d(t)}^{t}\int_{\theta}^{t}\dot{e}(s)\,ds\,d\theta\right) \\ &= -\frac{2}{d^2(t)}\left(d(t)\,e(t) - \int_{t-d(t)}^{t}e(s)\,ds\right)^T \\ &\quad\cdot Z\left(d(t)\,e(t) - \int_{t-d(t)}^{t}e(s)\,ds\right) \\ &= -2\left(e(t) - \int_{t-d(t)}^{t}\frac{e(s)}{d(t)}ds\right)^T \\ &\quad\cdot Z\left(e(t) - \int_{t-d(t)}^{t}\frac{e(s)}{d(t)}ds\right).\end{aligned} \tag{27}$$

Similarly, the estimation of the second integral term can be done as

$$\begin{aligned}&-\int_{t-h}^{t-d(t)}\int_{\theta}^{t-d(t)}\dot{e}^T(s)\,Z\dot{e}(s)\,ds\,d\theta \\ &\le -\frac{2}{(h-d(t))^2}\left(\int_{t-h}^{t-d(t)}\int_{\theta}^{t-d(t)}\dot{e}(s)\,ds\,d\theta\right)^T \\ &\quad\cdot Z\left(\int_{t-h}^{t-d(t)}\int_{\theta}^{t-d(t)}\dot{e}(s)\,ds\,d\theta\right) \\ &= -2\left(e(t-d(t)) - \int_{t-h}^{t-d(t)}\frac{e(s)}{h-d(t)}ds\right)^T \\ &\quad\cdot Z\left(e(t-d(t)) - \int_{t-h}^{t-d(t)}\frac{e(s)}{h-d(t)}ds\right).\end{aligned} \tag{28}$$

And by utilizing Lemma 3, if LMI (12) holds, we obtain

$$\begin{aligned}&-(h-d(t))\int_{t-d(t)}^{t}\dot{e}^T(s)\,Z\dot{e}(s)\,ds \le (h-d(t)) \\ &\quad\cdot\left(h\chi_1^T\left(Z_1 + \frac{1}{3}Z_3\right)\chi_1\right. \\ &\quad\left.+ \mathrm{Sym}\left\{\chi_1^T G_1\chi_2 + \chi_1^T G_2\chi_3\right\}\right).\end{aligned} \tag{29}$$

From (26) to (29), we get

$$\dot{V}_4(e_t) \le \xi^T(t)\,\Phi_4(d(t))\,\xi(t). \tag{30}$$

Then, taking assumption of the activation function (3) into account yields

$$\begin{aligned}0 \le 2g^T(t)\,\Lambda\,&[L(We(t-d(t)) - K_1Ce(t) \\ &- K_1De(t-d(t)) - K_1B_2\omega(t)) - g(t)],\end{aligned} \tag{31}$$

where

$$\begin{aligned}V_1 &= \Lambda LK_1 \\ &\Longrightarrow 0 \\ &\le 2e_6^T\Lambda(LWe_2 - e_6) - 2e_6^T V_1(Ce_1 + De_2 + B_2e_8).\end{aligned} \tag{32}$$

Based on the filtering error system (5), for any appropriately dimensioned matrix T, the following equation holds:

$$\begin{aligned}0 = 2(e(t) + \dot{e}(t))^T T\,&[\dot{e}(t) + (A + K_2C)e(t) \\ &+ K_2De(t-d(t)) - g(t) - (B_1 - K_2B_2)\omega(t)],\end{aligned} \tag{33}$$

where

$$\begin{aligned}V_2 &= TK_2 \\ &\Longrightarrow 0 \\ &= 2(e_1 + e_7)^T T(e_7 + Ae_1 - e_6 - B_1e_8) \\ &\quad + 2(e_1 + e_7)^T V_2(Ce_1 + De_2 + B_2e_8).\end{aligned} \tag{34}$$

Combining (19), (20), (21), (22), (23), (25), (26), (27), (28), (29), (30), (32), and (34), one can easily yield

$$\dot{V}\left(e_t\right) \le \xi^T(t)\,\Gamma\left(d(t)\right)\xi(t). \tag{35}$$

If $\Gamma(d(t)) < 0$, then $\dot{V}(e_t) < 0$. Thus, if $\Gamma(0) < 0$ and $\Gamma(h) < 0$ are satisfied, then $\dot{V}(e_t) \le -\epsilon\|e(t)\|^2$ for a sufficient small scalar $\epsilon > 0$, which implies the filtering error system (5) with $\omega(t) = 0$, is asymptotically stable.

Considering the definition of H_2 performance, we define

$$J(t) = V\left(e_t\right) - \int_0^t \omega^T(s)\,\omega(s)\,ds. \tag{36}$$

Then, under the zero-initial conditions $V(e_t)|_{t=0} = 0$ and $V(e_t) > 0$ for $t > 0$, the following inequality is given:

$$\begin{aligned} J(t) &= V\left(e_t\right) - V\left(e_t\right)\big|_{t=0} - \int_0^t \omega^T(s)\,\omega(s)\,ds \\ &= \int_0^t \left[\dot{V}\left(e(s)\right) - \omega^T(s)\,\omega(s)\right]ds < 0. \end{aligned} \tag{37}$$

That is,

$$V\left(e_t\right) < \int_0^t \omega^T(s)\,\omega(s)\,ds. \tag{38}$$

In addition, it follows that LMI (13) and Schur complement that

$$\begin{bmatrix} H^TH & O \\ * & O \end{bmatrix} \le \gamma^2 \begin{bmatrix} P_1 & P_2 \\ * & P_3 \end{bmatrix}. \tag{39}$$

Then, the following holds:

$$\begin{aligned} z_e^T(t)\,z_e(t) &= e^T(t)\,H^THe(t) \\ &= \begin{bmatrix} x(t) \\ \int_{t-h}^t e(s)\,ds \end{bmatrix}^T \begin{bmatrix} H^TH & O \\ * & O \end{bmatrix} \begin{bmatrix} x(t) \\ \int_{t-h}^t e(s)\,ds \end{bmatrix} \\ &\le \gamma^2 \begin{bmatrix} x(t) \\ \int_{t-h}^t e(s)\,ds \end{bmatrix}^T \begin{bmatrix} P_1 & P_2 \\ * & P_3 \end{bmatrix} \begin{bmatrix} x(t) \\ \int_{t-h}^t e(s)\,ds \end{bmatrix} \\ &= \gamma^2 V_1\left(e_t\right) \le \gamma^2 V\left(e_t\right) \le \gamma^2 \int_0^t \omega^T(s)\,\omega(s)\,ds \\ &\le \gamma^2 \int_0^\infty \omega^T(s)\,\omega(s)\,ds. \end{aligned} \tag{40}$$

Taking the supremum over $t > 0$, one has $\|z_e(t)\|_\infty^2 \le \gamma\|\omega(t)\|_2^2$, which means $\|z_e(t)\|_\infty \le \gamma\|\omega(t)\|_2$. Therefore, when (10)–(14) hold, the generalized H_2 filtering problem of NN (1) with time-varying delay satisfying (2) is solved with $\gamma_{\min}$. This completes the proof. □

Remark 6. The generalized H_2 design of a type of static NN with a time-varying delay is solved in Theorem 5. Different from [8–10, 12–15], we solve the filtering problem based on an Arcak-type filter, in which there are two gain matrices to be determined. Compared with the widely used Luenberger-type filter, it contains an additional gain matrix K_1 included in the activation function. So, it can be expected to lead a better generalized H_2 performance. And if we set $K_1 = 0$, the Arcak-type filter is then reduced to the Luenberger-type filter.

Remark 7. The triple integral term is introduced into the LKF in this paper. When bounding its derivative, the derived double integral term $-\int_{t-h}^t \int_\theta^t \dot{e}^T(s)Z\dot{e}(s)ds\,d\theta$ is divided into three parts, two double integral terms and a single integral term. By using the double Jensen inequality to estimate the double integral terms and using the free-matrix-based integral inequality to estimate the single integral term, the derivation of the triple term is accomplished without ignoring any terms. It should be pointed out that this technique is more effective than the ones used in [10], in which the derived double integral term $-\int_{t-h}^t \int_\theta^t \dot{e}^T(s)Z\dot{e}(s)ds\,d\theta$ is estimated in its entirety.

Remark 8. To reduce the conservatism of the derived conditions, Wirtinger integral inequality was used to estimate single integral terms in [16], while in the presented study, the free-matrix-based integral inequality is employed. The use of the free-matrix-based integral inequality brings several advantages for Theorem 5. On the one hand, by introducing some free matrices, it gives more degrees of freedom to the derived condition. On the other hand, it has been proved in [17] that the free-matrix-based integral inequality contains Wirtinger integral inequality as a special case. That means, it can provide a tighter bound than Wirtinger integral inequality. And if the same LKF is chosen, our designed filter will be better than the one designed in [16].

Remark 9. There is some room for further improvement of our proposed method:

(i) Notice that when the free-matrix-based integral inequality is employed to improve the proposed condition, the number of decision variables is increased, which further increases the computation complexity of the condition. It has been pointed out in [3] that the calculation complexity is also an important consideration during the application of the proposed LMI-based condition to physical systems. Thus, the results considering both the conservatism and the computation complexity need more investigation.

(ii) Recently, some new approaches have been developed for the stability analysis of delayed neural networks, which can be applied into the generalized H_2 filtering problem of neural networks, such as the delay-decomposition approach [21] and the free-matrix-based double integral inequality [22].

Notice that, in many applications, the derivative bound of the time delay is unknown. By setting $Q_1 = 0$, we can easily derive the delay-dependent but delay derivative-independent

condition of the generalized H_2 filtering problem of neural network (1) based on Theorem 5.

Theorem 10. *For given scalars h, the H_2 filtering problem of NN (1) with time-varying delay satisfying $0 \le d(t) \le h$ is solved with $\gamma_{\min}$ if there exist positive definite matrices $P = \begin{bmatrix} P_1 & P_2 \\ * & P_3 \end{bmatrix} \in \mathcal{R}^{2n}$, $Q_2, R, Z \in \mathcal{R}^n$, positive definite diagonal matrices $\Lambda = \mathrm{diag}\{\lambda_1, \lambda_2, \ldots, \lambda_n\} \in \mathcal{R}^n$, symmetric matrices $X_1, X_3, Y_1, Y_3, Z_1, Z_3 \in \mathcal{R}^{3n}$, and any matrices $X_2, Y_2, Z_2 \in \mathcal{R}^{3n}$, $M_1, M_2, N_1, N_2, G_1, G_2 \in \mathcal{R}^{3n\times n}$, $T \in \mathcal{R}^n$, $V_1, V_2 \in \mathcal{R}^{n\times p}$, satisfying LMIs (10)–(14).*

4. Numerical Examples

In this section, we provide a well-used numerical example to demonstrate the effectiveness of the proposed approach.

Example 1. Consider the delayed static NN (1) with the following parameters:

$$A = \begin{bmatrix} 0.96 & 0 & 0 \\ 0 & 1.22 & 0 \\ 0 & 0 & 0.78 \end{bmatrix},$$

$$W = \begin{bmatrix} -0.32 & 0.75 & -1.42 \\ 1.21 & 0.41 & -0.50 \\ 0.42 & 0.82 & -1.06 \end{bmatrix},$$

$$B_1 = \begin{bmatrix} 0.2 \\ 0.3 \\ 0.5 \end{bmatrix},$$

$$H = \begin{bmatrix} 0.8 & 0 & 0.5 \\ 1 & 0 & 1 \\ 0 & -1 & 1 \end{bmatrix}, \quad (41)$$

$$C = \begin{bmatrix} 1 & 0.5 & 0 \\ 0 & -0.5 & 0.6 \end{bmatrix},$$

$$D = \begin{bmatrix} 0 & -1.2 & 0.2 \\ 0 & 0 & 0.5 \end{bmatrix},$$

$$B_2 = \begin{bmatrix} 0.4 \\ -0.3 \end{bmatrix}.$$

This example has been studied in [10, 16], and we take these literatures for comparison study. To verify the advantages of our proposed approach, we calculate the optimal H_2 performance bounds index $\gamma_{\min}$ for various h, μ, and L such that filtering error system (5) is globally asymptotically stable with generalized H_2 performance.

Firstly, let $L = \mathrm{diag}\{l_1, l_2, \ldots, l_n\} = I$; for given h and μ, the optimal generalized H_2 performance index $\gamma_{\min}$ derived by Theorem 5 and the ones reported in [10, 16] are given in Table 1, where (α, β) represents $h = \alpha$, $\mu = \beta$ and "infeasible" means that no feasible solution can be found in the corresponding criteria.

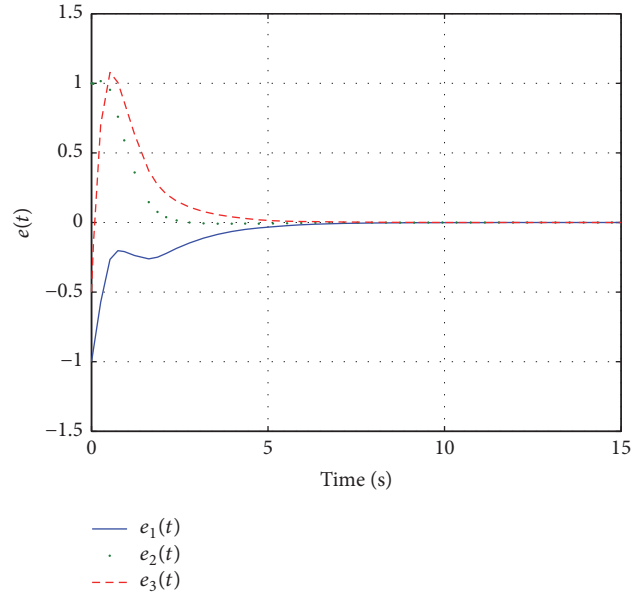

Figure 1: State response of the error $e(t)$.

It is clearly shown from Table 1 that, compared with [10, 16], much better generalized H_2 performance is achieved by Theorem 5 proposed in this paper. It should be noticed that, in this paper, we choose the same filter as [10, 16]; thus, the better H_2 performance effectively illustrates the superiority of our proposed approaches, which is mainly based on the free-matrix-based integral inequality.

Then let $f(x) = 1.57\tanh(x)$, $d(t) = 0.3\sin(1.5t) + 1.2$, and $w(t) = \sin(t)e^{-5t}$, for $h = 1.5$, $\mu = 0.3$; by solving the LMIs in Theorem 5, the gain matrices of our designed filter (4) are obtained as

$$K_1 = \begin{bmatrix} 1.0591 & 1.2990 \\ 0.1519 & 0.2687 \\ 2.4379 & 3.3466 \end{bmatrix},$$

$$K_2 = \begin{bmatrix} 0.0944 & -0.6005 \\ 0.3315 & -0.5100 \\ 2.1756 & 1.2563 \end{bmatrix}. \quad (42)$$

with the optimal generalized H_2 performance index $\gamma = 0.0505$. Figure 1 shows the state responses of error system (5) under initial condition $e(0) = [-1, 1, -0.5]^T$. The resulting responses obviously demonstrate the asymptotic stability of the simulated error system.

In addition, the optimal generalized H_2 performance index $\gamma_{\min}$ for $h = 0.5$, $\mu = 0.7$ and different L is listed in Table 2, from which one can see that Theorem 5 in this paper outperforms the ones in [10, 16].

Moreover, the optimal generalized H_2 performance index $\gamma_{\min}$ derived by Theorem 10 for $h = 0.8$, unknown μ, and different L is listed in Table 3.

Table 1: Optimal generalized H_2 performance index $\gamma_{\min}$ for $L = I$ and different (h, μ).

(h, μ)	$(1, 0.4)$	$(1.5, 0.3)$	$(3, 0.8)$	$(5, 1.2)$	$(6, 1.5)$
Theorem 1 [10]	0.7981	Infeasible	Infeasible	Infeasible	Infeasible
Theorem 2 [16]	1.34×10^{-4}	1.2763	Infeasible	Infeasible	Infeasible
Theorem 5	1.33×10^{-4}	0.0505	0.6639	0.9137	1.9523

Table 2: Optimal generalized H_2 performance index $\gamma_{\min}$ for $h = 0.5$, $\mu = 0.7$, and different L.

L	$1.6I$	$1.8I$	$2.5I$	$3.4I$
Theorem 1 [10]	3.3728	Infeasible	Infeasible	Infeasible
Theorem 2 [16]	0.5983	1.5563	Infeasible	Infeasible
Theorem 5	0.2765	0.4015	0.6896	4.7676

Table 3: Optimal generalized H_2 performance index $\gamma_{\min}$ for $h = 0.5$, unknown μ, and different L.

L	$1.6I$	$1.8I$	$2.5I$	$2.91I$
Theorem 10	0.5156	0.5868	1.0891	5.1122

5. Conclusion

In this paper, the generalized H_2 filtering problem of static NNs with a time-varying delay has been investigated. First, an Arcak-type filter has been constructed. Then, based on an augmented LKF, the free-matrix-based integral inequality, the free-weighting matrix approach, and Jensen inequality, a suitable delay-dependent condition expressed in terms of LMIs has been derived such that the filtering error system of the considered static NNs is globally asymptotically stable with guaranteed H_2 performance index. Moreover, by solving some coupled LMIs, the optimal performance index and the gain matrices of the designed H_2 filter have been obtained. The effectiveness and advantages of the proposed method have been demonstrated by an illustrative example finally.

Conflicts of Interest

The authors declare that there are no conflicts of interest regarding this paper.

References

[1] L. O. Chua and L. Yang, "Cellular Neural Networks: Applications," *IEEE Transactions on Circuits and Systems II: Express Briefs*, vol. 35, no. 10, pp. 1273–1290, 1988.

[2] X.-M. Zhang, Q.-L. Han, and X. Yu, "Survey on Recent Advances in Networked Control Systems," *IEEE Transactions on Industrial Informatics*, vol. 12, no. 5, pp. 1740–1752, 2016.

[3] C.-K. Zhang, Y. He, L. Jiang, and M. Wu, "Stability analysis for delayed neural networks considering both conservativeness and complexity," *IEEE Transactions on Neural Networks and Learning Systems*, vol. 27, no. 7, pp. 1486–1501, 2016.

[4] H.-B. Zeng, Y. He, P. Shi, M. Wu, and S.-P. Xiao, "Dissipativity analysis of neural networks with time-varying delays," *Neurocomputing*, vol. 168, pp. 741–746, 2015.

[5] C.-K. Zhang, Y. He, L. Jiang, Q. H. Wu, and M. Wu, "Delay-dependent stability criteria for generalized neural networks with two delay components," *IEEE Transactions on Neural Networks and Learning Systems*, vol. 25, no. 7, pp. 1263–1276, 2014.

[6] Y. He, Q. G. Wang, and C. Lin, "An improved H8 filter design for systems with time-varying interval delay," *IEEE Trans. Circuits Syst. II*, vol. 53, p. 1235, 2006.

[7] Y. He, G. P. Liu, D. Rees, and M. Wu, "Improved Hoo filtering for systems with a time-varying delay," *Circuits, Systems and Signal Processing*, vol. 29, no. 3, pp. 377–389, 2010.

[8] H. Huang and G. Feng, "Delay-dependent Hoo and generalized H2 filtering for delayed neural networks," *IEEE Transactions on Circuits and Systems I: Regular Papers*, vol. 56, no. 4, pp. 846–857, 2009.

[9] C. K. Ahn and M. K. Song, "L2-Loo filtering for time-delayed switched hopfield neural networks," *International Journal of Innovative Computing, Information and Control*, vol. 7, no. 4, pp. 1831–1844, 2011.

[10] D. Hu, H. Huang, and T. Huang, "Design of Arcak-type generalized H2 filter for delayed static neural networks," *Circuits, Systems and Signal Processing*, vol. 33, no. 11, pp. 3635–3648, 2014.

[11] M. Hua, H. Tan, and J. Chen, "Delay-dependent H^{∞} and generalized H^2 filtering for stochastic neural networks with time-varying delay and noise disturbance," *Neural Computing and Applications*, vol. 25, no. 3-4, pp. 613–624, 2014.

[12] Y. J. Li and Y. N. Liang, "Delay-dependent Hoo filtering for neural networks with time delay," *Applied Mechanics and Materials*, vol. 511-512, pp. 875–879, 2014.

[13] Y. He, G. P. Liu, D. Rees, and M. Wu, "Stability analysis for neural networks with time-varying interval delay," *IEEE Transactions on Neural Networks and Learning Systems*, vol. 18, no. 6, pp. 1850–1854, 2007.

[14] Y. Li, J. Li, and M. Hua, "New results of H8 filtering for neural network with time-varying delay," *Int. J. Innov. Comput. Inf. Control*, vol. 10, pp. 2309–2323, 2014.

[15] G. Liu, S. Zhou, X. Luo, and K. Zhang, "New filter design for static neural networks with mixed time-varying delays," *Lecture Notes in Computer Science (including subseries Lecture Notes in Artificial Intelligence and Lecture Notes in Bioinformatics): Preface*, vol. 9772, pp. 117–129, 2016.

[16] Y. Shu, X.-G. Liu, Y. Liu, and J. H. Park, "Improved Results on Guaranteed Generalized H2 Performance State Estimation for Delayed Static Neural Networks," *Circuits, Systems and Signal Processing*, vol. 36, no. 8, pp. 3114–3142, 2017.

[17] H.-B. Zeng, Y. He, M. Wu, and J. She, "Free-matrix-based integral inequality for stability analysis of systems with time-varying delay," *Institute of Electrical and Electronics Engineers Transactions on Automatic Control*, vol. 60, no. 10, pp. 2768–2772, 2015.

[18] C.-K. Zhang, Y. He, L. Jiang, M. Wu, and H.-B. Zeng, "Stability analysis of systems with time-varying delay via relaxed integral inequalities," *Systems & Control Letters*, vol. 92, pp. 52–61, 2016.

[19] C.-K. Zhang, Y. He, L. Jiang, W.-J. Lin, and M. Wu, "Delay-dependent stability analysis of neural networks with time-varying delay: a generalized free-weighting-matrix approach," *Applied Mathematics and Computation*, vol. 294, pp. 102–120, 2017.

[20] J. Sun, G. P. Liu, J. Chen, and D. Rees, "Improved delay-range-dependent stability criteria for linear systems with time-varying delays," *Automatica*, vol. 46, no. 2, pp. 466–470, 2010.

[21] C. Ge, C. Hua, and X. Guan, "New delay-dependent stability criteria for neural networks with time-varying delay using delay-decomposition approach," *IEEE Transactions on Neural Networks and Learning Systems*, vol. 25, no. 7, pp. 1378–1383, 2014.

[22] C. Hua, S. Wu, X. Yang, and X. Guan, "Stability analysis of time-delay systems via free-matrix-based double integral inequality," *International Journal of Systems Science*, vol. 48, no. 2, pp. 257–263, 2017.

Hindawi
Mathematical Problems in Engineering
Volume 2018, Article ID 9572927, 14 pages
https://doi.org/10.1155/2018/9572927

Research Article

Observer Design for Delayed Markovian Jump Systems with Output State Saturation

Guoliang Wang and Bo Feng

School of Information and Control Engineering, Liaoning Shihua University, Fushun, Liaoning 113001, China

Correspondence should be addressed to Guoliang Wang; gliangwang@aliyun.com

Received 16 June 2017; Accepted 17 December 2017; Published 22 January 2018

Academic Editor: Renming Yang

This paper considers the observer design problem of continuous-time delayed Markovian jump systems with output state saturation. Different from the traditionally observer-based saturation control methods, a kind of system output state saturation with a partially delay-dependent property is proposed, where both nondelay and delay states exist at the same time but happen asynchronously. By exploiting the Bernoulli variable, the probability distributions of such two states are described and considered in the observer design. Based on an improved equality applied to deal with saturation terms, sufficient conditions for the designed observer with three kinds of output saturations are all provided with LMI forms. Finally, a numerical example is given to indicate the effectiveness of the obtained results.

1. Introduction

As we know, Markovian jump system (MJS) is a special kind of stochastic hybrid dynamical systems. Because of two kinds of mechanisms contained, it is very suitable to model such actual systems whose structures or parameters change [1, 2]. Over the past years, many research topics on MJSs have been extensively studied, like stability analysis [3–6], stabilization [7–11], robust control [12–15], adaptive control [16–19], H_∞ filtering and control [20, 21], state estimation [22–25], synchronization [26–30], and so on.

On the other hand, saturation problem is commonly encountered in many physical systems. It is mainly because the transmitted signal is usually affected by environmental factors, physical factors, and even technical factors. When signal occurs with saturation, the system performance will be reduced. Therefore, the effect of saturation is necessarily studied, as in [31–35]. By investigating the above results, it is found that they mainly focused on the estimate of domain of attraction, in which an equivalent description of saturation actuator is necessary. However, the introduction of this transformation will make the computation complexity very large, especially for an MJS with N operation modes. Recently, one inequality was introduced in [36] and applied to deal with saturation. In the modern control theory, it is obvious that the state feedback control has advantages in solving the problems of system stability, pole placement, stabilization, and optimal control. However, system state usually cannot be measured directly, or the measurement is limited by objective conditions. In this case, it is not easy to achieve the object by state feedback control. The better way is to make full use of system output. When output is saturated, some results were presented in [37, 38]. By investigating these references, it is found that there are still many problems to be considered. For example, there is no time delay in the saturated output, while time delay is usually associated with most system states and could lead to unstable system. Thus, it is necessary to consider them together. To our best knowledge, very few results are available to study the above problems. All observations motivate current research.

In this paper, the observer design problem of continuous-time delayed Markovian jump systems with output state saturation is studied, where the output state saturation is partially delay-dependent. The main contributions of this paper are generalized as follows: (1) A kind of observer based on partially delay-dependent output is proposed. Here, both nondelay and delay states are contained in output saturation simultaneously, but their occurrences are asynchronous. (2)

The probability distributions of such two states are embodied by the Bernoulli variable and fully considered in the observe design. (3) Sufficient conditions of the designed observer are obtained by applying an improved inequality to deal with the saturation terms. In order to make the computation solved easily and directly, the existence conditions are presented within LMI framework by introducing some additional variables and inequalities. (4) Based on the proposed methods and techniques, another two kinds of observers based on different output saturations are proposed, whose conditions are all LMIs.

Notation 1. $\mathbb{R}^n$ denotes the n-dimensional Euclidean space; $\mathbb{R}^{q\times n}$ is the set of all $q \times n$ real matrices. $\|\cdot\|$ refers to the Euclidean vector norm or spectral matrix norm. Ω is the sample space, $\mathscr{F}$ is the σ-algebra of subsets of the sample space, and $\mathbb{P}$ is the probability measure on $\mathscr{F}$. In symmetric block matrices, we use "$*$" as an ellipsis for the terms induced by symmetry, diag$\{\cdots\}$ for a block-diagonal matrix, and $(M)^\star \triangleq M + M^T$.

2. Problem Formulation

Consider the following continuous-time delayed Markovian jump systems with output state saturation:

$$\begin{aligned}\dot{x}(t) &= A(r_t)\,x(t),\\ y(t) &= C(r_t)\,\mathrm{sat}\left[\alpha(t)\,x(t) + (1-\alpha(t))\,x(t-d)\right],\\ x(t) &= \phi(t), \quad -d \le t \le 0,\end{aligned} \tag{1}$$

where $x(t) \in \mathbb{R}^n$ is the state vector, $y(t) \in \mathbb{R}^q$ is the output, and $\phi(t) \in \mathbb{R}^n$ is the initial condition. Matrices $A(r_t)$ and $C(r_t)$ are known matrices of compatible dimensions. $\{r_t,\ t \ge 0\}$ is a continuous-time Markov process taking values in a finite set $\mathbb{S} = \{1, 2, \ldots, N\}$ with transition rate matrix (TRM) $\Pi \triangleq (\pi_{ij}) \in \mathbb{R}^{N\times N}$ given by

$$\Pr\{r_{t+\Delta t} = j \mid r_t = i\} = \begin{cases}\pi_{ij}\Delta t + o(\Delta t), & i \ne j\\ 1 + \pi_{ii}\Delta t + o(\Delta t), & i = j,\end{cases} \tag{2}$$

where $\Delta t > 0$, $\pi_{ij} \ge 0$, if $i \ne j$, and $\pi_{ii} = -\sum_{j\ne i}\pi_{ij}$ for all $i, j \in \mathbb{S}$. Time delay d satisfies $d > 0$, and $\alpha(t)$ is the Bernoulli stochastic variable and defined as

$$\alpha(t) = \begin{cases}1, & \text{if } x(t) \text{ is available}\\ 0, & \text{if } x(t-d) \text{ is available.}\end{cases} \tag{3}$$

It is satisfied as

$$\begin{aligned}\Pr\{\alpha(t) = 1\} &= \mathscr{E}\{\alpha(t)\} = \alpha,\\ \Pr\{\alpha(t) = 0\} &= 1 - \alpha.\end{aligned} \tag{4}$$

Function sat$(\cdot)$: $\mathbb{R}^n \to \mathbb{R}^n$ is the standard saturation function and defined as

$$\mathrm{sat}(u_i) = \begin{cases}\mu_i, & u_i > \mu_i\\ u_i, & -\mu_i \le u_i \le \mu_i\\ -\mu_i, & u_i < -\mu_i,\end{cases} \quad i \in 1, 2, \ldots, n, \tag{5}$$

where

$$\begin{aligned}\mathrm{sat}(u) &= \left[\mathrm{sat}(u_1) \quad \cdots \quad \mathrm{sat}(u_n)\right]^T,\\ \mu &= \left[\mu_1 \quad \cdots \quad \mu_n\right]^T.\end{aligned} \tag{6}$$

Remark 1. It is worth mentioning that saturation in output is more general and has some advantages. Firstly, compared with saturations described in [36, 39–42] where nondelay state should be available online, system state $x(t)$ in output is not necessary and could be replaced by delay state $x(t-d)$. Secondly, compared with the saturated controllers designed for delayed systems without delay state [43, 44], both nondelay and delay states are included in output, whose distribution probabilities are also considered. Because all the delay terms could affect delayed systems, the obtained results are more conservative without considering them. In this sense, it is said that our formulation about output saturation has a larger application scope and less conservatism.

By letting $\eta = x - \mathrm{sat}(x)$ and $\eta_d = x_d - \mathrm{sat}(x_d)$ and considering the definition of $\alpha(t)$, it is known that

$$\begin{aligned}&\mathrm{sat}\left[\alpha(t)\,x(t) + (1-\alpha(t))\,x(t-d)\right]\\ &\quad= \alpha(t)\,x(t) + (1-\alpha(t))\,x(t-d)\\ &\qquad- \left[\alpha(t)\,\eta + (1-\alpha(t))\,\eta_d\right]\\ &\quad= \alpha x(t) + (1-\alpha)\,x(t-d)\\ &\qquad+ (\alpha(t)-\alpha)\,(x(t) - x(t-d))\\ &\qquad- \left[\alpha\eta + (1-\alpha)\,\eta_d + (\alpha(t)-\alpha)\,(\eta - \eta_d)\right].\end{aligned} \tag{7}$$

Then, system (1) is rewritten to be

$$\begin{aligned}\dot{x}(t) &= A(r_t)\,x(t),\\ y(t) &= C(r_t)\left\{\alpha x(t) + (1-\alpha)\,x(t-d)\right.\\ &\qquad+ (\alpha(t)-\alpha)\,(x(t) - x(t-d))\\ &\qquad\left.- \left[\alpha\eta + (1-\alpha)\,\eta_d + (\alpha(t)-\alpha)\,(\eta - \eta_d)\right]\right\},\\ x(t) &= \phi(t), \quad -d \le t \le 0.\end{aligned} \tag{8}$$

In this paper, the designed state observer system is described by

$$\begin{aligned}\dot{\hat{x}}(t) &= A(r_t)\,\hat{x}(t) + G(r_t)\left(y(t) - \hat{y}(t)\right),\\ \hat{y}(t) &= C(r_t)\,\hat{x}(t),\end{aligned} \tag{9}$$

where $\hat{x}(t) \in \mathbb{R}^n$ is the estimation of $x(t)$, and $\hat{y}(t) \in \mathbb{R}^q$ is the corresponding output. Define $e(t) = x(t) - \hat{x}(t)$; the resulting error system is rewritten to be

$$\begin{aligned}\dot{e}(t) &= \left(A(r_t) - G(r_t)\,C(r_t)\right)e(t)\\ &\quad+ (1-\alpha)\,G(r_t)\,C(r_t)\,x(t)\end{aligned}$$

$$
\begin{aligned}
&-(1-\alpha)G(r_t)C(r_t)x(t-d)\\
&+\alpha G(r_t)C(r_t)\eta+(1-\alpha)G(r_t)C(r_t)\eta_d\\
&+(\alpha(t)-\alpha)G(r_t)C(r_t)\\
&\times\left(x(t-d)-x(t)+\eta-\eta_d\right).
\end{aligned}
\tag{10}
$$

Here, it is assumed that stochastic variables $\alpha(t)$ and r_t are independent.

Proposition 2. *Let $u=\alpha(t)Kx(t)+(1-\alpha(t))K_dx(t-d)$ and $\eta=u-sat(u)$. Then, there exist real numbers $\varepsilon\in(0,1)$ and $\varepsilon_d\in(0,1)$ such that*

$$
\begin{aligned}
\eta^T\eta\le{}&\alpha(t)\varepsilon x^T(t)K^TKx(t)\\
&+(1-\alpha(t))\varepsilon_d x^T(t-d)K_d^TK_dx(t-d),
\end{aligned}
\tag{11}
$$

where $\eta=[\eta_1\ \cdots\ \eta_n]^T$, and η_i is the dead-zone nonlinearity function, $i=\{1,2,\ldots,n\}$.

Proof. Based on the formulation of $u(t)$, it is obtained that

$$
\begin{aligned}
\eta^T\eta={}&\{\alpha(t)Kx(t)+(1-\alpha(t))K_dx(t-d)\\
&-\operatorname{sat}[\alpha(t)Kx(t)+(1-\alpha(t))K_dx(t-d)]\}^T\\
&\cdot\{\alpha(t)Kx(t)+(1-\alpha(t))\times K_dx(t-d)\\
&-\operatorname{sat}[\alpha(t)Kx(t)+(1-\alpha(t))K_dx(t-d)]\}.
\end{aligned}
\tag{12}
$$

On the one hand, if $\alpha(t)=1$, one has $u=Kx(t)$. Similar to [36], we have the following.

(i) If $u_i>\mu_i$, it is obtained that

$$
\begin{aligned}
\eta^T\eta&=(Kx(t)-\operatorname{sat}(Kx(t)))^T(Kx(t)-\operatorname{sat}(Kx(t)))\\
&=x^T(t)K^TKx(t)-2x^T(t)K^T\operatorname{sat}(Kx(t))\\
&\quad+(\operatorname{sat}(Kx(t)))^T(\operatorname{sat}(Kx(t)))\\
&=x^T(t)K^TKx(t)-2x^T(t)K^T\mu+\mu^T\mu\\
&<x^T(t)K^TKx(t)-\mu^T\mu\le\varepsilon x^T(t)K^TKx(t),
\end{aligned}
\tag{13}
$$

where $\varepsilon\in(0,1)$ could be selected.

(ii) If $u_i<-\mu_i$, it is found that

$$
\begin{aligned}
\eta^T\eta&=(Kx(t)-\operatorname{sat}(Kx(t)))^T(Kx(t)-\operatorname{sat}(Kx(t)))\\
&=x^T(t)K^TKx(t)-2x^T(t)K^T\operatorname{sat}(Kx(t))\\
&\quad+(\operatorname{sat}(Kx(t)))^T(\operatorname{sat}(Kx(t)))\\
&=x^T(t)K^TKx(t)+2x^T(t)K^T\mu+\mu^T\mu\\
&<x^T(t)K^TKx(t)-\mu^T\mu\le\varepsilon x^T(t)K^TKx(t),
\end{aligned}
\tag{14}
$$

where $\varepsilon\in(0,1)$ could be obtained too.

(iii) If $-\mu_i\le u_i\le\mu_i$, we have $\eta^T\eta=0$. Then, there is always a scalar $\varepsilon\in(0,1)$ such that

$$
\eta^T\eta\le\varepsilon x^T(t)K^TKx(t).
\tag{15}
$$

On the other hand, when $\alpha(t)=0$, it is obtained that $u=K_dx(t-d)$. Similarly, we have the following cases.

(i) If $u_i>\mu_i$, it is obtained that

$$
\begin{aligned}
\eta^T\eta&=\{K_dx(t-d)-\operatorname{sat}[K_dx(t-d)]\}^T\\
&\quad\cdot\{K_dx(t-d)-\operatorname{sat}[K_dx(t-d)]\}=x^T(t-d)\\
&\quad\cdot K_d^TK_dx(t-d)-2x^T(t)K_d^T\operatorname{sat}[K_dx(t-d)]\\
&\quad+(\operatorname{sat}[K_dx(t-d)])^T\operatorname{sat}[K_dx(t-d)]\\
&=x^T(t-d)K_d^TK_dx(t-d)-2x^T(t-d)K_d^T\mu\\
&\quad+\mu^T\mu<x^T(t-d)K_d^TK_dx(t-d)-\mu^T\mu\\
&\le\varepsilon_dx^T(t-d)K_d^TKx(t-d),
\end{aligned}
\tag{16}
$$

where $\varepsilon_d\in(0,1)$.

(ii) If $u_i<-\mu_i$, it is found that

$$
\begin{aligned}
\eta^T\eta&=\{K_dx(t-d)-\operatorname{sat}[K_dx(t-d)]\}^T\\
&\quad\cdot\{K_dx(t-d)-\operatorname{sat}[K_dx(t-d)]\}=x^T(t-d)\\
&\quad\cdot K_d^TK_dx(t-d)-2x^T(t)K_d^T\operatorname{sat}[K_dx(t-d)]\\
&\quad+(\operatorname{sat}[K_dx(t-d)])^T\operatorname{sat}[K_dx(t-d)]\\
&=x^T(t-d)K_d^TK_dx(t-d)+2x^T(t-d)K_d^T\mu\\
&\quad+\mu^T\mu<x^T(t-d)K_d^TK_dx(t-d)-\mu^T\mu\\
&\le\varepsilon_dx^T(t-d)K_d^TKx(t-d),
\end{aligned}
\tag{17}
$$

where $\varepsilon_d\in(0,1)$.

(iii) If $-\mu_i\le u_i\le\mu_i$, we have $\eta^T\eta=0$. Then, there is always a scalar $\varepsilon_d\in(0,1)$ such that

$$
\eta^T\eta\le\varepsilon_dx^T(t-d)K_d^TK_dx(t-d).
\tag{18}
$$

This completes the proof. □

3. Main Results

Theorem 3. *Given system (1) with $d>0$, there exists an observer (9) such that system (1) and error system (12) are asymptotically stable, if for given positive scalars $\alpha\in[0,1]$, $\varepsilon_i\in(0,1)$, and $\varepsilon_{di}\in(0,1)$, there exist $P_i>0$, $Q>0$, $Z>0$, $\gamma_i>0$, $\lambda_i>0$, and Y_i such that*

$$\begin{bmatrix} \Theta_{i1} & \Theta_{i2} & Z & 0 & \Theta_{i3} & \Theta_{i4} \\ * & \Theta_{i5} & \Theta_{i6} & Z & 0 & \Theta_{i7} \\ * & * & \Theta_{i8} & 0 & \Theta_{i9} & \Theta_{i10} \\ * & * & * & \Theta_{11} & 0 & 0 \\ * & * & * & * & \Theta_{i12} & 0 \\ * & * & * & * & * & \Theta_{i12} \end{bmatrix} < 0, \tag{19}$$

$$\begin{bmatrix} -\gamma_i I & C_i^T Y_i^T \\ * & -P_i \end{bmatrix} \leq 0, \tag{20}$$

$$\begin{bmatrix} -\lambda_i I & C_i^T Y_i^T \\ * & \Theta_{i12} \end{bmatrix} \leq 0, \tag{21}$$

where

$$\begin{aligned} \Theta_{i1} &= \left(P_i A_i\right)^\star + \sum_{j=1}^{N} \pi_{ij} P_j + \alpha\varepsilon_i\gamma_i I + Q + d^2 A_i^T Z A_i \\ &\quad - Z + 2\alpha d^2 \varepsilon_i \lambda_i I + 4\alpha\overline{\alpha} d^2 \varepsilon_i \lambda_i I, \\ \Theta_{i2} &= \overline{\alpha} C_i^T Y_i^T, \\ \Theta_{i3} &= -\sqrt{2\alpha\overline{\alpha}} d C_i^T Y_i^T, \\ \Theta_{i4} &= \sqrt{2}\overline{\alpha} d C_i^T Y_i^T, \\ \Theta_{i5} &= \left(P_i A_i - Y_i C_i\right)^\star + P_i + \sum_{j=1}^{N} \pi_{ij} P_j + Q - Z, \\ \Theta_{i6} &= -\overline{\alpha} Y_i C_i, \\ \Theta_{i7} &= \sqrt{2} d \left(A_i^T P_i - C_i^T Y_i^T\right), \\ \Theta_{i8} &= \overline{\alpha}\varepsilon_{di}\gamma_i I + 2\overline{\alpha} d^2 \varepsilon_{di} \lambda_i I + 4\alpha\overline{\alpha} d^2 \varepsilon_{di} \lambda_i I - Q - Z, \\ \Theta_{i9} &= \sqrt{2\alpha\overline{\alpha}} d C_i^T Y_i^T, \\ \Theta_{i10} &= -\sqrt{2}\overline{\alpha} d C_i^T Y_i^T, \\ \Theta_{11} &= -Q - Z, \\ \Theta_{i12} &= -2P_i + Z, \\ \overline{\alpha} &= 1 - \alpha. \end{aligned} \tag{22}$$

Then, the gain of observer (9) is computed by

$$G_i = Y_i P_i^{-1}. \tag{23}$$

Proof. For systems (1) and (12), choose the following Lyapunov function:

$$V\left(x_t\right) = V_1\left(x_t\right) + V_2\left(x_t\right), \tag{24}$$

where

$$\begin{aligned} V_1\left(x_t, r_t\right) &= x^T(t) P\left(r_t\right) x(t) + \int_{t-d}^{t} x^T(s) Q x(s)\, ds \\ &\quad + d \int_{-d}^{0} \int_{t+\theta}^{t} \dot{x}^T(s) Z \dot{x}(s)\, ds\, d\theta, \\ V_2\left(x_t, r_t\right) &= e^T(t) P\left(r_t\right) e(t) + \int_{t-d}^{t} e^T(s) Q e(s)\, ds \\ &\quad + d \int_{-d}^{0} \int_{t+\theta}^{t} \dot{e}^T(s) Z \dot{e}(s)\, ds\, d\theta. \end{aligned} \tag{25}$$

Let $\mathscr{L}$ be the weak infinitesimal generator of random process $\{x_t, r_t\}$, for each $r_t = i \in \mathbb{S}$; it is defined as

$$\begin{aligned} \mathscr{L}V\left(x_t, t, i\right) &= \lim_{\Delta t \to 0^+} \\ &\quad \cdot \frac{1}{\Delta t} \left\{\mathscr{E}\left[V\left(x_{t+\Delta t}, r_{t+\Delta t}, t + \Delta t\right) \mid x_t, r_t = i\right]\right. \\ &\quad \left. - V\left(x_t, i, t\right)\right\}. \end{aligned} \tag{26}$$

Then, it is further obtained that

$$\begin{aligned} &\mathscr{L}V_1\left(x_t\right) \\ &\quad = x^T(t) \left(P_i A_i\right)^\star x(t) + x^T(t) \sum_{j=1}^{N} \pi_{ij} P_j x(t) \\ &\qquad + x^T(t) Q x(t) - x^T(t-d) Q x(t-d) \\ &\qquad + d^2 x^T(t) A_i^T Z A_i x(t) - \int_{t-d}^{t} \dot{x}^T(\theta) Z \dot{x}(\theta)\, d\theta, \\ &\mathscr{L}V_2\left(x_t\right) \\ &\quad = e^T(t) \left[P_i\left(A_i - G_i C_i\right)\right]^\star e(t) \\ &\qquad + 2\overline{\alpha} e^T(t) P_i G_i C_i x(t) \\ &\qquad - 2\overline{\alpha} e^T(t) P_i G_i C_i x(t-d) + 2\alpha e^T(t) P_i G_i C_i \eta \\ &\qquad + 2\overline{\alpha} e^T(t) P_i G_i C_i \eta_d + e^T(t) \sum_{j=1}^{N} \pi_{ij} P_j e(t) \\ &\qquad - \int_{t-d}^{t} \dot{e}^T(\theta) Z \dot{e}(\theta)\, d\theta + e^T(t) Q e(t) \\ &\qquad - e^T(t-d) Q e(t-d) \\ &\qquad + d^2 \left(f_{i1} + f_{i2}\right)^T Z \left(f_{i1} + f_{i2}\right) \\ &\qquad + \alpha\overline{\alpha} d^2 \left[G_i C_i\left(x(t-d) - x(t) + \eta - \eta_d\right)\right]^T \\ &\qquad \times Z \left[G_i C_i\left(x(t-d) - x(t) + \eta - \eta_d\right)\right], \end{aligned} \tag{27}$$

where

$$\begin{aligned} f_{i1} &= \left(A_i - G_iC_i\right)e(t) + \overline{\alpha}G_iC_ix(t) \\ &\quad - \overline{\alpha}G_iC_ix(t-d), \\ f_{i2} &= \alpha G_iC_i\eta + \overline{\alpha}G_iC_i\eta_d. \end{aligned} \tag{28}$$

Based on the Jensen inequality, one has

$$\begin{aligned} &-\int_{t-d}^{t}\dot{x}^T(\theta)Z\dot{x}(\theta)\,d\theta \\ &\quad\le -x^T(t)Zx(t) + 2x^T(t)Zx(t-d) \\ &\qquad - x^T(t-d)Zx(t-d), \end{aligned} \tag{29}$$

$$\begin{aligned} &-\int_{t-d}^{t}\dot{e}^T(\theta)Z\dot{e}(\theta)\,d\theta \\ &\quad\le -e^T(t)Ze(t) + 2e^T(t)Ze(t-d) \\ &\qquad - e^T(t-d)Ze(t-d). \end{aligned} \tag{30}$$

Moreover, it is concluded that

$$\begin{aligned} &2\alpha e^T(t)P_iG_iC_i\eta \le \alpha e^T(t)P_ie(t) \\ &\quad + \alpha\eta^TC_i^TG_i^TP_iG_iC_i\eta, \end{aligned} \tag{31}$$

$$\begin{aligned} &2\overline{\alpha}e^T(t)P_iG_iC_i\eta_d \le \overline{\alpha}e^T(t)P_ie(t) \\ &\quad + \overline{\alpha}\eta_d^TC_i^TG_i^TP_iG_iC_i\eta_d, \end{aligned} \tag{32}$$

$$\begin{aligned} &2d^2\left(\alpha G_iC_i\eta + \overline{\alpha}G_iC_i\eta_d\right)^TZ\left(\alpha G_iC_i\eta + \overline{\alpha}G_iC_i\eta_d\right) \\ &\quad\le 2\alpha d^2\eta^TC_i^TG_i^TZG_iC_i\eta + 2\overline{\alpha}d^2\eta_d^TC_i^TG_i^TZG_iC_i\eta_d, \end{aligned} \tag{33}$$

$$\begin{aligned} &2\alpha\overline{\alpha}d^2\left(G_iC_i\eta - G_iC_i\eta_d\right)^TZ\left(G_iC_i\eta - G_iC_i\eta_d\right) \\ &\quad\le 4\alpha\overline{\alpha}d^2\eta^TC_i^TG_i^TZG_iC_i\eta \\ &\quad + 4\alpha\overline{\alpha}d^2\eta_d^TC_i^TG_i^TZG_iC_i\eta_d, \end{aligned} \tag{34}$$

$$\begin{aligned} &d^2\left(f_{i1}+f_{i2}\right)^TZ\left(f_{i1}+f_{i2}\right) \le 2d^2f_{i1}^TZf_{i1} \\ &\quad + 2d^2\left(\alpha G_iC_i\eta + \overline{\alpha}G_iC_i\eta_d\right)^T \\ &\quad\cdot Z\left(\alpha G_iC_i\eta + \overline{\alpha}G_iC_i\eta_d\right), \end{aligned} \tag{35}$$

$$\begin{aligned} &\alpha\overline{\alpha}d^2\left[G_iC_i\left(x(t-d) - x(t) + \eta - \eta_d\right)\right]^T \\ &\quad\cdot Z\left[G_iC_i\left(x(t-d) - x(t) + \eta - \eta_d\right)\right] \\ &\quad\le 2\alpha\overline{\alpha}d^2\left[G_iC_i\left(x(t-d) - x(t)\right)\right]^T \\ &\quad\cdot Z\left[G_iC_i\left(x(t-d) - x(t)\right)\right] \\ &\quad + 2\alpha\overline{\alpha}d^2\left(G_iC_i\eta - G_iC_i\eta_d\right)^TZ\left(G_iC_i\eta - G_iC_i\eta_d\right). \end{aligned} \tag{36}$$

Based on these conditions, the following is computed:

$$\begin{aligned} \mathscr{L}V(x_t) &\le x^T(t)\left(P_iA_i\right)^\star x(t) + x^T(t)\sum_{j=1}^{N}\pi_{ij}P_jx(t) \\ &\quad + e^T(t)\left[P_i\left(A_i - G_iC_i\right)\right]^\star e(t) + 2\overline{\alpha}e^T(t) \\ &\quad\cdot P_iG_iC_ix(t) - 2\overline{\alpha}e^T(t)P_iG_iC_ix(t-d) + e^T(t) \\ &\quad\cdot P_ie(t) + \alpha\eta^TC_i^TG_i^TP_iG_iC_i\eta + \overline{\alpha}\eta_d^TC_i^TG_i^TP_iG_iC_i\eta_d \\ &\quad + e^T(t)\sum_{j=1}^{N}\pi_{ij}P_je(t) + x^T(t)Qx(t) - x^T(t-d) \\ &\quad\cdot Qx(t-d) + e^T(t)Qe(t) - e^T(t-d)Qe(t-d) \\ &\quad + d^2x^T(t)A_i^TZA_ix(t) - x^T(t)Zx(t) + 2x^T(t) \\ &\quad\cdot Zx(t-d) - x^T(t-d)Zx(t-d) \\ &\quad + 2\alpha d^2\eta^TC_i^TG_i^TZG_iC_i\eta + 2\overline{\alpha}d^2\eta_d^TC_i^TG_i^TZG_iC_i\eta_d \\ &\quad + 2d^2\left[\left(A_i - G_iC_i\right)e(t) + \overline{\alpha}G_iC_ix(t)\right. \\ &\quad\left. - \overline{\alpha}G_iC_ix(t-d)\right]^T\times Z\left[\left(A_i - G_iC_i\right)e(t)\right. \\ &\quad\left. + \overline{\alpha}G_iC_ix(t) - \overline{\alpha}G_iC_ix(t-d)\right] \\ &\quad + 2\alpha\overline{\alpha}d^2\left[G_iC_i\left(x(t-d) - x(t)\right)\right]^T \\ &\quad\cdot Z\left[G_iC_i\left(x(t-d) - x(t)\right)\right] \\ &\quad + 4\alpha\overline{\alpha}d^2\eta^TC_i^TG_i^TZG_iC_i\eta \\ &\quad + 4\alpha\overline{\alpha}d^2\eta_d^TC_i^TG_i^TZG_iC_i\eta_d - e^T(t)Ze(t) + 2e^T(t) \\ &\quad\cdot Ze(t-d) - e^T(t-d)Ze(t-d). \end{aligned} \tag{37}$$

Moreover, the other conditions are assumed to be

$$C_i^TG_i^TP_iG_iC_i \le \gamma_iI, \tag{38}$$

$$C_i^TG_i^TZG_iC_i \le \lambda_iI. \tag{39}$$

Based on the above conditions and applying Proposition 2, it is obtained that (37) is implied by

$$\begin{aligned} \mathscr{L}V(x_t) &\le \xi^T(t)\left(\begin{bmatrix} \Theta_{i1} & \Theta_{i2} & Z & 0 \\ * & \Theta_{i5} & \Theta_{i6} & Z \\ * & * & \Theta_{i8} & 0 \\ * & * & * & \Theta_{11} \end{bmatrix}\right. \\ &\quad\left. + 2\alpha\overline{\alpha}d^2\begin{bmatrix} -C_i^TG_i^T \\ 0 \\ C_i^TG_i^T \\ 0 \end{bmatrix}Z\begin{bmatrix} -C_i^TG_i^T \\ 0 \\ C_i^TG_i^T \\ 0 \end{bmatrix}^T\right. \end{aligned}$$

$$+ 2d^2 \begin{bmatrix} \overline{\alpha} C_i^T G_i^T \\ \left(A_i - C_i^T G_i\right)^T \\ -\overline{\alpha} C_i^T G_i^T \\ 0 \end{bmatrix} Z \begin{bmatrix} \overline{\alpha} C_i^T G_i^T \\ \left(A_i - C_i^T G_i\right)^T \\ -\overline{\alpha} C_i^T G_i^T \\ 0 \end{bmatrix}^T \Bigg) \cdot \xi(t), \tag{40}$$

where

$$\xi^T(t) = \left[x^T(t) \quad e^T(t) \quad x^T(t-d) \quad e^T(t-d)\right]. \tag{41}$$

By using the Schur complement lemma, it is further obtained that

$$\begin{bmatrix} \Theta_{i1} & \Theta_{i2} & Z & 0 & \overline{\Theta}_{i3} & \overline{\Theta}_{i4} \\ * & \Theta_{i5} & \Theta_{i6} & Z & 0 & \overline{\Theta}_{i7} \\ * & * & \Theta_{i8} & 0 & \overline{\Theta}_{i9} & \overline{\Theta}_{i10} \\ * & * & * & \Theta_{11} & 0 & 0 \\ * & * & * & * & -Z^{-1} & 0 \\ * & * & * & * & * & -Z^{-1} \end{bmatrix} < 0, \tag{42}$$

where

$$\begin{aligned} \overline{\Theta}_{i3} &= -\sqrt{2\alpha\overline{\alpha}} d C_i^T G_i^T, \\ \overline{\Theta}_{i4} &= \sqrt{2}\overline{\alpha} d C_i^T G_i^T, \\ \overline{\Theta}_{i9} &= \sqrt{2\alpha\overline{\alpha}} d C_i^T G_i^T, \\ \overline{\Theta}_{i7} &= \sqrt{2} d \left(A_i^T - C_i^T G_i^T\right), \\ \overline{\Theta}_{i10} &= -\sqrt{2}\overline{\alpha} d C_i^T G_i^T. \end{aligned} \tag{43}$$

By pre- and postmultiplying both its sides with diag$\{I, I, I, I, P_i, P_i\}$ and its transpose, respectively, one gets

$$\begin{bmatrix} \Theta_{i1} & \Theta_{i2} & Z & 0 & \Theta_{i3} & \Theta_{i4} \\ * & \Theta_{i5} & \Theta_{i6} & Z & 0 & \Theta_{i7} \\ * & * & \Theta_{i8} & 0 & \Theta_{i9} & \Theta_{i10} \\ * & * & * & \Theta_{11} & 0 & 0 \\ * & * & * & * & -\overline{Z} & 0 \\ * & * & * & * & * & -\overline{Z} \end{bmatrix} < 0, \tag{44}$$

where $\overline{Z} = P_i Z^{-1} P_i$. It is further obtained that $\overline{Z} > 0$ could be guaranteed by

$$-P_i Z^{-1} P_i \le -2P_i + Z < 0. \tag{45}$$

As for conditions (38) and (39), they are equivalent to

$$\begin{aligned} -\gamma_i I + C_i^T G_i^T P_i G_i C_i &\le 0, \\ -\lambda_i I + C_i^T G_i^T Z G_i C_i &\le 0. \end{aligned} \tag{46}$$

By applying the Schur complement lemma and considering representation (23), it is known that condition (38) is equivalent to condition (20). As for condition (39), by pre- and postmultiplying both its sides with diag$\{I, P_i\}$ and applying inequality (45), one could easily get condition (21) with representation (23) implying condition (39). This completes the proof. □

Remark 4. Due to α included obviously, it plays important roles in analysis and synthesis of systems with output saturation. With two special cases that only system state with $\alpha = 0$ or delay state with $\alpha = 1$ is contained in output saturation, our results could be viewed as extension results on the saturation output problem from output without time delay to stochastic delay output. On the other hand, from the proof process, it is seen that some inequalities, like (31), (33), (35), and so on, have been used to get the LMI conditions and could lead to more conservatism. In order to reduce its conservatism, some additional variables could be introduced in these inequalities. However, such variables will lead to larger computation complexity. Moreover, the conservatism of inequality (45) could be further reduced by applying similar methods in [45]. Similarly, much larger computation complexity in terms of more variables and inequalities should be needed. Based on these facts, it is said that whether to choose these methods or not should be considered in concrete situations.

Remark 5. It is seen from this theorem that such a probability should be given exactly. It will be impossible or of high cost in some practical applications. Instead, only its estimation is available, even if it is totally unknown. In other words, there will be a uncertainty between the real and estimated values. As we know, such a uncertainty will degrade the system performance and even lead to unstable system. So, it is necessary and meaningful to consider this general case. Moreover, some necessarily additional variables and inequalities are introduced to obtain LMI conditions, where the variables are to be computed instead of being given beforehand. Because of the given results with LMI forms, the above general case could be handled by exploiting the methods in this paper and [46, 47] together.

Next, we consider another state observer system described as

$$\begin{aligned} \dot{\widehat{x}}(t) &= A(r_t)\widehat{x}(t) + G(r_t)\left(y(t) - \widehat{y}(t)\right), \\ \widehat{y}(t) &= C(r_t)\left[\alpha(t)\widehat{x}(t) + (1-\alpha(t))\widehat{x}(t-d)\right]. \end{aligned} \tag{47}$$

Then, the resulting error system is rewritten to be

$$\begin{aligned} \dot{e}(t) = {} & \left(A(r_t) - \alpha G(r_t) C(r_t)\right) e(t) - (1-\alpha) G(r_t) \\ & \cdot C(r_t) e(t-d) + \alpha G(r_t) C(r_t)\eta + (1-\alpha) \\ & \cdot G(r_t) C(r_t)\eta_d + (\alpha(t) - \alpha) G(r_t) C(r_t) \\ & \cdot \left(x(t-d) - x(t) + \eta - \eta_d\right). \end{aligned} \tag{48}$$

Similarly, we have the following theorem.

Theorem 6. *Given system (1) with $d > 0$, there exists observer (47) such that system (1) and error system (48) are asymptotically stable, if for given positive scalars $\alpha \in [0,1]$, $\varepsilon_i \in (0,1)$, and $\varepsilon_{di} \in (0,1)$, there exist $P_i > 0$, $Q > 0$, $Z > 0$, $\gamma_i > 0$, $\lambda_i > 0$, and Y_i satisfying conditions (20) and (21) and*

$$\begin{bmatrix} \Theta_{i1} & 0 & Z & 0 & 0 & 0 \\ * & \Psi_{i1} & 0 & \Psi_{i2} & \Theta_{i3} & \Psi_{i3} \\ * & * & \Theta_{i8} & 0 & 0 & 0 \\ * & * & * & \Theta_{11} & \Theta_{i9} & \Theta_{i10} \\ * & * & * & * & \Theta_{i12} & 0 \\ * & * & * & * & * & \Theta_{i12} \end{bmatrix} < 0, \tag{49}$$

where

$$\begin{aligned} \Psi_{i1} &= \left(P_i A_i - \alpha Y_i C_i\right)^{\star} + P_i + \sum_{j=1}^{N} \pi_{ij} P_j + Q - Z, \\ \Psi_{i2} &= -\overline{\alpha} Y_i C_i + Z, \\ \Psi_{i3} &= \sqrt{2} d \left(A_i^T P_i - \alpha C_i^T Y_i^T\right). \end{aligned} \tag{50}$$

Then, the gain of observer (47) could be computed by (23).

Proof. For systems (1) and (48), choose the same Lyapunov function (24). Similar to (35) and (36), it is obtained that

$$\begin{aligned} d^2 \left(f_{i3} + f_{i2}\right)^T Z \left(f_{i3} + f_{i2}\right) &\le 2d^2 f_{i3}^T Z f_{i3} \\ &+ 2d^2 \left(\alpha G_i C_i \eta + \overline{\alpha} G_i C_i \eta_d\right)^T \\ &\cdot Z \left(\alpha G_i C_i \eta + \overline{\alpha} G_i C_i \eta_d\right), \end{aligned} \tag{51}$$

where

$$f_{i3} = \left(A_i - \alpha G_i C_i\right) e(t) - \overline{\alpha} G_i C_i e(t-d), \tag{52}$$

$$\begin{aligned} &\alpha\overline{\alpha} d^2 \left[G_i C_i \left(e(t-d) - e(t) + \eta - \eta_d\right)\right]^T \\ &\quad \cdot Z \left[G_i C_i \left(e(t-d) - e(t) + \eta - \eta_d\right)\right] \\ &\quad \le 2\alpha\overline{\alpha} d^2 \left[G_i C_i \left(e(t-d) - e(t)\right)\right]^T \\ &\quad \cdot Z \left[G_i C_i \left(e(t-d) - e(t)\right)\right] \\ &\quad + 2\alpha\overline{\alpha} d^2 \left(G_i C_i \eta - G_i C_i \eta_d\right)^T Z \left(G_i C_i \eta - G_i C_i \eta_d\right). \end{aligned} \tag{53}$$

Then, it is obtained that

$$\begin{aligned} \mathscr{L}V\left(x_t\right) &\le x^T(t) \left(P_i A_i\right)^{\star} x(t) + x^T(t) \sum_{j=1}^{N} \pi_{ij} P_j x(t) \\ &+ e^T(t) \left[P_i \left(A_i - G_i C_i\right)\right]^{\star} e(t) - 2\overline{\alpha} e^T(t) \\ &\cdot P_i G_i C_i e(t-d) + e^T(t) P_i e(t) \\ &+ \alpha \eta^T C_i^T G_i^T P_i G_i C_i \eta + \overline{\alpha} \eta_d^T C_i^T G_i^T P_i G_i C_i \eta_d + e^T(t) \\ &\cdot \sum_{j=1}^{N} \pi_{ij} P_j e(t) + x^T(t) Q x(t) - x^T(t-d) \\ &\cdot Q x(t-d) + e^T(t) Q e(t) - e^T(t-d) Q e(t-d) \\ &+ d^2 x^T(t) A_i^T Z A_i x(t) - x^T(t) Z x(t) + 2x^T(t) \\ &\cdot Z x(t-d) - x^T(t-d) Z x(t-d) \\ &+ 2\alpha d^2 \eta^T C_i^T G_i^T Z G_i C_i \eta + 2\overline{\alpha} d^2 \eta_d^T C_i^T G_i^T Z G_i C_i \eta_d \\ &+ 2d^2 \left[\left(A_i - \alpha G_i C_i\right) e(t) - \overline{\alpha} G_i C_i e(t-d)\right]^T \\ &\times Z \left[\left(A_i - \alpha G_i C_i\right) e(t) - \overline{\alpha} G_i C_i e(t-d)\right] \\ &+ 2\alpha\overline{\alpha} d^2 \left[G_i C_i \left(e(t-d) - e(t)\right)\right]^T \\ &\cdot Z \left[G_i C_i \left(e(t-d) - e(t)\right)\right] \\ &+ 4\alpha\overline{\alpha} d^2 \eta^T C_i^T G_i^T Z G_i C_i \eta \\ &+ 4\alpha\overline{\alpha} d^2 \eta_d^T C_i^T G_i^T Z G_i C_i \eta_d - e^T(t) Z e(t) + 2e^T(t) \\ &\cdot Z e(t-d) - e^T(t-d) Z e(t-d). \end{aligned} \tag{54}$$

Based on conditions (20), (21), (51), and (53), it is obtained that (54) is implied by

$$\begin{aligned} \mathscr{L}V\left(x_t\right) \le \xi^T(t) \Bigg(& \begin{bmatrix} \Theta_{i1} & 0 & Z & 0 \\ * & \Psi_{i1} & 0 & \Psi_{i2} \\ * & * & \Theta_{i8} & 0 \\ * & * & * & \Theta_{11} \end{bmatrix} \\ &+ 2\alpha\overline{\alpha} d^2 \begin{bmatrix} 0 \\ -C_i^T G_i^T \\ 0 \\ C_i^T G_i^T \end{bmatrix} Z \begin{bmatrix} 0 \\ -C_i^T G_i^T \\ 0 \\ C_i^T G_i^T \end{bmatrix}^T \\ &+ 2d^2 \begin{bmatrix} 0 \\ \left(A_i - \alpha C_i^T G_i\right)^T \\ 0 \\ -\overline{\alpha} C_i^T G_i^T \end{bmatrix} Z \begin{bmatrix} 0 \\ \left(A_i - \alpha C_i^T G_i\right)^T \\ 0 \\ -\overline{\alpha} C_i^T G_i^T \end{bmatrix}^T \Bigg) \\ &\cdot \xi(t). \end{aligned} \tag{55}$$

By using similar methods given in Theorem 3, it is known that condition (55) could be guaranteed by inequality (49). This completes the proof. □

Finally, we consider the following state observer system described by

$$\begin{aligned} \dot{\widehat{x}}(t) &= A\left(r_t\right) \widehat{x}(t) + G\left(r_t\right) \left(y(t) - \widehat{y}(t)\right), \\ \widehat{y}(t) &= C\left(r_t\right) \mathrm{sat}\left(\alpha(t) \widehat{x}(t) + (1 - \alpha(t)) \widehat{x}(t-d)\right) \end{aligned} \tag{56}$$

which is equivalent to

$$\begin{aligned}\dot{\widehat{x}}(t) &= A(r_t)\widehat{x}(t) + G(r_t)(y(t) - \widehat{y}(t)),\\ \widehat{y}(t) &= C(r_t)\{\alpha\widehat{x}(t) + \overline{\alpha}\widehat{x}(t-d)\\ &\quad + (\alpha(t) - \alpha)(\widehat{x}(t) - \widehat{x}(t-d))\\ &\quad - [\alpha\widehat{\eta} + \overline{\alpha}\widehat{\eta}_d + (\alpha(t) - \alpha)(\widehat{\eta} - \widehat{\eta}_d)]\}.\end{aligned} \tag{57}$$

Then, the resulting error system is rewritten to be

$$\begin{aligned}\dot{e}(t) &= (A(r_t) - \alpha G(r_t)C(r_t))e(t) - \overline{\alpha}G(r_t)C(r_t)\\ &\quad \cdot e(t-d) + \alpha G(r_t)C(r_t)(\eta - \widehat{\eta}) + \overline{\alpha}G(r_t)\\ &\quad \cdot C(r_t)(\eta_d - \widehat{\eta}_d) + (\alpha(t) - \alpha)G(r_t)C(r_t)\\ &\quad \cdot (x(t-d) - x(t) + \eta - \widehat{\eta} - \eta_d + \widehat{\eta}_d).\end{aligned} \tag{58}$$

Theorem 7. *Given system (1) with $d > 0$, there exists observer (56) such that system (1) and error system (58) are asymptotically stable, if for given positive scalars $\alpha \in [0,1]$, $\varepsilon_i \in (0,1)$, and $\varepsilon_{di} \in (0,1)$, there exist $P_i > 0$, $Q > 0$, $Z > 0$, $\gamma_i > 0$, $\lambda_i > 0$, and Y_i satisfying conditions (20) and (21) and*

$$\begin{bmatrix}\Omega_{i1} & \Omega_{i2} & Z & 0 & 0 & 0\\ * & \Omega_{i3} & 0 & \Psi_{i2} & \Theta_{i3} & \Psi_{i3}\\ * & * & \Omega_{i4} & \Omega_{i5} & 0 & 0\\ * & * & * & \Omega_{i6} & \Theta_{i9} & \Theta_{i10}\\ * & * & * & * & \Theta_{i12} & 0\\ * & * & * & * & * & \Theta_{i12}\end{bmatrix} < 0, \tag{59}$$

where

$$\begin{aligned}\Omega_{i1} &= (P_iA_i)^{\star} + \sum_{j=1}^{N}\pi_{ij}P_j + 2\alpha\varepsilon_i\gamma_iI + Q + d^2A_i^TZA_i\\ &\quad - Z + 8\alpha d^2\varepsilon_i\lambda_iI + 16\alpha\overline{\alpha}d^2\varepsilon_i\lambda_iI,\\ \Omega_{i2} &= -\alpha\varepsilon_i\gamma_iI - 4\alpha d^2\varepsilon_i\lambda_iI - 8\alpha\overline{\alpha}d^2\varepsilon_i\lambda_iI,\\ \Omega_{i3} &= (P_iA_i - \alpha Y_iC_i)^{\star} + 2P_i + \sum_{j=1}^{N}\pi_{ij}P_j + Q - Z\\ &\quad + \alpha\varepsilon_i\gamma_iI + 4\alpha d^2\varepsilon_i\lambda_iI + 8\alpha\overline{\alpha}d^2\varepsilon_i\lambda_iI,\\ \Omega_{i4} &= 2\overline{\alpha}\varepsilon_{di}\gamma_iI + 8\overline{\alpha}d^2\varepsilon_{di}\lambda_iI + 16\alpha\overline{\alpha}d^2\varepsilon_{di}\lambda_iI - Q\\ &\quad - Z,\\ \Omega_{i5} &= -\overline{\alpha}\varepsilon_{di}\gamma_iI - 4\overline{\alpha}d^2\varepsilon_{di}\lambda_iI - 8\alpha\overline{\alpha}d^2\varepsilon_{di}\lambda_iI,\\ \Omega_{i6} &= \overline{\alpha}\varepsilon_{di}\gamma_iI + 4\overline{\alpha}d^2\varepsilon_{di}\lambda_iI + 8\alpha\overline{\alpha}d^2\varepsilon_{di}\lambda_iI - Q - Z.\end{aligned} \tag{60}$$

Then, (23) could be used to compute the gain of observer (56).

Proof. Firstly, the same Lyapunov function is also selected for systems (1) and (56). Similar to computation process of Theorems 3 and 6, the corresponding terms are handled as

$$\begin{aligned}&-2\alpha e^T(t)P_iG_iC_i\widehat{\eta}\\ &\quad \le \alpha e^T(t)P_ie(t) + \alpha\widehat{\eta}^TC_i^TG_i^TP_iG_iC_i\widehat{\eta},\\ &-2\overline{\alpha}e^T(t)P_iG_iC_i\widehat{\eta}_d\\ &\quad \le \overline{\alpha}e^T(t)P_ie(t) + \overline{\alpha}\widehat{\eta}_d^TC_i^TG_i^TP_iG_iC_i\widehat{\eta}_d,\\ &d^2(f_{i3} + f_{i4})^TZ(f_{i3} + f_{i4})\\ &\quad \le 2d^2f_{i3}^TZf_{i3} + 2d^2f_{i4}^TZf_{i4},\end{aligned} \tag{61}$$

where

$$\begin{aligned}f_{i4} &= \alpha G_iC_i(\eta - \widehat{\eta}) + \overline{\alpha}G_iC_i(\eta_d - \widehat{\eta_d}),\\ 2d^2f_{i4}^TZf_{i4} &\le 2\alpha d^2(\eta - \widehat{\eta})^TC_i^TG_i^TZG_iC_i(\eta - \widehat{\eta})\\ &\quad + 2\overline{\alpha}d^2(\eta_d - \widehat{\eta_d})^TC_i^TG_i^TZG_iC_i(\eta_d - \widehat{\eta_d})\\ &\le 4\alpha d^2\eta^TC_i^TG_i^TZC_i^TG_i^T\eta + 4\alpha d^2\widehat{\eta}^TC_i^TG_i^TZG_iC_i\widehat{\eta}\\ &\quad + 4\overline{\alpha}d^2\eta_d^TC_i^TG_i^TZG_iC_i\eta_d + 4\overline{\alpha}d^2\widehat{\eta}_d^TC_i^TG_i^TZG_iC_i\widehat{\eta}_d,\\ d^2(f_{i3} + f_{i4})^TZ(f_{i3} + f_{i4}) &\le 2d^2f_{i3}^TZf_{i3}\\ &\quad + 2d^2f_{i4}^TZf_{i4},\\ \alpha\overline{\alpha}d^2&\{G_iC_i[e(t-d) - e(t) + (\eta - \widehat{\eta}) - (\eta_d - \widehat{\eta_d})]\}^T\\ &\quad \times Z\{G_iC_i[e(t-d) - e(t) + (\eta - \widehat{\eta}) - (\eta_d - \widehat{\eta_d})]\}\\ &\quad \le 2\alpha\overline{\alpha}d^2[G_iC_i(e(t-d) - e(t))]^T\\ &\quad \cdot Z[G_iC_i(e(t-d) - e(t))] + 2\alpha\overline{\alpha}d^2[G_iC_i(\eta - \widehat{\eta})\\ &\quad - G_iC_i(\eta_d - \widehat{\eta_d})]^TZ \times [G_iC_i(\eta - \widehat{\eta}) - G_iC_i(\eta_d\\ &\quad - \widehat{\eta_d})].\end{aligned} \tag{62}$$

Moreover, it is obtained that

$$\begin{aligned}&2\alpha\overline{\alpha}d^2[G_iC_i(\eta - \widehat{\eta}) - G_iC_i(\eta_d - \widehat{\eta_d})]^T\\ &\quad \cdot Z[G_iC_i(\eta - \widehat{\eta}) - G_iC_i(\eta_d - \widehat{\eta_d})]\\ &\quad \le 8\alpha\overline{\alpha}d^2\eta^TC_i^TG_i^TZC_i^TG_i^T\eta\\ &\quad + 8\alpha\overline{\alpha}d^2\widehat{\eta}^TC_i^TG_i^TZG_iC_i\widehat{\eta}\\ &\quad + 8\alpha\overline{\alpha}d^2\eta_d^TC_i^TG_i^TZG_iC_i\eta_d\\ &\quad + 8\alpha\overline{\alpha}d^2\widehat{\eta}_d^TC_i^TG_i^TZG_iC_i\widehat{\eta}_d.\end{aligned} \tag{63}$$

Based on these conditions, it is obtained that

$$\begin{aligned}
\mathscr{L}V(x_t) &\le x^T(t)(P_iA_i)^{\star}x(t) + x^T(t)\sum_{j=1}^{N}\pi_{ij}P_jx(t)\\
&+ e^T(t)\left[P_i(A_i - G_iC_i)\right]^{\star}e(t) - 2\overline{\alpha}e^T(t)\\
&\cdot P_iG_iC_ie(t-d) + 2e^T(t)P_ie(t)\\
&+ \alpha\eta^TC_i^TG_i^TP_iG_iC_i\eta + \overline{\alpha}\eta_d^TC_i^TG_i^TP_iG_iC_i\eta_d\\
&+ \alpha\widehat{\eta}^TC_i^TG_i^TP_iG_iC_i\widehat{\eta} + \overline{\alpha}\widehat{\eta}_d^TC_i^TG_i^TP_iG_iC_i\widehat{\eta}_d + e^T(t)\\
&\cdot\sum_{j=1}^{N}\pi_{ij}P_je(t) + x^T(t)Qx(t) - x^T(t-d)\\
&\cdot Qx(t-d) + e^T(t)Qe(t) - e^T(t-d)Qe(t-d)\\
&+ d^2x^T(t)A_i^TZA_ix(t) - x^T(t)Zx(t) + 2x^T(t)\\
&\cdot Zx(t-d) - x^T(t-d)Zx(t-d)\\
&+ 4\alpha d^2\eta^TC_i^TG_i^TZG_iC_i\eta + 4\overline{\alpha}d^2\eta_d^TC_i^TG_i^TZG_iC_i\eta_d\\
&+ 4\alpha d^2\widehat{\eta}^TC_i^TG_i^TZG_iC_i\widehat{\eta} + 4\overline{\alpha}d^2\widehat{\eta}_d^TC_i^TG_i^TZG_iC_i\widehat{\eta}_d\\
&+ 2d^2\left[(A_i - \alpha G_iC_i)e(t) - \overline{\alpha}G_iC_ie(t-d)\right]^T\\
&\times Z\left[(A_i - \alpha G_iC_i)e(t) - \overline{\alpha}G_iC_ie(t-d)\right]\\
&+ 2\alpha\overline{\alpha}d^2\left[G_iC_i(e(t-d) - e(t))\right]^T\\
&\cdot Z\left[G_iC_i(e(t-d) - e(t))\right]\\
&+ 8\alpha\overline{\alpha}d^2\eta^TC_i^TG_i^TZG_iC_i\eta\\
&+ 8\alpha\overline{\alpha}d^2\eta_d^TC_i^TG_i^TZG_iC_i\eta_d\\
&+ 8\alpha\overline{\alpha}d^2\widehat{\eta}^TC_i^TG_i^TZG_iC_i\widehat{\eta}\\
&+ 8\alpha\overline{\alpha}d^2\widehat{\eta}_d^TC_i^TG_i^TZG_iC_i\widehat{\eta}_d - e^T(t)Ze(t) + 2e^T(t)\\
&\cdot Ze(t-d) - e^T(t-d)Ze(t-d).
\end{aligned} \tag{64}$$

Based on conditions (20) and (21) and above inequalities, it is obtained that (64) is implied by

$$\begin{aligned}
\mathscr{L}V(x_t) &\le \xi^T(t)\left(\begin{bmatrix}\Omega_{i1} & \Omega_{i2} & Z & 0\\ * & \Omega_{i3} & 0 & \Psi_{i3}\\ * & * & \Omega_{i4} & \Omega_{i5}\\ * & * & * & \Omega_{i6}\end{bmatrix}\right.\\
&+ 2\alpha\overline{\alpha}d^2\begin{bmatrix}0\\ -C_i^TG_i^T\\ 0\\ C_i^TG_i^T\end{bmatrix}Z\begin{bmatrix}0\\ -C_i^TG_i^T\\ 0\\ C_i^TG_i^T\end{bmatrix}^T\\
&+ 2d^2\left.\begin{bmatrix}0\\ \left(A_i - \alpha C_i^TG_i\right)^T\\ 0\\ -\overline{\alpha}C_i^TG_i^T\end{bmatrix}Z\begin{bmatrix}0\\ \left(A_i - \alpha C_i^TG_i\right)^T\\ 0\\ -\overline{\alpha}C_i^TG_i^T\end{bmatrix}^T\right)\\
&\cdot\xi(t).
\end{aligned} \tag{65}$$

By using similar methods given in Theorems 3 and 6, condition (65) is obtained easily from inequality (59) with representation (23). This completes the proof. □

4. Numerical Examples

Example 1. Consider a delayed Markovian jump system of form (1), whose parameters are described to be

$$\begin{aligned}
A_1 &= \begin{bmatrix}-1.5 & 0.1\\ 1 & -0.8\end{bmatrix},\\
C_1 &= \begin{bmatrix}0.1 & 0.6\\ 0.4 & 0.1\end{bmatrix},\\
A_2 &= \begin{bmatrix}-0.9 & -0.2\\ 0.8 & -0.9\end{bmatrix},\\
C_2 &= \begin{bmatrix}-0.2 & 0.5\\ -0.3 & -0.2\end{bmatrix}.
\end{aligned} \tag{66}$$

The transition rate matrix is given as

$$\Pi = \begin{bmatrix}-0.5 & 0.5\\ 0.6 & -0.6\end{bmatrix}. \tag{67}$$

Firstly, we design an observer with form (9). Letting $d = 0.3$, $\varepsilon_1 = 0.3$, $\varepsilon_2 = 0.2$, $\varepsilon_{d1} = 0.4$, and $\varepsilon_{d2} = 0.1$, by Theorem 3, the gains of observer (9) are computed as

$$\begin{aligned}
G_1 &= \begin{bmatrix}0.0902 & 0.2853\\ 0.2443 & 0.2980\end{bmatrix},\\
G_2 &= \begin{bmatrix}-0.1308 & -0.0389\\ -0.0230 & -0.4683\end{bmatrix}.
\end{aligned} \tag{68}$$

Applying the above designed observer, under the initial condition $x_0 = [1 \quad -1 \quad -1 \quad 1]^T$, we have the state responses of systems (1) and (10) given in Figure 1, while the simulation of the corresponding operation mode is given in Figure 2.

When another observer (47) is designed, its gains could be computed by Theorem 6 and given as

$$\begin{aligned}
G_1 &= \begin{bmatrix}0.0855 & 0.3848\\ 0.3415 & 0.2380\end{bmatrix},\\
G_2 &= \begin{bmatrix}-0.1079 & -0.0338\\ -0.0148 & -0.5234\end{bmatrix},
\end{aligned} \tag{69}$$

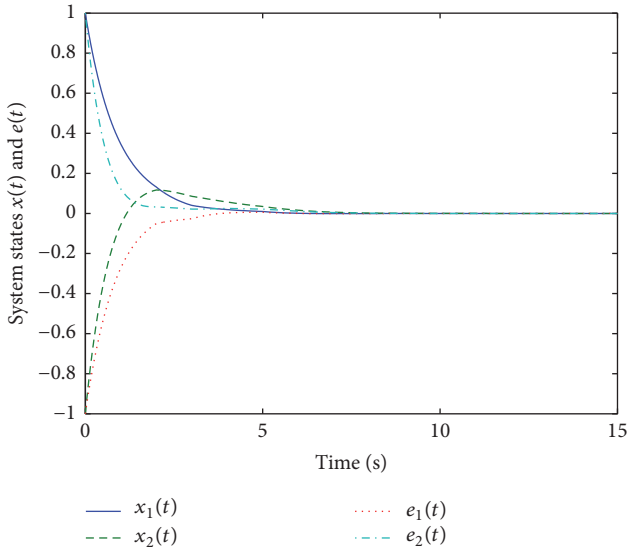

Figure 1: The state responses of systems (1) and (10).

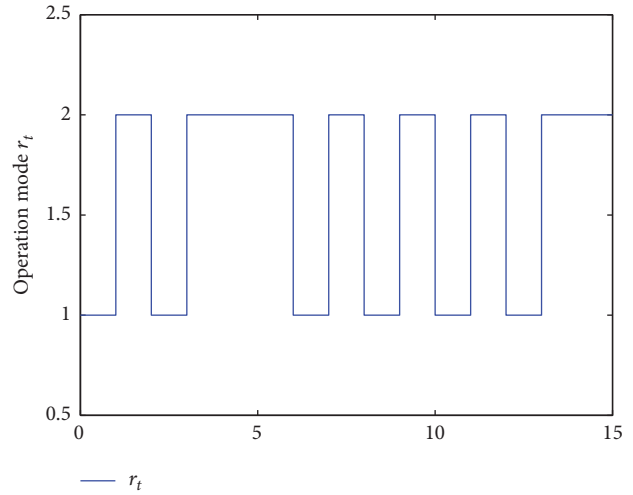

Figure 2: The simulation of operation mode.

where the corresponding parameters are the same as the above ones. At the same time, by Theorem 7, the gains of observer (57) are computed to be

$$G_1 = \begin{bmatrix} 0.2832 & 0.9648 \\ 0.2265 & 0.1486 \end{bmatrix}, \quad G_2 = \begin{bmatrix} 0.1489 & 0.8130 \\ -0.3814 & -2.0525 \end{bmatrix}. \tag{70}$$

Under the same initial condition, the state curves of the corresponding systems are simulated in Figures 3 and 4, respectively. Based on these simulations, it is seen that the designed observers are all useful and also demonstrate the utility of the proposed methods.

In order to further demonstrate the effects of output saturation existing in different forms, more comparisons among

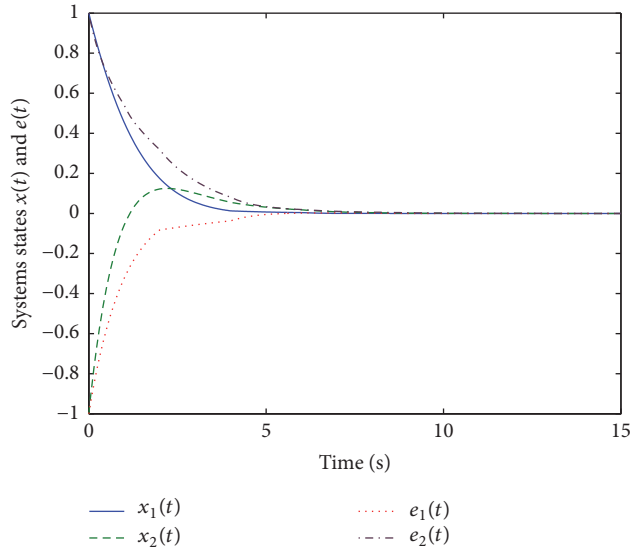

Figure 3: The state responses of systems (1) and (47).

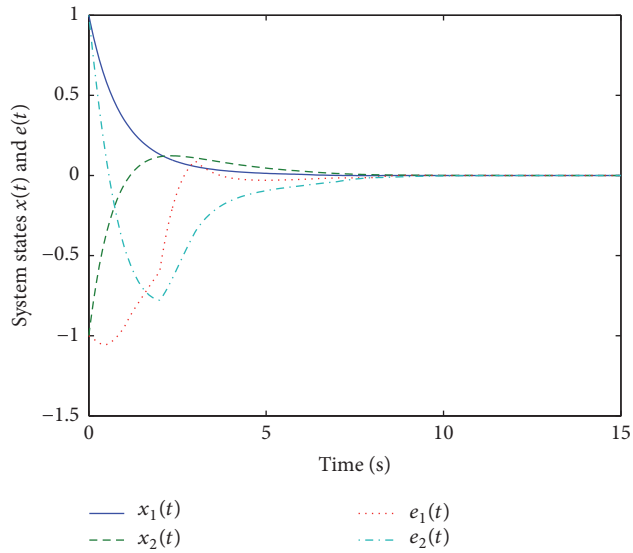

Figure 4: The state responses of systems (1) and (57).

them will be done in the following. Firstly, we consider the relationship between probability α and allowable maximum d. Based on Theorems 3–7, the maximum allowable d along with α is given in Table 1, whose simulation is carried out in Figure 5. From this simulation, it is seen that observer (9) is the least conservative, while observer (56) has the largest conservatism.

Next, we consider the effects of parameters ε_i and ε_{di}. In order to demonstrate their effects clearly, without loss of generality, matrix A_1 is assumed to be

$$A_1 = \begin{bmatrix} -1 & 0.1 + \delta \\ 1 & -0.8 \end{bmatrix}, \tag{71}$$

where δ is a positive scalar to be determined, and the other matrices are constant. Based on Theorem 3, the allowable

Table 1: The allowable maximum d for different α.

α	0	0.3	0.5	0.8	1
Theorem 3	0.927	0.943	0.955	0.976	0.999
Theorem 6	0.918	0.928	0.936	0.958	0.999
Theorem 7	0.207	0.273	0.313	0.390	0.470

Table 2: The allowable $\delta_{\max}$ for different pair $(\varepsilon_1, \varepsilon_2)$.

	$\varepsilon_2 = 0.1$	$\varepsilon_2 = 0.4$	$\varepsilon_2 = 0.6$	$\varepsilon_2 = 0.9$
$\varepsilon_1 = 0.1$	0.9450	0.9370	0.9340	0.9300
$\varepsilon_1 = 0.4$	0.9000	0.8930	0.8900	0.8860
$\varepsilon_1 = 0.6$	0.8760	0.8690	0.8650	0.8610
$\varepsilon_1 = 0.9$	0.8440	0.8370	0.8340	0.8300

Table 3: The allowable $\delta_{\max}$ for different pair $(\varepsilon_1, \varepsilon_2)$.

	$\varepsilon_2 = 0.1$	$\varepsilon_2 = 0.4$	$\varepsilon_2 = 0.6$	$\varepsilon_2 = 0.9$
$\varepsilon_1 = 0.1$	0.9390	0.9330	0.9300	0.9260
$\varepsilon_1 = 0.4$	0.8950	0.8900	0.8870	0.8830
$\varepsilon_1 = 0.6$	0.8710	0.8660	0.8630	0.8590
$\varepsilon_1 = 0.9$	0.8400	0.8350	0.8320	0.8280

Table 4: The allowable $\delta_{\max}$ for different pair $(\varepsilon_1, \varepsilon_2)$.

	$\varepsilon_2 = 0.1$	$\varepsilon_2 = 0.4$	$\varepsilon_2 = 0.6$	$\varepsilon_2 = 0.9$
$\varepsilon_1 = 0.01$	0.1960	0.1220	0.0870	0.0430
$\varepsilon_1 = 0.05$	0.1690	0.1020	0.0690	0.0260
$\varepsilon_1 = 0.10$	0.1410	0.0800	0.0480	0.0050
$\varepsilon_1 = 0.40$	0.0390	—	—	—

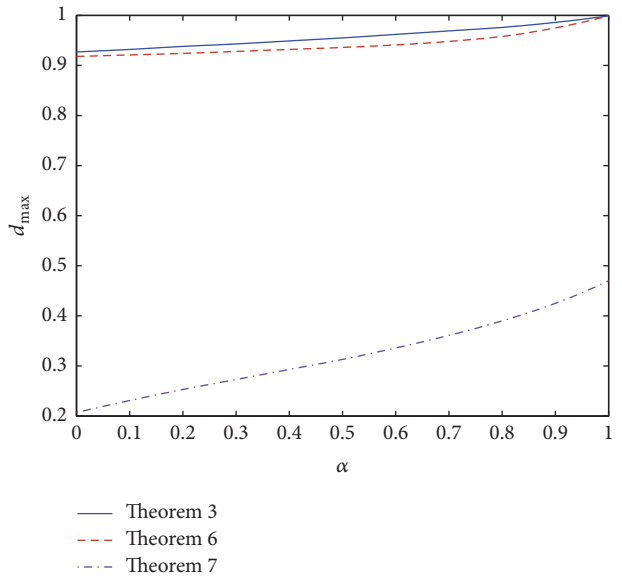

Figure 5: The curves of $d_{\max}$ along with α.

maximum $\delta \triangleq \delta_{\max}$ along with different pair $(\varepsilon_1, \varepsilon_2)$ is listed in Table 2. Similarly, Tables 3 and 4 are obtained by applying Theorems 6 and 7, respectively. Based on these tables, the simulation of correlation between pair $(\varepsilon_1, \varepsilon_2)$ and $\delta_{\max}$ is shown Figures 6 and 7. From Figure 6, it is seen that Theorem 3 related to observer (10) is less conservative than Theorem 6 corresponding to observer (47). From their forms, it is seen in this example that the delay term in output has a negative effect. However, the differences between them are very small. To the contrary, there is an advantage that the nondelay state of observer (47) is not necessarily available online, which could be replaced by a delay one with some probability. In this sense, it is said that observer (47) is better in terms of having less application constraints. As for Figure 7, it is concluded that observer (57) is the most conservative. The main reason is that a more output saturation is included and has a large negative effect in reducing performance. Similarly, we could also make a correlation between pair $(\varepsilon_{d1}, \varepsilon_{d2})$ and $\delta_{\max}$. Based on Theorems 3–7, the allowable $\delta_{\max}$ for different pair $(\varepsilon_{d1}, \varepsilon_{d2})$ are presented in Tables 5–7. From these tables, a similar conclusion could be obtained where Theorem 3 designed for observer (10) is superior over Theorems 6 and 7. Among them, it is found that the most conservative one is observer (57) obtained from Theorem 7. In addition, the corresponding simulations of such correlations between pair $(\varepsilon_{d1}, \varepsilon_{d2})$ and $\delta_{\max}$ could be obtained easily and will give the same conclusion, which are omitted here.

Table 5: The allowable $\delta_{\max}$ for different pair $(\varepsilon_{d1}, \varepsilon_{d2})$.

	$\varepsilon_{d2} = 0.1$	$\varepsilon_{d2} = 0.4$	$\varepsilon_{d2} = 0.6$	$\varepsilon_{d2} = 0.9$
$\varepsilon_{d1} = 0.1$	0.9470	0.9420	0.9390	0.9350
$\varepsilon_{d1} = 0.4$	0.9110	0.9080	0.9060	0.9030
$\varepsilon_{d1} = 0.6$	0.8890	0.8860	0.8840	0.8820
$\varepsilon_{d1} = 0.9$	0.8580	0.8550	0.8540	0.8510

Table 6: The allowable $\delta_{\max}$ for different pair $(\varepsilon_{d1}, \varepsilon_{d2})$.

	$\varepsilon_{d2} = 0.1$	$\varepsilon_{d2} = 0.4$	$\varepsilon_{d2} = 0.6$	$\varepsilon_{d2} = 0.9$
$\varepsilon_{d1} = 0.1$	0.9440	0.9390	0.9370	0.9330
$\varepsilon_{d1} = 0.4$	0.9060	0.9020	0.9000	0.8960
$\varepsilon_{d1} = 0.6$	0.8830	0.8790	0.8770	0.8730
$\varepsilon_{d1} = 0.9$	0.8510	0.8470	0.8450	0.8420

Table 7: The allowable $\delta_{\max}$ for different pair $(\varepsilon_{d1}, \varepsilon_{d2})$.

	$\varepsilon_{d2} = 0.1$	$\varepsilon_{d2} = 0.4$	$\varepsilon_{d2} = 0.6$	$\varepsilon_{d2} = 0.9$
$\varepsilon_{d1} = 0.01$	0.1950	0.1490	0.1210	0.0850
$\varepsilon_{d1} = 0.05$	0.1830	0.1380	0.1100	0.0730
$\varepsilon_{d1} = 0.10$	0.1660	0.1220	0.0940	0.0570
$\varepsilon_{d1} = 0.40$	0.0470	0.0110	—	—

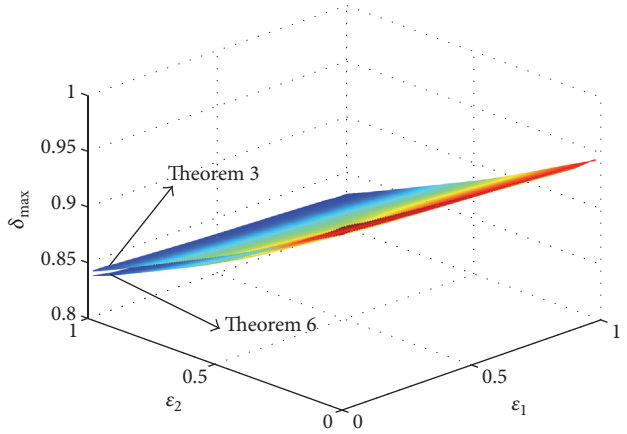

Figure 6: The simulation of correlation between pair $(\varepsilon_1, \varepsilon_2)$ and $\delta_{\max}$.

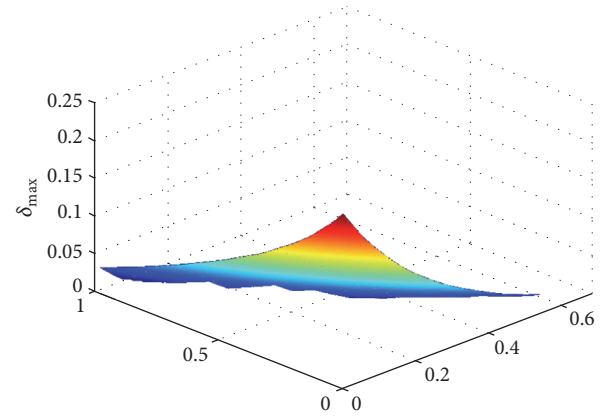

Figure 7: The simulation of correlation between pair (ϵ_1, ϵ_2) and $\delta_{\max}$.

5. Conclusion

In this paper, we have studied observer design problem of continuous-time Markovian jump systems with saturated output. First of all, a kind of state observer with output state saturation is proposed to be partially dependent. More precisely, both nondelay and delay sates are contained but occur asynchronously, whose probability distributions are embodied by the Bernoulli variable and taken into account in the observer design. By applying an improved inequality to deal with saturation terms, the existence conditions for observers with three kinds of output state saturations have been proposed with LMIs. Finally, a numerical example is used to testify the effectiveness and advantages of the presented methods.

Conflicts of Interest

The authors declare that there are no conflicts of interest regarding the publication of this paper.

Acknowledgments

This work was supported by the National Natural Science Foundation of China under Grants 61374043 and 61473140, the Program for Liaoning Excellent Talents in University under Grant LJQ2013040, and the Natural Science Foundation of Liaoning Province under Grant 2014020106.

References

[1] S.-L. Kong and Z.-S. Zhang, "Optimal control of stochastic system with Markovian jumping and multiplicative noises," *Acta Automatica Sinica*, vol. 38, no. 7, pp. 1113–1118, 2012.

[2] W. Li and Z. Wu, "Output tracking of stochastic high-order nonlinear systems with Markovian switching," *Institute of Electrical and Electronics Engineers Transactions on Automatic Control*, vol. 58, no. 6, pp. 1585–1590, 2013.

[3] S. Lakshmanan, F. A. Rihan, R. Rakkiyappan, and J. H. Park, "Stability analysis of the differential genetic regulatory networks model with time-varying delays and Markovian jumping parameters," *Nonlinear Analysis: Hybrid Systems*, vol. 14, pp. 1–15, 2014.

[4] J. Xiong, J. Lam, Z. Shu, and X. Mao, "Stability analysis of continuous-time switched systems with a random switching signal," *Institute of Electrical and Electronics Engineers Transactions on Automatic Control*, vol. 59, no. 1, pp. 180–186, 2014.

[5] J. Duan, M. Hu, Y. Yang, and L. Guo, "A delay-partitioning projection approach to stability analysis of stochastic Markovian jump neural networks with randomly occurred nonlinearities," *Neurocomputing*, vol. 128, pp. 459–465, 2014.

[6] C.-D. Zheng, Y. Zhang, and Z. Wang, "Stability analysis of stochastic reaction-diffusion neural networks with Markovian switching and time delays in the leakage terms," *International Journal of Machine Learning and Cybernetics*, vol. 5, no. 1, pp. 3–12, 2014.

[7] N. K. Kwon, B. Y. Park, and P. Park, "Less conservative stabilization conditions for Markovian jump systems with incomplete knowledge of transition probabilities and input saturation," *Optimal Control Applications and Methods*, vol. 37, no. 6, pp. 1207–1216, 2016.

[8] B. Y. Park, N. K. Kwon, and P. Park, "Stabilization of Markovian jump systems with incomplete knowledge of transition probabilities and input quantization," *Journal of The Franklin Institute*, vol. 352, no. 10, pp. 4354–4365, 2015.

[9] Y. Kao, J. Xie, and C. Wang, "Stabilization of singular Markovian jump systems with generally uncertain transition rates," *Institute of Electrical and Electronics Engineers Transactions on Automatic Control*, vol. 59, no. 9, pp. 2604–2610, 2014.

[10] H. Fan, B. Liu, W. Wang, and C. Wen, "Adaptive fault-tolerant stabilization for nonlinear systems with Markovian jumping actuator failures and stochastic noises," *Automatica*, vol. 51, pp. 200–209, 2015.

[11] M. Shen, J. H. Park, and D. Ye, "A Separated Approach to Control of Markov Jump Nonlinear Systems with General Transition Probabilities," *IEEE Transactions on Cybernetics*, vol. 46, no. 9, pp. 2010–2018, 2016.

[12] P. Shi, Y. Yin, F. Liu, and J. Zhang, "Robust control on saturated Markov jump systems with missing information," *Information Sciences*, vol. 265, pp. 123–138, 2014.

[13] L. Qiu, Y. Shi, F. Q. Yao, G. Xu, and B. G. Xu, "Network-based robust control for linear system With two-channel random packet dropout and time delays," *IEEE Transactions on Cybernetics*, vol. 45, no. 8, pp. 1450–1462, 2015.

[14] H. Zhang, Y. Shi, and J. Wang, "Observer-based tracking controller design for networked predictive control systems with uncertain Markov delays," *International Journal of Control*, vol. 86, no. 10, pp. 1824–1836, 2013.

[15] E. Tian, D. Yue, and G. Wei, "Robust control for Markovian jump systems with partially known transition probabilities and nonlinearities," *Journal of The Franklin Institute*, vol. 350, no. 8, pp. 2069–2083, 2013.

[16] H. Li, P. Shi, D. Yao, and L. Wu, "Observer-based adaptive sliding mode control for nonlinear Markovian jump systems," *Automatica*, vol. 64, pp. 133–142, 2016.

[17] X. Zhong, H. He, H. Zhang, and Z. Wang, "Optimal control for unknown discrete-time nonlinear markov jump systems using adaptive dynamic programming," *IEEE Transactions on Neural Networks and Learning Systems*, vol. 25, no. 12, pp. 2141–2155, 2014.

[18] R. Chang, Y. Fang, L. Liu, and J. Li, "Decentralized prescribed performance adaptive tracking control for Markovian jump uncertain nonlinear systems with input saturation," *International Journal of Adaptive Control and Signal Processing*, vol. 31, no. 2, pp. 255–274, 2017.

[19] M. Liu, D. W. C. Ho, and P. Shi, "Adaptive fault-tolerant compensation control for Markovian jump systems with mismatched external disturbance," *Automatica*, vol. 58, pp. 5–14, 2015.

[20] M. Q. Shen, D. Ye, and Q. G. Wang, "Event-triggered H8 filtering of Markov jump systems with general transition probabilities," *Information Sciences*, vol. 418, pp. 635–651, 2017.

[21] H. Shen, L. Su, and J. H. Park, "Reliable mixed H∞ passive control for T-S fuzzy delayed systems based on a semi-Markov jump model approach," *Fuzzy Sets and Systems*, vol. 314, pp. 79–98, 2017.

[22] F. Li, L. Wu, P. Shi, and C.-C. Lim, "State estimation and sliding mode control for semi-Markovian jump systems with mismatched uncertainties," *Automatica*, vol. 51, pp. 385–393, 2015.

[23] P. Shi, Y. Zhang, and R. Agarwal, "Stochastic finite-time state estimation for discrete time-delay neural networks with Markovian jumps," *Neurocomputing*, vol. 151, part 1, pp. 168–174, 2014.

[24] H. Zhang and J. Wang, "State estimation of discrete-time Takagi-Sugeno fuzzy systems in a network environment," *IEEE Transactions on Cybernetics*, vol. 45, no. 8, pp. 1525–1536, 2014.

[25] J. Hu, D. Chen, and J. Du, "State estimation for a class of discrete nonlinear systems with randomly occurring uncertainties and distributed sensor delays," *International Journal of General Systems*, vol. 43, no. 3-4, pp. 387–401, 2014.

[26] Z. G. Wu, P. Shi, H. Su, and J. Chu, "Stochastic synchronization of Markovian jump neural networks with time-varying delay using sampled data," *IEEE Transactions on Cybernetics*, vol. 43, no. 6, pp. 1796–1806, 2013.

[27] X. Wang, J. A. Fang, Y. H, and A. D. Dai, "Finite-time global synchronization for a class of Markovian jump complex networks with partially unknown transition rates under feedback control," *Nonlinear Dynamics*, vol. 79, no. 1, pp. 47–61, 2015.

[28] C. Allefeld and S. Bialonski, "Detecting synchronization clusters in multivariate time series via coarse-graining of Markov chains," *Physical Review E: Statistical, Nonlinear, and Soft Matter Physics*, vol. 76, no. 6, Article ID 066207, 2007.

[29] Z.-X. Li, J. H. Park, and Z.-G. Wu, "Synchronization of complex networks with nonhomogeneous Markov jump topology," *Nonlinear Dynamics*, vol. 74, no. 1-2, pp. 65–75, 2013.

[30] H. Shen, J. H. Park, Z.-G. Wu, and Z. Zhang, "Finite-time H∞ synchronization for complex networks with semi-Markov jump topology," *Communications in Nonlinear Science and Numerical Simulation*, vol. 24, no. 1-3, pp. 40–51, 2015.

[31] H. Michael, Z. Chen, X. Wang, and J. Lam, "Semi-global observer-based leader-following consensus with input saturation," *IEEE Transactions on Industrial Electronics*, vol. 61, no. 6, pp. 2842–2850, 2014.

[32] Q. Zhang, C. Schaaf, and K. C. Seto, "The Vegetation adjusted NTL Urban Index: A new approach to reduce saturation and increase variation in nighttime luminosity," *Remote Sensing of Environment*, vol. 129, pp. 32–41, 2013.

[33] W. Sun, H. Gao, and O. Kaynak, "Vibration isolation for active suspensions with performance constraints and actuator saturation," *IEEE/ASME Transactions on Mechatronics*, vol. 20, no. 2, pp. 675–683, 2015.

[34] S. Gao, H. Dong, Y. Chen, B. Ning, G. Chen, and X. Yang, "Approximation-based robust adaptive automatic train control: an approach for actuator saturation," *IEEE Transactions on Intelligent Transportation Systems*, vol. 14, no. 4, pp. 1733–1742, 2013.

[35] H. Y. Li, J. H. Hui, and P. Shi, "Output-feedback based sliding mode control for fuzzy systems with actuator saturation," *IEEE Transactions on Fuzzy Systems*, vol. 24, no. 6, pp. 1282–1293, 2016.

[36] L. Sun, Y. Wang, and G. Feng, "Control design for a class of affine nonlinear descriptor systems with actuator saturation," *Institute of Electrical and Electronics Engineers Transactions on Automatic Control*, vol. 60, no. 8, pp. 2195–2200, 2015.

[37] J. Klamkin, Y.-C. Chang, A. Ramaswamy et al., "Output saturation and linearity of waveguide unitraveling-carrier photodiodes," *IEEE Journal of Quantum Electronics*, vol. 44, no. 4, pp. 354–359, 2008.

[38] J. Klamkin, A. Ramaswamy, L. A. Johansson et al., "High output saturation and high-linearity uni-traveling-carrier waveguide photodiodes," *IEEE Photonics Technology Letters*, vol. 19, no. 3, pp. 149–151, 2007.

[39] X. Ji, Y. Sun, and H. Su, "Analysis and design for singular discrete linear systems subject to actuator saturation," *Asian Journal of Control*, vol. 13, no. 2, pp. 350–355, 2011.

[40] H. Liu, E.-K. Boukas, F. Sun, and D. W. C. Ho, "Controller design for Markov jumping systems subject to actuator saturation," *Automatica*, vol. 42, no. 3, pp. 459–465, 2006.

[41] S. Ma and C. Zhang, "H∞ control for discrete-time singular Markov jump systems subject to actuator saturation," *Journal of The Franklin Institute*, vol. 349, no. 3, pp. 1011–1029, 2012.

[42] C. A. C. Gonzaga and O. L. V. Costa, "Stochastic stabilization and induced $\ell 2$-gain for discrete-time Markov jump Lur'e systems with control saturation," *Automatica*, vol. 50, no. 9, pp. 2397–2404, 2014.

[43] L. Zhang, E.-K. Boukas, and A. Haidar, "Delay-range-dependent control synthesis for time-delay systems with actuator saturation," *Automatica*, vol. 44, no. 10, pp. 2691–2695, 2008.

[44] B. Y. Zhang, S. Y. Xu, Y. S. Zhang, and Y. M. Chu, "Delay-dependent stabilization for delayed Markovian jump systems subject to input saturation," in *Proceedings of the 29th Chinese Control Conference (CCC'10)*, pp. 5981–5986, Beijing, China, 2010.

[45] Y. S. Moon, P. Park, W. H. Kwon, and Y. S. Lee, "Delay-dependent robust stabilization of uncertain state-delayed systems," *International Journal of Control*, vol. 74, no. 14, pp. 1447–1455, 2001.

[46] G. Wang, S. Xu, and Y. Zou, "Stabilisation of hybrid stochastic systems by disordered controllers," *IET Control Theory & Applications*, vol. 8, no. 13, pp. 1154–1162, 2014.

[47] G. Wang, P. Zhang, and Q. Zhang, "A generalized robust H∞ filtering for singular Markovian jump systems and its applications," *International Journal of Robust and Nonlinear Control*, vol. 24, no. 18, pp. 3491–3507, 2014.

Hindawi
Mathematical Problems in Engineering
Volume 2017, Article ID 4163729, 14 pages
https://doi.org/10.1155/2017/4163729

Research Article

The Feedback Mechanism of Carbon Emission Reduction in Power Industry of Delayed Systems

Xiaobao Yu,[1] Zhongfu Tan,[1,2] Yuxie Zhang,[1] Daoxin Peng,[3] and Hui Xia[4]

[1]*North China Electric Power University, Beijing, China*
[2]*Yan'an University, Shaanxi, China*
[3]*China Southern Power Grid, Guangdong, China*
[4]*State Grid Cangzhou Company, Hebei, China*

Correspondence should be addressed to Zhongfu Tan; tanzhongfubeijing@126.com

Received 22 July 2017; Revised 12 October 2017; Accepted 19 October 2017; Published 10 December 2017

Academic Editor: Libor Pekař

Carbon emissions of power industry in China have accounted for more than half of the total emissions. How to decrease them is important for realizing carbon emission reduction. This paper proposes a carbon market feedback mechanism to power market, comprehensively considering the influence of generation structure, carbon intension, and technological progress on carbon emission reduction in power industry, and builds a potential model based on dynamic system. Operation system results show that the increasing trend of carbon emission can be controlled effectively but always with a lag. At the same time, sensitivity analysis results show that carbon emission reduction can be better realized by adjusting power structure and improving technological level; the former can reduce 32% and the latter can reduce 60% at most.

1. Introduction

In the 21st century, climate change has been one of the most serious problems; carbon dioxide, discharged by fossil fuel combustion, plays the main role in causing global greenhouse effect, in which discharge by thermal power accounts for more than half of the total emissions. Facing increasing environmental costs, environmental pollution treatment simply depending on administrative control lacks persistence [1]. Greenhouse gas emission reduction needs close international cooperation because of its wide scope, so environmental problems can be solved effectively by market mechanism [2–4].

In the research of controlling carbon dioxide emissions through market mechanism, international and domestic academics have made some valuable achievements. Emissions trading is an effective measure to promote carbon emission reduction. The theory of emissions trading comes from the "Pigovian Tax." Pigou, who is welfare economist, advocates punitive emissions or rewards for emission-controlled enterprises, which could control pollution and protect the environment more effectively [5]. The pioneering research in the field of air pollution control, made by Croker, further promotes the development of emissions trade theory [6]. Initial carbon emission allocation system, proposed by Hahn, is an important mechanism, which will affect transactional efficiency under imperfect competition [7]. Further researches show that the initial allocation will affect enterprise's financial burden and competitiveness, and the key factors that affect competitiveness include energy intensity, emissions reduction technology, and market demand elasticity [8, 9].

China's research on carbon emission reduction mechanism is slightly later than other countries. From the perspective of China's carbon market, it is appropriate to adopt an allocation method at present, which is free allocation as the main and paid quotas for the auxiliary [10, 11]. Changsheng et al. modeled a two-stage dynamic game, taking two typical iron and steel enterprises as research object, and investigated the effects of unified carbon tax and differential carbon tax on reduction cost, social economic benefit, and enterprise competitiveness [12]. Chen and Teng developed an international cooperation carbon reduction mechanism, which can deal with perfect competition and monopoly carbon market

structure [13]. Wu et al. examined CO_2 emission efficiency and productivity in 286 Chinese cities under different production scenarios using a nonradial directional distance function approach and found that total-factor emission efficiency varies considerably across regional and different-sized city groups [14]. Wong et al. examined various energy-related carbon dioxide (CO_2) reduction measures and demonstrated that the influence of users on CO_2 reduction is significant and compatible with the influence of water-efficient showerheads [15].

This paper puts forward a set of feedback mechanisms, which applies to the status quo of domestic power industry carbon emissions. Through the carbon market feedback to the electricity market, it restrains carbon emissions growth in power industry. With system dynamics as a platform, this paper builds carbon emission reduction potential model in power industry, sets related parameters according to different scenarios, takes power structure, carbon intensity, and technology progress for sensitivity analysis, and verifies the feasibility and effectiveness of the feedback mechanism according to the operation results.

2. Materials and Methods

2.1. Carbon Market Feedback Structure. China's per unit electricity carbon emission is 1.3–1.4 times that of the United States; in the meantime, the power industry is one of the larger proportion industries in total carbon emissions. How to effectively control carbon emission is the key point for future time. Exploring carbon reduction potential and realization path in power industry is the critical path in the process of developing low carbon economy in our country [16–19]. Considering the affinity between carbon market and power market, this paper builds a carbon market feedback structure to power market through controlling important factors in carbon market; it affects the carbon emissions in power market adversely. The feedback structure mainly includes two feedback loops, which was shown in Figure 1.

Loop 1. The growth of thermal power generation increases coal consumption and pollution emissions, reduces the opportunities and income, which comes from power suppliers to participate in the emissions reduction trading, thus improving carbon emission trading cost, reduces the proportion of thermal power generation relatively, and reduces thermal power generation, which constitutes the negative feedback loop in carbon emission trading link.

Loop 2. The growth of power consumption increases thermal power generation and then increases carbon emission in power industry, which results in an increase of carbon emissions throughout the market. Under the condition that GDP growth remains the same, carbon emissions intensity was relatively increased and power consumption growth slows down and thus reduces electricity consumption, which constitutes the negative feedback loop in carbon emission intensity control link.

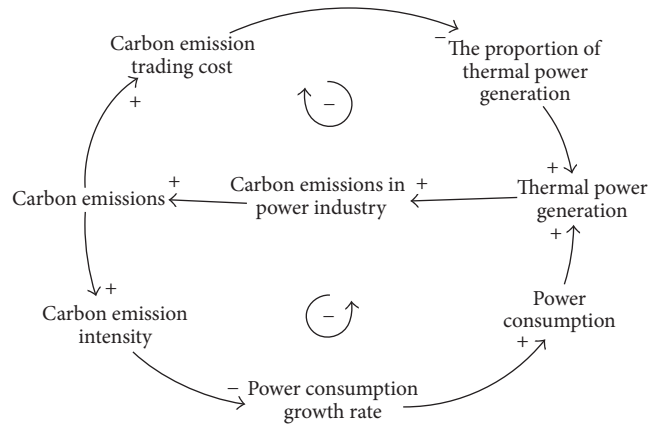

Figure 1: System basic variable causal loop diagram.

2.2. Carbon Reduction Potential System Dynamics Model. According to the analysis of system structure and the modeling principle of system dynamics, the software Vensim was used to draw carbon reduction potential analysis model in power industry [20–23]. The model includes power generation subsystem and carbon emissions subsystem; the former is divided into two modules, power demand and power generation structure, and the latter is also divided into two modules, carbon emissions trading and carbon emission intensity control.

Modeling language adopts DYNAMO; in the equation, L expresses state variable, R expresses rate variable, A expresses auxiliary variable, and DT expresses time step between moment J and moment K.

2.2.1. Power Demand Module. The system dynamic model of power demand module was shown at the bottom-right part in Figure 2. Power demand, affected by social economic level, is the main factor to define generation, which in turn affects the power generation coal consumptions and emissions. This module calculates power demand on the basis of accumulating GDP by industry [24, 25]. In the meantime, considering the consumer power sensitivity to price changes, the energy price elasticity coefficient was introduced to calculate power demand changes caused by price changes, expressed in the following formulas:

$$T_P.JK = \mathrm{INTEG}\left(D * \left(P_B.J - P_D.J\right), T_P.J\right) \tag{1}$$

$$P_B.K = T_P.K * \xi_B \tag{2}$$

$$P_D.K = T_P.K * \xi_D \tag{3}$$

$$\begin{aligned}&\mathrm{GDP}.JK\\ &\quad = \mathrm{INTEG}\left(D * \left(\Delta\mathrm{GDP}.K - \Delta\mathrm{GDP}.J\right), \mathrm{GDP}.J\right)\end{aligned} \tag{4}$$

$$\Delta\mathrm{GDP}.K = \mathrm{GDP}.J * \alpha \tag{5}$$

$$P_{\mathrm{GDP}}.K = \frac{\mathrm{GDP}.K}{T_P.K} \tag{6}$$

$$\beta = \beta_1 P_{\mathrm{GDP}}.K + \beta_2 * \alpha + \beta_3 * \chi + \varepsilon \tag{7}$$

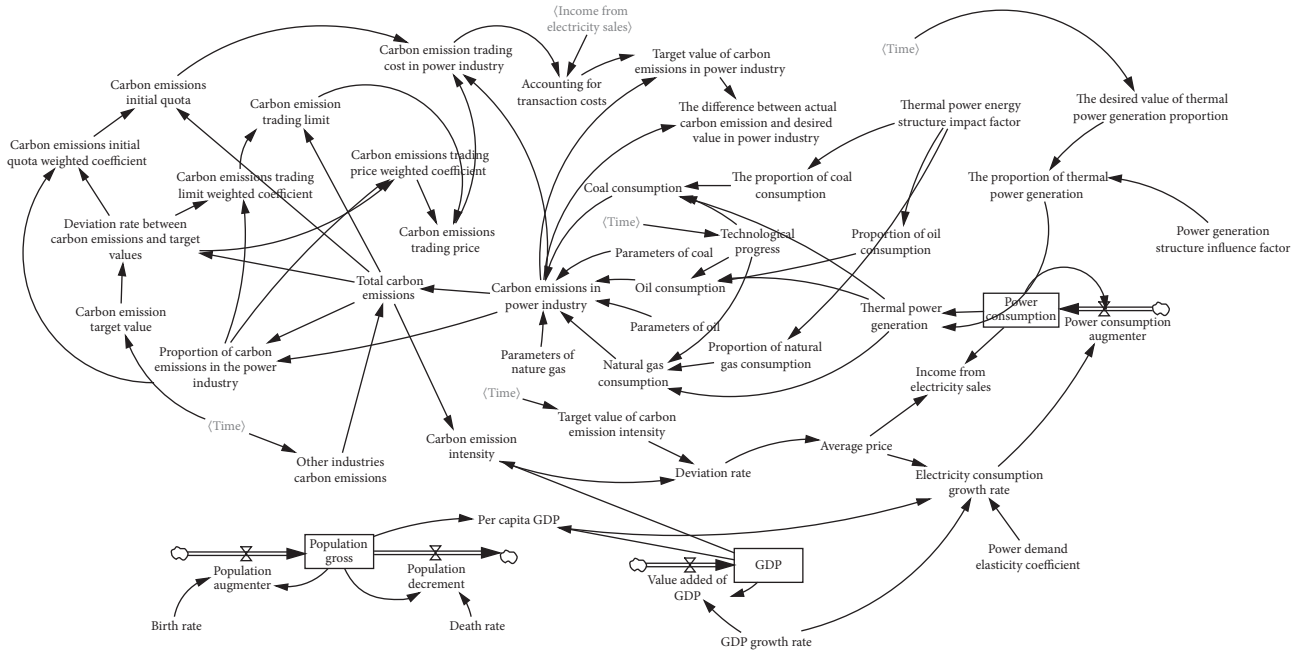

Figure 2: Carbon reduction potential system dynamics model in power industry.

$$\Delta C_E.K = C_E.J * (1 + \beta) \tag{8}$$

$$C_E.K = \text{INTEG}\left(D * \left(\Delta C_E.K - \Delta C_E.J\right), C_E.J\right), \tag{9}$$

where T_P expresses population gross; $.K$ expresses K time node; $.J$ expresses J time node; D expresses time period from J to K; P_B expresses population augmenter; ξ_B expresses birth rate; P_D expresses population decrement; ξ_D expresses death rate; GDP expresses gross domestic product; ΔGDP expresses value added of gross domestic product; α expresses GDP growth rate; P_{GDP} expresses per capita GDP; β expresses electricity consumption growth rate; $\beta_1, \beta_2, \beta_3$, respectively, express the fitting parameters of per capita GDP, GDP growth rate, and power demand elasticity; χ expresses power demand elasticity coefficient; ε expresses error coefficient of fitting function; ΔC_E expresses power consumption augmenter; C_E expresses power consumption.

2.2.2. Power Generation Structure Module. The system dynamic model of power generation structure module was shown at the upper-right part in Figure 2. This paper mainly researches the carbon reduction potential in power industry, so only the thermal power generating part was studied. This module introduces power generation structure impact factors to represent the desired thermal power ratio; for thermal power generation energy structure, thermal power energy structure impact factors were used to express the proportion of each fuel.

$$P_E.K = C_E.K * \phi \tag{10}$$

$$\delta_C = \eta * \kappa_1 \tag{11}$$

$$\delta_O = \eta * \kappa_2 \tag{12}$$

$$\delta_G = \eta * \kappa_3 \tag{13}$$

$$T_C.K = P_E.K * \delta_C \tag{14}$$

$$T_O.K = P_E.K * \delta_O \tag{15}$$

$$T_G.K = P_E.K * \delta_G \tag{16}$$

$$\phi.K = \text{DELAY}\left(o_\phi.K - \rho_{E_P}.J * \gamma, DT\right), \tag{17}$$

where P_E expresses thermal power generation; ϕ expresses the proportion of thermal power generation; δ_C expresses the proportion of coal consumption; δ_O expresses the proportion of oil consumption; δ_G expresses the proportion of natural gas consumption; η expresses power generation structure impact factors; $\kappa_1, \kappa_2, \kappa_3$, respectively, express the proportion parameters of three kinds of energy; T_C expresses coal consumption; T_O expresses oil consumption; T_G expresses natural gas consumption; o_ϕ expresses the desired value of thermal power generation proportion; ρ_{E_P} expresses the difference between actual carbon emission and desired value in power industry; γ expresses delay coefficient; DELAY1(f, t) is the delay function of system dynamics, f is the delay value, and t is delay time. In tape (17), considering the lag nature of enacting the actual proportion of thermal power generation, the delay link was set in the power generation structure model; the delay time is the interval from moment J to moment K.

2.2.3. Carbon Emissions Trading Module. The system dynamic model of carbon emissions trading module was shown at the upper-left part in Figure 2, which mainly studies the influence of carbon emissions on the carbon emissions trading market, including carbon emissions initial quota,

transaction amount, and transaction price, expressed in the following formulas:

$$\begin{aligned} E_C.K &= T_C.K * \mu_C + T_O.K * \mu_O + T_G.K * \mu_G \\ \Delta E_C.K &= E_C.K - E_C.J \\ \Delta I_C.K &= \mathrm{DELAY}\left(\Delta E_C.J + \Delta E_U.J, DT\right) \\ I_C.K &= \mathrm{INTEG}\left(\Delta I_C.K, I_C, J\right), \end{aligned} \tag{18}$$

where E_C expresses carbon emissions in power industry; μ_C, μ_O, μ_G, respectively, express the carbon emissions coefficient of three kinds of energy; ΔE_C expresses value added of carbon emissions in power industry; ΔI_C expresses value added of industrial carbon emissions; ΔE_U expresses value added of other industries carbon emissions; I_C expresses total carbon emissions.

Because of the delay when counting up the value added of carbon emissions, a delay link needs to be set; the delay time is the interval from moment J to moment K. The value added of other industries was forecasted according to history values.

In order to better study the influence of carbon emissions on the carbon emissions trading market, this paper sets a desired value of carbon emissions and, according to the deviation rate between the carbon emission actual value and the carbon emission target value, calculates the carbon emissions initial quota weighted coefficient, the carbon emissions trading limit weighted coefficient, and the carbon emissions trading price weighted coefficient. Because of the deviation rate, delay link was introduced.

$$\begin{aligned} \rho_{E_P}.K &= \mathrm{DELAY}\left(I_C.K - O_{I_C}.J, DT\right) \\ \varpi_1.K &= \frac{\rho_{E_P}}{E_P}.K * \sigma_1 \\ \varpi_2.K &= \frac{\rho_{E_P}}{E_P}.K * \sigma_2 \\ \varpi_3.K &= \frac{\rho_{E_P}}{E_P}.K * \sigma_3, \end{aligned} \tag{19}$$

where O_{I_C} expresses the carbon emission target value; ϖ_1 expresses the carbon emissions initial quota weighted coefficient; ϖ_2 expresses the carbon emissions trading limit weighted coefficient; ϖ_3 expresses the carbon emissions trading price weighted coefficient; $\sigma_1, \sigma_2, \sigma_3$ express corrected parameter of three weighted coefficients.

One thing to note is that these weighting coefficients refer in particular to the distributable initial quota of power industry, tradable credits of power industry, and trading price of power industry.

$$E_{\mathrm{QC}}.K = I_C.K * \varpi_1 \tag{20}$$

$$E_{\mathrm{TRC}}.K = I_C.K * \varpi_2 \tag{21}$$

$$E_{PC}.K = I_C.K * \varpi_3 * \left(1 + \vartheta * \frac{E_{\mathrm{TRC}}}{I_C}\right) \tag{22}$$

$$C_{\mathrm{EC}}.K = \left(E_C.K - E_{\mathrm{QC}}.K\right) * E_{PC}.K \tag{23}$$

$$\begin{aligned} O_{\mathrm{EC}}.K = E_C.K * \mathrm{IF\_THEN\_ELSE}\Bigg(&\frac{C_{\mathrm{EC}}.K - C_{\mathrm{EC}}.J}{C_{\mathrm{EC}}.J} \\ &\leq 0.05, 1.05, 0.95\Bigg) \end{aligned} \tag{24}$$

$$\rho_{E_C}.K = E_C.K - O_{\mathrm{EC}}.K, \tag{25}$$

where E_{QC} expresses the carbon emissions initial quota; E_{TRC} expresses the carbon emission trading limit; C_{EC} expresses the carbon emission trading cost in power industry; O_{EC} expresses the difference between the carbon emission actual value and the carbon emission target value in power industry.

IF THEN ELSE (a, b, c) is the conditional function of system dynamics, a expresses condition, b expresses variable value when the condition is satisfied, and c expresses variable value when the condition is not satisfied. Tape (24) shows that when the transaction variable cost ratio is not greater than 5%, carbon emissions in power industry will increase, setting coefficient as 1.05; if the ratio is greater than 1%, carbon emission in power industry will decrease, setting coefficient as 0.95. This is because when the change of carbon emission trading cost is very small, the power industry will not consider the carbon trading cost; when the change ratio is greater than 5%, the power industry will consider reducing carbon trading cost, thus reducing carbon emissions and thermal power generation.

2.2.4. Carbon Emission Intensity Control Module. The system dynamic model of carbon emissions intensity module was shown at the center part in Figure 2, which mainly studies the fact that carbon emissions affect carbon emission intensity and, in turn, affect power demand growth rate. Carbon emission intensity desired value represents expected intensity through comparing the difference between actual value and desired value to analyze the change of power demand growth rate; the formula is as follows:

$$\begin{aligned} e_C.K &= \frac{I_C.K}{\mathrm{GDP}.K} * 100\% \\ \xi &= \frac{e_C.K - O_{e_c}.K}{O_{e_c}.K} \\ \beta.K &= \beta.J * \mathrm{IF\_THEN\_ELSE}\left(\xi \leq 0, 1, 0.95\right), \end{aligned} \tag{26}$$

where e_C expresses carbon emission intensity; ξ expresses the deviation rate between the carbon emission intensity actual value and the carbon emission intensity desired value; O_{e_c} expresses the carbon emission intensity desired value.

Here, changes of power consumption growth rate are revised on the basis of power consumption growth rate calculated by per capita GDP, GDP growth rate, and power demand elasticity. When the difference between carbon emission intensity actual value and the desired value is less than zero, power consumption growth rate stays the same; if the difference is greater than zero, a weight, which is 0.95, is added to the power consumption growth rate.

Table 1: Some indicators statistics from the 2003 to 2011.

Years	Electricity consumption growth (%)	GDP per capita (ten thousand yuan/people)	GDP growth rate (%)	Electricity demand elasticity
2003	15.30	1.04	10.00	1.56
2004	15.46	1.23	10.10	1.52
2005	13.90	1.40	11.30	1.19
2006	14.16	1.64	12.70	1.15
2007	14.42	2.02	14.20	1.01
2008	5.49	2.38	9.60	0.58
2009	6.44	2.55	9.20	0.78
2010	14.77	2.98	10.40	1.27
2011	11.97	3.50	9.30	1.30

The results show that there are significant and stable positive correlations among GDP per capita, GDP growth rate, and electricity demand elasticity.

3. Results and Discussion

3.1. Parameters Setting. The data of the China economy and the power industry in 2010 are taken as a benchmark in the model; the model researched effects of carbon emission reduction in electric power industry and key influencing factors in the systems from 2015 to 2050. Among them, the growth rate forecast of electricity consumption primary considered GDP per capita, GDP growth rate, and electricity demand elasticity of the three factors. Table 1 showed the domestic GDP growth, GDP per capita, electricity demand elasticity, and electricity consumption growth in China from 2003 to 2011. On the basis of data and prediction model, in the future, Chinese power consumption growth can be expressed as

$$Y = -12.005 + 0.228X_1 + 1.101X_2 + 10.528X_3, \quad (27)$$

where X_1 expresses GDP per capita, X_2 expresses GDP growth rate, X_3 expresses electricity demand elasticity, and Y expresses electricity consumption growth.

For the control measures of carbon market can be effectively fed back to the electricity market, this model considers the deviation between the actual carbon emission and the target value and develops some weighting coefficients, including power industry carbon emissions initial quota weighted coefficient, trade quota weighted coefficient, and carbon trading price weighted coefficient. By adjusting the weighting coefficient, the model adjusts the carbon emission target and then controls the power industry carbon emissions [26, 27].

(1) Initial Quotas Weighting Factor of Power Industry Carbon Emissions. Firstly, in the case without considering other factors, initial quotas weighting factor of power industry carbon emissions is formulated in accordance with the grandfather model, which is

$$\varpi_1 = \frac{E_C}{I_C} \times 100\%. \quad (28)$$

Then, the model takes into account the goal of reducing carbon emissions to formulate a carbon emissions target; combined with the actual carbon emissions to compare, the power industry carbon emissions quotas initial weighting coefficient is adjusted based on the deviation rate, detailed as follows:

$$\varpi_1' = \frac{E_C}{I_C} \times \rho_{E_C} \times 100\%. \quad (29)$$

(2) Power Industry Carbon Emissions Trading Credits Weighting Factor. Firstly, in the case without considering other factors, initial quotas weighting factor of power industry carbon emissions is allocated in accordance with the following formula:

$$\varpi_2 = \frac{E_C}{I_C} \times 100\% \times 1.1. \quad (30)$$

Then, the model takes into account the goal of reducing carbon emissions to formulate a carbon emissions target; combined with the actual carbon emissions to compare, the power industry carbon emissions trading credits weighting factor is adjusted based on the deviation rate, detailed as follows:

$$\varpi_2' = \frac{E_C}{I_C} \times \rho_{E_C} \times 100\% \times 1.1. \quad (31)$$

(3) Power Industry Carbon Emissions Trading Price Weighting Coefficients. In order to establish an effective carbon market feedback mechanism, this model takes into account the unit power generation cost of thermal power in formulating the power sector carbon emission trading price weighted coefficient and sets a ratio of 10%, which can control the proportion of thermal power generation through the feedback of carbon emission trading price.

$$\varpi_3 = \zeta \times 10\%, \quad (32)$$

where ζ represents generation cost of thermal power.

Then, the model takes into account the goal of reducing carbon emissions to develop a carbon emissions target;

Table 2: Multiple scenarios parameter design.

	The impact factor of the power structure	Carbon intensity target factor	Impact factor of technological advances
BASE	1	1	1
CASE 1	0.9	1	1
CASE 2	0.8	1	1
CASE 3	0.7	1	1
CASE 4	0.6	1	1
CASE 5	1	0.9	1
CASE 6	1	0.8	1
CASE 7	1	0.7	1
CASE 8	1	0.6	1
CASE 9	1	1	0.9
CASE 10	1	1	0.8
CASE 11	1	1	0.7
CASE 12	1	1	0.6

combined with the actual carbon emissions to compare, power industry carbon emissions trading price weighting coefficient is adjusted based on the deviation rate, detailed as follows:

$$\varpi_3 = \zeta \times 10\% \times \rho_{E_p}. \tag{33}$$

(4) Multiple Scenarios Parameter Design. In order to analyze the impact of the key carbon emission reduction factors on the carbon emission reduction effect, which contains impact factor of power generation structure, carbon emission intensity target value, and technological progress, the model sets different parameter values to explore the system operating conditions in different scenarios (Table 2).

Among them, the impact factors of the power structure adjust the whole system by affecting thermal power generation ratio; then carbon emissions and carbon intensity are changed; the impact factors of carbon intensity target adjust the whole system by affecting carbon emission target; then carbon emissions of power industry were affected; impact factors of technical progress adjust the whole system by reducing coal consumption rate and other parameters; then carbon emissions of power industry were affected.

3.2. Baseline Conditions. Based on the simulation system constructed in this paper, parameters under the basic situation and data in 2010 are input; the operating system obtains relevant factors as shown in Table 3 (ten thousand tons/one hundred million yuan was abbreviated as T/O).

Figure 3 shows the trend situation of thermal power plants electricity generated proportion over the years; it can be seen from the figure that, in the constraints of feedback mechanisms, the proportion of thermal power plants is declining,, but the rate of decline slowed; it is explained that the proportion of thermal power plants reached a stable value; feedback system regional balance shows that feedback mechanism played a role that reduces the proportion of thermal power generation effect. Figure 4 shows the carbon intensity trends over the years; the carbon intensity target value is set to help reduce carbon emissions intensity; it can be seen from Figure 4 that the intensity of carbon emission shows a trend of first increasing and then decreasing; it is explained that the construction feedback mechanism has a period of instability; after a feedback mechanism enters into the stable phase, the carbon emission intensity is declining; it is suggested that control action of feedback mechanism to carbon emissions has hysteresis quality.

Figure 5 shows the trend of electricity consumption growth over the years; the growth of power consumption also shows a trend of first increasing and then decreasing. The growth stage is due to the rapid growth of GDP, which leads to the rapid growth of electricity consumption demand. However, due to the suppression of the growth of electricity consumption by the carbon emission intensity in the feedback mechanism, this results in decreasing part of the growth rate of power consumption. Figure 6 shows the trend of power industry carbon emissions over the years; even under constraints of feedback mechanisms, carbon emissions from the power industry are still growing year after year, which is related to the growth in demand for electricity consumption.

Figure 7 shows the trend of proportion of the power industry carbon emissions over the years; the proportion of carbon emissions from the power industry experienced a trend that first increased and then decreased; the proportion of thermal power feedback mechanism leads to slowdown of coal consumption growth; the growth rate of coal consumption is constant in other industries, so proportion of the power industry carbon emissions is declining. However, due to the cleanliness of electric power, the role of electric energy replacement appears gradually, leading to a decrease of coal consumption in other industries. As a result, the proportion of carbon emissions in the power industry has been increasing.

Table 3: Some parameters operating results under basic scenario.

Year	The proportion of thermal power generation (1)	Carbon emissions intensity (T/O)	Electricity consumption growth (1)	The proportion of the power industry carbon emission (1)	Power industry carbon emissions (ten thousand tons)	Deviation rate and the target of carbon emission intensity (1)	Cost ratio of carbon trading (1)
2010	0.800	3.1983	0.0687	0.4677	224029	0.3153	0.0043
2015	0.710	3.4633	0.0717	0.2912	279351	0.3821	0.0080
2020	0.680	3.3796	0.0717	0.2550	378294	0.3816	0.0112
2025	0.661	3.1620	0.0705	0.2533	518953	0.3548	0.0149
2030	0.648	2.9223	0.0688	0.2671	712318	0.3190	0.0200
2035	0.637	2.7073	0.0672	0.2905	974315	0.2834	0.0275
2040	0.628	2.5312	0.0659	0.3211	1326818	0.2533	0.0389
2045	0.621	2.3943	0.0649	0.3579	1800051	0.2315	0.0562
2050	0.614	2.2912	0.0643	0.3999	2436133	0.2187	0.0828

(1) refers to the unit of each parameter.

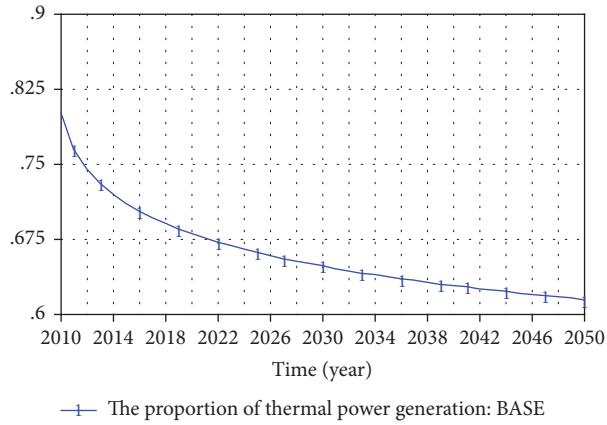

Figure 3: The trend of thermal power plants electricity generated proportion under the baseline scenario.

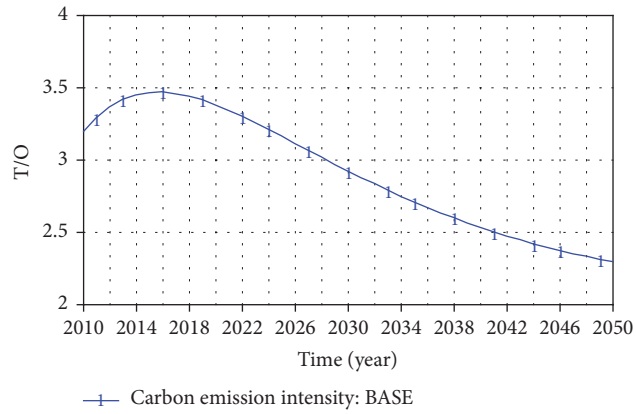

Figure 4: The trend of carbon intensity under the baseline scenario.

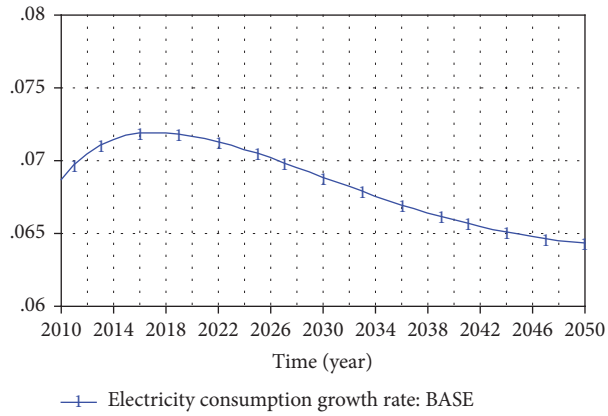

Figure 5: The trend of electricity consumption growth rate under the baseline scenario.

3.3. Key Elements Analysis. In order to study the key elements of carbon emission reduction in power industry, this paper performs sensitivity analysis on impact factors-generation structure, carbon intension, and technological progress and gets relevant conclusions according to the analysis results.

3.3.1. Generation Structure. According to the parameters in Table 3, different generation structure impact factors and operation systems were set for five scenarios, BASE, CASE 1, CASE 2, CASE 3, and CASE 4; relevant results were shown as attached list. Figure 8 shows the trend of ratio of thermal power generation under different parameters. With the adjustment of power generation structure, especially the feedback control of thermal power, the ratio shows a downward trend. In 2050, the ratio is 0.466 in CASE 4, which decreases by 24% compared with 0.614 in the baseline

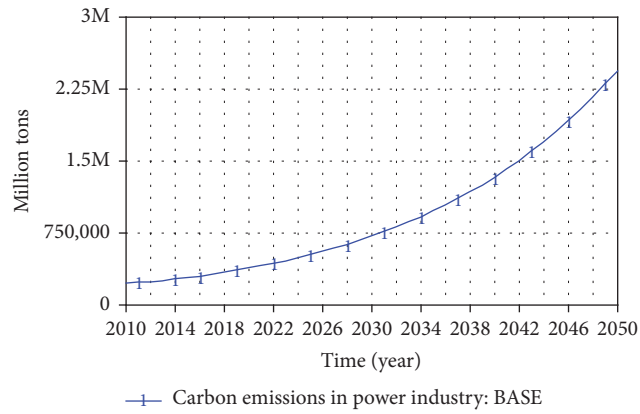

Figure 6: The trend of power industry carbon emissions under the baseline scenario.

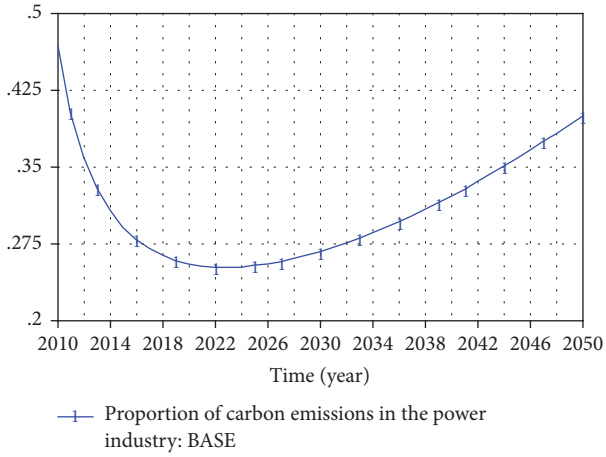

Figure 7: The trend of proportion of power industry carbon emissions under the baseline scenario.

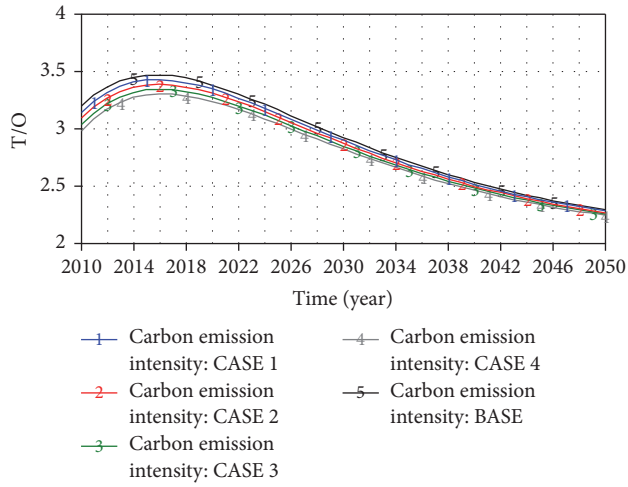

Figure 8: The trend of carbon emission intensity under different scenarios.

scenario. The control effect on thermal power is obvious, and the growth trend of carbon emission in thermal power generation is effectively suppressed.

Figure 9 shows the trend of power consumption growth under different parameter settings. With the adjustment of power generation structure, the change in electricity consumption growth is small, which was 6.38% under CASE 4, compared with 6.43% in the baseline scenario. This shows that the influence of power generation impact factor on it can be neglected.

Figure 10 shows the trend of carbon emissions in power industry under different parameter settings; Figure 11 shows the trend of carbon emission ratio in power industry; combined with attached list 3 and attached list 4, it can be seen that the adjustment of generation structure has some influence on carbon emissions and emission ratio. In 2050, carbon emission is 18.16448 billion tons under CASE 4, reduces 25%, and is lower than the baseline scenario, 24.36133 billion tons. In 2050, the emission ratio reduces 16.8%. That shows that adjusting generation structure can reduce carbon emissions, and the effect is obvious.

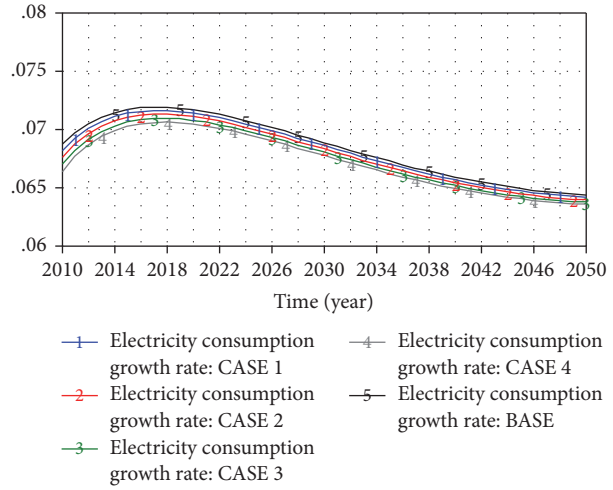

Figure 9: The trend of electricity consumption growth rate under different scenarios (1). The result is under generation structure.

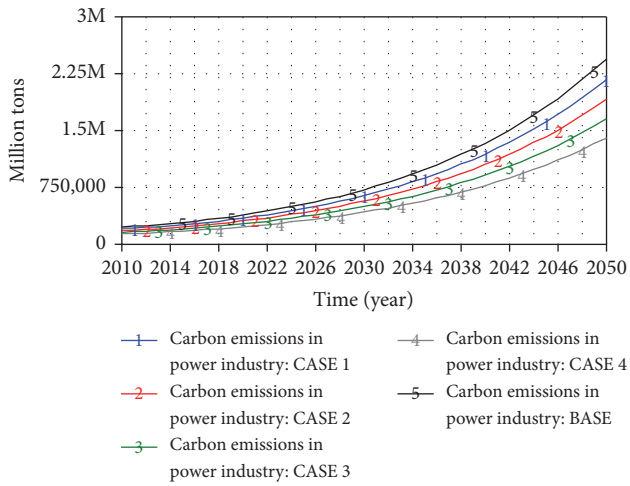

Figure 10: The trend of carbon emissions in power industry under different scenarios (1). The result is under generation structure.

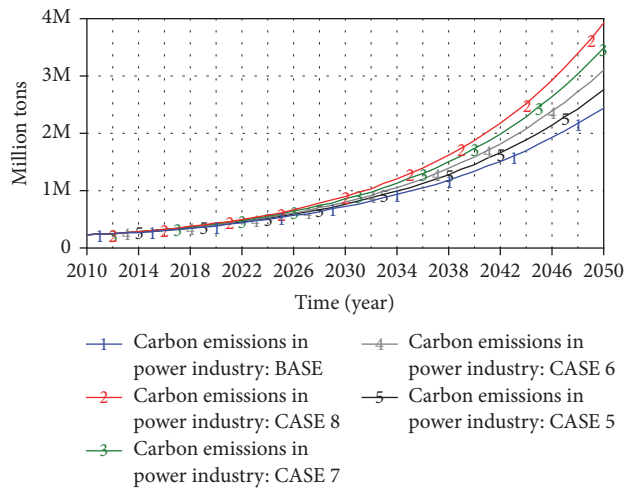

Figure 12: The trend of carbon emissions in power industry under different scenarios (2). The result is under carbon intension.

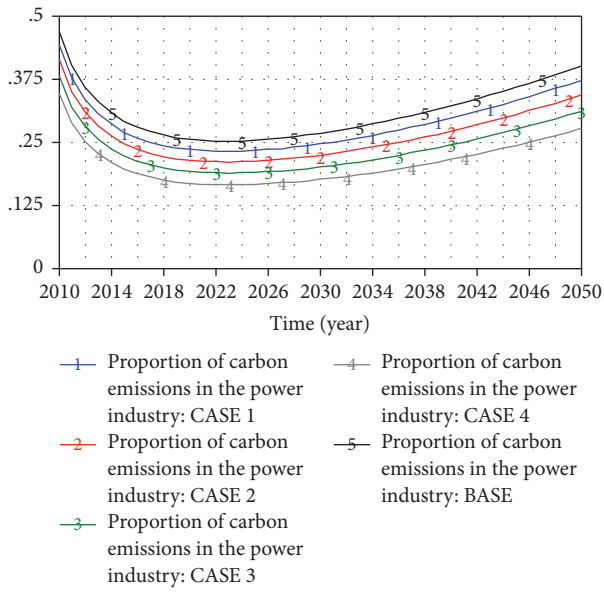

Figure 11: The trend of proportion of carbon emissions in power industry (1). The result is under generation structure.

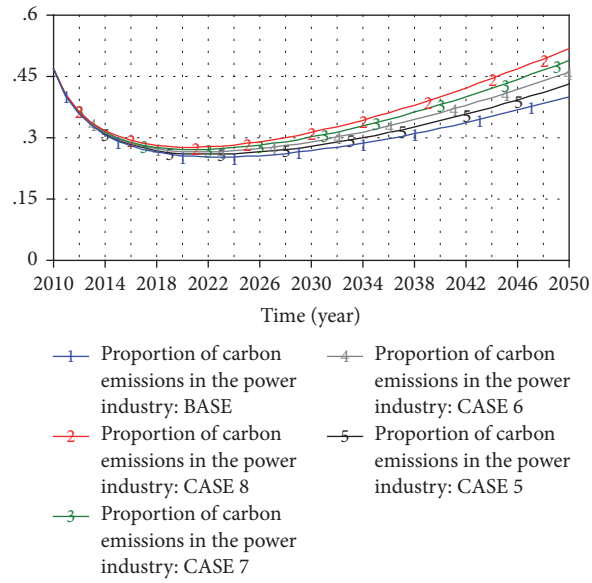

Figure 13: The trend of proportion of carbon emissions in power industry under different scenarios (2). The result is under carbon intension.

3.3.2. Carbon Intension. According to the parameters in Table 3, different carbon intension impact factors and operation systems were set for five scenarios, BASE, CASE 5, CASE 6, CASE 7, and CASE 8; relevant results were shown as attached list. Figure 12 shows the trend of carbon emissions in power industry under different scenarios; combined with attached list 5, it can be seen that carbon emissions in power industry under CASE 8 in 2050 increase 60% compared with baseline scenario. This shows that adjusting carbon intension cannot reduce carbon emission and increases it instead, which is due to the fact that the reduction of carbon intension desired value results in the increase of deviation ratio and thus influences power consumption growth and power demand growth and leads to the increase of carbon emissions. Figure 13 shows the trend of carbon emission ratio in power industry under different scenarios; the ratio under CASE 8 is obviously higher than baseline scenario, the same reason as carbon emission.

Figure 14 shows the trend of carbon intension under different parameter settings; combined with attached list 7, it can be seen that the adjustment of carbon intension impact factor has little influence on carbon intension. Figure 15 shows the trend of electricity consumption growth in different scenarios, which is 7.9% in CASE 8 in 2050 and decreases by 23% compared with 6.4% in the baseline scenario. This shows that adjusting carbon intension impact factor will

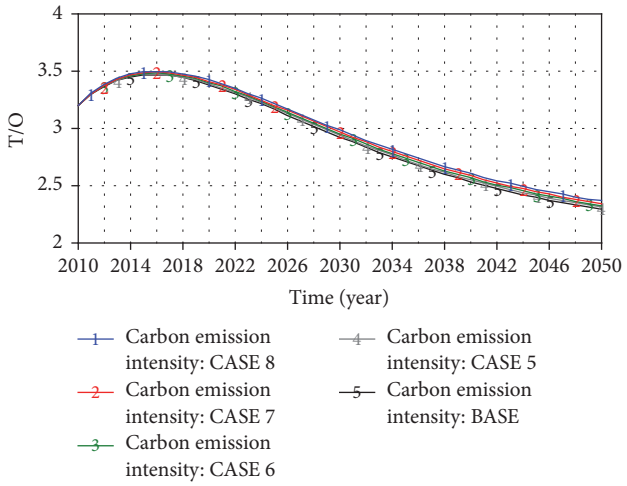

Figure 14: The trend of carbon emission intensity under different scenarios (1). The result is under carbon intension.

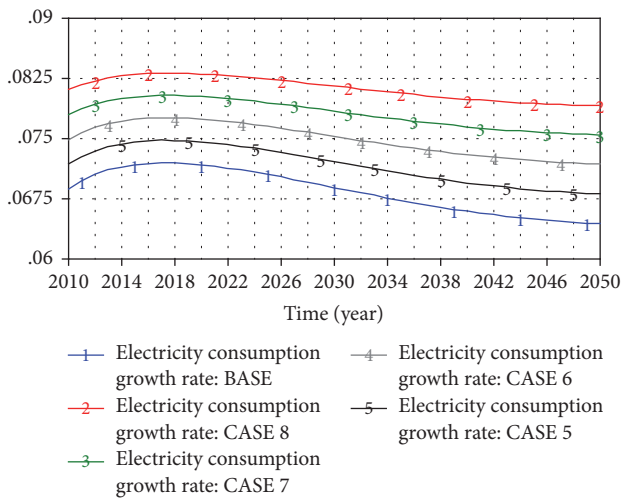

Figure 15: The trend of electricity consumption growth rate under different scenarios (2). The result is under carbon intension.

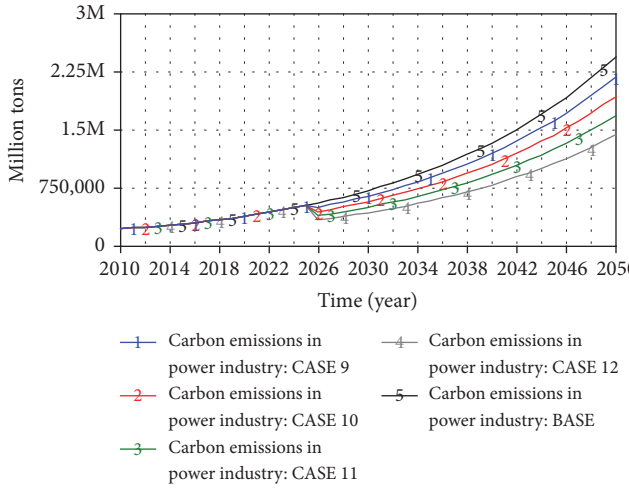

Figure 16: The trend of carbon emissions in power industry under different scenarios (3). The result is under technological progress.

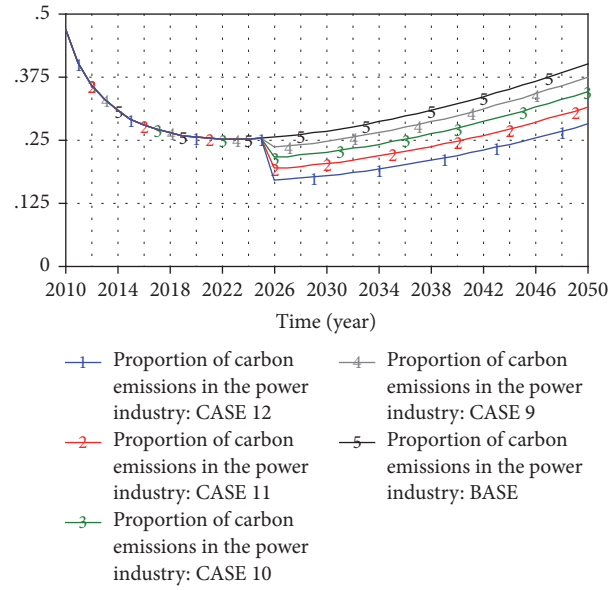

Figure 17: The trend of proportion of carbon emissions in power industry under different scenarios (2). The result is under technological progress.

increase power demand and power consumption growth and thus increase carbon emissions.

3.3.3. Technological Progress. According to the parameters in Table 3, different technological progress impact factors and operation systems were set for five scenarios, BASE, CASE 9, CASE 10, CASE 11, and CASE 12; relevant results were shown as attached list. It should be noted that the starting point of technological progress is in 2025. Figure 16 shows the trend of carbon emissions in power industry under different scenarios; it can be seen that technological progress reduces carbon emissions in power industry through affecting coal consumption rate and so forth. Carbon emission under CASE 12 in 2050 reduces by 41% compared with baseline scenario; the effect is obvious. Figure 17 shows the trend of carbon emission ratio in power industry under different scenarios; combined with attached list 10, it can be seen that the effect of reducing carbon emission ratio by technological progress is obvious, declining by up to 30%.

Figure 18 shows the trend of carbon intension under different parameter settings; combined with attached list 11, it can be seen that the adjustment of technological progress impact factor has a common influence on carbon intension; the decrease is 2%. Figure 19 shows the trend of power consumption growth under different parameter settings; combined with attached list 12, it can be seen that the adjustment of technological progress impact factor also has a common influence on power consumption growth; the range is less than 1%. Therefore, under the situation that technological progress impact factor does not affect power

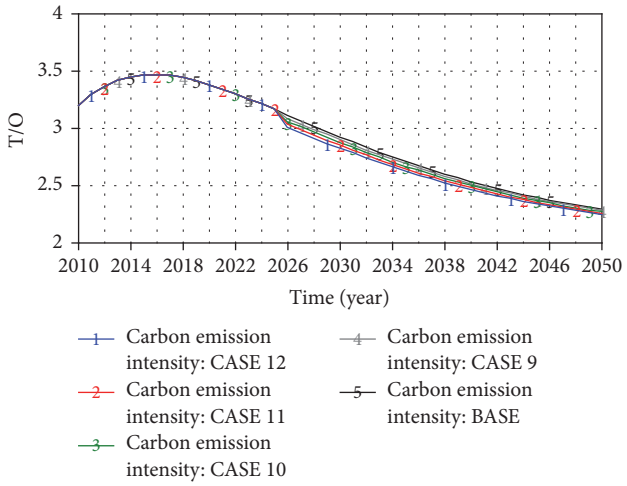

Figure 18: The trend of carbon emission intensity under different scenarios (2). The result is under technological progress.

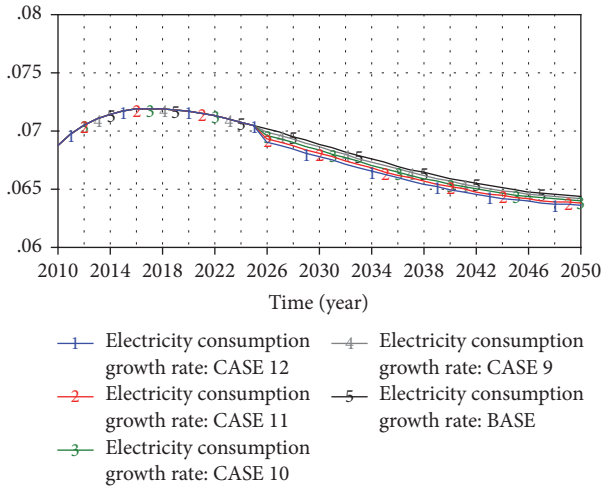

Figure 19: The trend of electricity consumption growth rate under different scenarios (3). The result is under technological progress.

consumption growth, it can effectively inhibit the growth of the carbon emissions in power industry.

3.4. Sensitivity Analysis. Through the sensitivity analysis for the key factors of carbon emission reduction in power industry, the carbon emission reduction effect of adjusting technological progress is the most obvious, the adjustment of generation structure takes second place, and the adjustment of carbon intension is the worst, which may even increase carbon emissions. The emission reduction effect of three key factors was shown in Figure 20. It can be seen from the figure that, among them, the effect of technological progress is the best (can be up to 60%); the effect of generation structure is second (can be up to 32%); the effect of carbon intension is the worst (can increase carbon emission up to 41%).

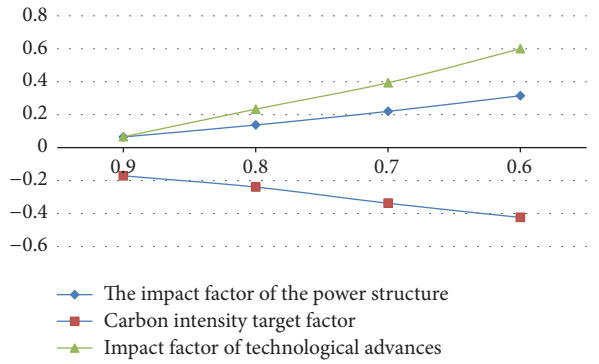

Figure 20: The trend of emission reduction factor sensitivity results.

4. Conclusions and Suggestions

Through building carbon reduction potential analysis model in power industry, this paper discusses the effectiveness of the carbon market feedback mechanism on power market, conducts the sensitivity analysis for the key factors of carbon emission reduction, and draws the following conclusions.

(1) Through running the system under the baseline scenario, the results show that the feedback mechanism constructed in this paper plays a certain role in suppressing the increase of carbon emissions in power industry, and it can be seen that there is a lag in the carbon emission feedback mechanism; from the long-term carbon emission situation, the carbon emission reduction effect in power industry is obvious.

(2) Through the sensitivity analysis of the generation structure factor, the results show that, on the basis of the carbon emission reduction feedback mechanism constructed in this paper, the adjustment of generation structure can play a better role in reducing carbon emissions, and in the best case it can reduce 32% of carbon emissions in power industry.

(3) Through the sensitivity analysis of the carbon emission intensity factor, the results show that, on the basis of the carbon emission reduction feedback mechanism constructed in this paper, the reduction of the carbon emission intensity cannot play a role in reducing carbon emissions; on the contrary, due to the increase of electricity consumption growth rate, it will lead to the increase of carbon emissions.

(4) Through the sensitivity analysis of technological progress factor, the results show that, on the basis of the carbon emission reduction feedback mechanism constructed in this paper, the improvement of technological progress level can largely realize the carbon emission reduction goal, and in the best case it can reduce 60% of carbon emissions in power industry.

Nomenclature

Symbols

T: Total value
ξ: Birth or death rate
α: GDP growth rate
β: Electricity consumption growth rate

χ: Power demand elasticity coefficient
ε: Error coefficient of fitting function
C: Consumption
ϕ: Proportion of thermal power
δ: The proportion of each energy
η: Power generation structure impact factors
κ: Proportion parameters of each energy
ϖ: Weighted coefficient
e: Emission intensity
o: The desired value of thermal power generation proportion
ρ: The difference between actual carbon emission and desired value
γ: Delay coefficient
E: Carbon emissions in power industry
μ: Carbon emissions coefficient
I: Total carbon emissions
O: Target value.

Acronyms

$.K$: K time node
$.J$: J time node
D: Time period from J to K
Δ: The amount of change
DELAY1: Delay function
INTEG: Integral function.

Conflicts of Interest

The authors declare that there are no conflicts of interest.

Acknowledgments

This paper is supported by the Fundamental Research Funds for the Central Universities (2016XS82), the National Natural Science Foundation of China (Grants nos. 71273090 and 71573084), and the Beijing Municipal Social Science Foundation (16JDYJB044).

References

[1] W. Sufeng, *Research on Allocation of Carbon Emission Rights and Abatement Mechanism for China*, Hefei University of Technology, Anhui, China, 2014.

[2] Y. Li and Y. Yu, "The use of freight apps in road freight transport for CO_2 reduction," *European Transport Research Review*, vol. 9, no. 3, 2017.

[3] S.-m. Yu and L. Zhu, "Impact of firms' observation network on the carbon market," *Energies*, vol. 10, no. 8, 2017.

[4] B. Koo, "Preparing hydropower projects for the post-paris regime: an econometric analysis of the main drivers for registration in the clean development mechanism," *Renewable & Sustainable Energy Reviews*, vol. 73, pp. 868–877, 2017.

[5] A. C. Pigou, *Wealth and Welfare*, Macmillan and collimated, New York, NY, USA, 1912.

[6] T. D. Crocker, "The structuring of atmospheric pollution control systems," *The Economics of Air Pollution*, pp. 61–86, 1966.

[7] R. W. Hahn, "Market power and transferable property rights," *The Quarterly Journal of Economics*, vol. 99, no. 4, pp. 753–765, 1984.

[8] S. Felder and R. Schleiniger, "Environmental tax reform: efficiency and political feasibility," *Ecological Economics*, vol. 42, no. 1, pp. 107–116, 2002.

[9] T. H. Edwards and J. P. Hutton, "Allocation of carbon permits within a country: a general equilibrium analysis of the United Kingdom," *Energy Economics*, vol. 23, no. 4, pp. 371–836, 2001.

[10] L. Shoude and H. Tongcheng, "A multi-objectives decision model of initial emission permits allocation," *Chinese Journal of Management Science*, vol. 11, no. 6, pp. 40–44, 2003.

[11] Z. Wenhui, "The review of initial emission permits allocation theory," *Industrial Technology and Economy*, vol. 27, no. 8, pp. 111–113, 2008.

[12] L. Changsheng, F. Ying, and Z. Lei, "The study of carbon dioxide emission intensity abatement mechanism of iron and steel industry based on two-stage game model," *Chinese Journal of Management Science*, vol. 20, no. 2, pp. 93–101, 2012.

[13] W. Chen and F. Teng, "International cooperation mechanisms for carbon reduction," *Journal of Tsinghua University (Science and Technology)*, vol. 45, no. 6, pp. 854–857, 2005.

[14] J. Wu, Z. Kang, and N. Zhang, "Carbon emission reduction potentials under different polices in Chinese cities: a scenario-based analysis," *Journal of Cleaner Production*, vol. 161, pp. 1226–1236, 2017.

[15] L.-t. Wong, K.-w. Mui, and Y. Zhou, "Carbon dioxide reduction targets of hot water showers for people in Hong Kong," *Water*, vol. 9, no. 8, p. 576, 2017.

[16] Y. Yang, W. Qiu, and D. He, "Carbon abatement game between regulator and firms under command-and-control scheme," *Systems Engineering*, vol. 30, no. 2, pp. 110–114, 2012.

[17] J. Zhou and Y. Diandian, "Studies on provincial differences, influential factors and reduction mechanisms of China's carbon dioxide emission," *Shanghai Journal of Economics*, vol. 11, pp. 65–80, 2012.

[18] L. Yalu, *System Dynamics Model on the Urban Low-Carbon Development Process*, Tianjin University, Tianjin, China, 2012.

[19] Y. Chao, *Study on Cost Optimization Models of Power Generation's Energy Consumption and Emission under Different Emission Mechanisms*, North China Electric Power University, Beijing, China, 2012.

[20] Y. Liu, L. Han, Z. Yin, and K. Luo, "A competitive carbon emissions scheme with hybrid fiscal incentives: The evidence from a taxi industry," *Energy Policy*, vol. 102, pp. 414–422, 2017.

[21] S. Zeng, X. Nan, C. Liu, and J. Chen, "The response of the Beijing carbon emissions allowance price (BJC) to macroeconomic and energy price indices," *Energy Policy*, vol. 106, pp. 111–121, 2017.

[22] R. J. Plevin, M. A. Delucchi, and M. O'Hare, "Fuel carbon intensity standards may not mitigate climate change," *Energy Policy*, vol. 105, pp. 93–97, 2017.

[23] Z. Wang, J. Zhao, and M. Li, "Analysis and optimization of carbon trading mechanism for renewable energy application in buildings," *Renewable & Sustainable Energy Reviews*, vol. 73, pp. 435–451, 2017.

[24] S. Ghosh, "Electricity supply, employment and real GDP in India: evidence from cointegration and Granger-causality tests," *Energy Policy*, vol. 37, no. 8, pp. 2926–2929, 2009.

[25] Y. Liu, X. Hu, and K. Feng, "Economic and environmental implications of raising China's emission standard for thermal power plants: an environmentally extended CGE analysis," *Resources, Conservation & Recycling*, vol. 121, pp. 64–72, 2017.

[26] L. Preusser, "Development of a thermal model for a heated steering wheel to compensate defective feedback variables," in *Proceedings of the WCX™ 17: SAE World Congress Experience*, 2017.

[27] K. Safarzyńska and J. C. van den Bergh, "Financial stability at risk due to investing rapidly in renewable energy," *Energy Policy*, vol. 108, pp. 12–20, 2017.

Hindawi
Mathematical Problems in Engineering
Volume 2017, Article ID 2505086, 12 pages
https://doi.org/10.1155/2017/2505086

Research Article

Proportional Retarded Controller to Stabilize Underactuated Systems with Measurement Delays: Furuta Pendulum Case Study

T. Ortega-Montiel,[1] R. Villafuerte-Segura,[1] C. Vázquez-Aguilera,[2] and L. Freidovich[3]

[1]*Research Center on Information Technology and Systems, Hidalgo State University, Pachuca, HGO, Mexico*
[2]*Control System Team, Ålö AB, Umeå, Sweden*
[3]*Department of Applied Physics and Electronics, Umeå University, Umeå, Sweden*

Correspondence should be addressed to R. Villafuerte-Segura; villafuerte@uaeh.edu.mx

Received 15 June 2017; Accepted 16 August 2017; Published 10 December 2017

Academic Editor: Libor Pekař

The design and tuning of a simple feedback strategy with delay to stabilize a class of underactuated mechanical systems with dead time are presented. A linear time-invariant (LTI) model with time delay of fourth order and a Proportional Retarded (PR) controller are considered. The PR controller is shown as an appealing alternative to the application of observer-based controllers. This paper gives a step forward to obtain a better understanding of the effect of output delays and related phenomena in mechatronic systems, making it possible to design resilient control laws under the presence of uncertain time delays in measurements and obtain an acceptable performance without using a derivative action. The Furuta pendulum is a standard two-degrees-of-freedom benchmark example from the class of underactuated mechanical systems. The configuration under study includes an inherent output delay due to wireless communication used to transmit measurements of the pendulum's angular position. Our approach offers a constructive design and a procedure based on a combination of root loci and Mikhailov methods for the analysis of stability. Experiments over a laboratory platform are reported and a comparison with a standard linear state feedback control law shows the advantages of the proposed scheme.

1. Introduction

Underactuated mechatronic systems have been a subject of intensive research during the past three decades, where partial feedback linearization, normal forms, and energy-based methods have offered successful results as well as breakthrough paradigms [1–9]. Experiments with pendulums having one or more degrees of underactuation play an important role in control theory. One important challenge concerning the construction of such equipment is how to send the measurements from the encoders located in the underactuated links without adding restrictions to the movement; one possible solution is wireless communication [10, 11]. Nowadays, wireless sensor networks are a feasible option when mobility and flexibility are requirements. However, when the sensor signals are transmitted through a wireless network, the time-delay phenomena are unavoidable, representing an important as well as an open challenge [11–13]. Time delays in measurements are often neglected. Moreover, when only positions are instrumented, the corresponding velocities are often required to be reconstructed, either with an observer or with the use of on-line differentiators or filters (see, e.g., [14, 15]). It is well known that noise, time delays, sampling, and unmodeled dynamics deteriorate the performance of such estimators. Hence, it is of relevance to understand the effect of time delays in measurements as well as the potential of such delays as a second degree of freedom for control design (see [16, 17]). For this aim, a PR controller design will be presented together with the Mikhailov stability approach. Furthermore, a Furuta pendulum case study, where the underactuated variable is subject to an inherent output delay due to wireless signal transmission, is presented. The analysis of time delays in control systems is not a new topic; particularly, the addition of time delays in the control design has been studied for many years (see, e.g., [18–27]). In particular, the introduction of time delays in the control

law avoids the use of techniques for estimating the derivative action, which is not an easy task under the presence of noise and delays in measurements and increases the cost and complexity of the overall controller design and tuning of the gains [16]. On the other hand, the implementation of a retarded control law requires only memory registers and is relatively simple to program, since it is based on a sum of a proportional signal and the corresponding delayed one. However, the stability analysis of a closed-loop system with a retarded feedback control law requires dealing with infinite-dimensional systems even if the initial plant model is not. This analysis is studied in the framework of two approaches: time domain and frequency domain [28, 29]. In the first approach, the analysis is based on the well-known Lyapunov's criteria using linear matrix inequalities (LMIs) via convex optimization. However, this approach provides only sufficient conditions of stability or stabilization, which are usually conservative for some systems, while for other systems the LMIs are unfeasible. Besides, in our experience for similar problems, the parameters tuning by a frequency method using LMIs sometimes is not feasible. In the second approach, the analysis is based on the root locus of its corresponding characteristic equation in the complex plane. Unlike the temporal approach, the frequency approach can provide necessary and sufficient conditions that are not conservative. In [30–32], some numerical methods to approximate the roots of these quasi-polynomial or analytic functions are displayed. Furuta pendulum is a well-known academic example that is used as a benchmark for the study of underactuated mechanical systems [33, 34]. Recently, in [17], the control design of a PR controller for the stabilization of Furuta pendulum was introduced; however, the effect of the inherent delay, present in the unactuated variable, was not studied. In contrast to the previous work [17], this paper presents a more detailed analysis for the tuning of control gains; also new experiments and graphs are presented, as well as experimental tests of robustness under external disturbances. In addition, the organization of the document is better and more natural; also a more comprehensive bibliographic review is performed and the introduction presents a better justification of the topic of study. Besides, to the best of our knowledge, the stability analysis including the inherent time delay as well as the enhancement of the PR control parameters has not been presented for Furuta pendulum. In addition, the Mikhailov procedure [35] is described and formalized for the present case study; concerning application of the method to systems with delay, see, for example, [36, 37]. The proposed control design is composed of two elements: a PD controller for the actuated variable and PR controller for the stabilization of the unactuated link. The main difference with respect to other works is that the stability analysis incudes two delays, one is inherent of the wireless communication and the other is introduced in the control law for stabilization purposes. Moreover, the time derivative of the unactuated variable or its on-line estimation is not required in the proposed control law. Thus, the characteristic equation analyzed is an analytical function or quasi-polynomial with two transcendental terms of the form

$$\begin{aligned} Q\left(s,\alpha,\beta,k_p,k_r,\tau,\tau_2\right) &= P_1\left(s,k_p,\alpha,\beta\right) + P_2\left(s,k_p\right)e^{-\tau s} \\ &\quad + P_3\left(s,k_r\right)e^{-(\tau+\tau_2)s}, \end{aligned} \tag{1}$$

where τ_2 is the inherent delay of the angular position measurements due to the wireless communication, $P_i(\cdot)$, $i = 1, 2, 3$, are polynomials with real coefficients, k_p, k_r, τ are the parameters of PR controller, and α, β are the parameter of PD controller. The first stability analysis is using the D-partition method [38] and the root continuity property [39, 40]. A growing body of literature has analyzed the stability of quasi polynomials (see [23, 26, 41–44]). Particularly in [26], the delay phenomena have been studied for a fully actuated cart-pendulum system, introducing a full-state feedback controller with feedforward term, assuming that all velocities and positions are measurable.

The present paper focuses on the delay phenomena in an underactuated system called Furuta pendulum. The main result introduces a methodology for the optimal selection of the controller gains and a procedure based on Mikhailov method for the study of complete stability under the presence of measurement delays. Here, it is assumed that only angular positions are available for measurement. For comparison purposes, a design of a state feedback controller, which includes the on-line estimation of velocities, is presented. All the proposed algorithms are verified with simulations and experiments over a laboratory test bench, obtaining the desired performance.

The outline of this paper is distributed as follows. In Section 2, the mathematical model of the Furuta pendulum is introduced. The proposed control design is presented in Section 3. Experimental results are found in Section 4. The conclusions of this study are drawn in Section 5.

2. Mathematical Model

The Furuta pendulum test bench consists of a passive pendulum attached to the end of an actuated rotating arm as shown in Figure 1. The coordinates of the centers of mass of both links are given by $(x_1, y_1, z_1) = (l_1\cos\phi, l_1\sin\phi, 0)$ and $(x_2, y_2, z_2) = (L_1\cos\phi - l_2\sin\phi\sin\theta, L_1\sin\phi + l_2\cos\phi\sin\theta, l_2\cos\theta)$, where θ is the angular position of the pendulum and ϕ is the angle of the rotational arm; and both variables represent the generalized coordinates that describe the motion. The following notation is used: m_1 is the mass of the arm, m_2 is the pendulum mass, J_1 and J_2 are the moments of inertia of the arm and of the pendulum, respectively, L_1 and L_2 are the lengths of the arm and the pendulum, respectively, and g is the acceleration due to gravity. Note that with the chosen coordinated system the unstable equilibrium point is located at $(\theta, \dot\theta, \phi, \dot\phi) = (0, 0, 0, 0)$. Note that the equilibrium does not depend on ϕ and every real value of ϕ corresponds to an unstable equilibrium. A model of the Furuta pendulum can be obtained applying the Euler-Lagrange formalism (see, e.g., [45–47]). The corresponding Lagrangian is given by $\mathscr{L} = T - V$, with $T = (1/2)m_1(\dot x^2 + \dot y^2) + (1/2)m_2(\dot x_2^2 + \dot y_2^2 + \dot z_2^2)$

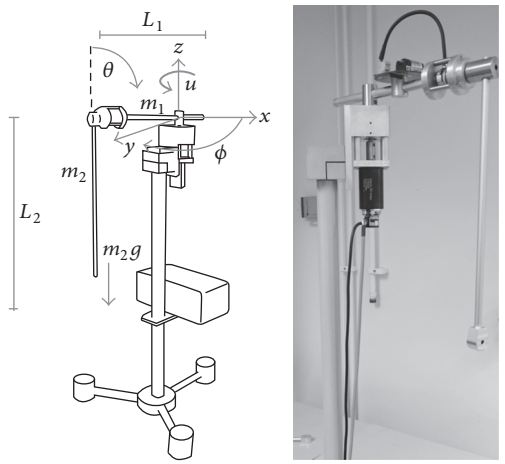

Figure 1: Scheme of the Furuta pendulum model by [10].

Table 1: Physical parameters of Furuta pendulum.

Mass of the horizontal rod (m_1)	0.431 kg
Length of the horizontal rod (L_1)	0.262 m
Distance to center of gravity (l_1)	0.131 m
Moment of inertia of the rod (J_1)	0.012 kg m^2
Mass of the pendulum (m_2)	0.128 kg
Length of the pendulum (L_2)	0.47 m
Distance to center of gravity (l_2)	0.185 m
Moment of inertia of pendulum (J_2)	0.0035 kg m^2
Friction on θ (d_{11})	0.0032 kg m^2/s
Friction on ϕ (d_{22})	0.004 kg m^2/s
Motor constant (κ)	1.07 rad kg m^2/s^2

$+ (1/2)J_1\dot{\phi}^2 + (1/2)J_2\dot{\theta}^2$ and $V = m_2 g l_2 \cos\theta$ leading to the following expression:

$$M\ddot{q} + (C + D)\,\dot{q} + h = f, \tag{2}$$

where the related terms are $q = \begin{bmatrix} \theta \\ \phi \end{bmatrix}$, $M = \begin{bmatrix} m_{11} & m_{12} \\ m_{12} & m_{22} \end{bmatrix}$, $h = \begin{bmatrix} 0 \\ \kappa u \end{bmatrix}$, $C = \begin{bmatrix} 0 & c_{12} \\ c_{21} & c_{22} \end{bmatrix}$, and $D = \begin{bmatrix} d_{11} & 0 \\ 0 & d_{22} \end{bmatrix}$. The elements of the inertia matrix are $m_{11} = J_2 + m_2 l_2^2$, $m_{12} = m_2 L_1 l_2 \cos\theta$, and $m_{22} = J_1 + m_1 l_1^2 + m_2(L_1^2 + l_2^2 \sin^2\theta)$; the Coriolis matrix is formed by $c_{12} = -m_2 l_2^2 \sin\theta\cos\theta\dot{\phi}$, $c_{21} = m_2 l_2^2 \sin\theta\cos\theta\dot{\phi} - m_2 l_2 L_1 \sin\theta\dot{\theta}$, and $c_{22} = m_2 L_2^2 \sin\theta\cos\theta\dot{\theta}$; the parameters of viscous friction are included in matrix D. For the particular laboratory test bench in Figure 1, static friction does not play an important role, because it is small and bounded, and it is neglected in the plant model.

The external torque that allows the control of the arm is produced by a DC motor. The motor induces a torque $M_a = c_a\kappa_i u = \kappa u$, where u is the normalized input voltage of the PWM amplifier, κ_i is constant, and $\kappa = c_a\kappa_i$.

There are two control problems commonly associated with the Furuta pendulum: stabilization around one of the two equilibrium points and the swing-up [48, 49]. In order to study the inherent delay due to the wireless communication together with the design of a retarded control law, here we are going to focus on the problem of stabilization.

In this context, the equation of motion (2) can be linearized around the unstable equilibrium point $(\theta, \dot{\theta}, \phi, \dot{\phi}) = (0, 0, 0, 0)$, obtaining the following controllable linear system:

$$\begin{aligned} \ddot{\theta}(t) &= a\theta(t) + b\dot{\theta}(t) + c\dot{\phi}(t) + du(t), \\ \ddot{\phi}(t) &= e\theta(t) + f\dot{\theta}(t) + g\dot{\phi}(t) + hu(t), \end{aligned} \tag{3}$$

$$y(t, t-\tau_2) = \left[\theta(t-\tau_2), \phi(t)\right]^T, \tag{4}$$

where $y(t, t-\tau_2)$ is the available output subject to communication delay τ_2. The total delay τ_2 involved in the sensor communication can be divided into three parts: the communication delay from sensor to controller, the computation delay at the controller, and the communication delay from controller to actuator. Here, any delay from the sensor to the controller is assumed to be small relative to the sampling period, since short delays are typical for optical encoders. Also, the computation delay is relatively small compared with the communication delay that normally is affected by the physical distance between the communication nodes. As a result, τ_2 is modeled as a static delay within a bounded set; that is, $\tau_2 \in [0, \tau_2^*]$. The other system parameters are $a = 37.377$, $b = -0.515$, $c = 0.142$, $d = -35.42$, $e = -8.228$, $f = 0.113$, $g = -0.173$, and $h = 43.28$. Here, the physical parameters of the experimental platform given in Table 1 are employed.

3. Controller Design and Tuning

Using classical techniques, stabilization of the Furuta pendulum requires measurements of variables θ and ϕ and the estimation of the corresponding time derivatives $\dot{\theta}$ and $\dot{\phi}$ (see, e.g., [33, 48, 49]). However, when wireless communication is considered, delays in the measurement deteriorate the accuracy of estimation of time derivatives. The system under study includes two encoders for measurements of θ and ϕ, where the communication for θ is via a wireless link. Since the wireless communication introduces a variable time delay in the measurement, the estimation of time derivative for variable θ is not a trivial task and we aim to avoid this by using a PR control action. The control methodology includes the design of a PR controller to stabilize the passive degree of freedom associated with θ together with a low-gain PD controller for variable ϕ. The D-partition method, root locus, and method of Mikhailov are implemented for gain design and stability analysis. Some preliminaries of Mikhailov method and second-order PR controllers are given in Appendices A and B, respectively.

3.1. Control Scheme. Consider the following control law:

$$u(t) = U(t-\tau_2) + \alpha\phi(t) + \left(\beta - \frac{c}{d}\right)\dot{\phi}(t), \tag{5}$$

where $U(t-\tau_2) = k_p\theta(t-\tau_2) - k_r\theta(t-\tau-\tau_2)$; τ_2 represents the inherent delay of the angular position measurements due to the wireless communication, and k_p, k_r, and τ are parameters

of design. For application of this control law, a method for derivative estimation is necessary for variable ϕ; in this case, either a high-gain observer or a super twisting differentiator can been used in order to obtain $\dot{\phi}$ (see [15, 50]). Thus, the closed-loop system, (3)–(5), is

$$\begin{aligned}\ddot{\theta}(t) &= a\theta(t) + b\dot{\theta}(t) + dk_p\theta(t-\tau_2) \\ &\quad - dk_r\theta(t-\tau_2-\tau) + d\alpha\phi(t) + d\beta\dot{\phi}(t), \\ \ddot{\phi}(t) &= h\alpha\phi(t) + (g + h\beta - (hc)/(d))\dot{\phi}(t) + e\theta(t) \\ &\quad + f\dot{\theta}(t) + hk_p\theta(t-\tau_2) \\ &\quad - hk_r\theta(t-\tau-\tau_2),\end{aligned} \tag{6}$$

and its representation in state space is given as follows:

$$\dot{x}(t) = A_0x(t) + A_1x(t-\tau_2) + A_2x(t-\tau-\tau_2), \tag{7}$$

where

$$\begin{aligned}x &= \left[\theta, \dot{\theta}, \phi, \dot{\phi}\right], \\ A_0 &= \begin{bmatrix} 0 & 1 & 0 & 0 \\ a & b & d\alpha & d\beta \\ 0 & 0 & 0 & 1 \\ e & f & h\alpha & g - \dfrac{hc}{d} + h\beta \end{bmatrix}, \\ A_1 &= \begin{bmatrix} 0 & 0 & 0 & 0 \\ dk_p & 0 & 0 & 0 \\ 0 & 0 & 0 & 0 \\ hk_p & 0 & 0 & 0 \end{bmatrix}, \\ A_2 &= \begin{bmatrix} 0 & 0 & 0 & 0 \\ -dk_r & 0 & 0 & 0 \\ 0 & 0 & 0 & 0 \\ -hk_r & 0 & 0 & 0 \end{bmatrix}.\end{aligned} \tag{8}$$

Thus, the characteristic quasi polynomial of system (7) is

$$\begin{aligned}&q\left(s, k_p, k_r, \tau, \tau_2, \alpha, \beta\right) \\ &= \det\left\{sI - A_0 - A_1e^{-s\tau_2} - A_2e^{-s(\tau+\tau_2)}\right\} = s^4 + \left(\frac{hc}{d}\right. \\ &\left. - h\beta - b - g\right)s^3 + \left((bh - fd)\beta - h\alpha + bg - \frac{bhc}{d}\right. \\ &\left. - a - dk_pe^{-s\tau_2} + dk_re^{-s(\tau+\tau_2)}\right)s^2 + \left((ah - de)\beta\right. \\ &+ (bh - fd)\alpha + ag - \frac{ahc}{d} + k_r(hc - gd)e^{-s(\tau+\tau_2)} \\ &\left. + k_p(gd - hc)e^{-s\tau_2}\right)s + (ah - de)\alpha.\end{aligned} \tag{9}$$

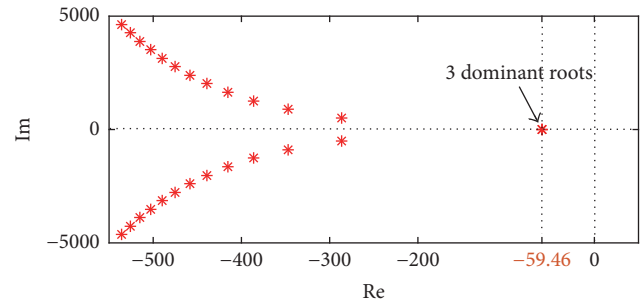

Figure 2: Root of quasi polynomial (11).

Note that, for $\alpha = \beta = 0$ and $\tau_2 = 0$, it reduces to

$$\begin{aligned}q\left(s, k_p, k_r, \tau, 0, 0, 0\right) &= \left(s^2 - bs - a - dk_p + dk_re^{-s\tau}\right) \\ &\times \left(s^2 + \left(\frac{hc}{d} - g\right)s\right).\end{aligned} \tag{10}$$

Clearly, the first factor of the above quasi polynomial is identical to the one for a decoupled one-degree-of-freedom mechanical system under a PR feedback (see (A.3) from Appendix A). Then, as a first step, let us assume small values for α, β, and τ_2, proceeding with the design of k_p, k_r, and τ with the help of Lemmas A.1 and A.2 given in Appendix B, placing some of the roots into the optimal locations for the reduced system. Lemmas A.1 and A.2 bring σ-stability to the dynamics of the variable θ. Then, choosing the right values for α and β, one should not expect σ-stability for the full fourth-order system but may expect asymptotic stability under sufficiently small and appropriately chosen α and β, which appears only in the terms associated with A_0 in (9). This is expected due to continuous dependence of the roots of a quasi polynomial on the coefficients and will be quantified in the next section with the analysis of root locus.

As a second step, the Mikhailov analysis will provide the stability conditions under the presence of an inherent sufficiently small delay τ_2.

3.2. Tuning and Stability Analysis. In this section, the tuning of the controller gains proposed in the previous section and an analysis of stability of closed-loop system (7) with $\tau_2 = 0$ are presented.

Consider the second-order quasi polynomial, roots of which cover all the roots of (10) except for $s = 0$ and $s = g - hc/d$:

$$p\left(s, k_p^*, k_r^*, \tau^*\right) = s^2 - bs - a - dk_p^* + dk_r^*e^{-s\tau^*}, \tag{11}$$

where k_p^*, k_r^*, and τ^* are tuned for the reduced system (see Lemma A.2). This choice provides three dominant roots in the same point at $-\sigma^*$, as can be seen in Figure 2. Suppose that α and β are small and $\tau_2 = 0$; then quasi polynomial (9) has five dominant roots, three close to $-\sigma^*$ and two close to zero, as can be seen in Figure 3. Therefore, system (7) is close to be marginally stable.

To determine stability of quasi polynomial (9), in Figure 4, a root locus is presented. Here, α and β are varied.

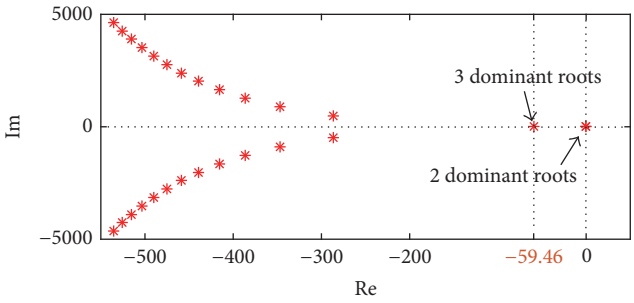

Figure 3: Roots of (9) when $\alpha = \beta = \tau_2 = 0$.

Observe that if $\alpha = 0$ and β is varied or $\beta = 0$ and α is varied, then quasi polynomial (9) remains unstable. The case where $\alpha \neq 0$ and $\beta \neq 0$ can be handled with the same method; however, for some combination of values, it can be exhaustive to find the stability condition or quasi polynomial (9) can turn unstable. Meanwhile, if the value of $\alpha = \beta$ is increased simultaneously, then quasi polynomial (9) can be stabilized relatively easier.

Next, the root locus of quasi polynomial (9) is presented when $\alpha = \beta > 0$ are simultaneously varied as can be seen in Figure 5. Here, two of the three dominant roots in $-\sigma^*$ are moved to the right and one root is moved to the left, while the two dominant roots at zero and at $g - hc/d \approx 0$ are moved to the left. Clearly, there is a breaking point γ^* such that quasi polynomial (9) becomes unstable; this occurs when $\gamma^* \approx 0.9$. Thus, the stability of system (3) in closed loop with control law (5) is ensured, when $\alpha = \beta \in (0, \gamma^*)$. The above analysis enables a proper selection of the gains α and β such that quasi polynomial (9) is stable. Without loss of generality, the gains have been set at $\alpha = \beta = 0.5$. Here, the five dominant roots are $s_1 = -130.3$, $s_{2,3} = -15.85 \pm 39i$, and $s_{4,5} = -0.358 \pm 0.78i$ (see roots marked with blue asterisk in Figure 5). Note that if $\alpha = \beta < 0$, then quasi polynomial (9) is unstable.

3.3. Robustness Analysis under the Presence of $\tau_2 > 0$. Now, Mikhailov's criterion [35] to corroborate the stability under the presence of $\tau_2 \neq 0$ and $\alpha = \beta = 0.5$ is implemented (see Appendix B). For this purpose, consider the next closed curve in the complex plane:

$$C = C_0 + C_1, \tag{12}$$

where $C_0 \subset \mathbb{C}$ is the interval $[-r, r]$ on the imaginary axis and $C_1 \subset \mathbb{C}$ is a semicircle of radius r in the right-half complex plane, where r is sufficiently large (we take $r = 100$). Mikhailov's criterion is used to analyze robustness when $\tau_2 \in [0, \tau_2^*]$. In Figures 6(a) and 6(b), one clockwise turn and one counterclockwise turn around zero are depicted. In Figures 6(c), 6(d), and 6(e), two clockwise turns and two counterclockwise turns around zero are observed. It should be mentioned that such behavior is verified for $\tau_2 = 0.004, \ldots, 0.007$. Nevertheless, the figures have been omitted to save the space. Thus, due to continuous dependence of the roots on the parameter τ_2 and due to the above observations, it can be concluded that the change of argument of quasi polynomial (9) is $N = 0$ when $\tau_2 \in [0, 0.008]$. However, in Figure 6(f), two clockwise turns and one counterclockwise turn around zero are observed when $\tau_2^* \approx 0.009$. Here, $N = 1$. Therefore, quasi polynomial (9) remains stable if $\tau_2 \in [0.008]$.

On the other hand, in Figure 7, the root locus of quasi polynomial (9) when $\tau_2 = 0.008$ and $\alpha = \beta \in [0, 0.9]$ is shown. Observe that (9) remains stable if $\tau_2 = 0.008$ and $\alpha = \beta \in [0, 0.524]$; and it is unstable if $\tau_2 = 0.008$ and $\alpha = \beta \in [0.524, 0.9]$.

Therefore, we have the following result.

Proposition 1. *Consider a quasi polynomial of the form (9) and a positive constant $\sigma > -b$. Then, the control law (5) stabilizes a fourth-order system of the form (6) if*

$$k_p^* = -\frac{\left(2\left(a + \sigma^2 + \sigma b\right) + b^2\right)}{(2d)},$$
$$\tau^* = \frac{(2\sigma + b)}{\left(\sigma^2 + b\sigma - a - dk_p^*\right)}, \tag{13}$$
$$k_r^* = -\frac{(2\sigma + b)}{\left(d\tau^* e^{\sigma\tau^*}\right)};$$

and α, β, and τ_2 are such that $\alpha = \beta \in (0, \gamma^*)$ and $\tau_2 \in [0, \tau_2^*)$. Here, k_p^* follows from (A.5) and γ^* is given in Section 3.2; $\tau_2^* = 0.008$.

4. Experiments

The experimental results were obtained in the Robotics and Control Lab at the Department of Applied Physics and Electronics, Umeå University, Umeå, Sweden. The system used for the experiments is from the PendCon Advanced series [10] with the configuration for rotary pendulum or Furuta pendulum (see Figure 1). In this hardware setup, signals from the encoders with resolution of 4096 pulses per revolution are transmitted wirelessly, and for the actuated link the motor MAXON RE40 (40 mm) is used, which is a graphite brushless DC motor (150 W) with nominal voltage of 24 V. The real-time controller is on a dedicated target PC that communicates with the host PC; it has one PCI slot for the encoder card and four interfaces for RS-232 signals; this PC has Intel Core i5 processor with real-time workshop; the host-target environment is a PC with MATLAB real-time workshop compiler installed on Intel Core i5 processor with Window 7. Both communicate with the Conversion Unit via a Matlab-compatible Quatech RS-232 card. The control system is developed in MATLAB R2015a/Simulink and downloaded to the target PC.

The control goal is to stabilize the pendulum at its unstable equilibrium point ($\theta^* = 0$), that is, vertically pointing up. For comparison purposes, a state feedback controller is designed: $u_{sf} = Kx(t)$ with $x(t) = [\theta(t), \dot{\theta}(t), \phi(t), \dot{\phi}(t)]^T$. In order to have a reasonable comparison, the gain K is designed such that the poles in closed loop of the linearized system are located at $-15.85 \pm 39i$ and $-0.3581 \pm 0.78i$. Note that these values correspond with the dominant complex conjugate poles obtained with the PR controller. In Figure 8, the performance of regulation of the angular positions $\theta(t)$

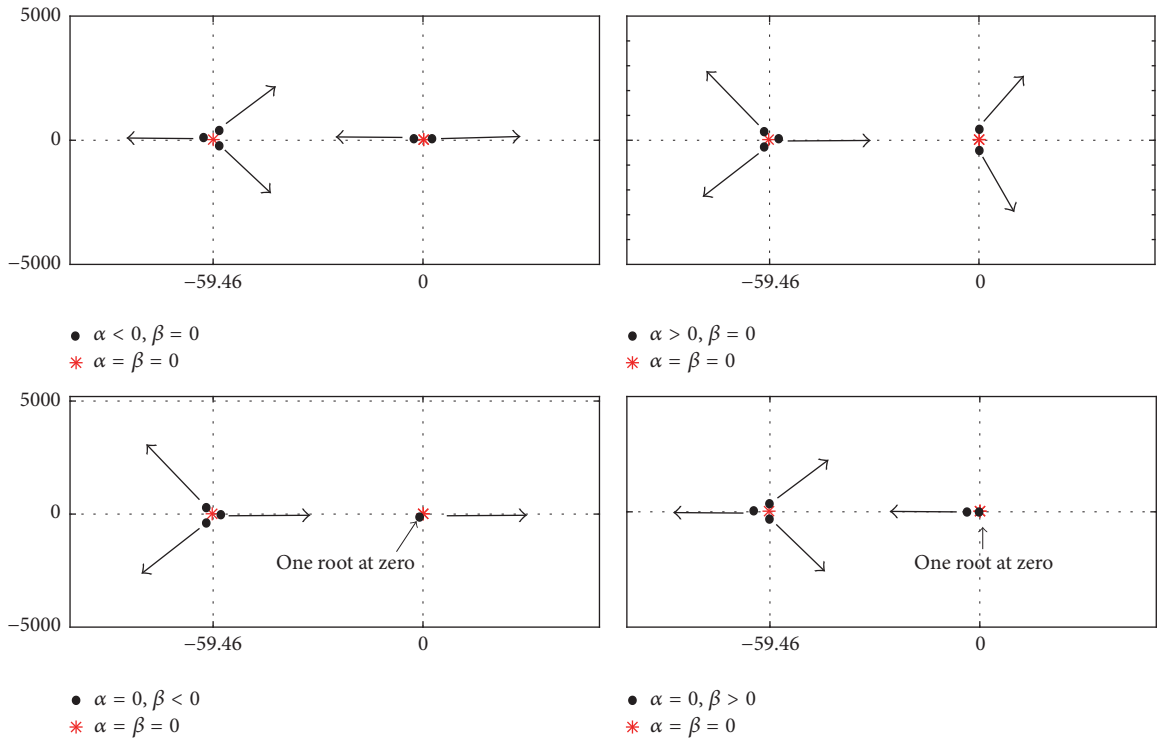

Figure 4: Root locus of (9) when $\tau_2 = 0$ and α and β are varied.

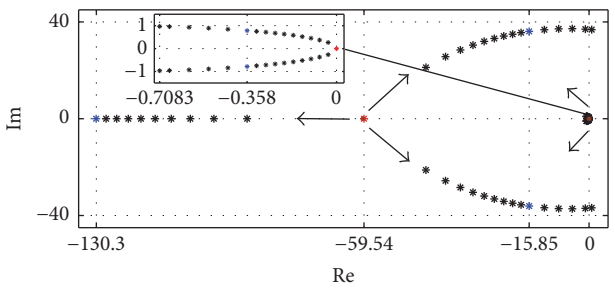

Figure 5: Root locus of (9) when $\tau_2 = 0$ and $\alpha = \beta \in [0, 0.9]$.

and $\phi(t)$ with the PR and state feedback controller are presented. Here, the initial position is close to the unstable equilibrium point θ^*. Figure 9 presents the control signals.

The design and tuning of the controller are done as follows:

(1) Consider a system of the form (3)-(4) in closed loop with a control law of the form (5) and its corresponding quasi polynomial of 4th order $q(s, k_p, k_r, \tau, \tau_2, \alpha, \beta)$, specified in (9).

(2) Factor the quasi polynomial of 4th order in one quasi polynomial of 2nd order and one polynomial of 2nd order, when $\alpha = \beta = 0$ and $\tau_2 = 0$ (see (10)):

$$q\left(s, k_p, k_r, \tau, 0, 0, 0\right) = p\left(s, k_p, k_r, \tau\right) f\left(s\right). \quad (14)$$

(3) Use Lemma A.2 to σ-stabilize the quasi polynomial of 2nd order and obtain the parameters (k_p^*, k_r^*, τ^*) of the PR controller (see (11)):

$$p\left(s, k_p, k_r, \tau\right) = p\left(s, k_p^*, k_r^*, \tau^*\right). \quad (15)$$

(4) Obtain α, β, and τ_2 such that quasi polynomial (9) remains stable, as depicted in Figures 6 and 7.

Remark 2. It is important to remark that there is an inherent unknown delay $\tau_2 > 0$, in the measurement of pendulum position; that is, at time t, we obtain $\theta(t - \tau_2)$. However, if τ_2 remains inside a small range, stability is still preserved as we have shown.

In order to compute the estimation of the first derivative for both position variables, θ and ϕ, two methods were explored: high gain and super twisting differentiators (see [15, 50]).

These methods are designed to be used on-line. For comparison purposes, it is obvious that better velocity estimation can be achieved with an off-line method when both previous and future values of the position are used. Then, we propose to postprocess the measured position to obtain an off-line estimation. For this purpose, the measured signal is fitted with a smoothing spline and next the off-line estimation of velocity is obtained as an analytical differentiation of the spline (see, e.g., [51], page 194). Using this off-line estimation as the true value of the velocity, we compare the performances of high gain (with different gains: HG1 and HG2) and super twisting (ST) differentiators, computing the estimation errors

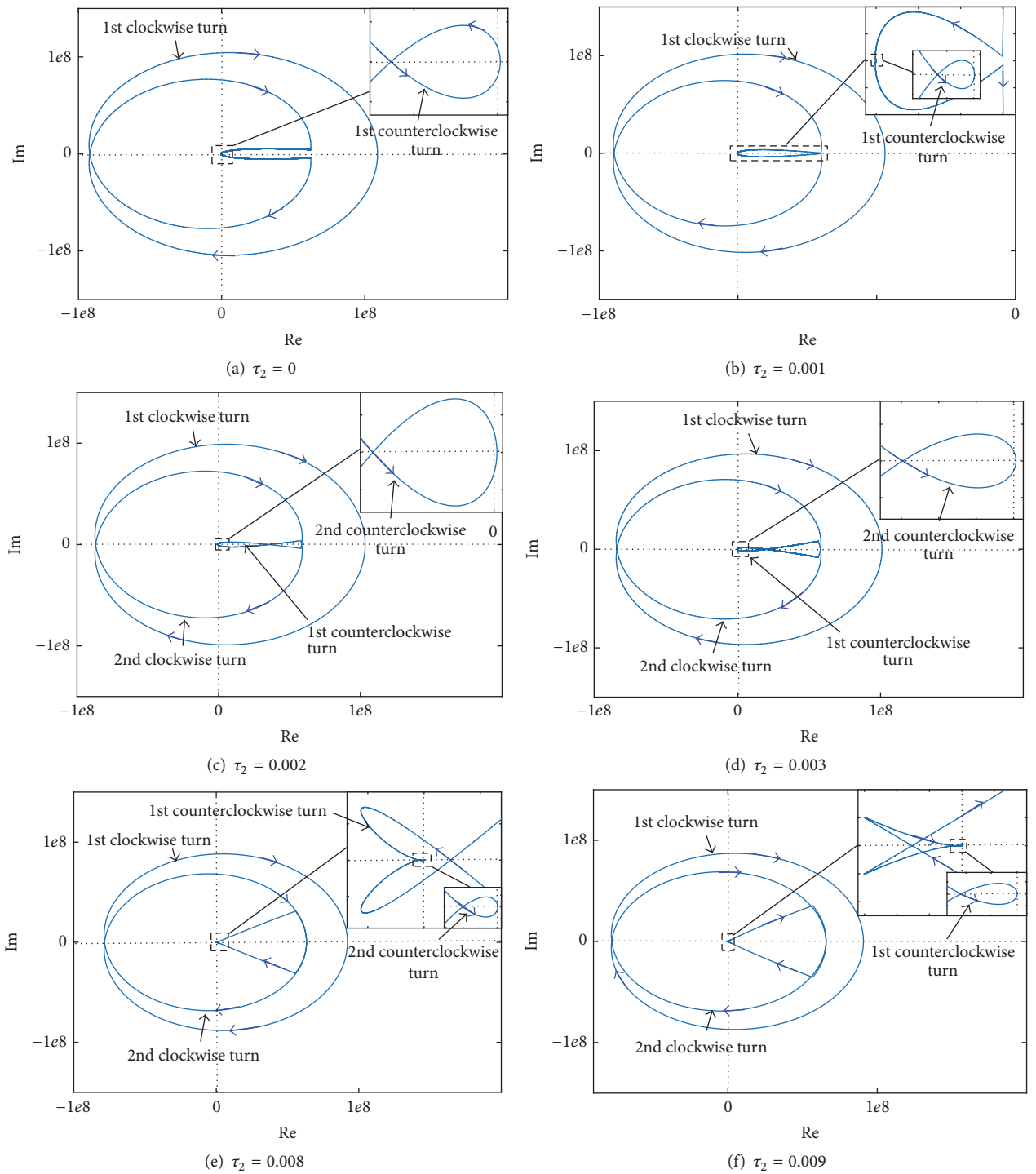

Figure 6: Mikhailov criterion for quasi polynomial (9) when $\alpha = \beta = 0.5$ and $\tau_2 \in [0, 0.009]$.

as is shown in Table 2. From Table 2, it is clear that, due to the wireless communication, the estimation of $\dot{\theta}$ is deteriorated, resulting in a bigger error and decreased closed-loop performance when we use this estimation with a state feedback controller.

Remark 3. With the proposed PR controller, the use of the estimation of $\dot{\theta}$ is not required. This is desirable in applications where the estimation of velocity deteriorates the overall performance.

An additional experiment was performed in order to test the robustness against external perturbations. For this aim, several impacts were applied to the pendulum at the time instants t_i, $i = 1, \ldots, 6$, as can be seen in Figures 10 and 11.

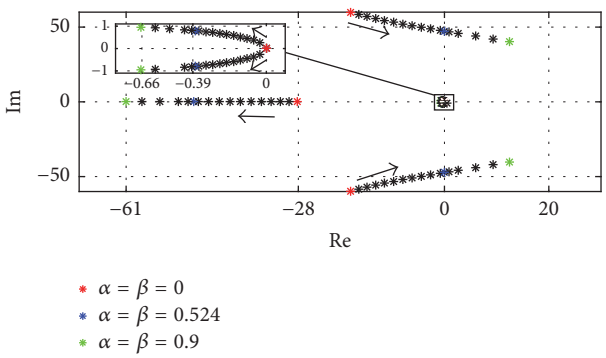

Figure 7: Root locus of (9) when $\tau_2 = 0.008$ and $\alpha = \beta \in [0, 0.9]$.

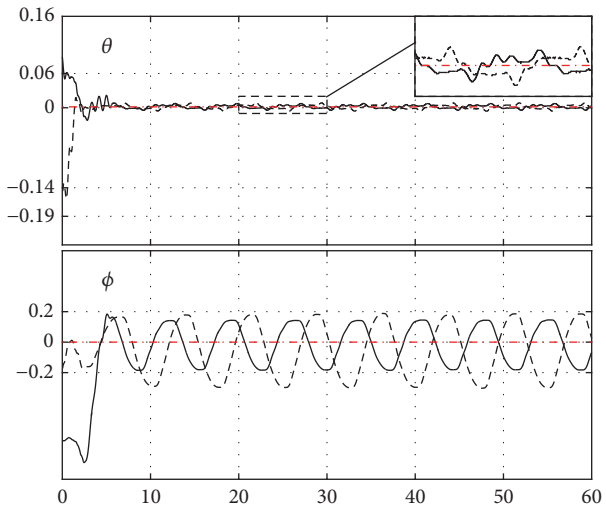

Figure 8: Angular positions (rad) $\theta(t)$ and $\phi(t)$ versus time (s): (solid line) PR controller, (dashed line) state feedback controller, and (dashed dotted line) reference.

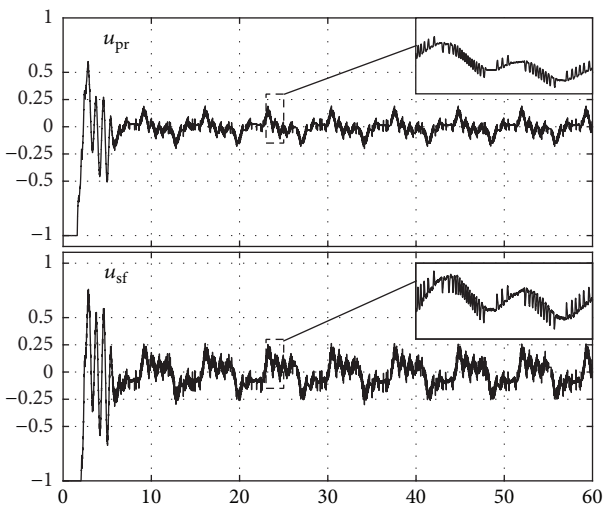

Figure 9: Control actions (N), PR controller (u_{pr}), and state feedback controller (u_{sf}).

Table 2: Table of error comparison.

		Differentiators		
		HG1	HG2	ST
Error $\dot{\theta}$	Norm 2	1.4167	1.1556	1.349
	Norm inf	24.9879	25.0273	10.0679
Error $\dot{\phi}$	Norm 2	.3888	.1292	.0634
	Norm inf	.8410	3.2624	.5597

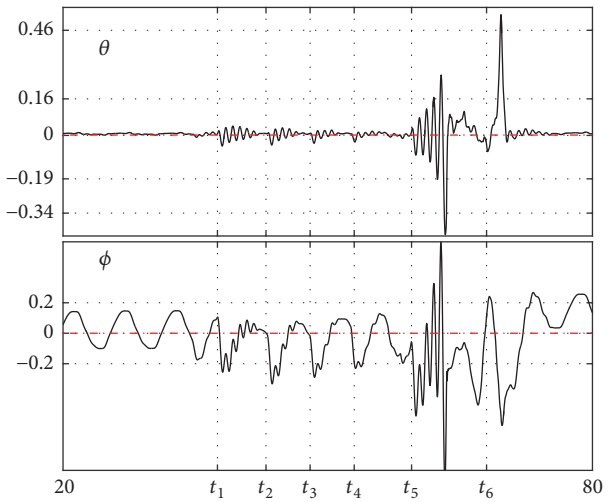

Figure 10: Angular positions (rad) $\theta(t)$ and $\phi(t)$ versus time (s) under external perturbations with PR controller.

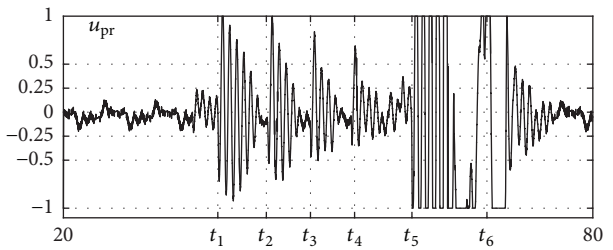

Figure 11: Control action (N) under external perturbations with PR controller.

From the experimental results, the recovery of performance with the proposed PR controller is verified. Besides, it is important to highlight that a better transient, a smoother response, and chattering attenuation in the control signal are observed with the proposed approach under the presence of delays in measurements. A video of the recorded experiments is available in the following link: https://www.youtube.com/watch?v=F9QbPVkagwE.

5. Conclusion

Presence of time delays, quantization errors of encoders, and errors of the wireless communication make the design of a robust control law difficult. The design and stability analysis of a PR action-based controller for stabilization of the Furuta pendulum under the presence of time delays

in measurements is introduced in this work. With the proposed approach, the design of observers for the passive variable is avoided simplifying the control algorithm and recovering an acceptable performance without relying on accurate estimates of the derivative for feedback. Since a retarded action is included in the control law, the closed-loop dynamics are represented by a characteristic quasi polynomial and the stability analysis was successfully done with Mikhailov's criterion and a root locus of the corresponding quasi polynomial. Furthermore, the stability analysis includes an inherent time delay due to the wireless communication. Besides, a two-step constructive procedure for tuning the four parameters of a controller is presented. Experimental results and a comparison with a state feedback controller show the advantages of the proposed methodology. We are aware that a possible extension of the proposed controller is the addition of a PR controller in the actuated variable as well; however, this is considered as a future work, since the order of the quasi polynomial will increase significantly, losing the scope of the actual contribution. Additionally, extension for a wider class of underactuated mechanical systems and the inclusion of nonlinearities is considered for future work.

Appendix

A. PR Controller for a Second-Order Plant

Consider the next second-order system,

$$\ddot{\theta}(t) - b\dot{\theta} - a\theta(t) = dU(t), \tag{A.1}$$

and the PR control law,

$$U(t) = k_p\theta(t) - k_r\theta(t-\tau), \tag{A.2}$$

where the design parameters are as follows: k_p is the proportional gain, k_r is the retarded gain, and τ is the time delay. Thus, the characteristic quasi polynomial of closed-loop system (A.1)-(A.2) is

$$p\left(s, k_p, k_r, \tau\right) = s^2 - bs - \left(a + dk_p\right) + dk_r e^{s\tau}. \tag{A.3}$$

We say that the triplet (k_p, k_r, τ) σ-stabilizes quasi polynomial (A.3) if

$$\alpha_0 \leq \sigma, \quad \sigma \in \mathbb{R}^+, \tag{A.4}$$

with $\alpha_0 = \sup\{\mathrm{Re}\{s_j\} : p(s_j, k_p, k_r, \tau) = 0,\ s_j \in \mathbb{C}\}$, where $\mathrm{Re}\{s_j\}$ is the real part of s_j, $j = 1, 2, \ldots, \infty$. In [16], the parameter space (k_p, k_r, τ) of control law [13] to σ-stabilize system [12] is determined.

Lemma A.1 (see [16]). *Let k_p be such that $-dk_p > a + (b/2)^2$ and $\sigma \in [-b/2, \sigma^*]$, where*

$$\sigma^* = -\frac{b}{2} + \sqrt{-a - (b/2)^2 - dk_p}. \tag{A.5}$$

Then, the parametric equations delimiting the regions of σ-stabilizability of closed-loop system (A.1)-(A.2) are given by the following:

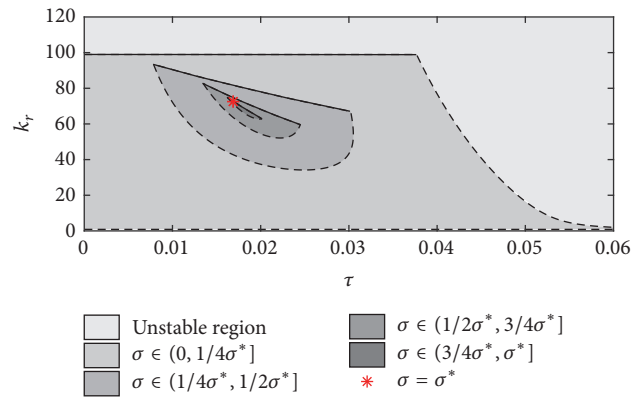

Figure 12: σ-Stability regions of closed-loop system (A.1)-(A.2). Here, $\sigma^* = 59.4573$, $\tau^* = 0.0169$, and $k_r^* = 72.4822$.

Lower Boundary

$$k_r(\omega, \tau) = -\frac{\left(\sigma^2 + \sigma b - a - dk_p\right)}{\left(de^{\tau\sigma}\right)}, \tag{A.6}$$

for τ defined as for the upper boundary.

Upper Boundary

$$\tau(\omega) = \begin{cases} \dfrac{1}{\omega}\cot^{-1}\left(\dfrac{\left(\sigma^2 + \sigma b - \omega^2 - a - dk_p\right)}{\left(2\left(\sigma + (b/2)\right)\omega\right)}\right), & \omega \in (0, \omega_e], \\ \dfrac{1}{\omega}\cot^{-1}\left(\dfrac{\left(\sigma^2 + \sigma b - \omega^2 - a - dk_p\right)}{\left(2\left(\sigma + (b/2)\right)\omega\right)}\right) + \dfrac{\pi}{\omega}, & \omega \in (\omega_e, \omega_0], \end{cases}$$

$$k_r(\omega, \tau) = -\left(\frac{2\omega\left(\sigma + (b/2)\right)}{\left(de^{\sigma\tau}\sin(\omega\tau)\right)}\right), \tag{A.7}$$

$$\omega_0 = \sqrt{-2\left[a + \sigma^2 + \sigma b + dk_p - b^2\right]},$$

$$\omega_e = \min\{\omega_0, \omega_\pi\},$$

$$\omega_\pi = \sqrt{\sigma^2 + \sigma b - a - dk_p}.$$

In Figure 12, the upper boundary (solid line) and lower bounds (dashed line) using $k_p = 100$ and the parameters given in Table 1 are shown. These bounds delimit the σ-stability regions for quasi polynomials of the form (A.3).

Also, note that these regions collapse into a single point (red asterisk) which correspond to the unique maximum achievable decay σ^*. The following result characterized analytically this point.

Lemma A.2 (see [16]). *Let k_p be such that $-k_p > +(b/2)^2$. Then, the maximum exponential decay σ^* of the closed-loop system (A.1)-(A.2) is given in (A.5). Moreover, the values*

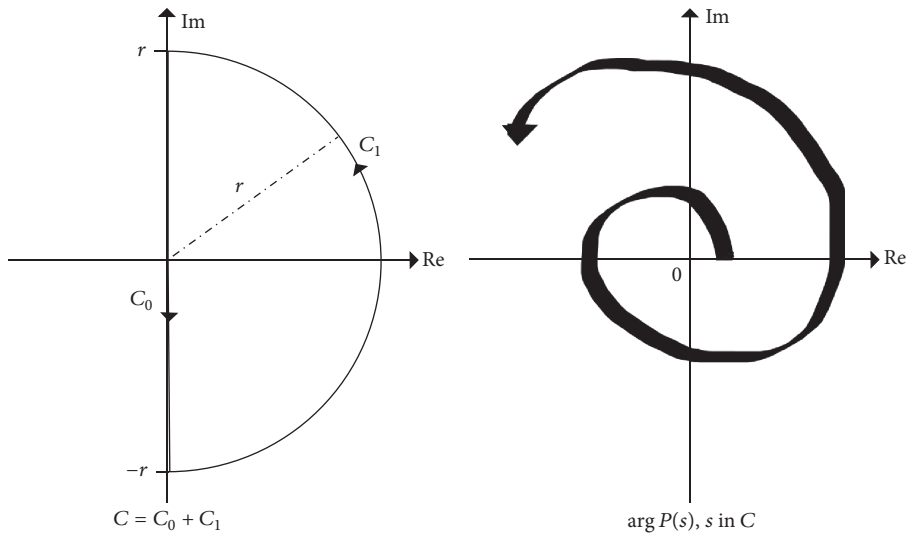

FIGURE 13: Example of $\Delta_C \arg\{P(s)\}$ along a curve C_0.

(k_r^*, τ^*) that σ-stabilize system (A.1)-(A.2) with the best possible exponential decay σ^* are

$$\tau^* = \left(\frac{(2\sigma^* + b)}{\left((\sigma^*)^2 + b\sigma^* - a - dk_p\right)} \right),$$
$$k_r^* = -\left(\frac{(2\sigma^* + b)}{(d\tau^* e^{\sigma^* \tau^*})} \right). \tag{A.8}$$

For illustrative purposes, for Figure 12, we take $k_p = 100$.

B. Summary of Mikhailov's Criterion

Stability conditions stated in terms of hodographs (frequency plots) have a long history. In their most general form, these conditions were given by Cauchy's principle of the argument around 1829. The graphical use of the argument principle was introduced to the engineering community by Nyquist in 1932 and Mikhailov in 1938 for linear time-independent systems; see [36, 37, 52–54] for extensions to the case with time delays. Mikhailov's criterion gives necessary and sufficient conditions for the stability of a quasi polynomial for a time-delay system. Let us formulate one of some possible versions of this criterion.

Theorem B.1. *Consider the following quasi polynomial for a time-delay system:*

$$P(s) = \sum_{k=0}^{m} A_k(s)\, e^{-h_i s}, \quad s \in C \subset \mathbb{C}, \tag{B.1}$$

where C is a closed curve in the complex plane $\mathbb{C}$, $0 = h_0 < h_1 < \cdots < h_m$, $A_K(s) = \sum_{j=0}^{n_k} a_{jk} s^j$, $a_{jk} \in \mathbb{R}$, $n_0 \geq 1$, and $n_k \leq n_0$, for $k = 1, \ldots, m$. If $P(s)$ has no roots on the curve $\mathbb{C}$, then the number N of its roots inside of C is

$$N = \frac{1}{2\pi} \Delta_C \arg\{P(s)\}, \tag{B.2}$$

where $\Delta_C \arg\{P(s)\}$ denotes the changes of the argument of P along C.

Immediately, the above theorem is used to determine stability or instability of quasi polynomials of Section 3, exploiting the well-known fact that the number of unstable roots is always finite (see [55], page 9) and therefore can be trapped by a large enough semicircle in the right-half plane.

Let $C = C_0 + C_1$ denote one closed curve in the complex plane, as depicted in Figure 13. Here, C_0 is the interval $[-r, r]$ on the imaginary axis and C_1 is the semicircle of the radius r in the right-half (left-half) complex plane. It follows from the above theorem that

$$N = 1/(2\pi)\left(\Delta_{C_0} \arg\{P(s)\} + \Delta_{C_1} \arg\{P(s)\}\right), \tag{B.3}$$

where $\Delta_{C_0} \arg\{P(s)\}$ and $\Delta_{C_1} \arg\{P(s)\}$ denote the changes of argument of P along C_0 and C_1, respectively. Assuming that the radius r is sufficiently large, to claim stability, one must just verify that $N = 0$, that is, verify that the number of the turns around the origin in the clockwise direction is equal to the number of turns in the counterclockwise direction.

It should be noted, however, that application of Mikhailov's method in the case of quasi polynomials must be done with great care, since there is typically no monotonicity of rotation of the curve along C_0, as in Figure 13, which can be proven only for the case of polynomials with a finite number of roots.

Nomenclature

θ: Angular position of the pendulum
ϕ: Angle of the rotational rod
m_1: Mass of the rotational rod
m_2: Pendulum mass
J_1: Moment of inertia of the rod
J_2: Moment of inertia of the pendulum
L_1: Length of the horizontal rod

L_2: Pendulum length
l_1: Distance to rod center of gravity
l_2: Distance to pendulum center of gravity
g: Gravity acceleration
M_a: Induced torque.

Conflicts of Interest

The authors declare that there are no conflicts of interest regarding the publication of this paper.

References

[1] M. Spong, "Partial feedback linearization of underactuated mechanical systems," in *Proceedings of the IEEE/RSJ/GI International Conference on Intelligent Robots and Systems (IROS'94)*, pp. 314–321, IEEE, Munich, Germany.

[2] M. Reyhanoglu, A. van der Schaft, N. H. McClamroch, and I. Kolmanovsky, "Dynamics and control of a class of underactuated mechanical systems," *Institute of Electrical and Electronics Engineers Transactions on Automatic Control*, vol. 44, no. 9, pp. 1663–1671, 1999.

[3] A. M. Bloch, N. E. Leonard, and J. E. Marsden, "Controlled Lagrangians and the stabilization of mechanical systems i: the first matching theorem," *Institute of Electrical and Electronics Engineers Transactions on Automatic Control*, vol. 45, no. 12, pp. 2253–2270, 2000.

[4] R. Ortega, M. W. Spong, F. Gómez-Estern, and G. Blankenstein, "Stabilization of a class of underactuated mechanical systems via interconnection and damping assignment," *Institute of Electrical and Electronics Engineers Transactions on Automatic Control*, vol. 47, no. 8, pp. 1218–1233, 2002.

[5] R. Olfati-Saber, "Normal forms for underactuated mechanical systems with symmetry," *Institute of Electrical and Electronics Engineers Transactions on Automatic Control*, vol. 47, no. 2, pp. 305–308, 2002.

[6] J. A. Acosta, R. Ortega, A. Astolfi, and A. D. Mahindrakar, "Interconnection and damping assignment passivity-based control of mechanical systems with underactuation degree one," *Institute of Electrical and Electronics Engineers Transactions on Automatic Control*, vol. 50, no. 12, pp. 1936–1955, 2005.

[7] A. S. Shiriaev, L. B. Freidovich, and S. V. Gusev, "Transverse linearization for controlled mechanical systems with several passive degrees of freedom," *Institute of Electrical and Electronics Engineers Transactions on Automatic Control*, vol. 55, no. 4, pp. 893–906, 2010.

[8] Y. Liu and H. Yu, "A survey of underactuated mechanical systems," *IET Control Theory & Applications*, vol. 7, no. 7, pp. 921–935, 2013.

[9] A. S. Shiriaev, L. B. Freidovich, and M. W. Spong, "Controlled invariants and trajectory planning for underactuated mechanical systems," *Institute of Electrical and Electronics Engineers Transactions on Automatic Control*, vol. 59, no. 9, pp. 2555–2561, 2014.

[10] PendCon, "PendCon Advanced: Rotary Pendulum, Germany".

[11] N. J. Ploplys, P. A. Kawka, and A. G. Alleyne, "Closed-loop control over wireless networks," *IEEE Control Systems Magazine*, vol. 24, no. 3, pp. 58–71, 2004.

[12] V. C. Gungor and G. P. Hancke, "Industrial wireless sensor networks: challenges, design principles, and technical approaches," *IEEE Transactions on Industrial Electronics*, vol. 56, no. 10, pp. 4258–4265, 2009.

[13] D.-I. Curiac, "Towards wireless sensor, actuator and robot networks: conceptual framework, challenges and perspectives," *Journal of Network and Computer Applications*, vol. 63, no. 1, pp. 14–23, 2009.

[14] A. Levant, "Higher-order sliding modes, differentiation and output-feedback control," *International Journal of Control*, vol. 76, no. 9-10, pp. 924–941, 2003.

[15] H. K. Khalil and L. Praly, "High-gain observers in nonlinear feedback control," *International Journal of Robust and Nonlinear Control*, vol. 24, no. 6, pp. 993–1015, 2014.

[16] R. Villafuerte, S. Mondié, and R. Garrido, "Tuning of proportional retarded controllers: theory and experiments," *IEEE Transactions on Control Systems Technology*, vol. 21, no. 3, pp. 983–990, 2013.

[17] T. Ortega, R. Villafuerte, C. Vázquez, and L. Freidovich, "Performance without tweaking differentiators via a PR controller: furuta pendulum case study," in *Proceedings of the 2016 IEEE International Conference on Robotics and Automation, (ICRA '16)*, pp. 3777–3782, IEEE, Stockholm, Sweden, May 2016.

[18] I. H. Suh and Z. Bien, "Proportional minus delay controller," *Institute of Electrical and Electronics Engineers Transactions on Automatic Control*, vol. 24, no. 2, pp. 370–372, 1979.

[19] I. H. Suh and Z. Bien, "Use of time-delay actions in the controller design," *IEEE Transactions on Automatic Control*, vol. 25, no. 3, pp. 600–603, 1980.

[20] G. M. Swisher and T. Shing, "Design of proportional-minus-delay action feedback controllers for second- and third-order systems," in *Proceedings of the 1988 American Control Conference*, pp. 254–260, 1998.

[21] C. Abadallah, P. Dorato, J. Benites-Read, and R. Byrne, "Delayed positive feedback can stailize oscillatory systems," in *Proceedings of the American Control Conference*, 1993.

[22] Q. Zhong and H. Li, "A delay-type pid controller," in *IFAC Proceedings Volumes*, vol. 35 of *15th Triennial World Congress*, pp. 265–270, Barcelona, Spain, 1 edition, 2002.

[23] S.-I. Niculescu and W. Michiels, "Stabilizing a chain of integrators using multiple delays," *Institute of Electrical and Electronics Engineers Transactions on Automatic Control*, vol. 49, no. 5, pp. 802–807, 2004.

[24] V. L. Kharitonov, S.-I. Niculescu, J. Moreno, and W. Michiels, "Static output feedback stabilization: necessary conditions for multiple delay controllers," *Institute of Electrical and Electronics Engineers Transactions on Automatic Control*, vol. 50, no. 1, pp. 82–86, 2005.

[25] M. Krstic, *Delay Compensation for Nonlinear, Adaptative, and PDE Systems*, Birkhäuser, Basel, Switzerland, 2009.

[26] N. Olgac and M. E. Cavdaroglu, "Full-state feedback controller design with "delay scheduling" for cart-and-pendulum dynamics," *Mechatronics*, vol. 21, no. 1, pp. 38–47, 2011.

[27] F. Mazenc and M. Malisoff, "New control design for bounded backstepping under input delays," *Automatica*, vol. 66, pp. 48–55, 2016.

[28] E. Fridman, *Introduction to Time-delay Systems: Analysis and Control*, Springer, Berlin, Germany, 2014.

[29] K. Gu, V. L. Kharitonov, and J. Chen, *Stability of Time Delay Systems*, Control eniginnering, Sprnger, Berlin, Germany, 2003.

[30] K. Engelborghs, T. Luzyanina, and D. Roose, "Numerical bifurcation analysis of delay differential equations using DDE-BIFTOOL," *IEEE Transactions on Automatic Control*, vol. 54, no. 1, pp. 171–177, 2002.

[31] M. Dellnitz, O. Schutze, and Q. Zheng, "Locating all the zeros of an analytic function in one complex variable," *Journal of Computational and Applied Mathematics*, vol. 138, no. 2, pp. 325–333, 2002.

[32] T. Vyhlídal and P. Zítek, "Mapping based algorithm for large-scale computation of quasi-polynomial zeros," *IEEE Transactions on Automatic Control*, vol. 28, no. 1, pp. 1–21, 2009.

[33] K. Aström and K. Furuta, "Swining up a pendulum by energy control," *FAC 13th World Congress*, 1996, San Francisco, USA.

[34] M. Ramírez-Neria, H. Sira-Ramírez, R. Garrido-Moctezuma, and A. Luviano-Juárez, "Linear active disturbance rejection control of underactuated systems: the case of the Furuta pendulum," *ISA Transactions*, vol. 53, no. 4, pp. 920–928, 2014.

[35] A. Mikhailov, "Method of harmonic analysis in control theory," *Avtomatika i Telemekhanika*, vol. 3, no. 1, pp. 27–81, 1938.

[36] I. Kabaknov, "Concerning the control process for the steam pressure," *Inzenernyj Sobrnik*, vol. 2, no. 2, pp. 27–60, 1946 (Russian).

[37] U. Forys, "Biological delay systems and the mikhailov criterion of stability," *Journal of Biological Systems*, vol. 12, no. 1, pp. 45–60, 2004.

[38] J. Neimark, "D-subdivisions and spaces of quasi-polynomials," *Prikl. Mat. Meh*, vol. 13, no. 1, pp. 349–380, 1949.

[39] W. Michiels and S.-I. Niculescu, "Stability, control, and computation for time-delay systems: an eigenvalue-based approach," *SIAM: Advances in Design and Control*, vol. 27, 2014.

[40] X.-G. Li, S.-I. Niculescu, and A. Cela, "Analytic curve frequency-sweeping stability tests for systems with commensurate delays," *Springer Briefs in Electrical and Computer Engineering: Control, Automation and Robotics*, 2015.

[41] K. Cooke and P. Van Den Driessche, "On the zeros of some elementary transcendental functions," *American Mathematical Society Translations*, vol. 2, no. 1, pp. 95–110, 1955.

[42] K. L. Cooke and P. Van den Driessche, "On zeroes of some transcendental equations," *Funkcialaj Ekvacioj*, vol. 29, no. 1, pp. 77–90, 1986.

[43] V. L. Kharitonov and A. P. Zhabko, "Robust stability of time-delay systems," *Institute of Electrical and Electronics Engineers Transactions on Automatic Control*, vol. 39, no. 12, pp. 2388–2397, 1994.

[44] N. Olgac and R. Sipahi, "An exact method for the stability analysis of time-delayed linear time-invariant (LTI) systems," *Institute of Electrical and Electronics Engineers Transactions on Automatic Control*, vol. 47, no. 5, pp. 793–797, 2002.

[45] L. Freidovich, A. Shiriaev, F. Gordillo, F. Gómez-Estern, and J. Aracil, "Partial-energy-shaping control for orbital stabilization of high-frequency oscillations of the furuta pendulum," *IEEE Transactions on Control Systems Technology*, vol. 17, no. 4, pp. 853–858, 2009.

[46] P. X. La Hera, L. B. Freidovich, A. S. Shiriaev, and U. Mettin, "New approach for swinging up the furuta pendulum: theory and experiments," *Mechatronics*, vol. 19, no. 8, pp. 1240–1250, 2009.

[47] S. Mori, H. Nishihara, and K. Furuta, "Control of unstable systems," *International Journal of Control*, vol. 23, no. 5, pp. 673–692, 1976.

[48] A. Ferreira, F. J. Bejarano, and L. M. Fridman, "Robust control with exact uncertainties compensation: with or without chattering?" *IEEE Transactions on Control Systems Technology*, vol. 19, no. 5, pp. 969–975, 2011.

[49] J. Aracil, J. Á. Acosta, and F. Gordillon, "A nonlinear hybrid controller for swinging-up and stabilizing the Furuta pendulum," *Control Engineering Practice*, vol. 21, no. 8, pp. 989–993, 2013.

[50] A. Levant, "Robust exact differentiation via sliding mode technique," *Automatica*, vol. 34, no. 3, pp. 379–384, 1998.

[51] L. Biagiotti and C. Melchiorri, *Trajectory Planning for Automatic Machines and Robots*, Springer, Berlin, Germany, 2008.

[52] Y. Tzypkin, "Stability of systems with delayed feedback," *Automation and Remote Control*, vol. 7, no. 2-3, pp. 107–129, 1946.

[53] A. Drozd and Z. Filer, "Application of the Mikhailov criterion to the study of stability of systems with delay," *Journal of Computer and Systems Sociences International*, vol. 38, no. 3, pp. 339–342, 1998.

[54] L. Pekar, R. Prokop, and R. Maturu, "A stability test for control systems with delays based on the nyquist criterion," *International Journal of Mathematical Models and Methods in Applied Sciences*, vol. 5, no. 7, pp. 1213–1224, 2011.

[55] W. Michiels and S.-I. Niculescu, "Stability and stailization of time-delay systems advances in design and control," *Society for Industrial and Applied Mathematics*, 2007.

Hindawi
Mathematical Problems in Engineering
Volume 2017, Article ID 4907520, 8 pages
https://doi.org/10.1155/2017/4907520

Research Article

Response of Duffing Oscillator with Time Delay Subjected to Combined Harmonic and Random Excitations

D. N. Hao[1] and N. D. Anh[2,3]

[1] *University of Information Technology, VNU-HCM, KP6, Linh Trung, Thu Duc, Ho Chi Minh City, Vietnam*
[2] *Institute of Mechanics, VAST, 18 Hoang Quoc Viet, Cau Giay, Hanoi, Vietnam*
[3] *University of Engineering and Technology, VNU, Hanoi, Vietnam*

Correspondence should be addressed to D. N. Hao; haodn@uit.edu.vn

Received 25 June 2017; Revised 3 September 2017; Accepted 25 October 2017; Published 20 November 2017

Academic Editor: Radek Matušů

This paper aims to investigate the stationary probability density functions of the Duffing oscillator with time delay subjected to combined harmonic and white noise excitation by the method of stochastic averaging and equivalent linearization. By the transformation based on the fundamental matrix of the degenerate Duffing system, the paper shows that the displacement and the velocity with time delay in the Duffing oscillator can be computed approximately in non-time delay terms. Hence, the stochastic system with time delay is transformed into the corresponding stochastic non-time delay equation in Ito sense. The approximate stationary probability density function of the original system can be found by combining the stochastic averaging method, the equivalent linearization method, and the technique of auxiliary function. The response of Duffing oscillator is investigated. The analytical results are verified by numerical simulation results.

1. Introduction

It is known that time delay in real active control systems is unavoidable due to the time spent in calculating and executing the control forces, performing online computation, and so on. Hence, time delay causes unsynchronized application of a control force and often leads to poor performance or instability of controlled systems [1]. In the theory of random vibration, much attention has been paid to the study of the oscillator system with time delay under random excitation extensively. For the case of systems with time delay excited by Gaussian white noise, some methods/techniques have been developed to treat these such systems [1–6]. For instance, in [1], Di Paola and Pirrotta used the Taylor expansion of the control force and another approach to finding exact stationary solution to study the effects of time delay on the controlled linear systems. In 2009, Li et al. [2] studied effects of time delay in feedback control on the first-passage failure of controlled systems under stochastic excitation by using the stochastic averaging method for quasi-integrable Hamiltonian systems. In 2012, Liu and Zhu [3] proposed a procedure based on the stochastic averaging method for the time delay stochastic optimal control and stabilization of quasi-integrable Hamiltonian systems subject to Gaussian white noise excitation to study the response and stability of systems. They converted the problem of time delay stochastic optimal control of quasi-integrable Hamiltonian systems into the problem of stochastic optimal control without time delay and the result problem is solved by applying the stochastic averaging method for quasi-integrable Hamiltonian systems and the stochastic dynamical programming principle. In Feng and Liu's work [6], they used stochastic averaging method with assumptions that state variables are slowly varying processes and then solved the Fokker-Planck (FP) equation by finite difference method to yield the stationary joint probability density. To authors' knowledge, this assumption is based on no appropriate reason/proof from now on. Maybe the assumption is based on authors' experiences. In our work, we showed that this assumption is acceptable.

In the present work we investigate Duffing oscillator under time delay state feedback, involving both displacement and velocity feedback, and under combined harmonic and

random excitation. Through this study, a new approximate procedure for vibration systems with time delay under harmonic and random excitation is proposed. The system is expressed equivalently in terms without time delay. Then the equivalent system is transformed into Ito stochastic equations which are treated by using the stochastic averaging method. The solution of the FP equation associated with the Ito stochastic system is a very difficult problem. To overcome the arising problem, the technique of combining the linear equivalent method and the auxiliary function technique proposed in [7–9] is utilized. The paper is organized as follows: in Section 2, the approximate technique for Duffing oscillator with time delay is discussed. In Section 3, effects of system's parameters on the response are investigated and compared with Monte-Carlo simulation (MCS). Finally, in Section 4, summary and conclusions are given.

2. Duffing with Time Delay Subjected to Combined Periodic and Random Excitations

Let us consider the Duffing system subjected to a harmonic force $\varepsilon Q\cos\nu t$ and the white noise $\xi(t)$:

$$\ddot{x}+\varepsilon h\dot{x}+\omega^2 x+\varepsilon\gamma x^3=\varepsilon\lambda_1 x_\tau+\varepsilon\lambda_2\dot{x}_\tau+\varepsilon Q\cos\nu t+\sqrt{\varepsilon}\sigma\xi(t), \tag{1}$$

where ω, h, γ, Q, ν, σ, λ_1, λ_2, $\tau > 0$ are constants, ε is a small positive parameter, $x_\tau = x(t-\tau)$, $\dot{x}_\tau = \dot{x}(t-\tau)$, dot denotes differentiation with respect to time, and function $\xi(t)$ is a Gaussian white noise process of unit intensity with the correlation function $R_\xi(s) = E[\xi(t)\xi(t+s)] = \delta(s)$, where $\delta(\tau)$ is the Dirac delta function, and notation $E(\cdot)$ denotes the mathematical expectation operator. Consider the primary resonant domain where there is a relation between ω and ν as

$$\omega^2=\nu^2+\varepsilon\Delta, \tag{2}$$

where Δ is a detuning parameter. Substituting (2) into (1) one obtains

$$\ddot{x}+\nu^2 x=\varepsilon\left(-\Delta x-h\dot{x}-\gamma x^3+\lambda_1 x_\tau+\lambda_2\dot{x}_\tau+Q\cos\nu t\right)+\sqrt{\varepsilon}\sigma\xi(t). \tag{3}$$

To the authors' knowledge, the stochastic averaging technique is developed for non-time delay systems which are in standard form and derivatives of their variables are proportional to the small parameter. There is no version for systems with the time delay. Thus, so as to apply this technique, the system with time delay should be replaced appropriately by the non-time delay one.

In order to employ the theory of stochastic differential equations, in many works, time delay terms were approximated by non-time delay ones under some assumptions such as "small time delay," for example, Bilello et al. (2002) [10], Feng et al. (2009) [5], Feng et al. (2011) [11], and Liu and Zhu (2012) [3], or "small parameter," for example, Li et al. (2009) [2] and Li and Feng (2010) [4]. Under such assumptions, the amplitude $a(t)$ of the system's response can be treated as a slow varying term. Thus, one obtains the approximation: $a(t-\tau)\approx a(t)$. Then, the time delay terms are approximated by non-time delay ones. Maybe these assumptions are based on the authors' experiences. In the next paragraph, it is showed that these assumptions are acceptable because they come from the fact that the new variables are, as shown in (8) and (10), varying slowly processes since their derivatives are proportional to the small parameter ε. To do that, (3) is rewritten in matrix form as follows:

$$\frac{d}{dt}\begin{bmatrix}x(t)\\ \dot{x}(t)\end{bmatrix}=A\begin{bmatrix}x(t)\\ \dot{x}(t)\end{bmatrix}+\varepsilon B\begin{bmatrix}x_\tau\\ \dot{x}_\tau\end{bmatrix}+\varepsilon\begin{bmatrix}0\\ f\end{bmatrix}+\sqrt{\varepsilon}\sigma\begin{bmatrix}0\\ 1\end{bmatrix}\xi(t), \tag{4}$$

where

$$A=\begin{bmatrix}0 & 1\\ -\nu^2 & 0\end{bmatrix},\quad B=\begin{bmatrix}0 & 0\\ \lambda_1 & \lambda_2\end{bmatrix},\quad f=-\Delta x-h\dot{x}-\gamma x^3+Q\cos\nu t. \tag{5}$$

Make the following transformation in (4):

$$\begin{bmatrix}x(t)\\ \dot{x}(t)\end{bmatrix}=H(t)\,z(t), \tag{6}$$

where $z(t) = [z_1(t)\ \ z_2(t)]^t$, $H(t)=\begin{bmatrix}\cos\nu t & \nu^{-1}\sin\nu t\\ -\nu\sin\nu t & \cos\nu t\end{bmatrix}$ is the fundamental matrix of ordinary differential equation (7), obtained from (6) for $\varepsilon = 0$:

$$\frac{d}{dt}\begin{bmatrix}x(t)\\ \dot{x}(t)\end{bmatrix}=A\begin{bmatrix}x(t)\\ \dot{x}(t)\end{bmatrix}. \tag{7}$$

Substituting (6) into (4) one obtains

$$\frac{d}{dt}z(t)=\varepsilon H(t)^{-1}\left\{BH(t-\tau)\,z(t-\tau)+\begin{bmatrix}0\\ f\end{bmatrix}\right\}+\sqrt{\varepsilon}\sigma\begin{bmatrix}0\\ 1\end{bmatrix}\xi(t), \tag{8}$$

where

$$H(t)^{-1}=\begin{bmatrix}\cos\nu t & -\nu^{-1}\sin\nu t\\ \nu\sin\nu t & \cos\nu t\end{bmatrix}. \tag{9}$$

It is observed from (8) that $z(t)$ can be assumed to be a slowly varying random process since ε is the small parameter; that is, one has the following approximation:

$$z(t-\tau)\approx z(t). \tag{10}$$

Using (6) and (10) with noting that $H(t-\tau) = H(-\tau)H(t)$ gives

$$B\begin{bmatrix} x_\tau \\ \dot{x}_\tau \end{bmatrix} = BH(t-\tau)\, z(t-\tau) \approx BH(-\tau)\, H(t)\, z(t) = BH(-\tau)\begin{bmatrix} x(t) \\ \dot{x}(t) \end{bmatrix}, \tag{11}$$

where

$$BH(-\tau) = \begin{bmatrix} 0 & 0 \\ \lambda_1 \cos \nu t + \lambda_2 \nu \sin \nu t & -\lambda_1 \nu^{-1} \sin \nu t + \lambda_2 \cos \nu t \end{bmatrix}. \tag{12}$$

Substituting (11) into (4) gives the equivalent system with (4) without time delay as follows:

$$\frac{d}{dt}\begin{bmatrix} x(t) \\ \dot{x}(t) \end{bmatrix} = A\begin{bmatrix} x(t) \\ \dot{x}(t) \end{bmatrix} + \varepsilon BH(-\tau)\begin{bmatrix} x(t) \\ \dot{x}(t) \end{bmatrix} + \varepsilon \begin{bmatrix} 0 \\ f \end{bmatrix} + \sqrt{\varepsilon}\sigma \begin{bmatrix} 0 \\ 1 \end{bmatrix} \xi(t). \tag{13}$$

Rewriting obtained (13), with noting (12), in second-order stochastic differential equation yields

$$\ddot{x} + \nu^2 x = \varepsilon \left[-\Delta x - h\dot{x} - \gamma x^3 + \left(\lambda_1 \cos \nu t + \lambda_2 \nu \sin \nu t\right) x + \left(-\frac{\lambda_1}{\nu} \sin \nu t + \lambda_2 \cos \nu t \right) \dot{x} + Q \cos \nu t \right] + \sqrt{\varepsilon}\sigma \xi(t). \tag{14}$$

Let us denote

$$\delta_1 = -\Delta + \lambda_1 \cos \nu\tau + \nu\lambda_2 \sin \nu\tau, \qquad \delta_2 = -h - \frac{\lambda_1}{\nu} \sin \nu\tau + \lambda_2 \cos \nu\tau. \tag{15}$$

Then (14) becomes

$$\ddot{x} + \nu^2 x = \varepsilon \left[\delta_1 x + \delta_2 \dot{x} - \gamma x^3 + Q \cos \nu t \right] + \sqrt{\varepsilon}\sigma \xi(t). \tag{16}$$

It is noted that (16) is non-time delay one which is an approximation of original system (1).

We seek the solution of (16) in the form of

$$x = a_1 \cos \nu t + a_2 \sin \nu t, \qquad \dot{x} = -a_1 \nu \sin \nu t + a_2 \nu \cos \nu t, \tag{17}$$

where a_1 and a_2 are random processes satisfying an additional condition

$$\dot{a}_1 \cos \nu t + \dot{a}_2 \sin \nu t = 0. \tag{18}$$

Substituting (17) into (16) and then solving the resulting equation and (18) with respect to the derivatives $\dot{a}_1$ and $\dot{a}_1$ yield

$$\begin{aligned} \dot{a}_1 &= -\frac{\sin \nu t}{\nu} \left\{ \varepsilon \left[\delta_1 \left(a_1 \cos \nu t + a_2 \sin \nu t \right) + \delta_2 \left(-a_1 \nu \sin \nu t + a_2 \nu \cos \nu t \right) - \gamma \left(a_1 \cos \nu t + a_2 \sin \nu t \right)^3 + Q \cos \nu t \right] + \sqrt{\varepsilon}\sigma \xi(t) \right\} \\ \dot{a}_2 &= \frac{\cos \nu t}{\nu} \left\{ \varepsilon \left[\delta_1 \left(a_1 \cos \nu t + a_2 \sin \nu t \right) + \delta_2 \left(-a_1 \nu \sin \nu t + a_2 \nu \cos \nu t \right) - \gamma \left(a_1 \cos \nu t + a_2 \sin \nu t \right)^3 + Q \cos \nu t \right] + \sqrt{\varepsilon}\sigma \xi(t) \right\}. \end{aligned} \tag{19}$$

This pair of stochastic differential equations can be simplified by using the stochastic averaging method [9, 12, 13]:

$$\dot{a}_1 = \varepsilon H_1(a_1, a_2) + \frac{\sqrt{\varepsilon}\sigma}{\nu\sqrt{2}} \xi_1(t), \qquad \dot{a}_2 = \varepsilon H_2(a_1, a_2) + \frac{\sqrt{\varepsilon}\sigma}{\nu\sqrt{2}} \xi_2(t). \tag{20}$$

Here $\xi_1(t)$ and $\xi_2(t)$ are independent white noises with unit intensity, and the drift coefficients $H_1(a_1, a_2)$ and $H_2(a_1, a_2)$ are determined as follows:

$$\begin{aligned} H_1(a_1, a_2) &= -\frac{1}{\nu} \left\langle \left[\delta_1 \left(a_1 \cos \nu t + a_2 \sin \nu t \right) + \delta_2 \left(-a_1 \nu \sin \nu t + a_2 \nu \cos \nu t \right), - \gamma \left(a_1 \cos \nu t + a_2 \sin \nu t \right)^3 + Q \cos \nu t \right] \sin \nu t \right\rangle \\ H_2(a_1, a_2) &= \frac{1}{\nu} \left\langle \left[\delta_1 \left(a_1 \cos \nu t + a_2 \sin \nu t \right) + \delta_2 \left(-a_1 \nu \sin \nu t + a_2 \nu \cos \nu t \right), - \gamma \left(a_1 \cos \nu t + a_2 \sin \nu t \right)^3 + Q \cos \nu t \right] \cos \nu t \right\rangle, \end{aligned} \tag{21}$$

where $\langle \cdot \rangle$ is a time-averaging operator over one period T defined by

$$\langle \cdot \rangle = \frac{1}{T} \int_0^T (\cdot)\, dt. \tag{22}$$

From (21), one obtains the drift coefficients of system (20):

$$H_1(a_1, a_2) = \frac{\delta_2}{2} a_1 - \frac{\delta_1}{2\nu} a_2 + \frac{3\gamma}{8\nu} \left(a_1^2 a_2 + a_2^3 \right), \qquad H_2(a_1, a_2) = \frac{\delta_1}{2\nu} a_1 + \frac{\delta_2}{2} a_2 - \frac{3\gamma}{8\nu} \left(a_1^3 + a_1 a_2^2 \right) + \frac{Q}{2\nu}. \tag{23}$$

The FP equation written for the stationary PDF $p(a_1, a_2)$ associated with system (20) has the form

$$\frac{\partial}{\partial a_1} \left(H_1(a_1, a_2)\, p \right) + \frac{\partial}{\partial a_2} \left(H_2(a_1, a_2)\, p \right) = \frac{\sigma^2}{4\nu^2} \left[\frac{\partial^2}{\partial a_1^2}(p) + \frac{\partial^2}{\partial a_2^2}(p) \right]. \tag{24}$$

Solution of (24) is still a difficult problem because functions $H_1(a_1, a_2)$ and $H_2(a_1, a_2)$ are nonlinear functions in a_1, a_2 and they do not fulfill the potential condition as showed in [12, 14]. To overcome this difficulty, the equivalent linearization method [15–17] is employed. Following this method, the nonlinear functions H_1, H_2 are replaced by linear ones. Denote

$$g_1(a_1, a_2) = \frac{3\gamma}{8\nu}\left(a_1^2 a_2 + a_2^3\right),$$
$$g_2(a_1, a_2) = -\frac{3\gamma}{8\nu}\left(a_1^3 + a_1 a_2^2\right). \tag{25}$$

According to the stochastic equivalent linearization method, nonlinear terms (25) are replaced by

$$\overline{g}_1(a_1, a_2) = \eta_{11} a_1 + \eta_{12} a_2 + \eta_{13},$$
$$\overline{g}_2(a_1, a_2) = \eta_{21} a_1 + \eta_{22} a_2 + \eta_{23}, \tag{26}$$

where equivalent coefficients η_{ij}, $i = 1, 2$, $j = 1, 2, 3$, are to be determined by an optimization criterion. Thus, the functions H_i, $i = 1, 2$, in (23) are replaced by linear functions

$$\overline{H}_1(a_1, a_2) = \left(\frac{\delta_2}{2} + \eta_{11}\right) a_1 + \left(-\frac{\delta_1}{2\nu} + \eta_{12}\right) a_2 + \eta_{13},$$
$$\overline{H}_2(a_1, a_2) = \left(\frac{\delta_1}{2\nu} + \eta_{21}\right) a_1 + \left(\frac{\delta_2}{2} + \eta_{22}\right) a_2 + \frac{Q}{2\nu} + \eta_{23}. \tag{27}$$

So far, it is seen that (24), where $H_1(a_1, a_2)$ and $H_2(a_1, a_2)$ are replaced by (27), is still hard to solve because it does not fulfill the potential condition [12]. In order to integrate (24), where $H_1(a_1, a_2)$ and $H_2(a_1, a_2)$ are replaced by (27), following the technique of auxiliary function [8, 9], we introduce an auxiliary function $u(a_1, a_2) = u_0 = \text{const}$ as follows:

$$\frac{\partial}{\partial a_1}\left\{\left(\overline{H}_1 p\right) - \frac{\sigma^2}{4\nu^2}\frac{\partial}{\partial a_1} p + \frac{\partial}{\partial a_2}\left(u_0 p\right)\right\} + \frac{\partial}{\partial a_2}\left\{\left(\overline{H}_2 p\right) - \frac{\sigma^2}{4\nu^2}\frac{\partial}{\partial a_2} p - \frac{\partial}{\partial a_1}\left(u_0 p\right)\right\} = 0. \tag{28}$$

We will choose the function $u(a_1, a_2) = u_0$ so that the equalities below are fulfilled:

$$\left(\overline{H}_1 p\right) - \frac{\sigma^2}{4\nu^2}\frac{\partial}{\partial a_1} p + u_0 \frac{\partial}{\partial a_2} p = 0,$$
$$\left(\overline{H}_2 p\right) - \frac{\sigma^2}{4\nu^2}\frac{\partial}{\partial a_2} p - u_0 \frac{\partial}{\partial a_1} p = 0. \tag{29}$$

Denote

$$\Phi(a_1, a_2) = \ln p(a_1, a_2). \tag{30}$$

Substituting (30) into system (29) one obtains

$$\overline{H}_1 - \frac{\sigma^2}{4\nu^2}\frac{\partial \Phi}{\partial a_1} + u_0 \frac{\partial \Phi}{\partial a_2} = 0,$$
$$\overline{H}_2 - \frac{\sigma^2}{4\nu^2}\frac{\partial \Phi}{\partial a_2} - u_0 \frac{\partial \Phi}{\partial a_1} = 0. \tag{31}$$

Solving system (31) in $\partial\Phi/\partial a_1$ and $\partial\Phi/\partial a_2$ yields

$$\frac{\partial \Phi}{\partial a_1} = M(a_1, a_2, u_0),$$
$$\frac{\partial \Phi}{\partial a_2} = N(a_1, a_2, u_0), \tag{32}$$

where

$$M(a_1, a_2, u_0) = \frac{\left(\sigma^2/4\nu^2\right)\overline{H}_1 + u_0 \overline{H}_2}{u_0^2 + \sigma^4/16\nu^4},$$
$$N(a_1, a_2, u_0) = \frac{\left(\sigma^2/4\nu^2\right)\overline{H}_2 - u_0 \overline{H}_1}{u_0^2 + \sigma^4/16\nu^4}. \tag{33}$$

Eliminating $\Phi(a_1, a_2)$ from system (32) gives the equation for the auxiliary function

$$u_0 = \frac{\sigma^2}{4\nu^2}\frac{\delta_1/\nu + \eta_{21} - \eta_{12}}{\delta_2 + \eta_{11} + \eta_{22}}. \tag{34}$$

After finding the function $u(a_1, a_2) = u_0$, the stationary PDF $p(a_1, a_2)$ can be found from (30), (32), and (33) by the quadrature

$$p(a_1, a_2) = C \exp\left\{\int M(a_1, a_2, u_0)\, da_1 + \int M(a_1, a_2, u_0)\, da_2\right\}, \tag{35}$$

where C is a normalization constant [9, 18]. Hence, the corresponding FP equation to (24), where drift coefficients are the linear functions (27), has the following solution:

$$p(a_1, a_2) = C \exp\left\{-\zeta_1 a_1^2 - \zeta_2 a_2^2 + \zeta_3 a_1 a_2 + \zeta_4 a_1 + \zeta_5 a_2\right\}, \tag{36}$$

where C is a normalization constant and coefficients ζ_i, $i = \overline{1, 5}$ are determined as follows:

$$\zeta_1 = -\rho\left(\left(\frac{\delta_2}{2} + \eta_{11}\right)(\delta_2 + \eta_{11} + \eta_{22}) + \left(\frac{\delta_1}{2\nu} + \eta_{21}\right)\left(\frac{\delta_1}{\nu} + \eta_{21} - \eta_{12}\right)\right),$$
$$\zeta_2 = -\rho\left((\delta_2 + \eta_{11} + \eta_{22})\left(\frac{\delta_2}{2} + \eta_{22}\right) - \left(\frac{\delta_1}{\nu} + \eta_{21} - \eta_{12}\right)\left(\frac{-\delta_1}{2\nu} + \eta_{12}\right)\right),$$
$$\zeta_3 = 2\rho\left(\left(\frac{-\delta_1}{2\nu} + \eta_{12}\right)\left(\frac{\delta_2}{2} + \eta_{11}\right) + \left(\frac{\delta_1}{2\nu} + \eta_{21}\right)\left(\frac{\delta_2}{2} + \eta_{22}\right)\right),$$

$$\zeta_4 = 2\rho\left(\eta_{13}\left(\delta_2+\eta_{11}+\eta_{22}\right)+\left(\frac{Q}{2\nu}+\eta_{23}\right)\left(\frac{\delta_1}{\nu}+\eta_{21}-\eta_{12}\right)\right),$$

$$\zeta_5 = 2\rho\left(\left(\frac{-\delta_1}{\nu}+\eta_{12}-\eta_{21}\right)\eta_{13}+\left(\delta_2+\eta_{11}+\eta_{22}\right)\left(\frac{Q}{2\nu}+\eta_{23}\right)\right),$$

$$\rho = \frac{2\nu^2\left(\delta_2+\eta_{11}+\eta_{22}\right)}{\sigma^2\left[\left(\delta_1/\nu+\eta_{21}-\eta_{12}\right)^2+\left(\delta_2+\eta_{11}+\eta_{22}\right)^2\right]}. \tag{37}$$

It is noted that the joint PDF $p(a_1,a_2)$ determined by (36) has finite integral if coefficients ζ_1 and ζ_2 are positive. This condition is always fulfilled because (24), where drift coefficients are linear functions (27), is associated with a linear system under Gaussian white noise in the form of (20). Therefore, the approximate stationary PDF of (24) is determined by (36) whose coefficients are given in (37). It is seen from (36) that random variables a_1 and a_2 are jointly Gaussian [19]. Thus, from (36), one obtains

$$E\left(a_1\right) = \frac{2\zeta_2\zeta_4+\zeta_3\zeta_5}{4\zeta_1\zeta_2-\zeta_3^2},$$

$$E\left(a_2\right) = \frac{2\zeta_1\zeta_5+\zeta_3\zeta_4}{4\zeta_1\zeta_2-\zeta_3^2},$$

$$\sigma_{a_1}^2 = \frac{2\zeta_2}{4\zeta_1\zeta_2-\zeta_3^2}, \tag{38}$$

$$\sigma_{a_2}^2 = \frac{2\zeta_1}{4\zeta_1\zeta_2-\zeta_3^2},$$

$$k_{a_1a_2} = \frac{\zeta_3}{4\zeta_1\zeta_2-\zeta_3^2},$$

where $\sigma_{a_1}^2$ and $\sigma_{a_2}^2$ are variance of a_1 and a_2, respectively, and $k_{a_1a_2}$ is covariance of a_1 and a_2. It is seen from (38) that necessary statistics of processes a_1 and a_2 can be computed algebraically based on coefficients of joint PDF $p(a_1,a_2)$.

Thus, the approximate solution (36) of (1) is completely determined when the linearization coefficients η_{ij}, $i=1,2$; $j=1,2,3$ are found. There are some criteria for determining the coefficients η_{ij}, $i=1,2$, $j=1,2,3$. The most extensively used criterion is the mean square error criterion which requires that the mean square of the following errors be minimum [17]. From (23), (25), (26), and (27), the errors in this problem will be

$$e_i = g_i\left(a_1,a_2\right) - \left(\eta_{i1}a_1+\eta_{i2}a_2+\eta_{i3}\right), \quad i=1,2. \tag{39}$$

So, the mean square error criterion leads to

$$E\left(e_i^2\right) = E\left\{\left[g_i\left(a_1,a_2\right)-\left(\eta_{i1}a_1+\eta_{i2}a_2+\eta_{i3}\right)\right]^2\right\} \longrightarrow \min_{\eta_{ij}}, \quad i=1,2;\ j=1,2,3. \tag{40}$$

From

$$\frac{\partial}{\partial\eta_{ij}}E\left(e_i^2\right) = 0, \quad i=1,2;\ j=1,2,3, \tag{41}$$

it follows that

$$\begin{aligned}
E\left(a_1g_1\right)-E\left(a_1^2\right)\eta_{11}-E\left(a_1a_2\right)\eta_{12}-E\left(a_1\right)\eta_{13} &= 0,\\
E\left(a_2g_1\right)-E\left(a_1a_2\right)\eta_{11}-E\left(a_2^2\right)\eta_{12}-E\left(a_2\right)\eta_{13} &= 0,\\
E\left(g_1\right)-E\left(a_1\right)\eta_{11}-E\left(a_2\right)\eta_{12}-\eta_{13} &= 0,\\
E\left(a_1g_2\right)-E\left(a_1^2\right)\eta_{21}-E\left(a_1a_2\right)\eta_{22}-E\left(a_1\right)\eta_{23} &= 0,\\
E\left(a_2g_2\right)-E\left(a_1a_2\right)\eta_{21}-E\left(a_2^2\right)\eta_{22}-E\left(a_2\right)\eta_{23} &= 0,\\
E\left(g_2\right)-E\left(a_1\right)\eta_{21}-E\left(a_2\right)\eta_{22}-\eta_{23} &= 0,
\end{aligned} \tag{42}$$

where $g_1(a_1,a_2)$, $g_2(a_1,a_2)$ are given by (25). Solving system (42) in η_{ij}, $i=1,2$, $j=1,2,3$, with noting that higher moments of a_1 and a_2 can be expressed in the first and second moments because a_1 and a_2 are jointly Gaussian [16], gives

$$\begin{aligned}
\eta_{11} &= -\frac{3\gamma}{4\nu}\left(k_{a_1a_2}+E\left(a_1\right)E\left(a_2\right)\right),\\
\eta_{12} &= -\frac{3\gamma}{8\nu}\left(E\left(a_1\right)+\sigma_{a_1}^2+3E\left(a_2\right)+3\sigma_{a_2}^2\right),\\
\eta_{13} &= \frac{3\gamma}{4\nu}E\left(a_2\right)\left(E^2\left(a_1\right)+E^2\left(a_2\right)\right),\\
\eta_{21} &= \frac{3\gamma}{8\nu}\left(3E\left(a_2\right)+3\sigma_{a_2}^2+E\left(a_2\right)+\sigma_{a_2}^2\right),\\
\eta_{22} &= \frac{3\gamma}{4\nu}\left(k_{a_1a_2}+E\left(a_1\right)E\left(a_2\right)\right),\\
\eta_{23} &= -\frac{3\gamma}{4\nu}E\left(a_1\right)\left(E^2\left(a_1\right)+E^2\left(a_2\right)\right).
\end{aligned} \tag{43}$$

Thus, η_{ij}, $i=1,2$, $j=1,2,3$, are determined from the system of nonlinear equations obtained by combining (37), (38), and (43). After being found, the values of coefficients η_{ij}, $i=1,2$, $j=1,2,3$, are substituted into (36) to obtain the approximate stationary PDF in a_1 and a_2 of (1).

From transformation (17), the mean response of the oscillator can be rewritten in the form

$$\begin{aligned}
E\left(x\right) &= \sqrt{E^2\left(a_1\right)+E^2\left(a_2\right)}\left[\frac{E\left(a_1\right)}{\sqrt{E^2\left(a_1\right)+E^2\left(a_2\right)}}\cos\nu t\right.\\
&\left.+\frac{E\left(a_2\right)}{\sqrt{E^2\left(a_1\right)+E^2\left(a_2\right)}}\sin\nu t\right]\\
&= \sqrt{E^2\left(a_1\right)+E^2\left(a_2\right)}\cos\left(\nu t+\theta\right),
\end{aligned} \tag{44}$$

where $\tan\theta = -E(a_2)/E(a_1)$. Thus it is periodic with amplitude A, where

$$A^2 = E^2(a_1) + E^2(a_2). \tag{45}$$

Also from transformation (17), the mean square response of (1) can be determined as follows:

$$E\left(x^2(t)\right) = E\left(a_1^2\right)\cos^2\nu t + E\left(a_2^2\right)\sin^2\nu t + E(a_1a_2)\sin 2\nu t. \tag{46}$$

Taking averaging with respect to time (46) gives

$$\begin{aligned}\left\langle E\left(x^2\right)\right\rangle &= \frac{1}{2\pi}\int_0^{2\pi} E\left[x^2(t)\right]d(\nu t)\\ &= \frac{1}{2}\left[E\left(a_1^2\right) + E\left(a_2^2\right)\right]\\ &= \frac{1}{2}\left[E^2(a_1) + \sigma_{a_1}^2 + E^2(a_2) + \sigma_{a_2}^2\right].\end{aligned} \tag{47}$$

Substituting (38) into (47) and reducing the obtained result yield the time-averaging of mean square response to be

$$\left\langle E\left(x^2\right)\right\rangle = \frac{\left(2\zeta_2\zeta_4 + \zeta_3\zeta_5\right)^2 + \left(2\zeta_1\zeta_5 + \zeta_3\zeta_4\right)^2}{2\left(4\zeta_1\zeta_2 - \zeta_3^2\right)^2} + \frac{\zeta_1 + \zeta_2}{4\zeta_1\zeta_2 - \zeta_3^2}, \tag{48}$$

where ζ_i, $i = \overline{1,5}$, are given by (37). It is noted from (48) that the approximate time-averaging value of mean square response of the Duffing oscillator is calculated algebraically.

Moreover, from transformation (17), one obtains

$$\begin{aligned}a_1 &= x\cos\nu t - \frac{\dot{x}}{\nu}\sin\nu t,\\ a_2 &= x\sin\nu t + \frac{\dot{x}}{\nu}\cos\nu t.\end{aligned} \tag{49}$$

It follows from transformation (49) and PDF (36) that the joint PDF of x and $\dot{x}$ takes the form of

$$\begin{aligned}\overline{p}(x,\dot{x},t) = \frac{C}{\nu}\exp\Bigg\{&-A_1\left(x\cos\nu t - \frac{\dot{x}}{\nu}\sin\nu t\right)^2\\ &- A_2\left(x\sin\nu t + \frac{\dot{x}}{\nu}\cos\nu t\right)^2\\ &+ A_3\left(x\cos\nu t - \frac{\dot{x}}{\nu}\sin\nu t\right)\left(x\sin\nu t + \frac{\dot{x}}{\nu}\cos\nu t\right)\\ &+ A_4\left(x\cos\nu t - \frac{\dot{x}}{\nu}\sin\nu t\right)\\ &+ A_5\left(x\sin\nu t + \frac{\dot{x}}{\nu}\cos\nu t\right)\Bigg\}.\end{aligned} \tag{50}$$

From (50), one gets the marginal PDF of x as

$$\overline{p}(x,t) = \int_{-\infty}^{\infty}\overline{p}(x,\dot{x},t)\,d\dot{x}. \tag{51}$$

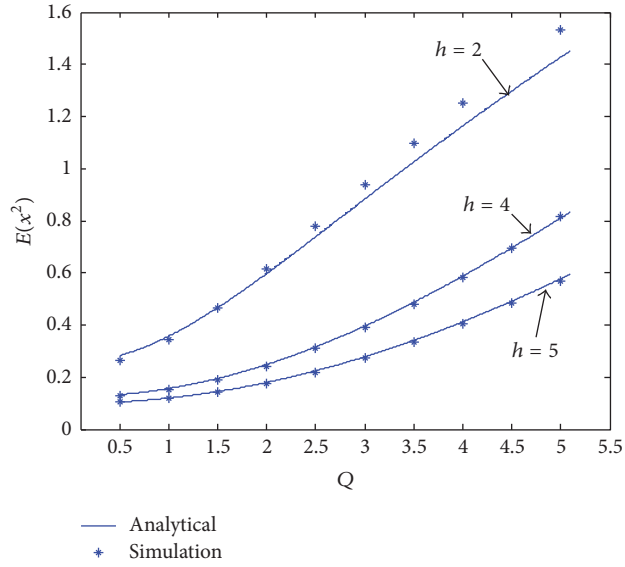

Figure 1: Plot of the time-averaging of mean square response $E(x^2(t))$ versus the parameters Q, $\varepsilon = 0.2$, $\gamma = 1$, $\omega = 1$, $\sigma^2 = 1$, $\nu = 1.01$, $\lambda_1 = \lambda_2 = 0.1$, and $\tau = 0.1$.

It is seen from (36), (50), and (51) that the joint PDF of x and $\dot{x}$ and the marginal PDF of x depend on time t, although two variables a_1 and a_2 are described in a stationary joint PDF.

3. Numerical Results

In the paper, the obtained results are compared to ones obtained from the Monte-Carlo simulation which is "often the sole tool available for assessing the accuracy of random vibration solutions generated by approximate methods of analysis," as pointed out in Robert and Spanos (2003) [17]. The various values of response of Duffing equation (1) are compared to the numerical simulation results versus the particular parameter. The numerical simulation of the mean square response is obtained by 10,000-realization Monte-Carlo simulation (MCS) with the time from zero to 300 seconds. The time-averaged mean square response of the Duffing oscillator obtained by formula (48) is compared to a numerical result obtained by MCS in Figure 1.

To obtain theoretical results below, algebraic system (43) is solved with initial values $\eta_{11} = -2$, $\eta_{12} = -0.5$, $\eta_{13} = 2$, $\eta_{21} = 1.5$, $\eta_{22} = -1$, $\eta_{23} = 2$. With the input parameters $\varepsilon = 0.2$, $\gamma = 1$, $\omega = 1$, $\sigma^2 = 1$, $\nu = 1.01$, $\lambda_1 = \lambda_2 = 0.1$, $\tau = 0.1$, in Figure 1, we present the effect of periodic force's amplitude Q on time-averaging mean square response. It may be seen that the theoretical predictions and the simulations compare very well. Moreover, it can be observed from Figure 1 that the time-averaging mean square response increases when harmonic excitation increases and decreases when the damping coefficient h increases.

In Figure 2, we present graphs of PDF of x plotting the time $t = 298$ (sec). In order to get the simulation of PDF of x by MCS, 20,000 sample paths have been used and counted at the time $t = 298$ (sec). Figure 2 shows that the proposed technique gives a good prediction.

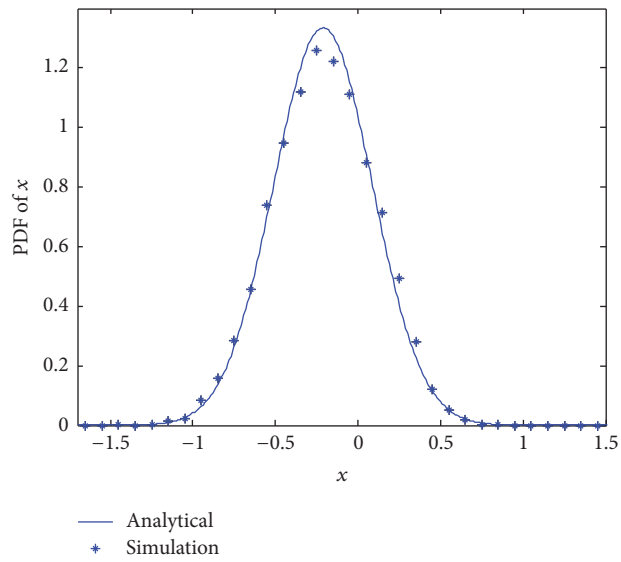

Figure 2: Graph of the marginal PDF of x at $t = 298$ (sec) with input parameters $\varepsilon = 0.2$, $\gamma = 1$, $\omega = 1$, $h = 5$, $Q = 2$, $\sigma^2 = 1$, $\nu = 1.01$, $\lambda_1 = \lambda_2 = 0.1$, and $\tau = 0.1$.

In Tables 1 and 2, effects of the delay coefficient λ_2 and the time delay τ on time-averaging of mean square response of the system are considered. The analytical approximate results obtained by the proposed technique are compared to simulation results $\langle E(x^2)\rangle_{\text{sim}}$ by MCS. The errors in the tables are defined as

$$\text{Error} = \frac{\left|\left\langle E\left(x^2\right)\right\rangle_{\text{sim}} - \left\langle E\left(x^2\right)\right\rangle\right|}{\left\langle E\left(x^2\right)\right\rangle_{\text{sim}}} \times 100\%. \quad (52)$$

In Table 1, the time-averaging mean square response of the system is performed for computation with various values of the parameter λ_2 while the system parameters are chosen to be $\varepsilon = 0.2$, $\gamma = 1$, $\omega = 1$, $h = 4$, $Q = 2$, $\sigma^2 = 1$, $\nu = 1.01$, $\lambda_1 = 0.1$, and $\tau = 1$. It is seen that the time-averaging mean square response of the system slightly increases as the delay coefficient λ_2 decreases from 0.01 to 0.2. Table 2 presents time-averaging values of the mean square response of the system evaluated versus the parameter τ in the primary resonant region with the system parameters chosen to be $\varepsilon = 0.2$, $\gamma = 1$, $\omega = 1$, $h = 5$, $Q = 2$, $\sigma^2 = 1$, $\nu = 1.01$, and $\lambda_1 = \lambda_2 = 0.1$. In Table 2, one expects that the error will decrease as the time delay decreases. However, sometimes this does not often happen in analysis of a stochastic system with time delay; for example, see Figure 1 in Feng et al. (2009) [5]. In the paper, the Duffing oscillator under studying is subjected to both periodic and random excitation. The random excitation would make the diversity of the system's response unpredictable. On the other hand, the error in the paper consists of 3 errors from replacing the time delay system with the non-time delay one, applying the stochastic averaging method, and applying the equivalent linearization method. Thus, in a particular range of the time delay, the values of error may be fluctuated. However, the errors in Table 2 are quite small (from 0.34% to 3.86%) as the time delay in [0.05, 1]. It shows that when the time delay increases from 0.05 to 1, the time-averaging values of the mean square response of the system slightly decrease. The two tables show that the proposed technique gives a good prediction.

Table 1: The error between the simulation result and approximate values of the time-averaging of mean square response versus the parameter λ_2.

λ_2	$\langle E(x^2)\rangle_{\text{sim}}$	$\langle E(x^2)\rangle$	Error (%)
0.01	0.2288	0.2362	3.23
0.03	0.2294	0.2353	2.57
0.05	0.2301	0.2361	2.61
0.07	0.2316	0.2368	2.25
0.09	0.2322	0.2375	2.28
0.1	0.2328	0.2397	2.96
0.15	0.2355	0.2396	1.74
0.2	0.2378	0.2414	1.51

Table 2: The error between the simulation result and approximate values of the time-averaging of mean square response versus the parameter τ.

τ	$\langle E(x^2)\rangle_{\text{sim}}$	$\langle E(x^2)\rangle$	Error (%)
0.05	0.1768	0.1808	2.27
0.15	0.1761	0.1795	1.91
0.2	0.1760	0.1792	1.81
0.25	0.1759	0.1788	1.64
0.3	0.1756	0.1785	1.63
0.35	0.1750	0.1782	1.83
0.4	0.1746	0.1778	1.82
0.5	0.1743	0.1749	0.34
0.7	0.1728	0.1736	0.46
1	0.1709	0.1775	3.86

4. Summary and Conclusions

In the present paper, a technique for predicting the response of the Duffing system with time delay under combined harmonic and white noise excitation has been proposed. The technique can be summarized as follows. Firstly, the time delay terms are expressed approximately in terms of the system state variables without time delay and, correspondingly, the original system with time delay is approximately transformed into one without time delay. The paper has shown this transformation in detail by (6), (7), (8), (10), (11), (12), (13), (14), (15), and (16). Secondly, the state coordinates $(x, \dot{x})$ are transformed to Cartesian coordinates (a_1, a_2). In these coordinates, the averaged equations obtained by the stochastic averaging method are nonlinear ones whose solution is still a difficult problem. Thirdly, the stochastic equivalent linearization method and the technique of auxiliary function are employed to solve approximately the Fokker-Planck equation associated with the averaged equations. The linearization coefficients of the equivalent linear system are determined from a closed nonlinear algebraic system as presented. Finally, the response of the system is obtained

from several algebraic and integral expressions (44)–(51). It has been shown that the results obtained by using the proposed procedure agree well with those from the numerical simulation of the original system. For the given parameters, the time-averaging of mean square response of the system is increasing with the periodic force's amplitude Q and the delay coefficient of velocity λ_2; and it decreases when the time delay τ increases from 0.05 to 1.

A significant contribution of the present paper is that the technique gained through it can be helpful for other nonlinear systems with time delay under harmonic and random excitation. Furthermore, the paper shows that the new variables are, as shown in (8), varying slowly processes since their derivatives are proportional to the small parameter ε. This approach allows simplifying the research by averaging procedure and getting analytical expression for solution.

Conflicts of Interest

The authors declare that there are no conflicts of interest regarding the publication of this paper.

Acknowledgments

This research is funded by Vietnam National University, HCM City, under Grant no. C2016-26-04.

References

[1] M. Di Paola and A. Pirrotta, "Time delay induced effects on control of linear systems under random excitation," *Probabilistic Engineering Mechanics*, vol. 16, no. 1, pp. 43–51, 2001.

[2] X. P. Li, Z. H. Liu, and W. Q. Zhu, "First-passage failure of quasi linear systems subject to multi-time-delayed feedback control and wide-band random excitation," *Probabilistic Engineering Mechanics*, vol. 24, no. 2, pp. 144–150, 2009.

[3] Z. H. Liu and W. Q. Zhu, "Time-delay stochastic optimal control and stabilization of quasi-integrable Hamiltonian systems," *Probabilistic Engineering Mechanics*, vol. 27, no. 1, pp. 29–34, 2012.

[4] J. Li and C. S. Feng, "First-passage failure of a business cycle model under time-delayed feedback control and wide-band random excitation," *Physica A: Statistical Mechanics and its Applications*, vol. 389, no. 24, pp. 5557–5562, 2010.

[5] C. S. Feng, Y. J. Wu, and W. Q. Zhu, "Response of Duffing system with delayed feedback control under combined harmonic and real noise excitations," *Communications in Nonlinear Science and Numerical Simulation*, vol. 14, no. 6, pp. 2542–2550, 2009.

[6] C. Feng and R. Liu, "Response of Duffing system with delayed feedback control under bound noise excitation," *Archive of Applied Mechanics*, 2012.

[7] N. D. Anh, "On the study of random oscillations in non-autonomous mechanical systems using the Fokker-Planck-Kolmogorov equation," *Journal of Applied Mathematics and Mechanics*, vol. 49, no. 3, pp. 392–397, 1985.

[8] N. D. Anh, "Two methods of integration of the Kolmogorov-Fokker-Planck equations," *Ukrainian Mathematical Journal*, vol. 38, no. 3, pp. 331–334, 1986.

[9] N. D. Anh, V. L. Zakovorotny, and D. N. Hao, "Response analysis of Van der Pol oscillator subjected to harmonic and random excitations," *Probabilistic Engineering Mechanics*, vol. 37, pp. 51–59, 2014.

[10] C. Bilello, M. Di Paola, and A. Pirrotta, "Time delay induced effects on control of non-linear systems under random excitation," *Meccanica*, vol. 37, pp. 207–220, 2002.

[11] J. Feng, W.-Q. Zhu, and Z.-H. Liu, "Stochastic optimal time-delay control of quasi-integrable Hamiltonian systems," *Communications in Nonlinear Science and Numerical Simulation*, vol. 16, no. 8, pp. 2978–2984, 2011.

[12] R. Stratonovich, *Topics in the Theory of Random Noise*, vol. 1, Gordon and Breach Science Publishers, New York, NY, USA, 1963.

[13] I. A. Mitropolsky, "Averaging method in non-linear mechanics," *International Journal of Non-Linear Mechanics*, vol. 2, no. 1, pp. 69–96, 1967.

[14] C. S. Manohar and R. N. Iyengar, "Entrainment in van der Pol's oscillator in the presence of noise," *International Journal of Non-Linear Mechanics*, vol. 26, no. 5, pp. 679–686, 1991.

[15] I. E. Kazakov, "An approximate method for the statistical investigation for nonlinear systems," *Trudy VVIA im Prof. N. E. Zhukovskogo*, p. 394, 1954.

[16] L. Socha, *Linearization Methods for Stochastic Dynamic Systems*, vol. 730 of *Lecture Notes in Physics*, Springer, Berlin, Germany, 2008.

[17] J. B. Roberts and P. D. Spanos, *Random Vibration and Statistical Linearization*, Dover, Mineola, NY, USA, 2003.

[18] N. D. Anh, V. L. Zakovorotny, and D. N. Hao, "Van der polduffing oscillator under combined harmonic and random excitations," *Vietnam Journal of Mechanics*, vol. 36, no. 3, 2014.

[19] L. Lutes and S. Sarkani, *Random vibration: analysis of Structural and Mechanical Systems. Elsevier ButterworthHeinemann*, Elsevier Butterworth–Heinemann, 2004.

Hindawi
Mathematical Problems in Engineering
Volume 2017, Article ID 3793157, 11 pages
https://doi.org/10.1155/2017/3793157

Research Article

New Stability Criterion for Takagi-Sugeno Fuzzy Cohen-Grossberg Neural Networks with Probabilistic Time-Varying Delays

Xiongrui Wang,[1] Ruofeng Rao,[2] and Shouming Zhong[3]

[1]*Department of Mathematics, Yibin University, Yibin 644000, China*
[2]*Department of Mathematics, Chengdu Normal University, Chengdu, Sichuan 611130, China*
[3]*College of Mathematics, University of Electronic Science and Technology of China, Chengdu 611731, China*

Correspondence should be addressed to Ruofeng Rao; ruofengrao@163.com

Received 2 July 2017; Revised 10 October 2017; Accepted 24 October 2017; Published 16 November 2017

Academic Editor: Renming Yang

A new global asymptotic stability criterion of Takagi-Sugeno fuzzy Cohen-Grossberg neural networks with probabilistic time-varying delays was derived, in which the diffusion item can play its role. Owing to deleting the boundedness conditions on amplification functions, the main result is a novelty to some extent. Besides, there is another novelty in methods, for Lyapunov-Krasovskii functional is the positive definite form of p powers, which is different from those of existing literature. Moreover, a numerical example illustrates the effectiveness of the proposed methods.

1. Introduction

Cohen-Grossberg neural networks (CGNNs) have many practical applications, like artificial intelligence, parallel computing, image processing and recovery, and so on ([1–6]). But the success of these applications largely depends on whether the system has some stability, and so people began to be interested in the stability analysis of the system. In recent decades, reaction-diffusion neural networks have received much attention ([7–13]), including various Laplacian diffusion ([6, 14–20]). Besides, people are paying more and more attention to fuzzy neural network system ([21–34]), due to encountering always some inconveniences such as the complicity, the uncertainty, and vagueness ([27, 35–37]). For example, in [27], Zhu and Li investigated the following fuzzy CGNNs model:

$$\begin{aligned} dx_i(t) = {} & \left\{ -a_i(x_i(t)) \left[b_i(x_i(t)) - \bigwedge_{j=1}^{n} a_{ij} f_j\left(x_j(t)\right) \right.\right. \\ & \left. - \bigvee_{j=1}^{n} b_{ij} g_j\left(x_j(t)\right) - \bigwedge_{j=1}^{n} c_{ij} f_j\left(x_j(t-\tau)\right) \right. \\ & \left.\left. - \bigvee_{j=1}^{n} d_{ij} g_j\left(x_j(t-\tau)\right) \right] \right\} dt \\ & + \sum_{j=1}^{n} \sigma_{ij}\left(x_j(t), x_j(t-\tau)\right) dw_j(t), \\ & x_i(t) = \phi_i(t), \quad -\tau \leqslant t \leqslant 0. \end{aligned} \tag{1}$$

In [36], Muralisankar and Gopalakrishnan studied the following T-S fuzzy neutral type CGNNs with distributed delays:

$$\begin{aligned} dx_i(t) = {} & \sum_{j=1}^{r} h_j(\omega(t)) \left\{ -A_j(x(t)) \left[B_j(x(t)) \right.\right. \\ & \left. - C_j f(x(t-\tau(t))) - M_j \int_{t-\rho(t)}^{t} f(x(s))\, ds \right. \\ & \left.\left. - D_j \dot{x}(t-r(t)) \right] \right\}. \end{aligned} \tag{2}$$

Besides, Balasubramaniam and Syed Ali discussed Takagi-Sugeno fuzzy Cohen-Grossberg BAM neural networks with discrete and distributed time-varying delays in [37].

Note that there is the following bounded condition on amplification functions in many literatures (see, e.g., [38, Theorem 4]) related to CGNNs:

$$0 < \underline{a}_i \leqslant a_i(r) \leqslant \overline{a}_i, \quad r \in R,\ i = 1, 2, \ldots, n. \tag{3}$$

So, in this paper, we try to delete this bounded condition on amplification functions. This is the main purpose of this paper.

2. Preliminaries

Consider the following fuzzy Takagi-Sugeno p-Laplace partial differential equations with distributed delay.

Fuzzy Rule j. IF $\omega_1(t)$ is μ_{j1} and $\cdots$ $\omega_s(t)$ is μ_{js} *THEN*

$$\begin{aligned}
&\frac{\partial u}{\partial t} = \nabla \cdot \left(\mathscr{D}(t,x,u) \circ \nabla_p u\right) - A(u) \Bigg[B(u) \\
&\quad - C_j f(u(t-\tau(t),x)) - M_j \int_{t-\rho(t)}^{t} f(u(s,x))\, ds \Bigg], \\
&u(\theta,x) = \phi(\theta,x), \quad (\theta,x) \in (-\infty,0] \times \Omega, \\
&u(t,x) = 0 \in R^n, \quad (t,x) \in R \times \partial\Omega,
\end{aligned} \tag{4}$$

where Ω is an arbitrary open bounded subset in R^m. $\omega_k(t)$ $(k = 1, 2, \ldots, s)$ is the premise variable and μ_{jk} $(j = 1, 2, \ldots, r;\ k = 1, 2, \ldots, s)$ is the fuzzy set that is characterized by membership function. And r is the number of the *IF-THEN* rules; s is the number of the premise variables. $u(t,x) = (u_1(t,x), u_2(t,x), \ldots, u_n(t,x))^T \in R^n$, where $u_i(t,x)$ is the state variable of the ith neuron and the jth neuron at time t and in space variable x. Matrix $\mathscr{D}(t,x,u) = (\mathscr{D}_{ij}(t,x,u))_{n\times m}$ with each $\mathscr{D}_{ij}(t,x,u) \geqslant 0$, and $\mathscr{D}_{ij}(t,x,u)$ is diffusion operator. $\mathscr{D}(t,x,u) \circ \nabla_p u = (\mathscr{D}_{jk}(t,x,u))|\nabla u_i|^{p-2}(\partial u_i/\partial x_k)_{n\times m}$ denotes the Hadamard product of matrix $\mathscr{D}(t,x,u)$ and $\nabla_p u$ (see [39] for details). Matrices $A(u) = \mathrm{diag}(a_1(u_1), a_2(u_2), \ldots, a_n(u_n))$ and $B(u) = \mathrm{diag}(b_1(u_1), b_2(u_2), \ldots, b_n(u_n))$, where $a_i(u_i)$ and $b_i(u_i)$ represent an amplification function at time t and an appropriate behavior function at time t. $C_j = (c_{ik}^{(j)})_{n\times n}$ is the connection matrix. Time delays $\tau(t) \in [0, +\infty)$. $f(u(t-\tau(t),x)) = (f_1(u_1(t-\tau(t)t,x)), f_2(u_2(t-\tau(t),x)), \ldots, f_n(u_n(t-\tau(t),x)))^T$ is the activation function of the neurons. And the second and third equations of (4) imply the initial condition and the Dirichlet boundary condition, respectively.

By way of a standard fuzzy inference method, (4) can be inferred as follows.

$$\begin{aligned}
&\frac{\partial u}{\partial t} = \nabla \cdot \left(\mathscr{D}(t,x,u) \circ \nabla_p u\right) - A(u(t,x)) \Bigg[B(u(t,x)) \\
&\quad - \sum_{j=1}^{r} h_j(\omega(t)) \Bigg(C_j f(u(t-\tau(t),x)) \\
&\quad + M_j \int_{t-\rho(t)}^{t} f(u(s,x))\, ds \Bigg) \Bigg], \\
&u(\theta,x) = \phi(\theta,x), \quad (\theta,x) \in (-\infty,0] \times \Omega, \\
&u(t,x) = 0 \in R^n, \quad (t,x) \in R \times \partial\Omega,
\end{aligned} \tag{5}$$

where $\omega(t) = [\omega_1(t), \omega_2(t), \ldots, \omega_s(t)]^T$ and $h_j(\omega(t)) = w_j(\omega(t))/\sum_{k=1}^{r} w_k(\omega(t))$, $w_j(\omega(t)) : R^s \to [0,1]$ $(j = 1, 2, \ldots, r)$ is the membership function of the system with respect to the fuzzy rule j. h_j can be regarded as the normalized weight of each *IF-THEN* rule, satisfying $h_j(\omega(t)) \geqslant 0$ and $\sum_{j=1}^{r} h_j(\omega(t)) = 1$.

Next, we consider the following information for probability distribution of time delays $\tau(t)$:

$$\begin{aligned}
&\mathbb{P}\left(0 \leqslant \tau(t) \leqslant \tau_1\right) = c_0, \\
&\mathbb{P}\left(\tau_1 < \tau(t) \leqslant \tau_2\right) = 1 - c_0.
\end{aligned} \tag{6}$$

Here the nonnegative scalar $c_0 \leqslant 1$. Define a random variable as follows:

$$\mathfrak{C}(t) = \begin{cases} 1, & 0 \leqslant \tau(t) \leqslant \tau_1; \\ 0, & \tau_1 < \tau(t) \leqslant \tau_2. \end{cases} \tag{7}$$

So, in this paper, we consider the following Takagi-Sugeno (T-S) fuzzy system with probabilistic time-varying delays:

$$\begin{aligned}
&\frac{\partial u}{\partial t} = \nabla \cdot \left(\mathscr{D}(t,x,u) \circ \nabla_p u\right) - A(u(t,x)) \Bigg\{ B(u(t,x)) \\
&\quad - \sum_{j=1}^{r} h_j(\omega(t)) \Big[c_0 C_j f\left(u\left(t-\tau_1(t),x\right)\right) + \left(1-c_0\right) \\
&\quad \cdot C_j f\left(u\left(t-\tau_2(t),x\right)\right) + \left(\mathfrak{C}-c_0\right) \\
&\quad \cdot \left(C_j f\left(u\left(t-\tau_1(t),x\right)\right) - C_j f\left(u\left(t-\tau_2(t),x\right)\right)\right) \\
&\quad + M_j \int_{t-\rho(t)}^{t} f(u(s,x))\, ds \Big] \Bigg\}, \\
&u(\theta,x) = \phi(\theta,x), \quad (\theta,x) \in (-\infty,0] \times \Omega, \\
&u(t,x) = 0 \in R^n, \quad (t,x) \in R \times \partial\Omega.
\end{aligned} \tag{8}$$

System (8) includes the following integrodifferential equations:

$$\begin{aligned}\frac{dx(t)}{dt} &= -A(x(t))\left\{B(x(t)) - \sum_{j=1}^{r} h_j(\omega(t))\right.\\ &\cdot\left[c_0 C_j f\left(x\left(t-\tau_1(t)\right)\right) + \left(1-c_0\right)\right.\\ &\cdot C_j f\left(x\left(t-\tau_2(t)\right)\right) + \left(\mathfrak{C}-c_0\right)\\ &\cdot\left(C_j f\left(x\left(t-\tau_1(t)\right)\right) - C_j f\left(x\left(t-\tau_2(t)\right)\right)\right)\\ &\left.\left.+ M_j\int_{t-\rho(t)}^{t} f(x(s))\,ds\right]\right\}, \quad t \geqslant 0,\\ x(\theta) &= \phi(\theta), \quad \theta \in (-\infty, 0].\end{aligned} \tag{9}$$

Particularly when $p = 2$, system (8) degenerates into the so-called reaction-diffusion CGNNs:

$$\begin{aligned}\frac{\partial u}{\partial t} &= \nabla\cdot(\mathscr{D}(t,x,u)\circ\nabla u) - A(u(t,x))\left\{B(u(t,x))\right.\\ &- \sum_{j=1}^{r} h_j(\omega(t))\left[c_0 C_j f\left(u\left(t-\tau_1(t),x\right)\right) + \left(1-c_0\right)\right.\\ &\cdot C_j f\left(u\left(t-\tau_2(t),x\right)\right) + \left(\mathfrak{C}-c_0\right)\\ &\cdot\left(C_j f\left(u\left(t-\tau_1(t),x\right)\right) - C_j f\left(u\left(t-\tau_2(t),x\right)\right)\right)\\ &\left.\left.+ M_j\int_{t-\rho(t)}^{t} f(u(s,x))\,ds\right]\right\},\\ u(\theta,x) &= \phi(\theta,x), \quad (\theta,x) \in (-\infty,0]\times\Omega,\\ u(t,x) &= 0 \in R^n, \quad (t,x) \in R\times\partial\Omega.\end{aligned} \tag{10}$$

Throughout this paper, we assume $p = p_1/p_2 > 1$ with p_1 being even number and p_2 being odd number. Besides, suppose that the following conditions hold:

(H1) There exist positive definite matrices $\underline{A} = \mathrm{diag}(\underline{a}_1, \underline{a}_2, \ldots, \underline{a}_n)$ and $\overline{A} = \mathrm{diag}(\overline{a}_1, \overline{a}_2, \ldots, \overline{a}_n)$ such that

$$0 < \underline{a}_i \leqslant \frac{a_i(s)}{s^{p-2}} \leqslant \overline{a}_i, \quad 0 \neq s \in R,\ i = 1,2,\ldots,n, \tag{11}$$

where $A(u) = \mathrm{diag}(a_1(u_1), a_2(u_2), \ldots, a_n(u_n))$ and $u = (u_1, u_2, \ldots, u_n)^T \in R^n$.

(H2) There exists a positive definite matrix $\mathbb{B} = \mathrm{diag}(b_1, b_2, \ldots, b_n)$ such that $b_i(0) = 0$ and

$$\frac{b_i(s)}{s} \geqslant b_i, \quad 0 \neq s \in R,\ i = 1,2,\ldots,n. \tag{12}$$

(H3) There is a positive definite matrix $F = \mathrm{diag}(F_1, F_2, \ldots, F_n)$ such that

$$\left|f_i(s)\right| \leqslant F_i|s|, \quad s \in R,\ i = 1,2,\ldots,n. \tag{13}$$

From (H1)–(H3), we know that $b_i(0) = f_i(0) = 0$ and $u = 0$ is an equilibrium of fuzzy system (8).

Remark 1. There are numerous functions satisfying (H1). For example, if $p = 4/3$, we may set

$$a_i(s) = \frac{0.1\left(1+e^{-s^2}\right)}{\sqrt[3]{s^2}}, \quad \forall 0 \neq s \in R,\ a_i(0) = 0.2. \tag{14}$$

It is obvious that

$$\lim_{s\to 0} a_i(s) = \lim_{s\to 0}\frac{0.1\left(1+e^{-s^2}\right)}{\sqrt[3]{s^2}} = +\infty. \tag{15}$$

So the function $a_i(s)$ is unbounded for $s \in R$. Moreover,

$$0.1 \leqslant \frac{a_i(s)}{s^{p-2}} = 0.1\left(1+e^{-s^2}\right) \leqslant 0.2. \tag{16}$$

One can know from (16) that $0.1 \leqslant a_i(s)/s^{p-2} \leqslant 0.2$ with $\underline{a}_i = 0.1$ and $\overline{a}_i = 0.2$.

Remark 2. The amplification function $a_i(s)$ defined as (7) is actually unbounded for $s \in R$. However, various bounded conditions always imposed restrictions on the amplification functions of existing literature ([3–6, 9, 10, 24, 27, 28]). Hence, our condition (H1) is weaker, which will make a corollary with regard to ordinary integrodifferential equations (9) become novel.

For convenience's sake, we need to introduce the following standard notations similarly as [38]:

$$\begin{aligned} &Q = \left(q_{ij}\right)_{n\times n} > 0\,(<0),\\ &Q = \left(q_{ij}\right)_{n\times n} \geqslant 0\,(\leqslant 0),\\ &Q_1 \geqslant Q_2\,(Q_1 \leqslant Q_2),\\ &Q_1 > Q_2\,(Q_1 < Q_2),\\ &\lambda_{\max}(\Phi),\\ &\lambda_{\min}(\Phi),\\ &|C| = \left(\left|c_{ij}\right|\right)_{n\times n},\\ &|u(t,x)|, \end{aligned} \tag{17}$$

and the identity matrix with compatible I.

(i) The Sobolev space $= \{u \in L^p : \mathscr{D}u \in L^p\}$ (see [40] for details).

(ii) Denote by λ_1 the lowest positive eigenvalue of the boundary value problem (see [40] for details).

$$-\Delta_p \varphi(t,x) = \lambda \varphi(t,x), \quad x \in \Omega$$
$$\varphi(t,x) = 0, \quad x \in \partial\Omega. \tag{18}$$

Lemma 3. *One has*

$$a^{q-1}b \leqslant \frac{q-1}{q}a^q + \frac{b^q}{q}, \quad \forall a,b \in (0,+\infty),\ q>1. \tag{19}$$

Note that Lemma 3 is the particular case of the famous Young inequality.

3. Results and Discussion

Lemma 4. *Let $P = \mathrm{diag}(p_1, p_2, \ldots, p_n)$ be a positive definite matrix and u be a solution of the fuzzy system (8). Then one has*

$$\int_\Omega u^T P\left(\nabla \cdot \left(D(t,x,u) \circ \nabla_p u\right)\right) dx \leqslant -\lambda_1 \underline{p} D \|u\|_p^p, \tag{20}$$

where $D = \min_{ik}(\inf_{t,x,u} | D_{ij}(t,x,u))$, $\|u\|_p^p = \sum_{i=1}^n \int_\Omega |u_i|^p dx$, and $\underline{p}$ is a positive scalar, satisfying $P > \underline{p} I$.

Proof. Since u is a solution of system (8), it follows by Gauss formula and the Dirichlet zero-boundary condition that

$$\begin{aligned}
&\int_\Omega \sum_{j=1}^n p_j u_j \sum_{k=1}^m \frac{\partial}{\partial x_k}\left(D_{jk}\left|\nabla u_j\right|^{p-2}\frac{\partial u_j}{\partial x_k}\right) dx \\
&= -\sum_{k=1}^m \sum_{j=1}^n \int_\Omega p_j D_{jk}\left|\nabla u_j\right|^{p-2}\left(\frac{\partial u_j}{\partial x_k}\right)^2 dx \\
&\leqslant -\lambda_1 D \underline{p} \sum_{j=1}^n \int_\Omega \left|u_j\right|^p dx = -\lambda_1 \underline{p} D \|u\|_p^p.
\end{aligned} \tag{21}$$

□

Remark 5. Lemma 4 extends the conclusion of [2, Lemma 2.1] and [10, Lemma 2.4] from Hilbert space $H_0^1(\Omega)$ to Banach space $W_0^{1,p}(\Omega)$. Particularly, in the case of $\Omega = (0,T) \subset R^1$ or $W_0^{1,p}(0,T)$, the first eigenvalue $\lambda_1 = ((2/T)\int_0^{(p-1)^{1/p}} (dt/(1 - t^p/(p-1))^{1/p}))^p$ (see, e.g., [40]).

Theorem 6. *If there exists a positive definite matrix $P = \mathrm{diag}(p_1, p_2, \ldots, p_n)$ and two positive scalars $\underline{p}$, $\overline{p}$ such that the following inequalities hold:*

$$\begin{aligned}
&\lambda_1 D \underline{p} + \underline{p}\lambda_{min}(\underline{A}\mathbb{B}) > \frac{n\overline{p}}{p}\sum_{j=1}^r \Bigg((p-1)\left|c_j\right| \\
&\quad + \rho(p-1)\left|m_j\right| + \frac{c_0\left|c_j\right|}{1-\tau_1} + \frac{(1-c_0)\left|c_j\right|}{1-\tau_2} + \rho\left|m_j\right| \Bigg) \\
&\quad \cdot \lambda_{max}\overline{A}\lambda_{max}F,
\end{aligned} \tag{22}$$

$$\begin{aligned}
&P > \underline{p} I, \\
&P < \overline{p} I,
\end{aligned} \tag{23}$$

then the null solution of fuzzy system (8) is globally asymptotically stable, where matrices $C_j = (c_{ik}^{(j)})_{n\times n}$, $M_j = (m_{ik}^{(j)})_{n\times n}$, $|c_j| = \max_{ik}|c_{ik}^{(j)}|$, $|m_j| = \max_{ik}|m_{ik}^{(j)}|$, and $\tau_1'(t) \leqslant \tau_1 < 1$, $\tau_2'(t) \leqslant \tau_2 < 1$, $0 \leqslant \rho(t) \leqslant \rho$.

Proof. Firstly, we can conclude from (H1)–(H3) that $u = 0$ is an equilibrium point for system (8).

Next, consider the Lyapunov-Krasovskii functional:

$$V(t) = V_1(t) + \frac{1}{1-\tau_1}V_2(t) + \frac{1}{1-\tau_2}V_3(t) + V_4(t), \tag{24}$$

where

$$\begin{aligned}
V_1(t) &= \int_\Omega u^T(t,x) P u(t,x)\, dx = \sum_{i=1}^n \int_\Omega p_i u_i^2 dx, \\
V_2(t) &= 2c_0 n \frac{\overline{p}}{p}\left(\sum_{j=1}^r \left|c_j\right|\right) \\
&\quad \cdot \lambda_{\max}\overline{A}\lambda_{\max}F \sum_{k=1}^n \int_{t-\tau_1(t)}^t \int_\Omega \left|u_k(s,x)\right|^p dx\, ds, \\
V_3(t) &= 2(1-c_0) n \frac{\overline{p}}{p}\left(\sum_{j=1}^r \left|c_j\right|\right) \\
&\quad \cdot \lambda_{\max}\overline{A}\lambda_{\max}F \sum_{k=1}^n \int_{t-\tau_2(t)}^t \int_\Omega \left|u_k(s,x)\right|^p dx\, ds, \\
V_4(t) &= 2\frac{\overline{p}}{p}\left(\sum_{j=1}^r \left|m_j\right|\right) \\
&\quad \cdot \lambda_{\max}\overline{A}\lambda_{\max}F \sum_{i=1}^n \sum_{k=1}^n \int_\Omega \left(\int_{-\rho}^0 d\zeta \int_{t+\zeta}^t \left|u_k(s,x)\right|^p ds\right) dx.
\end{aligned} \tag{25}$$

Here, $u(t,x) = (u_1(t,x), u_2(t,x), \ldots, u_n(t,x))^T$ is a solution for stochastic fuzzy system (8). Below, we may denote $u(t,x)$ by u and $u_i(t,x)$ by u_i for simplicity. □

Remark 7. It is obvious that our Lyapunov-Krasovskii functional is the positive definite form of p powers, which is different from those of existing literature ([41–43]). For example, in [41], the model is also neural networks with discrete time delay and distributed delays:

$$\begin{aligned}
dx(t) &= \Bigg[-C_i x(t) + A_i f\left(y(t-\tau(t), i)\right) \\
&\quad + B_i \int_{t-\rho(t)}^t f\left(y(s), r(s)\right)\Bigg] dt + \sigma_t dw_1(t), \\
dy(t) &= \Bigg[-\widetilde{C}_i y(t) + \widetilde{A}_i g\left(x(t-\widetilde{\tau}(t), i)\right) \\
&\quad + \widetilde{B}_i \int_{t-\widetilde{\rho}(t)}^t g\left(x(s), r(s)\right)\Bigg] dt + \widetilde{\sigma}_t dw_2(t).
\end{aligned} \tag{26}$$

In [42, Theorem 1], the corresponding Lyapunov-Krasovskii functional is as follows:

$$\widetilde{V}_2 = \int_{-\rho}^{0} d\theta \int_{t+\theta}^{t} f^T\left(y(s), r(s)\right) Lf\left(y(s), r(s)\right) ds + \int_{-\tilde{\rho}}^{0} d\theta \int_{t+\theta}^{t} g^T\left(x(s), r(s)\right) Lg\left(x(s), r(s)\right) ds, \tag{27}$$

which is the positive definite form of 2 powers. And the conclusion of [42, Theorem 1] is the asymptotical stability in the mean square, which is also similar to that of our Theorem 6. However, by means of our Lyapunov-Krasovskii functional with the positive definite form of p powers, we shall derive the asymptotical stability in the mean square for nonlinear p-Laplacian diffusion system (8).

Evaluating the time derivation of $V_1(t)$ along the trajectory of the fuzzy system (8), we can get by [38, Lemma 6] and Lemma 4

$$\begin{aligned} V_1'(t) &= 2\int_\Omega \left[u^T P\left(\nabla\cdot\left(D(t,x,u)\circ\nabla_p u\right)\right) - u^T PA(u)B(u)\right]dx + 2\sum_{j=1}^{r} h_j(\omega(t)) \\ &\cdot\left(\int_\Omega u^T PA(u)c_0 C_j f\left(u\left(t-\tau_1(t),x\right)\right)dx + \int_\Omega u^T PA(u)\left(1-c_0\right)C_j f\left(u\left(t-\tau_2(t),x\right)\right)dx \right. \\ &\left. + \int_\Omega u^T PA(u)M_j\int_{t-\rho(t)}^{t} f(u(s,x))\,ds\,dx\right) \\ &\leqslant -2\lambda_1 \underline{p} D\|u\|_p^p - 2\int_\Omega u^T PA(u)B(u)\,dx + 2c_0\sum_{j=1}^{r}\int_\Omega \left|u^T\right| PA(u)\left|C_j\right| \\ &\cdot\left|f\left(u\left(t-\tau_1(t),x\right)\right)\right|dx + 2\left(1-c_0\right)\sum_{j=1}^{r}\int_\Omega \left|u^T\right| \\ &\cdot PA(u)\left|C_j\right|\left|f\left(u\left(t-\tau_2(t),x\right)\right)\right|dx \\ &+ 2\sum_{j=1}^{r}\int_\Omega \left|u^T\right| PA(u)\left|M_j\right|\int_{t-\rho(t)}^{t}\left|f(u(s,x))\right|ds\,dx. \end{aligned} \tag{28}$$

Besides, gathering (H1) and (H2) gives

$$\int_\Omega u^T PA(u)B(u)\,dx \geqslant \underline{p}\lambda_{\min}\left(\underline{A}\mathbb{B}\right)\|u\|_p^p. \tag{29}$$

It follows by (H1), (H3), and Lemma 3 that

$$\begin{aligned} c_0\int_\Omega \left|u^T\right| PA(u)\left|C_j\right|\left|f\left(u\left(t-\tau_1(t),x\right)\right)\right|dx &= c_0\sum_{k=1}^{n}\sum_{i=1}^{n}\int_\Omega p_i\left|u_i a_i(u_i)\right|\left|c_{ik}^{(j)}\right|\left|f_k\left(u_k\left(t-\tau_1(t),x\right)\right)\right|dx \\ &\leqslant c_0\overline{p}\sum_{k=1}^{n}\sum_{i=1}^{n}\int_\Omega \overline{a}_i\left|c_j\right|\left|u_i\right|^{p-1}F_k\left|u_k\left(t-\tau_1(t),x\right)\right|dx \\ &\leqslant c_0\overline{p}\left|c_j\right|\lambda_{\max}\overline{A}\lambda_{\max}F\sum_{k=1}^{n}\sum_{i=1}^{n}\int_\Omega\left(\frac{p-1}{p}\left|u_i\right|^p + \frac{\left|u_k\left(t-\tau_1(t),x\right)\right|^p}{p}\right)dx \\ &= c_0\frac{(p-1)\overline{p}}{p}n\left|c_j\right|\lambda_{\max}\overline{A}\lambda_{\max}F\|u\|_p^p \\ &\quad + c_0\frac{\overline{p}}{p}n\left|c_j\right|\lambda_{\max}\overline{A}\lambda_{\max}F\sum_{k=1}^{n}\int_\Omega\left|u_k\left(t-\tau_1(t),x\right)\right|^p dx. \end{aligned} \tag{30}$$

Similarly,

$$\begin{aligned} \left(1-c_0\right)\int_\Omega \left|u^T\right| PA(u)\left|C_j\right|\left|f\left(u\left(t-\tau_2(t),x\right)\right)\right|dx &\leqslant \left(1-c_0\right)\frac{(p-1)\overline{p}}{p}n\left|c_j\right|\lambda_{\max}\overline{A}\lambda_{\max}F\|u\|_p^p \\ &+ \left(1-c_0\right)\frac{\overline{p}}{p}n\left|c_j\right|\lambda_{\max}\overline{A}\lambda_{\max}F\sum_{k=1}^{n}\int_\Omega\left|u_k\left(t-\tau_2(t),x\right)\right|^p dx, \end{aligned}$$

$$\int_\Omega \left|u^T\right| PA(u) \left|M_j\right| \int_{t-\rho(t)}^{t} \left|f(u(s,x))\right| ds\, dx = \sum_{k=1}^{n}\sum_{i=1}^{n} \int_\Omega p_i \left|u_i a_i(u_i)\right| \left|m_{ik}^{(j)}\right| \int_{t-\rho(t)}^{t} \left|f_k(u_k(s,x))\right| ds\, dx$$

$$\leqslant \overline{p} \sum_{k=1}^{n}\sum_{i=1}^{n} \int_\Omega \int_{t-\rho(t)}^{t} \overline{a}_i \left|m_j\right| \left|u_i(t,x)\right|^{p-1} F_k \left|u_k(s,x)\right| ds\, dx$$

$$\leqslant \overline{p} \left|m_j\right| \lambda_{\max}\overline{A}\lambda_{\max} F \sum_{k=1}^{n}\sum_{i=1}^{n} \int_\Omega \int_{t-\rho(t)}^{t} \left(\frac{p-1}{p}\left|u_i(t,x)\right|^p + \frac{\left|u_k(s,x)\right|^p}{p}\right) ds\, dx \leqslant \rho \frac{(p-1)\overline{p}}{p} n \left|m_j\right| \lambda_{\max}\overline{A}\lambda_{\max} F \|u\|_p^p$$

$$+ \frac{\overline{p}}{p} \left|m_j\right| \lambda_{\max}\overline{A}\lambda_{\max} F \sum_{i=1}^{n}\sum_{k=1}^{n} \int_\Omega \int_{t-\rho(t)}^{t} \left|u_k(s,x)\right|^p ds\, dx. \tag{31}$$

On the other hand,

$$\begin{aligned} V_2'(t) &= 2c_0 n \frac{\overline{p}}{p} \left(\sum_{j=1}^{r} \left|c_j\right|\right) \\ &\cdot \lambda_{\max}\overline{A}\lambda_{\max} F \left(\sum_{k=1}^{n} \int_\Omega \left|u_k(t,x)\right|^p dx \right. \\ &\left. - \sum_{k=1}^{n} \left(1 - \tau_1'(t)\right) \int_\Omega \left|u_k(t-\tau_1(t),x)\right|^p dx\right) \\ &\leqslant 2c_0 n \frac{\overline{p}}{p} \left(\sum_{j=1}^{r} \left|c_j\right|\right) \lambda_{\max}\overline{A}\lambda_{\max} F \|u\|_p^p - 2c_0 n \\ &\cdot \frac{\overline{p}}{p} \left(\sum_{j=1}^{r} \left|c_j\right|\right) \lambda_{\max}\overline{A}\lambda_{\max} F (1-\tau_1) \\ &\cdot \sum_{k=1}^{n} \int_\Omega \left|u_k(t-\tau_1(t),x)\right|^p dx. \end{aligned} \tag{32}$$

Similarly,

$$\begin{aligned} V_3'(t) &\leqslant 2(1-c_0) n \frac{\overline{p}}{p} \left(\sum_{j=1}^{r} \left|c_j\right|\right) \lambda_{\max}\overline{A}\lambda_{\max} F \|u\|_p^p \\ &- 2(1-c_0) n \frac{\overline{p}}{p} \left(\sum_{j=1}^{r} \left|c_j\right|\right) \\ &\cdot \lambda_{\max}\overline{A}\lambda_{\max} F (1-\tau_2) \\ &\cdot \sum_{k=1}^{n} \int_\Omega \left|u_k(t-\tau_2(t),x)\right|^p dx. \end{aligned} \tag{33}$$

Next, we need to recall some facts derived by mathematical analysis. Assume that $\eta(t,s)$ is continuous on variables t and s, and $\partial\eta/\partial t$ exists, utilizing the integral middle value theorem reaches

$$\begin{aligned} \frac{d}{dt} \int_{\xi(t)}^{\varpi(t)} \eta(t,s)\, ds &= \varpi'(t)\, \eta(t,\varpi(t)) \\ &- \xi'(t)\, \eta(t,\xi(t)) \\ &+ \int_{\xi(t)}^{\varpi(t)} \frac{\partial \eta(t,s)}{\partial t} ds, \end{aligned} \tag{34}$$

where both $\xi(\cdot)$ and $\varpi(\cdot)$ are differentiable.

Moreover, we can derive by employing (32) time and again

$$\begin{aligned} V_4'(t) &= 2\frac{\overline{p}}{p} \left(\sum_{j=1}^{r} \left|m_j\right|\right) \lambda_{\max}\overline{A}\lambda_{\max} F \sum_{i=1}^{n}\sum_{k=1}^{n} \int_\Omega \left(\int_{-\rho}^{0} \left|u_k(t,x)\right|^p ds - \int_{-\rho}^{0} \left|u_k(t+s,x)\right|^p ds\right) dx \\ &= 2\frac{\overline{p}}{p} \left(\sum_{j=1}^{r} \left|m_j\right|\right) \lambda_{\max}\overline{A}\lambda_{\max} F \sum_{i=1}^{n}\sum_{k=1}^{n} \int_\Omega \left(\rho \left|u_k(t,x)\right|^p - \int_{t-\rho(t)}^{t} \left|u_k(s,x)\right|^p ds\right) dx \\ &= 2\frac{\overline{p}}{p} \left(\sum_{j=1}^{r} \left|m_j\right|\right) \lambda_{\max}\overline{A}\lambda_{\max} F \left(n\rho \|u\|_p^p - \sum_{i=1}^{n}\sum_{k=1}^{n} \int_\Omega \int_{t-\rho(t)}^{t} \left|u_k(s,x)\right|^p ds\, dx\right). \end{aligned} \tag{35}$$

Combining (28)–(35) results in

$$V'(t) \leqslant -2\Bigg[\lambda_1 D\underline{p} + \underline{p}\lambda_{\min}(\underline{A}\mathbb{B}) - \frac{n}{p} \cdot \sum_{j=1}^{r}\Bigg(\overline{p}(p-1)\left|c_j\right| + \rho(p-1)\overline{p}\left|m_j\right| + c_0\frac{\overline{p}}{1-\tau_1}\left|c_j\right| + (1-c_0)\frac{\overline{p}}{1-\tau_2}\left|c_j\right| + \rho\overline{p}\left|m_j\right|\Bigg) \cdot \lambda_{\max}\overline{A}\lambda_{\max}F\Bigg]\|u\|_p^p \leqslant 0. \tag{36}$$

Now the standard Lyapunov functional theory derives that the null solution of the fuzzy system (8) is globally asymptotically stable.

Remark 8. In the case of Takagi-Sugeno fuzzy model, our Theorem 6 is better than [38, Theorem 4] because the condition (H1) is weaker than the bounded assumption (2).

Remark 9. In Theorem 6, (22) illustrates the influence of nonlinear diffusion on the stability of system (8) while its role was always ignored in existing results (see, e.g., [5, 39, 44]).

Theorem 6 derives the following corollary.

Corollary 10. *If there exists a positive definite matrix* $P = \mathrm{diag}(p_1, p_2, \ldots, p_n)$ *and two positive scalars* $\underline{p}$, $\overline{p}$ *such that the following inequalities hold:*

$$\underline{p}\lambda_{min}(\underline{A}\mathbb{B}) > \frac{n\overline{p}}{p}\sum_{j=1}^{r}\Bigg((p-1)\left|c_j\right| + \rho(p-1)\left|m_j\right| + \frac{c_0\left|c_j\right|}{1-\tau_1} + \frac{(1-c_0)\left|c_j\right|}{1-\tau_2} + \rho\left|m_j\right|\Bigg)\lambda_{max}\overline{A}\lambda_{max}F, \tag{37}$$

$$P > \underline{p}I,$$

$$P < \overline{p}I,$$

then the null solution of the ordinary integrodifferential equations (9) is globally asymptotically stable.

Furthermore, if both diffusion behaviors and distributed delay are ignored, we derive from Corollary 10.

Corollary 11. *If there exists a positive definite matrix* $P = \mathrm{diag}(p_1, p_2, \ldots, p_n)$ *and two positive scalars* $\underline{p}$, $\overline{p}$ *such that the following inequalities hold:*

$$\underline{p}\lambda_{min}(\underline{A}\mathbb{B}) > \frac{n\overline{p}}{p} \cdot \sum_{j=1}^{r}\Bigg((p-1)\left|c_j\right| + \frac{c_0\left|c_j\right|}{1-\tau_1} + \frac{(1-c_0)\left|c_j\right|}{1-\tau_2}\Bigg) \cdot \lambda_{max}\overline{A}\lambda_{max}F,$$

$$P > \underline{p}I,$$

$$P < \overline{p}I, \tag{38}$$

then the null solution of the following fuzzy system

$$\frac{dx(t)}{dt} = -A(x(t))\Bigg\{B(x(t)) - \sum_{j=1}^{r}h_j(\omega(t)) \cdot \left[c_0C_jf(x(t-\tau_1(t))) + (1-c_0) \cdot C_jf(x(t-\tau_2(t))) + (\mathfrak{C}-c_0) \cdot \left(C_jf(x(t-\tau_1(t))) - C_jf(x(t-\tau_2(t)))\right)\right]\Bigg\}, \tag{39}$$

$$t \geqslant 0,$$

$$x(\theta) = \phi(\theta), \quad \theta \in (-\infty, 0]$$

is globally asymptotically stable.

Remark 12. Condition (H1) is weaker than the bounded conditions on amplification functions of existing literature ([3–6, 9, 10, 24, 27, 28]).

Discussion 1. In recent related literature ([27, 45–51]), some new conditions and methods were presented, and their results were very good. However, some of the methods and conditions are not applicable for system (8) with nonlinear p-Laplacian diffusion. How to apply the new conditions and methods of [45–49] to our system (8) is an interesting problem.

4. Methods and Numerical Example

4.1. Methods. In this paper, Lyapunov functional method is employed to derive the stability criterion. In this process, the integral middle value theorem together with the derivation formula on integral upper limit functions plays the important roles.

Example 1. Consider the following Takagi-Sugeno p-Laplace fuzzy T-S dynamic equations.

Fuzzy Rule 1. IF $\omega_1(t)$ is μ_{11}, and $\omega_2(t)$ is μ_{12}, *THEN*

$$\frac{\partial u}{\partial t} = \nabla\cdot\left(\mathscr{D}(t,x,u)\circ\nabla_p u\right) - A(u)\Bigg[B(u) - c_0C_1f(u(t-\tau_1(t),x)) - (1-c_0) \cdot C_1f(u(t-\tau_2(t),x)) - (\mathfrak{C}-c_0) \cdot \left(C_1f(u(t-\tau_1(t),x)) - C_1f(u(t-\tau_2(t),x))\right) - M_1\int_{t-\rho(t)}^{t} f(u(s,x))\,ds\Bigg],$$

$$u(\theta, x) = \phi(\theta, x), \quad (\theta, x) \in (-\infty, 0] \times \Omega,$$
$$u(t, x) = 0 \in R^2, \quad (t, x) \in R \times \partial\Omega. \tag{40}$$

Fuzzy Rule 2. IF $\omega_1(t)$ is μ_{21}, and $\omega_2(t)$ is μ_{22}, *THEN*

$$\begin{aligned}\frac{\partial u}{\partial t} &= \nabla \cdot \left(\mathscr{D}(t, x, u) \circ \nabla_p u\right) - A(u) \Big[B(u) \\ &\quad - c_0 C_2 f\left(u\left(t - \tau_1(t), x\right)\right) - \left(1 - c_0\right) \\ &\quad \cdot C_2 f\left(u\left(t - \tau_2(t), x\right)\right) - \left(\mathfrak{C} - c_0\right) \\ &\quad \cdot \left(C_2 f\left(u\left(t - \tau_1(t), x\right)\right) - C_2 f\left(u\left(t - \tau_2(t), x\right)\right)\right) \\ &\quad - M_2 \int_{t-\rho(t)}^{t} f(u(s, x))\, ds \Big], \\ u(\theta, x) &= \phi(\theta, x), \quad (\theta, x) \in (-\infty, 0] \times \Omega, \\ u(t, x) &= 0 \in R^2, \quad (t, x) \in R \times \partial\Omega,\end{aligned} \tag{41}$$

where $u(t, x) = (u_1(t, x), u_2(t, x))^T$, $\Omega = (0, \pi)$, $p = 4/3$, and then Remark 1 gives

$$\lambda_1 = \left(\frac{2}{\pi} \int_0^{(p-1)^{1/p}} \frac{dt}{\left(1 - t^p/(p-1)\right)^{1/p}}\right)^p = 0.7915. \tag{42}$$

Let $\tau_1(t) = t/3$, $\tau_2(t) = t/2$, and then $\tau_1 = 1/3$, $\tau_2 = 1/2$. Let $a_i(u_i) = 0.1u_i^{-2/3}(1 + e^{-iu_i^2})$, $i = 1, 2$, $b_1(u_1) = 2u_1(1+\sin^2 u_1)$, $b_2(u_2) = 1.95u_2$, $f_1(u_1(t-\tau(t))) = 0.16u_1(t-\tau(t))\sin u_1(t-\tau(t))$, $f_2(u_2(t-\tau(t))) = 0.166u_2(t-\tau(t))$, $\tau = 0.5$, $D = 0.003$, $c_0 = 0.75$, $c_1 = 0.2$, $c_2 = 0.3$, $m_1 = 0.02$, $m_2 = 0.03$, and

$$\underline{A} = \begin{pmatrix} 0.01 & 0 \\ 0 & 0.02 \end{pmatrix},$$
$$\overline{A} = \begin{pmatrix} 0.1 & 0 \\ 0 & 0.2 \end{pmatrix},$$
$$\mathbb{B} = \begin{pmatrix} 2 & 0 \\ 0 & 1.95 \end{pmatrix},$$
$$D(t, x, u) = \begin{pmatrix} 0.003 & 0.005 \\ 0.004 & 0.006 \end{pmatrix},$$
$$M_1 = \begin{pmatrix} 0.02 & 0.01 \\ 0 & 0.01 \end{pmatrix},$$
$$F = \begin{pmatrix} 0.16 & 0 \\ 0 & 0.166 \end{pmatrix},$$
$$C_1 = \begin{pmatrix} 0.2 & 0.1 \\ 0 & 0.15 \end{pmatrix},$$
$$C_2 = \begin{pmatrix} 0.2 & 0.1 \\ 0 & 0.3 \end{pmatrix},$$
$$M_2 = \begin{pmatrix} 0.01 & 0.01 \\ 0 & 0.03 \end{pmatrix}. \tag{43}$$

Now we use MATLAB to solve LMIs (22)-(23), obtaining the feasibility data

$$P = \begin{pmatrix} 0.9381 & 0 \\ 0 & 1.013 \end{pmatrix},$$
$$\underline{p} = 0.9103, \tag{44}$$
$$\overline{p} = 1.023.$$

Now Theorem 6 derives that the null solution of this Takagi-Sugeno fuzzy equations is globally asymptotically stable (see Figures 1 and 2).

5. Conclusions

By constructing a novel Lyapunov function, we employed Young inequality and LMI technique to derive the asymptotic stability criteria for CGNNs with distributed delays and nonlinear diffusion. Since the stability of nonlinear p-Laplacian diffusion neural networks was originally investigated in [2], various p-Laplacian diffusion neural networks have attracted a lot of interest ([6, 17, 34, 39, 44]). As pointed out in Discussion 1, some new conditions and methods may not be applicable to CGNNs model with nonlinear p-Laplacian diffusion. So our results are a novelty to some extent.

Conflicts of Interest

The authors declare that there are no conflicts of interest regarding the publication of this paper.

Authors' Contributions

Xiongrui Wang wrote the original manuscript, carrying out the main part of this paper. Shouming Zhong checked it, and Ruofeng Rao is in charge of correspondence. All authors read and approved the final manuscript.

Acknowledgments

This work is supported by Scientific Research Fund of Science Technology Department of Sichuan Province (2011JYZ010,

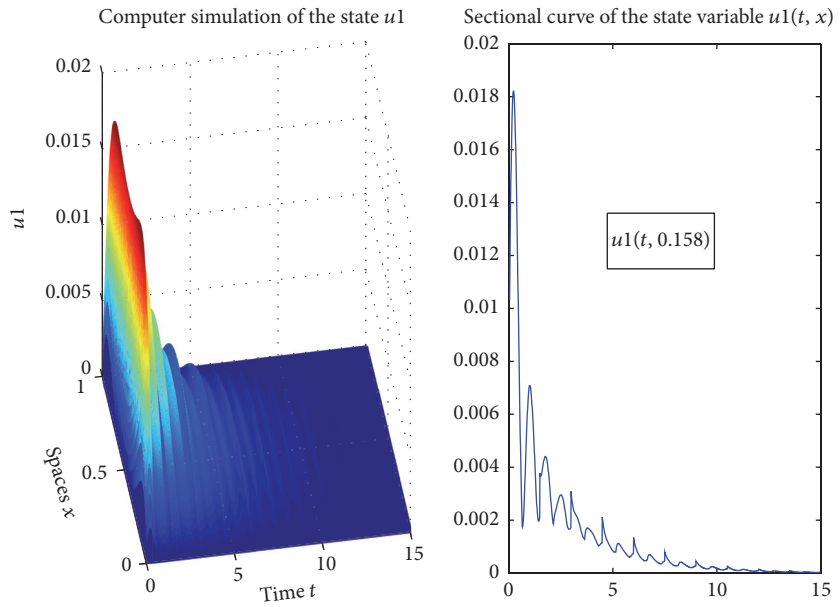

FIGURE 1: Computer simulations of the state $u_1(t, x)$.

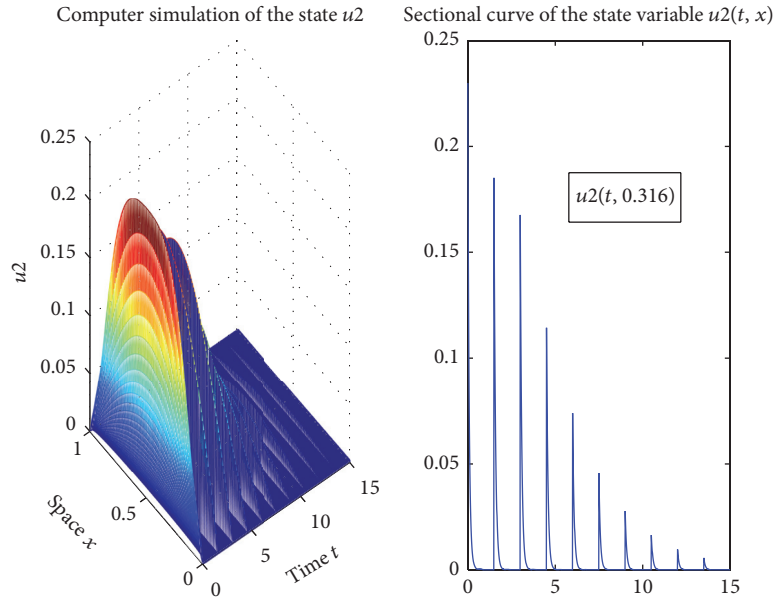

FIGURE 2: Computer simulations of the state $u_2(t, x)$.

2012JY010) and Scientific Research Fund of Sichuan Provincial Education Department (14ZA0274, 12ZB349, 11ZA172, and 08ZB002).

References

[1] X. Zhang, S. Wu, and K. Li, "Delay-dependent exponential stability for impulsive Cohen-Grossberg neural networks with time-varying delays and reaction-diffusion terms," *Communications in Nonlinear Science and Numerical Simulation*, vol. 16, no. 3, pp. 1524–1532, 2011.

[2] R. Rao, S. Zhong, and X. Wang, "Stochastic stability criteria with LMI conditions for Markovian jumping impulsive BAM neural networks with mode-dependent time-varying delays and nonlinear reaction-diffusion," *Communications in Nonlinear Science and Numerical Simulation*, vol. 19, no. 1, pp. 258–273, 2014.

[3] Q. Liu and R. Xu, "Periodic solutions of a cohen-grossberg-type BAM neural networks with distributed delays and impulses," *Journal of Applied Mathematics*, vol. 2012, Article ID 643418, 17 pages, 2012.

[4] H. Song, D. Chen, W. Li, and Y. Qu, "Graph-theoretic approach to exponential synchronization of stochastic reaction-diffusion

Cohen-Grossberg neural networks with time-varying delays," *Neurocomputing*, vol. 177, pp. 179–187, 2016.

[5] H. Xiang and J. Cao, "Periodic oscillation of fuzzy cohen-grossberg neural networks with distributed delay and variable coefficients," *Journal of Applied Mathematics*, vol. 2008, Article ID 453627, 18 pages, 2008.

[6] P. Qingfei, Z. Zifang, and H. Jingchang, "Stability of the stochastic reaction-diffusion neural network with time-varying delays and p-laplacian," *Journal of Applied Mathematics*, vol. 2012, Article ID 405939, 10 pages, 2012.

[7] Q. Song, H. Yan, Z. Zhao, and Y. Liu, "Global exponential stability of impulsive complex-valued neural networks with both asynchronous time-varying and continuously distributed delays," *Neural Networks*, vol. 81, pp. 1–10, 2016.

[8] K. Li, L. Zhang, X. Zhang, and Z. Li, "Stability in impulsive Cohen-Grossberg-type BAM neural networks with distributed delays," *Applied Mathematics and Computation*, vol. 215, no. 11, pp. 3970–3984, 2010.

[9] K. Li and Q. Song, "Exponential stability of impulsive Cohen-Grossberg neural networks with time-varying delays and reaction-diffusion terms," *Neurocomputing*, vol. 72, no. 1–3, pp. 231–240, 2008.

[10] J. Pan and S. Zhong, "Dynamic analysis of stochastic reaction-diffusion Cohen-Grossberg neural networks with delays," *Advances in Difference Equations*, vol. 2009, Article ID 410823, pp. 1–18, 2009.

[11] R. Rao, X. Wang, and S. Zhong, "LMI-based stability criterion for impulsive delays Markovian jumping time-delays reaction-diffusion BAM neural networks via Gronwall-Bellman-type impulsive integral inequality," *Mathematical Problems in Engineering*, vol. 2015, Article ID 185854, 11 pages, 2015.

[12] Q. Song, J. Cao, and Z. Zhao, "Periodic solutions and its exponential stability of reaction-diffusion recurrent neural networks with continuously distributed delays," *Nonlinear Analysis: Real World Applications*, vol. 7, no. 1, pp. 65–80, 2006.

[13] R. Rao, Z. Pu, S. Zhong, and X. Li, "Fixed points and exponential stability for impulsive time-delays BAM neural networks via LMI approach and contraction mapping principle," *Mathematical Problems in Engineering*, vol. 2016, Article ID 3154683, 8 pages, 2016.

[14] Y. Li, Y. Mi, and C. Mu, "Properties of positive solutions for a nonlocal nonlinear diffusion equation with nonlocal nonlinear boundary condition," *Acta Mathematica Scientia*, vol. 34, no. 3, pp. 748–758, 2014.

[15] R. Rao and S. Zhong, "Stability analysis of impulsive stochastic reaction-diffusion cellular neural network with distributed delay via fixed point theory," *Complexity*, Article ID 6292597, 9 pages, 2017.

[16] V. A. Galaktionov, "On asymptotic self-similar behaviour for a quasilinear heat equation: single point blow-up," *SIAM Journal on Mathematical Analysis*, vol. 26, no. 3, pp. 675–693, 1995.

[17] R. Rao and S. Zhong, "Existence of exponential p-stability nonconstant equilibrium of markovian jumping nonlinear diffusion equations via ekeland variational principle," *Advances in Mathematical Physics*, vol. 2015, Article ID 812150, 10 pages, 2015.

[18] R. Rao, S. Zhong, and Z. Pu, "On the role of diffusion factors in stability analysis for p-Laplace dynamical equations involved to BAM Cohen-Grossberg neural network," *Neurocomputing*, vol. 223, pp. 54–62, 2017.

[19] J. Ding and B.-Z. Guo, "Global existence and blow-up solutions for quasilinear reactiondiffusion equations with a gradient term," *Applied Mathematics Letters*, vol. 24, no. 6, pp. 936–942, 2011.

[20] R. Rao and Z. Pu, "Stability analysis for impulsive stochastic fuzzy p-Laplace dynamic equations under Neumann or Dirichlet boundary condition," *Boundary Value Problems*, vol. 2013, article no. 133, 2013.

[21] Y. H. Xia, Z. Yang, and M. Han, "Lag synchronization of unknown chaotic delayed yang-yang-type fuzzy neural networks with noise perturbation based on adaptive control and parameter identification," *IEEE Transactions on Neural Networks and Learning Systems*, vol. 20, no. 7, pp. 1165–1180, 2009.

[22] Y. Xia, Z. Yang, and M. Han, "Synchronization schemes for coupled identical YANg-YANg type fuzzy cellular neural networks," *Communications in Nonlinear Science and Numerical Simulation*, vol. 14, no. 9-10, pp. 3645–3659, 2009.

[23] D. He and D. Xu, "Attracting and invariant sets of fuzzy Cohen-Grossberg neural networks with time-varying delays," *Physics Letters A*, vol. 372, no. 47, pp. 7057–7062, 2008.

[24] Y. Liu and W. Tang, "Exponential stability of fuzzy cellular neural networks with constant and time-varying delays," *Physics Letters A*, vol. 323, no. 3-4, pp. 224–233, 2004.

[25] C. K. Ahn, "Delay-dependent state estimation for T-S fuzzy delayed Hopfield neural networks," *Nonlinear Dynamics*, vol. 61, no. 3, pp. 483–489, 2010.

[26] Q. Song and J. Cao, "Impulsive effects on stability of fuzzy Cohen-Grossberg neural networks with time-varying delays," *IEEE Transactions on Systems, Man, and Cybernetics, Part B: Cybernetics*, vol. 37, no. 3, pp. 733–741, 2007.

[27] Q. Zhu and X. Li, "Exponential and almost sure exponential stability of stochastic fuzzy delayed Cohen-Grossberg neural networks," *Fuzzy Sets and Systems*, vol. 203, pp. 74–94, 2012.

[28] M. A. Cohen and S. Grossberg, "Absolute stability of global pattern formation and parallel memory storage by competitive neural networks," *IEEE Transactions on Systems, Man, and Cybernetics*, vol. 13, no. 5, pp. 815–826, 1983.

[29] A.-T. Nguyen, T. Laurain, R. Palhares, J. Lauber, C. Sentouh, and J.-C. Popieul, "LMI-based control synthesis of constrained Takagi-Sugeno fuzzy systems subject to L2 or L∞ disturbances," *Neurocomputing*, vol. 207, pp. 793–804, 2016.

[30] R. Mrquez, T. M. Guerra, M. Bernal, and A. Kruszewski, "Asymptotically necessary and sufficient conditions for Takagi–Sugeno models using generalized non-quadratic parameter-dependent controller design," *Fuzzy Sets and Systems*, vol. 306, pp. 48–62, 2017.

[31] S. Xu, G. Sun, and W. Sun, "Takagi–Sugeno fuzzy model based robust dissipative control for uncertain flexible spacecraft with saturated time-delay input," *ISA Transactions*, vol. 66, pp. 105–121, 2017.

[32] X. M. Ding, Z. K. Xu, N. J. Cheung, and X. H. Liu, "Parameter estimation of Takagi-Sugeno fuzzy system using heterogeneous cuckoo search algorithm," *Neurocomputing*, vol. 151, no. 3, pp. 1332–1342, 2015.

[33] H. D. Choi, C. K. Ahn, P. Shi, M. T. Lim, and M. K. Song, "L2-L∞ Filtering for takagi-sugeno fuzzy neural networks based on wirtinger-type inequalities," *Neurocomputing*, vol. 153, pp. 117–125, 2015.

[34] X. Wang, R. Rao, and S. Zhong, "LMI approach to stability analysis of Cohen-Grossberg neural networks with p-Laplace diffusion," *Journal of Applied Mathematics*, vol. 2012, Article ID 523812, 12 pages, 2012.

[35] X. Li, R. Rakkiyappan, and P. Balasubramaniam, "Existence and global stability analysis of equilibrium of fuzzy cellular neural networks with time delay in the leakage term under impulsive perturbations," *Journal of The Franklin Institute*, vol. 348, no. 2, pp. 135–155, 2011.

[36] S. Muralisankar and N. Gopalakrishnan, "Robust stability criteria for Takagi-Sugeno fuzzy Cohen-Grossberg neural networks of neutral type," *Neurocomputing*, vol. 144, pp. 516–525, 2014.

[37] P. Balasubramaniam and M. Syed Ali, "Stability analysis of Takagi-Sugeno fuzzy Cohen-Grossberg BAM neural networks with discrete and distributed time-varying delays," *Mathematical and Computer Modelling*, vol. 53, no. 1-2, pp. 151–160, 2011.

[38] P. Lindqvist, "On the equation $\mathrm{div}(|\nabla u|^{p-2}) + \lambda |u|^{p-2}u = 0$," *Proceedings of the American Mathematical Society*, vol. 109, no. 1, pp. 159–164, 1990.

[39] R. Rao, "Delay-dependent exponential stability for nonlinear reaction-diffusion uncertain Cohen-Grossberg neural networks with partially known transition rates via Hardy-Poincare inequality," *Chinese Annals of Mathematics, Series B*, vol. 35, no. 4, pp. 575–598, 2014.

[40] R. F. Rao and X. R. Wang, "Infinitely many solutions for the resonant quasi-linear equation without landesman-lazer conditions," *Acta Mathematica Scientia (Chinese Series)*, vol. 32, no. 4, pp. 744–752, 2012.

[41] Q. Zhu, C. Huang, and X. Yang, "Exponential stability for stochastic jumping BAM neural networks with time-varying and distributed delays," *Nonlinear Analysis: Hybrid Systems*, vol. 5, no. 1, pp. 52–77, 2011.

[42] Z. Chen, X. Wang, S. Zhong, and J. Yang, "Improved delay-dependent robust passivity criteria for uncertain neural networks with discrete and distributed delays," *Chaos, Solitons & Fractals*, vol. 103, pp. 23–32, 2017.

[43] R. Yang and R. Guo, "Adaptive finite-time robust control of nonlinear delay hamiltonian systems via lyapunov-krasovskii method," *Asian Journal of Control*, vol. 20, no. 2, article 1C11, 2008.

[44] R. Rao, Z. Pu, S. Zhong, and J. Huang, "On the role of diffusion behaviors in stability criterion for p-laplace dynamical equations with infinite delay and partial fuzzy parameters under dirichlet boundary value," *Journal of Applied Mathematics*, vol. 2013, Article ID 940845, 8 pages, 2013.

[45] C. K. Ahn, "Passive and exponential filter design for fuzzy neural networks," *Information Sciences*, vol. 238, pp. 126–137, 2013.

[46] X. Li and J. Wu, "Stability of nonlinear differential systems with state-dependent delayed impulses," *Automatica*, vol. 64, pp. 63–69, 2016.

[47] J. Cheng, H. Zhu, S. Zhong, Q. Zhong, and Y. Zeng, "Finite-time H_∞ estimation for discrete-time Markov jump systems with time-varying transition probabilities subject to average dwell time switching," *Communications in Nonlinear Science and Numerical Simulation*, vol. 20, no. 2, pp. 571–582, 2015.

[48] Q. K. Song and Z. J. Zhao, "Stability criterion of complex-valued neural networks with both leakage delay and time-varying delays on time scales," *Neurocomputing*, vol. 171, pp. 179–184, 2016.

[49] X. Li and F. Deng, "Razumikhin method for impulsive functional differential equations of neutral type," *Chaos, Solitons & Fractals*, vol. 101, pp. 41–49, 2017.

[50] J. Tian, W. Xiong, and F. Xu, "Improved delay-partitioning method to stability analysis for neural networks with discrete and distributed time-varying delays," *Applied Mathematics and Computation*, vol. 233, pp. 152–164, 2014.

[51] X. Li and J. Cao, "An impulsive delay inequality involving unbounded time-varying delay and applications," *Institute of Electrical and Electronics Engineers Transactions on Automatic Control*, vol. 62, no. 7, pp. 3618–3625, 2017.

Hindawi
Mathematical Problems in Engineering
Volume 2017, Article ID 4157256, 16 pages
https://doi.org/10.1155/2017/4157256

Research Article

Stability Analysis of Delayed Genetic Regulatory Networks via a Relaxed Double Integral Inequality

Fu-Dong Li,[1,2] Qi Zhu,[3,4] Hao-Tian Xu,[4] and Lin Jiang[4]

[1] *The Office of Science and Technology Development, Peking University, Beijing 100871, China*
[2] *The Energy Research Institute, State Grid Corporation of China, Beijing, China*
[3] *School of Electronic Engineering, Xi'an Shiyou University, Xi'an 710065, China*
[4] *Department of Electrical Engineering & Electronics, University of Liverpool, Liverpool L69 3GJ, UK*

Correspondence should be addressed to Qi Zhu; qzhu@xsyu.edu.cn

Received 29 June 2017; Accepted 12 October 2017; Published 13 November 2017

Academic Editor: Radek Matušů

Time delay arising in a genetic regulatory network may cause the instability. This paper is concerned with the stability analysis of genetic regulatory networks with interval time-varying delays. Firstly, a relaxed double integral inequality, named as Wirtinger-type double integral inequality (WTDII), is established to estimate the double integral term appearing in the derivative of Lyapunov-Krasovskii functional with a triple integral term. And it is proved theoretically that the proposed WTDII is tighter than the widely used Jensen-based double inequality and the recently developed Wiringter-based double inequality. Then, by applying the WTDII to the stability analysis of a delayed genetic regulatory network, together with the usage of useful information of regulatory functions, several delay-range- and delay-rate-dependent (or delay-rate-independent) criteria are derived in terms of linear matrix inequalities. Finally, an example is carried out to verify the effectiveness of the proposed method and also to show the advantages of the established stability criteria through the comparison with some literature.

1. Introduction

In the past few years, genetic regulatory networks (GRNs), which describe the interactions of many molecules (DNA, RNA, proteins, etc.), have been becoming a new research area of biological and biomedical sciences [1–4]. Mathematical modelling based on the extracted functional information from the time-series data provides a useful tool for studying gene regulation processes in living organisms [5, 6], and a large variety of formalisms have been proposed to model and simulate GRNs, such as directed graphs, Boolean networks, and nonlinear differential equations [7]. Among them, the nonlinear differential equation model can provide more detailed understanding and insights into the nonlinear dynamical behavior exhibited by GRNs [8].

Since mRNAs and proteins in the GRNs may be synthesized at different locations, an important issue in modelling GRNs is that the slow processes of transcription, translation, and translocation result in sizable delays [9–11]. Time delays arising in the GRNs may lead to wrong prediction of dynamic behaviors [12, 13], which may lead to very serious consequences. The stability is essential for designing or controlling genetic regulatory networks [14]; it is of a great significance to study the influence of delays on the stability of the GRNs.

Up to now, a huge number of results on the stability of the delayed GRNs have been reported in the literature (see, e.g., [15–58]). The sufficient and necessary local stability criteria were firstly given for the GRNs with constant delay in [15, 16]. However, local stability is not enough for understanding nonlinear GRNs; the globally asymptotical stability of GRNs with SUM regulatory functions has been widely investigated [17–22]. Meanwhile, by taking into account the unavoidable uncertainties caused by modelling errors and parameter fluctuations, many scholars paid attentions to the robust stability analysis of the delayed GRNs [23–36]. Moreover, both the intrinsic noise derived from the random births and deaths of individual molecules and the extrinsic noise due to environment fluctuations make the gene regulation process

an intrinsically noisy process [59]. Thus, many researches aimed at the robust stability analysis of the GRNs in consideration of those noises [37–46]. Also, some results have considered both the uncertainties and the noises [47–52]. In addition, based on the definition of convergence rate index, the exponential stability problem was also studied in [53–57].

On the other hand, no matter what type of stability problems is concerned, the analysis methods for finding stability criteria have always been an important topic. To the best of the authors' knowledge, there are mainly two methods that have been used for the delayed GRNs. The first type of method is the M-matrix-based method. For example, the delay- and rate-independent stability criteria were proposed in [20], the delay-independent but rate-dependent criteria were established in [23, 44], and the delay- and rate-dependent criteria were developed in [21, 22]. The stability of the GRNs through those M-matrix-based criteria is judged by verifying whether or not a matrix is a nonsingular M-matrix. Although the computational complexity is low, those criteria are just available for slow-varying delay case [20–23, 44]. However, the time delays encountered in GRNs may be fast-varying or random changing. The M-matrix-based method is inapplicable for those cases. The second type of method is based on the framework of Lyapunov-Krasovskii functional (LKF) and linear matrix inequality (LMI). The LKF-based method can be used to handle all time delays mentioned before and it is available for not only stability analysis but also many other problems, like controller synthesis, state estimation, filter design, passivity analysis, and so on [13, 59–70]. Meanwhile, the LMI-based criteria can be easily checked through MATLAB/LMI toolbox for determining the system stability. Therefore, most existing researches for the GRNs are based on this type of method [17–19, 25–43, 45–56].

The problem of stability analysis by using the LKF and the LMI is that the criterion obtained has more or less conservatism. It is well-known that the criterion with less conservatism means that it can derive an admissible maximum upper bound such that the understudied GRNs maintains global asymptotical stability. It is predictable that the form of the LKF candidate is tightly related to the conservatism of the obtained criteria. Thus, the key point of the stability analysis based on such framework is to find an LKF satisfying some requirements for ensuring the globally asymptotical stability of the GRNs.

In most researches, the used LKFs were constructed by introducing delay-based single and/or double integral terms into the typical nonintegral quadratic form of Lyapunov function for delay-free systems [17, 18, 28–33, 35–42, 46–50, 53–55]. Based on a predictable fact that the conservatism-reducing of criteria can be achieved by constructing more general LKF, two types of more general LKFs have been developed to reduce the conservatism. The first one is the delay-partition-based LKFs, which is constructed by dividing the delay interval into several small subintervals and then replacing the original integral terms with multiple new integral terms based on delay subintervals. This type of LKF has been used to investigate the robust stability of various GRNs [25, 26, 51], the exponential stability of switch GRNs [56], and the stochastic stability of jumping GRNs [27, 43, 45]. The other is the augmented LKF constructed by using various state vectors (current and delayed and/or integrated state vectors, etc.) to augment the quadratic terms of original LKFs, and it has been used to derive the improved stability criteria of the GRNs [19, 34, 52].

Beside the above-mentioned two types of improved LKFs, a new LKF including triple integral terms firstly developed in [71] is proved to be very useful to reduce the conservatism. However, only a few researches of the GRNs have applied such type of LKF. The LKF with triple integral terms was used to discuss the asymptotical stability of the GRNs [19, 34]. The following form of double integral term will be introduced into the derivative of the LKF with a triple integral term:

$$-\int_a^b \int_s^b y^T(u) Z y(u)\, du\, ds, \quad Z > 0. \tag{1}$$

As mentioned in [72], the effective estimation of the above term is strongly linked to the conservatism of the criteria. To the best of the authors' knowledge, for the researches referring to the triple integral term in the LKFs, most literature directly applied the Jensen-based double integral inequality (JBDII) (see (17) for details) to achieve the estimation task [34]. Although an improved integral inequality was developed in [19], it is also derived based on Jensen inequality. Very recently, a Wirtinger-based double integral inequality (WBDII) was developed to general linear time-delay system and it was proved to be less conservative than the JBDII [72]. However, such inequality has not been used to discuss the GRNs. Furthermore, the gap between term (1) and its estimated value obtained by the WBDII still leads to conservatism. Therefore, it can be expected that the results may be further improved if a new estimation method that brings tighter gap is applied for term (1). This is the motivation of the paper.

This paper further investigates the delay-dependent stability of the GRNs by developing a more effective inequality to estimate the double integral term (1). The contributions of the paper are summarized as follows:

(1) A relaxed double integral inequality, that is, Wiringter-type double integral inequality (WTDII), is established to estimate the double integral term. Compared with the widely used JBDII and the recently developed WTDII, the presented WTDII is theoretically proved to be the tightest.

(2) Two less conservative stability criteria of the GRNs are derived. For the GRNs with time-varying delays satisfying different conditions, two stability criteria are, respectively, established by applying the proposed WTDII to estimate the double integral terms appearing in the derivative of the LKFs.

The rest of the paper is organized as follows. Problem statements and preliminaries are presented in Section 2. In Section 3, the development and the comparison of the WTDII approach are discussed in detail. Two stability criteria of the GRN with time-varying delay are derived through the WTDII in Section 4. An example is given to show the validity

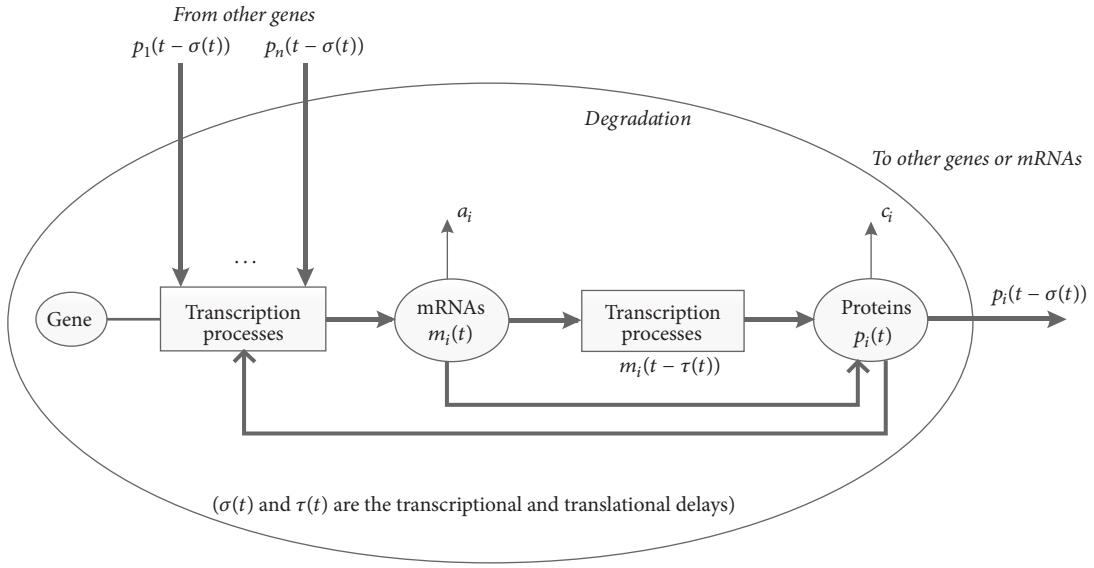

Figure 1: GRNs with time-varying feedback regulation delays and translational delays.

of the obtained results in Section 5. Finally, in Section 6, the conclusions are drawn.

In the Notations, the list of notations and abbreviations used throughout this paper is shown.

2. Problem Formulation and Preliminary

This section describes the problem to be investigated and gives some necessary preliminaries.

2.1. Problem Formulation. The following nonlinear differential equations have been used recently to describe the GRNs with time-varying feedback regulation delays and translational delays [28]:

$$\begin{aligned}\dot{m}_i(t) &= -a_i m_i(t) \\ &\quad + b_i\left(p_1(t-\sigma(t)), p_2(t-\sigma(t)), \ldots, p_n(t-\sigma(t))\right), \\ \dot{p}_i(t) &= -c_i p_i(t) + d_i m_i(t-\tau(t))\end{aligned} \tag{2}$$

as shown in Figure 1, where $m_i(t)$ and $p_i(t)$ are the concentrations of the ith mRNA and protein, respectively. $a_i > 0$ and $c_i > 0$ are the positive real numbers that represent the degradation rate of the ith mRNA and protein, respectively. $d_i > 0$ is the positive real number that represents the translating rate from mRNA i to protein i. b_i is the regulatory function of the ith gene. $\sigma(t)$ and $\tau(t)$ are the transcriptional and translational delays, respectively.

Since each transcription factor acts additively to regulate the gene, it is usual to assume that the regulatory function b_i satisfies the following SUM logic [37]:

$$b_i\left(p_1(t), p_2(t), \ldots, p_n(t)\right) = \sum_{j=1}^{n} b_{ij} p_j(t) \tag{3}$$

and b_{ij} is a monotonic function of the Hill form; that is,

$$b_{ij} = \begin{cases} \dfrac{\alpha_{ij}}{1+\left(x/\beta_j\right)^{H_j}}, & \text{if transcription factor } j \text{ represses gene } i \\ \dfrac{\alpha_{ij}\left(x/\beta_j\right)^{H_j}}{1+\left(x/\beta_j\right)^{H_j}}, & \text{if transcription factor } j \text{ activates gene } i, \end{cases} \tag{4}$$

where α_{ij} is bounded constant that denotes the dimensionless transcriptional rate of transcription factor j to gene i, β_j is a positive scalar, and H_j is the Hill coefficient that represents the degree of cooperativity.

The transcriptional and translational delays, $\sigma(t)$ and $\tau(t)$, are assumed to satisfy the following two different conditions.

Case 1. $\tau(t)$ and $\sigma(t)$ satisfy

$$\begin{aligned} 0 \le \tau_1 \le \tau(t) \le \tau_2, \\ 0 \le \sigma_1 \le \sigma(t) \le \sigma_2, \\ \dot{\tau}(t) \le \tau_d, \\ \dot{\sigma}(t) \le \sigma_d. \end{aligned} \tag{5}$$

Case 2. $\tau(t)$ and $\sigma(t)$ satisfy

$$\begin{aligned} 0 \le \tau_1 \le \tau(t) \le \tau_2, \\ 0 \le \sigma_1 \le \sigma(t) \le \sigma_2. \end{aligned} \tag{6}$$

Clearly, based on (3), GRN (2) can be rewritten as [19]

$$\begin{aligned}\dot{m}_i(t) &= -a_i m_i(t) + \sum_{j=1}^{n} w_{ij} g_j\left(p_j(t-\sigma(t))\right) + l_i, \\ \dot{p}_i(t) &= -c_i p_i(t) + d_i m_i(t-\tau(t)),\end{aligned} \tag{7}$$

where $l_i = \sum_{j\in\mathscr{V}_i}\alpha_{ij}$ with $\mathscr{V}_i$ being the set of all the transcription factors j which are repressors of gene i; $w_{ij} = \alpha_{ij}$ if transcription factor j activates gene i, $w_{ij} = 0$ if there is no connection between j and i, and $w_{ij} = -\alpha_{ij}$ if transcription factor j represses gene i; and $g_j(x) = (x/\beta_j)^{H_j}/(1 + (x/\beta_j)^{H_j})$, $x \geq 0$ is a monotonically increasing function satisfying

$$\rho \leq \frac{g_j(s_1) - g_j(s_2)}{s_1 - s_2} \leq \rho_i \tag{8}$$

with $\rho = \min_{s\geq 0}\dot{g}_j(s) = 0$ and

$$\rho_i = \max_{s\geq 0}\dot{g}_j(s) = \frac{\left(H_j - 1\right)^{(H_j-1)/H_j}\left(H_j + 1\right)^{(H_j+1)/H_j}}{4\beta_j H_j}. \tag{9}$$

GRN (7) can be expressed as the following vector-matrix form:

$$\begin{aligned}\dot{m}(t) &= -Am(t) + Wg\left(p\left(t - \sigma(t)\right)\right) + l,\\ \dot{p}(t) &= -Cp(t) + Dm\left(t - \tau(t)\right),\end{aligned} \tag{10}$$

where $m(t) = [m_1(t), m_2(t), \ldots, m_n(t)]^T$, $p(t) = [p_1(t), p_2(t), \ldots, p_n(t)]^T$, $A = \mathrm{diag}\{a_1, a_2, \ldots, a_n\} > 0$, $C = \mathrm{diag}\{c_1, c_2, \ldots, c_n\} > 0$, $D = \mathrm{diag}\{d_1, d_2, \ldots, d_n\} > 0$, $g(p(t)) = [g_1(p_1(t)), g_2(p_2(t)), \ldots, g_n(p_n(t))]^T$, $W = [w_{ij}]_{n\times n}$, and $l = [l_1, l_2, \ldots, l_n]$.

Let (m^*, p^*) be the equilibrium point (steady state) of (10); that is, $-Am^* + Wg(p^*) + l = 0$ and $-Cp^* + Dm^* = 0$. Using the transformations $x(t) = m(t) - m^*$ and $y(t) = p(t) - p^*$, one can shift the equilibrium point (m^*, p^*) to the origin and rewrite (10) as the following GRN:

$$\begin{aligned}\dot{x}(t) &= -Ax(t) + Wf\left(y\left(t - \sigma(t)\right)\right),\\ \dot{y}(t) &= -Cy(t) + Dx\left(t - \tau(t)\right),\end{aligned} \tag{11}$$

where $f(s) = [f_1(s), f_2(s), \ldots, f_n(s)]^T$ and $f_i(y(t)) = g_i(y(t) + p^*) - g_i(p^*)$ with $f_i(0) = 0$. Then,

$$\frac{f_i(s_1) - f_i(s_2)}{s_1 - s_2} = \frac{g_i(s_1 + p^*) - g_i(s_2 + p^*)}{s_1 + p^* - (s_2 + p^*)}. \tag{12}$$

Thus, it follows from (8) and $f_i(0) = 0$ that

$$0 \leq \frac{f_i(s_1) - f_i(s_2)}{s_1 - s_2} \leq \rho_i, \quad s_1 \neq s_2, \tag{13}$$

$$0 \leq \frac{f_i(s)}{s} \leq \rho_i, \quad s \neq 0. \tag{14}$$

This paper aims to analyze the asymptotical stability of GRN (2) and to determine the delay bounds, named as maximal admissible delay bounds (MADBs), under which the GRN is asymptotically stable. In order to achieve this aim, this paper will develop a new double integral inequality (i.e., WTDII) for estimating the double integral term (1) so as to derive some less conservative stability criteria.

2.2. Preliminaries. Several lemmas used to obtain the main results are given as follows.

For the estimation of single integral term, the most popular technique is Wirtinger-based inequality, shown as Lemma 1.

Lemma 1 (Wirtinger-based inequality [73]). *For symmetric positive-definite matrix $R \in \mathscr{R}^{n\times n}$, scalars $a < b$, and vector $\omega : [a,b] \mapsto \mathscr{R}^n$ such that the integration concerned is well defined, the following inequality holds:*

$$\int_a^b \omega^T(s) R\omega(s)\, ds \geq \frac{1}{b-a}\begin{bmatrix}\chi_a\\ \chi_b\end{bmatrix}^T\begin{bmatrix}R & 0\\ 0 & 3R\end{bmatrix}\begin{bmatrix}\chi_a\\ \chi_b\end{bmatrix}, \tag{15}$$

where $\chi_a = \int_a^b \omega(s)ds$ and $\chi_b = \chi_a - (2/(b-a))\int_a^b\int_a^s \omega(u)du\, ds = -\chi_a + (2/(b-a))\int_a^b\int_s^b \omega(u)du\, ds$.

The auxiliary function-based integral inequality, which encompasses the Wirtinger-based inequality, has been developed in recent years.

Lemma 2 (auxiliary function-based integral inequality [74]). *For symmetric positive-definite matrix $R \in \mathscr{R}^{n\times n}$, scalars $a < b$, and vector $\omega : [a,b] \mapsto \mathscr{R}^n$ such that the integration concerned is well defined, the following inequality holds*

$$\begin{aligned}&(b-a)\int_a^b \dot{\omega}^T(s) R\dot{\omega}(s)\, ds\\ &\quad\geq \chi_1^T R\chi_1 + 3\chi_2^T R\chi_2 + 5\chi_3^T R\chi_3,\end{aligned} \tag{16}$$

where $\chi_1 = \omega(b) - \omega(a)$, $\chi_2 = \omega(b) + \omega(a) - (2/(b-a))\int_a^b \omega(s)ds$, and $\chi_3 = \omega(b) - \omega(a) + (6/(b-a))\int_a^b \omega(s)ds - (12/(b-a)^2)\int_a^b\int_s^b \omega(u)du\, ds$.

For the estimation of double integral term, the JBDII is widely applied in [71], and, with its improvement, the WBDII was developed in [72] very recently, respectively shown as Lemmas 3 and 4.

Lemma 3 (Jensen-based double integral inequality (JBDII) [71]). *For symmetric positive-definite matrix $Z \in \mathscr{R}^{n\times n}$, scalars $a < b$, and vector $\nu : [a,b] \mapsto \mathscr{R}^n$ such that the integration concerned is well defined, the following inequality holds:*

$$\frac{(b-a)^2}{2}\int_a^b\int_s^b \nu^T(u) Z\nu(u)\, du\, ds \geq \chi_4^T Z\chi_4, \tag{17}$$

where $\chi_4 = \int_a^b\int_s^b \nu(u)du\, ds$.

Lemma 4 (Wirtinger-based double integral inequality (WBDII) [72]). *For symmetric positive-definite matrix $Z \in \mathscr{R}^{n\times n}$, scalars $a < b$, and vector $\nu : [a,b] \mapsto \mathscr{R}^n$ such*

that the integration concerned is well defined, the following inequality holds:

$$\frac{(b-a)^2}{2}\int_a^b\int_s^b \nu^T(u)\,Z\nu(u)\,du\,ds \geq \chi_4^T Z\chi_4 + 2\chi_5^T Z\chi_5, \tag{18}$$

where $\chi_5 = -\chi_4 + (3/(b-a))\int_a^b\int_s^b\int_\theta^b \nu(u)du\ d\theta\,ds$ *with* χ_4 *given in Lemma 3.*

For time-varying delay, when using the integral inequality, the reciprocally convex lemma is needed, and its simple form can be reformulated as Lemma 5.

Lemma 5 (reciprocally convex combination lemma [75]). *For any vectors* β_1 *and* β_2*, symmetric matrix* R*, any matrix* S*, and real scalar* $0 \leq \alpha \leq 1$ *satisfying* $\left[\begin{smallmatrix} R & S \\ * & R \end{smallmatrix}\right] \geq 0$*, the following inequality holds:*

$$\frac{1}{\alpha}\beta_1^T R\beta_1 + \frac{1}{1-\alpha}\beta_2^T R\beta_2 \geq \begin{bmatrix}\beta_1\\ \beta_2\end{bmatrix}^T \begin{bmatrix} R & S \\ * & R\end{bmatrix}\begin{bmatrix}\beta_1\\ \beta_2\end{bmatrix}. \tag{19}$$

3. A Relaxed Double Integral Inequality and Its Advantages

This section develops a new integral inequality, that is, the WTDII, to estimate the double integral terms existing. The comparison of the WTDII and the existing double integral inequalities is also given.

Based on the technique of integral in parts, the following WTDII is given.

Lemma 6. *For symmetric positive-definite matrix* $Z \in \mathscr{R}^{n\times n}$*, scalars* $a < b$*, and vector* $\nu : [a,b] \mapsto \mathscr{R}^n$ *such that the integration concerned is well defined, the following inequality holds:*

$$\frac{(b-a)^2}{2}\int_a^b\int_s^b \nu^T(u)\,Z\nu(u)\,du\,ds \geq \chi_4^T Z\chi_4 + 8\chi_5^T Z\chi_5, \tag{20}$$

where χ_4 *and* χ_5 *are defined in Lemmas 3 and 4.*

Proof. For a function $\lambda(u) = k_1 + k_2 u$, the calculation through integration by parts leads to

$$\begin{aligned}\int_a^b\int_s^b \lambda(u)\,\nu(u)\,du\,ds &= \lambda(a)\int_a^b\int_s^b \nu(u)\,du\,ds \\ &\quad + 2k_2\int_a^b\int_s^b\int_\theta^b x(u)\,du\,d\theta\,ds.\end{aligned} \tag{21}$$

By setting $\lambda(a) = -1$, $2k_2 = 3/(b-a)$, that is, $\lambda(u) = (-a-2b)/2(b-a) + (3/2(b-a))u$, the above equality is rewritten as

$$\int_a^b\int_s^b \lambda(u)\,\nu(u)\,du\,ds = \chi_5. \tag{22}$$

Then the following equality is obtained for any vector χ_0 and any matrix M:

$$\int_a^b\int_s^b \lambda(u)\,\chi_0^T M\nu(u)\,du\,ds = \chi_0^T M\chi_5. \tag{23}$$

Similarly, the following equalities are derived:

$$\begin{aligned}&\int_a^b\int_s^b \chi_0^T L\nu(u)\,du\,ds = \chi_0^T L\chi_4,\\ &\int_a^b\int_s^b \chi_0^T LR^{-1}L^T\chi_0 du\,ds = \frac{(b-a)^2}{2}\chi_0^T LR^{-1}L^T\chi_0,\\ &\int_a^b\int_s^b \chi_0^T LR^{-1}M^T\lambda(u)\,\chi_0 du\,ds = 0,\\ &\int_a^b\int_s^b \lambda^2(u)\,\chi_0^T MR^{-1}M^T\chi_0 du\,ds\\ &\quad = \frac{(b-a)^2}{16}\chi_0^T MR^{-1}M^T\chi_0.\end{aligned} \tag{24}$$

Therefore, using the above five equalities and the Schur complement derives the following equality:

$$\begin{aligned}&\int_a^b\int_s^b \begin{bmatrix}\chi_0\\ \lambda(u)\,\chi_0\\ \nu(u)\end{bmatrix}^T \\ &\cdot\begin{bmatrix} LZ^{-1}L^T & LZ^{-1}M^T & L\\ * & MZ^{-1}M^T & M\\ * & * & Z\end{bmatrix}\begin{bmatrix}\chi_0\\ \lambda(u)\,\chi_0\\ \nu(u)\end{bmatrix} du\,ds\\ &= \int_a^b\int_s^b \nu^T(u)\,R\nu(u)\,du\,ds + \mathrm{Sym}\left\{\chi_0^T L\chi_4 + \chi_0^T M\chi_5\right\} + \frac{(b-a)^2}{2}\\ &\cdot\chi_0^T\left(\frac{8LZ^{-1}L^T + MZ^{-1}M^T}{8}\right)\chi_0 \geq 0.\end{aligned} \tag{25}$$

By letting $\chi_0^T = [\chi_4^T, \chi_5^T]$, $L = -(2/(b-a)^2)[Z,0]^T$, and $M = -(16/(b-a)^2)[0,Z]$, that is, $\chi_0^T L = -(2/(b-a)^2)\chi_4^T Z$ and $\chi_0^T M = -(16/(b-a)^2)\chi_5^T Z$, then (25) leads to

$$\int_a^b\int_s^b \nu^T(u)\,Z\nu(u)\,du\,ds \geq \frac{2}{(b-a)^2}\left(\chi_4^T Z\chi_4 + 8\chi_5^T Z\chi_5\right). \tag{26}$$

Thus (20) holds. This completes the proof. □

Remark 7. Based on the comparison of the proposed WTDII (20) with the widely used JBDII (17) and the recently developed WBDII (18), it can be found that WTDII (20) provides the tightest estimation value of the double integral term (1).

More specifically, compared with the widely used JBDII (17), the extra positive term $8\chi_5^T Z\chi_5$ reduces the gap between the original double integral term (1) and its estimated value; and, compared with the recently developed WBDII (18), the extra positive term $6\chi_5^T Z\chi_5$ reduces the estimation gap. As mentioned in [72–74], it is helpful to reduce the conservatism by reducing such estimation gap. Therefore, the proposed WTDII (20) will lead to less conservative criteria than the ones derived by JBDII (17) [19] or WBDII (18).

By setting $\nu(u) = \dot{\omega}(u)$, the following lemma can be directly obtained from Lemma 6.

Lemma 8. *For symmetric positive-definite matrix $Z \in \mathscr{R}^{n\times n}$, scalars $a < b$, and vector $\dot{\omega} : [a,b] \mapsto \mathscr{R}^n$ such that the integration concerned is well defined, the following inequality holds:*

$$\int_a^b \int_s^b \dot{\omega}^T(u) Z \dot{\omega}(u)\, du\, ds \geq 2\theta_1^T Z \theta_1 + 16\theta_2^T Z \theta_2, \quad (27)$$

where $\theta_1 = (1/(b-a))\chi_4|_{\nu(u)=\dot{\omega}(u)} = \omega(b) - \int_a^b(\omega(s)/(b-a))ds$ and $\theta_2 = (1/(b-a))\chi_5|_{\nu(u)=\dot{\omega}(u)} = -(1/2)\omega(b) - \int_a^b(\omega(s)/(b-a))ds + 3\int_a^b\int_s^b(\omega(u)/(b-a)^2)du\, ds$.

4. Delay-Dependent Stability Analysis of GRN

This section derives delay-dependent stability criteria of GRN (2) by constructing the LKF with triple integral terms and applying the proposed WTDII (20) to estimate the double integral terms appearing in its derivative.

The following notations are introduced at first for simplifying the representation of subsequent parts:

$$\begin{aligned}
&\tau_{1\tau}(t) = \tau(t) - \tau_1,\\
&\tau_{2\tau}(t) = \tau_2 - \tau(t),\\
&\sigma_{1\sigma}(t) = \sigma(t) - \sigma_1,\\
&\sigma_{2\sigma}(t) = \sigma_2 - \sigma(t),\\
&x_{\tau_1}(t) = x(t-\tau_1),\\
&y_{\sigma_1}(t) = y(t-\sigma_1),\\
&x_{\tau}(t) = x(t-\tau(t)),\\
&y_{\sigma}(t) = y(t-\sigma(t)),\\
&x_{\tau_2}(t) = x(t-\tau_2),\\
&y_{\sigma_2}(t) = y(t-\sigma_2),\\
&\nu_1(t) = \int_{t-\tau_1}^{t} \frac{x(s)}{\tau_1} ds,\\
&\nu_4(t) = \int_{t-\tau_1}^{t}\int_{s}^{t} \frac{x(u)}{\tau_1^2} du\, ds,\\
&\nu_2(t) = \int_{t-\tau(t)}^{t-\tau_1} \frac{x(s)}{\tau_{1\tau}(t)} ds,\\
&\nu_5(t) = \int_{t-\tau(t)}^{t-\tau_1}\int_{s}^{t-\tau_1} \frac{x(u)}{\tau_{1\tau}^2(t)} du\, ds,\\
&\nu_3(t) = \int_{t-\tau_2}^{t-\tau(t)} \frac{x(s)}{\tau_{2\tau}(t)} ds,\\
&\nu_6(t) = \int_{t-\tau_2}^{t-\tau(t)}\int_{s}^{t-\tau(t)} \frac{x(u)}{\tau_{2\tau}^2(t)} du\, ds,\\
&\nu_7(t) = \int_{t-\sigma_1}^{t} \frac{x(s)}{\sigma_1} ds,\\
&\nu_{10}(t) = \int_{t-\sigma_1}^{t}\int_{s}^{t} \frac{x(u)}{\sigma_1^2} du\, ds,\\
&\nu_8(t) = \int_{t-\sigma(t)}^{t-\sigma_1} \frac{x(s)}{\sigma_{1\sigma}(t)} ds,\\
&\nu_{11}(t) = \int_{t-\sigma(t)}^{t-\sigma_1}\int_{s}^{t-\sigma_1} \frac{x(u)}{\sigma_{1\sigma}^2(t)} du\, ds,\\
&\nu_9(t) = \int_{t-\sigma_2}^{t-\sigma(t)} \frac{x(s)}{\sigma_{2\sigma}(t)} ds,\\
&\nu_{12}(t) = \int_{t-\sigma_2}^{t-\sigma(t)}\int_{s}^{t-\sigma(t)} \frac{x(u)}{\sigma_{2\sigma}^2(t)} du\, ds,\\
&\zeta(t) = \left[x^T(t), x^T(t-\tau_1), x^T(t-\tau(t)), x^T(t-\tau_2),\right.\\
&\quad \nu_1^T(t), \nu_2^T(t), \ldots, \nu_6^T(t), y^T(t), y^T(t-\sigma_1),\\
&\quad y^T(t-\sigma(t)), y^T(t-\sigma_2), \nu_7^T(t), \nu_8^T(t), \ldots, \nu_{12}^T(t),\\
&\quad f^T(y(t)), f^T(y(t-\sigma_1)), f^T(y(t-\sigma(t))),\\
&\quad \left. f^T(y(t-\sigma_2))\right]^T,
\end{aligned} \quad (28)$$

$$\begin{aligned}
&e_x = [-A, 0_{n\times 21n}, W, 0_{n\times n}],\\
&e_y = [0_{n\times 2n}, D, 0_{n\times 7n}, -C, 0_{n\times 13n}],\\
&e_0 = [0_{n\times 24n}],\\
&e_i = [0_{n\times(i-1)n}, I_{n\times n}, 0_{n\times(24-i)n}], \quad i = 1,2,\ldots,24,\\
&\Sigma = \operatorname{diag}\{\rho_1, \rho_2, \ldots, \rho_n\}.
\end{aligned} \quad (29)$$

4.1. Stability of GRN (2) with Delay Satisfying (5). For GRN (2) with a delay satisfying (5), the following stability criterion is derived by using the proposed WTDII (27), together with Lemmas 1, 2, and 5, to estimate the derivative of the LKF.

Theorem 9. *For given scalars τ_i, σ_i, $i = 1,2$, τ_d, and σ_d, GRN (2) with the time delay satisfying (5) and regulatory function satisfying (3) is asymptotically stable, if there exist symmetric matrices $P > 0$, $Q_i > 0$, $R_j > 0$, $Z_k > 0$, $i = 1,2,\ldots,6$, $j = 1,2,\ldots,5$, and $k = 1,2,\ldots,4$; diagonal matrices $\Lambda_1 > 0$, $\Lambda_2 > 0$, $H_j > 0$, $j = 1,2,\ldots,4$, $U_{lk} >$*

0, $l = 1, 2, \ldots, 4$, *and* $k = l + 1, \ldots, 4$; *and any matrices* S_i, $i = 1, 2$, *such that the following LMIs hold:*

$$\begin{bmatrix} \widetilde{R}_{2i+1} & S_i \\ * & \widetilde{R}_{2i+1} \end{bmatrix} > 0, \quad i = 1, 2, \tag{30}$$

$$\Psi_1 = \Xi_{\tau(t)}\big|_{\tau(t)=\tau_1} + \sum_{i=1}^{8} \Xi_i \leq 0, \tag{31}$$

$$\Psi_2 = \Xi_{\tau(t)}\big|_{\tau(t)=\tau_2} + \sum_{i=1}^{8} \Xi_i \leq 0, \tag{32}$$

where $\tau_{12} = \tau_2 - \tau_1$, $\sigma_{12} = \sigma_2 - \sigma_1$, *and*

$$\begin{aligned} \Xi_{\tau(t)} = {} & -\tau_{1\tau}(t)\left[e_6^T R_2 e_6 + 3\left(2e_9 - e_6\right)^T R_2 \left(2e_9 - e_6\right)\right] \\ & - \tau_{2\tau}(t)\left[e_7^T R_2 e_7 + 3\left(2e_{10} - e_7\right)^T R_2 \left(2e_{10} - e_7\right)\right], \end{aligned} \tag{33}$$

$$\Xi_1 = \Xi_{11} + \Xi_{11}^T, \tag{34}$$

$$\begin{aligned} \Xi_{11} = {} & \begin{bmatrix} e_1 \\ e_{11} \end{bmatrix}^T P \begin{bmatrix} e_x \\ e_y \end{bmatrix} + \left[\left(\Sigma e_{11} - e_{21}\right)^T \Lambda_1 + e_{21}^T \Lambda_2\right] \\ & \cdot e_y, \end{aligned} \tag{35}$$

$$\begin{aligned} \Xi_2 = {} & e_1^T Q_1 e_1 - e_2^T \left(Q_1 - Q_2 - Q_3\right) e_2 - e_4^T Q_2 e_4 - (1 \\ & - \tau_d) e_3^T Q_3 e_3, \end{aligned} \tag{36}$$

$$\Xi_3 = \Xi_{31} + \Xi_{32} + \Xi_{33}, \tag{37}$$

$$\Xi_{31} = e_x^T \left(\tau_1^2 R_1 + \tau_{12}^2 R_3\right) e_x + \tau_{12} e_1^T R_2 e_1, \tag{38}$$

$$\Xi_{32} = E_1^T \widetilde{R}_1 E_1, \quad \widetilde{R}_1 = \operatorname{diag}\left\{R_1, 3R_1, 5R_1\right\}, \tag{39}$$

$$\begin{aligned} \Xi_{33} = {} & \begin{bmatrix} E_2 \\ E_3 \end{bmatrix}^T \begin{bmatrix} \widetilde{R}_3 & S_1 \\ * & \widetilde{R}_3 \end{bmatrix} \begin{bmatrix} E_2 \\ E_3 \end{bmatrix}, \\ & \widetilde{R}_3 = \operatorname{diag}\left\{R_3, 3R_3, 5R_3\right\}, \end{aligned} \tag{40}$$

$$\Xi_4 = \Xi_{41} + \Xi_{42} + \Xi_{43}, \tag{41}$$

$$\Xi_{41} = e_x^T \left(\frac{\tau_1^2}{2} Z_1 + \frac{\tau_2^2 - \tau_1^2}{2} Z_2 - \tau_1 \tau_{12} Z_2\right) e_x, \tag{42}$$

$$\begin{aligned} \Xi_{42} = {} & -2\left[e_1 - e_5\right]^T Z_1 \left[e_1 - e_5\right] - 16\left[3e_8 - \frac{e_1}{2}\right. \\ & \left. - e_5\right]^T Z_1 \left[3e_8 - \frac{e_1}{2} - e_5\right], \end{aligned} \tag{43}$$

$$\begin{aligned} \Xi_{43} = {} & -2\left[e_2 - e_6\right]^T Z_2 \left[e_2 - e_6\right] - 16\left[3e_9 - \frac{e_2}{2}\right. \\ & \left. - e_6\right]^T Z_2 \left[3e_9 - \frac{e_2}{2} - e_6\right] - 2\left[e_3 - e_7\right]^T Z_2 \left[e_3\right. \\ & \left. - e_7\right] - 16\left[3e_{10} - \frac{e_3}{2} - e_7\right]^T Z_2 \left[3e_{10} - \frac{e_3}{2} - e_7\right], \end{aligned} \tag{44}$$

$$\begin{aligned} \Xi_5 = {} & \begin{bmatrix} e_{11} \\ e_{21} \end{bmatrix}^T Q_4 \begin{bmatrix} e_{11} \\ e_{21} \end{bmatrix} + \begin{bmatrix} e_{12} \\ e_{22} \end{bmatrix}^T \left(Q_5 + Q_6 - Q_4\right) \\ & \cdot \begin{bmatrix} e_{12} \\ e_{22} \end{bmatrix} - \begin{bmatrix} e_{14} \\ e_{24} \end{bmatrix}^T Q_5 \begin{bmatrix} e_{14} \\ e_{24} \end{bmatrix} - \left(1 - \sigma_d\right) \begin{bmatrix} e_{13} \\ e_{23} \end{bmatrix}^T \\ & \cdot Q_6 \begin{bmatrix} e_{13} \\ e_{23} \end{bmatrix}, \end{aligned} \tag{45}$$

$$\Xi_6 = \Xi_{61} + \Xi_{62} + \Xi_{63}, \tag{46}$$

$$\Xi_{61} = e_y^T \left(\sigma_1^2 R_4 + \sigma_{12}^2 R_5\right) e_y, \tag{47}$$

$$\Xi_{62} = E_4^T \widetilde{R}_4 E_4, \quad \widetilde{R}_4 = \operatorname{diag}\left\{R_4, 3R_4, 5R_4\right\}, \tag{48}$$

$$\begin{aligned} \Xi_{63} = {} & \begin{bmatrix} E_5 \\ E_6 \end{bmatrix}^T \begin{bmatrix} \widetilde{R}_5 & S_2 \\ * & \widetilde{R}_5 \end{bmatrix} \begin{bmatrix} E_5 \\ E_6 \end{bmatrix}, \\ & \widetilde{R}_5 = \operatorname{diag}\left\{R_5, 3R_5, 5R_5\right\}, \end{aligned} \tag{49}$$

$$\Xi_7 = \Xi_{71} + \Xi_{72} + \Xi_{73}, \tag{50}$$

$$\Xi_{71} = e_y^T \left(\frac{\sigma_1^2}{2} Z_3 + \frac{\sigma_2^2 - \sigma_1^2}{2} Z_4 - \sigma_1 \sigma_{12} Z_4\right) e_y, \tag{51}$$

$$\begin{aligned} \Xi_{72} = {} & -2\left[e_{11} - e_{15}\right]^T Z_3 \left[e_{11} - e_{15}\right] - 16\left[3e_{18} - \frac{e_{11}}{2}\right. \\ & \left. - e_{15}\right]^T Z_3 \left[3e_{18} - \frac{e_{11}}{2} - e_{15}\right], \end{aligned} \tag{52}$$

$$\begin{aligned} \Xi_{73} = {} & -2\left[e_{12} - e_{16}\right]^T Z_4 \left[e_{12} - e_{16}\right] - 16\left[3e_{19} - \frac{e_{12}}{2}\right. \\ & \left. - e_{16}\right]^T Z_4 \left[3e_{19} - \frac{e_{12}}{2} - e_{16}\right] - 2\left[e_{13} - e_{17}\right]^T \\ & \cdot Z_4 \left[e_{13} - e_{17}\right] - 16\left[3e_{20} - \frac{e_{13}}{2} - e_{17}\right]^T \\ & \cdot Z_4 \left[3e_{20} - \frac{e_{13}}{2} - e_{17}\right], \end{aligned} \tag{53}$$

$$\Xi_8 = \Xi_{81} + \Xi_{81}^T, \tag{54}$$

$$\begin{aligned} \Xi_{81} = {} & \sum_{i=1}^{4} \left[\left(\Sigma e_{1i} - e_{2i}\right)^T H_i e_{2i}\right] \\ & + \sum_{i=1}^{4} \sum_{j=i+1}^{4} \left[\Sigma\left(e_{1i} - e_{1j}\right) - \left(e_{2i} - e_{2j}\right)\right]^T \\ & \cdot U_{ij}\left(e_{2i} - e_{2j}\right), \end{aligned} \tag{55}$$

$$E_1 = \begin{bmatrix} e_1 - e_2 \\ e_1 + e_2 - 2e_5 \\ e_1 - e_2 + 6e_5 - 12e_8 \end{bmatrix}, \tag{56}$$

$$E_2 = \begin{bmatrix} e_2 - e_3 \\ e_2 + e_3 - 2e_6 \\ e_2 - e_3 + 6e_6 - 12e_9 \end{bmatrix}, \quad (57)$$

$$E_3 = \begin{bmatrix} e_3 - e_4 \\ e_3 + e_4 - 2e_7 \\ e_3 - e_4 + 6e_7 - 12e_{10} \end{bmatrix}, \quad (58)$$

$$E_4 = \begin{bmatrix} e_{11} - e_{12} \\ e_{11} + e_{12} - 2e_{15} \\ e_{11} - e_{12} + 6e_{15} - 12e_{18} \end{bmatrix}, \quad (59)$$

$$E_5 = \begin{bmatrix} e_{12} - e_{13} \\ e_{12} + e_{13} - 2e_{16} \\ e_{12} - e_{13} + 6e_{16} - 12e_{19} \end{bmatrix}, \quad (60)$$

$$E_6 = \begin{bmatrix} e_{13} - e_{14} \\ e_{13} + e_{14} - 2e_{17} \\ e_{13} - e_{14} + 6e_{17} - 12e_{20} \end{bmatrix}. \quad (61)$$

Proof. Construct the following LKF candidate:

$$V(t) = \sum_{i=1}^{7} V_i(t), \quad (62)$$

where

$$V_1(t) = \begin{bmatrix} x(t) \\ y(t) \end{bmatrix}^T P \begin{bmatrix} x(t) \\ y(t) \end{bmatrix} + \sum_{i=1}^{n} \int_0^{y_i} \left[\lambda_{1i}(\rho_i s - f_i(s)) + \lambda_{2i} f_i(s)\right] ds,$$

$$V_2(t) = \int_{t-\tau_1}^{t} x^T(s) Q_1 x(s)\, ds + \int_{t-\tau_2}^{t-\tau_1} x^T(s) \cdot Q_2 x(s)\, ds + \int_{t-\tau(t)}^{t-\tau_1} x^T(s) Q_3 x(s)\, ds,$$

$$V_3(t) = \tau_1 \int_{-\tau_1}^{0} \int_{t+\theta}^{t} \dot{x}^T(s) R_1 \dot{x}(s)\, ds\, d\theta + \int_{-\tau_2}^{-\tau_1} \int_{t+\theta}^{t} \left[x^T(s) R_2 x(s) + \tau_{12} \dot{x}^T(s) R_3 \dot{x}(s)\right] ds\, d\theta,$$

$$V_4(t) = \int_{-\tau_1}^{0} \int_{\theta}^{0} \int_{t+s}^{t} \dot{x}^T(u) Z_1 \dot{x}(u)\, du\, ds\, d\theta + \int_{-\tau_2}^{-\tau_1} \int_{\theta}^{-\tau_1} \int_{t+s}^{t} \dot{x}^T(u) Z_2 \dot{x}(u)\, du\, ds\, d\theta,$$

$$V_5(t) = \int_{t-\sigma_1}^{t} \begin{bmatrix} y(s) \\ f(y(s)) \end{bmatrix}^T Q_4 \begin{bmatrix} y(s) \\ f(y(s)) \end{bmatrix} ds + \int_{t-\sigma_2}^{t-\sigma_1} \begin{bmatrix} y(s) \\ f(y(s)) \end{bmatrix}^T Q_5 \begin{bmatrix} y(s) \\ f(y(s)) \end{bmatrix} ds + \int_{t-\sigma(t)}^{t-\sigma_1} \begin{bmatrix} y(s) \\ f(y(s)) \end{bmatrix}^T Q_6 \begin{bmatrix} y(s) \\ f(y(s)) \end{bmatrix} ds,$$

$$V_6(t) = \sigma_1 \int_{-\sigma_1}^{0} \int_{t+\theta}^{t} \dot{y}^T(s) R_4 \dot{y}(s)\, ds\, d\theta + \sigma_{12} \int_{-\sigma_2}^{-\sigma_1} \int_{t+\theta}^{t} \dot{y}^T(s) R_5 \dot{y}(s)\, ds\, d\theta,$$

$$V_7(t) = \int_{-\sigma_1}^{0} \int_{\theta}^{0} \int_{t+s}^{t} \dot{y}^T(u) Z_3 \dot{y}(u)\, du\, ds\, d\theta + \int_{-\sigma_2}^{-\sigma_1} \int_{\theta}^{-\sigma_1} \int_{t+s}^{t} \dot{y}^T(u) Z_4 \dot{y}(u)\, du\, ds\, d\theta \quad (63)$$

and $P > 0$, $Q_i > 0$, $R_j > 0$, $Z_k > 0$, $i = 1, 2, \ldots, 6$, $j = 1, 2, \ldots, 5$, and $k = 1, 2, \ldots, 4$ are the symmetric positive-definite matrices and $\Lambda_i = \mathrm{diag}\{\lambda_{i1}, \lambda_{i2}, \ldots, \lambda_{in}\} > 0$, $i = 1, 2$, are the symmetric positive-definite diagonal matrices.

Calculating the derivative of the LKF along the solutions of GRN (11) yields

$$\dot{V}(t) = \sum_{i=1}^{7} \dot{V}_i(t), \quad (64)$$

where

$$\dot{V}_1(t) = 2 \begin{bmatrix} x(t) \\ y(t) \end{bmatrix}^T P \begin{bmatrix} \dot{x}(t) \\ \dot{y}(t) \end{bmatrix} + 2\left\{\left[\Sigma y(t) - f(y(t))\right]^T \Lambda_1 + f^T(y(t)) \Lambda_2\right\} \cdot \dot{y}(t) = \zeta^T(t) \left(\Xi_{11} + \Xi_{11}^T\right) \zeta(t),$$

$$\dot{V}_2(t) = x^T(t) Q_1 x(t) + x_{\tau_1}^T(t) \left(Q_2 + Q_3 - Q_1\right) x_{\tau_1}(t) - x_{\tau_2}^T(t) Q_2 x_{\tau_2}(t) - (1 - \dot{\tau}(t)) x_{\tau}^T(t) Q_3 x_{\tau}(t)$$
$$\leq x^T(t) Q_1 x(t) + x_{\tau_1}^T(t) \left(Q_2 + Q_3 - Q_1\right) x_{\tau_1}(t) - x_{\tau_2}^T(t) Q_2 x_{\tau_2}(t) - \left(1 - \tau_d\right) x_{\tau}^T(t) Q_3 x_{\tau}(t) = \zeta^T(t) \Xi_2 \zeta(t),$$

$$\dot{V}_3(t) = \dot{x}^T(t) \left(\tau_1^2 R_1 + \tau_{12}^2 R_3\right) \dot{x}(t) + \tau_{12} x^T(t) R_2 x(t) - \tau_1 \int_{t-\tau_1}^{t} \dot{x}^T(s) R_1 \dot{x}(s)\, ds - \int_{t-\tau_2}^{t-\tau_1} \left(x^T(s) R_2 x(s) + \tau_{12} \dot{x}^T(s) R_3 \dot{x}(s)\right) ds,$$

$$\begin{aligned}
\dot{V}_4(t) &= \dot{x}^T(t)\left(\frac{\tau_1^2}{2}Z_1 + \frac{\tau_2^2-\tau_1^2}{2}Z_2 - \tau_1\tau_{12}Z_2\right)\dot{x}(t) \\
&\quad - \int_{t-\tau_1}^{t}\int_{s}^{t}\dot{x}^T(u)Z_1\dot{x}(u)\,du\,ds \\
&\quad - \int_{t-\tau_2}^{t-\tau_1}\int_{s}^{t-\tau_1}\dot{x}^T(u)Z_2\dot{x}(u)\,du\,ds, \\
\dot{V}_5(t) &= \begin{bmatrix} y(t) \\ f(y(t)) \end{bmatrix}^T Q_4 \begin{bmatrix} y(t) \\ f(y(t)) \end{bmatrix} \\
&\quad + \begin{bmatrix} y_{\sigma_1}(t) \\ f(y(t-\sigma_1)) \end{bmatrix}^T (Q_5 + Q_6 - Q_4) \\
&\quad \cdot \begin{bmatrix} y_{\sigma_1}(t) \\ f(y(t-\sigma_1)) \end{bmatrix} - \begin{bmatrix} y_{\sigma_2}(t) \\ f(y(t-\sigma_2)) \end{bmatrix}^T \\
&\quad \cdot Q_5 \begin{bmatrix} y_{\sigma_2}(t) \\ f(y(t-\sigma_2)) \end{bmatrix} - (1-\dot{\sigma}(t)) \\
&\quad \cdot \begin{bmatrix} y_{\sigma}(t) \\ f(y(t-\sigma(t))) \end{bmatrix}^T Q_6 \begin{bmatrix} y_{\sigma}(t) \\ f(y(t-\sigma(t))) \end{bmatrix} \\
&\quad \le \zeta^T(t)\Xi_5\zeta(t), \\
\dot{V}_6(t) &= \dot{y}^T(t)\left(\sigma_1^2 R_4 + \sigma_{12}^2 R_5\right)\dot{y}(t) \\
&\quad - \sigma_1\int_{t-\sigma_1}^{t}\dot{y}^T(s)R_4\dot{y}(s)\,ds \\
&\quad - \sigma_{12}\int_{t-\sigma_2}^{t-\sigma_1}\dot{y}^T(s)R_5\dot{y}(s)\,ds, \\
\dot{V}_7(t) &= \dot{y}^T(t)\left(\frac{\sigma_1^2}{2}Z_3 + \frac{\sigma_2^2-\sigma_1^2}{2}Z_4 - \sigma_1\sigma_{12}Z_4\right)\dot{y}(t) \\
&\quad - \int_{t-\sigma_1}^{t}\int_{s}^{t}\dot{y}^T(u)Z_3\dot{y}(u)\,du\,ds \\
&\quad - \int_{t-\sigma_2}^{t-\sigma_1}\int_{s}^{t-\sigma_1}\dot{y}^T(u)Z_4\dot{y}(u)\,du\,ds,
\end{aligned} \tag{65}$$

where Ξ_{11}, Ξ_2, and Ξ_5 are defined in (35), (36), and (45), respectively.

Using Lemma 2 to estimate the R_1-dependent single integral terms in $\dot{V}_3(t)$ yields

$$\begin{aligned}
-\tau_1\int_{t-\tau_1}^{t}\dot{x}^T(s)R_1\dot{x}(s)\,ds &\le -\eta_1^T(t)\widetilde{R}_1\eta_1(t) \\
&= \zeta^T(t)\Xi_{32}\zeta(t),
\end{aligned} \tag{66}$$

where $\widetilde{R}_1$ and Ξ_{32} are defined in (39) and

$$\eta_1(t) = \begin{bmatrix} x(t) - x_{\tau_1}(t) \\ x(t) + x_{\tau_1}(t) - 2v_1(t) \\ x(t) - x_{\tau_1}(t) + 6v_1(t) - 12v_4(t) \end{bmatrix}. \tag{67}$$

Using Lemma 1 to estimate the R_2-dependent single integral terms in $\dot{V}_3(t)$ yields

$$\begin{aligned}
&-\int_{t-\tau_2}^{t-\tau_1}x^T(s)Rx(s)\,ds = -\int_{t-\tau(t)}^{t-\tau_1}x^T(s)Rx(s)\,ds \\
&\quad - \int_{t-\tau_2}^{t-\tau(t)}x^T(s)Rx(s)\,ds \le -\tau_{1\tau}(t) \\
&\quad \cdot \left[v_2^T(t)R_2v_2(t)\right. \\
&\quad \left. + 3\left(2v_5(t) - v_2(t)\right)^T R_2\left(2v_5(t) - v_2(t)\right)\right] \\
&\quad - \tau_{2\tau}(t)\left[v_3^T(t)R_2v_3(t)\right. \\
&\quad \left. + 3\left(2v_6(t) - v_3(t)\right)^T R_2\left(2v_6(t) - v_3(t)\right)\right] \\
&\quad = \zeta^T(t)\Xi_{\tau(t)}\zeta(t),
\end{aligned} \tag{68}$$

where $\Xi_{\tau(t)}$ is defined in (33).

Using Lemmas 2 and 5, together with (30), to estimate the R_3-dependent single integral terms in $\dot{V}_3(t)$ yields

$$\begin{aligned}
&-\tau_{12}\int_{t-\tau_2}^{t-\tau_1}\dot{x}^T(s)R_3\dot{x}(s)\,ds \\
&\quad = -\tau_{12}\int_{t-\tau(t)}^{t-\tau_1}\dot{x}^T(s)R_3\dot{x}(s)\,ds \\
&\qquad - \tau_{12}\int_{t-\tau_2}^{t-\tau(t)}\dot{x}^T(s)R_3\dot{x}(s)\,ds \\
&\quad \le -\frac{\tau_{12}}{\tau(t)-\tau_1}\left\{\eta_2^T(t)\widetilde{R}_3\eta_2(t)\right\} \\
&\qquad - \frac{\tau_{12}}{\tau_2-\tau(t)}\left\{\eta_3^T(t)\widetilde{R}_3\eta_3(t)\right\} \\
&\quad \le -\begin{bmatrix}\eta_2(t) \\ \eta_3(t)\end{bmatrix}^T\begin{bmatrix}\widetilde{R}_3 & S_1 \\ * & \widetilde{R}_3\end{bmatrix}\begin{bmatrix}\eta_2(t) \\ \eta_3(t)\end{bmatrix} = \zeta^T(t)\Xi_{33}\zeta(t),
\end{aligned} \tag{69}$$

where $\widetilde{R}_3$ and Ξ_{33} are defined in (40) and

$$\begin{aligned}
\eta_2(t) &= \begin{bmatrix} x_{\tau_1}(t) - x_{\tau}(t) \\ x_{\tau_1}(t) + x_{\tau}(t) - 2v_2(t) \\ x_{\tau_1}(t) - x_{\tau}(t) + 6v_2(t) - 12v_5(t) \end{bmatrix}, \\
\eta_3(t) &= \begin{bmatrix} x_{\tau}(t) - x_{\tau_2}(t) \\ x_{\tau}(t) + x_{\tau_2}(t) - 2v_3(t) \\ x_{\tau}(t) - x_{\tau_2}(t) + 6v_3(t) - 12v_6(t) \end{bmatrix}.
\end{aligned} \tag{70}$$

Using Lemma 8 to estimate the Z_1-dependent double integral terms in $\dot{V}_4(t)$ yields

$$\begin{aligned}
&-\int_{t-\tau_1}^{t}\int_{s}^{t}\dot{x}^T(u)Z_1\dot{x}(u)\,du\,ds \le -2\left[x(t)-v_1(t)\right]^T \\
&\cdot Z_1\left[x(t)-v_1(t)\right]+16\left[3v_4(t)-\frac{x(t)}{2}-v_1(t)\right]^T \\
&\cdot Z_1\left[3v_4(t)-\frac{x(t)}{2}-v_1(t)\right]=\zeta^T(t)\Xi_{42}\zeta(t),
\end{aligned} \tag{71}$$

where Ξ_{42} is defined in (43).

Using Lemma 8 to estimate the Z_2-dependent double integral terms in $\dot{V}_4(t)$ yields

$$\begin{aligned}
&-\int_{t-\tau_2}^{t-\tau_1}\int_{s}^{t-\tau_1}\dot{x}^T(u)Z_2\dot{x}(u)\,du\,ds \\
&=-\int_{t-\tau(t)}^{t-\tau_1}\int_{s}^{t-\tau_1}\dot{x}^T(u)Z_2\dot{x}(u)\,du\,ds \\
&-\int_{t-\tau_2}^{t-\tau(t)}\int_{s}^{t-\tau_1}\dot{x}^T(u)Z_2\dot{x}(u)\,du\,ds \\
&\le-\int_{t-\tau(t)}^{t-\tau_1}\int_{s}^{t-\tau_1}\dot{x}^T(u)Z_2\dot{x}(u)\,du\,ds \\
&-\int_{t-\tau_2}^{t-\tau(t)}\int_{s}^{t-\tau(t)}\dot{x}^T(u)Z_2\dot{x}(u)\,du\,ds \\
&\le-2\left[x_{\tau_1}(t)-v_2(t)\right]^T Z_2\left[x_{\tau_1}(t)-v_2(t)\right] \\
&-16\left[3v_5(t)-\frac{x_{\tau_1}(t)}{2}-v_2(t)\right]^T \\
&\cdot Z_2\left[3v_5(t)-\frac{x_{\tau_1}(t)}{2}-v_2(t)\right] \\
&-2\left[x_\tau(t)-v_3(t)\right]^T Z_2\left[x_\tau(t)-v_3(t)\right] \\
&-16\left[3v_6(t)-\frac{x_\tau(t)}{2}-v_3(t)\right]^T \\
&\cdot Z_2\left[3v_6(t)-\frac{x_\tau(t)}{2}-v_3(t)\right]=\zeta^T(t)\Xi_{43}\zeta(t),
\end{aligned} \tag{72}$$

where Ξ_{43} is defined in (44).

Similarly, using Lemmas 2, 5, and 8 to estimate the single and double integral terms in $\dot{V}_6(t)$ and $\dot{V}_7(t)$ yields

$$\begin{aligned}
&-\sigma_1\int_{t-\sigma_1}^{t}\dot{x}^T(s)R_4\dot{x}(s)\,ds\le\zeta^T(t)\Xi_{62}\zeta(t), \\
&-\sigma_{12}\int_{t-\sigma_2}^{t-\sigma_1}\dot{x}^T(s)R_5\dot{x}(s)\,ds\le\zeta^T(t)\Xi_{63}\zeta(t), \\
&-\int_{t-\sigma_1}^{t}\int_{s}^{t}\dot{x}^T(u)Z_3\dot{x}(u)\,du\,ds\le\zeta^T(t)\Xi_{72}\zeta(t), \\
&-\int_{t-\sigma_2}^{t-\sigma_1}\int_{s}^{t-\sigma_1}\dot{x}^T(u)Z_4\dot{x}(u)\,du\,ds\le\zeta^T(t)\Xi_{73}\zeta(t),
\end{aligned} \tag{73}$$

where Ξ_{62}, Ξ_{63}, Ξ_{72}, and Ξ_{73} are defined in (48)–(53).

Taking into account the assumption of the activation function, (13) and (14), the following inequalities hold [76, 77]:

$$\begin{aligned}
&h_i(s)=2\left[\Sigma y(s)-f\left(y(s)\right)\right]^T H_i f\left(y(s)\right)\ge 0, \\
&u_{ij}(s_1,s_2)=2\left[\Sigma\left(y(s_1)-y(s_2)\right)\right. \\
&\quad\left.-\left(f\left(y(s_1)\right)-f\left(y(s_2)\right)\right)\right]^T U_{ij}\times\left(f\left(y(s_1)\right)\right. \\
&\quad\left.-f\left(y(s_2)\right)\right)\ge 0,
\end{aligned} \tag{74}$$

where H_i, $i=1,2,\ldots,4$, and U_{ij}, $i=1,2,\ldots,4$, $j=i+1,\ldots,4$, are the symmetric diagonal matrices. Thus, the following inequality holds:

$$\begin{aligned}
H(t)+U(t)&=h_1(t)+h_2(t-\sigma_1)+h_3(t-\sigma(t)) \\
&\quad+h_4(t-\sigma_2)+u_{12}(t,t-\sigma_1) \\
&\quad+u_{13}(t,t-\sigma(t))+u_{14}(t,t-\sigma_2) \\
&\quad+u_{23}(t-\sigma_1,t-\sigma(t)) \\
&\quad+u_{24}(t-\sigma_1,t-\sigma_2) \\
&\quad+u_{34}(t-\sigma(t),t-\sigma_2) \\
&=\zeta^T(t)\Xi_8\zeta(t)\ge 0,
\end{aligned} \tag{75}$$

where Ξ_8 is defined in (54).

Finally, combining (64), (65), (66), (68), (69), (71), (72), (73), and (75) yields

$$\dot{V}(t)\le\zeta^T(t)\left[\Xi_{\tau(t)}+\sum_{i=1}^{8}\Xi_i\right]\zeta(t), \tag{76}$$

where the related notations are defined in (31).

Therefore, if LMIs (31) and (32) hold, then the following holds for a sufficiently small scalar $\epsilon>0$ based on convex combination method [78, 79]:

$$\dot{V}(t)\le-\epsilon\left(\|x(t)\|^2+\|y(t)\|^2\right) \tag{77}$$

which shows the asymptotical stability of GRN (2) with time delay satisfying (5). This completes the proof. □

4.2. Stability of GRN (11) with Delay Satisfying (6). For some cases, the change rates of the time-varying delays are unmeasurable, that is, time delay satisfying (6). For this case, the following stability criterion can be derived by using the proposed WTDII (27), together with Lemmas 1, 2, 5, and 8, to estimate the derivative of the LKF.

Theorem 10. *For given scalars τ_i and σ_i, $i=1,2$, GRN (2) with the time delay satisfying (6) and regulatory function satisfying (3) is asymptotically stable, if there exist symmetric matrices $P>0$, $Q_i>0$, $R_j>0$, $Z_k>0$, $i=1,2,4,5$, $j=1,2,\ldots,5$, and $k=1,2,\ldots,4$; diagonal matrices $\Lambda_1>0$, $\Lambda_2>0$, $H_j>$*

0, $j = 1,2,3,4$, $U_{lk} > 0$, $l = 1,2,\ldots,4$, *and* $k = l+1,\ldots,4$; *and any matrices* S_i, $i = 1,2$, *such that the following LMIs hold:*

$$\begin{bmatrix} \widetilde{R}_{2i+1} & S_i \\ * & \widetilde{R}_{2i+1} \end{bmatrix} > 0, \quad i = 1,2,$$

$$\begin{aligned} \Psi_3 &= \Xi_{\tau(t)}\big|_{\tau(t)=\tau_1} + \sum_{i=1,3,4,6,7} \Xi_i + \overline{\Xi}_2 + \overline{\Xi}_5 \\ &\le 0, \\ \Psi_4 &= \Xi_{\tau(t)}\big|_{\tau(t)=\tau_2} \sum_{i=1,3,4,6,7} \Xi_i + \overline{\Xi}_2 + \overline{\Xi}_5 \\ &\le 0, \end{aligned} \tag{78}$$

where Ξ_i, $i = 1,3,4,6,7$, *are defined in Theorem 9 and*

$$\begin{aligned} \overline{\Xi}_2 &= e_1^T Q_1 e_1 - e_2^T (Q_1 - Q_2) e_2 - e_4^T Q_2 e_4, \\ \overline{\Xi}_5 &= \begin{bmatrix} e_{11} \\ e_{21} \end{bmatrix}^T Q_4 \begin{bmatrix} e_{11} \\ e_{21} \end{bmatrix} + \begin{bmatrix} e_{12} \\ e_{22} \end{bmatrix}^T (Q_5 - Q_4) \begin{bmatrix} e_{12} \\ e_{22} \end{bmatrix} \\ &\quad - \begin{bmatrix} e_{14} \\ e_{24} \end{bmatrix}^T Q_5 \begin{bmatrix} e_{14} \\ e_{24} \end{bmatrix}. \end{aligned} \tag{79}$$

Proof. The above stability criterion can be obtained by setting $Q_3 = 0$ and $Q_6 = 0$ in Theorem 9. □

4.3. Some Remarks. This part gives some remarks for the above criteria.

Remark 11. During the proof of the above two stability criteria, the double integral terms arising in the derivative of the LKFs are estimated by using the proposed WTDII, that is, Lemma 8. As discussed in Section 3, the WTDII is tighter than the widely used JBDII (17), which was used for the GRN [19, 34], and the recently developed WBDII (18), which has not been used for the GRN. Thus, the proposed criteria are less conservative than the ones reported in [19, 34].

Remark 12. Compared with the literature, more information of regulatory function has been used during the proof of criteria. Specifically, in the literature, only (14) is used during the estimation of the derivative of the LKF, while, in this paper, extra information of regulatory function (13) is also used for estimating task. It has been proved in [77] that such additional information is helpful to reduce the conservatism.

Remark 13. The conditions given in Theorems 9 and 10 are in the form of LMI. Such LMI conditions can be easily checked by using MATLAB/LMI toolbox [80]. One can refer to [81–83] for more details.

Remark 14. Although this paper has just investigated the asymptotical stability, the proposed method can be extended to the robust stability analysis by taking into account the parameter uncertainties and/or noises of the GRNs. Moreover, the proposed method can also be extended to other problems discussed in Section 2, like controller synthesis, state estimation, filter design, passivity analysis, and so on [13, 59–70].

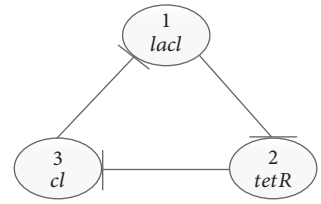

Figure 2: The repressilator network.

5. Illustrative Example

In this section, an example will be presented to illustrate the effectiveness of our results. As mentioned in Section 2, the important aim of the stability analysis of delayed GRNs is to determine the MADBs. And the stability criterion that provides bigger MADBs is less conservative than the one that gives smaller ones. Therefore, the advantages of the proposed criteria are demonstrated via the comparison of the MADBs calculated by various criteria. Moreover, the index of the number of variables (NoV) is applied to show the complexity of criteria.

Example 1. For the GRN model which is theoretically predicted and experimentally investigated in *Escherichia coli* in [4], the genetic network is composed of three repressilators *(lacl*, *tetR*, and *cl)* which form a cyclic negative feedback loop, each repressor protein inhibits the transcription of its downstream repressor gene, as shown in Figure 2, the protein of *lacl* represses the gene transcription of *tetR*, and the protein of *tetR* inhibits the gene transcription of *cl* simultaneously, and, finally, the transcription of *lacl* is inhibited by *cl*, which completes the cycle.

The kinetics of the genetic network are modelled as the GRN (2) with the following parameters [19]:

$$\begin{aligned} A &= \operatorname{diag}\{3,3,3\}, \\ C &= \operatorname{diag}\{2.5,2.5,2.5\}, \\ W &= \begin{bmatrix} 0 & 0 & -2.5 \\ -2.5 & 0 & 0 \\ 0 & -2.5 & 0 \end{bmatrix}, \\ D &= \begin{bmatrix} 0.8 \\ 0.8 \\ 0.8 \end{bmatrix}, \\ b_i(x) &= \frac{x^2}{1+x^2}, \quad i = 1,2,\ldots,n. \end{aligned} \tag{80}$$

It follows from (9) and (29) that

$$\Sigma = \operatorname{diag}\left\{\frac{3\sqrt{3}}{8}, \frac{3\sqrt{3}}{8}, \frac{3\sqrt{3}}{8}\right\}. \tag{81}$$

Table 1: The MADBs of τ_2 for various τ_1 and the NoVs of various criteria.

Criteria	NoVs	τ_1 0.1	0.5	1
[29, 31, 34]	—	<5.5	<5.9	<6.4
[19]	$40.5n^2 + 16.5n$	5.5	5.91	6.41
Theorem 9	$32n^2 + 22n$	9.2681	9.6682	10.1681

Table 2: The MADBs of τ_2 for various τ_1 and the NoVs of various criteria.

Criteria	NoVs	τ_1 0	1	2
[19]	$38n^2 + 15n$	2.3101	3.3101	4.3102
[19]	$29.5n^2 + 20.5n$	4.1647	5.1647	6.1646

(1) Calculation Results. The first study case is that the changing rates of the time-varying delays are measurable; that is, delays satisfy (5). Assume that $\sigma_1 = 0.1$, $\sigma_2 = 0.3$, $\sigma_d = 0.7$, and $\tau_d = 1.5$ [19], and the MADBs of τ_2 with respect to various τ_1 obtained by the proposed criteria are given in Table 1, where the MADBs reported in the literature are also listed for comparison.

The second study case is that the changing rates of the time-varying delays are nonmeasurable; that is, delays satisfy (6). Assume that $\sigma_1 = 1$ and $\sigma_2 = 2$, and the MADBs of τ_2 with respect to various τ_1 obtained by the proposed criteria, together with the ones provided by the least literature [19], are given in Table 2.

Moreover, the NoVs of criteria reported in the least literature [19] and that of criteria established in this paper are also given in tables to compare the computation complexity.

From the results in the tables, it can be easily found that the proposed stability criteria can provide the larger MADBs for two cases compared to those given in the existing literature. It shows that the proposed criteria are indeed less conservative than the ones reported in the literature. On the other hand, it is found that the NoV of the proposed criteria (Theorem 9) is smaller than the one reported in [19], $(40.5n^2 + 16.5n) - (32n^2 + 22n) = 8.5n^2 - 5.5n > 0$ and $(38n^2 + 15n) - (29.5n^2 + 20.5n) = 8.5n^2 - 5.5n > 0$ for any n. Both of those observations show the advantages of the proposed criterion.

(2) Simulation Verification. From the given parameters, the equilibrium points of the GRN can be obtained as

$$m^* = [0.7840, 0.7840, 0.7840]^T,$$
$$p^* = [0.2509, 0.2509, 0.2509]^T. \quad (82)$$

Simulation studies for the following two types of time-varying delays are carried out.

Case 1. The initial conditions $m(t) = [0.70, 0.85, 0.80]^T$, $t \in [-10.1681, 0]$, and $p(t) = [0.15, 0.20, 0.30]^T$, $t \in [-0.3, 0]$, and the following delays satisfy $\sigma_1 = 0.1$, $\sigma_2 = 0.3$, $\sigma_d = 0.7$, $\tau_1 = 1$, $\tau_2 = 10.1681$, and $\tau_d = 1.5$:

$$\tau(t) = 9.1681 \sin^2(0.1636t) + 1,$$
$$\sigma(t) = 0.2 \sin^2(3.5t) + 0.1. \quad (83)$$

Case 2. The initial conditions $m(t) = [0.70, 0.85, 0.80]^T$, $t \in [-6.1746, 0]$, and $p(t) = [0.15, 0.20, 0.30]^T$, $t \in [-2, 0]$, and the random delays satisfy $\sigma_1 = 1$, $\sigma_2 = 2$, $\tau_1 = 2$, $\tau_2 = 6.1746$.

Based on Tables 1 and 2, the GRN with the above delays, respectively, is stable. The trajectories of the concentrations of mRNA and protein are shown in Figures 3 and 4. The results show that they are stable at their equilibrium points.

6. Conclusions

This paper has investigated the stability of the GRN with time-varying delays, and its contributions have been revealed from two aspects. The novel WTDII has been developed for the estimation of the double integral terms, and it has been also proved to be tighter than the widely used JBDII and the recently developed WBDII for the same task. Then, with benefit from the WTDII, two LMI-based stability criteria with less conservatism have been derived for checking the stability of the GRN with time delays. Finally, the advantages of the proposed inequality and the established criteria have been verified through an example.

Notations

$\|\cdot\|$: The Euclidean vector norm
$\mathcal{R}^{n\times m}$: The set of all $n \times m$ real matrices
N^T (N^{-1}): The transpose (inverse) of the matrix N
$P > 0$: P is a real positive-definite matrix
diag$\{\cdots\}$: A block-diagonal matrix
I (0): The identity (zero) matrix
Sym$\{X\}$: $X + X^T$
$\begin{bmatrix} X & Y \\ * & Z \end{bmatrix}$: $\begin{bmatrix} X & Y \\ Y^T & Z \end{bmatrix}$

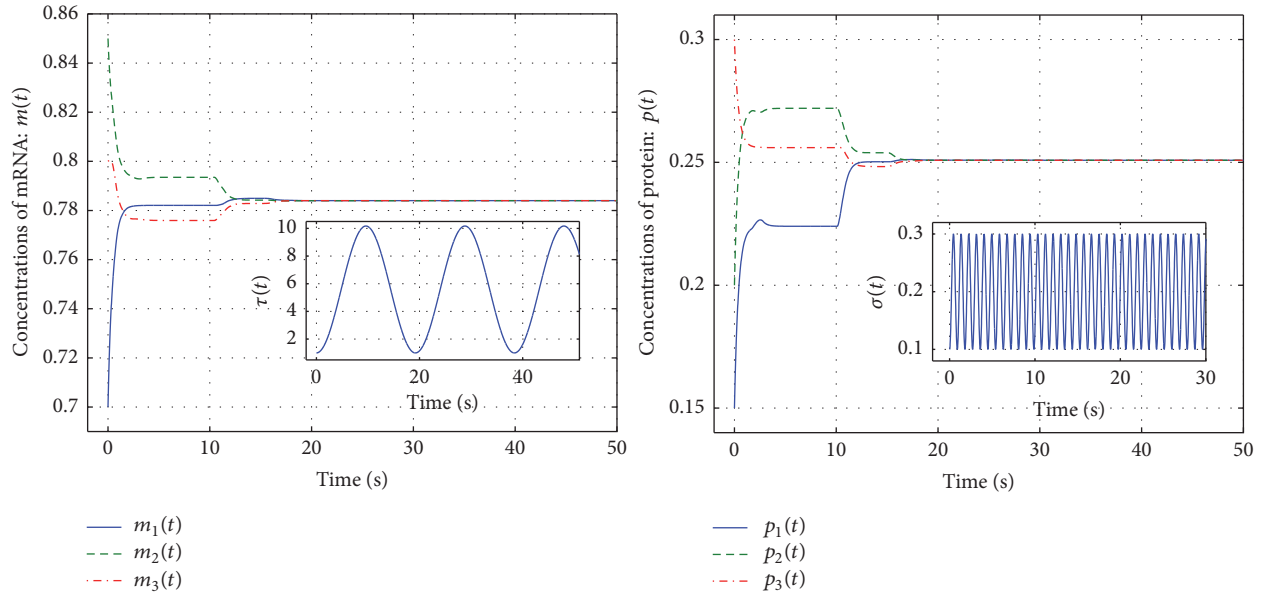

Figure 3: The trajectories of concentrations of mRNA and protein for Case 1.

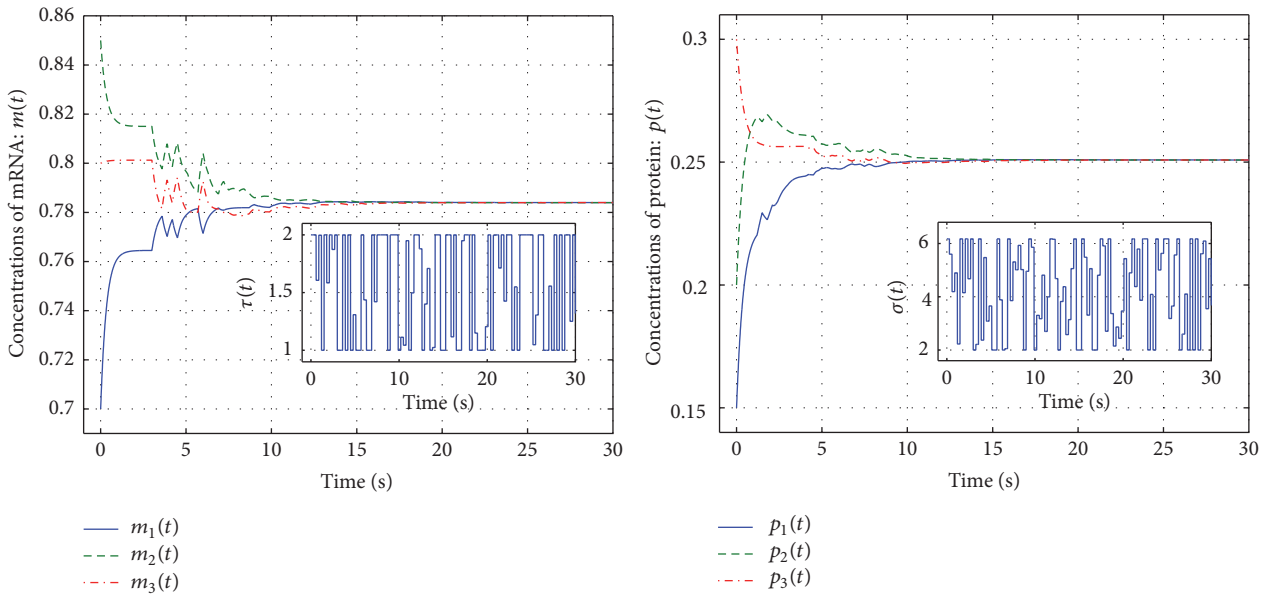

Figure 4: The trajectories of concentrations of mRNA and protein for Case 2.

GRNs: Genetic regulatory networks
LKF: Lyapunov-Krasovskii function
LMI: Linear matrix inequality
JBDII: Jensen-based double integral inequality
WBDII: Wirtinger-based double integral inequality
WTDII: Wiringter-type double integral inequality
MADB: Maximal admissible delay bounds
NoV: The number of variables.

Conflicts of Interest

The authors declare that they have no conflicts of interest.

Acknowledgments

This work was supported by the Provincial Scientific Research Project "Research on Power Prediction and Optimal Control of New Energy Generation" under Grant no. 12C0915 and the 61st Postdoctoral Science Fund Project of China under Grant no. 163612.

References

[1] Z. Wang, X. Liu, Y. Liu, J. Liang, and V. Vinciotti, "An extended Kalman filtering approach to modeling nonlinear dynamic gene

regulatory networks via short gene expression time series," *IEEE Transactions on Computational Biology and Bioinformatics*, vol. 6, no. 3, pp. 410–419, 2009.

[2] S. Mitra, R. Das, and Y. Hayashi, "Genetic networks and soft computing," *IEEE Transactions on Computational Biology and Bioinformatics*, vol. 8, no. 1, pp. 94–107, 2011.

[3] N. Noman and H. Iba, "Inferring gene regulatory networks using differential evolution with local search heuristics," *IEEE Transactions on Computational Biology and Bioinformatics*, vol. 4, no. 4, pp. 634–647, 2007.

[4] M. B. Elowitz and S. Leibier, "A synthetic oscillatory network of transcriptional regulators," *Nature*, vol. 403, no. 6767, pp. 335–338, 2000.

[5] P. Smolen, D. A. Baxter, and J. H. Byrne, "Mathematical modeling of gene networks," *Neuron*, vol. 26, no. 3, pp. 567–580, 2000.

[6] Z. Wang, F. Yang, D. W. C. Ho, S. Swift, A. Tucker, and X. Liu, "Stochastic dynamic modeling of short gene expression time-series data," *IEEE Transactions on NanoBioscience*, vol. 7, no. 1, pp. 44–55, 2008.

[7] T. Schlitt and A. Brazma, "Current approaches to gene regulatory network modelling," *BMC Bioinformatics*, vol. 8, no. 6, article no. S9, 2007.

[8] L. Qian, H. Wang, and E. R. Dougherty, "Inference of noisy nonlinear differential equation models for gene regulatory networks using genetic programming and Kalman filtering," *IEEE Transactions on Signal Processing*, vol. 56, no. 7, part 2, pp. 3327–3339, 2008.

[9] H. Hirata, S. Yoshiura, T. Ohtsuka et al., "Oscillatory expression of the BHLH factor Hes1 regulated by a negative feedback loop," *Science*, vol. 298, no. 5594, pp. 840–843, 2002.

[10] P. Smolen, D. A. Baxter, and J. H. Byrne, "A reduced model clarifies the role of feedback loops and time delays in the Drosophila circadian oscillator," *Biophysical Journal*, vol. 83, no. 5, pp. 2349–2359, 2002.

[11] I. Hoteit, N. Kharma, and L. Varin, "Computational simulation of a gene regulatory network implementing an extendable synchronous single-input delay flip-flop," *BioSystems*, vol. 109, no. 1, pp. 57–71, 2012.

[12] D. Bratsun, D. Volfson, L. S. Tsimring, and J. Hasty, "Delay-induced stochastic oscillations in gene regulation," *Proceedings of the National Acadamy of Sciences of the United States of America*, vol. 102, no. 41, pp. 14593–14598, 2005.

[13] X. Wan, L. Xu, H. Fang, and G. Ling, "Robust non-fragile H∞ state estimation for discrete-time genetic regulatory networks with Markov jump delays and uncertain transition probabilities," *Neurocomputing*, vol. 154, pp. 162–173, 2015.

[14] A. Becskel and L. Serrano, "Engineering stability in gene networks by autoregulation," *Nature*, vol. 405, no. 6786, pp. 590–593, 2000.

[15] L. Chen and K. Aihara, "Stability of genetic regulatory networks with time delay," *IEEE Transactions on Circuits and Systems I: Fundamental Theory and Applications*, vol. 49, no. 5, pp. 602–608, 2002.

[16] F.-X. Wu, "Stability and bifurcation of ring-structured genetic regulatory networks with time delays," *IEEE Transactions on Circuits and Systems I: Regular Papers*, vol. 59, no. 6, pp. 1312–1320, 2012.

[17] F. Ren and J. Cao, "Asymptotic and robust stability of genetic regulatory networks with time-varying delays," *Neurocomputing*, vol. 71, no. 4–6, pp. 834–842, 2008.

[18] W. Zhang, J.-A. Fang, and Y. Tang, "New robust stability analysis for genetic regulatory networks with random discrete delays and distributed delays," *Neurocomputing*, vol. 74, no. 14-15, pp. 2344–2360, 2011.

[19] X. Zhang, L. Wu, and S. Cui, "An improved integral inequality to stability analysis of genetic regulatory networks with interval time-varying delays," *IEEE Transactions on Computational Biology and Bioinformatics*, vol. 12, no. 2, pp. 398–409, 2015.

[20] F.-X. Wu, "Delay-independent stability of genetic regulatory networks," *IEEE Transactions on Neural Networks and Learning Systems*, vol. 22, no. 11, pp. 1685–1693, 2011.

[21] X. Zhang, A. Yu, and G. Zhang, "M-matrix-based delay-range-dependent global asymptotical stability criterion for genetic regulatory networks with time-varying delays," *Neurocomputing*, vol. 113, pp. 8–15, 2013.

[22] X. Zhang, L. Wu, and J. Zou, "Globally asymptotic stability analysis for genetic gegulatory networks with mixed delays: An M-matrix-based approach," *IEEE/ACM Transactions on Computational Biology and Bioinformatics*, pp. 10–1109, 2015.

[23] F. Wu, "Global and robust stability analysis of genetic regulatory networks with time-varying delays and parameter uncertainties," *IEEE Transactions on Biomedical Circuits and Systems*, vol. 5, no. 4, pp. 391–398, 2011.

[24] Y. Wang, Z. Wang, and J. Liang, "On robust stability of stochastic genetic regulatory networks with time delays: A delay fractioning approach," *IEEE Transactions on Systems, Man, and Cybernetics, Part B: Cybernetics*, vol. 40, no. 3, pp. 729–740, 2010.

[25] Q. Zhu, L. Jiang, W. Yao, C.-K. Zhang, and C. Luo, "Robust Load Frequency Control with Dynamic Demand Response for Deregulated Power Systems Considering Communication Delays," *Electric Power Components and Systems*, vol. 45, no. 1, pp. 75–87, 2017.

[26] P. Balasubramaniam and R. Sathy, "Robust asymptotic stability of fuzzy Markovian jumping genetic regulatory networks with time-varying delays by delay decomposition approach," *Communications in Nonlinear Science and Numerical Simulation*, vol. 16, no. 2, pp. 928–939, 2011.

[27] P. Balasubramaniam, R. Sathy, and R. Rakkiyappan, "A delay decomposition approach to fuzzy Markovian jumping genetic regulatory networks with time-varying delays," *Fuzzy Sets and Systems*, vol. 164, no. 1, pp. 82–100, 2011.

[28] Z. Wang, H. Gao, J. Cao, and X. Liu, "On delayed genetic regulatory networks with polytopic uncertainties: Robust stability analysis," *IEEE Transactions on NanoBioscience*, vol. 7, no. 2, article no. 8, pp. 154–163, 2008.

[29] H. Wu, X. Liao, W. Feng, S. Guo, and W. Zhang, "Robust stability for uncertain genetic regulatory networks with interval time-varying delays," *Information Sciences*, vol. 180, no. 18, pp. 3532–3545, 2010.

[30] J. H. Koo, D. H. Ji, S. C. Won, and J. H. Park, "An improved robust delay-dependent stability criterion for genetic regulatory networks with interval time delays," *Communications in Nonlinear Science and Numerical Simulation*, vol. 17, no. 8, pp. 3399–3405, 2012.

[31] W. Wang and S. Zhong, "Delay-dependent stability criteria for genetic regulatory networks with time-varying delays and nonlinear disturbance," *Communications in Nonlinear Science and Numerical Simulation*, vol. 17, no. 9, pp. 3597–3611, 2012.

[32] L.-P. Tian, J. Wang, and F.-X. Wu, "Robust and global delay-dependent stability for genetic regulatory networks with parameter uncertainties," *IEEE Transactions on NanoBioscience*, vol. 11, no. 3, pp. 251–258, 2012.

[33] J. Liu and D. Yue, "Asymptotic and robust stability of T-S fuzzy genetic regulatory networks with time-varying delays," *International Journal of Robust and Nonlinear Control*, vol. 22, no. 8, pp. 827–840, 2012.

[34] W. Wang, S. Zhong, and F. Liu, "New delay-dependent stability criteria for uncertain genetic regulatory networks with time-varying delays," *Neurocomputing*, vol. 93, pp. 19–26, 2012.

[35] P.-L. Liu, "Robust stability analysis of genetic regulatory network with time delays," *ISA Transactions®*, vol. 52, no. 3, pp. 326–334, 2013.

[36] W. Wang, S. Zhong, S. Kiong Nguang, and F. Liu, "Novel delay-dependent stability criterion for uncertain genetic regulatory networks with interval time-varying delays," *Neurocomputing*, vol. 121, pp. 170–178, 2013.

[37] C. Li, L. Chen, and K. Aihara, "Stability of genetic networks with SUM regulatory logic: Lur'e system and LMI approach," *IEEE Transactions on Circuits and Systems I: Regular Papers*, vol. 53, no. 11, pp. 2451–2458, 2006.

[38] C. Li, L. Chen, and K. Aihara, "Stochastic stability of genetic networks with disturbance attenuation," *IEEE Transactions on Circuits and Systems II: Express Briefs*, vol. 54, no. 10, pp. 892–896, 2007.

[39] H. Wu, X. Liao, S. Guo, W. Feng, and Z. Wang, "Stochastic stability for uncertain genetic regulatory networks with interval time-varying delays," *Neurocomputing*, vol. 72, no. 13-15, pp. 3263–3276, 2009.

[40] Q. Zhou, S. Xu, B. Chen, H. Li, and Y. Chu, "Stability analysis of delayed genetic regulatory networks with stochastic disturbances," *Physics Letters A*, vol. 373, no. 41, pp. 3715–3723, 2009.

[41] Y. He, L.-Y. Fu, J. Zeng, and M. Wu, "Stability of genetic regulatory networks with interval time-varying delays and stochastic perturbation," *Asian Journal of Control*, vol. 13, no. 5, pp. 625–634, 2011.

[42] W. Zhang, J.-a. Fang, and Y. Tang, "Robust stability for genetic regulatory networks with linear fractional uncertainties," *Communications in Nonlinear Science and Numerical Simulation*, vol. 17, no. 4, pp. 1753–1765, 2012.

[43] W. Zhang, J.-a. Fang, and Y. Tang, "Stochastic stability of Markovian jumping genetic regulatory networks with mixed time delays," *Applied Mathematics and Computation*, vol. 217, no. 17, pp. 7210–7225, 2011.

[44] L.-P. Tian, Z.-K. Shi, L.-Z. Liu, and F.-X. Wu, "M-matrix-based stability conditions for genetic regulatory networks with time-varying delays and noise perturbations," *IET Systems Biology*, vol. 7, no. 5, pp. 214–222, 2013.

[45] Y. Zhu, Q. Zhang, Z. Wei, and L. Zhang, "Robust stability analysis of Markov jump standard genetic regulatory networks with mixed time delays and uncertainties," *Neurocomputing*, vol. 110, pp. 44–50, 2013.

[46] W. Wang, S. Zhong, F. Liu, and J. Cheng, "Robust delay-probability-distribution-dependent stability of uncertain stochastic genetic regulatory networks with random discrete delays and distributed delays," *International Journal of Robust and Nonlinear Control*, vol. 24, no. 16, pp. 2574–2596, 2014.

[47] Y. Sun, G. Feng, and J. Cao, "Stochastic stability of Markovian switching genetic regulatory networks," *Physics Letters A*, vol. 373, no. 18-19, pp. 1646–1652, 2009.

[48] R. Rakkiyappan and P. Balasubramaniam, "Delay-probability-distribution-dependent stability of uncertain stochastic genetic regulatory networks with mixed time-varying delays: an LMI approach," *Nonlinear Analysis: Hybrid Systems*, vol. 4, no. 3, pp. 600–607, 2010.

[49] Y. Sun, G. Feng, and J. Cao, "Robust stochastic stability analysis of genetic regulatory networks with disturbance attenuation," *Neurocomputing*, vol. 79, pp. 39–49, 2012.

[50] W. Wang and S. Zhong, "Stochastic stability analysis of uncertain genetic regulatory networks with mixed time-varying delays," *Neurocomputing*, vol. 82, no. 1, pp. 143–156, 2012.

[51] Y. Wang, A. Yu, and X. Zhang, "Robust stability of stochastic genetic regulatory networks with time-varying delays: A delay fractioning approach," *Neural Computing and Applications*, vol. 23, no. 5, pp. 1217–1227, 2013.

[52] W. Wang, S. K. Nguang, S. Zhong, and F. Liu, "Robust stability analysis of stochastic delayed genetic regulatory networks with polytopic uncertainties and linear fractional parametric uncertainties," *Communications in Nonlinear Science and Numerical Simulation*, vol. 19, no. 5, pp. 1569–1581, 2014.

[53] X. Lou, Q. Ye, and B. Cui, "Exponential stability of genetic regulatory networks with random delays," *Neurocomputing*, vol. 73, no. 4-6, pp. 759–769, 2010.

[54] Z. Wang, X. Liao, S. Guo, and H. Wu, "Mean square exponential stability of stochastic genetic regulatory networks with time-varying delays," *Information Sciences*, vol. 181, no. 4, pp. 792–811, 2011.

[55] W. Zhang, J.-a. Fang, and W. Cui, "Exponential stability of switched genetic regulatory networks with both stable and unstable subsystems," *Journal of The Franklin Institute*, vol. 350, no. 8, pp. 2322–2333, 2013.

[56] Y. Yao, J. Liang, and J. Cao, "Stability analysis for switched genetic regulatory networks: an average dwell time approach," *Journal of The Franklin Institute*, vol. 348, no. 10, pp. 2718–2733, 2011.

[57] W. Zhang, Y. Tang, X. Wu, and J.-A. Fang, "Stochastic stability of switched genetic regulatory networks with time-varying delays," *IEEE Transactions on NanoBioscience*, vol. 13, no. 3, pp. 336–342, 2014.

[58] Q. Zhou, X. Shao, H. Reza Karimi, and J. Zhu, "Stability of genetic regulatory networks with time-varying delay: delta operator method," *Neurocomputing*, vol. 149, pp. 490–495, 2015.

[59] Z. Wang, J. Lam, G. Wei, K. Fraser, and X. Liu, "Filtering for nonlinear genetic regulatory networks with stochastic disturbances," *Institute of Electrical and Electronics Engineers Transactions on Automatic Control*, vol. 53, no. 10, pp. 2448–2457, 2008.

[60] J. Liang, J. Lam, and Z. Wang, "State estimation for Markov-type genetic regulatory networks with delays and uncertain mode transition rates," *Physics Letters A*, vol. 373, no. 47, pp. 4328–4337, 2009.

[61] W. Yu, J. Lu, Z. D. Wang, J. Cao, and Q. Zhou, "Robust H∞ control and uniformly bounded control for genetic regulatory network with stochastic disturbance," *IET Control Theory & Applications*, vol. 4, no. 9, pp. 1687–1706, 2010.

[62] D. Zhang and L. Yu, "Passivity analysis for stochastic Markovian switching genetic regulatory networks with time-varying delays," *Communications in Nonlinear Science and Numerical Simulation*, vol. 16, no. 8, pp. 2985–2992, 2011.

[63] P. Li and J. Lam, "Disturbance analysis of nonlinear differential equation models of genetic SUM regulatory networks," *IEEE Transactions on Computational Biology and Bioinformatics*, vol. 8, no. 1, pp. 253–259, 2011.

[64] Y. He, J. Zeng, M. Wu, and C.-K. Zhang, "Robust stabilization and H∞ controllers design for stochastic genetic regulatory networks with time-varying delays and structured uncertainties," *Mathematical Biosciences*, vol. 236, no. 1, pp. 53–63, 2012.

[65] Y. Liu and H. Jiang, "Exponential stability of genetic regulatory networks with mixed delays by periodically intermittent control," *Neural Computing and Applications*, vol. 21, no. 6, pp. 1263–1269, 2012.

[66] L. Chen, Y. Zhou, and X. Zhang, "Guaranteed cost control for uncertain genetic regulatory networks with interval time-varying delays," *Neurocomputing*, vol. 131, pp. 105–112, 2014.

[67] C. Ma, Q. Zeng, L. Zhang, and Y. Zhu, "Passivity and passification for Markov jump genetic regulatory networks with time-varying delays," *Neurocomputing*, vol. 136, pp. 321–326, 2014.

[68] L. Lu, Z. Xing, and B. He, "Non-uniform sampled-data control for stochastic passivity and passification of Markov jump genetic regulatory networks with time-varying delays," *Neurocomputing*, vol. 171, pp. 434–443, 2016.

[69] L. Li and Y. Yang, "On sampled-data control for stabilization of genetic regulatory networks with leakage delays," *Neurocomputing*, vol. 149, pp. 1225–1231, 2015.

[70] R. Anbuvithya, K. Mathiyalagan, R. Sakthivel, and P. Prakash, "Sampled-data state estimation for genetic regulatory networks with time-varying delays," *Neurocomputing*, vol. 151, no. 2, pp. 737–744, 2015.

[71] J. Sun, G. P. Liu, J. Chen, and D. Rees, "Improved delay-range-dependent stability criteria for linear systems with time-varying delays," *Automatica*, vol. 46, no. 2, pp. 466–470, 2010.

[72] M. Park, O. Kwon, J. H. Park, S. Lee, and E. Cha, "Stability of time-delay systems via Wirtinger-based double integral inequality," *Automatica*, vol. 55, pp. 204–208, 2015.

[73] A. Seuret and F. Gouaisbaut, "Wirtinger-based integral inequality: Application to time-delay systems," *Automatica*, vol. 49, no. 9, pp. 2860–2866, 2013.

[74] P. Park, W. I. Lee, and S. Y. Lee, "Auxiliary function-based integral inequalities for quadratic functions and their applications to time-delay systems," *Journal of The Franklin Institute*, vol. 352, no. 4, pp. 1378–1396, 2015.

[75] P. Park, J. W. Ko, and C. Jeong, "Reciprocally convex approach to stability of systems with time-varying delays," *Automatica*, vol. 47, no. 1, pp. 235–238, 2011.

[76] C.-K. Zhang, Y. He, L. Jiang, Q. H. Wu, and M. Wu, "Delay-dependent stability criteria for generalized neural networks with two delay components," *IEEE Transactions on Neural Networks and Learning Systems*, vol. 25, no. 7, pp. 1263–1276, 2014.

[77] C.-K. Zhang, Y. He, L. Jiang, and M. Wu, "Stability analysis for delayed neural networks considering both conservativeness and complexity," *IEEE Transactions on Neural Networks and Learning Systems*, vol. 27, no. 7, pp. 1486–1501, 2016.

[78] C. Zhang, Y. He, L. Jiang, and M. Wu, "Notes on Stability of Time-Delay Systems: Bounding Inequalities and Augmented Lyapunov-Krasovskii Functionals," *IEEE Transactions on Automatic Control*, vol. 62, no. 10, pp. 5331–5336, 2017.

[79] C.-K. Zhang, Y. He, L. Jiang, M. Wu, and H.-B. Zeng, "Summation inequalities to bounded real lemmas of discrete-time systems with time-varying delay," *Institute of Electrical and Electronics Engineers Transactions on Automatic Control*, vol. 62, no. 5, pp. 2582–2588, 2017.

[80] G. Balas, R. Chiang, A. Packard, and M. Safonov, *Robust Control Toolbox Users Guide*, MathWorks, 2010.

[81] W. Yao, L. Jiang, Q. H. Wu, J. Y. Wen, and S. J. Cheng, "Delay-dependent stability analysis of the power system with a wide-area damping controller embedded," *IEEE Transactions on Power Systems*, vol. 26, no. 1, pp. 233–240, 2011.

[82] C.-K. Zhang, L. Jiang, Q. H. Wu, Y. He, and M. Wu, "Delay-dependent robust load frequency control for time delay power systems," *IEEE Transactions on Power Systems*, vol. 28, no. 3, pp. 2192–2201, 2013.

[83] C.-K. Zhang, L. Jiang, Q. H. Wu, Y. He, and M. Wu, "Further results on delay-dependent stability of multi-area load frequency control," *IEEE Transactions on Power Systems*, vol. 28, no. 4, pp. 4465–4474, 2013.

Hindawi
Mathematical Problems in Engineering
Volume 2017, Article ID 4936490, 12 pages
https://doi.org/10.1155/2017/4936490

Research Article

An Improved Car-Following Model Accounting for Impact of Strong Wind

Dawei Liu, Zhongke Shi, and Wenhuan Ai

College of Automation, Northwestern Polytechnical University, Xi'an, Shaanxi 710072, China

Correspondence should be addressed to Zhongke Shi; shizknwpu@163.com

Received 17 March 2017; Revised 18 June 2017; Accepted 13 July 2017; Published 24 October 2017

Academic Editor: Renming Yang

In order to investigate the effect of strong wind on dynamic characteristic of traffic flow, an improved car-following model based on the full velocity difference model is developed in this paper. Wind force is introduced as the influence factor of car-following behavior. Among three components of wind force, lift force and side force are taken into account. The linear stability analysis is carried out and the stability condition of the newly developed model is derived. Numerical analysis is made to explore the effect of strong wind on spatial-time evolution of a small perturbation. The results show that the strong wind can significantly affect the stability of traffic flow. Driving safety in strong wind is also studied by comparing the lateral force under different wind speeds with the side friction of vehicles. Finally, the fuel consumption of vehicle in strong wind condition is explored and the results show that the fuel consumption decreased with the increase of wind speed.

1. Introduction

As an important part of modern traffic flow theory, car-following theory describes how the vehicle follows the vehicle ahead. The principle of the car-following model is that the acceleration or deceleration of the vehicle depends entirely on the driver's response to the stimuli from the surrounding vehicles. Because the research of car-following model is of great significance to traffic management and traffic safety analysis, it has been proposed as early as 1950s. Pipes [1] presented the first car-following model in 1953. Subsequently, researchers have developed some classic models [2–5]. Newell [2] derived a car-following model with time delay which is important to exploring the evolution of traffic jam. Bando et al. [3] proposed an optimal velocity model (OVM) to reveal the complex dynamic characteristics of traffic flow. To solve the problem of excessively high acceleration and unrealistic deceleration in OVM, generalized force model (GFM) has been developed by Helbing and Tilch [4]. Based on the GFM, Jiang et al. [5] developed a car-following model called full velocity difference model (FVDM). In recent years, car-following theory has been rapidly developed and many models have been proposed to describe traffic phenomena and driving behavior. These new models focused on many different factors that influence car-following behavior, like the effects of time delay [6–9], multiple-vehicle in front [10–13], lane changing [14–19], the heavy vehicles [20–23], driver's behaviors [24–33], and some other factors in the literatures [34–44]. Nagatani [12] found that the car interaction before the next car ahead can stabilize the traffic flow. Tang et al. [14] presented a car-following model on two lanes by considering the lateral effects in traffic. They believed that vehicle drivers always worry about the lane changing actions from neighbor lane and the consideration of lateral effects could stabilize the traffic flows on both lanes. Peng and Cheng [27] developed an extended model based on FVDM through substituting an anticipation optimal velocity with optimal velocity and discussed the impact of driver's forecast on traffic flow stability. Liu et al. [31] believed that short-term driving memory can influence the driver's anticipation behavior. Yu and Shi [33] put forward an improved car-following model in the connected cruise control strategy to investigate the effects of multiple preceding cars' velocity changes with memory on each car's speed and acceleration, the relative distance, fuel consumption, and CO, HC, and NOX emissions.

However, in these car-following models mentioned above, little effort has been made to study the effect of inclement weather on driving behavior. Inclement weather,

especially strong winds, has important influence on traffic safety, and traffic accidents caused by strong winds often appear in the news. A British study showed that up to 318 accidents were caused by strong winds from January 2002 to June 2007. In the case of driving in strong wind, drivers will always consider the impact of it to avoid traffic accident, so it is necessary to study the effect of strong wind on the driving behavior. Many researches have been done to investigate the effect of wind. Kwon et al. [45] explored that wind force acting on the vehicle has great effect on occurrence of traffic accidents. Baker [46, 47] found that overturning accidents, sideslip accidents, and rotation accidents are three most common types of traffic accident which can be induced by wind. In addition, they further presented the mathematical model of wind-induced accident risk. Xu et al. [48] explored the vehicle stability driving model with considering crosswind and obtained the limit minimum radii of horizontal curve in the conditions of different wind speeds.

However, the above works on strong wind only focus on studying the impact of strong wind from the perspective of traffic safety. To investigate the effect of strong wind on the micro driving behavior of vehicle, we develop an extended car-following model in this paper. This paper is organized as follows. In Section 2, a new improved car-following model based on FVDM is proposed by taking into account the effect of strong wind. In Section 3, linear stability analysis is carried out and the stability condition of this model is obtained. In Section 4, a series of numerical simulations is proposed to confirm the theoretical results. Conclusions are given in Section 5.

2. Model

Among the existing car-following models, the full velocity difference model (FVDM) proposed by Jiang et al. [5] is the most effective one, which can describe many car-following behaviors appearing in the real traffic. FVDM can be written as follows:

$$\frac{dx_n^2(t)}{dt^2} = a\left[V(\Delta x) - v_n\right] + \lambda \Delta v_n, \tag{1}$$

where $x_n(t)$ is the position of the nth vehicle at time t; $\Delta x = x_{n+1} - x_n$ and $\Delta v_n = v_{n+1} - v_n$ are the headway and the velocity difference between successive vehicles, respectively. $V(\Delta x)$ is the nth vehicle's optimal velocity which is a function of headway and can be expressed as follows:

$$V(\Delta x) = V_1 + V_2 \tanh\left(C_1\left(\Delta x_n - Lc\right) - C_2\right), \tag{2}$$

Where V_1, V_2, C_1, C_2 are parameters, respectively, and their values are the same as those in [5].

In the case of driving in the weather of strong wind, driving behavior always has been affected not only by the vehicle ahead, but also in a large degree by the wind force on vehicle. Driver in the vehicle behind will keep following with the leading vehicle. At the same time, he will consider the impact from strong wind especially lateral wind which can make the vehicle's control harder. When the wind force is great enough to make the driver feel uncomfortable to control the vehicle, adjusting the driving speed will be done by the driver to reduce the impact of wind.

According to automobile aerodynamics [49], the wind force on the stationary vehicle can be decomposed into drag force (F_X), lift force (F_Z), and the side force (F_Y), which can be formulated as follows:

$$\begin{aligned} F_X &= 0.5 C_D S \rho v_w^2, \\ F_Y &= 0.5 C_L S \rho v_w^2, \\ F_Z &= 0.5 C_Z S \rho v_w^2, \end{aligned} \tag{3}$$

where C_D, C_L, C_Z are, respectively, drag coefficient, lift coefficient, and side force coefficient. ρ and v_w are, respectively, air density and velocity of the wind. S represents windward area of vehicle. Windward area is related to the angle between the wind direction and the vehicle.

In this paper, we investigate the wind force on the running vehicle. In addition, we consider that there always exists an angle between the wind direction and the driving direction in real traffic. According to the above reasons, we rewrite (3) as follows:

$$\begin{aligned} F_X &= 0.5 C_D B H \rho \left(v_w \cos(\theta)\right)^2, \\ F_Y &= 0.5 C_Z L c H \rho \left(v_w \sin(\theta)\right)^2 \\ F_Z &= 0.5 C_L B L c \rho v_r^2, \end{aligned} \tag{4}$$

where $v_r = \sqrt{v_n^2 + v_w^2 - 2 v_n v_w \cos(\theta)}$ represents relative velocity of the wind and the vehicle. θ is the angle between the wind direction and the driving direction. Lc, B, and H are, respectively, length, width, and height of the vehicle.

Among three force components of wind force, side force (F_Y) has the greatest influence on the vehicle's driving stability [50]. Furthermore, lift force (F_Z) is also taken into account since it will gradually become strong with the increasing relative velocity of wind to the vehicle; as a result the actual weight of vehicle is reduced. That is why driver has the feeling of floating in the case of driving in a high speed. The greater lift force will also affect the vehicle's steering stability. Based on above consideration, we take side wind force and lift force into account and propose the car-following model under strong wind, which can be expressed as

$$\frac{dx_n^2}{dt^2} = a\left[\overline{V(\Delta x)} - v_n\right] + \lambda \Delta v_n, \tag{5}$$

where $\overline{V(\Delta x)}$ is modified optimal velocity with the consideration of the wind effect. For simplicity, we define $\overline{V(\Delta x)}$ as follows:

$$\overline{V(\Delta x)} = V(\Delta x) + \widetilde{v}, \tag{6}$$

where $\widetilde{v}$ is adjustable speed of optimal velocity under the influence of the wind force.

The influence of wind force on the vehicle can be measured by driver's driving comfort degree. In the case of driving

in wind, driver's driving comfort degree decreases with the increasing speed of wind. When the wind speed is small, drivers can not feel the impact of the wind. With the increase of wind speed, the driving comfort degree of the driver continues to reduce. When the degree reduced to a critical value, drivers need to adjust the driving state to reduce the impact caused by the wind and typically reduce the speed of vehicle. Thus, we define $\overline{v} = -\xi_n V(\Delta x_n)$; ξ_n is coefficient which varies with the change of driving comfort degree. Thus, the new car-following with the consideration of wind effect is as follows:

$$\frac{dx_n^2(t)}{dt^2} = a\left[\left(1-\xi_n\right)V\left(\Delta x\right) - v_n\right] + \lambda \Delta v_n. \tag{7}$$

Next, we define ξ_n as follows:

$$\xi_n = \begin{cases} 0, & \text{if } \mu < \mu_c, \\ k_1 + \dfrac{\left(1-k_1\right)\left(\mu-\mu_c\right)}{\left(k_2-1\right)\mu_c}, & \text{if } \mu_c < \mu < k_2\mu_c, \\ 1, & \text{if } \mu > k_2\mu_c, \end{cases} \tag{8}$$

where μ is sideway force coefficient which can measure the degree of driving comfort and the driving stability. μ_c is the critical value of sideway force coefficient when the driver feels uncomfortable, and $0 < k_1 < 1, k_2 > 1$ are coefficients. When the sideway force coefficient is smaller than μ_c, the driver does not need to consider the effect of the wind and just needs to pay attention to the driving state of the vehicle ahead. As the wind speed increases, the value of sideway force coefficient (μ) gradually increases. When the value of μ is bigger than μ_c, the driver will feel uncomfortable to control the vehicle, so he needs to slow down to reduce uncomfortable feeling caused by the wind. If the sideway force coefficient reaches $k_2\mu_c$, the vehicle will reach the maximum deceleration to avoid the accident.

Equation of sideway force coefficient is expressed as

$$\mu = \frac{v_n^2}{127r} - i_h + \frac{F_Y}{G}, \tag{9}$$

where v_n, r, i_h, G, and F_Y are vehicle speed, horizontal radius, super elevation, vehicle weight, and side force of wind, respectively. In the case of driving in the plane curve road section, we can set $i_h = 0$. Taking the influence of the lift force of the wind into account, the vehicle weight (G) can be rewritten as

$$\overline{G} = G - F_Z. \tag{10}$$

Thus, (9) can be rewritten as

$$\mu = \frac{v_n^2}{127r} + \frac{F_Y}{G - F_Z}. \tag{11}$$

Because (7) has taken the lift force and side force of the wind into account, it can be used to describe the driving behavior under varying speeds of wind.

3. The Linear Stability Analysis

Strong wind has great effect on traffic flow. However, little effort has been made to study the effects of strong wind on traffic flow from perspective of the linear stability analysis. In this section, the linear stability theory is applied to derive linear stability condition of the new proposed model in this section. The uniform traffic flow is defined by such a state that all vehicles move with the optimal velocity $\overline{V(\Delta x)}$ and the identical headway h.

Assuming $x_n(t) = x_n^{(0)}(t) + y_n(t)$, where $x_n^{(0)}(t) = hn + V(h)t$ and $y_n(t)$ is a small deviation from the steady state $x_n^{(0)}(t)$, then we can rewrite (7) as

$$\begin{aligned} \frac{d^2 y_n(t)}{dt^2} = a\left[\left(1-\xi_n\right)V'(h)\,\Delta y_n(t) - \frac{dy_n(t)}{dt}\right] \\ + \lambda \frac{d\Delta y_n(t)}{dt}, \end{aligned} \tag{12}$$

where $\Delta y_n(t) = y_{n+1}(t) - y_n(t)$. Expanding $y_n(t)$ in the Fourier-modes $y_n(t) \propto \exp(ikn + zt)$, we have

$$\begin{aligned} z^2 + z\left[a - \lambda\left(\exp(ik) - 1\right)\right] \\ - a\left(1-\xi_n\right)V'(h)\left(\exp(ik) - 1\right) = 0. \end{aligned} \tag{13}$$

Substituting $z = z_1(ik) + z_2(ik)^2 + \cdots$ into (13), we can obtain the first- and second-order terms of coefficients in the expression of z, respectively:

$$\begin{aligned} z_1 &= \left(1-\xi_n\right)V'(h), \\ z_2 &= \frac{z_1}{a}\left(\lambda + \frac{1}{2}a - z_1\right). \end{aligned} \tag{14}$$

For small perturbations with long waves, the uniform steady state will become unstable when z_2 is negative. Thus the neutral stability curve is given by

$$a_s = 2\left[\left(1-\xi_n\right)V'(h) - \lambda\right]. \tag{15}$$

The uniform traffic flow will be stable if

$$a_s > 2\left[\left(1-\xi_n\right)V'(h) - \lambda\right]. \tag{16}$$

Figure 1 shows the neutral stability line in the headway-sensitivity space $(\Delta x, a)$ with different sets of ξ_n. For the case of $\xi_n = 0$, the neutral stability line is the same as that of FVDM. The traffic flow is stable above the neutral stability line, while below the line traffic flow is unstable. The regime where the values of the headway give positive values of the stability function (see (15)) represents the unstable regime. The apex of each neutral stability curve represents the critical point (h_c, a_c), where h_c and a_c are, respectively, the safety distance and the critical sensitivity. It can be seen clearly from Figure 1 that, given the same values of headway, the critical point and the neutral stability curve obtained from our model are significantly lower than those of FVDM. The new model has a smaller unstable regime, which means the stability of

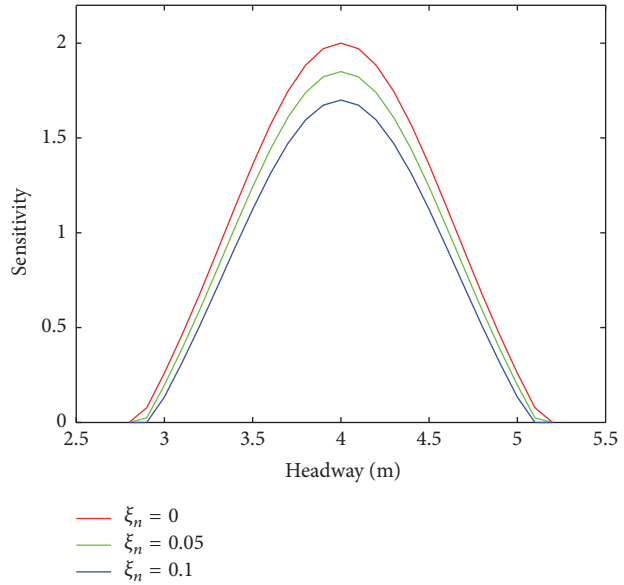

Figure 1: The neutral stability line in the headway-sensitivity space.

the traffic flow is improved as the value of ξ_n increases. The result of Figure 1 indicates that since FVDM did not consider the effect of strong wind, the vehicle velocity calculated by FVDM is still high even when the wind speed gets higher, which will decrease the stability of traffic flow. On the other hand, we believe that the strong wind will reduce the vehicle's velocity; as a result, stability of traffic flow will be improved.

4. Numerical Simulations

In this section, we explore the impacts of the strong wind on driving behavior by using numerical method. Simulation is made to investigate evolution of small perturbation, lateral stability of vehicle, and vehicle's fuel consumption, respectively.

4.1. Evolution of a Small Perturbation. We study spatial-time evolution of small perturbation with the effect of wind in this subsection. To compare with the FVDM which has not considered the impact of wind, we suppose that there are N vehicles running on a ring road whose length is $L = 1000$ m and those vehicles have same characters as $Lc = 5$, $B = 2$, $H = 1.5$, $G = 9800$. The initial state is set as

$$\begin{aligned} \Delta x_n(0) &= \Delta x_0 \quad \text{for } n = 1, 2, \ldots, N, \\ \Delta x_n(1) &= \Delta x_0 \quad \text{for } n \neq 1, N, \\ \Delta x_n(1) &= \Delta x_0 - 1 \quad \text{for } n = 1, \\ \Delta x_n(1) &= \Delta x_0 + 1 \quad \text{for } n = N. \end{aligned} \tag{17}$$

The total number of vehicles is $N = 60$, $\Delta x_0 = L/N - Lc$, and a periodic boundary condition is adopted in the simulation. Wind direction is always perpendicular to the direction of the vehicle, for simplicity. Other input parameters are set as follows:

$$\begin{aligned} a &= 0.41, \\ \lambda &= 0.5, \\ k_1 &= 0.02, \\ k_2 &= 2, \\ \mu_c &= 0.2, \\ \rho &= 1.293\ \text{kg/m}^3, \\ C_Z &= 0.629, \\ C_L &= 0.106. \end{aligned} \tag{18}$$

Figure 2 shows the space-time evolution of the velocity after 500 seconds and the velocity profile of the 30th vehicle for different wind speed. From Figure 2, we can observe the following:

(1) Using our model with the consideration of wind effect, the maximum speed in Figure 2(b) is approximately 12 m/s with wind speed at 20 m/s, which is significantly lower than that obtained by FVDM about 14 m/s in Figure 2(a) because FVDM did not consider the wind effect. Moreover, maximum speed is lower than 10 m/s with wind speed at 24 m/s in Figure 2(c). These indicate that strong wind could significantly inhibit driving speed; the higher the wind speed, the lower the vehicle speed. The result is consistent with the phenomenon observed in real traffic that driver will slow down when the wind force is powerful.

(2) Figures 2(b) and 2(c) are simulation results under our model and from them we can see that the oscillation

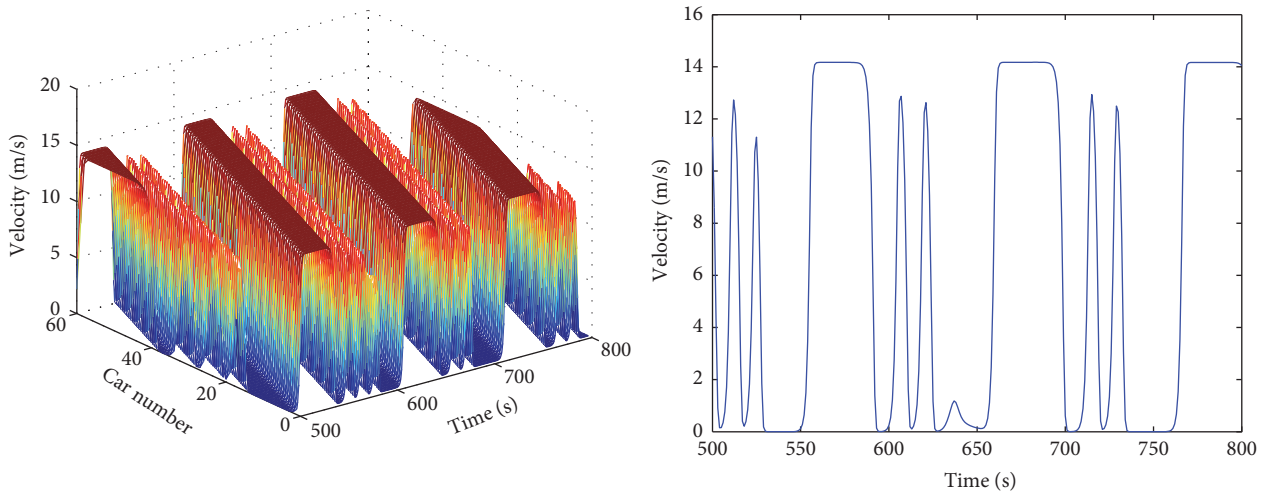

(a) FVDM

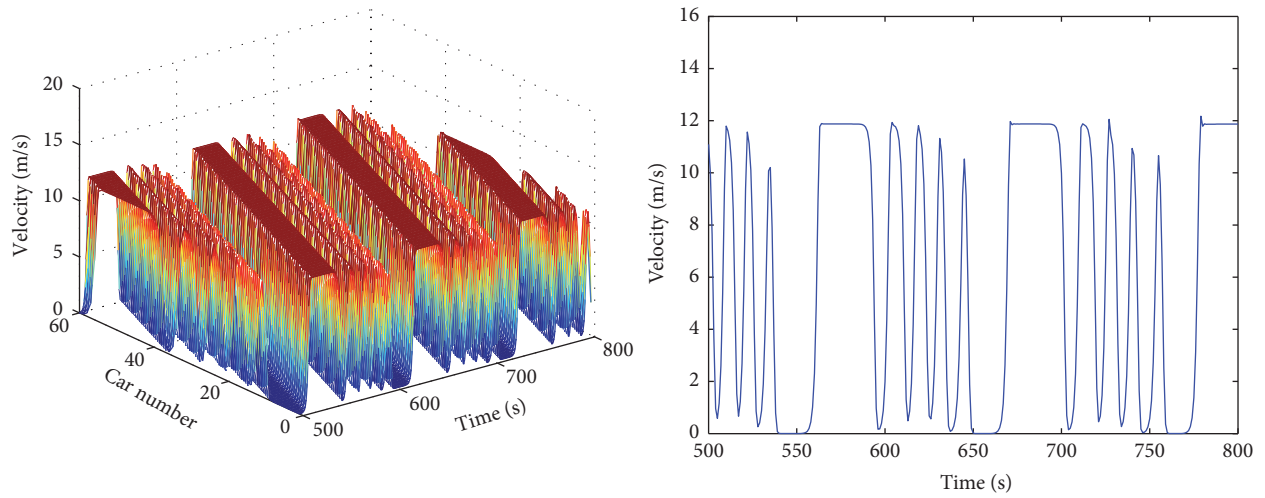

(b) Our model with wind speed at 20 m/s

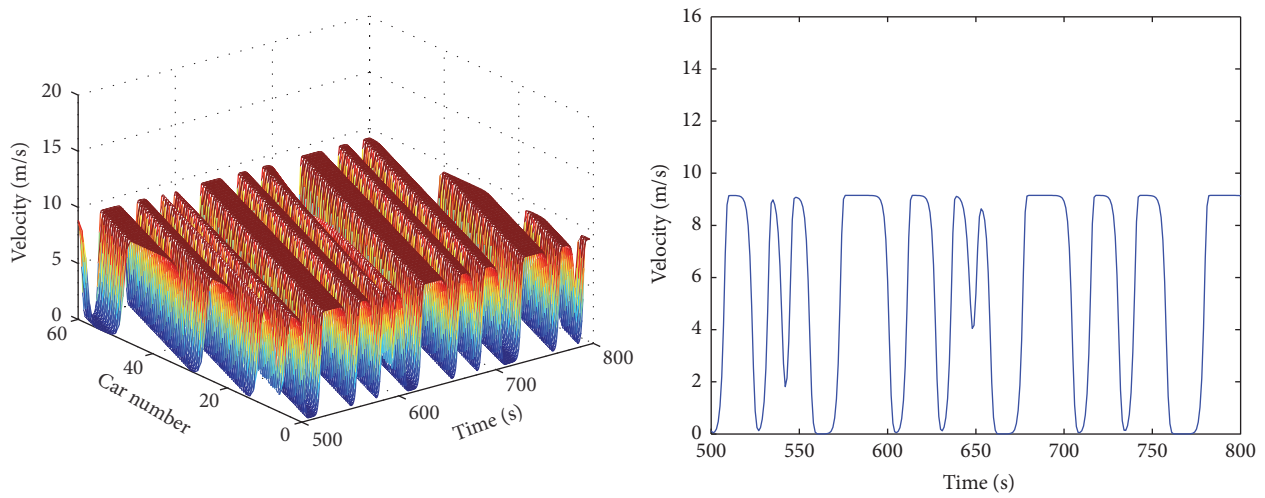

(c) Our model with wind speed at 24 m/s

FIGURE 2: Space-time evolution of the velocity and the velocity profile of the 30th vehicle for different wind speed from 500 seconds to 800 seconds, where (a) shows the results obtained by FVDM and (b) and (c) are the results of our model with wind speed at 20 m/s and 24 m/s, respectively.

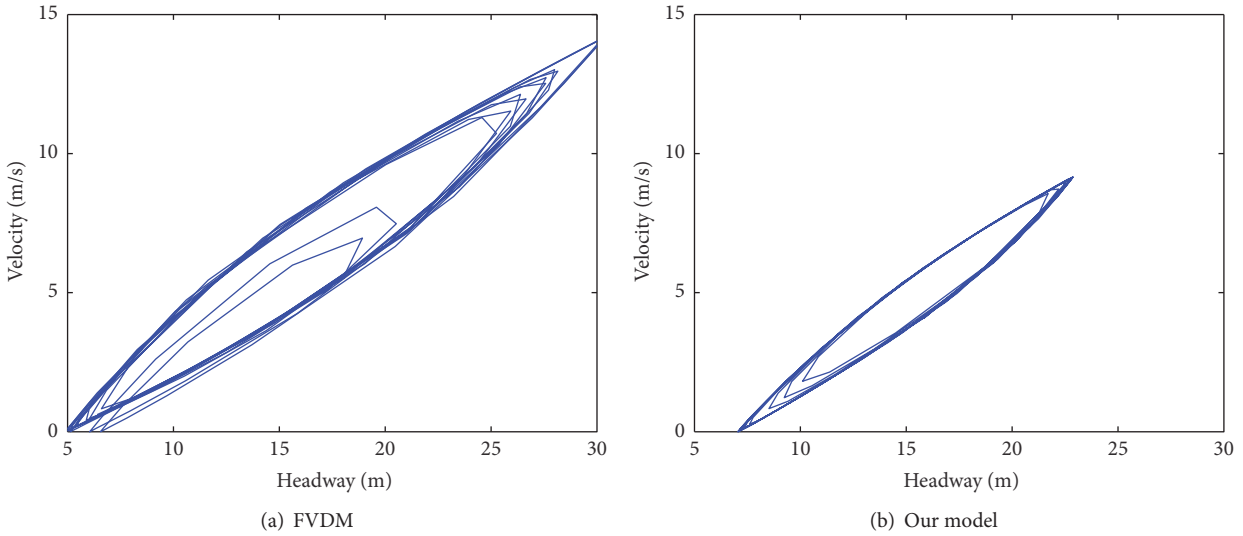

Figure 3: Hysteresis loops for FVDM and our model.

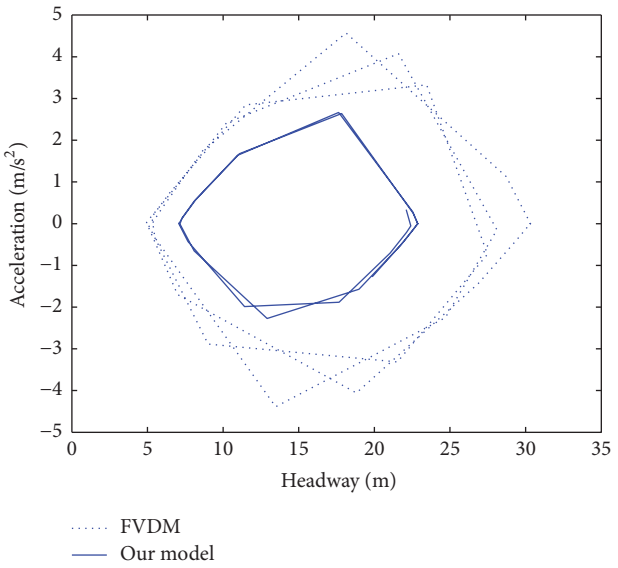

Figure 4: Vehicles' acceleration versus headway for FVDM and our model.

in Figure 2(c) is more gentle than those in Figure 2(b). It shows that drivers will be more careful to keep driving and try to stabilize the vehicle velocity when the wind speed gets higher.

(3) Stop-and-go traffic appears in Figure 2. The jam in Figure 2(a) is the most serious, followed by those in Figures 2(b) and 2(c). It explores that stop-and-go phenomenon is weakened since vehicle's velocity reduces with the increase of the wind speed.

We also use the hysteresis loops to demonstrate the relationship between velocity and space headway and the relationship between acceleration and space headway. Figure 3 exhibits the hysteresis loops after a sufficiently large time, where (a) and (b) are obtained from FVDM and our model. The 30th vehicle is selected as the target vehicle. Figure 4 represents the relationship between acceleration and space headway at time 600 s, where the dotted line and solid line are obtained from FVDM and our model. Hysteresis loop having a larger size means that the stability of traffic flow is lower, and the stability of traffic flow is improved with the decrease of the size of the loop. From Figures 3 and 4, we can find that the hysteresis loop obtained from our model is much smaller than that from the FVDM. The result indicates that, by taking the effect of strong wind into account, the stability of the traffic flow simulated by our model is superior to that simulated by FVDM, which is consistent with the conclusion of Figure 1.

4.2. Lateral Stability of Vehicle. In this subsection, we investigate the influence of strong wind on the lateral stability of vehicle. Lateral stability refers to the vehicle's performance of resisting lateral overturn and side slip. Researches show that,

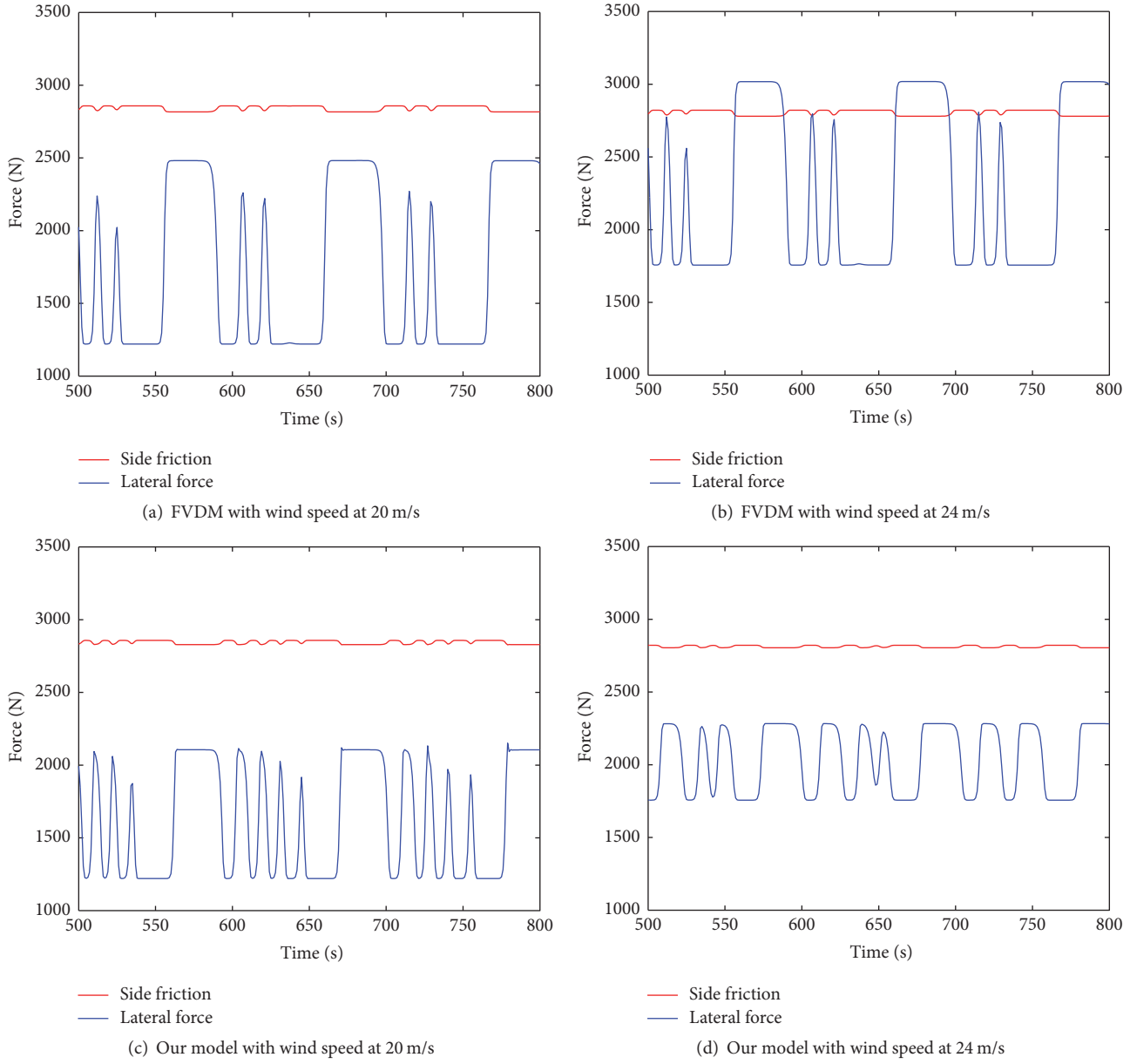

Figure 5: The force profile of the 30th vehicle with different wind speed from 500 seconds to 800 seconds, where (a) and (b) are the results without consideration of wind effect and (c) and (d) are the results with consideration of wind effect.

under the identical road conditions and driving speed, side slip occurs before overturn with the enhancement of cross wind [50]. In real traffic, vehicle side slip will occur when the lateral force is greater than the side friction between the vehicle and the road surface. In view of this, lateral stability of the driving vehicle will be ensured as long as side slip is prevented.

Maximum side friction can be expressed as

$$f_s = \zeta f, \tag{19}$$

where $f = \phi G$ is the maximum static friction force between vehicle and road. The permanents ϕ and ζ are, respectively, friction coefficient and sideway adhesion coefficient. In this paper ϕ, ζ are, respectively, set as 0.5 and 0.6.

In the case of driving on a ring road in the weather of strong winds, lateral force on vehicle is the resultant force of centrifugal force and wind force. When the wind force has same direction with the centrifugal force, lateral force will be a large increase with the increase of wind speed and possibly exceed the maximum side friction. Therefore, it is necessary to analyze the lateral force on vehicle in this situation.

Figure 5 shows the force evolution of the 30th vehicle for different wind speed after 500 seconds, where (a) and (b) are the results by FVDM with wind speed at 20 m/s and 24 m/s, respectively. Figures 5(c) and 5(d) are the results of our model with wind speed at 20 m/s and 24 m/s, respectively. The red curve is the curve of maximum side friction and the blue curve is the curve of lateral force on the vehicle. The

Table 1: The regression coefficients in (20).

$K^e_{i,j}$	j			
	0	1	2	3
i				
0	−0.679439	0.135273	0.015946	−0.001189
1	0.29665	0.004808	−0.000020535	$5.5409285E-8$
2	−0.000276	0.000083329	0.000000937	$-2.479644E-8$
3	0.000001487	−0.000061321	0.000000304	$-4.467234E-9$

initial conditions are set as (17). Comparing with the FVDM, we can draw the conclusions from Figure 5: (1) The lateral force increases with wind speed. Figures 5(a) and 5(b) are the results obtained by FVDM with different speed of wind. As the wind speed increases from 20 m/s in Figure 5(a) to 24 m/s in Figure 5(b), the maximum lateral force on the vehicle corresponding increases from about 2500 N to 3000 N. The curve of lateral force surpasses the curve of maximum side friction three times in Figure 5(b), so sideslip occurs three times. On the contrary, by using our model, the curve of lateral force is always significantly lower than the curve of maximum side friction in Figures 5(c) and 5(d), so the sideslip has not occurred. It is well known that vehicles should slow down to avoid the sideslip when the crosswind becomes powerful. Thus, the numerical results show that our model can better reproduce the real traffic phenomena with the effect of strong wind.

(2) The amplitude and the frequency of lateral force curve in Figure 5(d) are, respectively, smaller than those in Figure 5(c). It indicates that the increase of wind force plays a role in prompting driver to be more careful while driving and thereby leads to a more gentle curve of the lateral force.

4.3. Vehicle's Fuel Consumption. We explore the effect of strong wind on vehicle's fuel consumption because the existing studies show that fuel consumption can be affected by driving behavior [51–53]. Ahn [51] proposed a VT-micro model to formulate the vehicle's fuel consumption in 1998. The VT-micro model can be written as

$$\ln(\mathrm{MOEe}) = \sum_{i=0}^{3}\sum_{j=0}^{3}\left(K^e_{i,j}\times v^i\times\left(\frac{dv}{dt}\right)^j\right),$$
$$\mathrm{MOEe} = \exp\left(\sum_{i=0}^{3}\sum_{j=0}^{3}\left(K^e_{i,j}\times v^i\times\left(\frac{dv}{dt}\right)^j\right)\right), \tag{20}$$

where MOEe is the vehicle's fuel consumption rate and its unit is ml/s; $K^e_{i,j}$ is the regression coefficient (see Table 1).

To display the difference of the vehicle's fuel consumption under different wind speed, we calculate the evolution of the fuel consumption rate from 500 seconds to 800 seconds and the profile of the $30th$ vehicle under different wind speed. The initial conditions are set as (17).

Figure 6 shows the evolution of the fuel consumption rate and the profile of the 30th vehicle for different wind speed from 500 seconds to 800 seconds, where (a) shows the results obtained by FVDM; (b) and (c) are the results by our model with wind speed at 20 m/s and 24 m/s, respectively. From Figure 6, we can see that without the consideration of the wind effect, the amplitude of fuel consumption rate simulated by FVDM in Figure 6(a) is higher than that simulated by our model in Figures 6(b) and 6(c). Furthermore, the amplitude of fuel consumption rate is lower in Figure 6(c) when the wind speed is 24 m/s than that in Figure 6(b) when the wind speed is 20 m/s. It shows that the fuel consumption is affected by the wind. As the wind speed increases, the amplitude of fuel consumption rate decreases gradually.

Though we obtain the conclusion from Figure 6 that the wind can affect the amplitude of fuel consumption rate, we can not determine whether the effect of strong wind will reduce vehicle's fuel consumption. In order to further study the effect of strong wind on vehicle's fuel consumption, we simulated each vehicle's total fuel consumption for a period of time by using FVDM and our model, respectively. Figure 7 exhibits each vehicle's total fuel consumption for 1000 s with different wind speed, where (a) and (b) are, respectively, with wind speed at 20 m/s and 24 m/s. As can be seen from Figure 7, the curves of each vehicle's total fuel consumption simulated by our model are lower than the curve simulated by FVDM. Also, each vehicle's total fuel consumption with wind speed at 24 m/s is lower than that with 20 m/s. Simulation results indicate that by taking the effect of strong wind into account the driver will reduce the vehicle's velocity to avoid the traffic accident, so it leads to the reduction of fuel consumption. Therefore, the simulation results are consistent with the conclusions of Figure 6.

5. Conclusions

In this paper, we present an extended car-following model with the consideration of the wind effect based on the FVD model. Linear stability analysis is carried out to study the traffic characteristics by making use of linear stability analysis. Numerical analysis is made to explore the effect of strong wind on evolution of a small perturbation, lateral stability of vehicle, and vehicle's fuel consumption. The simulation result shows that the developed model can qualitatively reproduce the impact of the strong wind on traffic flow, which means the new developed model is reasonable. Nevertheless, there are still some limitations in this paper. For example, we do not consider the influence caused by wind changing direction, and, moreover, strong wind often causes low visibility, but it is not currently taken into account.

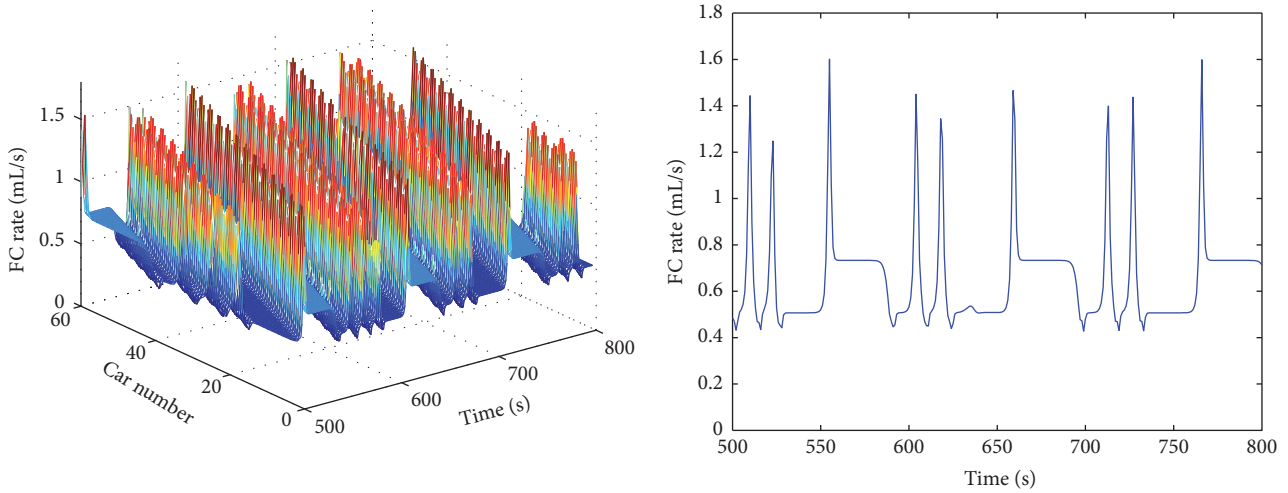

(a) FVDM

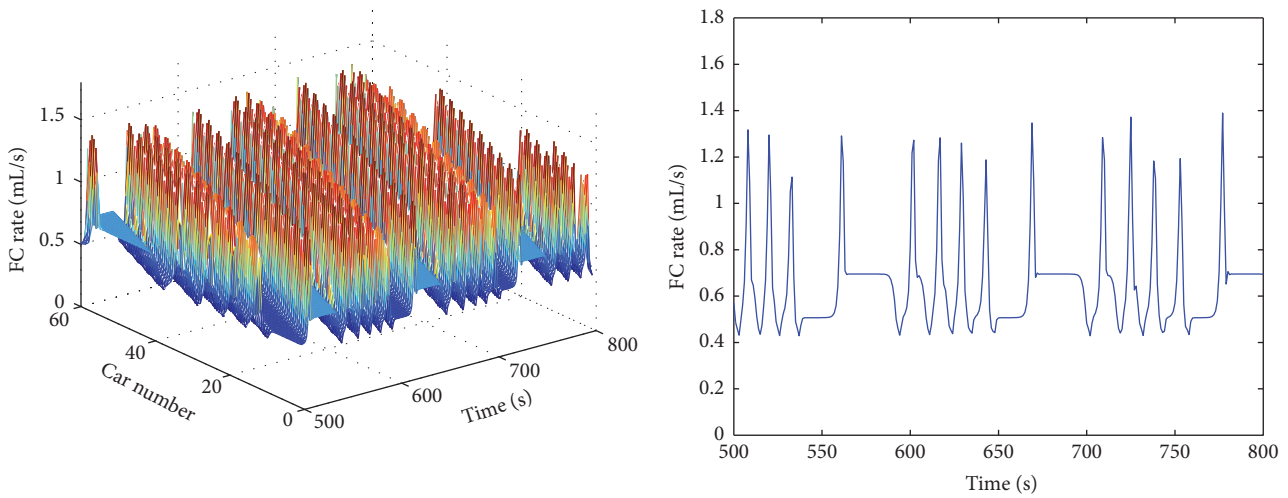

(b) Our model with wind speed at 20 m/s

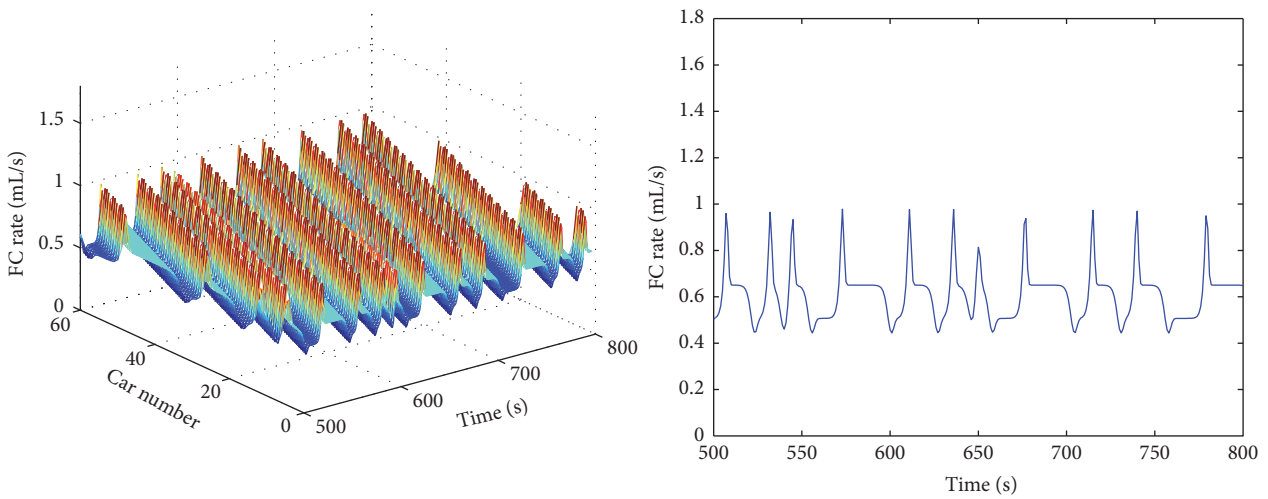

(c) Our model with wind speed at 24 m/s

Figure 6: Evolution of the fuel consumption rate and the profile of the single vehicle.

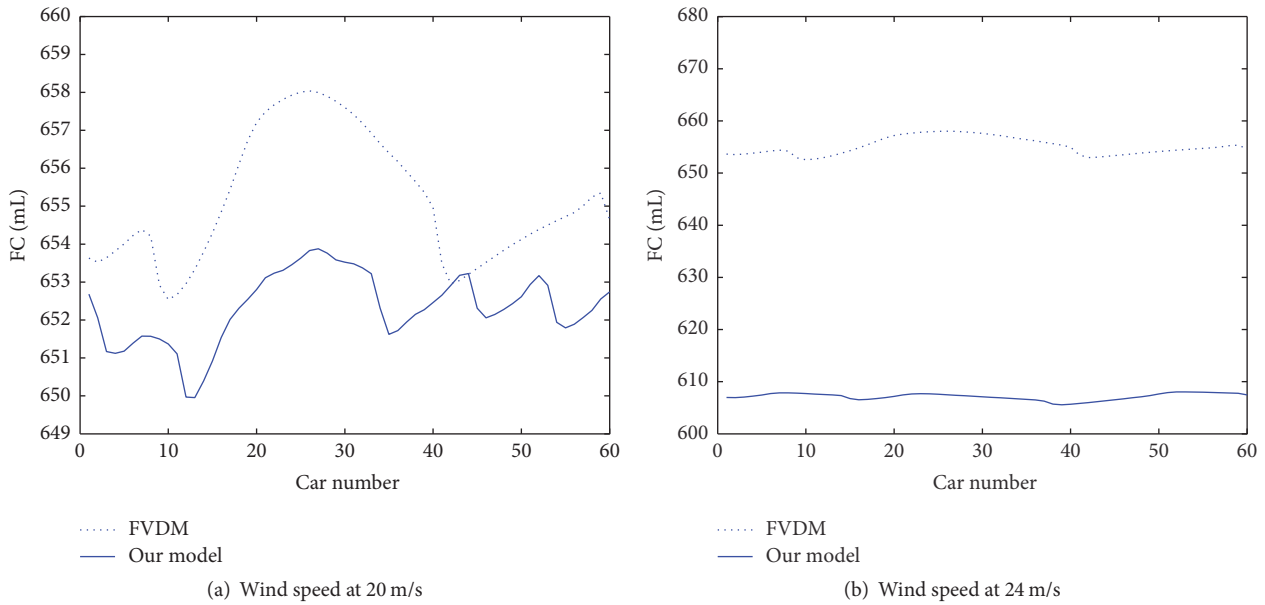

(a) Wind speed at 20 m/s

(b) Wind speed at 24 m/s

Figure 7: Each vehicle's total fuel consumption for a period of time.

In the further study, we will develop a new car-following model on the basis of the model presented in this paper to address the above limitations. Theoretical analysis and experimental study will be carried out to explore the effect of wind changing direction and low visibility on traffic flow.

Conflicts of Interest

The authors declare that there are no conflicts of interest regarding the publication of this paper.

Acknowledgments

This work is partially supported by the National Nature Science Foundation of China (Grant no. 61134004), Gansu Province Educational Research Project (Grant no. 2015B-130), and the Fundamental Research Funds for the Central Universities (no. 31920160045).

References

[1] L. A. Pipes, "An operational analysis of traffic dynamics," *Journal of Applied Physics*, vol. 24, no. 3, pp. 274–281, 1953.

[2] G. F. Newell, "Nonlinear effects in the dynamics of car following," *Operations Research*, vol. 9, pp. 209–229, 1961.

[3] M. Bando, K. Hasebe, A. Nakayama, A. Shibata, and Y. Sugiyama, "Dynamical model of traffic congestion and numerical simulation," *Physical Review E: Statistical, Nonlinear, and Soft Matter Physics*, vol. 51, no. 2, pp. 1035–1042, 1995.

[4] D. Helbing and B. Tilch, "Generalized force model of traffic dynamics," *Physical Review E: Statistical, Nonlinear, and Soft Matter Physics*, vol. 58, no. 1, pp. 133–138, 1998.

[5] R. Jiang, Q. Wu, and Z. Zhu, "Full velocity difference model for a car-following theory," *Physical Review E: Statistical, Nonlinear, and Soft Matter Physics*, vol. 64, article 017101, no. 1, Article ID 017101, 2001.

[6] L. C. Davis, "Modifications of the optimal velocity traffic model to include delay due to driver reaction time," *Physica A: Statistical Mechanics and its Applications*, vol. 319, pp. 557–567, 2003.

[7] R. Sipahi, F. M. Atay, and S.-I. Niculescu, "Stability of traffic flow behavior with distributed delays modeling the memory effects of the drivers," *SIAM Journal on Applied Mathematics*, vol. 68, no. 3, pp. 738–759, 2007/08.

[8] Y. Jin and M. Xu, "Stability analysis in a car-following model with reaction-time delay and delayed feedback control," *Physica A: Statistical Mechanics and its Applications*, vol. 459, pp. 107–116, 2016.

[9] D. Ngoduy, "Linear stability of a generalized multi-anticipative car following model with time delays," *Communications in Nonlinear Science and Numerical Simulation*, vol. 22, no. 1-3, pp. 420–426, 2015.

[10] C. Wagner, "Asymptotic solutions for a multi-anticipative car-following model," *Physica A: Statistical Mechanics and its Applications*, vol. 260, no. 1-2, pp. 218–224, 1998.

[11] K. Hasebe, A. Nakayama, and Y. Sugiyama, "Equivalence of linear response among extended optimal velocity models," *Physical Review E: Statistical, Nonlinear, and Soft Matter Physics*, vol. 69, article 017103, no. 1, 2004.

[12] T. Nagatani, "Stabilization and enhancement of traffic flow by the next-nearest-neighbor interaction," *Physical Review E: Statistical Physics, Plasmas, Fluids, and Related Interdisciplinary Topics*, vol. 60, pp. 6395–6401, 1999.

[13] H. X. Ge, S. Q. Dai, L. Y. Dong, and Y. Xue, "Stabilization effect of traffic flow in an extended car-following model based on an intelligent transportation system application," *Physical Review E: Statistical, Nonlinear, and Soft Matter Physics*, vol. 70, no. 6, Article ID 066134, 2004.

[14] T.-Q. Tang, H.-J. Huang, and Z.-Y. Gao, "Stability of the car-following model on two lanes," *Physical Review E: Statistical, Nonlinear, and Soft Matter Physics*, vol. 72, no. 6, Article ID 066124, 2005.

[15] G. Peng, "A new lattice model of two-lane traffic flow with the consideration of optimal current difference," *Communications*

in Nonlinear Science and Numerical Simulation, vol. 18, no. 3, pp. 559–566, 2013.

[16] G. Peng, "A new lattice model of the traffic flow with the consideration of the driver anticipation effect in a two-lane system," *Nonlinear Dynamics*, vol. 73, no. 1-2, pp. 1035–1043, 2013.

[17] T. Wang, Z. Gao, J. Zhang, and X. Zhao, "A new lattice hydrodynamic model for two-lane traffic with the consideration of density difference effect," *Nonlinear Dynamics*, vol. 75, no. 1-2, pp. 27–34, 2014.

[18] Y. Jia, Y. Du, and J. Wu, "Stability Analysis of a Car-Following Model on Two Lanes," *Mathematical Problems in Engineering*, vol. 2014, Article ID 727560, 2014.

[19] H.-x. Ge, X.-p. Meng, H.-b. Zhu, and Z.-P. Li, "Feedback control for car following model based on two-lane traffic flow," *Physica A: Statistical Mechanics and its Applications*, vol. 408, pp. 28–39, 2014.

[20] K. Aghabayk, M. Sarvi, and W. Young, "Attribute selection for modelling driver's car-following behaviour in heterogeneous congested traffic conditions," *Transportmetrica A: Transport Science*, vol. 10, no. 5, pp. 457–468, 2014.

[21] D. Ngoduy, "Effect of the car-following combinations on the instability of heterogeneous traffic flow," *Transportmetrica B*, vol. 3, no. 1, pp. 44–58, 2015.

[22] T. Nagatani, "Complex motion of a shuttle bus between two terminals with periodic inflows," *Physica A: Statistical Mechanics and its Applications*, vol. 449, pp. 254–264, 2016.

[23] T. Nagatani, "Effect of stoppage time on motion of a bus through a sequence of signals," *Physica A: Statistical Mechanics and its Applications*, vol. 465, pp. 297–304, 2017.

[24] M. Treiber, A. Kesting, and D. Helbing, "Delays, inaccuracies and anticipation in microscopic traffic models," *Physica A: Statistical Mechanics and its Applications*, vol. 360, no. 1, pp. 71–88, 2006.

[25] L.-J. Zheng, C. Tian, D.-H. Sun, and W.-N. Liu, "A new car-following model with consideration of anticipation driving behavior," *Nonlinear Dynamics*, vol. 70, no. 2, pp. 1205–1211, 2012.

[26] T. Q. Tang, C. Y. Li, and H. J. Huang, "A new car-following model with the consideration of the driver's forecast effect," *Physics Letters A*, vol. 374, no. 38, pp. 3951–3956, 2010.

[27] G.-h. Peng and R.-j. Cheng, "A new car-following model with the consideration of anticipation optimal velocity," *Physica A: Statistical Mechanics and its Applications*, vol. 392, no. 17, pp. 3563–3569, 2013.

[28] Y.-R. Kang, D.-H. Sun, and S.-H. Yang, "A new car-following model considering driver's individual anticipation behavior," *Nonlinear Dynamics*, vol. 82, no. 3, pp. 1293–1302, 2015.

[29] G. Peng, F. Nie, B. Cao, and C. Liu, "A driver's memory lattice model of traffic flow and its numerical simulation," *Nonlinear Dynamics*, vol. 67, no. 3, pp. 1811–1815, 2012.

[30] H.-X. Ge, F. Lv, P.-J. Zheng, and R.-J. Cheng, "The time-dependent Ginzburg-Landau equation for car-following model considering anticipation-driving behavior," *Nonlinear Dynamics*, vol. 76, no. 2, pp. 1497–1501, 2014.

[31] D.-W. Liu, Z.-K. Shi, and W.-H. Ai, "Enhanced stability of car-following model upon incorporation of short-term driving memory," *Communications in Nonlinear Science and Numerical Simulation*, vol. 47, pp. 139–150, 2017.

[32] G. Peng, W. Lu, H. He, and Z. Gu, "Nonlinear analysis of a new car-following model accounting for the optimal velocity changes with memory," *Communications in Nonlinear Science and Numerical Simulation*, vol. 40, pp. 197–205, 2016.

[33] S. Yu and Z. Shi, "Dynamics of connected cruise control systems considering velocity changes with memory feedback," *Measurement*, vol. 64, pp. 34–48, 2015.

[34] T.-Q. Tang, K.-W. Xu, S.-C. Yang, and H.-Y. Shang, "Influences of battery exchange on the vehicle's driving behavior and running time under car-following model," *Measurement*, vol. 59, pp. 30–37, 2015.

[35] D. Yang, P. Jin, Y. Pu, and B. Ran, "Safe distance car-following model including backward-looking and its stability analysis," *The European Physical Journal B*, vol. 86, no. 3, Art. 92, 11 pages, 2013.

[36] W.-X. Zhu, D. Jun, and L.-D. Zhang, "A compound compensation method for car-following model," *Communications in Nonlinear Science and Numerical Simulation*, vol. 39, pp. 427–441, 2016.

[37] T. Q. Tang, J. He, S. C. Yang, and H. Y. Shang, "A car-following model accounting for the driver's attribution," *Physica A*, vol. 419, pp. 293–300, 2015.

[38] T. Nagatani, "Effect of perception irregularity on chain-reaction crash in low visibility," *Physica A: Statistical Mechanics and its Applications*, vol. 427, pp. 92–99, 2015.

[39] T. Nagatani, "Traffic jam at adjustable tollgates controlled by line length," *Physica A: Statistical Mechanics and its Applications*, vol. 442, pp. 131–136, 2016.

[40] D.-H. Sun, G. Zhang, W.-N. Liu, M. Zhao, and S.-L. Cheng, "Analysis of anticipation driving effect in traffic lattice hydrodynamic model with on-ramp," *Nonlinear Dynamics*, vol. 81, no. 1-2, pp. 907–916, 2015.

[41] G. Peng, H. He, and W.-Z. Lu, "A new car-following model with the consideration of incorporating timid and aggressive driving behaviors," *Physica A: Statistical Mechanics and its Applications*, vol. 442, pp. 197–202, 2016.

[42] S. Yu and Z. Shi, "An extended car-following model considering vehicular gap fluctuation," *Measurement*, vol. 70, pp. 137–147, 2015.

[43] D. Sun, Y. Kang, and S. Yang, "A novel car following model considering average speed of preceding vehicles group," *Physica A: Statistical Mechanics and its Applications*, vol. 436, pp. 103–109, 2015.

[44] S. Yu and Z. Shi, "An improved car-following model considering relative velocity fluctuation," *Communications in Nonlinear Science and Numerical Simulation*, vol. 36, pp. 319–326, 2016.

[45] S. D. Kwon, D. H. Kim, and S. H. Lee, "Design criteria of wind barriers for traffic. part 1: wind barrier performance," *Wind and Structures*, vol. 14, pp. 55–70, 2011.

[46] C. J. Baker, "A simplified analysis of various types of wind-induced road vehicle accidents," *Journal of Wind Engineering & Industrial Aerodynamics*, vol. 22, no. 1, pp. 69–85, 1986.

[47] C. J. Baker, "The quantification of accident risk for road vehicles in cross winds," *Journal of Wind Engineering & Industrial Aerodynamics*, vol. 52, no. C, pp. 93–107, 1994.

[48] J. L. Xu, H. Wang, L. P. Zhao, and Y. J. Han, "Research on minimum radius of highway horizontal curve with crosswind considered," *China Journal of Highway and Transport*, vol. 27, no. 1, pp. 38–43, 2014.

[49] Z. Q. Gu, *Automobile Aerodynamics*, China Communications Press, Beijing, 2005.

[50] J. B. Pang, D. L. Wang, A. R. Chen, and Z. X. Lin, "Probability evaluating method of bridge deck side wind effects on driving safety," *China Journal of Highway and Transport*, vol. 19, pp. 59–64, 2006.

[51] K. Ahn, *Microscopic fuel consumption and emission modeling [Ph.D. thesis]*, Civil and Environmental Engineering, Virginia Polytechnic Institute and State University, Blacksburg, Va, USA, 1998.

[52] T. Q. Tang, J. G. Li, S. C. Yang, and H. Y. Shang, "Effects of on-ramp on the fuel consumption of the vehicles on the main road under car-following model," *Physica A*, vol. 419, no. 15, pp. 293–300, 2015.

[53] T.-Q. Tang, H.-J. Huang, and H.-Y. Shang, "Influences of the driver's bounded rationality on micro driving behavior, fuel consumption and emissions," *Transportation Research Part D: Transport and Environment*, vol. 41, pp. 423–432, 2015.

Hindawi
Mathematical Problems in Engineering
Volume 2017, Article ID 6798729, 4 pages
https://doi.org/10.1155/2017/6798729

Research Article

Stability Switches and Hopf Bifurcations in a Second-Order Complex Delay Equation

M. Roales and F. Rodríguez

Department of Applied Mathematics, University of Alicante, Apdo. 99, 03080 Alicante, Spain

Correspondence should be addressed to F. Rodríguez; f.rodriguez@ua.es

Received 21 July 2017; Accepted 19 September 2017; Published 15 October 2017

Academic Editor: Libor Pekař

The existence of stability switches and Hopf bifurcations for the second-order delay differential equation $x''(t)+ax'(t-\tau)+bx(t)=0,\ t>0$, with complex coefficients, is studied in this paper.

1. Introduction

The delayed friction equation

$$x''(t)+ax'(t)+bx'(t-\tau)+cx(t)=0, \tag{1}$$

where $c>0$, $\tau>0$, and a and b are nonnegative such that $a+b>0$, was considered by Minorsky [1, 2] for problems of ship stability and modeling of small vibrations of a pendulum. In [3, 4], the stability of the zero solution of more general forms of the delayed friction equation with real coefficients was characterized.

Delay differential equations (DDE) with complex coefficients have attracted increasing attention in the last years (e.g., [5–7]). In [8], Wei and Zhang characterized the stability of the zero solution of the retarded equation with complex coefficients

$$x'(t)=px(t)+qx(t-\tau), \tag{2}$$

by studying the distribution of the roots of the characteristic equation for the associated real differential system with delay and analyzed the existence of stability switches [3, 4, 9].

In [10], Li et al. presented a method for directly analyzing the stability of complex DDEs on the basis of stability switches. Their results generalize those for real DDEs, thus greatly reducing the complexity of the analysis. In [11], Roales and Rodríguez studied the stability switches of the zero solution of the neutral equation with complex coefficients

$$x'(t)+ax'(t-\tau)=bx(t)+cx(t-\tau), \tag{3}$$

using the results developed in [10].

The aim of this paper is to characterize the stability of the zero solution of the equation

$$x''(t)+ax'(t-\tau)+bx(t)=0, \tag{4}$$

where $\tau>0$ is a constant delay and a, b are complex parameters, with $b\neq 0$.

Using the results given by [10], the existence of stability switches and Hopf bifurcations for certain conditions on the parameters of (4) will be shown, discussing the conditions that may allow for delay dependent stabilization of the system.

2. Methods

To carry out our analysis, we will use some previous results that are recalled in this section (see, [4, 10, 12, 13]).

Following [10], and similar to the analysis carried out [11] for a first-order equation, we write the characteristic equation of a time-delay system with a single delay $\tau\geq 0$ in the form

$$\Delta(\lambda,\tau)=P(\lambda)+Q(\lambda)e^{-\lambda\tau}, \tag{5}$$

where $P(\lambda)$ and $Q(\lambda)$ are complex polynomial. To be able to apply the main result in [10], we will require the order of $P(\lambda)$ to be either higher than that of $Q(\lambda)$ or, if they have the same order, that $|\alpha|>|\beta|$, with $\alpha,\beta\in\mathbb{C}$ being, respectively, the highest order coefficients of $P(\lambda)$ and $Q(\lambda)$. Also, it is

necessary that $P(\lambda)$ and $Q(\lambda)$ have no roots on the imaginary axis simultaneously and that $\lambda = 0$ is not a root of (5): that is,

$$P(0) + Q(0) \neq 0. \tag{6}$$

In the next section, it will be shown that all these conditions hold in our problem.

As shown in [10], introducing the function

$$F(\omega) = |P(i\omega)|^2 - |Q(i\omega)|^2, \tag{7}$$

if $\omega^* \neq 0$ is a zero of $F(\omega)$, then there are an infinite number of delays τ_j corresponding to ω^* satisfying

$$\Delta\left(i\omega^*, \tau_j\right) = 0. \tag{8}$$

Based on a previous work of Lee and Hsu [14], Li et al. established the following theorem [10, Theorem 1], characterizing, for the critical values τ_j such that $\Delta(i\omega^*, \tau_j) = 0$, the variation of the number of zeros with nonnegative real parts of $\Delta(\lambda, \tau)$, in terms of the order and sign of the first nonzero derivate of $F(\omega^*)$.

Theorem 1. *Assume that $\Delta(i\omega^*, \tau_j) = 0$, $j = 0, 1, 2, \ldots$ Let $N(\tau)$ be the number of zeros with nonnegative real parts of $\Delta(\lambda, \tau)$, and let M be an integer such that $F^{(M)}(\omega^*) \neq 0$ and $F^m(\omega^*) = 0$ for all $m < M$. Then*

(a) *$N(\tau)$ keeps unchanged as τ increases along τ_j if M is even,*

(b) *when M is odd, $N(\tau)$ increases by one if $\omega^* F^{(M)}(\omega^*) > 0$, and decreases by one if $\omega^* F^{(M)}(\omega^*) < 0$, as τ increases along τ_j.*

This theorem facilitates the stability analysis with respect to the method used in [14] and extends to the complex coefficients setting a previous result which was only valid for real DDEs [15].

Hopf bifurcation theorem gives the conditions for the existence of local nontrivial periodic solutions (e.g., [4, 12, 13]). Basic conditions are the existence of a nonzero purely imaginary root of the characteristic equation, λ_0, that all other eigenvalues are not integer multiples of λ_0, and, in addition, it must hold that, if α is the bifurcation parameter, the branch of eigenvalues $\lambda(\alpha)$ which satisfies $\lambda(0) = \lambda_0$ is such that $\mathrm{Re}(\lambda'(0)) \neq 0$, which is called the transversality condition.

3. Stability Analysis of the Second-Order Complex DDE

Consider the complex DDE (4), where

$$\begin{aligned} a &= a_1 + ia_2, \\ b &= b_1 + ib_2. \end{aligned} \tag{9}$$

The characteristic equation associated with (4) is

$$\lambda^2 + a\lambda e^{-\lambda\tau} + b = 0, \tag{10}$$

so that for the function $\Delta(\lambda, \tau)$, as defined in (5), one has

$$\begin{aligned} P(\lambda) &= \lambda^2 + b, \\ Q(\lambda) &= a\lambda. \end{aligned} \tag{11}$$

Since $P(\lambda)$ is of higher order than $Q(\lambda)$, and since we assume $b \neq 0$, it also holds that $P(0) + Q(0) \neq 0$. Thus, the conditions to apply Theorem 1 are satisfied.

The following lemma gives $N(0)$, the number of zeros with nonnegative real parts of $\Delta(\lambda, \tau)$ when the delay is zero.

Lemma 2. *Consider the complex number*

$$z = (A, B) = \left(a_1^2 - a_2^2 - 4b_1, 2a_1a_2 - 4b_2\right). \tag{12}$$

If $z \neq 0$ and

$$|a_1| < \frac{|B|}{2\sqrt{(-A + |z|)/2}} \tag{13}$$

then $N(0) = 1$. Else, if $a_1 \leq 0$ then $N(0) = 2$, and if $a_1 > 0$ then $N(0) = 0$ when $z = 0$ or

$$|a_1| > \frac{|B|}{2\sqrt{(-A + |z|)/2}}, \tag{14}$$

and $N(0) = 1$ when $z \neq 0$ and

$$|a_1| = \frac{|B|}{2\sqrt{(-A + |z|)/2}}. \tag{15}$$

Proof. Consider the equation

$$\Delta(\lambda, 0) = P(\lambda) + Q(\lambda) = \lambda^2 + a\lambda + b = 0. \tag{16}$$

Then,

$$\begin{aligned} \lambda &= \frac{-a \pm \sqrt{a^2 - 4b}}{2} \\ &= \frac{-(a_1 + ia_2) \pm \sqrt{a_1^2 - a_2^2 + 2ia_1a_2 - 4b_1 - 4ib_2}}{2} \\ &= \frac{-(a_1 + ia_2) \pm \sqrt{z}}{2}. \end{aligned} \tag{17}$$

If $z = 0$, there is a double root with real part $-a_1/2$. If $z \neq 0$, λ can be written as

$$\lambda = \frac{-(a_1 + ia_2) \pm \left(B/\left(2\sqrt{(-A + |z|)/2}\right) + i\sqrt{(-A + |z|)/2}\right)}{2}, \tag{18}$$

and the conclusion of the lemma follows. □

Now consider the function $F(\omega)$ defined in (7),

$$\begin{aligned} F(\omega) &= \left(-\omega^2 + b_1\right)^2 + b_2^2 - |a|^2\omega^2 \\ &= \omega^4 - \left(|a|^2 + 2b_1\right)\omega^2 + |b|^2, \end{aligned} \tag{19}$$

and calculate its zeros. One gets

$$\omega_{\pm}^2 = \frac{|a|^2 + 2b_1 \pm \sqrt{\left(|a|^2 + 2b_1\right)^2 - 4|b|^2}}{2}. \tag{20}$$

We will consider two different cases and several subcases.

Case 1 ($|a|^2 + 2b_1 > 0$).

Case 1(a): $(|a|^2 + 2b_1)^2 > 4|b|^2$.

Case 1(b): $(|a|^2 + 2b_1)^2 = 4|b|^2$.

Case 1(c): $(|a|^2 + 2b_1)^2 < 4|b|^2$.

Case 2 ($|a|^2 + 2b_1 \leq 0$). First, we assume that $|a|^2 + 2b_1 > 0$ (Case 1).

If $(|a|^2 + 2b_1)^2 > 4|b|^2$ (Case 1(a)), then $F(\omega)$ has four real roots, ω_1^+, ω_2^+, ω_1^-, ω_2^-, such that

$$\begin{aligned} &\omega_1^+ > \omega_2^+ > 0 > \omega_2^- > \omega_1^-, \\ &\omega_1^+ = -\omega_1^-, \\ &\omega_2^+ = -\omega_2^-. \end{aligned} \tag{21}$$

If $(|a|^2 + 2b_1)^2 = 4|b|^2$ (Case 1(b)), then $F(\omega)$ has two double real roots, ω_1^+, ω_1^-, such that

$$\begin{aligned} &\omega_1^+ > 0 > \omega_1^-, \\ &\omega_1^+ = -\omega_1^-. \end{aligned} \tag{22}$$

If $(|a|^2 + 2b_1)^2 < 4|b|^2$ (Case 1(c)), then $F(\omega)$ has no real root, and therefore the stability of the zero solution of (4) does not change for any $\tau > 0$.

Consider now Case 1(a), where $\omega_1^+ > \omega_2^+ > 0 > \omega_2^- > \omega_1^-$. Substituting $\lambda = i\omega$ into (10), and separating the real and imaginary parts, one gets

$$\begin{aligned} -\omega^2 + a_1\omega\sin\omega\tau - a_2\omega\cos\omega\tau + b_1 = 0, \\ b_2 + a_1\omega\cos\omega\tau + a_2\omega\sin\omega\tau = 0, \end{aligned} \tag{23}$$

obtaining the following four sets of values of τ for which there are roots.

For ω_1^+ and ω_1^-, one gets

$$\begin{aligned} \cos\omega_1^+\tau &= \frac{\left(-\left(\omega_1^+\right)^2 + b_1\right)a_2 - b_2a_1}{|a|^2\,\omega_1^+}, \\ \sin\omega_1^+\tau &= \frac{\left(\left(\omega_1^+\right)^2 - b_1\right)a_1 - b_2a_2}{|a|^2\,\omega_1^+}, \\ \cos\omega_1^-\tau &= \frac{\left(-\left(\omega_1^-\right)^2 + b_1\right)a_2 - b_2a_1}{|a|^2\,\omega_1^-}, \\ \sin\omega_1^-\tau &= \frac{\left(\left(\omega_1^-\right)^2 - b_1\right)a_1 - b_2a_2}{|a|^2\,\omega_1^-}. \end{aligned} \tag{24}$$

As $\omega_1^+ = -\omega_1^-$, then $\cos\omega_1^+\tau = \cos\omega_1^-\tau$ and $\sin\omega_1^+\tau = -\sin\omega_1^-\tau$. By (24) $\cos\omega_1^+\tau = -\cos\omega_1^-\tau$ and $\sin\omega_1^+\tau = -\sin\omega_1^-\tau$. Therefore, $\cos\omega_1^+\tau = 0$ in what follows

$$\begin{aligned} \tau_{n,1}^+ &= \frac{\pi/2}{\omega_1^+} + \frac{n\pi}{\omega_1^+} \\ \tau_{n,1}^- &= \frac{-\pi/2}{\omega_1^-} - \frac{n\pi}{\omega_1^-}. \\ \tau_{n,1}^+ &= \tau_{n,1}^-, \quad n = 0, 1, 2, \ldots, \end{aligned} \tag{25}$$

Similarly for ω_2^+ and ω_2^-, we obtain the following set of values of τ for which there are roots,

$$\tau_{n,2}^+ = \tau_{n,2}^- = \frac{\pi/2}{\omega_2^+} + \frac{n\pi}{\omega_2^+} = \frac{-\pi/2}{\omega_2^-} - \frac{n\pi}{\omega_2^-}, \quad n = 0, 1, 2, \ldots. \tag{26}$$

Since

$$\begin{aligned} F'\left(\omega_1^+\right) &= -F'\left(\omega_1^-\right) = 2\omega_1^+\left[2\left(\omega_1^+\right)^2 - \left(|a|^2 + 2b_1\right)\right] \\ &> 0, \\ F'\left(\omega_2^+\right) &= -F'\left(\omega_2^-\right) = 2\omega_2^+\left[2\left(\omega_2^+\right)^2 - \left(|a|^2 + 2b_1\right)\right] \\ &< 0, \end{aligned} \tag{27}$$

one has

$$\begin{aligned} \omega_1^+F'\left(\omega_1^+\right) > 0 \\ \omega_1^-F'\left(\omega_1^-\right) > 0 \\ \omega_2^+F'\left(\omega_2^+\right) < 0 \\ \omega_2^-F'\left(\omega_2^-\right) < 0. \end{aligned} \tag{28}$$

Therefore, according to Theorem 1, as τ is increased, the number of the characteristic roots with nonnegative real parts increases by two as τ passes through $\tau_{n,1}^+$ and decreases by two as τ passes through $\tau_{n,2}^+$.

If $N(0) = 0$, that is, if the zero solution of (4) is stable for $\tau = 0$, as $\tau_{0,1}^+ < \tau_{0,2}^+$, there are stability switches when the delays are such that

$$\tau_{0,1}^+ < \tau_{0,2}^+ < \tau_{1,1}^+ < \tau_{1,2}^+ < \cdots. \tag{29}$$

Since

$$\tau_{n+1,1}^+ - \tau_{n,1}^+ = \frac{\pi/2}{\omega_1^+} < \frac{\pi/2}{\omega_2^+} = \tau_{n+1,2}^+ - \tau_{n,2}^+, \tag{30}$$

the intervals become smaller with increasing n, so that eventually, for a certain $k \geq 1$,

$$\tau_{k-1,1}^+ < \tau_{k,1}^+ \leq \tau_{k-1,2}^+. \tag{31}$$

Thus, the distribution of delays is

$$\begin{aligned} \tau_{0,1}^+ < \tau_{0,2}^+ < \tau_{1,1}^+ < \tau_{1,2}^+ < \cdots < \tau_{k-1,1}^+ < \tau_{k,1}^+ \leq \tau_{k-1,2}^+ \\ < \tau_{k+1,1}^+ < \cdots, \end{aligned} \tag{32}$$

and there is only a finite number of stability switches, with the system becoming unstable for $\tau > \tau^+_{k-1,1}$.

If $N(0) = 1$ or $N(0) = 2$, the system is always unstable because $\tau^+_{0,1} < \tau^+_{0,2}$ and a distribution of delays for stability switches to occur is not possible.

After the study of the stability, we wonder what happens, when there are stability switches, in the critical delays $\tau = \tau^\pm_{n,j}$. Denote $\lambda(\tau) = \alpha(\tau) + i\omega(\tau)$ as the root of (10) satisfying $\alpha(\tau^\pm_{n,j}) = 0$, $\omega(\tau^\pm_{n,j}) = \omega^\pm_{n,j}$, $j = 1, 2$. According to Theorem 1, one has

$$\operatorname{sgn}\left[\left(\frac{d\,\operatorname{Re}\lambda\left(\tau^\pm_{n,j}\right)}{d\tau}\right)\right] = \operatorname{sgn}\left(\omega^\pm_{n,j}\right)\operatorname{sgn}F'\left(\omega^\pm_{n,j}\right). \quad (33)$$

By (28), one gets that the transversality condition required by Hopf Theorem is satisfied. Therefore, a Hopf bifurcation occurs for these critical values.

Now we study Case 1(b), where $\omega^+_1 > 0 > \omega^-_1$ are two real roots. Proceeding as before, there are two sets of critical values of delays τ^+_n and τ^-_n, corresponding to ω^+_1 and ω^-_1, respectively, such that $\tau^+_n = \tau^-_n$, $n = 1, 2, \ldots$. Since $F'(\omega^+_1) = F'(\omega^-_1) = 0$, we consider the second derivative,

$$F''\left(\omega^\pm_1\right) = 4\left(|a|^2 + 2b_1\right) \neq 0. \quad (34)$$

By Theorem 1, since $M = 2$, $N(\tau)$ keeps unchanged as τ increases along τ_n. Consequently, the stability of zero solution of (4) does not change for any $\tau > 0$.

Finally, consider Case 2, where

$$|a|^2 + 2b_1 \leq 0. \quad (35)$$

The function $F(\omega)$ defined in (19) has no real root, and therefore the stability of the zero solution of (4) does not change for any $\tau > 0$. Thus, the following theorem has been established.

Theorem 3. *Consider the second-order complex delay equation (4). The following two cases may occur concerning its stability:*

(a) $(|a|^2 + 2b_1)^2 > 4|b|^2$. *In this case, if* $N(0) = 0$, *and the distribution of delays is* $0 < \tau^+_{0,1} < \tau^+_{0,2} < \cdots < \tau^+_{k-1,1} < \tau^+_{k,1} \leq \tau_{k-1,2} < \tau^+_{k+1,1} < \cdots$, *then the zero solution of (4) is asymptotically stable for* $\tau \in (0, \tau^+_{0,1})$ *and* $\tau \in \bigcup_{n=0}^{k-2}(\tau^+_{n,2}, \tau^+_{n+1,1})$, *and unstable for* $\tau \in \bigcup_{n=0}^{k-2}(\tau^+_{n,1}, \tau^+_{n,2})$ *and* $\tau > \tau^+_{k-1,1}$. *Otherwise, if* $N(0) = 1$ *or* $N(0) = 2$, *the zero solution of (4) is unstable for all* $\tau \geq 0$.

When there are stability switches, the critical delays $\tau = \tau^\pm_{n,1}$, $n = 0 \cdots k-1$, *and* $\tau = \tau^\pm_{n,2}$, $n = 0 \cdots k-2$, *are Hopf bifurcation values for (4).*

(b) $(|a|^2 + 2b_1)^2 \leq 4|b|^2$. *In this case, the stability of the zero solution of (4) does not change for any* $\tau > 0$.

Conflicts of Interest

The authors declare that there are no conflicts of interest regarding the publication of this paper.

References

[1] N. Minorsky, "Self-excited oscillations in dynamical systems possessing retarded actions," *Journal of Applied Mechanics*, vol. 9, pp. A65–A71, 1942.

[2] N. Minorsky, "Experiments with activated tanks," *Transactions of the American Society of Mechanical Engineers*, vol. 69, pp. 735–747, 1947.

[3] K. L. Cooke and Z. Grossman, "Discrete delay, distributed delay and stability switches," *Journal of Mathematical Analysis and Applications*, vol. 86, no. 2, pp. 592–627, 1982.

[4] Y. Kuang, *Delay Differential Equations with Applications in Population Dynamics*, Academic Press, New York, NY, USA, 1993.

[5] J. Y. Li and Z. H. Wang, "Local Hopf bifurcation of complex nonlinear systems with time-delay," *International Journal of Bifurcation and Chaos*, vol. 19, no. 3, pp. 1069–1079, 2009.

[6] Z. Zhang, C. Lin, and B. Chen, "Global stability criterion for delayed complex-valued recurrent neural networks," *IEEE Transactions on Neural Networks and Learning Systems*, vol. 25, no. 9, pp. 1704–1708, 2014.

[7] T. Fang and J. Sun, "Stability of complex-valued impulsive system with delay," *Applied Mathematics and Computation*, vol. 240, pp. 102–108, 2014.

[8] J. Wei and C. Zhang, "Stability analysis in a first-order complex differential equations with delay," *Nonlinear Analysis*, vol. 59, no. 5, pp. 657–671, 2004.

[9] E. Beretta and Y. Kuang, "Geometric stability switch criteria in delay differential systems with delay dependent parameters," *SIAM Journal on Mathematical Analysis*, vol. 33, no. 5, pp. 1144–1165, 2002.

[10] J. Li, L. Zhang, and Z. Wang, "Two effective stability criteria for linear time-delay systems with complex coefficients," *Journal of Systems Science & Complexity*, vol. 24, no. 5, pp. 835–849, 2011.

[11] M. Roales and F. Rodríguez, "Stability switches in a first-order complex neutral delay equation," *Journal of Applied Mathematics*, vol. 2013, 6 pages, Article ID 929186, 2013.

[12] J. K. Hale, *Theory of Functional Differential Equations*, Springer, New York, NY, USA, 1977.

[13] H. Smith, *An Introduction to Delay Differential Equations with Applications to the Life Sciences*, Springer, New York, NY, USA, 2011.

[14] M. S. Lee and C. S. Hsu, "On the τ-decomposition method of stability analysis for retarded dynamical system," *SIAM Journal on Control and Optimization*, vol. 7, pp. 242–259, 1969.

[15] K. L. Cooke and P. van den Driessche, "On zeroes of some transcendental equations," *Funkcialaj Ekvacioj*, vol. 29, no. 1, pp. 77–90, 1986.

Hindawi
Mathematical Problems in Engineering
Volume 2017, Article ID 6048365, 12 pages
https://doi.org/10.1155/2017/6048365

Research Article

Delayed Trilateral Teleoperation of a Mobile Robot

D. Santiago, E. Slawiñski, and V. Mut

Instituto de Automática (INAUT), Universidad Nacional de San Juan and CONICET, Av. Libertador San Martín 1109 (Oeste), J5400ARL San Juan, Argentina

Correspondence should be addressed to D. Santiago; dsantiago@inaut.unsj.edu.ar

Received 29 June 2017; Accepted 29 August 2017; Published 12 October 2017

Academic Editor: Libor Pekař

This paper analyzes the stability of a trilateral teleoperation system of a mobile robot. This type of system is nonlinear, time-varying, and delayed and includes a master-slave kinematic dissimilarity. To close the control loop, three $P + d$ controllers are used under a position master/slave velocity strategy. The stability analysis is based on Lyapunov-Krasovskii theory where a functional is proposed and analyzed to get conditions for the control parameters that assure a stable behavior, keeping the synchronism errors bounded. Finally, the theoretical result is verified in practice by means of a simple test, where two human operators both collaboratively and simultaneously drive a 3D simulator of a mobile robot to achieve an established task on a remote shared environment.

1. Introduction

Robot teleoperation allows the execution of a task in a remote environment; generally dangerous and harmful jobs for the human operator are addressed necessarily by these systems to improve the safety level. They are formed by a human operator, a device called master, a robot called slave acting on a remote environment, and a communication channel that connect user and environment. Besides, the term bilateral indicates that there is a physical coupled via force feedback additional to the common multimedia information such as video and audio. That is, the slave follows the motions carried out by the master while simultaneously the human operator receives multimodal information [1]. This feature about tact at distance increases the application field to varied areas such as telemedicine, health assistance, exploration, entertainment, teleservices, and telemanufacturing, among others. Besides, the use of the Internet as a low-cost communication channel allows easily connecting the master and slave devices. However, all Internet-like communication adds nonsymmetric time-varying delays, which if become larger could cause oscillations, low performance [2, 3], and poor transparency [4, 5]. In general, the teleoperation systems are represented by delayed time-varying nonlinear models. So, one of the research topics in delayed teleoperation systems is related to the analysis of different mathematical tools to get delay-dependent conditions for the controller parameters that allow assuring the stability of the delayed closed-loop system.

In the field about robot teleoperation, most control schemes are designed and analyzed considering two manipulators called master and slave [3–6] (and references therein). In general, energy is removed to assure stability or passivity [7]. A classic strategy is the use of scattering signals or wave transformations [8, 9], which adds an apparent damping to get passivity analyzing the system as a two- or four-channel port. In the last years, many researches were focused on the use of $P + d$ schemes to get a stable operation in the sense of Lyapunov by using a sufficiently large damping injected into master and slave [10–12]. Besides, many strategies designed for teleoperation of manipulators were tested also into bilateral teleoperation of WMR (wheeled mobile robots), for example, control based on impedance [13], control based on r-passivity [14, 15], schemes including prediction and augmented reality [16], haptic teledriving of a WMR coupled with slippage, where an acceleration-level control law is proposed to assure the passivity of the bilateral system [17, 18], and also $P + d$ control schemes [19, 20]. It is important to remark that the stability analysis of a master position/slave velocity coupling is different mathematically to the common position/position used in a teleoperation

between two manipulators due to the master-slave kinematic dissimilarity: master device (e.g., joystick) has a bounded workspace, while slave mobile robot can navigate by an unbounded workspace.

On the other hand, several applications, such as rehabilitation, surgical training, and safety [21, 22], require multiple users instead of a single operator due to the fact that a multilateral teleoperation provides various useful capabilities such as increased dexterity, improved loading, redundancy, and handling capacity, among others. For example, these systems can be addressed to training of human operators to learn the driving of industrial machines. However, the analysis about these systems is even more complex. With respect to the control of them, there are strategies for trilateral systems considering all devices as robot manipulators, for example, control based on passivity [23], where observers and controllers of passivity are added to retain the system energy bounded; adaptive fuzzy control scheme [24]; and $P + d$ controllers [25], where the stability of a dual-master/single slave teleoperation system is evaluated. On the other hand, few papers have been proposed to trilateral systems of WMR. In [26], a WMR trilateral teleoperation scheme is proposed but the time delays are not considered. Also, recently, many papers have been focused on teleoperation networks [27, 28]. This kind of system is an extension of the traditional bilateral teleoperation but includes multiple users working collaboratively and simultaneously from different locations on a shared remote environment, through robots. However, to the best of the authors' knowledge, the $P+d$-like strategies using a master position/WMR velocity mapping present in the current literature cannot be applied in a direct way to the delayed trilateral teleoperation of a mobile robot because both manipulator-manipulator and mobile-manipulator connections simultaneously occur, making difficult the energy analysis inside the system. That is, the application of $P + d$ controllers to a delayed trilateral teleoperation of a mobile robot requires a new analysis to get delay-dependent conditions that can be held from an adequate calibration of control parameters, to assure a stable behavior for the errors between master 1 position, master 2 position, and mobile robot velocity.

This paper presents a stability analysis based on a Lyapunov-Krasovskii functional applied to a delayed trilateral teleoperation of a mobile robot. The main contribution of this work involves a new functional which is analyzed along the system trajectories, allowing getting information about the evolution of velocity and position of both master 1 and master 2, velocity and acceleration of mobile robot, and synchronism errors. As a result of the mathematical analysis being exposed, depending-delay conditions for the calibration of the controller are achieved. Furthermore, a test about trilateral teleoperation using a 3D simulator is shown in order to verify that the evolution of the delayed trilateral system state is in agreement with the theoretical result achieved.

This work is organized as follows: Section 2 presents some preliminary aspects such as the employed dynamic models and the assumptions used. In Section 3, a control scheme applied to delayed trilateral teleoperation of a mobile robot is proposed and its stability analysis based on a Lyapunov-Krasovskii functional (LKF) is performed. Section 5 shows an experimental test, where two users drive simultaneously a wheeled robot simulator. Finally, in Section 6, the conclusions of this work are given.

2. Preliminary

This paper will analyze teleoperation systems in which two human operators generally called trainer and trainee, use each one a master device (called master 1 and master 2, resp.) to drive a mobile robot slave in a trilateral way, as it is illustrated in Figure 1.

Master Model. Each human operator drives a manipulator robot to generate velocity commands and also receive force feedback. The standard nonlinear dynamic model of a manipulator robot to represent each master is used [10, 11], that is,

$$\begin{aligned}\mathbf{M}_{\mathbf{m}_i}\left(\mathbf{q}_{\mathbf{m}_i}\right)\ddot{\mathbf{q}}_{\mathbf{m}_i} + \mathbf{C}_{\mathbf{m}_i}\left(\mathbf{q}_{\mathbf{m}_i}, \dot{\mathbf{q}}_{\mathbf{m}_i}\right)\dot{\mathbf{q}}_{\mathbf{m}_i} + \mathbf{g}_{\mathbf{m}_i}\left(\mathbf{q}_{\mathbf{m}_i}\right) \\ = \boldsymbol{\tau}_{\mathbf{m}_i} + \mathbf{f}_{\mathbf{h}_i},\end{aligned} \tag{1}$$

where index i indicates master 1 or master 2, $\mathbf{q}_{\mathbf{m}}(t) \in R^{n\times 1}$ is the joint position of the master; $\dot{\mathbf{q}}_{\mathbf{m}}(t)$ is the joint velocity; $\mathbf{M}_{\mathbf{m}}(\mathbf{q}_{\mathbf{m}}) \in R^{n\times n}$ is the inertia matrix; $\mathbf{C}_{\mathbf{m}}(\mathbf{q}_{\mathbf{m}}, \dot{\mathbf{q}}_{\mathbf{m}})$ is the matrix representing centripetal and Coriolis torques; $\mathbf{g}_{\mathbf{m}}(\mathbf{q}_{\mathbf{m}})$ is the gravitational torque; $\mathbf{f}_{\mathbf{h}}$ is the torque caused by the human operator force; and $\boldsymbol{\tau}_{\mathbf{m}}$ is the torque applied to the master by the controller. Commonly, master 1 is associated with the trainer and master 2 with the trainee.

Mobile Robot Model. For the case of teleoperation of a mobile robot, the dynamic model of a mobile robot with differential traction is considered [14]. It has two independently actuated rear wheels and is represented by

$$\mathbf{D}\dot{\boldsymbol{\eta}} + \mathbf{Q}\left(\boldsymbol{\eta}\right)\boldsymbol{\eta} = \boldsymbol{\tau}_{\mathbf{s}} + \mathbf{f}_{\mathbf{e}}, \tag{2}$$

where $\boldsymbol{\eta} = \begin{bmatrix} v & \omega \end{bmatrix}^T$ is the robot velocity vector with v and ω representing the linear and angular velocity of the mobile robot, $\mathbf{f}_{\mathbf{e}}$ is the force caused by the elements of the environment on the robot as well as other nonmodeled external forces such as static and dynamic frictions, $\mathbf{D} = \begin{bmatrix} m & 0 \\ 0 & i \end{bmatrix}$ is the inertia matrix and $\mathbf{Q} = \begin{bmatrix} 0 & -ma\omega \\ ma\omega & 0 \end{bmatrix}$ is the Coriolis matrix where m is the mass of the robot, i is the rotational inertia, and a is the distance between the mass center and the geometric center. In addition, the control action $\boldsymbol{\tau}_{\mathbf{s}} = \begin{bmatrix} u_1 & u_2 \end{bmatrix}^T$ involves a force u_1 and torque u_2 is applied to the robot.

The devices are numbered as follows: index 1 represents master 1; index 2 indicates master 2; and index 3 represents the mobile robot. Besides, to represent the communication channel of a trilateral system, a forward time delay h_{ij} (from device i to device j) and a backward time delay h_{ji} (from device j to device i) for each pair master 1-master 2, master 1-slave, and master 2-slave are taken as time-varying and nonpredictable.

Next, common properties, assumptions, and lemmas will be used in this paper [7, 10, 11].

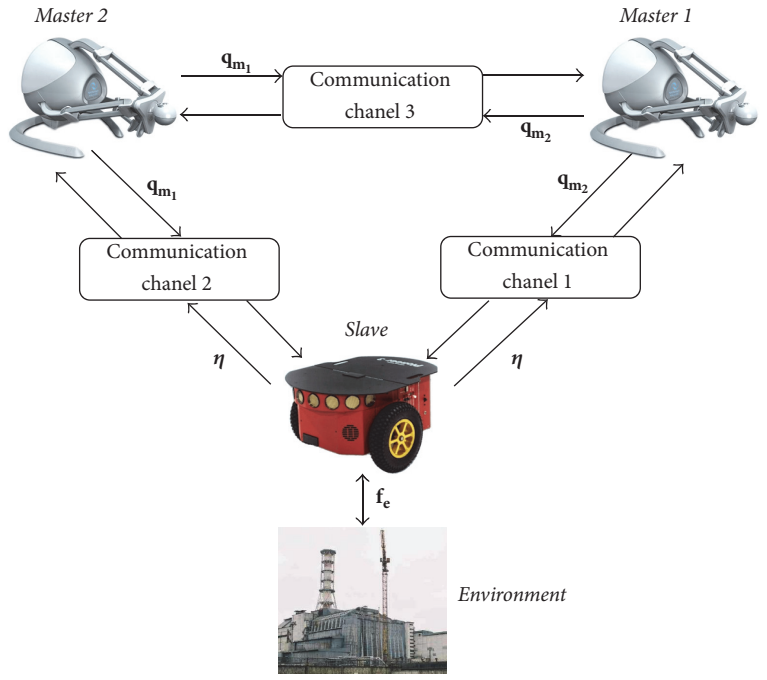

Figure 1: Delayed trilateral teleoperation system of a mobile robot.

Property 1. The inertia matrices $\mathbf{M}_{\mathbf{m}_i}(\mathbf{q}_{\mathbf{m}_i})$ and $\mathbf{D}$ are symmetric positive definite.

Property 2. Matrix $\dot{\mathbf{M}}_{\mathbf{m}_i}(\mathbf{q}_{\mathbf{m}_i}) - 2\mathbf{C}_{\mathbf{m}_i}(\mathbf{q}_{\mathbf{m}_i}, \dot{\mathbf{q}}_{\mathbf{m}_i})$ is skew-symmetric.

Property 3. There exists $k_r > 0$ such that $|\mathbf{C}_{\mathbf{m}_i}(\mathbf{q}_{\mathbf{m}_i}, \dot{\mathbf{q}}_{\mathbf{m}_i})\dot{\mathbf{q}}_{\mathbf{m}_i}| \leq k_r|\dot{\mathbf{q}}_{\mathbf{m}_i}|^2$ for all time t.

Property 4. The vector $\mathbf{g}_{\mathbf{m}_i}(\mathbf{q}_{\mathbf{m}_i})$ is bounded if $\mathbf{q}_{\mathbf{m}_i}$ is bounded.

Assumption 5. All time delays $h_{ij}(t)$ and $h_{ji}(t)$ are bounded. Therefore, there exist positive scalars $\overline{h}_{12}, \overline{h}_{13}, \overline{h}_{21}, \overline{h}_{23}, \overline{h}_{31}, \overline{h}_{32}$ such that $0 \leq h_{12}(t) \leq \overline{h}_{12}$, $0 \leq h_{13}(t) \leq \overline{h}_{13}$, $0 \leq h_{21}(t) \leq \overline{h}_{21}$, $0 \leq h_{23}(t) \leq \overline{h}_{23}$, $0 \leq h_{31}(t) \leq \overline{h}_{31}$, $0 \leq h_{32}(t) \leq \overline{h}_{32}$ for all t.

Assumption 6. The human operator has finite energy [7] and the environment is represented by a damping-like model plus a finite-energy perturbation [12]. Such models are mathematically represented as follows:

$$E_{h_i} = \varphi_{h_i} - \int_0^t \mathbf{f}_{\mathbf{h}_i}{}^T \dot{\mathbf{q}}_{\mathbf{m}_i} dt \geq 0, \tag{3}$$

$$\mathbf{f}_{\mathbf{e}} = -\alpha_e \boldsymbol{\eta} + \mathbf{f}_{\mathbf{a}_e}, \tag{4}$$

where $\mathbf{f}_{\mathbf{h}}$ is the human force, $\varphi_h > 0$ is a finite value that bounds the energy of the human operator, α_e is the environment's damping, and $\mathbf{f}_{\mathbf{a}_e}$ is assumed to be bounded with finite energy, that is $|\mathbf{f}_{\mathbf{a}_e}| \leq \overline{f}_{a_e}$, with $\overline{f}_{a_e}$ a positive constant and $\mathbf{f}_{\mathbf{a}_e} \in L_2$.

Lemma 7 (see [11]). *For real vector functions* $\mathbf{a}(\cdot)$ *and* $\mathbf{b}(\cdot)$ *and a time-varying scalar* $h(t)$ *with* $0 \leq h(t) \leq \overline{h}$, *the following inequality holds:*

$$\begin{aligned} &-2\mathbf{a}^T(t)\int_{t-h(t)}^{t}\mathbf{b}(\xi)\,d\xi - \int_{t-h(t)}^{t}\mathbf{b}^T(\xi)\,\mathbf{b}(\xi)\,d\xi \\ &\quad\leq h(t)\,\mathbf{a}^T(t)\,\mathbf{a}(t) \leq \overline{h}(t)\,\mathbf{a}^T(t)\,\mathbf{a}(t). \end{aligned} \tag{5}$$

Relation 8. The time delayed variable $x(t-h)$ can be written as follows:

$$x(t-h) = x(t) - \int_{t-h}^{t}\dot{x}(\xi)\,d\xi. \tag{6}$$

3. Trilateral Teleoperation of a Mobile Robot

The teleoperation trilateral system is used to control the velocity of a mobile robot, where the trainer and trainee (or in general two human operators) permanently send commands and perceive a force feedback. Based on the $P + d$ control schemes applied to bilateral teleoperation of manipulator robots [10–12] and mobile robots [19, 20], and its recent use in delayed trilateral teleoperation of manipulator robots [25], the stability of a dual-master single mobile robot system under a master position/slave velocity strategy will be analyzed in this work.

The set of control actions is established as follows:

$$\begin{aligned} \boldsymbol{\tau}_{\mathbf{m}_1} = k_{p_1}\big[&-k_g\mathbf{q}_{\mathbf{m}_1} + \alpha\boldsymbol{\eta}(t-h_{31}) \\ &+ (1-\alpha)\,k_g\mathbf{q}_{\mathbf{m}_2}(t-h_{21})\big] - k_{d_1}\dot{\mathbf{q}}_{\mathbf{m}_1} + \mathbf{g}_{\mathbf{m}_1}(\mathbf{q}_{\mathbf{m}_1}), \end{aligned}$$

$$\begin{aligned}\boldsymbol{\tau}_{\mathbf{m}_2} &= k_{p_2}\left[-k_g\mathbf{q}_{\mathbf{m}_2} + \alpha k_g\mathbf{q}_{\mathbf{m}_1}(t-h_{12})\right.\\ &\quad\left.+(1-\alpha)\boldsymbol{\eta}(t-h_{32})\right] - k_{d_2}\dot{\mathbf{q}}_{\mathbf{m}_2} + \mathbf{g}_{\mathbf{m}_2}\left(\mathbf{q}_{\mathbf{m}_2}\right),\\ \boldsymbol{\tau}_{\mathbf{s}} &= k_{p_3}\left[\beta k_g\mathbf{q}_{\mathbf{m}_1}(t-h_{13}) + (1-\beta)k_g\mathbf{q}_{\mathbf{m}_2}(t-h_{23})\right.\\ &\quad\left.-\boldsymbol{\eta}\right] - k_{d_3}\mathbf{z} + \mathbf{Q}(\boldsymbol{\eta})\boldsymbol{\eta},\end{aligned} \tag{7}$$

where the parameters k_{p_3} and k_{d_3} are positive constant and they represent the proportional gain and acceleration-dependent damping added by the velocity controller placed on the remote site, k_{d_1} and k_{d_2} are the damping injected in the masters, and k_{p_1} and k_{p_2} represent a relative spring depending on the mismatch between the master position and a reference feedback. Besides, the parameter k_g linearly maps the master position to a velocity reference, and $\mathbf{z}$ represents the available information about the mobile robot acceleration $\dot{\boldsymbol{\eta}}$ but an infinitesimal before the current time instant. It is assumed that this signal can be represented by the real mobile robot acceleration $\dot{\boldsymbol{\eta}}$ plus an infinitesimal error $g(t) \in L_\infty$ [20, 29]:

$$\mathbf{z} = \dot{\boldsymbol{\eta}} - g(t). \tag{8}$$

Furthermore, two dominance factors are used. The α factor determines the authority of trainer over trainee and $1-\alpha$ implies the supremacy of trainee over trainer. Moreover, the dominance factors β and $1-\beta$ indicate the supremacy of trainer and trainee over the mobile robot, respectively. The relation between them is defined in [25] as follows:

$$\beta = \frac{\alpha^2}{\alpha^2 + (1-\alpha)^2} \tag{9}$$

with $0 < \alpha < 1$. As α is closer to 1, the following occurs.

(i) On master device 1, the force feedback from the mobile robot is bigger than the feedback of master device 2; then the trainer has greater perception about the state of the mobile robot than about the command provided by the trainee.

(ii) On master device 2, the force feedback from master device 1 is bigger than the force feedback from the mobile robot; thus the trainee has greater perception about the command generated by the trainer than about the mobile robot state.

(iii) On mobile robot, β increases with α (Figure 2); thus the command of the trainer has higher priority than the command of the trainee.

Relation between α and β can be seen on Figure 2. To the best of the authors' knowledge, there is not a conceptual justification about the above definition, but from it the stability analysis can be completed. The study about different definitions of β that allow keeping the system stability is an open subject.

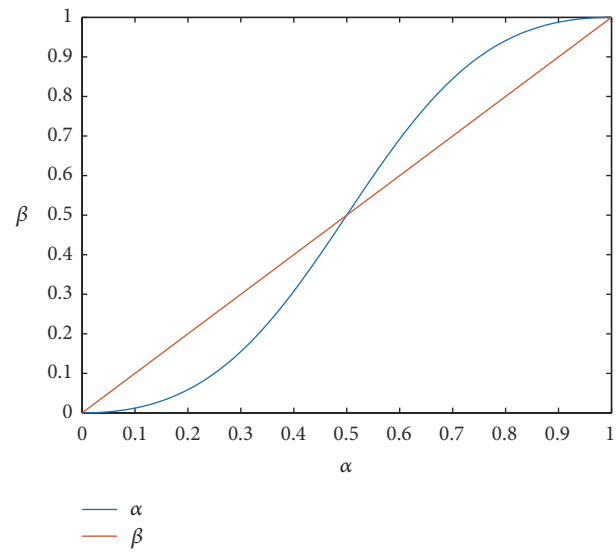

Figure 2: Relation between α and β.

4. Stability of the Delayed Closed-Loop System

The stability analysis of the control scheme is based on the Lyapunov-Krasovskii theory applied to trilateral teleoperation of a mobile robot in presence of time delays.

Theorem 9. *Consider a teleoperation system wherein two human operators (3) use two master devices (1) to drive a slave mobile robot (2) which interacts with an environment described by (4). If the control actions (7) are applied to such system, and if the controller gains hold with*

$$\begin{aligned}\lambda_1 &= \alpha\frac{k_{d_1}k_{p_3}}{p_1} - (1-\alpha)\alpha k_{p_3}k_g\overline{h}_{12} - \alpha^2 k_{p_3}\overline{h}_{13}\\ &\quad - \frac{\alpha^2 k_{p_3}}{4}\overline{h}_{31} - \frac{(1-\alpha)\alpha k_{p_3}k_g}{4}\overline{h}_{21} > 0,\\ \lambda_2 &= \frac{k_{d_2}k_{p_3}}{k_{p_2}}(1-\alpha) - \alpha(1-\alpha)k_{p_3}k_g\overline{h}_{21}\\ &\quad - (1-\alpha)^2 k_{p_3}\overline{h}_{23} - \frac{\alpha(1-\alpha)k_{p_3}k_g}{4}\overline{h}_{12}\\ &\quad - \frac{(1-\alpha)^2 k_{p_3}}{4}\overline{h}_{32} > 0,\\ \lambda_3 &= \frac{k_{d_3}}{k_g}\left[\alpha^2 + (1-\alpha)^2\right] - \alpha^2 k_{p_3}\overline{h}_{31}\\ &\quad - (1-\alpha)^2 k_{p_3}\overline{h}_{32} - \frac{\alpha^2 k_{p_3}}{4}\overline{h}_{13} - \frac{(1-\alpha)^2 k_{p_3}}{4}\overline{h}_{23}\\ &\quad > 0,\end{aligned} \tag{10}$$

then the vector $\mathbf{x} := [\dot{\mathbf{q}}_{\mathbf{m}_1}\ \dot{\mathbf{q}}_{\mathbf{m}_2}\ \boldsymbol{\eta}\ \dot{\boldsymbol{\eta}}\ \mathbf{z}\ (\boldsymbol{\eta} - k_g\mathbf{q}_{\mathbf{m}_1})\ (\boldsymbol{\eta} - k_g\mathbf{q}_{\mathbf{m}_2})\ (k_g\mathbf{q}_{\mathbf{m}1} - k_g\mathbf{q}_{\mathbf{m}_2})]^T$ *is bounded, and the variables vectors* $\dot{\mathbf{q}}_{\mathbf{m}_1}, \dot{\mathbf{q}}_{\mathbf{m}_2}, \dot{\boldsymbol{\eta}} \in L_2$.

Proof. A Lyapunov-Krasovskii functional $V(\mathbf{x}) = V_1 + V_2 + V_3 + V_4 + V_5 + V_6 + V_7 + V_8 > 0$ is proposed, in order to analyze its evolution along the system trajectories and then infer the behavior of $\mathbf{x} \coloneqq [\dot{\mathbf{q}}_{\mathbf{m}_1} \ \dot{\mathbf{q}}_{\mathbf{m}_2} \ \boldsymbol{\eta} \ \dot{\boldsymbol{\eta}} \ \mathbf{z} \ (\boldsymbol{\eta} - k_g \mathbf{q}_{\mathbf{m}_1}) \ (\boldsymbol{\eta} - k_g \mathbf{q}_{\mathbf{m}_2}) \ (k_g \mathbf{q}_{\mathbf{m}1} - k_g \mathbf{q}_{\mathbf{m}_2})]^T$ which includes the kinetic energy of the two masters and mobile robot as well as the potential energy of the synchronism errors of the trilateral system. Next each V_i is represented mathematically as follows:

$$V_1 = \frac{1}{2}\alpha \frac{k_{p_3}}{k_{p_1}} \dot{\mathbf{q}}_{\mathbf{m}_1}{}^{\mathbf{T}} \mathbf{M}_{\mathbf{m}_1}\left(\mathbf{q}_{\mathbf{m}_1}\right) \dot{\mathbf{q}}_{\mathbf{m}_1} + \alpha \frac{k_{p_3}}{k_{p_1}} E_{h_1}, \tag{11}$$

$$V_2 = \frac{1}{2}(1-\alpha) \frac{k_{p_3}}{k_{p_2}} \dot{\mathbf{q}}_{\mathbf{m}_2}{}^{\mathbf{T}} \mathbf{M}_{\mathbf{m}_2}\left(\mathbf{q}_{\mathbf{m}_2}\right) \dot{\mathbf{q}}_{\mathbf{m}_2} + (1-\alpha) \frac{k_{p_3}}{k_{p_2}} \cdot E_{h_2}, \tag{12}$$

$$V_3 = \frac{1}{2}\left[\alpha^2 + (1-\alpha)^2\right] \frac{\alpha_e}{k_g} \boldsymbol{\eta}^{\mathbf{T}} \boldsymbol{\eta}, \tag{13}$$

$$V_4 = \left[\alpha^2 + (1-\alpha)^2\right] \frac{1}{k_g} \int_0^t \dot{\boldsymbol{\eta}}^{\mathbf{T}} \mathbf{D} \dot{\boldsymbol{\eta}}, \tag{14}$$

$$V_5 = \frac{1}{2}\alpha^2 \frac{k_{p_3}}{k_g} \left(\boldsymbol{\eta} - k_g \mathbf{q}_{\mathbf{m}_1}\right)^{\mathbf{T}} \left(\boldsymbol{\eta} - k_g \mathbf{q}_{\mathbf{m}_1}\right), \tag{15}$$

$$V_6 = \frac{1}{2}(1-\alpha)^2 \frac{k_{p_3}}{k_g} \left(\boldsymbol{\eta} - k_g \mathbf{q}_{\mathbf{m}_2}\right)^{\mathbf{T}} \left(\boldsymbol{\eta} - k_g \mathbf{q}_{\mathbf{m}_2}\right), \tag{16}$$

$$V_7 = \frac{1}{2}\alpha(1-\alpha) \frac{k_{p_3}}{k_g} \left(k_g \mathbf{q}_{\mathbf{m}1} - k_g \mathbf{q}_{\mathbf{m}_2}\right)^{\mathbf{T}} \cdot \left(k_g \mathbf{q}_{\mathbf{m}1} - k_g \mathbf{q}_{\mathbf{m}_2}\right), \tag{17}$$

$$\begin{aligned} V_8 = {} & \alpha^2 k_{p_3} \int_{-h_{31}}^0 \int_{t+\theta}^t \dot{\boldsymbol{\eta}}^T(\xi)\, \dot{\boldsymbol{\eta}}(\xi)\, \mathbf{d}\xi + (1-\alpha) \\ & \cdot \alpha k_{p_3} k_g \int_{-h_{12}}^0 \int_{t+\theta}^t \dot{\mathbf{q}}_{\mathbf{m}_1}{}^T(\xi)\, \dot{\mathbf{q}}_{\mathbf{m}_1}(\xi)\, \mathbf{d}\xi + \alpha(1-\alpha) \\ & \cdot k_{p_3} k_g \int_{-h_{21}}^0 \int_{t+\theta}^t \dot{\mathbf{q}}_{\mathbf{m}_2}{}^T(\xi)\, \dot{\mathbf{q}}_{\mathbf{m}_2}(\xi)\, \mathbf{d}\xi + (1-\alpha)^2 \\ & \cdot k_{p_3} \int_{-h_{32}}^0 \int_{t+\theta}^t \dot{\boldsymbol{\eta}}^T(\xi)\, \dot{\boldsymbol{\eta}}(\xi)\, \mathbf{d}\xi \\ & + \alpha^2 k_{p_3} \int_{-h_{13}}^0 \int_{t+\theta}^t \dot{\mathbf{q}}_{\mathbf{m}_1}{}^T(\xi)\, \dot{\mathbf{q}}_{\mathbf{m}_1}(\xi)\, \mathbf{d}\xi + (1-\alpha)^2 \\ & \cdot k_{p_3} \int_{-h_{23}}^0 \int_{t+\theta}^t \dot{\mathbf{q}}_{\mathbf{m}_2}{}^T(\xi)\, \dot{\mathbf{q}}_{\mathbf{m}_2}(\xi)\, \mathbf{d}\xi, \end{aligned} \tag{18}$$

where k_{V_i} are arbitrary positive constants which will be determined later.

To get $\dot{V}$, the time derivative of (11)–(18) will be computed along the system trajectories. First, $\dot{V}_1$ is obtained from (11) as follows:

$$\begin{aligned} \dot{V}_1 = {} & \frac{1}{2}\alpha \frac{k_{p_3}}{k_{p_1}} \dot{\mathbf{q}}_{\mathbf{m}_1}{}^{\mathbf{T}} \dot{\mathbf{M}}_{\mathbf{m}_1} \dot{\mathbf{q}}_{\mathbf{m}_1} + \alpha \frac{k_{p_3}}{k_{p_1}} \dot{\mathbf{q}}_{\mathbf{m}_1}{}^{\mathbf{T}} \mathbf{M}_{\mathbf{m}_1} \ddot{\mathbf{q}}_{\mathbf{m}_1} \\ & - \alpha \frac{k_{p_3}}{k_{p_1}} \mathbf{f}_{\mathbf{h}_1}{}^{\mathbf{T}} \dot{\mathbf{q}}_{\mathbf{m}_1}. \end{aligned} \tag{19}$$

Next, the master dynamics (1) are inserted into (19) considering also Properties 1 and 2 of the master model:

$$\begin{aligned} \dot{V}_1 = {} & \frac{1}{2}\alpha \frac{k_{p_3}}{k_{p_1}} \dot{\mathbf{q}}_{\mathbf{m}_1}{}^{\mathbf{T}} \dot{\mathbf{M}}_{\mathbf{m}_1} \dot{\mathbf{q}}_{\mathbf{m}_1} + \alpha \frac{k_{p_3}}{k_{p_1}} \\ & \cdot \dot{\mathbf{q}}_{\mathbf{m}_1}{}^{\mathbf{T}} \mathbf{M}_{\mathbf{m}_1} \mathbf{M}_{\mathbf{m}_1}{}^{-1} \left(\boldsymbol{\tau}_{\mathbf{m}_1} + \mathbf{f}_{\mathbf{h}_1} - \mathbf{g}\left(\mathbf{q}_{\mathbf{m}_1}\right) \right. \\ & \left. - \mathbf{C}_{\mathbf{m}_1} \dot{\mathbf{q}}_{\mathbf{m}_1}\right) - \alpha \frac{k_{p_3}}{k_{p_1}} \mathbf{f}_{\mathbf{h}_1}{}^{\mathbf{T}} \dot{\mathbf{q}}_{\mathbf{m}_1} = \alpha \frac{k_{p_3}}{k_{p_1}} \dot{\mathbf{q}}_{\mathbf{m}_1}{}^{\mathbf{T}} \left(\boldsymbol{\tau}_{\mathbf{m}_1} \right. \\ & \left. - \mathbf{g}\left(\mathbf{q}_{\mathbf{m}_1}\right)\right). \end{aligned} \tag{20}$$

Now, the control action $\boldsymbol{\tau}_{\mathbf{m}_1}$ from (7) is included in (20) and Relation 8 (6) is applied over the delayed terms:

$$\begin{aligned} \dot{V}_1 = {} & -\frac{k_{d_1} k_{p_3}}{k_{p1}} \alpha \dot{\mathbf{q}}_{\mathbf{m}_1}{}^{\mathbf{T}} \dot{\mathbf{q}}_{\mathbf{m}_1} - k_{p_3} k_g \alpha \dot{\mathbf{q}}_{\mathbf{m}_1}{}^{\mathbf{T}} \mathbf{q}_{\mathbf{m}_1} \\ & + (1-\alpha) \alpha k_{p_3} k_g \dot{\mathbf{q}}_{\mathbf{m}_1}{}^{\mathbf{T}} \mathbf{q}_{\mathbf{m}_2} + \alpha^2 k_{p_3} \dot{\mathbf{q}}_{\mathbf{m}_1}{}^{\mathbf{T}} \boldsymbol{\eta} \\ & - \alpha^2 k_{p_3} \dot{\mathbf{q}}_{\mathbf{m}_1}{}^{\mathbf{T}} \int_{t-h_{31}}^t \dot{\boldsymbol{\eta}}(\xi)\, d\xi \\ & - (1-\alpha) \alpha k_{p_3} k_g \dot{\mathbf{q}}_{\mathbf{m}_1}{}^{\mathbf{T}} \int_{t-h_{21}}^t \dot{\mathbf{q}}_{\mathbf{m}_2}(\xi)\, d\xi. \end{aligned} \tag{21}$$

Following a similar procedure, the time derivative of (12) is given as follows:

$$\begin{aligned} \dot{V}_2 = {} & \frac{1}{2}(1-\alpha) \frac{k_{p_3}}{k_{p_2}} \dot{\mathbf{q}}_{\mathbf{m}_2}{}^{\mathbf{T}} \dot{\mathbf{M}}_{\mathbf{m}_2} \dot{\mathbf{q}}_{\mathbf{m}_2} \\ & + (1-\alpha) \frac{k_{p_3}}{k_{p_2}} \dot{\mathbf{q}}_{\mathbf{m}_2}{}^{\mathbf{T}} \mathbf{M}_{\mathbf{m}_2} \ddot{\mathbf{q}}_{\mathbf{m}_2} \\ & - (1-\alpha) \frac{k_{p_3}}{k_{p_2}} \mathbf{f}_{\mathbf{h}_2}{}^{\mathbf{T}} \dot{\mathbf{q}}_{\mathbf{m}_2}. \end{aligned} \tag{22}$$

Next, the dynamics (1) of master 2 are introduced into (22) while Properties 1 and 2 of the master model are used, too:

$$\begin{aligned} \dot{V}_2 = {} & \frac{1}{2}(1-\alpha) \frac{k_{p_3}}{k_{p_2}} \dot{\mathbf{q}}_{\mathbf{m}_2}{}^{\mathbf{T}} \dot{\mathbf{M}}_{\mathbf{m}_2} \dot{\mathbf{q}}_{\mathbf{m}_2} + (1-\alpha) \frac{k_{p_3}}{k_{p_2}} \\ & \cdot \dot{\mathbf{q}}_{\mathbf{m}_2}{}^{\mathbf{T}} \left(\boldsymbol{\tau}_{\mathbf{m}_2} + \mathbf{f}_{\mathbf{h}_2} - \mathbf{C}_{\mathbf{m}_2}\left(\mathbf{q}_{\mathbf{m}_2}, \dot{\mathbf{q}}_{\mathbf{m}_2}\right) \dot{\mathbf{q}}_{\mathbf{m}_2} \right. \\ & \left. - \mathbf{g}_{\mathbf{m}_2}\left(\mathbf{q}_{\mathbf{m}_2}\right)\right) - (1-\alpha) \frac{k_{p_3}}{k_{p_2}} \mathbf{f}_{\mathbf{h}_2}{}^{\mathbf{T}} \dot{\mathbf{q}}_{\mathbf{m}_2} = (1-\alpha) \frac{k_{p_3}}{k_{p_2}} \\ & \cdot \dot{\mathbf{q}}_{\mathbf{m}_2}{}^{\mathbf{T}} \left(\boldsymbol{\tau}_{\mathbf{m}_2} - \mathbf{g}\left(\mathbf{q}_{\mathbf{m}_2}\right)\right). \end{aligned} \tag{23}$$

If the control action $\boldsymbol{\tau}_{\mathbf{m}_2}$ from (7) is replaced into (23) and Relation 8 is applied again over delayed terms, the following expression is achieved:

$$\begin{aligned}\dot{V}_2 = &-k_{p_3}k_g(1-\alpha)\,\dot{\mathbf{q}}_{\mathbf{m}_2}{}^{\mathbf{T}}\mathbf{q}_{\mathbf{m}_2}\\ &-\frac{k_{d_2}k_{p_3}}{k_{p_2}}(1-\alpha)\,\dot{\mathbf{q}}_{\mathbf{m}_2}{}^{\mathbf{T}}\dot{\mathbf{q}}_{\mathbf{m}_2}\\ &+\alpha k_g k_{p_3}(1-\alpha)\,\dot{\mathbf{q}}_{\mathbf{m}_2}{}^{\mathbf{T}}\mathbf{q}_{\mathbf{m}_1}+k_{p_3}(1-\alpha)^2\,\dot{\mathbf{q}}_{\mathbf{m}_2}{}^{\mathbf{T}}\boldsymbol{\eta}\\ &-\alpha k_{p_3}k_g(1-\alpha)\,\dot{\mathbf{q}}_{\mathbf{m}_2}{}^{\mathbf{T}}\int_{t-h_{12}}^{t}\dot{\mathbf{q}}_{\mathbf{m}_1}(\xi)\,d\xi\\ &-k_{p_3}(1-\alpha)^2\,\dot{\mathbf{q}}_{\mathbf{m}_2}{}^{\mathbf{T}}\int_{t-h_{32}}^{t}\dot{\boldsymbol{\eta}}(\xi)\,d\xi.\end{aligned}\tag{24}$$

The functions $\dot{V}_3$ and $\dot{V}_4$ are easily reached from (13) and (14), respectively:

$$\dot{V}_3 = \left[\alpha^2+(1-\alpha)^2\right]\frac{\alpha_e}{k_g}\boldsymbol{\eta}^{\mathbf{T}}\dot{\boldsymbol{\eta}},\tag{25}$$

$$\dot{V}_4 = \left[\alpha^2+(1-\alpha)^2\right]\frac{1}{k_g}\dot{\boldsymbol{\eta}}^{\mathbf{T}}\mathbf{D}\dot{\boldsymbol{\eta}}.\tag{26}$$

Including the dynamics of the mobile robot (2) into (26) and then adding the control action $\boldsymbol{\tau}_{\mathbf{s}}$ from (7) and the environment force $\mathbf{f}_{\mathbf{e}}$ of (4) to the resulting equation, we get

$$\begin{aligned}\dot{V}_4 = &\,k_{p_3}\left[\alpha^2+(1-\alpha)^2\right]\frac{1}{k_g}\dot{\boldsymbol{\eta}}^{\mathbf{T}}\left[\beta k_g\mathbf{q}_{\mathbf{m}_1}(t-h_{13})\right.\\ &\left.+(1-\beta)\,k_g\mathbf{q}_{\mathbf{m}_2}(t-h_{23})-\boldsymbol{\eta}\right]-k_{d_3}\left[\alpha^2\right.\\ &\left.+(1-\alpha)^2\right]\frac{1}{k_g}\dot{\boldsymbol{\eta}}^{\mathbf{T}}\mathbf{z}+\left[\alpha^2+(1-\alpha)^2\right]\frac{1}{k_g}\dot{\boldsymbol{\eta}}^{\mathbf{T}}\mathbf{f}_{\mathbf{e}}.\end{aligned}\tag{27}$$

If relations (6) and (8) and β from (9) are considered, the terms of (27) can be reorganized as follows:

$$\begin{aligned}\dot{V}_4 = &-\left[\alpha^2+(1-\alpha)^2\right]\left(\frac{\alpha_e}{k_g}+\frac{k_{p_3}}{k_g}\right)\dot{\boldsymbol{\eta}}^{\mathbf{T}}\boldsymbol{\eta}\\ &+\left[\alpha^2+(1-\alpha)^2\right]\frac{1}{k_g}\dot{\boldsymbol{\eta}}^{\mathbf{T}}\mathbf{f}_{\mathbf{a}_e}\\ &+\frac{k_{d_3}}{k_g}\left[\alpha^2+(1-\alpha)^2\right]\dot{\boldsymbol{\eta}}^{\mathbf{T}}g\\ &-\frac{k_{d_3}}{k_g}\left[\alpha^2+(1-\alpha)^2\right]\dot{\boldsymbol{\eta}}^{\mathbf{T}}\dot{\boldsymbol{\eta}}+\alpha^2k_{p_3}\dot{\boldsymbol{\eta}}^{\mathbf{T}}\mathbf{q}_{\mathbf{m}_1}\\ &+(1-\alpha)^2k_{p_3}\dot{\boldsymbol{\eta}}^{\mathbf{T}}\mathbf{q}_{\mathbf{m}_2}\\ &-\alpha^2k_{p_3}\dot{\boldsymbol{\eta}}^{\mathbf{T}}\int_{t-h_{13}}^{t}\dot{\mathbf{q}}_{\mathbf{m}_1}(\xi)\,d\xi\\ &-(1-\alpha)^2k_{p_3}\dot{\boldsymbol{\eta}}^{\mathbf{T}}\int_{t-h_{23}}^{t}\dot{\mathbf{q}}_{\mathbf{m}_2}(\xi)\,d\xi.\end{aligned}\tag{28}$$

Next, the derivative of the synchronism errors of the trilateral system are obtained from (15), (16), and (17):

$$\begin{aligned}\dot{V}_5 &= \alpha^2\frac{k_{p_3}}{k_g}\left(\boldsymbol{\eta}-k_g\mathbf{q}_{\mathbf{m}_1}\right)^{\mathbf{T}}\left(\dot{\boldsymbol{\eta}}-k_g\dot{\mathbf{q}}_{\mathbf{m}_1}\right)\\ &= \alpha^2\frac{k_{p_3}}{k_g}\boldsymbol{\eta}^T\dot{\boldsymbol{\eta}}-\alpha^2k_{p_3}\boldsymbol{\eta}^T\dot{\mathbf{q}}_{\mathbf{m}_1}-\alpha^2k_{p_3}\mathbf{q}_{\mathbf{m}_1}{}^T\dot{\boldsymbol{\eta}}\\ &\quad+\alpha^2k_{p_3}k_g\mathbf{q}_{\mathbf{m}_1}{}^T\dot{\mathbf{q}}_{\mathbf{m}_1},\\ \dot{V}_6 &= (1-\alpha)^2\frac{k_{p_3}}{k_g}\left(\boldsymbol{\eta}-k_g\mathbf{q}_{\mathbf{m}_2}\right)^{\mathbf{T}}\left(\dot{\boldsymbol{\eta}}-k_g\dot{\mathbf{q}}_{\mathbf{m}_2}\right)\\ &= (1-\alpha)^2\frac{k_{p_3}}{k_g}\boldsymbol{\eta}^T\dot{\boldsymbol{\eta}}-(1-\alpha)^2k_{p_3}\boldsymbol{\eta}^T\dot{\mathbf{q}}_{\mathbf{m}_2}\\ &\quad-(1-\alpha)^2k_{p_3}\mathbf{q}_{\mathbf{m}_2}{}^T\dot{\boldsymbol{\eta}}+(1-\alpha)^2k_{p_3}k_g\mathbf{q}_{\mathbf{m}_2}{}^{\mathbf{T}}\dot{\mathbf{q}}_{\mathbf{m}_2},\\ \dot{V}_7 &= \alpha(1-\alpha)\frac{k_{p_3}}{k_g}\left(k_g\mathbf{q}_{\mathbf{m}1}-k_g\mathbf{q}_{\mathbf{m}_2}\right)^{\mathbf{T}}\left(k_g\dot{\mathbf{q}}_{\mathbf{m}1}-k_g\dot{\mathbf{q}}_{\mathbf{m}_2}\right)\\ &= \alpha(1-\alpha)k_{p_3}k_g\mathbf{q}_{\mathbf{m}1}{}^T\dot{\mathbf{q}}_{\mathbf{m}1}\\ &\quad-\alpha(1-\alpha)k_{p_3}k_g\mathbf{q}_{\mathbf{m}1}{}^T\dot{\mathbf{q}}_{\mathbf{m}_2}\\ &\quad-\alpha(1-\alpha)k_{p_3}k_g\mathbf{q}_{\mathbf{m}2}{}^T\dot{\mathbf{q}}_{\mathbf{m}1}\\ &\quad+\alpha(1-\alpha)k_{p_3}k_g\mathbf{q}_{\mathbf{m}_2}{}^T\dot{\mathbf{q}}_{\mathbf{m}_2}.\end{aligned}\tag{29}$$

Finally, $\dot{V}_8$ is deduced from (18) (see [11, 20] for further details) as follows:

$$\begin{aligned}\dot{V}_8 \le\;&\alpha^2k_{p_3}\overline{h}_{31}\dot{\boldsymbol{\eta}}^T\dot{\boldsymbol{\eta}}-\alpha^2k_{p_3}\int_{t-h_{31}}^{t}\dot{\boldsymbol{\eta}}^T(\xi)\,\dot{\boldsymbol{\eta}}(\xi)\,d\xi\\ &+(1-\alpha)\,\alpha k_{p_3}k_g\overline{h}_{12}\dot{\mathbf{q}}_{\mathbf{m}_1}{}^T\dot{\mathbf{q}}_{\mathbf{m}_1}\\ &-(1-\alpha)\,\alpha k_{p_3}k_g\int_{t-h_{12}}^{t}\dot{\mathbf{q}}_{\mathbf{m}_1}{}^T(\xi)\,\dot{\mathbf{q}}_{\mathbf{m}_1}(\xi)\,d\xi\\ &+\alpha(1-\alpha)\,k_{p_3}k_g\overline{h}_{21}\dot{\mathbf{q}}_{\mathbf{m}_2}{}^T\dot{\mathbf{q}}_{\mathbf{m}_2}\\ &-\alpha(1-\alpha)\,k_{p_3}k_g\int_{t-h_{21}}^{t}\dot{\mathbf{q}}_{\mathbf{m}_2}{}^T(\xi)\,\dot{\mathbf{q}}_{\mathbf{m}_2}(\xi)\,d\xi\\ &+(1-\alpha)^2\,k_{p_3}\overline{h}_{32}\dot{\boldsymbol{\eta}}^T\dot{\boldsymbol{\eta}}\\ &-(1-\alpha)^2\,k_{p_3}\int_{t-h_{32}}^{t}\dot{\boldsymbol{\eta}}^T(\xi)\,\dot{\boldsymbol{\eta}}(\xi)\,d\xi\\ &+\alpha^2k_{p_3}\overline{h}_{13}\dot{\mathbf{q}}_{\mathbf{m}_1}{}^T\dot{\mathbf{q}}_{\mathbf{m}_1}\\ &-\alpha^2k_{p_3}\int_{t-h_{13}}^{t}\dot{\mathbf{q}}_{\mathbf{m}_1}{}^T(\xi)\,\dot{\mathbf{q}}_{\mathbf{m}_1}(\xi)\,d\xi\end{aligned}$$

$$+ (1-\alpha)^2 k_{p_3} \overline{h}_{23} \dot{\mathbf{q}}_{\mathbf{m}_2}{}^T \dot{\mathbf{q}}_{\mathbf{m}_2} - (1-\alpha)^2 k_{p_3} \int_{t-h_{23}}^{t} \dot{\mathbf{q}}_{\mathbf{m}_2}{}^T(\xi)\, \dot{\mathbf{q}}_{\mathbf{m}_2}(\xi). \tag{30}$$

Now, observing the expressions obtained for $\dot{V}_i$, there are terms with integrals that difficult the analysis. To solve this, the terms with integrals can be linked by means of Lemma 7 (5) to get quadratic expressions which are convenient to compare the contribution of each factor on the stability.

If each integral term of (21), (24), and (28) is associated with one integral term of (30) through the structure of (5), the following relations can be stated:

$$\begin{aligned}
&-\alpha^2 k_{p_3} \dot{\mathbf{q}}_{\mathbf{m}_1}{}^{\mathbf{T}} \int_{t-h_{31}}^{t} \dot{\boldsymbol{\eta}}(\xi)\, d\xi \\
&\quad - \alpha^2 k_{p_3} \int_{t-h_{31}}^{t} \dot{\boldsymbol{\eta}}^T(\xi)\, \dot{\boldsymbol{\eta}}(\xi)\, d\xi \le \frac{\alpha^2 k_{p_3}}{4} \overline{h}_{31} \dot{\mathbf{q}}_{\mathbf{m}_1}{}^{\mathbf{T}} \dot{\mathbf{q}}_{\mathbf{m}_1}, \\
&-(1-\alpha)\,\alpha k_{p_3} k_g \dot{\mathbf{q}}_{\mathbf{m}_1}{}^{\mathbf{T}} \int_{t-h_{21}}^{t} \dot{\mathbf{q}}_{\mathbf{m}_2}(\xi)\, d\xi \\
&\quad - \alpha(1-\alpha) k_{p_3} k_g \int_{t-h_{21}}^{t} \dot{\mathbf{q}}_{\mathbf{m}_2}{}^T(\xi)\, \dot{\mathbf{q}}_{\mathbf{m}_2}(\xi)\, d\xi \\
&\quad \le \frac{(1-\alpha)\,\alpha k_{p_3} k_g}{4} \overline{h}_{21} \dot{\mathbf{q}}_{\mathbf{m}_1}{}^{\mathbf{T}} \dot{\mathbf{q}}_{\mathbf{m}_1}, \\
&-\alpha(1-\alpha) k_g k_{p_3} \dot{\mathbf{q}}_{\mathbf{m}_2}{}^{\mathbf{T}} \int_{t-h_{12}}^{t} \dot{\mathbf{q}}_{\mathbf{m}_1}(\xi)\, d\xi \\
&\quad - \alpha(1-\alpha) k_g k_{p_3} \int_{t-h_{12}}^{t} \dot{\mathbf{q}}_{\mathbf{m}_1}{}^T(\xi)\, \dot{\mathbf{q}}_{\mathbf{m}_1}(\xi)\, d\xi \\
&\quad \le \frac{\alpha(1-\alpha) k_{p_3} k_g}{4} \overline{h}_{12} \dot{\mathbf{q}}_{\mathbf{m}_2}{}^{\mathbf{T}} \dot{\mathbf{q}}_{\mathbf{m}_2}, \\
&-(1-\alpha)^2 k_{p_3} \dot{\mathbf{q}}_{\mathbf{m}_2}{}^{\mathbf{T}} \int_{t-h_{32}}^{t} \dot{\boldsymbol{\eta}}(\xi)\, d\xi \\
&\quad - (1-\alpha)^2 k_{p_3} \int_{t-h_{32}}^{t} \dot{\boldsymbol{\eta}}^T(\xi)\, \dot{\boldsymbol{\eta}}(\xi)\, d\xi \\
&\quad \le \frac{(1-\alpha)^2 k_{p_3}}{4} \overline{h}_{32} \dot{\mathbf{q}}_{\mathbf{m}_2}{}^{\mathbf{T}} \dot{\mathbf{q}}_{\mathbf{m}_2}, \\
&-\alpha^2 k_{p_3} \dot{\boldsymbol{\eta}}^{\mathbf{T}} \int_{t-h_{13}}^{t} \dot{\mathbf{q}}_{\mathbf{m}_1}(\xi)\, d\xi \\
&\quad - \alpha^2 k_{p_3} \int_{t-h_{13}}^{t} \dot{\mathbf{q}}_{\mathbf{m}_1}{}^T(\xi)\, \dot{\mathbf{q}}_{\mathbf{m}_1}(\xi)\, d\xi \le \frac{\alpha^2 k_{p_3}}{4} \overline{h}_{13} \dot{\boldsymbol{\eta}}^{\mathbf{T}} \dot{\boldsymbol{\eta}}, \\
&-(1-\alpha)^2 k_{p_3} \dot{\boldsymbol{\eta}}^{\mathbf{T}} \int_{t-h_{23}}^{t} \dot{\mathbf{q}}_{\mathbf{m}_2}(\xi)\, d\xi \\
&\quad - (1-\alpha)^2 k_{p_3} \int_{t-h_{23}}^{t} \dot{\mathbf{q}}_{\mathbf{m}_2}{}^T(\xi)\, \dot{\mathbf{q}}_{\mathbf{m}_2}(\xi) \\
&\quad \le \frac{(1-\alpha)^2 k_{p_3}}{4} \overline{h}_{23} \dot{\boldsymbol{\eta}}^{\mathbf{T}} \dot{\boldsymbol{\eta}}.
\end{aligned} \tag{31}$$

Joining the functions V_i and applying relations (31)–(37), the terms including integrals are replaced with expressions more adequate to comparison:

$$\begin{aligned}
\dot{V} \le\ & -\dot{\mathbf{q}}_{\mathbf{m}_1}{}^{\mathbf{T}} \lambda_1 \mathbf{I} \dot{\mathbf{q}}_{\mathbf{m}_1} - \dot{\mathbf{q}}_{\mathbf{m}_2}{}^{\mathbf{T}} \lambda_2 \mathbf{I} \dot{\mathbf{q}}_{\mathbf{m}_2} - \dot{\boldsymbol{\eta}}^{\mathbf{T}} \lambda_3 \mathbf{I} \dot{\boldsymbol{\eta}} \\
& + \left[\alpha^2 + (1-\alpha)^2\right] k_g{}^{-1} \dot{\boldsymbol{\eta}}^{\mathbf{T}} \mathbf{f}_{\mathbf{a}_e} \\
& + k_{d_3} k_g{}^{-1} \left[\alpha^2 + (1-\alpha)^2\right] \dot{\boldsymbol{\eta}}^{\mathbf{T}} g,
\end{aligned} \tag{32}$$

where the constants λ_i are given by

$$\begin{aligned}
-\lambda_1 =\ & -\alpha \frac{k_{d_1} k_{p_3}}{p_1} + (1-\alpha)\,\alpha k_{p_3} k_g \overline{h}_{12} + \alpha^2 k_{p_3} \overline{h}_{13} \\
& + \frac{\alpha^2 k_{p_3}}{4} \overline{h}_{31} + \frac{(1-\alpha)\,\alpha k_{p_3} k_g}{4} \overline{h}_{21}, \\
-\lambda_2 =\ & -\frac{k_{d_2} k_{p_3}}{k_{p_2}} (1-\alpha) + \alpha(1-\alpha) k_{p_3} k_g \overline{h}_{21} \\
& + (1-\alpha)^2 k_{p_3} \overline{h}_{23} + \frac{\alpha(1-\alpha) k_{p_3} k_g}{4} \overline{h}_{12} \\
& + \frac{(1-\alpha)^2 k_{p_3}}{4} \overline{h}_{32}, \\
-\lambda_3 =\ & -\frac{k_{d_3}}{k_g} \left[\alpha^2 + (1-\alpha)^2\right] + \alpha^2 k_{p_3} \overline{h}_{31} \\
& + (1-\alpha)^2 k_{p_3} \overline{h}_{32} + \frac{\alpha^2 k_{p_3}}{4} \overline{h}_{13} \\
& + \frac{(1-\alpha)^2 k_{p_3}}{4} \overline{h}_{23}.
\end{aligned} \tag{33}$$

As $\alpha^2 + (1-\alpha)^2 \le 1$, (32) can be rewritten as

$$\begin{aligned}
\dot{V} \le\ & -\dot{\mathbf{q}}_{\mathbf{m}_1}{}^{\mathbf{T}} \lambda_1 \mathbf{I} \dot{\mathbf{q}}_{\mathbf{m}_1} - \dot{\mathbf{q}}_{\mathbf{m}_2}{}^{\mathbf{T}} \lambda_2 \mathbf{I} \dot{\mathbf{q}}_{\mathbf{m}_2} - \dot{\boldsymbol{\eta}}^{\mathbf{T}} \lambda_3 \mathbf{I} \dot{\boldsymbol{\eta}} \\
& + k_g{}^{-1} \dot{\boldsymbol{\eta}}^{\mathbf{T}} \mathbf{f}_{\mathbf{a}_e} + k_{d_3} k_g{}^{-1} \dot{\boldsymbol{\eta}}^{\mathbf{T}} g.
\end{aligned} \tag{34}$$

Since $\mathbf{f}_{\mathbf{a}_e}(t) \in L_2, L_\infty$ (Assumption 6) and $g(t) \in L_\infty$, if the damping coefficients $k_{d_1}, k_{d_2}, k_{d_3}$ are sufficiently high such that $\lambda_1, \lambda_2, \lambda_3 > 0$ in (34) then it is possible to state that $\left[\dot{\mathbf{q}}_{\mathbf{m}_1} \ \ \dot{\mathbf{q}}_{\mathbf{m}_2} \ \ \dot{\boldsymbol{\eta}}\right] \in L_\infty$.

Then, if (34) is integrated from 0 to t, we have

$$\begin{aligned}
V(t) - V(0) \le\ & -\lambda_1 \left\|\dot{\mathbf{q}}_{\mathbf{m}_1}\right\|_2^2 - \lambda_2 \left\|\dot{\mathbf{q}}_{\mathbf{m}_2}\right\|_2^2 - \lambda_3 \left\|\dot{\boldsymbol{\eta}}\right\|_2^2 \\
& + k_g{}^{-1} \int_0^t \dot{\boldsymbol{\eta}}^{\mathbf{T}} \mathbf{f}_{\mathbf{a}_e}(\xi)\, d\xi \\
& + k_{d_3} k_g{}^{-1} \int_0^t \dot{\boldsymbol{\eta}}^{\mathbf{T}} g(\xi)\, d\xi.
\end{aligned} \tag{35}$$

Furthermore, as $g(t)$ is considered infinitesimal, the terms containing $g(t)$ in (34) and (35) can be neglected. Besides, the integral term $\int_0^t \dot{\boldsymbol{\eta}}^{\mathbf{T}} \mathbf{f}_{\mathbf{a}_e}(\xi) d\xi$ is bounded by

$$\begin{aligned}\int_0^t \dot{\boldsymbol{\eta}}^T \mathbf{f}_{\mathbf{a}_e} d\xi &\leq \left| \int_0^t \dot{\mathbf{x}}_{\mathbf{m}}{}^T \mathbf{f}_{\mathbf{a}_e} d\xi \right| \leq \int_0^t \left|\dot{\boldsymbol{\eta}}\right| \left|\mathbf{f}_{\mathbf{a}_e}\right| d\xi \\ &\leq \left\|\dot{\boldsymbol{\eta}}\right\|_\infty \int_0^t \left|\mathbf{f}_{\mathbf{a}_h}\right| d\xi \\ &\leq \left\|\dot{\boldsymbol{\eta}}\right\|_\infty \left(\int_0^t \left|\mathbf{f}_{\mathbf{a}_e}\right|^2 d\xi \right)^{1/2} \leq \left\|\dot{\boldsymbol{\eta}}\right\|_\infty \left\|\mathbf{f}_{\mathbf{a}_e}\right\|_2 .\end{aligned} \tag{36}$$

Therefore, (35) can be rewritten as

$$V(t) \leq \left\|\dot{\boldsymbol{\eta}}\right\|_\infty \left\|\mathbf{f}_{\mathbf{a}_e}\right\|_2 + V(0) . \tag{37}$$

As $V(\mathbf{x})$ is radially unbounded and from (37) also it is bounded for all t, then $\mathbf{x} \in L_\infty$. Thus, the synchronism errors are bounded. Even more, considering this result in (35), we get

$$-\lambda_1 \left\|\dot{\mathbf{q}}_{\mathbf{m}_1}\right\|_2^2 - \lambda_2 \left\|\dot{\mathbf{q}}_{\mathbf{m}_2}\right\|_2^2 - \lambda_3 \left\|\dot{\boldsymbol{\eta}}\right\|_2^2 \leq \left\|\mathbf{f}_{\mathbf{a}_e}\right\|_2^2 + V(0) . \tag{38}$$

In this way, relation (38) allows asserting that the variables $\dot{\mathbf{q}}_{\mathbf{m}_1}, \dot{\mathbf{q}}_{\mathbf{m}_2}, \dot{\boldsymbol{\eta}} \in L_2$. The proof is complete. □

Remark 10. Taking the result achieved in (34), as the parameters $k_{d_1}, k_{d_2}, k_{d_3}$ are larger, then $\dot{\mathbf{q}}_{\mathbf{m}_1}, \dot{\mathbf{q}}_{\mathbf{m}_2}, \dot{\boldsymbol{\eta}}$ (both master velocities and slave acceleration) will tend to a smaller convergence ball.

Remark 11. From the $\mathbf{x}$ vector boundness and employing Properties 2 and 3, Proving that the control actions (7) are bounded is direct.

Remark 12. The following procedure to calibrate the control parameters of a delayed trilateral teleoperation system formed by a single mobile robot and dual-master is proposed:

(1) Calibrate the gain parameters $k_{p_1}, k_{p_2}, k_{p_3}$ and map k_g for the nondelayed trilateral teleoperation system considering $\alpha = 0$ and $\alpha = 1$.

(2) Set α depending on some training process.

(3) According to (1), (2) and considering the maximum magnitude (estimated or predicted based on previous connections) of all time delays added by the trilateral communication channel $(\overline{h}_{12}, \overline{h}_{13}, \overline{h}_{21}, \overline{h}_{23}, \overline{h}_{31}, \overline{h}_{32})$, the damping level is calibrated to hold Theorem 9.

5. Experimental Results

In this section, the proposed control scheme is tested. Two human operators teleoperate a mobile robot, receiving visual and force feedback. Both master devices employed are a low-cost manipulator, Novint Falcon model http://www.novint.com/ which has 3DOF and force feedback. Two DOFs of each master device are used to generate velocity commands for the mobile robot: one for the linear velocity and the other to set the angular velocity reference. To implement the teleoperation system, the following tools are used: MATLAB/Simulink from https://www.mathworks.com/ running with the real-time module and the SAS library from https://drive.google.com/drive/folders/0B2jklwyyOJqPNVA2SWFSaGFSNnc?usp=sharing compatible with V-REP environment (http://www.coppeliarobotics.com/). The methodology used allows easily doing tests of a delayed trilateral teleoperation system using a simulated robot but considering the two human operators inside the system, which commonly is called human-in-the-loop simulations, as it is shown in Figure 3. The communication between the master devices, Simulink, and V-REP is made through shared memory.

For the test, all time delays $h_{12}, h_{13}, h_{21}, h_{23}, h_{31}, h_{32}$ are configured randomly with values from 0.35 seconds to 0.65 seconds while the control parameters are calibrated following the procedure described in Remark 12, obtaining the following setting:

$$\begin{aligned} \alpha &= 0.6 \\ k_g &= 10; \\ k_{p_1} &= 15; \\ k_{p_2} &= 15; \\ k_{p_3} &= \begin{bmatrix} 200 & 0 \\ 0 & 35 \end{bmatrix}; \\ k_{d_1} &= 100; \\ k_{d_2} &= 100; \\ k_{d_3} &= 1. \end{aligned} \tag{39}$$

The objective of the experiment is to navigate avoiding the walls for reaching the yellow cube. Then the yellow cube must be pushed from its initial position to the green painted floor, as it is shown in Figure 4. Both operators feel not only the motion exerted by the other operator but also the dynamics of the mobile robot and the box weight.

Figure 5 shows the evolution on the remote site of each component (linear and angular velocity references) of the references $k_g \mathbf{q}_{\mathbf{m}_1}(t - h_{13})$ and $k_g \mathbf{q}_{\mathbf{m}_2}(t - h_{23})$ as well as the mobile robot velocity $\boldsymbol{\eta}$ (where v is the linear velocity and ω is the angular velocity). It can be seen that the mobile robot velocity is closer to master 1 reference, due to $\alpha = 0.6$ and therefore from (8) we get $\beta \approx 0.7$. Last value establishes the priority level over the mobile robot. Figure 6 shows an image sequence captured from the test, in which it is possible to observe that the task is done adequately in spite of the delays added by the trilateral communication channel.

Finally, in Figures 7 and 8, the main signals of the system about its stability are shown, such that it was proven in the theoretical analysis (Theorem 9 and Remarks 10 and 11), the synchronism errors between: master 1 and master 2

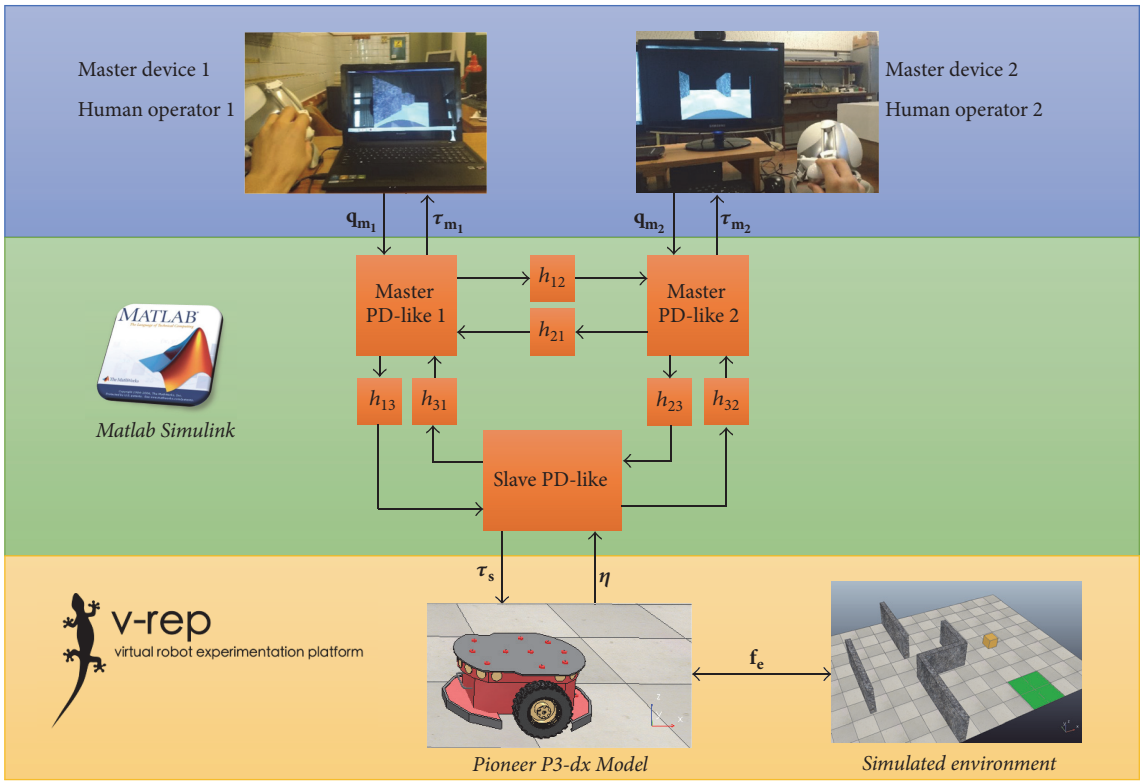

FIGURE 3: Delayed trilateral teleoperation implemented for testing.

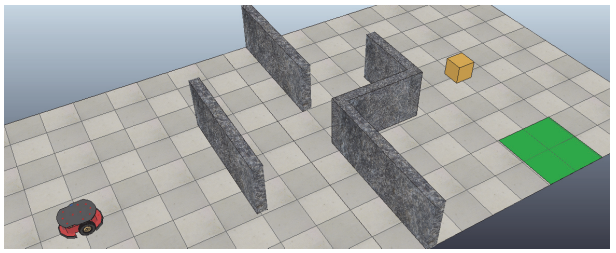

FIGURE 4: Setting of the test.

$\mathbf{e_3} = k_g\mathbf{q}_{\mathbf{m}_1}(t) - k_g\mathbf{q}_{\mathbf{m}_2}(t)$, master 1 and mobile robot $\mathbf{e_1} = k_g\mathbf{q}_{\mathbf{m}_1}(t) - \boldsymbol{\eta}(t)$, and master 2 and mobile robot $\mathbf{e_2} = k_g\mathbf{q}_{\mathbf{m}_2}(t) - \boldsymbol{\eta}(t)$, as well as the mobile robot acceleration $\mathbf{z}$, master 1 velocity $\dot{\mathbf{q}}_{\mathbf{m}_1}$, and master 2 velocity $\dot{\mathbf{q}}_{\mathbf{m}_2}$, remain bounded throughout the test. It is important to point out that about 53 seconds (subplot named T5 on Figure 5) the mobile robot, driven by the two human operators, starts to push the box. In the error signals $\mathbf{e_1}$ and $\mathbf{e_2}$ (Figure 7) as well as the mobile robot acceleration $\mathbf{z}$ (Figure 6), it is possible to appreciate such action. That is, two human operators both collaboratively and simultaneously drive a mobile robot, fulfilling the required task on the remote environment.

Discussion. The scheme control developed is addressed to keep the motion synchronism errors bounded, that is, $\mathbf{e_1}$, $\mathbf{e_2}$, and $\mathbf{e_3} \in L_\infty$. On the other, the controller is not designed to achieve force tracking but the control actions are bounded

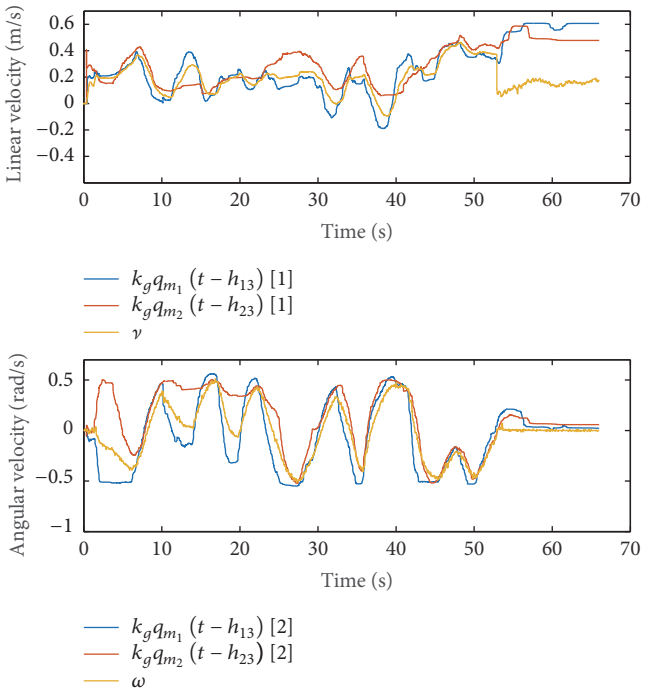

FIGURE 5: Linear and angular velocities of the mobile robot and the dual-references from masters 1 and 2.

(Remark 11) and therefore the force errors given by $\boldsymbol{\tau}_{\mathbf{m}_1} - \boldsymbol{\tau}_{\mathbf{m}_2}$, $\boldsymbol{\tau}_{\mathbf{m}_1} - \boldsymbol{\tau}_{\mathbf{s}}$, and $\boldsymbol{\tau}_{\mathbf{m}_2} - \boldsymbol{\tau}_{\mathbf{s}} \in L_\infty$. On the other hand, the

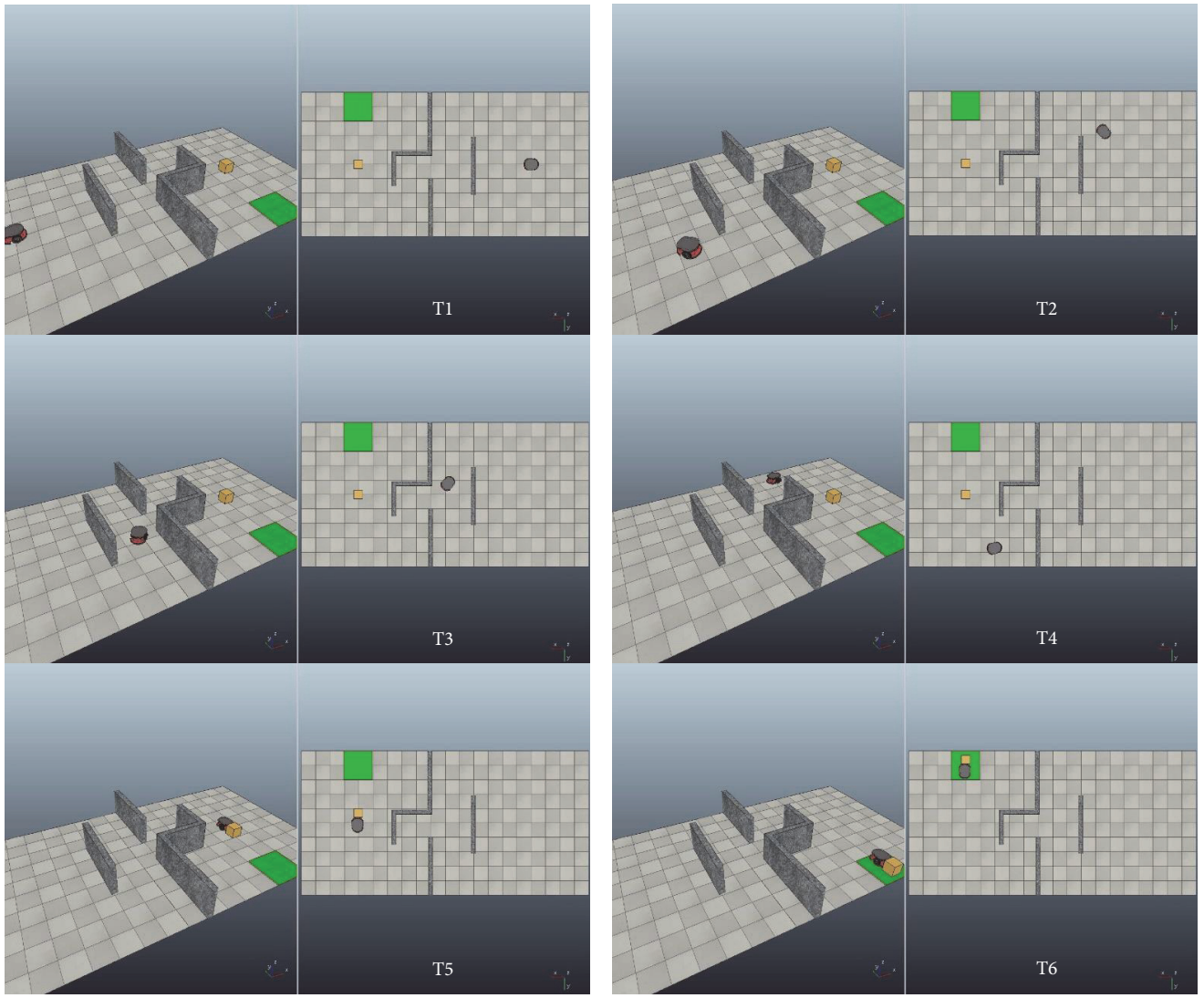

Figure 6: Sequence of images named T1, T2, T3, T4, T5, and T6 captured into the remote site.

human operator performance generally is quantified with indirect measures such as time to complete the task and position errors of the mobile robot with respect to a goal path (navigation task). These indexes could be used to allocate a training process where the expert (trainer) gradually will have less control (α and β are decreased) as the performance of the trainee will be better.

6. Conclusions

In this paper, the stability of a delayed trilateral teleoperation system of a single mobile robot-dual manipulator-like master is carried out. The kinematics and dynamics mismatch between the mobile robot and the type-manipulator masters makes the analysis presented different with respect to the one applied for the case where all robots are manipulator robots. To get a result about stability, a new Lyapunov-Krasovskii functional has been proposed, which is analyzed along the system trajectories. The result of the analysis exposed is formalized through Theorem 9, which establishes sufficient conditions to hold bounded the position and velocity of each master, velocity and acceleration of the mobile robot, motion synchronism errors, and all the control actions of the delayed trilateral system. Besides, a procedure suitable in practice for the parameters calibration is proposed considering the six values of time delays present on the trilateral system and some training process. A common training methodology requires that the trainer gradually sets the convenient level of α depending on the learning stage of the trainee, which could be evaluated from indexes such as time to complete the task. Furthermore, a simple test about trilateral teleoperation using a 3D simulator is shown, whose result agrees with the result achieved from the theoretical analysis proposed. Finally, it is important to remark that the main current application field is the remote training of operators to drive different types of mobile machines or robotic systems such as collaborative mobile manipulators.

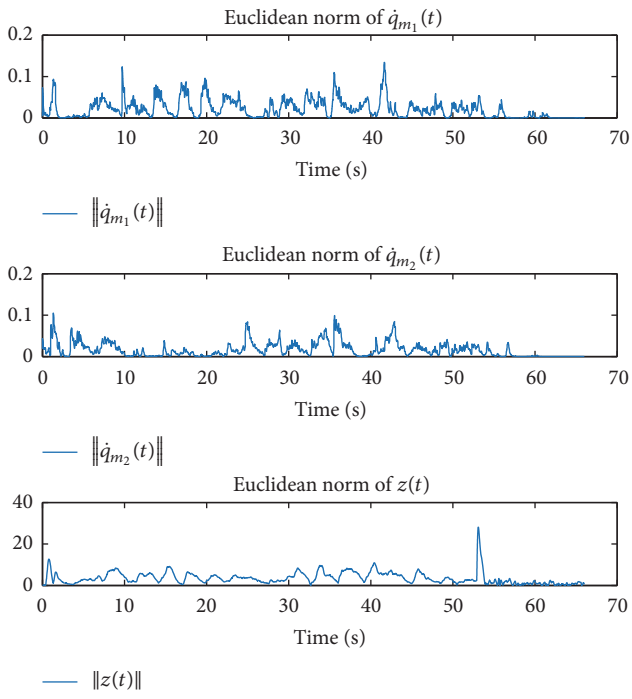

Figure 7: Velocities of both masters and acceleration of the mobile robot.

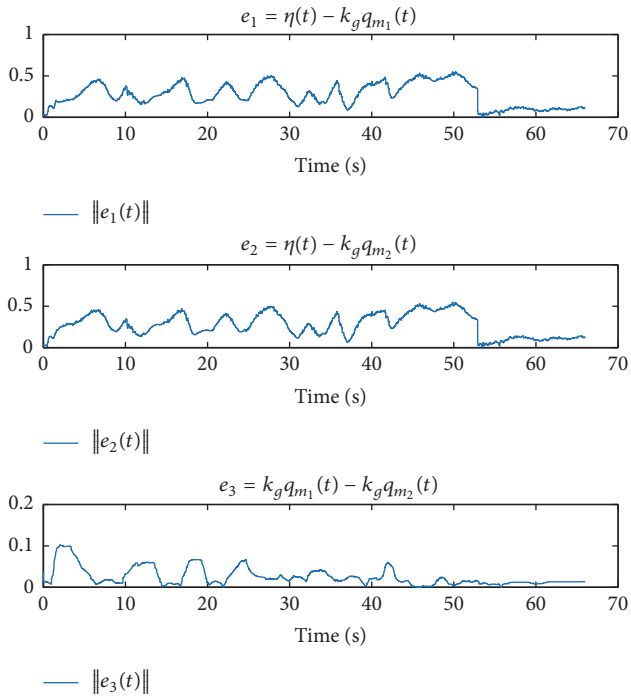

Figure 8: Errors of synchronism.

Conflicts of Interest

The authors declare that they have no conflicts of interest.

References

[1] T. B. Sheridan, *Telerobotics, Automation, and Human Supervisory Control*, MIT press, Cambridge, Mass, USA, 1992.

[2] T. A. Várkonyi, I. J. Rudas, P. Pausits, and T. Haidegger, "Survey on the control of time delay teleoperation systems," in *Proceedings of the 18th IEEE International Conference on Intelligent Engineering Systems, INES 2014*, pp. 89–94, Tihany, Hungary, July 2014.

[3] P. F. Hokayem and M. W. Spong, "Bilateral teleoperation: an historical survey," *Automatica*, vol. 42, no. 12, pp. 2035–2057, 2006.

[4] D. A. Lawrence, "Stability and transparency in bilateral teleoperation," *IEEE Transactions on Robotics and Automation*, vol. 9, no. 5, pp. 624–637, 1993.

[5] E. Slawiński, V. A. Mut, P. Fiorini, and L. R. Salinas, "Quantitative absolute transparency for bilateral teleoperation of mobile robots," *IEEE Transactions on Systems, Man, and Cybernetics Part A:Systems and Humans*, vol. 42, no. 2, pp. 430–442, 2012.

[6] R. Muradore and P. Fiorini, "A review of bilateral teleoperation algorithms riccardo muradore and paolo fiorini," *Acta Polytechnica Hungarica*, vol. 13, no. 1, pp. 191–208, 2016.

[7] E. Nuño, L. Basañez, and R. Ortega, "Passivity-based control for bilateral teleoperation: a tutorial," *Automatica*, vol. 47, no. 3, pp. 485–495, 2011.

[8] R. J. Anderson and M. W. Spong, "Bilateral control of teleoperators with time delay," *IEEE Transactions on Automatic Control*, vol. 34, no. 5, pp. 494–501, 1989.

[9] G. Niemeyer and J.-E. Slotine, "Stable adaptive teleoperation," *IEEE Journal of Oceanic Engineering*, vol. 16, no. 1, pp. 152–162, 1991.

[10] E. Nuño, R. Ortega, N. Barabanov, and L. Basañez, "A globally stable PD controller for bilateral teleoperators," *IEEE Transactions on Robotics*, vol. 24, no. 3, pp. 753–758, 2008.

[11] C. C. Hua and X. P. Liu, "Delay-dependent stability criteria of teleoperation systems with asymmetric time-varying delays," *IEEE Transactions on Robotics*, vol. 26, no. 5, pp. 925–932, 2010.

[12] S. Islam, P. X. Liu, A. El Saddik, J. Dias, and L. Seneviratne, "Bilateral shared autonomous systems with passive and nonpassive input forces under time varying delay," *ISA Transactions*, vol. 54, pp. 218–228, 2015.

[13] I. Farkhatdinov, J.-H. Ryu, and J. An, "A preliminary experimental study on haptic teleoperation of mobile robot with variable force feedback gain," in *Proceedings of the IEEE Haptics Symposium*, pp. 251–256, IEEE, Waltham, Mass, USA, March 2010.

[14] D. Lee, O. Martinez-Palafox, and M. W. Spong, "Bilateral teleoperation of a wheeled mobile robot over delayed communication network," in *Proceedings of the IEEE International Conference on Robotics and Automation (ICRA '06)*, pp. 3298–3303, May 2006.

[15] D. Lee and D. Xu, "Feedback r-passivity of Lagrangian systems for mobile robot teleoperation," in *Proceedings of the IEEE International Conference on Robotics and Automation (ICRA '11)*, pp. 2118–2123, Shanghai, China, May 2011.

[16] E. Slawiński and V. Mut, "Control scheme including prediction and augmented reality for teleoperation of mobile robots," *Robotica*, vol. 28, no. 1, pp. 11–22, 2010.

[17] W. Li, L. Ding, H. Gao, and M. Tavakoli, "Kinematic bilateral teleoperation of wheeled mobile robots subject to longitudinal slippage," *IET Control Theory & Applications*, vol. 10, no. 2, pp. 111–118, 2016.

[18] W. Li, L. Ding, Z. Liu, W. Wang, H. Gao, and M. Tavakoli, "Kinematic Bilateral Teledriving of Wheeled Mobile Robots Coupled with Slippage," *IEEE Transactions on Industrial Electronics*, vol. 64, no. 3, pp. 2147–2157, 2017.

[19] E. Slawiñski, S. García, L. Salinas, and V. Mut, "PD-like controller with impedance for delayed bilateral teleoperation of mobile robots," *Robotica*, vol. 34, no. 9, pp. 2151–2161, 2016.

[20] E. Slawiñski, V. Mut, and D. Santiago, "PD-like controller for delayed bilateral teleoperation of wheeled robots," *International Journal of Control*, vol. 89, no. 8, pp. 1622–1631, 2016.

[21] P. R. Culmer, A. E. Jackson, S. Makower et al., "A control strategy for upper limb robotic rehabilitation with a dual robot system," *IEEE/ASME Transactions on Mechatronics*, vol. 15, no. 4, pp. 575–585, 2010.

[22] K. Shamaei, L. H. Kim, and A. M. Okamura, "Design and evaluation of a trilateral shared-control architecture for teleoperated training robots," in *Proceedings of the 37th Annual International Conference of the IEEE Engineering in Medicine and Biology Society, EMBC 2015*, pp. 4887–4893, August 2015.

[23] M. Panzirsch, J. Artigas, A. Tobergte et al., "A peer-to-peer trilateral passivity control for delayed collaborative teleoperation," in *Proceedings of the Haptics: Perception, Devices, Mobility, and Communication*, vol. 7282, pp. 395–406, 2012.

[24] Z. Li, L. Ding, H. Gao, G. Duan, and C.-Y. Su, "Trilateral teleoperation of adaptive fuzzy force/motion control for nonlinear teleoperators with communication random delays," *IEEE Transactions on Fuzzy Systems*, vol. 21, no. 4, pp. 610–624, 2013.

[25] A. Ghorbanian, S. M. Rezaei, A. R. Khoogar, M. Zareinejad, and K. Baghestan, "A novel control framework for nonlinear time-delayed Dual-master/single-slave teleoperation," *ISA Transactions*, vol. 52, no. 2, pp. 268–277, 2013.

[26] W. Li, H. Gao, L. Ding, and M. Tavakoli, "Trilateral Predictor-Mediated Teleoperation of a Wheeled Mobile Robot with Slippage," *IEEE Robotics and Automation Letters*, vol. 1, no. 2, pp. 738–745, 2016.

[27] E. Nuño, C. I. Aldana, and L. Basañez, "Task space consensus in networks of heterogeneous and uncertain robotic systems with variable time-delays," *International Journal of Adaptive Control and Signal Processing*, vol. 31, no. 6, pp. 917–937, 2017.

[28] E. Nuno, "Consensus of Euler-Lagrange systems using only position measurements," *IEEE Transactions on Control of Network Systems*, 2016.

[29] D. Santiago, D. Herrera, E. Slawi, V. Mut, and E. Slawiñski, "Mapeos continuos para teleoperación de Manipuladores Móviles," *VIII Jornadas Argentinas de Robótica*, 2014.

Hindawi
Mathematical Problems in Engineering
Volume 2017, Article ID 9490142, 8 pages
https://doi.org/10.1155/2017/9490142

Research Article

A Method for Stability Analysis of Periodic Delay Differential Equations with Multiple Time-Periodic Delays

Gang Jin,[1,2] Houjun Qi,[1,2] Zhanjie Li,[1,2] Jianxin Han,[1,2] and Hua Li[3]

[1] *Tianjin Key Laboratory of High Speed Cutting and Precision Machining, Tianjin University of Technology and Education, Tianjin 300222, China*
[2] *National-Local Joint Engineering Laboratory of Intelligent Manufacturing Oriented Automobile Die & Mould, Tianjin University of Technology and Education, Tianjin 300222, China*
[3] *Tianjin Jinhang Institute of Technical Physics, Tianjin, China*

Correspondence should be addressed to Jianxin Han; hanjianxin@tju.edu.cn

Received 28 June 2017; Accepted 14 August 2017; Published 17 September 2017

Academic Editor: Renming Yang

Delay differential equations (DDEs) are widely utilized as the mathematical models in engineering fields. In this paper, a method is proposed to analyze the stability characteristics of periodic DDEs with multiple time-periodic delays. Stability charts are produced for two typical examples of time-periodic DDEs about milling chatter, including the variable-spindle speed milling system with one-time-periodic delay and variable pitch cutter milling system with multiple delays. The simulations show that the results gained by the proposed method are in close agreement with those existing in the past literature. This indicates the effectiveness of our method in terms of time-periodic DDEs with multiple time-periodic delays. Moreover, for milling processes, the proposed method further provides a generalized algorithm, which possesses a good capability to predict the stability lobes for milling operations with variable pitch cutter or variable-spindle speed.

1. Introduction

Time-delay systems widely exist in engineering and science, where the rate of change of state is determined by both present and past state variables, such as machining processes [1, 2], wheel dynamics [3, 4], feedback controller [5, 6], gene expression dynamics [7], and population dynamics [8, 9]. However, for some of above applications, the time delay in the dynamic system may lead to instability, poor performance, or other types of potential damage. Therefore, it is necessary for engineers and scientists to research the dynamics of these systems to reduce or avoid such problems.

Compared to the finite dimensional dynamics for systems without time delay, time-delay systems have infinite-dimensional dynamics and are usually described by delay differential equations (DDEs). Their stability properties can be analyzed through obtaining the stability charts that show the stable and unstable domains. For example, a stable milling process can be realized by choosing the corresponding parameter from a stability lobe diagram (SLD), which is a function of spindle speed and depth of cut parameters. Thus, more and more attention has been paid on this issue and many analytical and numerical methods have been developed to derive the stability conditions for the system parameters.

By using the D-subdivision method, Bhatt and Hsu [10] determined stability criteria for second-order scalar DDEs. Budak and Altıntaş [11, 12] and Merdol and Altintas [13] proposed a method in frequency domain called multifrequency solution. By employing a shifted Chebyshev polynomial approximation, Butcher et al. [14, 15] presented a new technique to study the stability properties of dynamic systems by obtaining an approximate monodromy matrix. Insperger and Stepan [16–18] proposed a known method called semidiscretization method (SDM), which is based on the discretization of the DDEs and approximates their infinite-dimensional phase space by a finite discrete map in time domain. Bayly et al. [19] carried out a temporal finite element analysis for solving the DDEs, which are written in

the form of a state space model and discretizing the time interval of interest into a finite number of temporal elements. Based on the direct integration scheme, Ding et al. [20], Liu et al. [21], and Jin et al. [22] used a full-discretization method to gain stability chart efficiently. Recently, Khasawneh and Mann [23] and Lehotzky et al. [24] presented a numerical algorithm called spectral element method. This method has good efficiency because of its highly accurate numerical quadratures for the integral terms.

SDM is a known and widely used method to determine stability charts for general time-periodic DDEs arising in different engineering problems. In this paper, based on SDM, a generalized method for periodic DDEs with multiple time-periodic delays is proposed to obtain the stability chart of DDEs. The structure of the paper is as follows. In Section 2, the mathematical model is introduced. In Section 3, two typical examples are used to verify the effectiveness of the proposed method. In Section 4, conclusions with a brief discussion are presented.

2. Mathematical Model

The general form of linear, time-periodic DDEs with multiple time-periodic delays can be expressed as

$$\begin{aligned}\dot{\mathbf{y}}(t) &= \mathbf{A}_0\mathbf{y}(t) + \mathbf{A}(t)\mathbf{y}(t) - \sum_{j=1}^{N}\mathbf{B}_j(t)\mathbf{u}\left(t-\tau_j(t)\right)\\ \mathbf{u}(t) &= \mathbf{D}\mathbf{y}(t),\end{aligned} \tag{1}$$

where $\mathbf{y}(t) \in \mathbb{R}^n$ is the state, $\mathbf{u}(t) \in \mathbb{R}^m$ is the input, $\mathbf{A}_0$ is a constant matrix, $\mathbf{A}(t)$ and $\mathbf{B}_j(t)$, respectively, are $n \times n$ and $n \times m$ periodic coefficient matrices that satisfy $\mathbf{A}(t) = \mathbf{A}(t+T)$ and $\mathbf{B}_j(t) = \mathbf{B}_j(t+T)$, $j = 1, 2, \ldots, N$, and $\tau_j(t) = \tau_j(t+T) > 0$, $\mathbf{D}$ is an $m \times n$ constant matrix, T is the time period, and N is the number of time-delays. Note that (1) can also be written in the form

$$\dot{\mathbf{y}}(t) = \mathbf{A}_0\mathbf{y}(t) + \mathbf{A}(t)\mathbf{y}(t) - \sum_{j=1}^{N}\mathbf{C}_j(t)\mathbf{y}\left(t-\tau_j(t)\right) \tag{2}$$

with $\mathbf{C}_j(t) = \mathbf{B}_j(t)D$.

Consider that the period T is divided into k number of discrete time intervals, such that each interval length $\Delta t = T/k$. Introduce symbol $[t_i, t_{i+1}]$ to represent the ith time interval, $i \in \mathbb{Z}^+$. Here, t_i means the ith time node and is equal to $i\Delta t$. Thus, considering the idea in [2], the averaged delay for the discretization interval $[t_i, t_{i+1}]$ is defined as follows:

$$\tau_{i,j} = \frac{1}{\Delta t}\int_{t_i}^{t_{i+1}}\tau_j(t)\,dt = \tau_{0,j} - \tau_{1,j}c_i, \tag{3}$$

where

$$c_i = \frac{k}{2\pi}\int_{i2\pi/k}^{(i+1)2\pi/k}\sin(t)\,dt, \quad i = 0, 1, \ldots, k-1. \tag{4}$$

The number of intervals $m_{i,j}$ related to the delay item $\tau_{i,j}$ can be approximately obtained by

$$m_{i,j} = \mathrm{int}\left(\frac{\tau_{i,j} + \Delta t/2}{\Delta t}\right), \tag{5}$$

where int$(*)$ indicates the operation that rounds positive number towards zero.

Substituting (3) into (2) and solving it as an ordinary differential equation over the discretization period $[t_i, t_{i+1}]$ with initial condition $x(t_i) = x_i$, the following equation is derived:

$$\begin{aligned}\mathbf{y}(t) = e^{\mathbf{A}_0(t-t_i)}\mathbf{y}_i + \int_{t_i}^{t}\Bigg\{e^{\mathbf{A}_0(t-\xi)}\Bigg[\mathbf{A}(\xi)\mathbf{y}(\xi)\\ - \sum_{j=1}^{N}\mathbf{C}_j(\xi)\mathbf{y}\left(\xi-\tau_{i,j}\right)\Bigg]\Bigg\}d\xi.\end{aligned} \tag{6}$$

Substituting $t = t_{i+1}$ into (6), then it can be equivalently expressed as

$$\begin{aligned}\mathbf{y}\left(t_{i+1}\right) = e^{\mathbf{A}_0\Delta t}\mathbf{y}_i + \int_{t_i}^{t_{i+1}}\Bigg\{e^{\mathbf{A}_0(t_{i+1}-\xi)}\Bigg[\mathbf{A}(\xi)\mathbf{y}(\xi)\\ - \sum_{j=1}^{N}\mathbf{C}_j(\xi)\mathbf{y}\left(\xi-\tau_{i,j}\right)\Bigg]\Bigg\}d\xi.\end{aligned} \tag{7}$$

In $[t_i, t_{i+1}]$, $\mathbf{A}(t)$, $\mathbf{C}_j(t)$, $\mathbf{y}(t)$, and $\mathbf{y}(t-\tau_{i,j})$ are defined as follows:

$$\begin{aligned}\mathbf{A}(t) &= \mathbf{A}_i + \frac{\mathbf{A}_{i+1}-\mathbf{A}_i}{\Delta t}(t-t_i),\\ \mathbf{C}_j(t) &= \mathbf{C}_{i,j} + \frac{\mathbf{C}_{i+1,j}-\mathbf{C}_{i,j}}{\Delta t}(t-t_i),\\ \mathbf{y}(t) &= \mathbf{y}_i + \frac{\mathbf{y}_{i+1}-\mathbf{y}_i}{\Delta t}(t-t_i),\\ \mathbf{y}\left(t-\tau_{i,j}\right) &= \beta_{i,j}\mathbf{y}_{i-m_{i,j}} + \alpha_{i,j}\mathbf{y}_{i+1-m_{i,j}},\end{aligned} \tag{8}$$

where $\mathbf{A}_i = \mathbf{A}(t_i)$, $\mathbf{C}_{i,j} = \mathbf{C}_j(t_i)$, $\mathbf{y}_i = \mathbf{y}(t_i)$, $\alpha_{i,j} = (m_{i,j}\Delta t + \Delta t/2 - \tau_{i,j})/\Delta t$, and $\beta_{i,j} = 1 - \alpha_{i,j}$. Here, it should be noted that the approximation of $\mathbf{y}(t-\tau_{i,j})$ in (8) is the same as that for the so-called zero-order SDM in [2].

Substituting (8) into (7) leads to

$$\begin{aligned}\mathbf{y}_{i+1} &= \left(\Phi_0 + \mathbf{F}_i\right)\mathbf{y}_i + \mathbf{P}_i\mathbf{y}_{i+1}\\ &\quad - \sum_{j=1}^{N}\left(\beta_{i,j}\mathbf{R}_{i,j}\mathbf{y}_{i-m_{i,j}} + \alpha_{i,j}\mathbf{R}_{i,j}\mathbf{y}_{i+1-m_{i,j}}\right),\end{aligned} \tag{9}$$

where

$$\begin{aligned}\mathbf{F}_i &= \left(\Phi_1 - \frac{2}{\Delta t}\Phi_2 + \frac{1}{\Delta t^2}\Phi_3\right)\mathbf{A}_i\\ &\quad + \left(\frac{1}{\Delta t}\Phi_2 - \frac{1}{\Delta t^2}\Phi_3\right)\mathbf{A}_{i+1},\\ \mathbf{P}_i &= \left(\frac{1}{\Delta t}\Phi_2 - \frac{1}{\Delta t^2}\Phi_3\right)\mathbf{A}_i + \left(\frac{1}{\Delta t^2}\Phi_3\right)\mathbf{A}_{i+1},\\ \mathbf{R}_{i,j} &= \left(\Phi_1 - \frac{1}{\Delta t}\Phi_2\right)\mathbf{C}_{i,j} + \left(\frac{1}{\Delta t}\Phi_2\right)\mathbf{C}_{i+1,j}.\end{aligned} \tag{10}$$

Clearly, Φ_0, Φ_1, Φ_2, and Φ_3 can be expressed as follows:

$$\begin{aligned}
\Phi_0 &= e^{\mathbf{A}_0 \Delta t},\\
\Phi_1 &= \int_0^{\Delta t} e^{\mathbf{A}_0(\Delta t - s)} ds = \mathbf{A}_0^{-1}\left(\Phi_0 - \mathbf{I}\right),\\
\Phi_2 &= \int_0^{\Delta t} s e^{\mathbf{A}_0(\Delta t - s)} ds = \mathbf{A}_0^{-1}\left(\Phi_1 - \Delta t \mathbf{I}\right),\\
\Phi_3 &= \int_0^{\Delta t} s^2 e^{\mathbf{A}_0(\Delta t - s)} ds = \mathbf{A}_0^{-1}\left(2\Phi_2 - \Delta t^2 \mathbf{I}\right),
\end{aligned} \tag{11}$$

where $\mathbf{I}$ denotes the identity matrix. Let $M = \max(m_{i.j})$ and

$$\mathbf{Z}_i = \operatorname{col}\left(\mathbf{y}_i, \mathbf{y}_{i-1} \cdots \mathbf{y}_{i-M}\right); \tag{12}$$

then combining (9) and (12), one can be recast into a discrete map as

$$\mathbf{Z}_{i+1} = \mathbf{D}_i \mathbf{Z}_i, \tag{13}$$

where each $\mathbf{D}_i$ matrix is given by

$$\begin{aligned}
\mathbf{D}_i = &\begin{bmatrix}
\mathbf{H}_{i+1}\left(\Phi_0 + \mathbf{F}_i\right) & 0 & \cdots & 0 & 0 & 0\\
\mathbf{I} & 0 & \cdots & 0 & 0 & 0\\
0 & \mathbf{I} & \cdots & 0 & 0 & 0\\
\vdots & \vdots & \ddots & \vdots & \vdots & \vdots\\
0 & 0 & \cdots & \mathbf{I} & 0 & 0\\
0 & 0 & \cdots & 0 & \mathbf{I} & 0
\end{bmatrix}\\
&+ \sum_{j=1}^{N} \begin{bmatrix}
0 & \cdots & -\mathbf{H}_{i+1}\alpha_{i,j}\mathbf{R}_{i,j} & -\mathbf{H}_{i+1}\beta_{i,j}\mathbf{R}_{i,j} & \cdots & 0\\
0 & \cdots & 0 & 0 & \cdots & 0\\
0 & \cdots & 0 & 0 & \cdots & 0\\
\vdots & \vdots & \ddots & \vdots & \vdots & \vdots\\
0 & \cdots & 0 & 0 & \cdots & 0\\
0 & \cdots & 0 & 0 & \cdots & 0
\end{bmatrix},
\end{aligned} \tag{14}$$

where $\mathbf{H}_{i+1} = (\mathbf{I} - \mathbf{P}_i)^{-1}$. The horizontal position of the discrete input matrices $\mathbf{H}_{i+1}\alpha_{i,j}\mathbf{R}_{i,j}$ and $\mathbf{H}_{i+1}\beta_{i,j}\mathbf{R}_{i,j}$ in (14) depends on the value of $m_{i,j}$ corresponding to $\tau_{i,j}$ and they, respectively, begin from the column of $2m_{i,j} - 1$ and $2m_{i,j} + 1$ for a single DOF system as opposed to the column of $4m_{i,j} - 3$ and $4m_{i,j} + 1$ for a two-DOF one.

Based on (13) and (14), the following mathematical expressions can be established by coupling the solutions of the k successive time intervals in period T:

$$\mathbf{V}_k = \mathbf{\Phi}\mathbf{V}_0 = \mathbf{D}_{k-1}\mathbf{D}_{k-2}\cdots\mathbf{D}_1\mathbf{D}_0\mathbf{V}_0, \tag{15}$$

where $\mathbf{\Phi}$ is the Floquet transition matrix that gives the connection between $\mathbf{V}_k$ and $\mathbf{V}_0$. According to the Floquet theory, the stability of the system is determined using the following criterion. If the moduli of all the eigenvalues of the transition matrix $\mathbf{\Phi}$ are less than unity, the system is stable. Otherwise, it is unstable.

Here, it should be noted that the matrix $\mathbf{V}_i$ can be reduced because only the delayed positions show up in the governing equation of the milling process. Thus, the size of the approximation vector in (14) could be reduced by removing the delayed values of the velocities, such that the size of vector $\mathbf{V}_i$ can be decreased to $M + 2$ for a single DOF system and $2M + 4$ for a two-DOF system. This can give some additional improvement in the computational time for the proposed method.

3. Verification of Method

There are several numerical and semianalytical techniques to determine the stability conditions for periodic DDEs. However, most of them were developed with the aim of constructing stability charts for milling processes, such as the analysis of the milling system with runout [25], with variable pitch/helix cutter [26–30], with variable-spindle speed [31–33], or with serrated cutter [34, 35]. In order to verify the proposed method, two typical milling operations are chosen and considered. The first is the varying spindle speed process, which can be described by a DDE with time-periodic delay in general. The other is the milling process with variable pitch cutters, which is often characterized by a DDE with multiple delays. Both methods are known means to influence and to prevent chatter vibration in milling.

3.1. Milling with Varying Spindle Speed. Generally, the mathematical models for milling processes with spindle speed variation can be written as

$$\dot{\mathbf{y}}(t) = \mathbf{A}_0\mathbf{y}(t) + \mathbf{A}(t)\,\mathbf{y}(t) - \mathbf{B}(t)\,\mathbf{y}(t - \tau(t)); \tag{16}$$

that is, (2) is degenerated into one with one-time-periodic delay. For a single DOF system in [2], the matrices in (16) have the form

$$\begin{aligned}
\mathbf{A}_0 &= \begin{bmatrix} 0 & 1 \\ -\omega_n^2 & -2\zeta\omega_n \end{bmatrix},\\
\mathbf{A}(t) = \mathbf{B}(t) &= \begin{bmatrix} 0 & 0 \\ \dfrac{-G(t)}{m} & 0 \end{bmatrix},
\end{aligned} \tag{17}$$

where m is the mode mass, ω_n is the natural frequency, ζ is *the* damping ratios, and $G(t)$ is the specific directional factor and has the form

$$\begin{aligned}
&G(t)\\
&= a_p \sum_{j=1}^{N} g_j(t) \sin\phi_j(t)\left(K_t \cos\phi_j(t) + K_r \sin\phi_j(t)\right),
\end{aligned} \tag{18}$$

where a_p is the axial depth of cut, N is the number of teeth, K_t and K_r are the linearized cutting coefficients in tangential and radial directions, $g_j(t)$ denotes whether the jth tooth is cutting, and the angular position of tooth j is

$$\phi_j(t) = \frac{2\pi}{60}\int_0^t \Omega(s)\, ds + j\frac{2\pi}{N}, \tag{19}$$

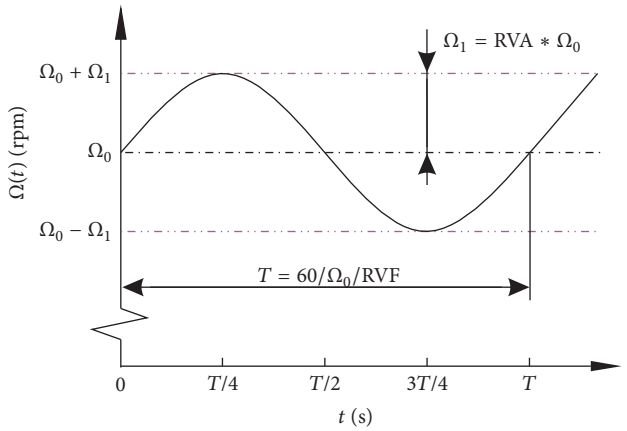

Figure 1: Schematic drawing of the sinusoidal modulation of the spindle speed.

where $\Omega(s)$ is the spindle speed and is assumed to change in the form of a sinusoidal wave, which is periodic at a time period $T = 60/\Omega_0/\text{RVF}$, with a nominal value, Ω_0, and an amplitude $\Omega_1 = \text{RVA} \times \Omega_0$, as shown in Figure 1. For this sinusoidal modulation, the shape function is modeled as

$$\begin{aligned}\Omega(t) &= \Omega_0 + \Omega_1 \sin\left(\frac{2\pi}{T}t\right) \\ &= \Omega_0\left[1 + \text{RVA} \cdot \sin\left(\text{RVF} \cdot \frac{2\pi}{60}\Omega_0 t\right)\right],\end{aligned} \tag{20}$$

where $\text{RVA} = \Omega_1/\Omega_0$ is the ratio of the speed variation amplitude to the nominal spindle speed and $\text{RVF} = 60/(\Omega_0 T)$ is the ratio of the speed variation frequency to the nominal spindle speed.

To illustrate the effectiveness of the approach method for milling with spindle speed, the method and results in [2] are taken into consideration. Here, it should be noted that the delayed term is approximated by a linear function of time and the periodic coefficient is approximated by a piecewise constant function for the method in [2]. However, for the proposed method, the delayed term $\mathbf{y}(\xi - \tau_{i,j})$, the state term $\mathbf{y}(\xi)$, and the periodic terms $\mathbf{A}(\xi)$ and $\mathbf{C}_j(\xi)$ in (7) are all discretized by linear interpolation (see (8)). Thus, different policies are utilized in the process of equation approximations for two methods. Figure 2 illustrates the stability charts that correspond to the milling processes for RVA = 0.1 and for four different RVF values using the proposed method and the method in [2]. The parameters are as follows. The cutting processes using a 4-flute tool ($N = 4$) with zero helix angles are considered under half-immersion up-milling. The cutting force coefficients are $K_t = 800 \times 10^6\,\text{N/m}^2$ and $K_r = 300 \times 10^6\,\text{N/m}^2$. The mode mass is $m = 3.1663\,\text{kg}$, the natural frequency is $\omega_n = 400\,\text{Hz}$, and damping ratios is $\xi = 0.02$. It can be seen from Figure 2 that the results obtained via the proposed method in this paper are in close agreement with those in [2].

Meanwhile, the computational times corresponding to every graphic in Figure 2 are also recorded to evaluate the efficiency of proposed method. Here, considering the assumption $q_1 T = q_2 \tau_0$ (τ_0 is the tooth passing period) with q_1 and q_2 being relatively prime [2] and the equation $q_1/q_2 = \text{RVF}/N$ obtained consequently, if the resolution of τ_0 is adopted as 40 and $q_1 = 1$, the resolutions of period T are 320, 800, 1600, and 3200 for RVF = 0.5, 0.2, 0.1, and 0.05, respectively. For a 200×100 grid of the spindle speed and the depth of cut and a personal computer (Intel(R) Core(TM) i5-2300, 2.8 GHz, 3 GB), the computational times are, respectively, 436 s, 1026 s, 2012 s, and 4132 s corresponding to RVF = 0.5, 0.2, 0.1, and 0.05 for the proposed method as opposed to 1953 s, 4757 s, 9185 s, and 18341 s for the method in [2] using our own codes. Time costs reduce nearly by 70% for every case. Obviously, the low computational cost of our method is illustrated. The reason about the cost reduction can be explained as follows. The matrices Φ_0, Φ_1, Φ_2, and Φ_3 in (11) are dependent on spindle speed but on depth of cut. Consequently, they are not needed to calculate in the process of sweeping the range of the depth of cut for the proposed method. However, this is also necessary for the method in [2]. Thus, for a parameter plane formed by the spindle speed and the cutting depth and divided into a $N_s \times N_d$ size grid, the method in [2] must be calculated $N_s \times N_d \times k$ times to obtain a stability chart, but only N_s times for the method in this paper.

3.2. Milling with Variable Pitch Cutter. Considering a system for milling process with variable pitch cutter [29, 30] as shown in Figure 3, the mathematical models can be written as

$$\dot{\mathbf{y}}(t) = \mathbf{A}_0\mathbf{y}(t) + \mathbf{A}(t)\,\mathbf{y}(t) - \sum_{j=1}^{N}\mathbf{B}_j(t)\,\mathbf{y}\left(t - \tau_j\right); \tag{21}$$

that is, the original system of (2) is degenerated into one with multiple delays in this case. τ_j is the pitch period corresponding to the pitch angle $\boldsymbol{\psi}$ (see the right graphic of Figure 3), and the matrices $\mathbf{A}_0$, $\mathbf{A}(t)$, and $\mathbf{B}_j(t)$ in (21) have the form

$$\begin{aligned}\mathbf{A}_0 &= \begin{bmatrix} 0 & 0 & 1 & 0 \\ 0 & 0 & 0 & 1 \\ -\omega_{nx}^2 & 0 & -2\zeta_x\omega_{nx} & 0 \\ 0 & -\omega_{ny}^2 & 0 & -2\zeta_y\omega_{ny} \end{bmatrix}, \\ \mathbf{A}(t) &= \sum_{j=1}^{N} B_j(t), \\ \mathbf{B}_j(t) &= \begin{bmatrix} 0 & 0 & 0 & 0 \\ 0 & 0 & 0 & 0 \\ -\dfrac{a_p}{m_x h_{xx,j}(t)} & -\dfrac{a_p}{m_y h_{xy,j}(t)} & 0 & 0 \\ -\dfrac{a_p}{m_x h_{yx,j}(t)} & -\dfrac{a_p}{m_y h_{yy,j}(t)} & 0 & 0 \end{bmatrix},\end{aligned} \tag{22}$$

where ζ_x and ζ_y are the damping ratios, ω_x and ω_y are the natural frequencies, and m_x and m_y are the modal masses of the cutter. $h_{xx,j}(t)$, $h_{xy,j}(t)$, $h_{yx,j}(t)$,, and $h_{yy,j}(t)$ are the cutting force coefficients for the jth tooth defined as

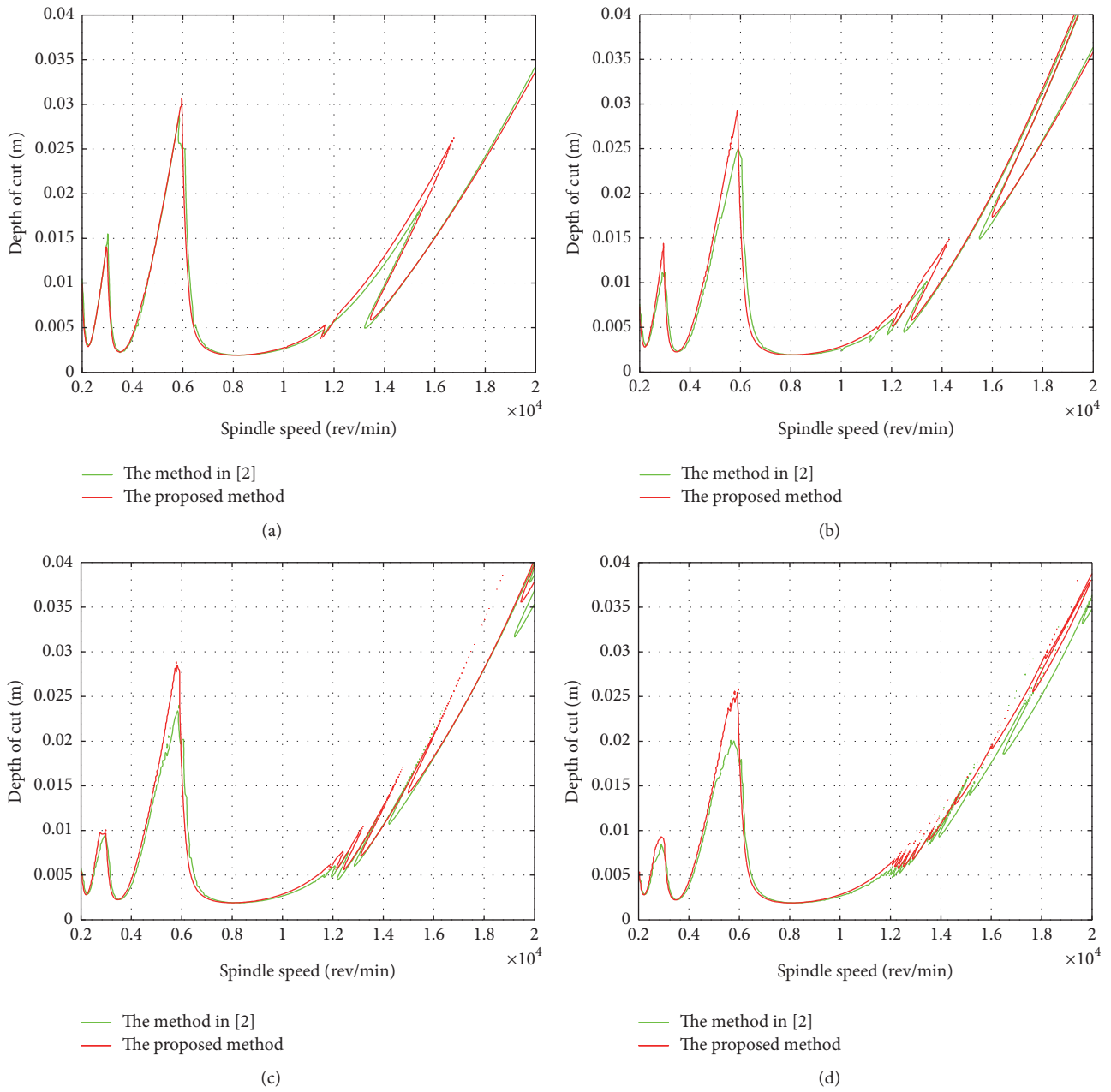

Figure 2: Comparison of stability charts for milling processes with sinusoidal spindle speed modulation with RVA = 0.1 in the high-speed domain: (a) RVF = 0.5; (b) RVF = 0.2; (c) RVF = 0.1; (d) RVF = 0.05.

$$
\begin{aligned}
h_{xx,j}(t) &= g\left(\phi_j(t)\right)\left(K_t\cos\left(\phi_j(t)\right)+K_r\sin\left(\phi_j(t)\right)\right)\\
&\quad\cdot\sin\left(\phi_j(t)\right),\\
h_{xy,j}(t) &= g\left(\phi_j(t)\right)\left(K_t\cos\left(\phi_j(t)\right)+K_r\sin\left(\phi_j(t)\right)\right)\\
&\quad\cdot\cos\left(\phi_j(t)\right),\\
h_{yx,j}(t) &= g\left(\phi_j(t)\right)\\
&\quad\cdot\left(-K_t\sin\left(\phi_j(t)\right)+K_r\cos\left(\phi_j(t)\right)\right)\sin\left(\phi_j(t)\right),\\
h_{yy,j}(t) &= g\left(\phi_j(t)\right)\\
&\quad\cdot\left(-K_t\sin\left(\phi_j(t)\right)+K_r\cos\left(\phi_j(t)\right)\right)\cos\left(\phi_j(t)\right).
\end{aligned}
\tag{23}
$$

To illustrate the performance of the proposed approach on uniform and variable pitch milling tools, the frequency-domain method published in [29] is considered. The comparison of the results using the proposed approach and the method [29] is carried out for both uniform and variable pitch cutter milling, as shown in Figure 4. The main system parameters are down-milling, half-immersion, the number of the cutter teeth which is $N = 4$, the natural frequencies which are $\omega_x = 563.6$ Hz and $\omega_y = 516.21$ Hz, the damping ratios which are $\zeta_x = 0.0558$ and $\zeta_y = 0.025$, the modal masses which are $m_x = 1.4986$ kg and $m_y = 1.199$ kg, and the cutting force coefficients which are $K_t = 679 \times 10^6$ N/m^2 and

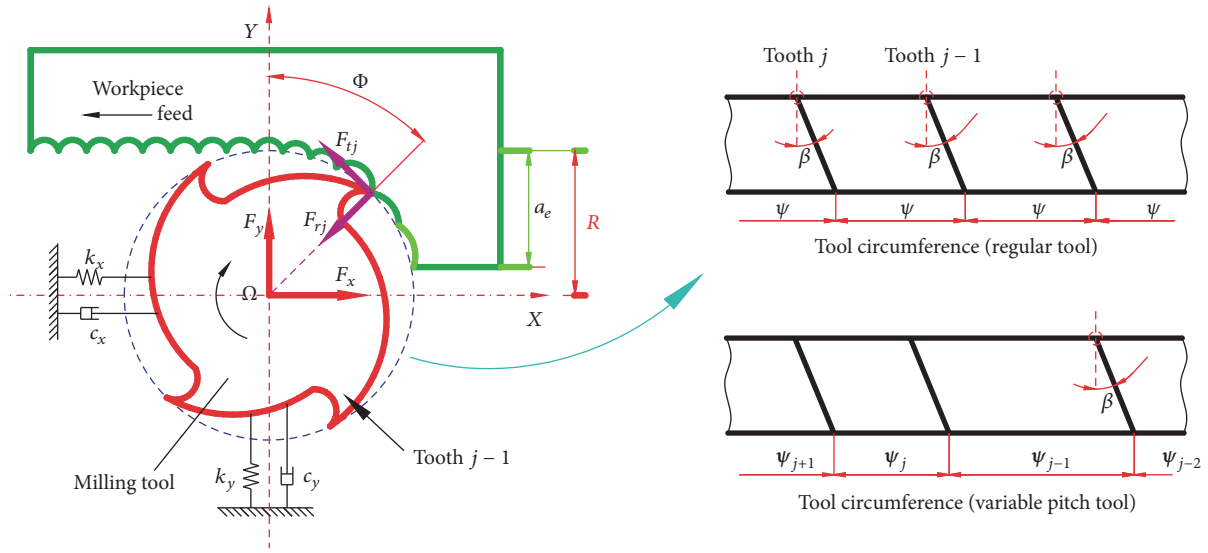

FIGURE 3: Schematic mechanical model of a system for milling process with variable pitch cutter.

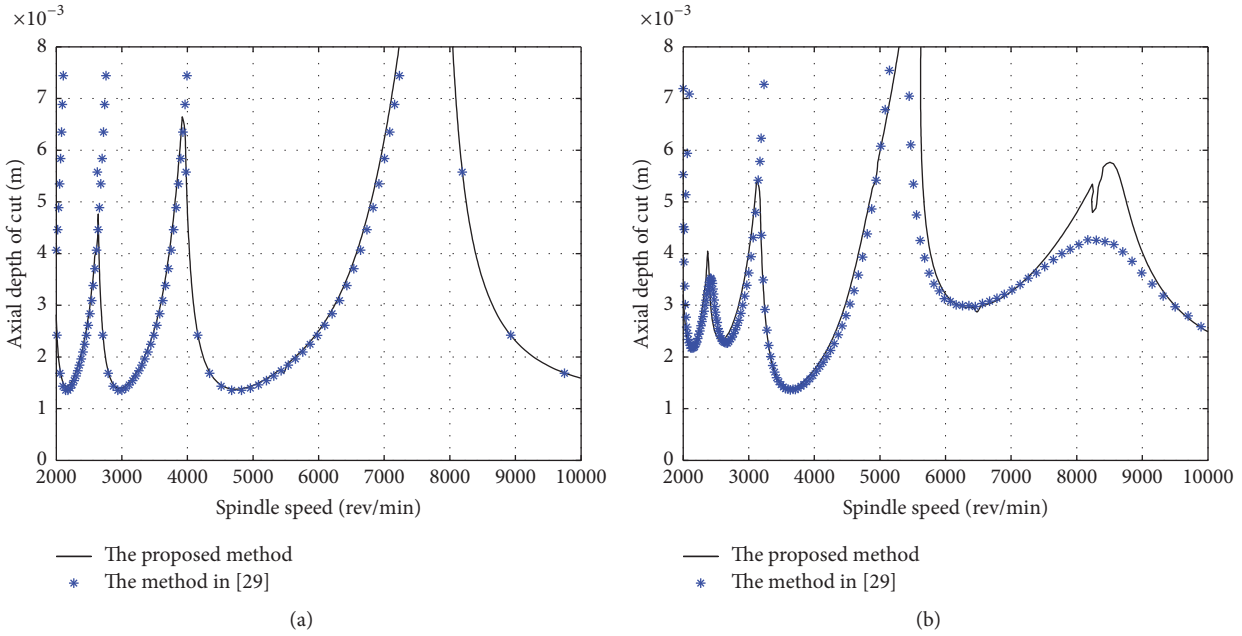

FIGURE 4: Comparison of the predicted stability lobes: (a) uniform pitch cutter with $\boldsymbol{\psi} = [90^\circ, 90^\circ, 90^\circ, 90^\circ]$ and (b) variable pitch cutter with $\boldsymbol{\psi} = [70^\circ, 110^\circ, 70^\circ, 110^\circ]$.

$K_t = 256 \times 10^6\,\mathrm{N/m^2}$. It can be seen from Figure 4(a) that the proposed method agrees closely with the results of analytical method for the uniform pitch cutter milling. For the variable pitch cutter as shown in Figure 4(b), two methods gain consistent predicting results, except for the high-speed domain at approximately 8500 rpm, where a clear deviation occurred. Reference [27] chose one point ($a_p = 5$ mm and $\Omega = 8500$ rpm) in this deviation and showed its stabilization by time-domain simulations. The reason of this phenomenon is as follows. The proposed method is based on the time-periodic cutting force coefficients (see (23)), rather than the simplified time-averaged ones in [29]. Thus, the stability prediction by our method is more reasonable and has better accuracy.

4. Conclusion

In this work, an improved semidiscretization algorithm is proposed to obtain the stability char for DDEs with multiple time-periodic delays. Two milling examples, variable-spindle speed milling system with one-time-periodic delay and variable pitch cutter milling system with multiple delays,

are utilized to demonstrate effectiveness of the proposed algorithm. Through the comparison with prior works, it is found that the results gained by the presented method in this paper are in close agreement with those existing in the past literature. Moreover, the proposed method also has good computational efficiency. Here, it should be noted that if discussing the milling process only, the proposed method is a generalized algorithm, which can consider the milling processes with variable pitch cutter and variable-spindle speed simultaneously.

Conflicts of Interest

The authors declare that there are no conflicts of interest regarding the publication of this paper.

Acknowledgments

This work was supported by the National Natural Science Foundation of China (51405343, 51505336, and 11702192), Tianjin Research Program of Application Foundation and Advanced Technology (15JCQNJC05000 and 15JCQNJC05200), Innovation Team Training Plan of Tianjin Universities and Colleges (TD12-5043), and Tianjin Science and Technology Planning Project (15ZXZNGX00220).

References

[1] Y. Altintas, *Manufacturing Automation*, vol. 298, Cambridge University Press, New York, NY, USA, 2012.

[2] T. Insperger and G. Stépán, *Semi-Discretization for Time-Delay Systems: Stability and Engineering Applications*, vol. 178 of *Applied Mathematical Sciences*, Springer Science & Business Media, New York, NY, USA, 2011.

[3] G. Stépán, "Delay, Nonlinear Oscillations and Shimmying Wheels," in *Proceedings of the IUTAM Symposium on New Applications of Nonlinear and Chaotic Dynamics in Mechanics*, vol. 63, pp. 373–386, Springer, New York, NY, USA.

[4] D. Takács, G. Stépán, and S. J. Hogan, "Isolated large amplitude periodic motions of towed rigid wheels," *Nonlinear Dynamics*, vol. 52, no. 1-2, pp. 27–34, 2008.

[5] J. Sun, "Delay-dependent stability criteria for time-delay chaotic systems via time-delay feedback control," *Chaos, Solitons & Fractals*, vol. 21, no. 1, pp. 143–150, 2004.

[6] J. H. Park and O. M. Kwon, "A novel criterion for delayed feedback control of time-delay chaotic systems," *Chaos, Solitons & Fractals*, vol. 23, no. 2, pp. 495–501, 2005.

[7] A. Verdugo and R. Rand, "Hopf bifurcation in a DDE model of gene expression," *Communications in Nonlinear Science and Numerical Simulation*, vol. 13, no. 2, pp. 235–242, 2008.

[8] A. Ruiz-Herrera, "Chaos in delay differential equations with applications in population dynamics," *Discrete and Continuous Dynamical Systems- Series A*, vol. 33, no. 4, pp. 1633–1644, 2013.

[9] J. Yan, A. Zhao, and L. Peng, "Oscillation of impulsive delay differential equations and applications to population dynamics," *The ANZIAM Journal*, vol. 46, no. 4, pp. 545–554, 2005.

[10] S. J. Bhatt and C. S. Hsu, "Stability criteria for second-order dynamical systems with time lag," vol. 33, pp. 113–118, 1966.

[11] E. Budak and Y. Altıntaş, "Analytical prediction of chatter stability in milling, Part I: General formulation," *Journal of Dynamic Systems, Measurement, and Control*, vol. 120, pp. 22–30, 1998.

[12] E. Budak and Y. Altıntaş, "Analytical prediction of chatter stability in milling, Part II: application of the general formulation to common milling systems," *Journal of Dynamic Systems, Measurement, and Control*, vol. 120, no. 1, pp. 31–36, 1998.

[13] S. D. Merdol and Y. Altintas, "Multi frequency solution of chatter stability for low immersion milling," *Journal of Manufacturing Science and Engineering*, vol. 126, no. 3, pp. 459–466, 2004.

[14] E. A. Butcher and O. A. Bobrenkov, "On the Chebyshev spectral continuous time approximation for constant and periodic delay differential equations," *Communications in Nonlinear Science and Numerical Simulation*, vol. 16, no. 3, pp. 1541–1554, 2011.

[15] E. A. Butcher, H. Ma, E. Bueler, V. Averina, and Z. Szabo, "Stability of linear time-periodic delay-differential equations via Chebyshev polynomials," *International Journal for Numerical Methods in Engineering*, vol. 59, no. 7, pp. 895–922, 2004.

[16] T. Insperger and G. Stepan, "Semi-discretization method for delayed systems," *International Journal for Numerical Methods in Engineering*, vol. 55, no. 5, pp. 503–518, 2002.

[17] T. Insperger and G. Stepan, "Updated semi-discretization method for periodic delay-differential equations with discrete delay," *International Journal for Numerical Methods in Engineering*, vol. 61, no. 1, pp. 117–141, 2004.

[18] T. Insperger, "Full-discretization and semi-discretization for milling stability prediction: some comments," *International Journal of Machine Tools and Manufacture*, vol. 50, no. 7, pp. 658–662, 2010.

[19] P. V. Bayly, J. E. Halley, B. P. Mann, and M. A. Davies, "Stability of interrupted cutting by temporal finite element analysis," *Transactions of the ASME—Journal of Manufacturing Science and Engineering*, vol. 125, no. 2, pp. 220–225, 2003.

[20] Y. Ding, L. Zhu, X. Zhang, and H. Ding, "A full-discretization method for prediction of milling stability," *International Journal of Machine Tools and Manufacture*, vol. 50, no. 5, pp. 502–509, 2010.

[21] Y. Liu, D. Zhang, and B. Wu, "An efficient full-discretization method for prediction of milling stability," *International Journal of Machine Tools and Manufacture*, vol. 63, pp. 44–48, 2012.

[22] G. Jin, H. Qi, Y. Cai, and Q. Zhang, "Stability prediction for milling process with multiple delays using an improved semi-discretization method," *Mathematical Methods in the Applied Sciences*, vol. 39, no. 4, pp. 949–958, 2016.

[23] F. A. Khasawneh and B. P. Mann, "Stability of delay integro-differential equations using a spectral element method," *Mathematical and Computer Modelling*, vol. 54, no. 9-10, pp. 2493–2503, 2011.

[24] D. Lehotzky, T. Insperger, and G. Stepan, "Extension of the spectral element method for stability analysis of time-periodic delay-differential equations with multiple and distributed delays," *Communications in Nonlinear Science and Numerical Simulation*, vol. 35, pp. 177–189, 2016.

[25] M. Wan, W.-H. Zhang, J.-W. Dang, and Y. Yang, "A unified stability prediction method for milling process with multiple delays," *International Journal of Machine Tools and Manufacture*, vol. 50, no. 1, pp. 29–41, 2010.

[26] N. D. Sims, B. Mann, and S. Huyanan, "Analytical prediction of chatter stability for variable pitch and variable helix milling tools," *Journal of Sound and Vibration*, vol. 317, pp. 664–686, 2008.

[27] G. Jin, Q. Zhang, S. Hao, and Q. Xie, "Stability prediction of milling process with variable pitch cutter," *Mathematical Problems in Engineering*, vol. 2013, Article ID 932013, 2013.

[28] G. Jin, Q. Zhang, S. Hao, and Q. Xie, "Stability prediction of milling process with variable pitch and variable helix cutters," *Proceedings of the Institution of Mechanical Engineers, Part C: Journal of Mechanical Engineering Science*, vol. 228, no. 2, pp. 281–293, 2014.

[29] Y. Altintaş, S. Engin, and E. Budak, "Analytical stability prediction and design of variable pitch cutters," *Transactions of the ASME—Journal of Manufacturing Science and Engineering*, vol. 121, no. 2, pp. 173–178, 1999.

[30] G. Jin, Q. Zhang, H. Qi, and B. Yan, "A frequency-domain solution for efficient stability prediction of variable helix cutters milling," *Proceedings of the Institution of Mechanical Engineers, Part C: Journal of Mechanical Engineering Science*, vol. 228, no. 15, pp. 2702–2710, 2014.

[31] T. Insperger and G. Stéfán, "Stability analysis of turning with periodic spindle speed modulation via semidiscretization," *Journal of Vibration and Control*, vol. 10, no. 12, pp. 1835–1855, 2004.

[32] M. Zatarain, I. Bediaga, J. Muñoa, and R. Lizarralde, "Stability of milling processes with continuous spindle speed variation: analysis in the frequency and time domains, and experimental correlation," *CIRP Annals—Manufacturing Technology*, vol. 57, no. 1, pp. 379–384, 2008.

[33] S. Seguy, T. Insperger, L. Arnaud, G. Dessein, and G. Peigné, "On the stability of high-speed milling with spindle speed variation," *International Journal of Advanced Manufacturing Technology*, vol. 48, no. 9-12, pp. 883–895, 2010.

[34] Z. Dombovari, Y. Altintas, and G. Stepan, "The effect of serration on mechanics and stability of milling cutters," *International Journal of Machine Tools and Manufacture*, vol. 50, no. 6, pp. 511–520, 2010.

[35] Z. Dombovari and G. Stepan, "The effect of helix angle variation on milling stability," *Journal of Manufacturing Science and Engineering, Transactions of the ASME*, vol. 134, no. 5, Article ID 051015, 2012.

Hindawi
Mathematical Problems in Engineering
Volume 2017, Article ID 1057909, 16 pages
https://doi.org/10.1155/2017/1057909

Research Article

Analysis and Design of Associative Memories for Memristive Neural Networks with Deviating Argument

Jin-E Zhang

Hubei Normal University, Hubei 435002, China

Correspondence should be addressed to Jin-E Zhang; zhang86021205@163.com

Received 19 April 2017; Revised 20 June 2017; Accepted 2 July 2017; Published 9 August 2017

Academic Editor: Radek Matušů

We investigate associative memories for memristive neural networks with deviating argument. Firstly, the existence and uniqueness of the solution for memristive neural networks with deviating argument are discussed. Next, some sufficient conditions for this class of neural networks to possess invariant manifolds are obtained. In addition, a global exponential stability criterion is presented. Then, analysis and design of autoassociative memories and heteroassociative memories for memristive neural networks with deviating argument are formulated, respectively. Finally, several numerical examples are given to demonstrate the effectiveness of the obtained results.

1. Introduction

In recent decades, analysis and design of neurodynamic systems have received much attention [1–16]. Specifically, neurodynamics of associative memories is a hot research issue [9–16]. Associative memories refer to brain-inspired computing designed to store a set of prototype patterns such that the stored patterns can be retrieved with the recalling probes containing sufficient information about the contents of patterns. In associative memories, for any given probe (e.g., noisy or corrupted version of a prototype pattern), the retrieval dynamics can converge to an ideal equilibrium point representing the prototype pattern. At present, system analysts have two main theories for explaining strange dynamical behaviors in recalling processes: autoassociative memories and heteroassociative memories [12, 13]. Two types of methods are usually used for solving problems in regard to analysis and synthesis of associative memories. The first is when neurodynamic systems are multistable, and then system states may converge to locally stable equilibrium points, and these equilibrium points are encoded as the memorized patterns. The second is when neurodynamic systems are globally monostable, and then the memorized patterns are associated with the external input patterns.

As we know, the human brain is believed to be the most powerful information processor because of its structure of synapses. Actually, there is always a high demand for a single device to emulate artificial synaptic functions. Using a memristor, essential synaptic plasticity and learning behaviors can be mimicked. By integrating memristors into a large-scale neuromorphic circuit, memristive neural networks based neuromorphic circuits demonstrate spike-timing-dependent plasticity (a form of the Hebbian learning rule) [17–21]. From the viewpoint of theory and experiment, a memristive neural network model is a state-dependent switching system. On the other hand, this new dynamical system shows many of the characteristic features of magnetic tunnel junction [19, 20]. For these reasons, system analysis and integration for memristive neural networks will be extremely tricky. For the moment, there are two major methods for qualitative analysis of memristive neural networks. One is the differential inclusions approach [17–20], and the other is the fuzzy uncertainty approach [21]. For the differential inclusions approach, the core idea is to integrate a switched network cluster. For the fuzzy uncertainty approach, the central idea is to divide multijump network flows into a continuous subsystem and bounded subsystem. The two kinds of analysis frameworks are just the type and level of points, not the merits of good points of difference. From the perspective of cybernetics, many reported analytical skills are merely a breakthrough of system theory more than substance. How to develop more

effective analysis methods for memristive neural networks is worth studying.

For the past few years, hybrid dynamic systems have remained one of the most active fields of research in the control community [22–30]. For instance, to describe the stationary distribution of temperature along the length of a wire that is bended, the nonlinear dynamic model with deviating argument is often used. The right-hand side in nonlinear systems with deviating argument features a combination of continuous and discrete systems. Thus, nonlinear systems with deviating argument unify the advanced and retarded systems. Because of this property, related works on the control strategies for nonlinear systems with deviating argument are relatively rare. Viewed from systems involving the interplay, differential equations and difference equations are included in the nonlinear systems with deviating argument [28–30]. However, it is still obvious that many basic issues on nonlinear systems with deviating argument remain to be addressed, such as nonlinear dynamics, systems design, and analysis.

Inspired by the above discussions, the goal of this paper is to formulate the analysis and design of associative memories for a class of memristive neural networks with deviating argument. On the whole, the highlights of this paper can be outlined as follows:

(1) Sufficient conditions are derived to ascertain the existence, uniqueness, and global exponential stability of the solution for memristive neural networks with deviating argument.

(2) The synthetic mechanism of the analysis and design of associative memories for a general class of memristive neural networks with deviating argument is revealed.

(3) A uniform associative memories model, which unites autoassociative memories and heteroassociative memories, is proposed for memristive neural networks with deviating argument.

In addition, it should be noted that when special and strict conditions are exerted, associative memories' performance of neural networks is usually limited. Therefore, the methods applicable to conventional stability analysis of neural networks cannot be directly employed to investigate the associative memories for memristive neural networks. Moreover, the study of dynamics for memristive neural networks with deviating argument is not an easy work, since the conditions for dynamics of neural networks cannot be simply utilized to analyze hybrid dynamic systems with deviating argument. In this paper, according to the fuzzy uncertainty approach, in combination with the theories of set-valued maps and differential inclusions, analysis and design of associative memories for memristive neural networks with deviating argument are described in detail.

The rest of the paper is arranged as follows. Design problem and preliminaries are given in Section 2. Main results are stated in Section 3. In Section 4, several numerical examples are presented. Finally, concluding remarks are given in Section 5.

2. Design Problem and Preliminaries

2.1. Problem Description. Let $\Omega = \{\beta = (\beta_1, \beta_2, \ldots, \beta_n)^T \mid \beta_i = \{-p, p\},\ i = 1, 2, \ldots, n\}$ be the set of n-dimensional bipolar vectors, where p is a positive constant and T denotes the transpose of a vector or matrix. The problem considered is described as follows.

Given l ($l \leq 2^n$) pairs of bipolar vectors $(u^{(1)}, q^{(1)})$, $(u^{(2)}, q^{(2)}), \ldots, (u^{(l)}, q^{(l)})$, where $u^{(r)}, q^{(r)} \in \Omega$, for $r = 1, 2, \ldots, l$, design an associative memory model which satisfies the notion that the output of the model will converge to the corresponding pattern $q^{(r)}$ when $u^{(r)}$ is fed to the model input as a memory pattern.

Definition 1. The neural network is said to be an autoassociative memory if $u^{(r)} = q^{(r)}$ and a heteroassociative memory if $u^{(r)} \neq q^{(r)}$, for $r = 1, 2, \ldots, l$.

In this paper, let N be the natural number set; the norm of vector $x = (x_1, x_2, \ldots, x_n)^T$ is defined as $\|x\| = \sum_{i=1}^{n} |x_i|$. Denote $\mathfrak{R}^n$ as the n-dimensional Euclidean space. Fix two real number sequences $\{\eta_k\}$, $\{\vartheta_k\}$, $k \in N$, satisfying $\eta_k < \eta_{k+1}$, $\eta_k \leq \vartheta_k \leq \eta_{k+1}$, and $\lim_{k \to +\infty} \eta_k = +\infty$.

2.2. Model. Consider the following neural network model:

$$\begin{aligned} \dot{x}(t) &= -Ax(t) + B(x(t))\, f(x(t)) \\ &\quad + C(x(t))\, f(x(\gamma(t))) + \mathbb{E}u^{(r)}, \\ w(t) &= f(x(t)), \\ &\qquad\qquad r = 1, 2, \ldots, l, \end{aligned} \tag{1}$$

where $x(t) = (x_1(t), x_2(t), \ldots, x_n(t))^T \in \mathfrak{R}^n$ is the neuron state, $A = \mathrm{diag}(a_1, a_2, \ldots, a_n)$, which is a constant diagonal matrix with $a_i > 0$, $i \in \{1, 2, \ldots, n\}$, indicates the self-inhibition matrix, $B(x(t)) = (b_{ij}(x_j(t)))_{n \times n}$ and $C(x(t)) = (c_{ij}(x_j(t)))_{n \times n}$ are connection weight matrices at time t and $\gamma(t)$, respectively, $b_{ij}(x_j(t))$ and $c_{ij}(x_j(t))$ are defined by

$$\begin{aligned} b_{ij}(x_j(t)) &= \begin{cases} \widehat{b}_{ij}, & |x_j(t)| > T_j, \\ \check{b}_{ij}, & |x_j(t)| < T_j, \end{cases} \\ c_{ij}(x_j(t)) &= \begin{cases} \widehat{c}_{ij}, & |x_j(t)| > T_j, \\ \check{c}_{ij}, & |x_j(t)| < T_j, \end{cases} \end{aligned} \tag{2}$$

for $i, j = 1, 2, \ldots, n$, and $b_{ij}(\pm T_j) = \widehat{b}_{ij}$ or $\check{b}_{ij}$, $c_{ij}(\pm T_j) = \widehat{c}_{ij}$ or $\check{c}_{ij}$, where $T_j > 0$ represents the switching jump, and $\widehat{b}_{ij}, \check{b}_{ij}, \widehat{c}_{ij}$, and $\check{c}_{ij}$ are all constants. $f(x(\cdot)) = (f_1(x_1(\cdot)), f_2(x_2(\cdot)), \ldots, f_n(x_n(\cdot)))^T$ is the activation function. The deviating function $\gamma(t) = \vartheta_k$, when $t \in [\eta_k, \eta_{k+1})$ for any $k \in N$. $\mathbb{E}$ stands for a transform matrix of order n satisfying $\mathbb{E}u^{(r)} = q^{(r)}$ for $r = 1, 2, \ldots, l$. $u^{(r)}$ and $q^{(r)}$ indicate the external input pattern and the corresponding memorized pattern, respectively. $w(t) = (w_1(t), w_2(t), \ldots, w_n(t))^T$ is the output of (1) corresponding to $u^{(r)}$.

Neural network model (1) is called an associative memory if the output $w(t)$ converges to $q^{(r)}$.

Obviously, neural network model (1) is of hybrid type: switching and mixed. When $|x_j(t)| > T_j$, $b_{ij}(x_j(t)) = \widehat{b}_{ij}$, $c_{ij}(x_j(t)) = \widehat{c}_{ij}$. When $|x_j(t)| < T_j$, $b_{ij}(x_j(t)) = \check{b}_{ij}$, $c_{ij}(x_j(t)) = \check{c}_{ij}$. From this perspective, (1) is a switching system. On the other hand, for any fixed interval $[\eta_k, \eta_{k+1})$, when $\gamma(t) = \vartheta_k < t < \eta_{k+1}$, neural network model (1) is a retarded system. When $\eta_k \le t < \gamma(t) = \vartheta_k$, neural network model (1) is an advanced system. Then. from this point of view, (1) is a mixed system.

For neural network model (1), the conventional definition of solution for differential equations cannot apply here. To tackle this problem, the solution concept for differential equations with deviating argument is introduced [24–30]. According to this theory, a solution $x(t) = (x_1(t), x_2(t), \ldots, x_n(t))^T$ of (1) is a consecutive function such that (1) $\dot{x}(t)$ exists on $[0, +\infty)$, except at the points η_k, $k \in N$, where a one-sided derivative exists, and (2) $x(t)$ satisfies (1) within each interval (η_k, η_{k+1}), $k \in N$.

In this paper, the activation functions are selected as

$$f_i(\chi) = \sum_{\ell=1}^{2} (-1)^{\ell} \frac{p}{2d} \left(\left| \chi + z_{\ell}^{(i)} \right| - \left| \chi - z_{\ell}^{(i)} \right| \right), \quad i = 1, 2, \ldots, n, \tag{3}$$

where $p > 0$ and $d > 0$ are used to adjust the slope and corner point of activation functions and $z_1^{(i)} = T_i$, $z_2^{(i)} = T_i + d$.

It is easy to see that $f_i(\cdot)$ satisfies $f_i(\pm T_i) = 0$ and

$$\left| f_i(l_1) - f_i(l_2) \right| \le \alpha \left| l_1 - l_2 \right|, \quad i = 1, 2, \ldots, n, \tag{4}$$

for any $l_1, l_2 \in (-\infty, +\infty)$, where $\alpha = p/d$.

For technical convenience, denote $\overline{b}_{ij} = \max\{|\widehat{b}_{ij}|, |\check{b}_{ij}|\}$, $b_{ij}^0 = (1/2)(\widehat{b}_{ij} + \check{b}_{ij})$, $b_{ij}^+ = (1/2)|\widehat{b}_{ij} + \check{b}_{ij}|$, $b_{ij}^- = (1/2)|\widehat{b}_{ij} - \check{b}_{ij}|$, $\overline{c}_{ij} = \max\{|\widehat{c}_{ij}|, |\check{c}_{ij}|\}$, $c_{ij}^0 = (1/2)(\widehat{c}_{ij} + \check{c}_{ij})$, $c_{ij}^+ = (1/2)|\widehat{c}_{ij} + \check{c}_{ij}|$, $c_{ij}^- = (1/2)|\widehat{c}_{ij} - \check{c}_{ij}|$, and $S_i = \max\{|\widehat{b}_{ii} p - a_i d|, |\check{b}_{ii} p - a_i d|\}$, for $i, j = 1, 2, \ldots, n$. Let $S_b = \max_{1 \le i \le n}(a_i + \sum_{j=1}^{n} \alpha(b_{ji}^+ + b_{ji}^-))$, $S_b^- = \min_{1 \le i \le n}(a_i - \sum_{j=1}^{n}(b_{ji}^+ + b_{ji}^-)\alpha)$, and $S_c = \max_{1 \le i \le n}(\sum_{j=1}^{n} \alpha(c_{ji}^+ + c_{ji}^-))$. $\overline{co}\{\widehat{\mathscr{M}}, \check{\mathscr{M}}\}$ denotes the convex closure of a set constituted by real numbers $\widehat{\mathscr{M}}$ and $\check{\mathscr{M}}$.

2.3. Autoassociative Memories. From Definition 1, matrix $\mathbb{E}$ is selected as an identity matrix when designing autoassociative memories (i.e., $\mathbb{E}u^{(r)} = u^{(r)} = q^{(r)}$ for $r = 1, 2, \ldots, l$). For the convenience of analysis and formulation in autoassociative memories, neural network model (1) can be rewritten in component form:

$$\dot{x}_i(t) = -a_i x_i(t) + \sum_{j=1}^{n} b_{ij}\left(x_j(t)\right) f_j\left(x_j(t)\right) + \sum_{j=1}^{n} c_{ij}\left(x_j(t)\right) f_j\left(x_j(\gamma(t))\right) + u_i,$$

$$w_i(t) = f_i\left(x_i(t)\right), \quad i = 1, 2, \ldots, n. \tag{5}$$

2.4. Properties. For neural network model (1), we consider the following set-valued maps:

$$K\left[b_{ij}\left(x_j(t)\right)\right] = \begin{cases} \widehat{b}_{ij}, & \left|x_j(t)\right| > T_j, \\ \overline{co}\left\{\widehat{b}_{ij}, \check{b}\right\}, & \left|x_j(t)\right| = T_j, \\ \check{b}_{ij}, & \left|x_j(t)\right| < T_j, \end{cases} \tag{6}$$

$$K\left[c_{ij}\left(x_j(t)\right)\right] = \begin{cases} \widehat{c}_{ij}, & \left|x_j(t)\right| > T_j, \\ \overline{co}\left\{\widehat{c}_{ij}, \check{c}\right\}, & \left|x_j(t)\right| = T_j, \\ \check{c}_{ij}, & \left|x_j(t)\right| < T_j, \end{cases} \tag{7}$$

for $i, j = 1, 2, \ldots, n$.

Based on the theory of differential inclusions [17–20], from (5), we can get

$$\dot{x}_i(t) \in -a_i x_i(t) + \sum_{j=1}^{n} K\left[b_{ij}\left(x_j(t)\right)\right] f_j\left(x_j(t)\right) + \sum_{j=1}^{n} K\left[c_{ij}\left(x_j(t)\right)\right] f_j\left(x_j(\gamma(t))\right) + u_i, \tag{8}$$

or, equivalently, there exist $b_{ij}^*(x_j(t)) \in K[b_{ij}(x_j(t))]$ and $c_{ij}^*(x_j(t)) \in K[c_{ij}(x_j(t))]$ such that

$$\dot{x}_i(t) = -a_i x_i(t) + \sum_{j=1}^{n} b_{ij}^*\left(x_j(t)\right) f_j\left(x_j(t)\right) + \sum_{j=1}^{n} c_{ij}^*\left(x_j(t)\right) f_j\left(x_j(\gamma(t))\right) + u_i, \quad i = 1, 2, \ldots, n, \tag{9}$$

for almost all $t \in [0, +\infty)$.

Employing the fuzzy uncertainty approach [21], neural network model (5) can be expressed as follows:

$$\dot{x}_i(t) = -a_i x_i(t) + \sum_{j=1}^{n} b_{ij}^0 f_j\left(x_j(t)\right) + \sum_{j=1}^{n} c_{ij}^0 f_j\left(x_j(\gamma(t))\right) + u_i + \sum_{j=1}^{n} \delta_{ij}^b\left(x_j(t)\right) b_{ij}^- f_j\left(x_j(t)\right) + \sum_{j=1}^{n} \delta_{ij}^c\left(x_j(t)\right) \times c_{ij}^- f_j\left(x_j(\gamma(t))\right), \tag{10}$$

where

$$\delta_{ij}^{b}\left(x_j(t)\right)=\begin{cases}\operatorname{sgn}\left(\widehat{b}_{ij}-\check{b}_{ij}\right), & \left|x_j(t)\right|>T_j,\\ -\operatorname{sgn}\left(\widehat{b}_{ij}-\check{b}_{ij}\right), & \left|x_j(t)\right|<T_j,\end{cases}$$
$$\delta_{ij}^{c}\left(x_j(t)\right)=\begin{cases}\operatorname{sgn}\left(\widehat{c}_{ij}-\check{c}_{ij}\right), & \left|x_j(t)\right|>T_j,\\ -\operatorname{sgn}\left(\widehat{c}_{ij}-\check{c}_{ij}\right), & \left|x_j(t)\right|<T_j,\end{cases}\tag{11}$$

and $\operatorname{sgn}(\cdot)$ is the sign function.

Definition 2. A constant vector $x^*=(x_1^*,x_2^*,\ldots,x_n^*)^T$ is said to be an equilibrium point of neural network model (5) if and only if

$$0\in -a_ix_i^*+\sum_{j=1}^{n}K\left[b_{ij}\left(x_j^*\right)\right]f_j\left(x_j^*\right)+\sum_{j=1}^{n}K\left[c_{ij}\left(x_j^*\right)\right]f_j\left(x_j^*\right)+u_i,\quad i=1,2,\ldots,n,\tag{12}$$

or, equivalently, there exist $\widetilde{b}_{ij}(x_j^*)\in K[b_{ij}(x_j^*)]$ and $\widetilde{c}_{ij}(x_j^*)\in K[c_{ij}(x_j^*)]$ such that

$$-a_ix_i^*+\sum_{j=1}^{n}\widetilde{b}_{ij}\left(x_j^*\right)f_j\left(x_j^*\right)+\sum_{j=1}^{n}\widetilde{c}_{ij}\left(x_j^*\right)f_j\left(x_j^*\right)+u_i=0,\tag{13}$$

for $i=1,2,\ldots,n$.

Definition 3. The equilibrium point $x^*=(x_1^*,x_2^*,\ldots,x_n^*)^T$ of neural network model (5) is globally exponentially stable if there exist constants $M>0$ and $\epsilon>0$ such that

$$\left\|x(t)-x^*\right\|\le M\left\|x^0-x^*\right\|\exp\{-\epsilon t\},\tag{14}$$

for any $t\ge 0$, where $x(t)$ is the state vector of neural network model (5) with initial condition x^0.

Lemma 4. *For neural network model (5), one has*

$$\begin{aligned}&\left|K\left[b_{ij}\left(x_j\right)\right]f_j\left(x_j\right)-K\left[b_{ij}\left(y_j\right)\right]f_j\left(y_j\right)\right|\\&\quad\le\bar{b}_{ij}\alpha\left|x_j-y_j\right|,\\&\left|K\left[c_{ij}\left(x_j\right)\right]f_j\left(x_j\right)-K\left[c_{ij}\left(y_j\right)\right]f_j\left(y_j\right)\right|\\&\quad\le\bar{c}_{ij}\alpha\left|x_j-y_j\right|,\end{aligned}\tag{15}$$

for $i,j=1,2,\ldots,n$, $x_j,y_j\in(-\infty,+\infty)$, where $K[b_{ij}(\cdot)]$ and $K[c_{ij}(\cdot)]$ are defined as those in (6) and (7), respectively.

Lemma 4 is a basic conclusion. To get more specific, please see [Neural Networks, vol. 51, pp. 1–8, 2014], or [Information Sciences, vol. 279, pp. 358–373, 2014], or others.

In the following, we end this section with some basic assumptions:

(A1) There exists a positive constant η satisfying

$$\eta_{k+1}-\eta_k<\eta,\quad k\in N.\tag{16}$$

(A2) $\eta(S_b+2S_c)\exp\{S_b\eta\}<1$.

(A3) $\eta[S_c+S_b(1+S_c\eta)\exp\{S_b\eta\}]<1$.

3. Main Results

In this section, we first present the conditions ensuring the existence and uniqueness of solution for neural network model (5) and then analyze its global exponential stability; finally, we discuss how to design the procedures of autoassociative memories and heteroassociative memories.

3.1. Existence and Uniqueness of Solution

Theorem 5. *Let (A1) and (A2) hold. Then, there exists a unique solution $x(t)=x(t,t_0,x^0)$, $t\ge t_0$, of (5) for every $(t_0,x^0)\in(\Re^+,\Re^n)$.*

Proof. The proof of the assertion is divided into two steps.

Firstly, we discuss the existence of solution.

For a fixed $k\in N$, assume that $\eta_k\le t_0\le\vartheta_k=\gamma(t)<t<\eta_{k+1}$ and the other case $\eta_k\le t_0<t<\vartheta_k=\gamma(t)<\eta_{k+1}$ can be discussed in a similar way.

Let $v(t)=x(t,t_0,x^0)$, and consider the following equivalent equation:

$$\begin{aligned}v_i(t)=x_i^0+\int_{t_0}^{t}\Bigg[&-a_iv_i(s)+\sum_{j=1}^{n}b_{ij}^0f_j\left(v_j(s)\right)+\sum_{j=1}^{n}c_{ij}^0\\&\times f_j\left(v_j\left(\vartheta_k\right)\right)+u_i+\sum_{j=1}^{n}\delta_{ij}^{b}\left(v_j(t)\right)b_{ij}^{-}f_j\left(v_j(s)\right)\\&+\sum_{j=1}^{n}\delta_{ij}^{c}\left(v_j(t)\right)c_{ij}^{-}f_j\left(v_j\left(\vartheta_k\right)\right)\Bigg]\mathrm{d}s,\\&i=1,2,\ldots,n.\end{aligned}\tag{17}$$

Construct the following sequence $\{v_i^m(t)\}$, $m\in N$, $i=1,2,\ldots,n$:

$$\begin{aligned}v_i^{m+1}(t)=x_i^0+\int_{t_0}^{t}\Bigg[&-a_iv_i^m(s)+\sum_{j=1}^{n}b_{ij}^0f_j\left(v_j^m(s)\right)\\&+\sum_{j=1}^{n}c_{ij}^0\times f_j\left(v_j^m\left(\vartheta_k\right)\right)+u_i\\&+\sum_{j=1}^{n}\delta_{ij}^{b}\left(v_j^m(t)\right)b_{ij}^{-}f_j\left(v_j^m(s)\right)\end{aligned}$$

$$+\sum_{j=1}^{n}\delta_{ij}^{c}\left(v_j^m(t)\right)c_{ij}^{-}f_j\left(v_j^m(\vartheta_k)\right)\Bigg]\mathrm{d}s,\quad i=1,2,\ldots,n, \tag{18}$$

and $v_i^0(t)=x_i^0$.

Define a norm $\|v(t)\|_M=\max_{[t_0,t]}\|v(t)\|$, and we can get

$$\left\|v^{m+1}(t)-v^m(t)\right\|_M\le\left[\left(S_b+S_c\right)\eta\right]^m\varsigma, \tag{19}$$

where $\varsigma=\eta[\sum_{i=1}^n a_i|x_i^0|+\sum_{i=1}^n\sum_{j=1}^n(b_{ij}^{+}+b_{ij}^{-}+c_{ij}^{+}+c_{ij}^{-})p+\sum_{i=1}^n|u_i|]$.

From (A2), we have $(S_b+S_c)\eta<1$, and hence

$$\lim_{m\to+\infty}\left\|v^{m+1}(t)-v^m(t)\right\|_M=0. \tag{20}$$

Therefore, there exists a solution $v(t)=x(t,t_0,x^0)$ on the interval $[t_0,\vartheta_k]$ for (17). From (4), the solution can be consecutive to η_{k+1}. Utilizing a similar method, $x(t)$ can be consecutive to ϑ_{k+1} and then to η_{k+2}. Applying the mathematical induction, the proof of existence of solution for (5) is completed.

Next, we analyze the uniqueness of solution.

Fix $k\in N$ and choose $t_0\in[\eta_k,\eta_{k+1}]$, $x^1\in\mathfrak{R}^n$, $x^2\in\mathfrak{R}^n$. Denote $x^1(t)=x(t,t_0,x^1)$ and $x^2(t)=x(t,t_0,x^2)$ as two solutions of (5) with different initial conditions (t_0,x^1) and (t_0,x^2), respectively.

Then, we get

$$\begin{aligned}&\left\|x^1(t)-x^2(t)\right\|\\&\le\left(\left\|x^1-x^2\right\|+S_c\eta\left\|x^1(\vartheta_k)-x^2(\vartheta_k)\right\|\right)\\&\quad+\int_{t_0}^{t}S_b\left\|x^1(s)-x^2(s)\right\|\mathrm{d}s.\end{aligned} \tag{21}$$

Based on the Gronwall-Bellman inequality,

$$\begin{aligned}&\left\|x^1(t)-x^2(t)\right\|\\&\le\left(\left\|x^1-x^2\right\|+S_c\eta\left\|x^1(\vartheta_k)-x^2(\vartheta_k)\right\|\right)\\&\quad\times\exp\left\{S_b\eta\right\},\end{aligned} \tag{22}$$

and, particularly,

$$\begin{aligned}&\left\|x^1(\vartheta_k)-x^2(\vartheta_k)\right\|\\&\le\left(\left\|x^1-x^2\right\|+S_c\eta\left\|x^1(\vartheta_k)-x^2(\vartheta_k)\right\|\right)\\&\quad\times\exp\left\{S_b\eta\right\}.\end{aligned} \tag{23}$$

Hence,

$$\left\|x^1(t)-x^2(t)\right\|\le\left(\frac{\exp\left\{S_b\eta\right\}}{1-S_c\eta\exp\left\{S_b\eta\right\}}\right)\left\|x^1-x^2\right\|. \tag{24}$$

Suppose that there exists some $\widetilde{t}\in[\eta_k,\eta_{k+1}]$ satisfying $x^1(\widetilde{t})=x^2(\widetilde{t})$; then,

$$\begin{aligned}\left\|x^1-x^2\right\|&\le S_c\eta\left\|x^1(\vartheta_k)-x^2(\vartheta_k)\right\|\\&\quad+\int_{t_0}^{\widetilde{t}}S_b\left\|x^1(s)-x^2(s)\right\|\mathrm{d}s.\end{aligned} \tag{25}$$

From (A2), we get

$$0<\eta\exp\left\{S_b\eta\right\}\left(S_b+S_c\right)<1-\eta S_c\exp\left\{S_b\eta\right\}; \tag{26}$$

that is,

$$0<\frac{\eta\exp\left\{S_b\eta\right\}\left(S_b+S_c\right)}{1-\eta S_c\exp\left\{S_b\eta\right\}}<1. \tag{27}$$

Substituting (24) into (25), from (27), we obtain

$$\begin{aligned}\left\|x^1-x^2\right\|&\le S_c\eta\frac{\exp\left\{S_b\eta\right\}}{1-S_c\eta\exp\left\{S_b\eta\right\}}\left\|x^1-x^2\right\|\\&\quad+S_b\eta\frac{\exp\left\{S_b\eta\right\}}{1-S_c\eta\exp\left\{S_b\eta\right\}}\left\|x^1-x^2\right\|\\&\le\frac{\eta\exp\left\{S_b\eta\right\}\left(S_b+S_c\right)}{1-\eta S_c\exp\left\{S_b\eta\right\}}\left\|x^1-x^2\right\|\\&<\left\|x^1-x^2\right\|.\end{aligned} \tag{28}$$

This poses a contradiction. Therefore, the uniqueness of solution is true. Taken together, the proof of the existence and uniqueness of solution for (5) is completed. □

3.2. Invariant Manifolds

Lemma 6. *The solution $x(t)$ of neural network model (5) will fall into $\prod_{i=1}^n[d+T_i,+\infty)$ ultimately if, for $i=1,2,\ldots,n$, the following conditions hold:*

$$u_i>S_i+a_iT_i+\sum_{j=1,j\ne i}^{n}\bar{b}_{ij}p+\sum_{j=1}^{n}\bar{c}_{ij}p. \tag{29}$$

Proof. We distinguish four cases to prove the lemma.

(1) If, for some t, $x_i(t)\in[T_i,d+T_i)$, $i\in\{1,2,\ldots,n\}$, then

$$\begin{aligned}\dot{x}_i(t)&=-a_ix_i(t)+\sum_{j=1}^{n}b_{ij}\left(x_j(t)\right)f_j\left(x_j(t)\right)\\&\quad+\sum_{j=1}^{n}c_{ij}\left(x_j(t)\right)\times f_j\left(x_j(\gamma(t))\right)+u_i\end{aligned}$$

$$\begin{aligned}
&\geq -a_i x_i(t) + b_{ii}(x_i(t))\frac{p}{d}[x_i(t) - T_i] \\
&\quad - \sum_{j=1,j\neq i}^{n} \overline{b}_{ij} p - \sum_{j=1}^{n} \overline{c}_{ij} p + u_i \\
&\geq -a_i[x_i(t) - T_i] + b_{ii}(x_i(t))\frac{p}{d}[x_i(t) - T_i] \\
&\quad - a_i T_i - \sum_{j=1,j\neq i}^{n} \overline{b}_{ij} p - \sum_{j=1}^{n} \overline{c}_{ij} p + u_i \\
&\geq \left[-a_i + b_{ii}(x_i(t))\frac{p}{d}\right][x_i(t) - T_i] - a_i T_i \\
&\quad - \sum_{j=1,j\neq i}^{n} \overline{b}_{ij} p - \sum_{j=1}^{n} \overline{c}_{ij} p + u_i \\
&\geq -\left|-a_i + b_{ii}(x_i(t))\frac{p}{d}\right| d - a_i T_i - \sum_{j=1,j\neq i}^{n} \overline{b}_{ij} p \\
&\quad - \sum_{j=1}^{n} \overline{c}_{ij} p + u_i \\
&\geq -|b_{ii}(x_i(t))\, p - a_i d| - a_i T_i - \sum_{j=1,j\neq i}^{n} \overline{b}_{ij} p \\
&\quad - \sum_{j=1}^{n} \overline{c}_{ij} p + u_i \\
&\geq -S_i - a_i T_i - \sum_{j=1,j\neq i}^{n} \overline{b}_{ij} p - \sum_{j=1}^{n} \overline{c}_{ij} p + u_i > 0.
\end{aligned} \tag{30}$$

That is to say, $\dot{x}_i(t) > 0$, when $x_i(t) \in [T_i, d + T_i)$.

(2) If, for some t, $x_i(t) \in (-T_i, T_i)$, $i \in \{1, 2, \ldots, n\}$, then

$$\begin{aligned}
\dot{x}_i(t) &\geq -a_i x_i(t) + b_{ii}(x_i(t))\, f_i(x_i(t)) - \sum_{j=1,j\neq i}^{n} \overline{b}_{ij} p \\
&\quad - \sum_{j=1}^{n} \overline{c}_{ij} p + u_i \\
&\geq -a_i T_i - \sum_{j=1,j\neq i}^{n} \overline{b}_{ij} p - \sum_{j=1}^{n} \overline{c}_{ij} p + u_i > S_i > 0.
\end{aligned} \tag{31}$$

That is to say, $\dot{x}_i(t) > 0$, when $x_i(t) \in (-T_i, T_i)$.

(3) If, for some t, $x_i(t) \in (-T_i - d, -T_i)$, $i \in \{1, 2, \ldots, n\}$, then

$$\begin{aligned}
\dot{x}_i(t) &\geq -a_i x_i(t) + b_{ii}(x_i(t))\, f_i(x_i(t)) - \sum_{j=1,j\neq i}^{n} \overline{b}_{ij} p \\
&\quad - \sum_{j=1}^{n} \overline{c}_{ij} p + u_i \\
&= -a_i[x_i(t) + T_i] + b_{ii}(x_i(t))\frac{p}{d}[x_i(t) + T_i] \\
&\quad - \sum_{j=1,j\neq i}^{n} \overline{b}_{ij} p - \sum_{j=1}^{n} \overline{c}_{ij} p + u_i + a_i T_i \\
&= \left[-a_i + b_{ii}(x_i(t))\frac{p}{d}\right][x_i(t) + T_i] - \sum_{j=1,j\neq i}^{n} \overline{b}_{ij} p \\
&\quad - \sum_{j=1}^{n} \overline{c}_{ij} p + u_i + a_i T_i \\
&\geq -|b_{ii}(x_i(t))\, p - a_i d| + a_i T_i - \sum_{j=1,j\neq i}^{n} \overline{b}_{ij} p \\
&\quad - \sum_{j=1}^{n} \overline{c}_{ij} p + u_i > 2a_i T_i > 0.
\end{aligned} \tag{32}$$

That is to say, $\dot{x}_i(t) > 0$, when $x_i(t) \in (-T_i - d_i, -T_i)$.

(4) If, for some t, $x_i(t) \in (-\infty, -T_i - d_i)$, $i \in \{1, 2, \ldots, n\}$, then

$$\begin{aligned}
\dot{x}_i(t) &\geq -a_i x_i(t) + b_{ii}(x_i(t))\, f_i(x_i(t)) - \sum_{j=1,j\neq i}^{n} \overline{b}_{ij} p \\
&\quad - \sum_{j=1}^{n} \overline{c}_{ij} p + u_i \\
&\geq a_i(T_i + d) - b_{ii}(x_i(t))\, p - \sum_{j=1,j\neq i}^{n} \overline{b}_{ij} p \\
&\quad - \sum_{j=1}^{n} \overline{c}_{ij} p + u_i \\
&\geq -|b_{ii}(x_i(t))\, p - a_i d| + a_i T_i - \sum_{j=1,j\neq i}^{n} \overline{b}_{ij} p \\
&\quad - \sum_{j=1}^{n} \overline{c}_{ij} p + u_i > 2a_i T_i > 0.
\end{aligned} \tag{33}$$

That is to say, $\dot{x}_i(t) > 0$, when $x_i(t) \in (-\infty, -T_i - d_i)$.

From the above analysis, we can get that any component $x_i(t)$ $(i = 1, 2, \ldots, n)$ of the solution $x(t)$ of neural network model (5) will fall into $[d + T_i, +\infty)$ ultimately. Hence, the proof is completed. □

Lemma 7. *The solution $x(t)$ of neural network model (5) will fall into $\prod_{i=1}^{n}(-\infty, -d - T_i]$ ultimately if, for $i = 1, 2, \ldots, n$, the following conditions hold:*

$$u_i < -S_i - a_i T_i - \sum_{j=1,j\neq i}^{n} \overline{b}_{ij} p - \sum_{j=1}^{n} \overline{c}_{ij} p. \tag{34}$$

Proof. We distinguish four cases to prove the lemma.

(1) If, for some t, $x_i(t) \in [d + T_i, +\infty)$, $i \in \{1, 2, \ldots, n\}$, then

$$\begin{aligned}
\dot{x}_i(t) &= -a_i x_i(t) + \sum_{j=1}^{n} b_{ij}\left(x_j(t)\right) f_j\left(x_j(t)\right) \\
&\quad + \sum_{j=1}^{n} c_{ij}\left(x_j(t)\right) f_j\left(x_j(\gamma(t))\right) + u_i \\
&\le -a_i x_i(t) + b_{ii}\left(x_i(t)\right) f_i\left(x_i(t)\right) + \sum_{j=1, j\neq i}^{n} \overline{b}_{ij} p \\
&\quad + \sum_{j=1}^{n} \overline{c}_{ij} p + u_i \\
&\le -a_i\left(d + T_i\right) + b_{ii}\left(x_i(t)\right) p + \sum_{j=1, j\neq i}^{n} \overline{b}_{ij} p \\
&\quad + \sum_{j=1}^{n} \overline{c}_{ij} p + u_i \\
&\le \left|a_i d - b_{ii}\left(x_i(t)\right) p\right| - a_i T_i + \sum_{j=1, j\neq i}^{n} \overline{b}_{ij} p \\
&\quad + \sum_{j=1}^{n} \left|\overline{c}_{ij}\right| p + u_i \\
&\le S_i - a_i T_i + \sum_{j=1, j\neq i}^{n} \overline{b}_{ij} p + \sum_{j=1}^{n} \overline{c}_{ij} p + u_i < -2a_i T_i \\
&< 0.
\end{aligned} \tag{35}$$

That is to say, $\dot{x}_i(t) < 0$, when $x_i(t) \in [d + T_i, +\infty)$.

(2) If, for some t, $x_i(t) \in (T_i, d + T_i)$, $i \in \{1, 2, \ldots, n\}$, then

$$\begin{aligned}
\dot{x}_i(t) &= -a_i x_i(t) + \sum_{j=1}^{n} b_{ij}\left(x_j(t)\right) f_j\left(x_j(t)\right) \\
&\quad + \sum_{j=1}^{n} c_{ij}\left(x_j(t)\right) f_j\left(x_j(\gamma(t))\right) + u_i \\
&\le -a_i\left[x_i(t) - T_i\right] + b_{ii}\left(x_i(t)\right) \frac{p}{d}\left[x_i(t) - T_i\right] \\
&\quad - a_i T_i + \sum_{j=1, j\neq i}^{n} \overline{b}_{ij} p + \sum_{j=1}^{n} \overline{c}_{ij} p + u_i \\
&\le \left[-a_i + b_{ii}\left(x_i(t)\right) \frac{p}{d}\right]\left[x_i(t) - T_i\right] - a_i T_i \\
&\quad + \sum_{j=1, j\neq i}^{n} \overline{b}_{ij} p + \sum_{j=1}^{n} \overline{c}_{ij} p + u_i \\
&\le \left|-a_i + b_{ii}\left(x_i(t)\right) \frac{p}{d}\right| d - a_i T_i + \sum_{j=1, j\neq i}^{n} \overline{b}_{ij} p \\
&\quad + \sum_{j=1}^{n} \overline{c}_{ij} p + u_i \\
&\le \left|b_{ii}\left(x_i(t)\right) p - a_i d\right| - a_i T_i + \sum_{j=1, j\neq i}^{n} \overline{b}_{ij} p \\
&\quad + \sum_{j=1}^{n} \overline{c}_{ij} p + u_i \\
&\le S_i - a_i T_i + \sum_{j=1, j\neq i}^{n} \overline{b}_{ij} p + \sum_{j=1}^{n} \overline{c}_{ij} p + u_i < -2a_i T_i \\
&< 0.
\end{aligned} \tag{36}$$

That is to say, $\dot{x}_i(t) < 0$, when $x_i(t) \in (T_i, d + T_i)$.

(3) If, for some t, $x_i(t) \in (-T_i, T_i)$, $i \in \{1, 2, \ldots, n\}$, then

$$\begin{aligned}
\dot{x}_i(t) &\le -a_i x_i(t) + b_{ii}\left(x_i(t)\right) f_i\left(x_i(t)\right) + \sum_{j=1, j\neq i}^{n} \overline{b}_{ij} p \\
&\quad + \sum_{j=1}^{n} \overline{c}_{ij} p + u_i \\
&\le a_i T_i + \sum_{j=1, j\neq i}^{n} \overline{b}_{ij} p + \sum_{j=1}^{n} \overline{c}_{ij} p + u_i < -S_i < 0.
\end{aligned} \tag{37}$$

That is to say, $\dot{x}_i(t) < 0$, when $x_i(t) \in (-T_i, T_i)$.

(4) If, for some t, $x_i(t) \in (-T_i - d, -T_i)$, $i \in \{1, 2, \ldots, n\}$, then

$$\begin{aligned}
\dot{x}_i(t) &\le -a_i x_i(t) + b_{ii}\left(x_i(t)\right) f_i\left(x_i(t)\right) + \sum_{j=1, j\neq i}^{n} \overline{b}_{ij} p \\
&\quad + \sum_{j=1}^{n} \overline{c}_{ij} p + u_i \\
&= -a_i\left[x_i(t) + T_i\right] + b_{ii}\left(x_i(t)\right) \frac{p}{d}\left[x_i(t) + T_i\right] \\
&\quad + \sum_{j=1, j\neq i}^{n} \overline{b}_{ij} p + \sum_{j=1}^{n} \overline{c}_{ij} p + u_i + a_i T_i \\
&= \left[-a_i + b_{ii}\left(x_i(t)\right) \frac{p}{d}\right]\left[x_i(t) + T_i\right] + \sum_{j=1, j\neq i}^{n} \overline{b}_{ij} p \\
&\quad + \sum_{j=1}^{n} \overline{c}_{ij} p + u_i + a_i T_i \\
&\le \left|b_{ii}\left(x_i(t)\right) p - a_i d\right| + a_i T_i + \sum_{j=1, j\neq i}^{n} \overline{b}_{ij} p \\
&\quad + \sum_{j=1}^{n} \overline{c}_{ij} p + u_i < 0.
\end{aligned} \tag{38}$$

That is to say, $\dot{x}_i(t) < 0$, when $x_i(t) \in (-T_i - d_i, -T_i)$.

From the above analysis, we can get that any component $x_i(t)$ $(i = 1, 2, \ldots, n)$ of the solution $x(t)$ of neural network model (5) will fall into $(-\infty, -d - T_i]$ ultimately. Hence, the proof is completed. □

3.3. Global Exponential Stability Analysis. Denote

$$\Delta_1 = \left\{ i \mid i \in \{1, 2, \ldots, n\},\ u_i > S_i + a_i T_i + \sum_{j=1, j\neq i}^{n} \overline{b}_{ij} p + \sum_{j=1}^{n} \overline{c}_{ij} p \right\},$$
$$\Delta_2 = \left\{ i \mid i \in \{1, 2, \ldots, n\},\ u_i > S_i + a_i T_i + \sum_{j=1, j\neq i}^{n} \overline{b}_{ij} p + \sum_{j=1}^{n} \overline{c}_{ij} p \right\}. \tag{39}$$

In order to guarantee the existence of equilibrium point for neural network model (5), the following assumption is needed:

(A4) For any $i \in \{1, 2, \ldots, n\}$, $i \in \Delta_1 \cup \Delta_2$.

Theorem 8. *Let (A4) hold. Then, neural network model (5) has at least one equilibrium point $x^* \in \Theta$, where*

$$\Theta = \left\{ x \in \mathfrak{R}^n \mid x_i \leq -T_i - d \text{ or } x_i \geq d + T_i,\ i \in \{1, 2, \ldots, n\} \right\}. \tag{40}$$

Proof. Define a mapping

$$F(x) = \left(F_1(x), F_2(x), \ldots, F_n(x)\right)^T, \tag{41}$$

where

$$F_i(x) = \frac{1}{a_i} \left[\sum_{j=1}^{n} K\left[b_{ij}\left(x_j\right)\right] f_j\left(x_j\right) + \sum_{j=1}^{n} K\left[c_{ij}\left(x_j\right)\right] f_j\left(x_j\right) + u_i \right], \quad i = 1, 2, \ldots, n. \tag{42}$$

It is obvious that $F(x)$ is equicontinuous.

When $i \in \Delta_1$, there exists a small enough positive number ε_1 satisfying

$$u_i > S_i + a_i T_i + \sum_{j=1, j\neq i} \overline{b}_{ij} p + \sum_{j=1} \overline{c}_{ij} p + a_i \varepsilon_1, \tag{43}$$

and when $i \in \Delta_2$, there exists a small enough positive number ε_2 satisfying

$$u_i < -S_i - a_i T_i - \sum_{j=1, j\neq i} \overline{b}_{ij} p - \sum_{j=1} \overline{c}_{ij} p - a_i \varepsilon_2. \tag{44}$$

Take $0 < \varepsilon < \min(\varepsilon_1, \varepsilon_2)$ and denote

$$\overline{\Theta} = \left\{ x \in \mathfrak{R}^n \mid x_i \in \left[d + T_i + \varepsilon, \frac{(d + T_i)}{\varepsilon} \right],\ i \in \Delta_1,\ \text{or } x_i \in \left[\frac{-(d + T_i)}{\varepsilon}, -d - T_i - \varepsilon \right],\ i \in \Delta_2 \right\}, \tag{45}$$

which is a bounded and closed set.

When $x_i \in [d + T_i + \varepsilon, (d + T_i)/\varepsilon]$, $i \in \Delta_1$,

$$\begin{aligned} F_i(x) &= \frac{1}{a_i} \left[\sum_{j=1}^{n} K\left[b_{ij}\left(x_j\right)\right] f_j\left(x_j\right) + \sum_{j=1}^{n} K\left[c_{ij}\left(x_j\right)\right] f_j\left(x_j\right) + u_i \right] \\ &\geq \frac{1}{a_i} \left[K\left[b_{ii}\left(x_i\right)\right] p - \sum_{j=1, j\neq i}^{n} \overline{b}_{ij} p - \sum_{j=1}^{n} \overline{c}_{ij} p + u_i \right] \\ &> \frac{1}{a_i} \left[\left(K\left[b_{ii}\left(x_i\right)\right] p - a_i d\right) + S_i + a_i T_i + a_i d + a_i \varepsilon \right] \\ &\geq T_i + d + \varepsilon. \end{aligned} \tag{46}$$

Similarly, we can obtain

$$F_i(x) < -T_i - d - \varepsilon \tag{47}$$

for $x_i \in [-(d + T_i)/\varepsilon, -d - T_i - \varepsilon]$, $i \in \Delta_2$.

From the above discussion, we can get $F(x) \in \Theta$ for $x \in \Theta$. Based on the generalized Brouwer's fixed point theorem, there exists at least one equilibrium $x^* \in \Theta$. This completes the proof. □

Recalling (10), for $i = 1, 2, \ldots, n$, then

$$\begin{aligned} \dot{x}_i(t) \in\ & -a_i x_i(t) + \sum_{j=1}^{n} b_{ij}^0 f_j\left(x_j(t)\right) + \sum_{j=1}^{n} c_{ij}^0 f_j\left(x_j(\gamma(t))\right) + u_i \\ & + \sum_{j=1}^{n} K\left[\delta_{ij}^b\left(x_j(t)\right)\right] b_{ij}^- f_j\left(x_j(t)\right) \\ & + \sum_{j=1}^{n} K\left[\delta_{ij}^c\left(x_j(t)\right)\right] c_{ij}^- f_j\left(x_j(\gamma(t))\right). \end{aligned} \tag{48}$$

Let $y_i(t) = x_i(t) - x_i^*$, $i = 1, 2, \ldots, n$,

$$\begin{aligned} \dot{y}_i(t) \in\ & -a_i y_i(t) + \sum_{j=1}^{n} b_{ij}^0 g_j\left(y_j(t)\right) + \sum_{j=1}^{n} c_{ij}^0 g_j\left(y_j(\gamma(t))\right) + \sum_{j=1}^{n} A_{ij}^b\left(y_j(t)\right) \\ & + \sum_{j=1}^{n} A_{ij}^c\left(y_j(\gamma(t))\right), \quad i = 1, 2, \ldots, n, \end{aligned} \tag{49}$$

where $g_j(y_j(t)) = f_j(y_j(t) + x_j^*) - f_j(x_j^*)$, $A_{ij}^b(y_j(t)) = b_{ij}^-(K[\delta_{ij}^b(y_j(t) + x_j^*)]f_j(y_j(t) + x_j^*) - K[\delta_{ij}^b(x_j^*)]f_j(x_j^*))$, or $A_{ij}^c(y_j(\gamma(t))) = c_{ij}^-(K[\delta_{ij}^c(y_j(\gamma(t)) + x_j^*)]f_j(y_j(\gamma(t)) + x_j^*) - K[\delta_{ij}^c(x_j^*)]f_j(x_j^*))$, or there exists $\varphi_{ij}^b(y_j(t)) \in A_{ij}^b(y_j(t))$, $\varphi_{ij}^c(y_j(t)) \in A_{ij}^c(y_j(t))$ for $i, j = 1, 2, \ldots, n$, such that

$$\begin{aligned}\dot{y}_i(t) = -a_i y_i(t) &+ \sum_{j=1}^{n} b_{ij}^0 g_j\left(y_j(t)\right) \\ &+ \sum_{j=1}^{n} c_{ij}^0 g_j\left(y_j(\gamma(t))\right) + \sum_{j=1}^{n} \varphi_{ij}^b\left(y_j(t)\right) \\ &+ \sum_{j=1}^{n} \varphi_{ij}^c\left(y_j(\gamma(t))\right), \quad i = 1, 2, \ldots, n.\end{aligned} \tag{50}$$

According to Lemma 4,

$$\begin{aligned}\left|A_{ij}^b\left(y_j(t)\right)\right| &\le b_{ij}^-\alpha\left|y_j(t)\right|, \\ \left|A_{ij}^c\left(y_j(\gamma(t))\right)\right| &\le c_{ij}^-\alpha\left|y_j(\gamma(t))\right|,\end{aligned} \tag{51}$$

for $i, j = 1, 2, \ldots, n$.

Lemma 9. *Let (A1)–(A3) hold and $y(t) = (y_1(t), y_2(t), \ldots, y_n(t))^T$ be a solution of (49) or (50). Then,*

$$\left\|y(\gamma(t))\right\| \le \mu\left\|y(t)\right\|, \tag{52}$$

for $t \ge 0$, where $\mu = (1 - \eta[S_c + S_b(1 + S_c\eta)\exp\{S_b\eta\}])^{-1}$.

Proof. For any $t > 0$, there exists a unique $k \in N$, such that $t \in [\eta_k, \eta_{k+1})$; then,

$$\begin{aligned}y_i(t) = y_i(\vartheta_k) + \int_{\vartheta_k}^{t} \Bigg[&-a_i y_i(s) + \sum_{j=1}^{n} b_{ij}^0 g_j\left(y_j(s)\right) \\ &+ \sum_{j=1}^{n} c_{ij}^0 g_j\left(y_j(\vartheta_k)\right) + \sum_{j=1}^{n} \varphi_{ij}^b\left(y_j(s)\right) \\ &+ \sum_{j=1}^{n} \varphi_{ij}^c\left(y_j(\vartheta_k)\right)\Bigg] \mathrm{d}s, \quad i = 1, 2, \ldots, n.\end{aligned} \tag{53}$$

Taking the absolute value on both sides of (53),

$$\begin{aligned}\left|y_i(t)\right| \le \left|y_i(\vartheta_k)\right| + \int_{\vartheta_k}^{t} \Bigg[&a_i\left|y_i(s)\right| \\ &+ \sum_{j=1}^{n} b_{ij}^+\left|g_j\left(y_j(s)\right)\right| + \sum_{j=1}^{n} c_{ij}^+\left|g_j\left(y_j(\vartheta_k)\right)\right| \\ &+ \sum_{j=1}^{n}\left|\varphi_{ij}^b\left(y_j(s)\right)\right| + \sum_{j=1}^{n}\left|\varphi_{ij}^c\left(y_j(\vartheta_k)\right)\right|\Bigg] \mathrm{d}s, \\ &i = 1, 2, \ldots, n,\end{aligned} \tag{54}$$

and then

$$\begin{aligned}\sum_{i=1}^{n}\left|y_i(t)\right| \le \sum_{i=1}^{n}\left|y_i(\vartheta_k)\right| + \int_{\vartheta_k}^{t} \Bigg[&\sum_{i=1}^{n} a_i\left|y_i(s)\right| \\ &+ \sum_{i=1}^{n}\sum_{j=1}^{n} b_{ij}^+\left|g_j\left(y_j(s)\right)\right| + \sum_{i=1}^{n}\sum_{j=1}^{n} c_{ij}^+\left|g_j\left(y_j(\vartheta_k)\right)\right| \\ &+ \sum_{i=1}^{n}\sum_{j=1}^{n}\left|\varphi_{ij}^b\left(y_j(s)\right)\right| + \sum_{i=1}^{n}\sum_{j=1}^{n}\left|\varphi_{ij}^c\left(y_j(\vartheta_k)\right)\right|\Bigg] \mathrm{d}s.\end{aligned} \tag{55}$$

Applying Lemma 4,

$$\begin{aligned}\sum_{i=1}^{n}\left|y_i(t)\right| &\le \sum_{i=1}^{n}\left|y_i(\vartheta_k)\right| + \int_{\vartheta_k}^{t} \Bigg[\sum_{i=1}^{n} a_i\left|y_i(s)\right| \\ &+ \sum_{i=1}^{n}\sum_{j=1}^{n} b_{ij}^+\alpha\left|y_j(s)\right| + \sum_{i=1}^{n}\sum_{j=1}^{n} c_{ij}^+\alpha\left|y_j(\vartheta_k)\right| \\ &+ \sum_{i=1}^{n}\sum_{j=1}^{n} b_{ij}^-\alpha\left|y_j(s)\right| + \sum_{i=1}^{n}\sum_{j=1}^{n} c_{ij}^-\alpha\left|y_j(\vartheta_k)\right|\Bigg] \mathrm{d}s \\ &= \sum_{i=1}^{n}\left|y_i(\vartheta_k)\right| + \int_{\vartheta_k}^{t} \Bigg[\sum_{i=1}^{n} a_i\left|y_i(s)\right| \\ &+ \sum_{i=1}^{n}\sum_{j=1}^{n} b_{ji}^+\alpha\left|y_i(s)\right| + \sum_{i=1}^{n}\sum_{j=1}^{n} c_{ji}^+\alpha\left|y_i(\vartheta_k)\right| \\ &+ \sum_{i=1}^{n}\sum_{j=1}^{n} b_{ji}^-\alpha\left|y_i(s)\right| + \sum_{i=1}^{n}\sum_{j=1}^{n} c_{ji}^-\alpha\left|y_i(\vartheta_k)\right|\Bigg] \mathrm{d}s;\end{aligned} \tag{56}$$

that is

$$\begin{aligned}\left\|y(t)\right\| &\le \sum_{i=1}^{n}\left|y_i(\vartheta_k)\right| \\ &+ \int_{\vartheta_k}^{t} \Bigg[\sum_{i=1}^{n}\left(a_i + \sum_{j=1}^{n}\alpha\left(b_{ji}^+ + b_{ji}^-\right)\right)\left|y_i(s)\right| \\ &+ \sum_{i=1}^{n}\left(\sum_{j=1}^{n}\alpha\left(c_{ji}^+ + c_{ji}^-\right)\right)\left|y_i(\vartheta_k)\right|\Bigg] \mathrm{d}s;\end{aligned} \tag{57}$$

then

$$\begin{aligned}\left\|y(t)\right\| &\le \left\|y(\vartheta_k)\right\| + \int_{\vartheta_k}^{t}\left[S_b\left\|y(s)\right\| + S_c\left\|y(\vartheta_k)\right\|\right] \mathrm{d}s \\ &\le (1 + S_c\eta)\left\|y(\vartheta_k)\right\| + \int_{\vartheta_k}^{t} S_b\left\|y(s)\right\| \mathrm{d}s.\end{aligned} \tag{58}$$

According to the Gronwall-Bellman inequality,

$$\begin{aligned}\left\|y(t)\right\| &\le (1 + S_c\eta)\left\|y(\vartheta_k)\right\| \exp\left\{\int_{\vartheta_k}^{t} S_b \mathrm{d}s\right\} \\ &\le (1 + S_c\eta)\exp\{S_b\eta\}\left\|y(\vartheta_k)\right\|.\end{aligned} \tag{59}$$

Exchanging the location of $y_i(t)$ and $y_i(\vartheta_k)$ in (53), we get

$$\begin{aligned}\|y(\vartheta_k)\| &\le \|y(t)\| + \int_{\vartheta_k}^{t} \left[S_b \|y(s)\| + S_c \left\|y_{\vartheta_k}\right\|\right] ds \\ &\le \|y(t)\| + \int_{\vartheta_k}^{t} \left[S_b \left((1 + S_c\eta)\exp\{S_b\eta\} \|y(\vartheta_k)\|\right)\right. \\ &\quad \left. + S_c \left\|y_{\vartheta_k}\right\|\right] ds \le \|y(t)\| + \eta \left[S_c + S_b (1 \right. \\ &\quad \left. + S_c\eta)\right] \|y(\vartheta_k)\|,\end{aligned} \tag{60}$$

and then

$$\|y(\vartheta_k)\| \le \mu \|y(t)\| \tag{61}$$

holds for $t \in [\eta_k, \eta_{k+1})$, so $\|y(\gamma(t))\| \le \mu\|y(t)\|$, where $\mu = (1 - \eta[S_c + S_b(1 + S_c\eta)\exp\{S_b\eta\}])^{-1}$. This completes the proof. □

Remark 10. Neural network model (49) is also of a hybrid type. The difficulty in investigating this class of neural networks lies in the existence of a switching jump and deviating argument. For the switching jump, we introduce the differential inclusions and fuzzy uncertainty approach to compensate state-jump uncertainty. For the deviating argument, by the aid of effective computational analysis, we estimate the norm of deviating state $y(\gamma(t))$ by the corresponding state $y(t)$.

In the following, the criterion to guarantee the global exponential stability of neural network model (5) based on the Lyapunov method is established.

Theorem 11. *Let (A1)–(A4) hold. The origin of neural network model (49) is globally exponentially stable, which implies that the equilibrium point $x^* = (x_1^*, x_2^*, \ldots, x_n^*)^T$ of neural network model (5) is globally exponentially stable, if the following condition is satisfied:*

$$\mu S_c - S_b^- < 0. \tag{62}$$

Proof. Denote

$$z_i(t) = \exp\{\lambda t\} \left|y_i(t)\right|, \quad i = 1, 2, \ldots, n, \tag{63}$$

where $\lambda = -(1/2)(\mu S_c - S_b^-) > 0$ is a positive constant satisfying

$$\lambda + \mu S_c - S_b^- = \frac{1}{2}\left(\mu S_c - S_b^-\right) < 0. \tag{64}$$

Then, for $t \ne \eta_k$, $k \in N$, calculate the derivative of $z_i(t)$ along the trajectory of (49) or (50):

$$\begin{aligned}\dot{z}_i(t) &= \lambda \exp\{\lambda t\} \left|y_i(t)\right| + \exp\{\lambda t\} \operatorname{sgn}\left(y_i(t)\right) \dot{y}_i(t) \\ &= \lambda \exp\{\lambda t\} \left|y_i(t)\right| + \exp\{\lambda t\} \operatorname{sgn}\left(y_i(t)\right) \\ &\quad \cdot \left(-a_i y_i(t) + \sum_{j=1}^{n} b_{ij}^0 g_j\left(y_j(t)\right)\right. \\ &\quad + \sum_{j=1}^{n} c_{ij}^0 g_j\left(y_j(\gamma(t))\right) + \sum_{j=1}^{n} \varphi_{ij}^b\left(y_j(t)\right) \\ &\quad \left. + \sum_{j=1}^{n} \varphi_{ij}^c\left(y_j(\gamma(t))\right)\right) \le \lambda \exp\{\lambda t\} \left|y_i(t)\right| \\ &\quad + \exp\{\lambda t\} \left(-a_i \left|y_i(t)\right| + \sum_{j=1}^{n} b_{ij}^+ \left|g_j\left(y_j(t)\right)\right|\right. \\ &\quad + \sum_{j=1}^{n} c_{ij}^+ \left|g_j\left(y_j(\gamma(t))\right)\right| + \sum_{j=1}^{n} \left|\varphi_{ij}^b\left(y_j(t)\right)\right| \\ &\quad \left. + \sum_{j=1}^{n} \left|\varphi_{ij}^c\left(y_j(\gamma(t))\right)\right|\right), \quad i = 1, 2, \ldots, n.\end{aligned} \tag{65}$$

Applying Lemma 4,

$$\begin{aligned}\dot{z}_i(t) &\le \exp\{\lambda t\} \left((\lambda - a_i) \left|y_i(t)\right| + \sum_{j=1}^{n} b_{ij}^+ \alpha \left|y_j(t)\right|\right. \\ &\quad + \sum_{j=1}^{n} c_{ij}^+ \alpha \left|y_j(\gamma(t))\right| + \sum_{j=1}^{n} b_{ij}^- \alpha \left|y_j(t)\right| \\ &\quad \left. + \sum_{j=1}^{n} c_{ij}^- \alpha \left|y_j(\gamma(t))\right|\right), \quad i = 1, 2, \ldots, n.\end{aligned} \tag{66}$$

Let

$$V(t) = \sum_{i=1}^{n} z_i(t); \tag{67}$$

then, for $t \ne \eta_k$, $k \in N$,

$$\begin{aligned}\dot{V}(t) &= \sum_{i=1}^{n} \dot{z}_i(t) \le \exp\{\lambda t\} \left(\sum_{i=1}^{n} (\lambda - a_i) \left|y_i(t)\right|\right. \\ &\quad + \sum_{i=1}^{n}\sum_{j=1}^{n} b_{ij}^+ \alpha \left|y_j(t)\right| + \sum_{i=1}^{n}\sum_{j=1}^{n} c_{ij}^+ \alpha \left|y_j(\gamma(t))\right| \\ &\quad \left. + \sum_{i=1}^{n}\sum_{j=1}^{n} b_{ij}^- \alpha \left|y_j(t)\right| + \sum_{i=1}^{n}\sum_{j=1}^{n} c_{ij}^- \alpha \left|y_j(\gamma(t))\right|\right) \\ &= \exp\{\lambda t\} \left(\sum_{i=1}^{n} (\lambda - a_i) \left|y_i(t)\right| + \sum_{i=1}^{n}\sum_{j=1}^{n} b_{ji}^+ \alpha \left|y_i(t)\right|\right. \\ &\quad \left. + \sum_{i=1}^{n}\sum_{j=1}^{n} c_{ji}^+ \alpha \left|y_i(\gamma(t))\right| + \sum_{i=1}^{n}\sum_{j=1}^{n} b_{ji}^- \alpha \left|y_i(t)\right|\right.\end{aligned}$$

$$+\sum_{i=1}^{n}\sum_{j=1}^{n}c_{ji}^{-}\alpha\left|y_i\left(\gamma\left(t\right)\right)\right|\Bigg)=\exp\left\{\lambda t\right\}$$
$$\cdot\left[\sum_{i=1}^{n}\left(\lambda-a_i+\sum_{j=1}^{n}\alpha\left(b_{ji}^{+}+b_{ji}^{-}\right)\right)\left|y_i\left(t\right)\right|\right.$$
$$\left.+\sum_{i=1}^{n}\left(\sum_{j=1}^{n}\alpha\left(c_{ji}^{+}+c_{ji}^{-}\right)\right)\left|y_i\left(\gamma\left(t\right)\right)\right|\right]\leq\exp\left\{\lambda t\right\}$$
$$\cdot\left[\left(\lambda-S_b^{-}\right)\left\|y\left(t\right)\right\|+S_c\left\|y\left(\gamma\left(t\right)\right)\right\|\right]. \tag{68}$$

Based on Lemma 9,

$$\dot{V}\left(t\right)\leq\exp\left\{\lambda t\right\}\left(\lambda-S_b^{-}+\mu S_c\right)\left\|y\left(t\right)\right\|. \tag{69}$$

From (64),

$$\lambda-S_b^{-}+\mu S_c<0; \tag{70}$$

then,

$$\dot{V}\left(t\right)\leq\exp\left\{\lambda t\right\}\left(\lambda-S_b^{-}+\mu S_c\right)\left\|y\left(t\right)\right\|\leq 0. \tag{71}$$

It is easy to see that

$$V\left(t\right)=\exp\left\{\lambda t\right\}\sum_{i=1}^{n}\left|y_i\left(t\right)\right|=\exp\left\{\lambda t\right\}\left\|y\left(t\right)\right\|\leq V\left(0\right)$$
$$=\left\|y\left(0\right)\right\|; \tag{72}$$

hence

$$\left\|y\left(t\right)\right\|\leq\left\|y\left(0\right)\right\|\exp\left\{-\lambda t\right\}; \tag{73}$$

that is

$$\left\|x\left(t\right)-x^{*}\right\|\leq\left\|x\left(0\right)-x^{*}\right\|\exp\left\{-\lambda t\right\}, \tag{74}$$

for $t\geq 0$. This completes the proof. □

3.4. Design Procedure of Autoassociative Memories. Given l ($l\leq 2^n$) vectors $u^{(1)}, u^{(2)},\ldots,u^{(l)}$ to be memorized, where $u^{(k)}\in\Omega$, for $k=1,2,\ldots,l$, the design procedure of autoassociative memories is stated as follows:

(1) Select matrix $\mathbb{E}$ as an identity matrix.

(2) According to (29) and (34), choose appropriate S_i, a_i, T_i, $\overline{b}_{ij}$, and $\overline{c}_{ij}$.

(3) Based on $S_i=\max(|\widehat{b}_{ii}p-a_id|,|\check{b}_{ii}p-a_id|)$, $\overline{b}_{ij}=\max(|\widehat{b}_{ij}|,|\check{b}_{ij}|)$, and $\overline{c}_{ij}=\max(|\widehat{c}_{ij}|,|\check{c}_{ij}|)$, the values of $\widehat{b}_{ij}$, $\check{b}_{ij}$, $\widehat{c}_{ij}$, and $\check{c}_{ij}$ can be selected.

(4) Calculate S_b, S_b^{-}, and S_c. Adjust the values of $\widehat{b}_{ij}$, $\check{b}_{ij}$, $\widehat{c}_{ij}$, and $\check{c}_{ij}$ to make sure that $S_c-S_b^{-}<0$.

(5) Solving the following inequalities: $\eta(S_b+2S_c)\exp\{S_b\eta\}<1$, $\eta(S_c+S_b(1+S_c\eta)\exp\{S_{b\eta}\})<1$, we can get $0<\eta<\overline{\eta}$.

(6) Take a proper $\eta\in(0,\overline{\eta})$ such that $\mu S_c-S_b^{-}<0$.

The output $w(t)$ will converge to the related memory pattern when matrices A, B, C, and $\mathbb{E}$ and scalar η are chosen as above.

3.5. Design Procedure of Heteroassociative Memories. Given l ($l\leq 2^n$) vectors to be memorized as $q^{(1)}, q^{(2)},\ldots,q^{(l)}$, which correspond to the external input patterns $u^{(1)}, u^{(2)},\ldots,u^{(l)}$, where $q^{(k)}\in\Omega$, $u^{(k)}\in\Omega$, $k=1,2,\ldots,l$, set $\mathbb{E}U=Q$, where $U=[u^{(1)},u^{(2)},\ldots,u^{(l)}]$, $Q=[q^{(1)},q^{(2)},\ldots,q^{(l)}]$. It is clear that heteroassociative memories can be treated as autoassociative memories when transform matrix $\mathbb{E}$ is obtained. Matrices A, B, and C and scalar η can be selected as the method used in autoassociative memories. The transform matrix $\mathbb{E}$ is obtained by the following steps:

(1) When $l=n$, that is, Q and U are square matrices, utilizing Matlab Toolbox, we can get inverse matrix of U as U^{-1}, and $\mathbb{E}$ can be obtained as $\mathbb{E}=QU^{-1}$.

(2) When $l<n$, add $n-l$ proper column vectors to U and Q, which constructs new matrices $\overline{U}$ and $\overline{Q}$, respectively, such that the ranks of matrices $\overline{U}$ and $\overline{Q}$ are full. And the transform matrix $\mathbb{E}$ can be obtained by $\mathbb{E}=\overline{Q}\,\overline{U}^{-1}$.

(3) When $n<l$, add $l-n$ proper row vectors to U and Q, which constructs new matrices $\widetilde{U}$ and $\widetilde{Q}$, such that the ranks of matrices $\widetilde{U}$ and $\widetilde{Q}$ are full. And the transform matrix $\mathbb{E}$ can be obtained by $\mathbb{E}=\widetilde{Q}\widetilde{U}^{-1}$. Note in particular, in this circumstance, that the dimensionality of each input and output pattern increases from n to l. And the front n values of each external input pattern carry out associative memories.

The output $w(t)$ will converge to the related memory pattern when matrices A, B, C, and $\mathbb{E}$ and scalar η are chosen as above.

4. Experimental Verification

In this section, in order to verify the effectiveness of the proposed results, several numerical examples are provided.

Example 12. The first example is state response of autoassociative memory.

Consider neural network model (5) with $n=12$, where $p=d=1$, $\eta=2/9$, $T_i=0.1$, $a_i=0.4$, and

$$\widehat{b}_{ij}=\widehat{c}_{ij}=\begin{cases}0.012, & i=j,\\ 0.01, & i\neq j,\end{cases}$$
$$\check{b}_{ij}=\check{c}_{ij}=\begin{cases}0.008, & i=j,\\ 0.006, & i\neq j,\end{cases} \tag{75}$$

with the activation functions

$$f_i\left(x_i\right)=-\frac{1}{2}\left(\left|x_i+0.1\right|-\left|x_i-0.1\right|\right)$$
$$+\frac{1}{2}\left(\left|x_i+1.1\right|-\left|x_i-1.1\right|\right) \tag{76}$$

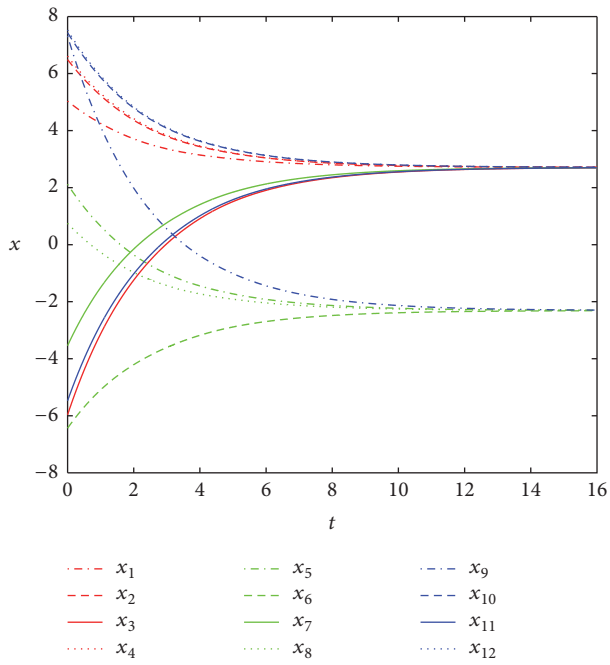

Figure 1: State response in neural network model (5) with external input u.

Table 1: The influences of a_i and d on the location of equilibrium points when $p = 1$ is a constant.

d		1.2	1.4	1.6	2.0	2.4	3.0
a_i	0.3	ν	ν	ν	ν	ν	—
	0.4	ν	ν	ν	ν	—	—
	0.5	ν	ν	ν	—	—	—
	0.6	ν	ν	—	—	—	—
	0.7	ν	—	—	—	—	—

"ν" ("—") denotes the equilibrium points located (not located) in the saturation regions.

Table 2: The influences of a_i and $\alpha = p/d$ on the location of equilibrium points when $d = 0.25$ is a constant.

$\alpha = \frac{p}{d}$		$\frac{1}{2}$	$\frac{2}{3}$	$\frac{3}{4}$	1	1.2	1.5
a_i	0.40	—	ν	ν	ν	ν	ν
	0.45	—	—	ν	ν	ν	ν
	0.60	—	—	—	ν	ν	ν
	0.70	—	—	—	—	ν	ν
	0.90	—	—	—	—	—	ν

"ν" ("—") denotes the equilibrium points located (not located) in the saturation region.

for $i, j = 1, 2, \ldots, 12$. Denote $u = q = (1, 1, 1, 1, -1, -1, 1, -1, -1, 1, 1, 1)^T$ as the external input vector and the memorized vector, respectively.

It follows from Theorem 11 that neural network model (5) has a unique equilibrium point, which is globally exponentially stable. The simulation result is shown in Figure 1.

It can be calculated easily that the equilibrium point in Figure 1 is

$$x^* = (2.71, 2.71, 2.71, 2.71, -2.31, -2.31, 2.71, -2.31, -2.31, 2.71, 2.71, 2.71)^T. \quad (77)$$

Clearly, the output pattern is

$$w^* = (1, 1, 1, 1, -1, -1, 1, -1, -1, 1, 1, 1)^T, \quad (78)$$

which is equivalent to the memorized pattern q. Hence, neural network model (5) can be implemented effectively as an autoassociative memory.

Remark 13. Because the equilibrium point is globally exponentially stable, the initial values can be selected randomly, and there is no influence on the performance of associative memories.

Example 14. The second example includes influences of a_i, d, and p on the location of equilibrium points.

The influences are divided into two cases to discuss.

Case 1. Let $p = 1$ be a constant and denote $u = q = (1, 1, 1, 1, -1, -1, 1, -1, -1, 1, 1, 1)^T$ as the external input vector and the memorized vector, respectively. Consider a_i and d as variables in neural network model (5), taking $\eta = 1/9$, and the rest of the parameters are the same as those in Example 12. The results are shown in Table 1, from which we can see that the smaller the value of a_i, the bigger the value range d can take for the sake of memorized pattern, and vice versa.

Case 2. Let $d = 0.25$ be a constant and denote $u = q = (p, p, p, p, -p, -p, p, -p, -p, p, p, p)^T$ as the external input vector and the memorized vector, respectively, where $p > 0$. Consider a_i and p (or $\alpha = p/d$) as variables in neural network model (5), taking $\eta = 1/9$, and the rest of the parameters are the same as those in Example 12. The results are shown in Table 2, from which we can see that α (or p) should increase when a_i increases for the sake of memorized pattern, and vice versa.

Remark 15. From Tables 1 and 2, it can be concluded that the associative memories performance becomes better with the increase of $\alpha = p/d$ when a_i is fixed, but not vice versa.

Example 16. The third example includes the influences of a_i and perturbed u on the recall success rate of memorized patterns.

Let $u = (1, 1, 1, 1, -1, -1, 1, -1, -1, 1, 1, 1)^T, \eta = 1/9$, and consider a_i $(i = 1, 2, \ldots, 12)$ as variables in neural network model (5). The other parameters are the same as those in Example 12. In this example, the influences of a_i and perturbed u are analyzed on the recall success rate of memorized vectors. Experimental results are illustrated in Table 3, which makes it clear that the robustness of neural network model (5) for perturbed input u will become stronger as a_i is small enough.

Table 3: The influences of a_i and perturbed u on the recall success rate.

a_i	0.3	0.4	0.5	0.6	0.7
0.9**u**	100%	100%	100%	100%	100%
0.84**u**	100%	100%	100%	100%	66.67%
0.63**u**	100%	100%	100%	66.67%	0
0.52**u**	100%	100%	66.67%	0	
0.41**u**	100%	66.67%	0		
0.25**u**	66.67%	0			
0.24**u**	0				

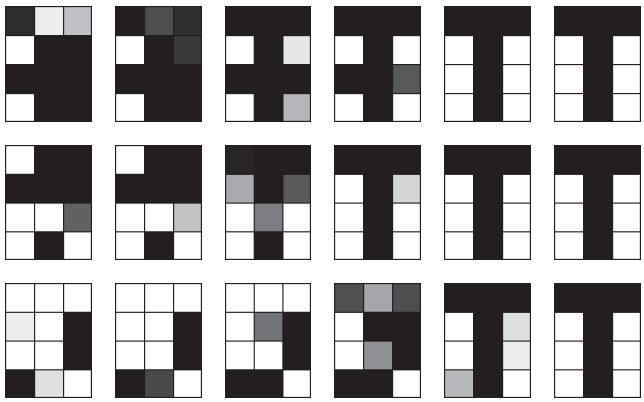

Figure 2: Typical evolutions of output pattern with input vector $u = q$ under three random initial values.

Remark 17. Table 3 illustrates that the robustness of associative memories on perturbed u becomes stronger with the decrease of a_i.

Example 18. The fourth example includes the application of autoassociative memory without input perturbation.

According to neural network model (5), design an autoassociative memory to memorize pattern "**T**" which is represented by a 4×3-pixel image (black pixel $= 1$; white pixel $= -1$) and the corresponding input pattern is $u = (1, 1, 1, -1, 1, -1, -1, 1, -1, -1, 1, -1)^T$. The parameters are the same as those in Example 12.

Simulation results with three random initial values are depicted in Figure 2, where the dark grey block indicates that the value of the related component of output $w(t)$ is in $(0, 1)$ and the light grey block indicates that the value of the related component of output $w(t)$ is in $(-1, 0)$. Obviously, the output pattern $w(t)$ converges to the memorized pattern correctly.

Example 19. The fifth example includes the application of autoassociative memory with input perturbation.

The aim of this experiment is to discuss the influence of input pattern perturbation on the output pattern. The parameters are the same as those in Example 12. Choose pattern "**T**" to be memorized, and the perturbed vector is selected as $u = k * q$, where $q = (1, 1, 1, -1, 1, -1, -1, 1, -1, -1, 1, -1)^T$ is the corresponding memorized vector and k is a perturbation coefficient.

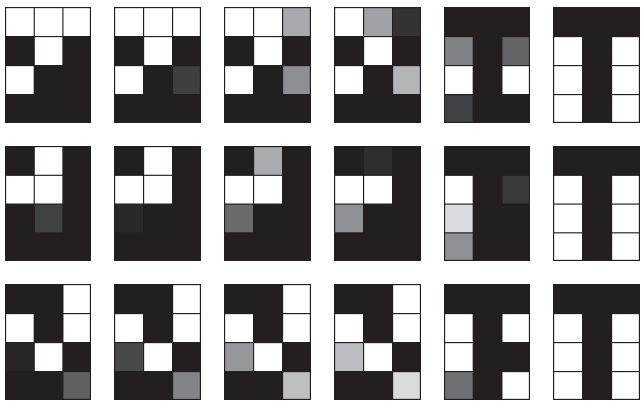

Figure 3: Typical evolutions of output pattern with input vector $u = 0.52 * q$ under three random initial values.

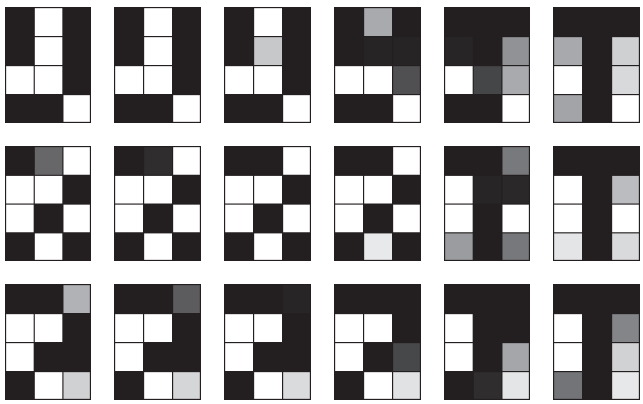

Figure 4: Typical evolutions of output pattern with input vector $u = 0.41 * q$ under three random initial values.

In what follows, the perturbed vector u is imposed on neural network model (5) as input vector with $k = 0.52$ and $k = 0.41$, respectively. Simulation results are shown in Figures 3 and 4. In Figure 3, the output pattern is exactly the same as the memorized pattern, and in Figure 4 the output pattern is different from the memorized pattern although they can be distinguished from the outlines.

Remark 20. From the analysis above, we can see that the output pattern will converge to the memorized pattern when the perturbation coefficient is not small enough. In fact, neural network model (5) is implemented well as an associative memory if the coefficient satisfying $k \geq 0.52$ and the other parameters are the same as those in Example 19.

Example 21. The sixth example includes the application of heteroassociative memory.

Consider neural network model (1), and the parameters are the same as those in Example 12 except the transform matrix $\mathbb{E}$, which will be given later. The aim of this experiment is to design a heteroassociative memory to memorize pattern "**U**" when the input pattern is "**C**." It is clear that the input vector is $u = (1, 1, 1, 1, -1, -1, 1, -1, -1, 1, 1, 1)^T$ and the corresponding output vector is $q = (1, -1, 1, 1, -1, 1, 1, -1, 1, 1, 1, 1,)^T$.

According to the heteroassociative memories design procedure, the matrices $\overline{U}$ and $\overline{Q}$ are constructed as

$$\overline{U} = \begin{bmatrix} 1 & 0 & 0 & 0 & 0 & 0 & 0 & 0 & 0 & 0 & 0 & 0 \\ 1 & 1 & 0 & 0 & 0 & 0 & 0 & 0 & 0 & 0 & 0 & 0 \\ 1 & 0 & 1 & 0 & 0 & 0 & 0 & 0 & 0 & 0 & 0 & 0 \\ 1 & 0 & 0 & 1 & 0 & 0 & 0 & 0 & 0 & 0 & 0 & 0 \\ -1 & 0 & 0 & 0 & 1 & 0 & 0 & 0 & 0 & 0 & 0 & 0 \\ -1 & 0 & 0 & 0 & 0 & 1 & 0 & 0 & 0 & 0 & 0 & 0 \\ 1 & 0 & 0 & 0 & 0 & 0 & 1 & 0 & 0 & 0 & 0 & 0 \\ -1 & 0 & 0 & 0 & 0 & 0 & 0 & 1 & 0 & 0 & 0 & 0 \\ -1 & 0 & 0 & 0 & 0 & 0 & 0 & 0 & 1 & 0 & 0 & 0 \\ 1 & 0 & 0 & 0 & 0 & 0 & 0 & 0 & 0 & 1 & 0 & 0 \\ 1 & 0 & 0 & 0 & 0 & 0 & 0 & 0 & 0 & 0 & 1 & 0 \\ 1 & 0 & 0 & 0 & 0 & 0 & 0 & 0 & 0 & 0 & 0 & 1 \end{bmatrix},$$

$$\overline{Q} = \begin{bmatrix} 1 & 0 & 0 & 0 & 0 & 0 & 0 & 0 & 0 & 0 & 0 & 0 \\ -1 & 1 & 0 & 0 & 0 & 0 & 0 & 0 & 0 & 0 & 0 & 0 \\ 1 & 0 & 1 & 0 & 0 & 0 & 0 & 0 & 0 & 0 & 0 & 0 \\ 1 & 0 & 0 & 1 & 0 & 0 & 0 & 0 & 0 & 0 & 0 & 0 \\ -1 & 0 & 0 & 0 & 1 & 0 & 0 & 0 & 0 & 0 & 0 & 0 \\ 1 & 0 & 0 & 0 & 0 & 1 & 0 & 0 & 0 & 0 & 0 & 0 \\ 1 & 0 & 0 & 0 & 0 & 0 & 1 & 0 & 0 & 0 & 0 & 0 \\ -1 & 0 & 0 & 0 & 0 & 0 & 0 & 1 & 0 & 0 & 0 & 0 \\ 1 & 0 & 0 & 0 & 0 & 0 & 0 & 0 & 1 & 0 & 0 & 0 \\ 1 & 0 & 0 & 0 & 0 & 0 & 0 & 0 & 0 & 1 & 0 & 0 \\ 1 & 0 & 0 & 0 & 0 & 0 & 0 & 0 & 0 & 0 & 1 & 0 \\ 1 & 0 & 0 & 0 & 0 & 0 & 0 & 0 & 0 & 0 & 0 & 1 \end{bmatrix}, \quad (79)$$

respectively.

Using the Matlab Toolbox, we can have

$$\mathbb{E} = \overline{Q}\,\overline{U}^{-1} = \begin{bmatrix} 1 & 0 & 0 & 0 & 0 & 0 & 0 & 0 & 0 & 0 & 0 & 0 \\ -2 & 1 & 0 & 0 & 0 & 0 & 0 & 0 & 0 & 0 & 0 & 0 \\ 0 & 0 & 1 & 0 & 0 & 0 & 0 & 0 & 0 & 0 & 0 & 0 \\ 0 & 0 & 0 & 1 & 0 & 0 & 0 & 0 & 0 & 0 & 0 & 0 \\ 0 & 0 & 0 & 0 & 1 & 0 & 0 & 0 & 0 & 0 & 0 & 0 \\ 2 & 0 & 0 & 0 & 0 & 1 & 0 & 0 & 0 & 0 & 0 & 0 \\ 0 & 0 & 0 & 0 & 0 & 0 & 1 & 0 & 0 & 0 & 0 & 0 \\ 0 & 0 & 0 & 0 & 0 & 0 & 0 & 1 & 0 & 0 & 0 & 0 \\ 2 & 0 & 0 & 0 & 0 & 0 & 0 & 0 & 1 & 0 & 0 & 0 \\ 0 & 0 & 0 & 0 & 0 & 0 & 0 & 0 & 0 & 1 & 0 & 0 \\ 0 & 0 & 0 & 0 & 0 & 0 & 0 & 0 & 0 & 0 & 1 & 0 \\ 0 & 0 & 0 & 0 & 0 & 0 & 0 & 0 & 0 & 0 & 0 & 1 \end{bmatrix}. \quad (80)$$

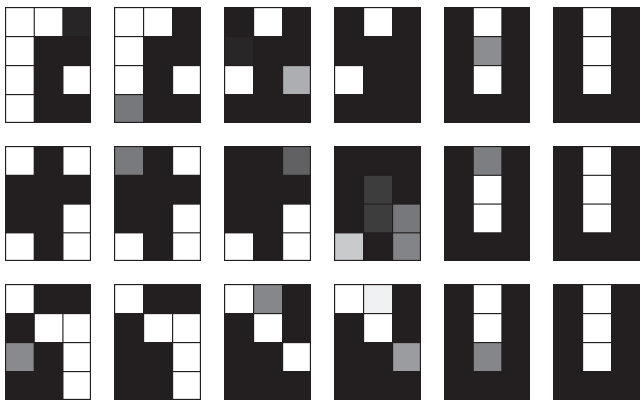

Figure 5: Typical evolutions of pattern "**U**" with input pattern "**C**" under three random initial values.

The simulation results are depicted in Figure 5, which shows that the output pattern "**U**" is memorized when the input pattern is "**C**" and the transform matrix $\mathbb{E}$ is selected as above. This indicates that neural network model (1) can perform well as a heteroassociative memory under a proper transform matrix $\mathbb{E}$, which can be easily obtained by using the Matlab Toolbox.

Remark 22. Simulation results in Figure 5 show that the associative memories model presented in this paper can be implemented well as autoassociative memories and heteroassociative memories. This model possesses the resistance capacity against external input perturbations and can be regarded as an extension and complement to the relevant results [10, 11, 16].

5. Concluding Remarks

Analysis and design of associative memories for recurrent neural networks have drawn considerable attention, whereas analysis and design of associative memories for memristive neural networks with deviating argument have not been well investigated. This paper presents a general class of memristive neural networks with deviating argument and discusses the analysis and design of autoassociative memories and heteroassociative memories. Meanwhile, the robustness of this class of neural networks is demonstrated when external input patterns are seriously perturbed. To the best of the author's knowledge, this is the first theoretical result on associative memories for memristive neural networks with deviating argument. Future works may aim at (1) studying associative memories based on multistability of memristive neural networks with deviating argument; (2) analyzing associative memories based on discrete-time memristive neural networks with deviating argument; (3) exploring high-capacity associative memories for memristive neural networks with deviating argument.

Conflicts of Interest

The author declares that there are no conflicts of interest regarding the publication of this paper.

Acknowledgments

This work is supported by the Research Project of Hubei Provincial Department of Education of China under Grant T201412.

References

[1] J. Tian and S. Zhong, "Improved delay-dependent stability criterion for neural networks with time-varying delay," *Applied Mathematics and Computation*, vol. 217, no. 24, pp. 10278–10288, 2011.

[2] Y. Du, S. Zhong, and N. Zhou, "Global asymptotic stability of Markovian jumping stochastic Cohen-Grossberg BAM neural networks with discrete and distributed time-varying delays," *Applied Mathematics and Computation*, vol. 243, pp. 624–636, 2014.

[3] W.-H. Chen, X. Lu, and W. X. Zheng, "Impulsive stabilization and impulsive synchronization of discrete-time delayed neural networks," *IEEE Transactions on Neural Networks and Learning Systems*, vol. 26, no. 4, pp. 734–748, 2015.

[4] H. Zhang, F. Yang, X. Liu, and Q. Zhang, "Stability analysis for neural networks with time-varying delay based on quadratic convex combination," *IEEE Transactions on Neural Networks and Learning Systems*, vol. 24, no. 4, pp. 513–521, 2013.

[5] S. Wen, T. Huang, Z. Zeng, Y. Chen, and P. Li, "Circuit design and exponential stabilization of memristive neural networks," *Neural Networks*, vol. 63, pp. 48–56, 2015.

[6] A. L. Wu, L. Liu, T. W. Huang, and Z. G. Zeng, "Mittag-Leffler stability of fractional-order neural networks in the presence of generalized piecewise constant arguments," *Neural Networks*, vol. 85, pp. 118–127, 2017.

[7] C. Hu, J. Yu, Z. H. Chen, H. J. Jiang, and T. W. Huang, "Fixed-time stability of dynamical systems and fixed-time synchronization of coupled discontinuous neural networks," *Neural Networks*, vol. 89, pp. 74–83, 2017.

[8] T. W. Huang, "Robust stability of delayed fuzzy Cohen-Grossberg neural networks," *Computers & Mathematics with Applications*, vol. 61, no. 8, pp. 2247–2250, 2011.

[9] G. Grass, "On discrete-time cellular neural networks for associative memories," *IEEE Transactions on Circuits and Systems I: Fundamental Theory and Applications*, vol. 48, no. 1, pp. 107–111, 2001.

[10] Q. Han, X. Liao, T. Huang, J. Peng, C. Li, and H. Huang, "Analysis and design of associative memories based on stability of cellular neural networks," *Neurocomputing*, vol. 97, pp. 192–200, 2012.

[11] M. S. Tarkov, "Oscillatory neural associative memories with synapses based on memristor bridges," *Optical Memory and Neural Networks*, vol. 25, no. 4, pp. 219–227, 2016.

[12] M. Baghelani, A. Ebrahimi, and H. B. Ghavifekr, "Design of RF MEMS based oscillatory neural network for ultra high speed associative memories," *Neural Processing Letters*, vol. 40, no. 1, pp. 93–102, 2014.

[13] M. Kobayashi, "Gradient descent learning rule for complex-valued associative memories with large constant terms," *IEEJ Transactions on Electrical and Electronic Engineering*, vol. 11, no. 3, pp. 357–363, 2016.

[14] A. R. Trivedi, S. Datta, and S. Mukhopadhyay, "Application of silicon-germanium source tunnel-fet to enable ultralow power cellular neural network-based associative memory," *IEEE Transactions on Electron Devices*, vol. 61, no. 11, pp. 3707–3715, 2014.

[15] Y. Wu and S. N. Batalama, "Improved one-shot learning for feedforward associative memories with application to composite pattern association," *IEEE Transactions on Systems, Man, and Cybernetics, Part B: Cybernetics*, vol. 31, no. 1, pp. 119–125, 2001.

[16] C. Zhou, X. Zeng, J. Yu, and H. Jiang, "A unified associative memory model based on external inputs of continuous recurrent neural networks," *Neurocomputing*, vol. 186, pp. 44–53, 2016.

[17] R. Zhang, D. Zeng, S. Zhong, and Y. Yu, "Event-triggered sampling control for stability and stabilization of memristive neural networks with communication delays," *Applied Mathematics and Computation*, vol. 310, pp. 57–74, 2017.

[18] G. Zhang and Y. Shen, "Exponential stabilization of memristor-based chaotic neural networks with time-varying delays via intermittent control," *IEEE Transactions on Neural Networks and Learning Systems*, vol. 26, no. 7, pp. 1431–1441, 2015.

[19] S. Wen, Z. Zeng, T. Huang, and Y. Zhang, "Exponential adaptive lag synchronization of memristive neural networks via fuzzy method and applications in pseudo random number generators," *IEEE Transactions on Fuzzy Systems*, 2013.

[20] A. Wu and Z. Zhigang, "Lagrange stability of memristive neural networks with discrete and distributed delays," *IEEE Transactions on Neural Networks and Learning Systems*, vol. 25, no. 4, pp. 690–703, 2014.

[21] S. B. Ding, Z. S. Wang, J. D. Wang, and H. G. Zhang, "H_∞ state estimation for memristive neural networks with time-varying delays: The discrete-time case," *Neural Networks*, vol. 84, pp. 47–56, 2016.

[22] Q. Zhong, J. Cheng, Y. Zhao, J. Ma, and B. Huang, "Finite-time H_∞ filtering for a class of discrete-time Markovian jump systems with switching transition probabilities subject to average dwell time switching," *Applied Mathematics and Computation*, vol. 225, pp. 278–294, 2013.

[23] K. Shi, X. Liu, H. Zhu, S. Zhong, Y. Zeng, and C. Yin, "Novel delay-dependent master-slave synchronization criteria of chaotic Lur'e systems with time-varying-delay feedback control," *Applied Mathematics and Computation*, vol. 282, pp. 137–154, 2016.

[24] M. U. Akhmet, D. Aruğaslan, and E. Yilmaz, "Stability analysis of recurrent neural networks with piecewise constant argument of generalized type," *Neural Networks*, vol. 23, no. 7, pp. 805–811, 2010.

[25] M. U. Akhmet, D. Aruğaslan, and E. Yılmaz, "Stability in cellular neural networks with a piecewise constant argument," *Journal of Computational and Applied Mathematics*, vol. 233, no. 9, pp. 2365–2373, 2010.

[26] M. U. Akhmet and E. Yılmaz, "Impulsive Hopfield-type neural network system with piecewise constant argument," *Nonlinear Analysis: Real World Applications*, vol. 11, no. 4, pp. 2584–2593, 2010.

[27] K.-S. Chiu, M. Pinto, and J.-C. Jeng, "Existence and global convergence of periodic solutions in recurrent neural network models with a general piecewise alternately advanced and retarded argument," *Acta Applicandae Mathematicae*, vol. 133, pp. 133–152, 2014.

[28] L. G. Wan and A. L. Wu, "Stabilization control of generalized type neural networks with piecewise constant argument," *Journal of Nonlinear Science and Applications*, vol. 9, no. 6, pp. 3580–3599, 2016.

[29] L. Liu, A. L. Wu, Z. G. Zeng, and T. W. Huang, "Global mean square exponential stability of stochastic neural networks with retarded and advanced argument," *Neurocomputing*, vol. 247, pp. 156–164, 2017.

[30] A. Wu and Z. Zeng, "Output convergence of fuzzy neurodynamic system with piecewise constant argument of generalized type and time-varying input," *IEEE Transactions on Systems, Man, and Cybernetics: Systems*, vol. 46, no. 12, pp. 1689–1702, 2016.

Hindawi
Mathematical Problems in Engineering
Volume 2017, Article ID 8123830, 16 pages
https://doi.org/10.1155/2017/8123830

Research Article

Delay-Dependent Stability Analysis of TS Fuzzy Switched Time-Delay Systems

Nawel Aoun,[1,2] Marwen Kermani,[1] and Anis Sakly[1]

[1]*Research Unit of Industrial Systems Study and Renewable Energy (ESIER), National Engineering School of Monastir (ENIM), University of Monastir, Ibn El Jazzar, Skaness, 5019 Monastir, Tunisia*
[2]*National Engineering School of Sousse (ENISo), University of Sousse, Pôle Technologique de Sousse, Route de Ceinture Sahloul, 4054 Sousse, Tunisia*

Correspondence should be addressed to Marwen Kermani; kermanimarwen@gmail.com

Received 14 February 2017; Revised 17 April 2017; Accepted 7 May 2017; Published 7 June 2017

Academic Editor: Radek Matušů

This paper proposes a new approach to deal with the problem of stability under arbitrary switching of continuous-time switched time-delay systems represented by TS fuzzy models. The considered class of systems, initially described by delayed differential equations, is first put under a specific state space representation, called arrow form matrix. Then, by constructing a pseudo-overvaluing system, common to all fuzzy submodels and relative to a regular vector norm, we can obtain sufficient asymptotic stability conditions through the application of Borne and Gentina practical stability criterion. The stability criterion, hence obtained, is algebraic, is easy to use, and permits avoiding the problem of existence of a common Lyapunov-Krasovskii functional, considered as a difficult task even for some low-order linear switched systems. Finally, three numerical examples are given to show the effectiveness of the proposed method.

1. Introduction

Switched systems, seen as an important class of hybrid dynamical systems, are defined as a family of subsystems described by differential or difference equations and a rule that governs the switching between them [1, 2]. They have a strong engineering background in various areas and are often used to suitably model a great number of real-world systems, such as mechanical systems, chemical processes, communication networks, robotic systems, and aircraft and air traffic.

On the other hand, since the significant development that has witnessed the field of fuzzy modeling and control and more particularly model-based control, a new theory about fuzzy switched systems has emerged as an answer to more complicated real systems analysis and synthesis requirements such as multiple nonlinear systems, switched nonlinear systems, and second-order nonholonomic systems [3–10].

Originally inspired from the concept of sector nonlinearity, the main idea of Takagi-Sugeno fuzzy modeling is to partition the nonlinear system dynamics into several locally linearized models so that the overall nonlinear system could be represented by a sufficiently accurate approximation [11]. Hence, model-based control is considered as a powerful universal approximation tool and a reliable approach to deal with complex and ill-determined systems [12–15].

A fuzzy switched system is defined as a switched system which involves fuzzy models among its subsystems.

Despite the considerable efforts made for the analysis of nonlinear systems, stability study of switched systems and in particular of fuzzy switched systems is still complex. Indeed, the example of asymptotically stable subsystems which, due to a specific switching sequence, yield to an unstable behavior of the overall system is well known. Besides, the case of unstable subsystems that, via a particular stabilizing switching law, lead to a stable global system also exists.

The stability problem of such systems becomes more challenging when time delay is involved [16]. In fact, time delay often occurs in many dynamical systems, namely, in biological systems, chemical systems, metallurgical processing systems, and network systems. Its existence, whether in the

state variables, control inputs, or the measurement outputs, is frequently a source of instability and poor performance.

The existing results on stability of TS fuzzy switched time-delay systems can be classified into two types: delay-independent criteria, which are applicable to delay of arbitrary size [17–20] and delay-dependent criteria, which include information on the size of the delay [21]. It is generally recognized that delay-dependent results are usually less conservative than delay-independent ones, especially when the size of the delay is small.

Stability analysis of switched systems in general has been conducted mainly on the basis of Lyapunov stability theory and concerns two major problems [22–24].

The first is related to the asymptotic stability of switched systems under arbitrary switching. An important result in this area states that a sufficient condition for the asymptotic stability of this class of systems is that all the subsystems share a common Lyapunov function [25–31]. Sufficient stability conditions are then derived through the resolution of a set of Linear Matrix Inequalities (LMIs).

In the case of switched time-delay systems, a common Lyapunov-Krasovskii functional is searched [32–34]. However, checking the existence of such a functional is a hard task even for some simple cases. Moreover, the method becomes less reliable when the number of subsystems switching between each other is important or when the number of fuzzy rules required to model each subsystem with a good accuracy is high.

A second problem concerns the stabilization of TS fuzzy switched systems by restricting the class of admissible switching signals to those in which the interval between any two consecutive switching instants is no smaller than a number τ called dwell time [35].

To overcome limitations due to the existence of Lyapunov-Krasovskii functionals, we propose, in this paper, to study the stability of TS fuzzy switched systems through the convergence of a regular vector norm, associated with a specific characteristic matrix, called arrow form matrix [36–43]. The proposed method is based on the construction of a common overvaluing/comparison system for all the fuzzy submodels and whose stability permits concluding to that of the original system. The obtained results, valuable for the case of arbitrary switching, are expressed in terms of simple algebraic conditions and explicitly involve the time delay.

The application of vector norms to switched systems has already been introduced in [44–47]. It has been extended later to switched time-delay systems in [48–53].

The remainder of the paper is organized as follows: Section 2 presents the problem formulation and some preliminaries. In Section 3, new delay-dependent stability conditions are derived for a class of TS fuzzy switched time-delay systems described by differential equations and having a single constant delay. Section 4 generalizes the main result to the case of TS fuzzy switched systems with multiple delays. Three numerical examples are provided in Section 5 to demonstrate the effectiveness of the proposed method. Finally, some concluding remarks are given in Section 6.

Notations. The notations used throughout this paper are fairly standard. $\Re^n$ denotes the n-dimensional Euclidean space, I_n is the identity matrix with appropriate dimensions, and $\|\cdot\|$ denotes Euclidean vector norm. For any $u = (u_i)_{1\le i\le n}$, $v = (v_i)_{1\le i\le n} \in \Re^n$, we define the scalar product of the vectors u and v as $\langle u, v\rangle = \sum_{i=1}^{n} u_i v_i$. $M = (m_{i,j})_{1\le i,j\le n}$, M^T and M^{-1} are its transpose and its inverse, respectively. We denote $M^* = ({m_{i,j}}^*)_{1\le i,j\le n}$ with ${m_{i,j}}^* = m_{i,j}$ if $i = j$ and ${m_{i,j}}^* = |m_{i,j}|$ if $i \ne j$ and $|M| = |m_{i,j}|$, $\forall 1 \le i, j \le n$.

2. Problem Formulation and Preliminaries

2.1. Problem Formulation. Let us consider the unforced switched nonlinear time-delay systems that are described by a differential equation of the form:

$$\begin{aligned} \dot{x}(t) &= f_{\sigma(t)}(x(t), x(t-\tau)) \\ x(t) &= \Phi(t), \quad t \in [-\tau, 0], \end{aligned} \tag{1}$$

where $x(t) \in \Re^n$ is the state vector, $\tau > 0$ is the time delay, $\Phi : [-\tau, 0] \to \Re^n$ is a differentiable vector valued initial function, $f_\sigma : \Re^n \to \Re^n$ are sufficiently regular functions that are parametrized by the index set $I = \{1, 2, \ldots, N\}$, $\sigma(t) : \Re^n \to I$ is a piecewise constant function depending on time, called switching signal and assumed to be available in real time, and N is the number of subsystems.

The switching sequence is defined through a switching vector $\xi(t) = [\xi_1(t), \ldots, \xi_N(t)]^T$ whose components $\xi_i(t)$ are given by

$$\xi_i(t) = \begin{cases} 1 & \text{if } \sigma(t) = i,\ i \in I \text{ (i.e. subsystem } i \text{ is active)} \\ 0 & \text{otherwise.} \end{cases} \tag{2}$$

It is obvious that $\sum_{i=1}^{N} \xi_i(t) = 1\ \forall t \ge 0$.

Therefore, the switched system is composed of N subsystems expressed as

$$\begin{aligned} \dot{x}(t) &= f_i(x(t), x(t-\tau)), \quad i \in I \\ x(t) &= \Phi(t), \quad t \in [-\tau, 0]. \end{aligned} \tag{3}$$

In addition, each subsystem $\sum_{f_i}$ is described by a set of IF-THEN rules; each rule is related to a region of the state space where the subsystem could be approximated by a local linear model.

Thus, the lth fuzzy rule associated with the ith subsystem is given by

$$\begin{aligned} R_i^l: \quad & \text{IF } z_1(t) \text{ is } M_{li}^1 \text{ and} \ldots \text{and } z_p(t) \text{ is } M_{li}^p \\ & \text{THEN} \begin{cases} \dot{x}(t) = A_{li}x(t) + D_{li}x(t-\tau) \\ x(t) = \Phi(t), \quad t \in [-\tau, 0], \end{cases} \end{aligned} \tag{4}$$

where $z_1(t), \ldots, z_p(t)$ are the premise variables, A_{li} and D_{li} ($l = 1, \ldots, r$ and $i = 1, \ldots, N$) are matrices of appropriate

dimensions, M_{li}^{j} $(j = 1, \ldots, p)$ are the fuzzy sets, and r and p are the number of fuzzy rules and premise variables, respectively.

By using the product inference engine and the center of average defuzzification, the ith TS fuzzy subsystem can be inferred as

$$\dot{x}(t) = \sum_{l=1}^{r} h_{li}(z(t)) \left(A_{li}x(t) + D_{li}x(t-\tau)\right), \tag{5}$$

where $z(t) = [z_1(t), \ldots, z_p(t)]^T$ and $h_{li}(z(t)) : \mathfrak{R}^p \to [0,1]$ are the normalized weighting functions expressed by

$$h_{li}(z(t)) = \frac{w_{li}(z(t))}{\sum_{l=1}^{r} w_{li}(z(t))} = \frac{\prod_{j=1}^{p} M_{li}^{j}\left(z_j(t)\right)}{\sum_{l=1}^{r}\prod_{j=1}^{p} M_{li}^{j}\left(z_j(t)\right)}. \tag{6}$$

$M_{li}^{j}(z_j(t))$ is the firing strength of the membership function M_{li}^{j}. It is assumed that $w_{li}(z_j(t)) \geq 0$ and $\sum_{l=1}^{r} w_{li}(z_j(t)) > 0$.

Hence, $h_{li}(z(t)) \geq 0$ and $\sum_{l=1}^{r} h_{li}(z(t)) = 1$.

Finally, the fuzzy switched system (3) can be represented by

$$\dot{x}(t) = \sum_{i=1}^{N}\sum_{l=1}^{r} \xi_i(t)\, h_{li}(z(t)) \left(A_{li}x(t) + D_{li}x(t-\tau)\right). \tag{7}$$

Equation (7) can also be written as

$$\dot{x}(t) = \sum_{l=1}^{r} h_{l\sigma(t)}(z(t)) \left(A_{l\sigma(t)}x(t) + D_{l\sigma(t)}x(t-\tau)\right). \tag{8}$$

By using the Newton-Leibniz formula,

$$x(t-\tau) = x(t) - \int_{t-\tau}^{t} \dot{x}(\theta)\, d\theta. \tag{9}$$

Equation (8) can be written as

$$\begin{aligned}\dot{x}(t) = \sum_{i=1}^{N} \xi_i(t) \sum_{l=1}^{r} h_{li} \Big\{ &\left(A_{li} + D_{li}\right)x(t) \\ &- \left(D_{li}A_{li}\right)\int_{t-\tau}^{t} x(\theta)\, d\theta - \left(D_{li}\right)^2 \int_{t-\tau}^{t} x(\theta-\tau)\, d\theta \Big\}.\end{aligned} \tag{10}$$

In the sequel, $h_{li}(z(t))$ will be simplified by h_{li}.

2.2. Preliminaries. This subsection recalls some of the definitions and remarks that will be useful throughout this paper.

Kotelyanski Lemma (see [54]). *The real parts of the eigenvalues of matrix A, with non-negative off-diagonal elements, are less than a real number μ if and only if all those of matrix M; $M = \mu I_n - A$ are positive, with I_n the n identity matrix.*

Definition 1 (see [43]). The matrix $A(\cdot) = (a_{i,j}(\cdot))_{1\leq i,j\leq n}$ is called an M-matrix, if the following conditions are met:

(i) $a_{ii}(\cdot) > 0$ $(i = 1, \ldots, n)$, $a_{ij}(\cdot) \leq 0$ $(i \neq j; i, j = 1, \ldots, n)$;

(ii) the principal minors of $A(\cdot)$ are all positive:

$$(A(\cdot))\begin{pmatrix} 1 & 2 & \cdots & j \\ 1 & 2 & \cdots & j \end{pmatrix} > 0, \quad j = 1, \ldots, n; \tag{11}$$

(iii) for any positive real vector $\eta = [\eta_1, \ldots, \eta_n]^T$, the algebraic equations $A(\cdot)x = \eta$ have a positive solution $w = [w_1, \ldots, w_n]^T$.

Remark 2. $A(\cdot) = (a_{i,j}(\cdot))_{1\leq i,j\leq n}$ is the opposite of an M-matrix if $(-A(\cdot))$ is an M-matrix.

Remark 3. A continuous-time system characterized by $A(\cdot)$ is stable if $A(\cdot)$ is the opposite of an M-matrix. In this case, the main minors of $A(\cdot)$ are of alternating signs (the first is negative) and the Kotelyanski lemma permits concluding to the stability of the system characterized by $A(\cdot)$.

Definition 4 (see [43, 55]). If $M_c(\cdot)$ is a pseudo-overvaluing matrix of the system $\dot{x}(t) = A_i(\cdot)x(t)$ with respect to the vector norm $p(x) = [|x_1|, \ldots, |x_n|]^T$, the following inequality is satisfied:

$$D^+ p(x) \leq M_c(\cdot)\, p(x), \tag{12}$$

where D^+ denotes the right hand derivative operator.

Consequently, the stability of the comparison system, $\dot{z}(t) = M_c(\cdot)z(t)$ with the initial conditions such as $z_0 = p(x_0)$, implies the same property for the initial system.

3. Delay-Dependent Stability Conditions for TS Fuzzy Switched Systems with Single Delay

3.1. Main Results. In this section, new delay-dependent conditions for global asymptotic stability of system (10) under arbitrary switching are stated.

Theorem 5. *System (10) is globally asymptotically stable under an arbitrary switching rule $\sigma(t) = i$, $i \in I$, if matrix*

$$T_m = \max_{\substack{1\leq i\leq N \\ 1\leq l\leq r}} \left(T_{li}\right) \tag{13}$$

is the opposite of an M-matrix, where

$$T_{li} = \left(A_{li} + D_{li}\right)^* + \tau\left(\left|D_{li}A_{li}\right| + \left|D_{li}{}^2\right|\right). \tag{14}$$

Proof. Let $w \in \mathfrak{R}_+^{*n}$ with components $(w_m > 0, \forall m = 1, \ldots, n)$ and consider the radially unbounded candidate Lyapunov functional for each fuzzy submodel $\sum_{A_{li},D_{li}}$ given by

$$V(t) = V_1(t) + V_2(t) + V_3(t) + V_4(t), \tag{15}$$

where

$$\begin{aligned} V_1(t) &= \langle |x(t)|, w\rangle \\ V_2(t) &= \left\langle \left|D_{li}A_{li}\right| \int_{-\tau}^{0}\int_{t+\theta}^{t} |x(s)|\, ds\, d\theta, w \right\rangle \\ V_3(t) &= \left\langle \left|D_{li}{}^2\right| \int_{-\tau}^{0}\int_{t+\theta}^{t} |x(s-\tau)|\, ds\, d\theta, w \right\rangle \\ V_4(t) &= \tau \left\langle \left|D_{li}{}^2\right| \int_{t-\tau}^{t} |x(s)|\, ds, w \right\rangle. \end{aligned} \tag{16}$$

It is clear that $V(t_0) < \infty$ and that a common Lyapunov functional for all the submodels can be given by

$$V_c(t) = \max_{\substack{1\le i\le N\\ 1\le l\le r}} (V(t)). \tag{17}$$

The right Dini derivative of $V(t)$ along the trajectory of system (10) gives

$$\begin{aligned} D^+V(t)\big|_{(10)} &= \sum_{j=1}^{4} D^+V_j(t)\big|_{(10)} \\ D^+V_1(t)\big|_{(10)} &= \left\langle \frac{d^+|x(t)|}{dt^+}, w \right\rangle \\ &= \left\langle \operatorname{sgn}(x(t)) \frac{d^+x(t)}{dt^+}, w \right\rangle \end{aligned} \tag{18}$$

with

$$\operatorname{sgn}(x(t)) = \begin{pmatrix} \operatorname{sgn} x_1(t) & & \\ & \ddots & \\ & & \operatorname{sgn} x_n(t) \end{pmatrix}. \tag{19}$$

Then,

$$\begin{aligned} D^+V_1(t)\big|_{(10)} &= \left\langle \operatorname{sgn}(x(t)) \left\{ (A_{li}+D_{li})x(t) \right.\right. \\ &\quad - (D_{li}A_{li}) \int_{t-\tau}^{t} x(\theta)\, d\theta \\ &\quad \left.\left. - (D_{li})^2 \int_{t-\tau}^{t} x(\theta-\tau)\, d\theta \right\}, w \right\rangle \le \left\langle (A_{li}+D_{li})^* \right. \\ &\quad \left. \cdot |x(t)|, w \right\rangle + \left\langle \left|D_{li}A_{li}\right| \int_{t-\tau}^{t} |x(\theta)|\, d\theta, w \right\rangle \\ &\quad + \left\langle \left|D_{li}{}^2\right| \int_{t-\tau}^{t} |x(\theta-\tau)|\, d\theta, w \right\rangle \\ D^+V_2(t)\big|_{(10)} &= \left\langle \left|D_{li}A_{li}\right| \left(\tau|x(t)| - \int_{t-\tau}^{t} |x(s)|\, ds \right), \right. \\ &\quad \left. w \right\rangle = \left\langle \tau \left|D_{li}A_{li}\right| |x(t)|, w \right\rangle - \left\langle \left|D_{li}A_{li}\right| \right. \\ &\quad \left. \cdot \int_{t-\tau}^{t} |x(s)|\, ds, w \right\rangle \\ D^+V_3(t)\big|_{(10)} &= \left\langle \left|D_{li}{}^2\right| \left(\tau|x(t-\tau)| \right.\right. \\ &\quad \left.\left. - \int_{t-\tau}^{t} |x(s-\tau)|\, ds \right), w \right\rangle = \left\langle \tau \left|D_{li}{}^2\right| |x(t-\tau)|, w \right\rangle \\ &\quad - \left\langle \left|D_{li}{}^2\right| \int_{t-\tau}^{t} |x(s-\tau)|\, ds, w \right\rangle \\ D^+V_4(t)\big|_{(10)} &= \left\langle \tau \left|D_{li}{}^2\right| (|x(t)| - |x(t-\tau)|), w \right\rangle \\ &= \left\langle \tau \left|D_{li}{}^2\right| |x(t)|, w \right\rangle - \left\langle \tau \left|D_{li}{}^2\right| |x(t-\tau)|, w \right\rangle. \end{aligned} \tag{20}$$

Finally, we obtain

$$\begin{aligned} &D^+V(t)\big|_{(10)} \\ &\le \left\langle \left\{ (A_{li}+D_{li})^* + \tau\left(\left|D_{li}A_{li}\right| + \left|D_{li}{}^2\right| \right) \right\} |x(t)|, w \right\rangle \\ &\le \langle T_m |x(t)|, w\rangle, \end{aligned} \tag{21}$$

where

$$T_m = \max_{\substack{1\le i\le N\\ 1\le l\le r}} \left\{ (A_{li}+D_{li})^* + \tau\left(\left|D_{li}A_{li}\right| + \left|D_{li}{}^2\right| \right) \right\}. \tag{22}$$

On the other hand, if we suppose that T_m is the opposite of an M-matrix and according to the M-matrices properties, we can find a vector $\rho \in \mathfrak{R}_+^{*n}$ ($\rho_l > 0\ \forall l = 1, \ldots, n$) satisfying the relation: ${T_m}^T w = -\rho$, $\forall w \in \mathfrak{R}_+^{*n}$.

Knowing that

$$\langle T_m |x(t)|, w\rangle = \left\langle {T_m}^T w, |x(t)| \right\rangle, \tag{23}$$

we can write

$$\begin{aligned} D^+V(t)\big|_{(10)} &\le \left\langle {T_m}^T w, |x(t)| \right\rangle = \langle -\rho, |x(t)| \rangle \\ &= -\sum_{l=1}^{n} \rho_l |x_l(t)| < 0. \end{aligned} \tag{24}$$

This completes the proof of Theorem 5. □

3.2. Extension of the Results to the Case of TS Fuzzy Switched Systems Described by Delayed Differential Equations with Single Delay. In this section, we consider the class of TS

fuzzy switched time-delay systems that are governed by the following differential equation:

$$y^{(n)}(t) + \sum_{i=1}^{N} \xi_i(t) \cdot \left\{ \sum_{l=1}^{r} h_{li} \left(\sum_{j=0}^{n-1} a_{li}^{j} y^{(j)}(t) + \sum_{j=0}^{n-1} d_{li}^{j} y^{(j)}(t-\tau) \right) \right\} = 0, \tag{25}$$

where $y(t) \in \Re^n$ is the state vector and a_{li}^{j} and d_{li}^{j} ($l = 1, \ldots, r$; $i = 1, \ldots, N$; and $j = 0, \ldots, n-1$) are constant coefficients.

A change of variable under the form $x_{j+1}(t) = y^{(j)}(t)$, $j = 0, \ldots, n-1$, allows system (25) to be represented in the state space as follows:

$$\begin{aligned} \dot{x}(t) &= \sum_{i=1}^{N} \xi_i(t) \sum_{l=1}^{r} h_{li} \left(A_{li} x(t) + D_{li} x(t-\tau) \right) \\ x(t) &= \Phi(t), \quad t \in [-\tau, 0], \end{aligned} \tag{26}$$

where matrices A_{li} and D_{li} are given by

$$\begin{aligned} A_{li} &= \begin{pmatrix} 0 & 1 & \cdots & 0 \\ \vdots & \ddots & \ddots & \vdots \\ 0 & \cdots & 0 & 1 \\ -a_{li}^{0} & \cdots & \cdots & -a_{li}^{n-1} \end{pmatrix}, \\ D_{li} &= \begin{pmatrix} 0 & \cdots & \cdots & 0 \\ \vdots & & & \vdots \\ 0 & \cdots & \cdots & 0 \\ -d_{li}^{0} & \cdots & \cdots & -d_{li}^{n-1} \end{pmatrix}. \end{aligned} \tag{27}$$

A change of base of the form $z(t) = Px(t)$ of (26) under the arrow form matrix gives

$$\begin{aligned} \dot{z}(t) &= \sum_{i=1}^{N} \xi_i(t) \sum_{l=1}^{r} h_{li} \left(M_{li} z(t) + N_{li} z(t-\tau) \right) \\ z(t) &= P\Phi(t), \quad t \in [-\tau, 0], \end{aligned} \tag{28}$$

where $M_{li} = P^{-1} A_{li} P$, $N_{li} = P^{-1} D_{li} P$, and P is the corresponding passage matrix such that

$$P = \begin{pmatrix} 1 & 1 & \cdots & 1 & 0 \\ \alpha_1 & \alpha_2 & \cdots & \alpha_{n-1} & 0 \\ (\alpha_1)^2 & (\alpha_2)^2 & \cdots & (\alpha_{n-1})^2 & \vdots \\ \vdots & \vdots & \cdots & \vdots & 0 \\ (\alpha_1)^{n-1} & (\alpha_2)^{n-1} & \cdots & (\alpha_{n-1})^{n-1} & 1 \end{pmatrix}. \tag{29}$$

Arrow form matrices M_{li}, $l = 1, \ldots, r$ and $i \in I$, are given by

$$M_{li} = \begin{pmatrix} \alpha_1 & & & \beta_1 \\ & \ddots & & \vdots \\ & & \alpha_{n-1} & \beta_{n-1} \\ \gamma_{li}^{1} & \cdots & \gamma_{li}^{n-1} & \gamma_{li}^{n} \end{pmatrix} \tag{30}$$

with

$$\begin{aligned} \beta_j &= \prod_{\substack{q=1 \\ q \neq j}}^{n-1} \left(\alpha_j - \alpha_q \right)^{-1} \quad \forall j = 1, \ldots, n-1 \\ \gamma_{li}^{j} &= -P_{A_{li}}(\alpha_j) \quad \forall j = 1, \ldots, n-1 \\ \gamma_{li}^{n} &= -a_{li}^{n-1} - \sum_{j=1}^{n-1} \alpha_j, \end{aligned} \tag{31}$$

whereas matrices N_{li} are given by

$$N_{li} = \begin{pmatrix} 0_{n-1,n-1} & & 0_{n-1,1} \\ \delta_{li}^{1} & \cdots \; \delta_{li}^{n-1} & \delta_{li}^{n} \end{pmatrix} \tag{32}$$

with

$$\begin{aligned} \delta_{li}^{j} &= -P_{D_{li}}(\alpha_j) \quad \forall j = 1, \ldots, n-1 \\ \delta_{li}^{n} &= -d_{li}^{n-1} \\ P_{D_{li}}(\lambda) &= \sum_{j=0}^{n-1} d_{li}^{j} \lambda^j. \end{aligned} \tag{33}$$

Note that α_j, $j = 1, \ldots, n-1$, are distinct constant parameters that can be chosen arbitrarily and $P_{A_{li}}(\lambda)$ is the instantaneous characteristic polynomial of matrix A_{li} given by

$$P_{A_{li}}(\lambda) = \lambda^n + \sum_{j=0}^{n-1} a_{li}^{j} \lambda^j. \tag{34}$$

Therefore, the expression of the common comparison matrix in the new base is given through the sum of the following terms:

$$\left(M_{li} + N_{li}\right)^* = \begin{pmatrix} \alpha_1 & & & |\beta_1| \\ & \ddots & & \vdots \\ & & \alpha_{n-1} & |\beta_{n-1}| \\ \left|\gamma_{li}^{1} + \delta_{li}^{1}\right| & \cdots & \left|\gamma_{li}^{n-1} + \delta_{li}^{n-1}\right| & \gamma_{li}^{n} + \delta_{li}^{n} \end{pmatrix}$$

$$\left|N_{li}M_{li}\right| = \begin{pmatrix} 0_{n-1,n-1} & 0_{n-1,1} \\ \left|\psi_{li}(\alpha_1)\right| \ \cdots \ \left|\psi_{li}(\alpha_{n-1})\right| & \left|\delta_{li}^{n}\gamma_{li}^{n} + \sum_{j=1}^{n-1}\delta_{li}^{j}\beta_j\right| \end{pmatrix}$$

$$\left|N_{li}^{2}\right| = \begin{pmatrix} 0_{n-1,n-1} & 0_{n-1,1} \\ \left|-\delta_{li}^{1}d_{li}^{n-1}\right| \ \left|-\delta_{li}^{n-1}d_{li}^{n-1}\right| & \left|\left(d_{li}^{n-1}\right)^2\right| \end{pmatrix}. \tag{35}$$

The new polynomial $\psi_{li}(\alpha_j)$ is defined by

$$\psi_{li}(\alpha_j) = -P_{D_{li}}(\alpha_j) \times \alpha_j + d_{li}^{n-1}P_{A_{li}}(\alpha_j). \tag{36}$$

Notice that $|N_{li}M_{li}|$ can be simplified. In fact, $\delta_{li}^{n}\gamma_{li}^{n} + \sum_{j=1}^{n-1}\delta_{li}^{j}\beta_j = \text{trace}(N_{li}M_{li})$. However, $\text{trace}(N_{li}M_{li}) = \text{trace}(D_{li}A_{li}) = a_{li}^{n-1}d_{li}^{n-1} - d_{li}^{n-2}$. Consequently, we can construct for each individual submodel $\sum_{A_{li},D_{li}}$ the following overvaluing system:

$$T_{li} = (M_{li} + N_{li})^{*} + \tau\left(\left|N_{li}M_{li}\right| + \left|N_{li}^{2}\right|\right), \tag{37}$$

where

$$T_{li} = \begin{pmatrix} \alpha_1 & & \left|\beta_1\right| \\ & \ddots & \vdots \\ & \alpha_{n-1} & \left|\beta_{n-1}\right| \\ t_{li}^{1} \ \cdots & t_{li}^{n-1} & t_{li}^{n} \end{pmatrix},$$

$$t_{li}^{j} = \left|\gamma_{li}^{j} + \delta_{li}^{j}\right| + \tau\left(\left|\psi_{li}(\alpha_j)\right| + \left|-\delta_{li}^{j}d_{li}^{n-1}\right|\right) \tag{38}$$

$$t_{li}^{n} = (\gamma_{li}^{n} + \delta_{li}^{n}) + \tau\left(\left|a_{li}^{n-1}d_{li}^{n-1} - d_{li}^{n-2}\right| + \left(d_{li}^{n-1}\right)^2\right).$$

Finally, the common overvaluing matrix is given by

$$T_m = \begin{pmatrix} \alpha_1 & & \left|\beta_1\right| \\ & \ddots & \vdots \\ & \alpha_{n-1} & \left|\beta_{n-1}\right| \\ t_1 \ \cdots & t_{n-1} & t_n \end{pmatrix} \tag{39}$$

with

$$t_j = \max_{\substack{1\le i\le N \\ 1\le l\le r}}\left(t_{li}^{j}\right) \quad \forall j = 1,\ldots,n. \tag{40}$$

At this level, we can state the following theorem.

Theorem 6. *System (26) is globally asymptotically stable under an arbitrary switching rule $\sigma(t) = i$, $i \in I$, if there exist $\alpha_j < 0$, $\forall j = 1,\ldots,n-1$, $\alpha_j \neq \alpha_q$, $\forall j \neq q$, satisfying the following condition:*

$$-t_n + \sum_{j=1}^{n-1} t_j \left|\beta_j\right| \alpha_j^{-1} > 0. \tag{41}$$

Proof. It is sufficient to check that the matrix

$$T_m = \max_{\substack{1\le i\le N \\ 1\le l\le r}}\left((M_{li} + N_{li})^{*} + \tau\left(\left|N_{li}M_{li}\right| + \left|N_{li}^{2}\right|\right)\right) \tag{42}$$

is the opposite of an M-matrix by verifying that all the successive principal minors of T_m, denoted by Δ_j, are of alternating signs; that is,

$$(-1)^j \Delta_j > 0 \quad \forall j = 1,\ldots,n-1. \tag{43}$$

It is clear that, for an arbitrary choice of $\alpha_j < 0$, relation (43) is satisfied for $j = 1,\ldots,n-1$.

Condition (43) becomes for $j = n$

$$\begin{aligned}(-1)^n \Delta_n &= (-1)^n \det(T_m) \\ &= (-1)^n\left[t_n - \sum_{j=1}^{n-1} t_j \left|\beta_j\right| \alpha_j^{-1}\right]\prod_{j=1}^{n-1}\alpha_j.\end{aligned} \tag{44}$$

By dividing (44) by $\kappa = (-1)^{n-1}\prod_{j=1}^{n-1}\alpha_j$, we obtain

$$-t_n + \sum_{j=1}^{n-1} t_j \left|\beta_j\right| \alpha_j^{-1} > 0. \tag{45}$$

This achieves the proof of Theorem 6. □

Remark 7. The maximum value of τ ensuring the asymptotic stability of each individual model $\sum_{A_{li},D_{li}}$ ($\tau < \tau_{\max}^{(li)}$) is computed by

$$\tau_{\max}^{(li)} = \frac{-\left(\gamma_{li}^{n} + \delta_{li}^{n}\right) + \sum_{j=1}^{n-1}\alpha_j^{-1}\left|-\left(P_{A_{li}}(\alpha_j) + P_{D_{li}}(\alpha_j)\right)\right|\left|\beta_j\right|}{\left(d_{li}^{n-1}\right)^2 + \left|a_{li}^{n-1}d_{li}^{n-1} - d_{li}^{n-2}\right| - \sum_{j=1}^{n-1}\alpha_j^{-1}\left(\left|\psi_{li}(\alpha_j)\right| + \left|P_{D_{li}}(\alpha_j)\,d_{li}^{n-1}\right|\right)\left|\beta_j\right|}. \tag{46}$$

Remark 8. Expression (46) can be widely simplified. We can give, for instance, two of the possible combinations.

Case 1. One has

$$\begin{aligned}\left(P_{D_{li}}\left(\alpha_j\right)+P_{A_{li}}\left(\alpha_j\right)\right)\beta_j<0\\ \psi_{li}\left(\alpha_j\right)\beta_j>0\\ P_{D_{li}}\left(\alpha_j\right)d_{li}^{n-1}\beta_j>0.\end{aligned}\tag{47}$$

Then, stability conditions will depend on the sign of $(a_{li}^{n-1}d_{li}^{n-1}-d_{li}^{n-2})$ as follows:

$$\begin{aligned}&\tau_{\max}^{(li)}\\ &=\frac{P_{A_{li}}(0)+P_{D_{li}}(0)}{2\kappa\left(d_{li}^{n-2}-a_{li}^{n-1}d_{li}^{n-1}\right)+d_{li}^{n-1}\left(P_{A_{li}}(0)+P_{D_{li}}(0)\right)}\\ &\qquad\text{if } a_{li}^{n-1}d_{li}^{n-1}<d_{li}^{n-2}\end{aligned}\tag{48}$$

$$\tau_{\max}^{(li)}=\frac{1}{d_{li}^{n-1}}\quad\text{if } a_{li}^{n-1}d_{li}^{n-1}>d_{li}^{n-2},\ d_{li}^{n-1}>0.$$

Case 2. One has

$$\begin{aligned}&\left(P_{D_{li}}\left(\alpha_j\right)+P_{A_{li}}\left(\alpha_j\right)\right)\beta_j<0\\ &\psi_{li}\left(\alpha_j\right)\beta_j<0\\ &P_{D_{li}}\left(\alpha_j\right)d_{li}^{n-1}\beta_j<0\end{aligned}\tag{49}$$

$$\begin{aligned}&\tau_{\max}^{(li)}\\ &=\frac{P_{A_{li}}(0)+P_{D_{li}}(0)}{2\kappa\left(\left(a_{li}^{n-1}d_{li}^{n-1}-d_{li}^{n-2}\right)+\left(d_{li}^{n-1}\right)^2\right)-d_{li}^{n-1}\left(P_{A_{li}}(0)+P_{D_{li}}(0)\right)}\\ &\qquad\text{if } a_{li}^{n-1}d_{li}^{n-1}>d_{li}^{n-2}\end{aligned}\tag{50}$$

$$\begin{aligned}\tau_{\max}^{(li)}=\frac{P_{A_{li}}(0)+P_{D_{li}}(0)}{2\kappa\left(d_{li}^{n-1}\right)^2-d_{li}^{n-1}\left(P_{A_{li}}(0)+P_{D_{li}}(0)\right)}\\ \text{if } a_{li}^{n-1}d_{li}^{n-1}<d_{li}^{n-2}.\end{aligned}\tag{51}$$

Proof. See the Appendix. □

4. Delay-Dependent Stability Conditions for TS Fuzzy Switched Systems with Multiple Delays

Stability criteria in Theorem 5 can be generalized to systems with multiple delays.

4.1. Main Result. Consider a switched system composed of N subsystems; each subsystem is a TS fuzzy time-delay system as shown in the following differential equation:

$$\begin{aligned}\dot{x}(t)&=\sum_{i=1}^{N}\xi_i(t)\sum_{l=1}^{r}h_{li}\left(A_{li}x(t)+\sum_{k=1}^{m}D_{li,k}x\left(t-\tau_k\right)\right)\\ x(t)&=\Phi(t),\quad t\in\left[-\max_{1\le k\le m}\tau_k,0\right],\end{aligned}\tag{52}$$

where A_{li}, $D_{li,k}$ ($l=1,\dots,r$; $i=1,\dots,N$; and $k=1,\dots,m$) are constant matrices of appropriate dimensions, h_{li} are fuzzy weighting factors, previously defined in (6), and $\tau_k>0\ \forall k=1,\dots,m$.

System (52) can also be put in the following form:

$$\begin{aligned}\dot{x}(t)&=A_{\sigma(t)}x(t)+\sum_{k=1}^{m}D_{\sigma(t),k}x\left(t-\tau_k\right)\\ x(t)&=\Phi(t),\quad t\in\left[-\max_{1\le k\le m}\tau_k,0\right],\end{aligned}\tag{53}$$

where

$$\begin{aligned}A_{\sigma(t)}&=\sum_{i=1}^{N}\xi_i(t)\sum_{l=1}^{r}h_{li}A_{li},\\ D_{\sigma(t),k}&=\sum_{i=1}^{N}\xi_i(t)\sum_{l=1}^{r}h_{li}D_{li,k}.\end{aligned}\tag{54}$$

Theorem 9. *System (52) is globally asymptotically stable under arbitrary switching rule $\sigma(t)=i\in I$, if matrix*

$$\begin{aligned}T_{m,M}=\max_{\substack{1\le i\le N\\1\le l\le r}}\left\{\left(A_{li}+\sum_{k=1}^{m}D_{li,k}\right)^*\right.\\ \left.+\sum_{k=1}^{m}\tau_k\left(\left|D_{li,k}A_{li}\right|+\left|D_{li,k}{}^2\right|\right)\right\}\end{aligned}\tag{55}$$

is the opposite of an M-matrix.

Proof. Following the same steps as those given in the proof of Theorem 5 and by choosing the common radially unbounded Lyapunov functional as follows,

$$V_{c,M}(t)=\max_{\substack{1\le i\le N\\1\le l\le r}}\left(V_M(t)\right)=\max_{\substack{1\le i\le N\\1\le l\le r}}\left(\sum_{p=1}^{4}V_{p,M}(t)\right),\tag{56}$$

where

$$\begin{aligned}&V_{1,M}(t)=\langle|x(t),w|\rangle\\ &V_{2,M}(t)=\sum_{k=1}^{m}\left\langle\left|D_{li,k}A_{li}\right|\int_{-\tau_k}^{0}\int_{t+\theta}^{t}|x(s)|\,ds\,d\theta,w\right\rangle\\ &V_{3,M}(t)\\ &\quad=\sum_{k=1}^{m}\left\langle\left|D_{li,k}{}^2\right|\int_{-\tau_k}^{0}\int_{t+\theta}^{t}\left|x\left(s-\tau_k\right)\right|ds\,d\theta,w\right\rangle\\ &V_{4,M}(t)=\sum_{k=1}^{m}\tau_k\left\langle\left|D_{li,k}{}^2\right|\int_{t-\tau_k}^{t}|x(s)|\,ds,w\right\rangle,\end{aligned}\tag{57}$$

we deduce that it suffices that $T_{m,M}$ is the opposite of an M-matrix to conclude to the asymptotic stability of system (52). □

4.2. Extension of the Results to the Case of TS Fuzzy Switched Systems Described by Differential Equations with Multiple Delays. The same method is applied to determine delay-dependent stability criteria for systems described by the following multiple time-delayed differential equation:

$$y^{(n)}(t) + \sum_{i=1}^{N} \xi_i(t) \sum_{l=1}^{r} h_{li} \cdot \left(\sum_{j=0}^{n-1} a_{li}^{j} y^{(j)}(t) + \sum_{k=1}^{m} \sum_{j=0}^{n-1} d_{li,k}^{j} y^{(j)}(t-\tau_k) \right) = 0 \tag{58}$$

$$y^{(j)}(t) = \Phi_j(t) \quad \forall t \in \left[-\max_{1\le k\le m} \tau_k, 0 \right], \ j = 0, \ldots, n-1.$$

The same change of variable $x_{j+1}(t) = y^{(j)}(t)$, $j = 0, \ldots, n-1$, as in Section 3.2 yields to the new state space representation:

$$\dot{x}(t) = \sum_{i=1}^{N} \xi_i(t) \sum_{l=1}^{r} h_{li} \left(A_{li} x(t) + \sum_{k=1}^{m} D_{li,k} x(t-\tau_k) \right)$$
$$x(t) = \Phi(t), \quad t \in \left[-\max_{1\le k\le m} \tau_k, 0 \right], \tag{59}$$

where $x(t) = [x_1(t), \ldots, x_n(t)]^T$ is the state vector and for each $i \in I$, $k \in [1, \ldots, m]$, A_{li} and $D_{li,k}$ are given by

$$A_{li} = \begin{pmatrix} 0 & 1 & \cdots & 0 \\ \vdots & \ddots & \ddots & \vdots \\ 0 & \cdots & 0 & 1 \\ -a_{li}^{0} & \cdots & \cdots & -a_{li}^{n-1} \end{pmatrix}$$
$$D_{li,k} = \begin{pmatrix} 0_{n-1,n-1} & 0_{n-1,1} \\ -d_{li,k}^{0} & \cdots \ -d_{li,k}^{n-1} \end{pmatrix}. \tag{60}$$

A change of base of the form $z(t) = Px(t)$ allows system (59) to be represented by the arrow form matrix:

$$\dot{z}(t) = \sum_{i=1}^{N} \xi_i(t) \sum_{l=1}^{r} h_{li} \left(M_{li} z(t) + \sum_{k=1}^{m} N_{li,k} z(t-\tau_k) \right)$$
$$z(t) = P\Phi(t), \quad t \in \left[-\max_{1\le k\le m} \tau_k, 0 \right], \tag{61}$$

where M_{li} is given by (30) and $N_{li,k}$ becomes

$$N_{li,k} = \begin{pmatrix} 0_{n-1,n-1} & 0_{n-1,1} \\ \delta_{li,k}^{1} \ \cdots \ \delta_{li,k}^{n-1} & \delta_{li,k}^{n} \end{pmatrix} \tag{62}$$

with

$$\delta_{li,k}^{j} = -P_{D_{li,k}}(\alpha_j)$$
$$\delta_{li,k}^{n} = -d_{li,k}^{n-1}. \tag{63}$$

Define the new polynomials:

$$P_{D_{li,k}}(\lambda) = \sum_{j=0}^{n-1} d_{li,k}^{j} \lambda^j,$$
$$\psi_{li,k}(\lambda) = -P_{D_{li,k}}(\lambda) \times \lambda + d_{li,k}^{n-1} P_{A_{li}}(\lambda). \tag{64}$$

Finally, we can compute the common overvaluing matrix as follows:

$$T_{m,M} = \begin{pmatrix} \alpha_1 & & |\beta_1| \\ & \ddots & \vdots \\ & & \alpha_{n-1} \ |\beta_{n-1}| \\ t_{1,M} \ \cdots \ t_{n-1,M} & & t_{n,M} \end{pmatrix} \tag{65}$$

with

$$t_{j,M} = \max_{\substack{1\le i\le N \\ 1\le l\le r}} \left(\left| \gamma_{li}^{j} + \sum_{k=1}^{m} \delta_{li,k}^{j} \right| + \sum_{k=1}^{m} \tau_k \left(\left| \psi_{li,k}(\alpha_j) \right| + \left| -d_{li,k}^{n-1} \delta_{li,k}^{j} \right| \right) \right), \quad \forall j = 1, \ldots, n-1, \tag{66}$$

$$t_{n,M} = \max_{\substack{1\le i\le N \\ 1\le l\le r}} \left(\left(\gamma_{li}^{n} + \sum_{k=1}^{m} \delta_{li,k}^{n} \right) + \sum_{k=1}^{m} \tau_k \left(\left| a_{li}^{n-1} d_{li,k}^{n-1} - d_{li,k}^{n-2} \right| + \left(d_{li,k}^{n-1} \right)^2 \right) \right).$$

Hence, we can state Theorem 10.

Theorem 10. *System (59) is globally asymptotically stable under an arbitrary switching rule $\sigma(t) = i \in I$, if there exist $\alpha_j < 0$, $j = 1, \ldots, n-1$, $\alpha_j \neq \alpha_q$, $\forall j \neq q$ such that*

$$-t_{n,M} + \sum_{j=1}^{n-1} t_{j,M} \left| \beta_j \right| \alpha_j^{-1} > 0. \tag{67}$$

Proof. The same proof is as in Theorem 6; just replace matrix T_m by $T_{m,M}$. □

5. Illustrative Examples

Example 1. Consider a switched system composed of three second-order subsystems $\sum_{A_i,D_i}$, $i \in \{1, 2, 3\}$; each subsystem

is represented by a TS fuzzy time-delay model as follows:

Subsystem (1)

$$A_{11} = \begin{pmatrix} 0 & 1 \\ -16 & -15 \end{pmatrix},$$
$$D_{11} = \begin{pmatrix} 0 & 0 \\ -1.5 & -0.02 \end{pmatrix}$$
$$A_{21} = \begin{pmatrix} 0 & 1 \\ -16 & -13.5 \end{pmatrix}, \quad (68)$$
$$D_{21} = \begin{pmatrix} 0 & 0 \\ -1.5 & 0 \end{pmatrix}.$$

Subsystem (2)

$$A_{12} = \begin{pmatrix} 0 & 1 \\ -20 & -18 \end{pmatrix},$$
$$A_{22} = \begin{pmatrix} 0 & 1 \\ -16 & -15 \end{pmatrix} \quad (69)$$
$$D_{12} = D_{22} = \begin{pmatrix} 0 & 0 \\ -0.5 & 0 \end{pmatrix}.$$

Subsystem (3)

$$A_{13} = \begin{pmatrix} 0 & 1 \\ -14 & -12 \end{pmatrix},$$
$$D_{13} = \begin{pmatrix} 0 & 0 \\ -1.75 & 0 \end{pmatrix}$$
$$A_{23} = \begin{pmatrix} 0 & 1 \\ -14.5 & -10 \end{pmatrix}, \quad (70)$$
$$D_{23} = \begin{pmatrix} 0 & 0 \\ -1 & 0 \end{pmatrix}.$$

A transformation of state matrices under the arrow form $F_{li} = P^{-1}A_{li}P$ and $N_{li} = P^{-1}D_{li}P$ ($l \in \{1,2\}$ and $i \in \{1,2,3\}$) with $P = \left(\begin{smallmatrix} 1 & 0 \\ \alpha & 1 \end{smallmatrix}\right)$ gives

$$F_{li} = \begin{pmatrix} \alpha & 1 \\ \gamma_{li}^1 & \gamma_{li}^2 \end{pmatrix},$$
$$N_{li} = \begin{pmatrix} 0 & 0 \\ \delta_{li}^1 & \delta_{li}^2 \end{pmatrix}. \quad (71)$$

For $i \in \{1,2,3\}$ and $l \in \{1,2\}$, parameters γ_{li} and δ_{li} are computed as follows:

$$\gamma_{11}^1 = -P_{A_{11}}(\alpha) = -\left(\alpha^2 + 15\alpha + 16\right)$$
$$\gamma_{11}^2 = -15 - \alpha;$$
$$\gamma_{21}^1 = -P_{A_{21}}(\alpha) = -\left(\alpha^2 + 13.5\alpha + 16\right)$$
$$\gamma_{21}^2 = -13.5 - \alpha;$$
$$\gamma_{12}^1 = -P_{A_{12}}(\alpha) = -\left(\alpha^2 + 18\alpha + 20\right)$$
$$\gamma_{12}^2 = -18 - \alpha;$$
$$\gamma_{22}^1 = -P_{A_{22}}(\alpha) = -\left(\alpha^2 + 15\alpha + 16\right)$$
$$\gamma_{22}^2 = -15 - \alpha;$$
$$\gamma_{13}^1 = -P_{A_{13}}(\alpha) = -\left(\alpha^2 + 12\alpha + 14\right)$$
$$\gamma_{13}^2 = -12 - \alpha;$$
$$\gamma_{23}^1 = -P_{A_{23}}(\alpha) = -\left(\alpha^2 + 10\alpha + 14.5\right)$$
$$\gamma_{23}^2 = -10 - \alpha;$$
$$\delta_{11}^1 = -P_{D_{11}}(\alpha) = -(0.02\alpha + 1.5)$$
$$\delta_{11}^2 = -0.02;$$
$$\delta_{21}^1 = -P_{D_{21}}(\alpha) = -1.5$$
$$\delta_{21}^2 = 0. \quad (72)$$

For an arbitrary choice of $\alpha = -1$, we obtain, for example, for subsystem (1)

$$F_{11} = \begin{pmatrix} -1 & 1 \\ -2 & -14 \end{pmatrix},$$
$$N_{11} = \begin{pmatrix} 0 & 0 \\ -1.48 & -0.02 \end{pmatrix};$$
$$F_{21} = \begin{pmatrix} -1 & 1 \\ -3.5 & -12.5 \end{pmatrix}, \quad (73)$$
$$N_{21} = \begin{pmatrix} 0 & 0 \\ -1.5 & 0 \end{pmatrix}.$$

For $h_2 = 1 - h_1$ and by using the center of average defuzzification, state matrix $F_i = h_1F_{1i} + h_2F_{2i}$ and delayed-state matrix $N_i = h_1N_{1i} + h_2N_{2i}$ ($i \in \{1,2,3\}$) are given, respectively, by

$$F_1 = \begin{pmatrix} -1 & 1 \\ 1.5h_1 - 3.5 & -(1.5h_1 + 12.5) \end{pmatrix},$$
$$N_1 = \begin{pmatrix} 0 & 0 \\ 0.02h_1 - 1.5 & -0.02h_1 \end{pmatrix},$$
$$F_2 = \begin{pmatrix} -1 & 1 \\ -(h_1 + 2) & -(3h_1 + 14) \end{pmatrix}, \quad (74)$$
$$N_2 = \begin{pmatrix} 0 & 0 \\ -0.5 & 0 \end{pmatrix},$$
$$F_3 = \begin{pmatrix} -1 & 1 \\ -(5.5 - 2.5h_1) & -(2h_1 + 9) \end{pmatrix},$$
$$N_3 = \begin{pmatrix} 0 & 0 \\ -(0.75h_1 + 1) & 0 \end{pmatrix}.$$

Table 1: Maximum allowable time delay for each submodel ($\tau_{\max}^{(li)}$).

Submodel (li)	(11)	(21)	(12)	(22)	(13)	(23)
$\tau_{\max}^{(li)}$(s)	3.83	2.5	13.5	11.5	1.78	1.25

Denote by T_{li}, $l \in \{1,2\}$ and $i \in \{1,2,3\}$, the minimal pseudo-overvaluing matrix of the fuzzy submodel $\sum_{A_{li},D_{li}}$ such that

$$T_{li} = \begin{pmatrix} -1 & 1 \\ t_{li}^1 & t_{li}^2 \end{pmatrix}, \tag{75}$$

where

$$\begin{aligned} T_{11} &= \begin{pmatrix} -1 & 1 \\ 3.48 + 1.5496\tau & -14.02 + 1.2\tau \end{pmatrix} \\ T_{21} &= \begin{pmatrix} -1 & 1 \\ 5 + 1.5\tau & -12.5 + 1.5\tau \end{pmatrix} \\ T_{12} &= \begin{pmatrix} -1 & 1 \\ 3.5 + 0.5\tau & -17 + 0.5\tau \end{pmatrix} \\ T_{22} &= \begin{pmatrix} -1 & 1 \\ 2.5 + 0.5\tau & -14 + 0.5\tau \end{pmatrix} \\ T_{13} &= \begin{pmatrix} -1 & 1 \\ 4.75 + 1.75\tau & -11 + 1.75\tau \end{pmatrix} \\ T_{23} &= \begin{pmatrix} -1 & 1 \\ 6.5 + \tau & -9 + \tau \end{pmatrix}. \end{aligned} \tag{76}$$

At this level, we can derive sufficient conditions for the asymptotic stability of each submodel individually as shown in Table 1.

From Table 1, we can already see that it is sufficient to have a time delay τ inferior to 1.25 s to ensure the asymptotic stability of all the submodels individually. Taking into account this value, we can notice that $\sum_{T_{23}}$ can be chosen as the common comparison system for the six submodels $\sum_{A_{li},D_{li}}$ ($l \in \{1,2\}$ and $i \in \{1,2,3\}$). Then, the TS fuzzy switched time-delay system is asymptotically stable under an arbitrary switching law if

$$\tau < 1.25\,\text{s}. \tag{77}$$

The switching signal is plotted on Figure 1. For a time delay equal to $\tau = 1.2$ s, a final simulation time $t_f = 4$ s, weighting factors $h_1 = h_2 = 0.5$, and an initial state vector $x(t) = [1 \ -2]^T \ \forall t \in [-1.2, 0]$, the evolution of state vectors, the system's trajectory, and the state's norm are illustrated on Figures 2, 3, and 4, respectively.

This example shows that the obtained stability conditions are sufficient and very close to be necessary. Moreover, the proposed method makes it possible to avoid searching a common Lyapunov-Krasovskii functional, which is very difficult in this case.

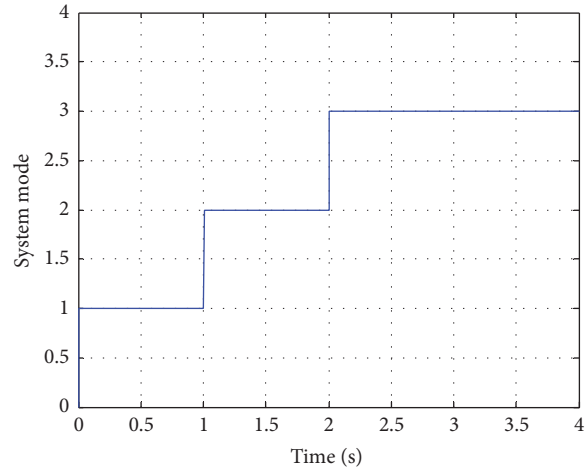

Figure 1: Switching signal (Example 1).

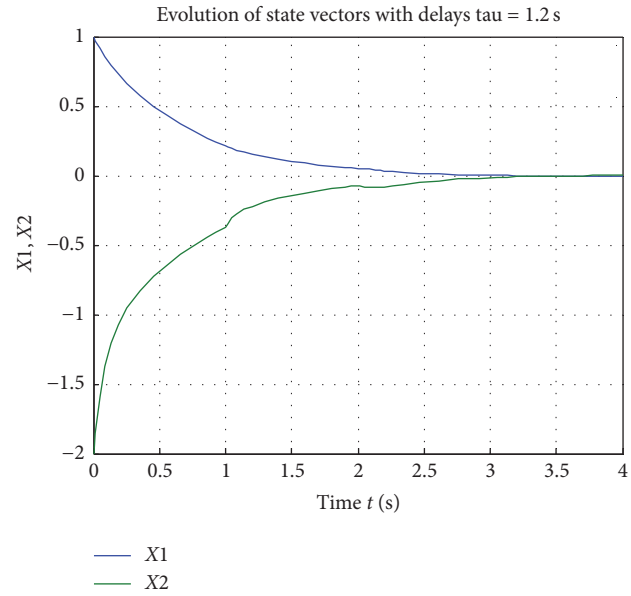

Figure 2: Evolution of the state vectors (Example 1).

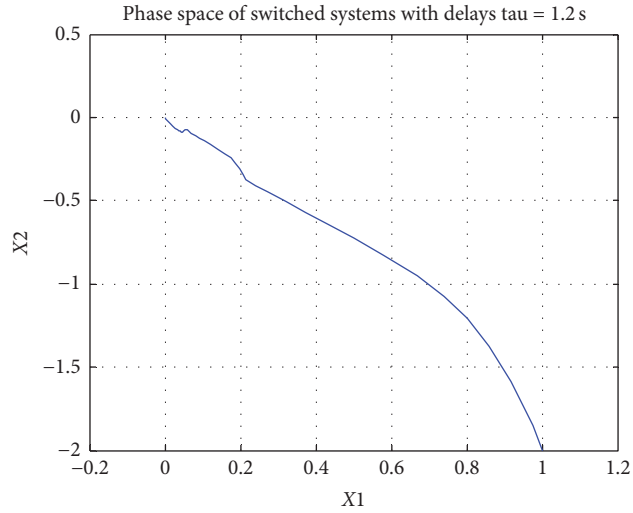

Figure 3: System's trajectory (Example 1).

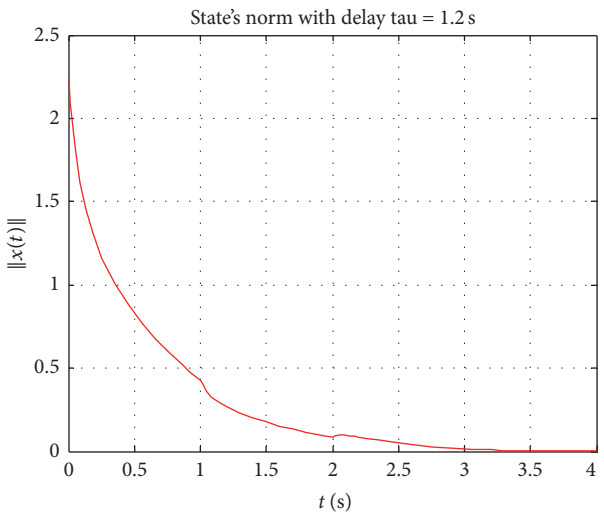

Figure 4: State's norm (Example 1).

Example 2. Consider the TS fuzzy switched system with two delays τ_1 and τ_2 as follows:

$$\dot{x}(t) = \sum_{i=1}^{2} \xi_i(t) \cdot \sum_{l=1}^{2} h_{li}\left(A_{li}x(t) + D_{li,1}x(t-\tau_1) + D_{li,2}x(t-\tau_2)\right) \quad (78)$$
$$x(t) = \Phi(t), \quad t \in \left[-\max_{1\le k\le 2}\tau_k, 0\right].$$

Subsystem (1)

$$A_{11} = \begin{pmatrix} 0 & 1 \\ -4 & -3 \end{pmatrix}, \quad D_{11,1} = \begin{pmatrix} 0 & 0 \\ 0 & -1 \end{pmatrix}, \quad D_{11,2} = \begin{pmatrix} 0 & 0 \\ -0.5 & 0 \end{pmatrix}$$
$$A_{21} = \begin{pmatrix} 0 & 1 \\ -3 & -3 \end{pmatrix}, \quad D_{21,1} = \begin{pmatrix} 0 & 0 \\ 0 & -1 \end{pmatrix}, \quad D_{21,2} = \begin{pmatrix} 0 & 0 \\ -0.2 & 0 \end{pmatrix}. \quad (79)$$

Subsystem (2)

$$A_{12} = \begin{pmatrix} 0 & 1 \\ -5 & -10 \end{pmatrix}, \quad D_{12,1} = \begin{pmatrix} 0 & 0 \\ -2 & -1 \end{pmatrix}, \quad D_{12,2} = \begin{pmatrix} 0 & 0 \\ -0.1 & 0 \end{pmatrix}$$
$$A_{22} = \begin{pmatrix} 0 & 1 \\ -7 & -12 \end{pmatrix}, \quad D_{22,1} = \begin{pmatrix} 0 & 0 \\ -3 & -1 \end{pmatrix}, \quad D_{22,2} = \begin{pmatrix} 0 & 0 \\ -0.1 & 0 \end{pmatrix}. \quad (80)$$

For $\alpha = -1$, a transformation under the arrow form matrices gives

$$F_{11} = \begin{pmatrix} -1 & 1 \\ -2 & -2 \end{pmatrix}, \quad N_{11,1} = \begin{pmatrix} 0 & 0 \\ 1 & -1 \end{pmatrix}, \quad N_{11,2} = \begin{pmatrix} 0 & 0 \\ -0.5 & 0 \end{pmatrix}$$
$$F_{21} = \begin{pmatrix} -1 & 1 \\ -1 & -2 \end{pmatrix}, \quad N_{21,1} = \begin{pmatrix} 0 & 0 \\ 1 & -1 \end{pmatrix}, \quad N_{21,2} = \begin{pmatrix} 0 & 0 \\ -0.2 & 0 \end{pmatrix}$$
$$F_{12} = \begin{pmatrix} -1 & 1 \\ 4 & -9 \end{pmatrix}, \quad N_{12,1} = \begin{pmatrix} 0 & 0 \\ -1 & -1 \end{pmatrix}, \quad N_{12,2} = \begin{pmatrix} 0 & 0 \\ -0.1 & 0 \end{pmatrix},$$
$$F_{22} = \begin{pmatrix} -1 & 1 \\ 4 & -11 \end{pmatrix},$$

Table 2: Maximum allowable time delay for each submodel ($\tau_{2,\max}^{(li)}$).

Submodel (li)	(11)	(21)	(12)	(22)
$\tau_{2,\max}^{(li)}$	$1.5 - 6\tau_1$	$7 - 12.5\tau_1$	$35.5 - 65\tau_1$	$50.5 - 70\tau_1$

$$N_{22,1} = \begin{pmatrix} 0 & 0 \\ -2 & -1 \end{pmatrix},$$
$$N_{22,2} = \begin{pmatrix} 0 & 0 \\ -0.1 & 0 \end{pmatrix}. \tag{81}$$

Denote by $T_{li,M}$, $l, i \in \{1, 2\}$, the minimal overvaluing matrix of subsystem of index (li) and relative to the vector norm $p(x) = [|x_1|, \ldots, |x_n|]^T$ such that

$$T_{li,M} = \begin{pmatrix} -1 & 1 \\ t_{li,M}^1 & t_{li,M}^2 \end{pmatrix}, \tag{82}$$

where

$$T_{11,M} = \begin{pmatrix} -1 & 1 \\ 1.5 + 2\tau_1 + 0.5\tau_2 & -3 + 4\tau_1 + 0.5\tau_2 \end{pmatrix}$$
$$T_{21,M} = \begin{pmatrix} -1 & 1 \\ 0.2 + \tau_1 + 0.2\tau_2 & -3 + 4\tau_1 + 0.2\tau_2 \end{pmatrix}$$
$$T_{12,M} = \begin{pmatrix} -1 & 1 \\ 2.9 + 4\tau_1 + 0.1\tau_2 & -10 + 9\tau_1 + 0.1\tau_2 \end{pmatrix}$$
$$T_{22,M} = \begin{pmatrix} -1 & 1 \\ 1.9 + 4\tau_1 + 0.1\tau_2 & -12 + 10\tau_1 + 0.1\tau_2 \end{pmatrix}. \tag{83}$$

Applying Theorem 10, we can draw Table 2 which gives a sufficient stability condition $0 < \tau_2 < \tau_{2,\max}^{(li)}$ for each submodel.

Finally, we can construct the following common comparison system $\sum_{T_{m,M}}$ such that

$$T_{m,M} = \begin{pmatrix} -1 & 1 \\ 2.9 + 4\tau_1 + 0.1\tau_2 & -3 + 4\tau_1 + 0.5\tau_2 \end{pmatrix}. \tag{84}$$

Consequently, the TS fuzzy switched time-delay system is asymptotically stable under arbitrary switching if

$$0 < \tau_2 < \frac{0.1 - 8\tau_1}{0.6}. \tag{85}$$

In this example, we can notice that maximum bounds found for the delays τ_1 and τ_2 are small. Indeed, this is justified by the multiplicity of time delay, by the choice of delay matrices $N_{li,k}$, $l, i, k \in \{1, 2\}$, and by the fact that arbitrary switching strategy brings conservativeness because of the "strict" condition that requires finding a comparison system which is common to all fuzzy local models.

Nevertheless, the simplicity of vector norms based approach makes the study almost feasible in most cases in the opposite of Lyapunov-based method which proves to be difficult when dealing with the problem of stability under arbitrary switching.

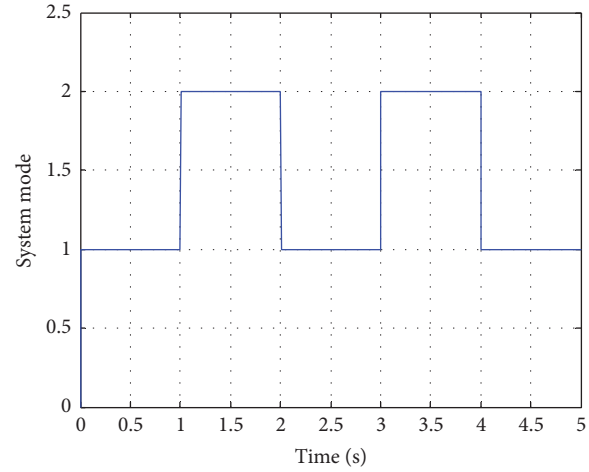

Figure 5: Switching signal (Example 2).

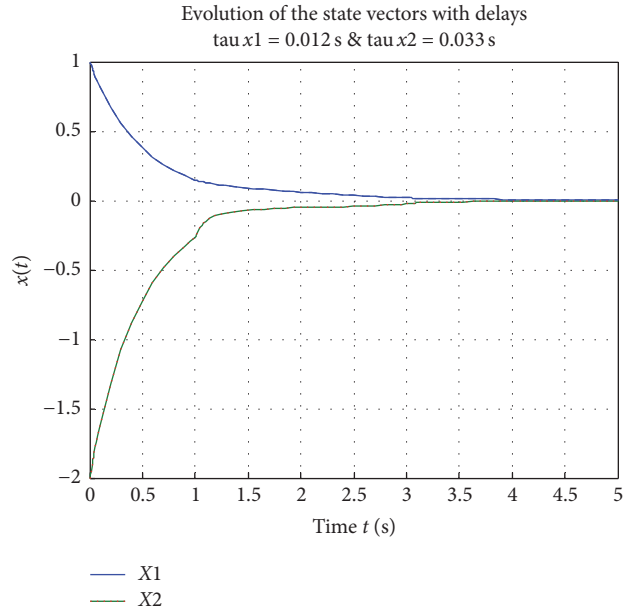

Figure 6: Evolution of state vectors (Example 2).

For a switching signal as shown on Figure 5, a choice of time delays $\tau_1 = 0.01$ s and $\tau_2 = 0.033$ s, particular values of weighting factors $h_1 = 0.2$ and $h_2 = 0.8$, and an initial state vector $x(t) = \begin{bmatrix} 1 & -2 \end{bmatrix}^T$ $\forall t \in [-0.033, 0]$, the evolution of state responses is illustrated on Figure 6 whereas Figures 7 and 8 show the system's trajectory and the norm's state, respectively.

Example 3 (see [38, 45]). Consider a DC motor with separate excitation (Figure 9). The system acts under variable mechanical load and is subject to a retarded state feedback control input. Our aim is to synthesize a state feedback control for each local model so that the overall system is asymptotically stable under arbitrary switching despite the time delay.

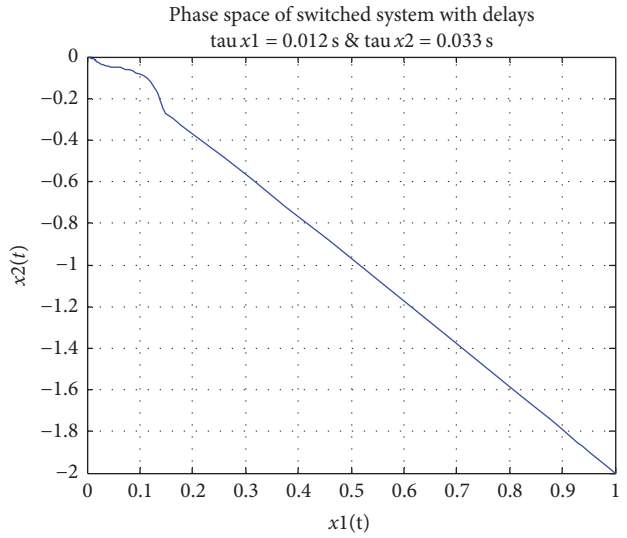

Figure 7: System's trajectory (Example 2).

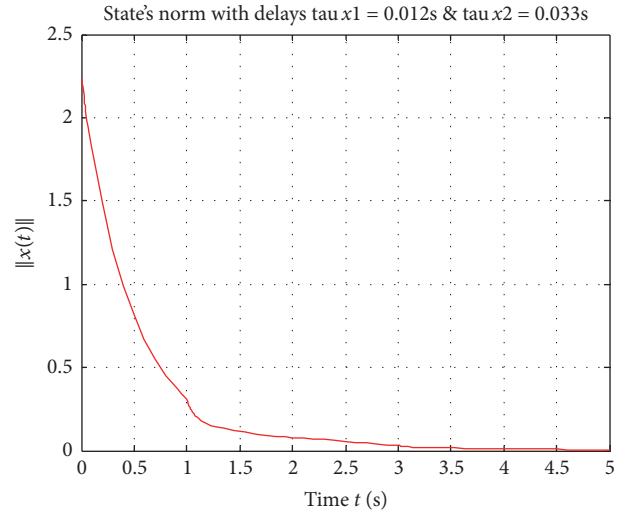

Figure 8: State's norm (Example 2).

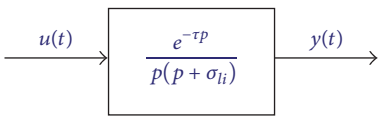

Figure 9: DC motor with separate excitation.

A PDC controller scheme is employed such that the lth controller fuzzy rule of the ith subsystem is given by

$$R_i^l: \quad \text{IF } z_1(t) \text{ is } M_{li}^1 \text{ and } z_2(t) \text{ is } M_{li}^2 \quad \text{THEN } u(t) = -K_{li}x(t), \tag{86}$$

where $K_{li} = [k_{li}^0 \;\; k_{li}^1]$, $l, i \in [1, 2]$, is the local feedback gain vector.

The TS fuzzy switched system is then represented in the state space by

$$\dot{x}(t) = \sum_{i=1}^{2}\xi_i(t)\sum_{l=1}^{2}h_{li}\left(A_{li}x(t) - \sum_{q=1}^{2}h_{qi}BK_{qi}x(t-\tau)\right), \tag{87}$$

where $A_{li} = \begin{pmatrix} 0 & 1 \\ 0 & -\sigma_{li} \end{pmatrix}$ and $B = \begin{pmatrix} 0 & 1 \end{pmatrix}^T$.

We can also write

$$\dot{x}(t) = \sum_{i=1}^{2}\xi_i(t) \cdot \left\{\sum_{l=1}^{2}h_{li}A_{li}x(t) - \sum_{q=1}^{2}h_{qi}\sum_{l=1}^{2}h_{li}BK_{qi}x(t-\tau)\right\}. \tag{88}$$

Hence,

$$\dot{x}(t) = \sum_{i=1}^{2}\xi_i(t)\left(\sum_{l=1}^{2}h_{li}\left(A_{li}x(t) - BK_{li}x(t-\tau)\right)\right). \tag{89}$$

Denote $D_{li} = -BK_{li}$, and the problem is then reduced to determining admissible values of parameters (k_{li}^0, k_{li}^1), $l, i \in [1, 2]$, for a given value of time delay τ.

A transformation under the arrow form matrix with $\alpha = -1$ yields

$$F_{li} = \begin{pmatrix} -1 & 1 \\ -(1-\sigma_{li}) & -\sigma_{li}+1 \end{pmatrix} \qquad N_{li} = \begin{pmatrix} 0 & 0 \\ k_{li}^1 - k_{li}^0 & -k_{li}^1 \end{pmatrix}. \tag{90}$$

To tune parameters (k_{li}^0, k_{li}^1), suppose that for $k_{li}^1 > 0$, $\sigma_{li} < 1$ we have

$$k_{li}^0 < \sigma_{li}k_{li}^1. \tag{91}$$

Thus, we can verify that

$$-\delta_{li}^1 d_{li}^1 = -\left(k_{li}^1 - k_{li}^0\right) \times k_{li}^1 < 0 \qquad \psi_{li}(-1) = k_{li}^0 - \sigma_{li}k_{li}^1 < 0. \tag{92}$$

Since all the assumptions of Remark 8 (Case 2) are met, this allows us, according to inequality (50), to write

$$\tau < \frac{k_{li}^0}{2\left[\left(\sigma_{li}k_{li}^1 - k_{li}^0\right) + \left(k_{li}^1\right)^2\right] - k_{li}^1k_{li}^0}. \tag{93}$$

Therefore, each fuzzy model is asymptotically stable individually if

$$k_{li}^0 > \frac{2\tau k_{li}^1\left(\sigma_{li} + k_{li}^1\right)}{1 + \tau\left(2 + k_{li}^1\right)}. \tag{94}$$

The pseudo-overvaluing matrix for each submodel is constructed as follows:

$$T_{li} = \begin{pmatrix} -1 & 1 \\ t_{li}^1 & t_{li}^2 \end{pmatrix} \tag{95}$$

with

$$\begin{aligned} t_{li}^1 &= \left(k_{li}^1 - k_{li}^0 + \sigma_{li} - 1\right) + \tau\left(\psi_{li}(-1) + k_{li}^1\left(k_{li}^1 - k_{li}^0\right)\right) \\ t_{li}^2 &= 1 - \sigma_{li} - k_{li}^1 + \tau\left(\sigma_{li}k_{li}^1 - k_{li}^0 + \left(k_{li}^1\right)^2\right). \end{aligned} \tag{96}$$

For instance, if the time delay τ is equal to 0.5 s, $\sigma_{11} = 0.86$, $\sigma_{21} = 0.97$, $\sigma_{12} = 0.76$, and $\sigma_{22} = 0.89$, and local feedback gains are chosen as $K_{11} = [0.7 \;\; 0.9]$, $K_{21} = [1.15 \;\; 1.2]$, $K_{12} = [0.92 \;\; 1.22]$, and $K_{22} = [0.8 \;\; 1]$, we obtain

$$\begin{aligned} T_{11} &= \begin{pmatrix} -1 & 1 \\ 0.187 & -0.318 \end{pmatrix} \\ T_{21} &= \begin{pmatrix} -1 & 1 \\ 0.057 & -0.443 \end{pmatrix} \\ T_{12} &= \begin{pmatrix} -1 & 1 \\ 0.233 & -0.2352 \end{pmatrix} \\ T_{22} &= \begin{pmatrix} -1 & 1 \\ 0.2350 & -0.345 \end{pmatrix}. \end{aligned} \tag{97}$$

Finally, the common comparison matrix that verifies the properties of the opposite of an M-matrix is given by

$$T_m = \begin{pmatrix} -1 & 1 \\ 0.2350 & -0.2352 \end{pmatrix}. \tag{98}$$

This example has shown that the proposed approach is appropriate for the synthesis of a stabilizing state feedback retarded control for an initially unstable nonlinear system described by a set of linear TS fuzzy local linear models.

6. Conclusion

In this paper, new delay-dependent stability conditions by using the vector norms approach have been presented. In fact, most of the research works that have been carried out on stability analysis of TS fuzzy switched time-delay systems under arbitrary switching are based on the research of a common Lyapunov-Krasovskii functional for all the fuzzy models, which is considered as a hard task. The idea of the proposed method consists in putting the switched system under a special form of state space representation using arrow form matrices and then finding a common pseudo-overvaluing system for all the constituent submodels. The stability analysis of this comparison system, based on the aggregation techniques and the M-matrices properties, permits concluding to that of the original TS fuzzy switched system.

Vector norms approach, applied to TS fuzzy switched time-delay systems, whether with single or multiple delay, is suitable for the case of arbitrary switching and provides delay-dependent algebraic criteria. The applicability of the obtained conditions is shown through three numerical examples. It would be interesting to generalize the study to the case of systems with control input.

Appendix

Demonstrations of (48), (50), and (51) are based on the following expressions:

$$\begin{aligned} -\gamma_{li}^n + \sum_{j=1}^{n-1} {\alpha_j}^{-1}\gamma_{li}^j\beta_j &= \frac{P_{A_{li}}(0)}{\prod_{j=1}^{n-1}\left(-\alpha_j\right)} = \frac{P_{A_{li}}(0)}{\kappa} \\ -\delta_{li}^n + \sum_{j=1}^{n-1} {\alpha_j}^{-1}\delta_{li}^j\beta_j &= \frac{P_{D_{li}}(0)}{\prod_{j=1}^{n-1}\left(-\alpha_j\right)} = \frac{P_{D_{li}}(0)}{\kappa} \\ d_{li}^{n-1} + \sum_{j=1}^{n-1} {\alpha_j}^{-1}\delta_{li}^j\beta_j &= \frac{P_{D_{li}}(0)}{\kappa} \\ -\left(a_{li}^{n-1}d_{li}^{n-1} - d_{li}^{n-2}\right) + \sum_{j=1}^{n-1} {\alpha_j}^{-1}\psi_{li}\left(\alpha_j\right)\beta_j & \\ = \frac{-d_{li}^{n-1}P_{A_{li}}(0)}{\kappa}. & \end{aligned} \tag{A.1}$$

Considering assumptions of Case 1 and the condition $a_{li}^{n-1}d_{li}^{n-1} > d_{li}^{n-2}$, these relations permit us to write

$$\begin{aligned} \tau_{\max}^{(li)} &= \frac{P_{A_{li}}(0) + P_{D_{li}}(0)}{\kappa\left[\left(a_{li}^{n-1}d_{li}^{n-1} - d_{li}^{n-2}\right) - \sum_{j=1}^{n-1}{\alpha_j}^{-1}\psi_{li}\left(\alpha_j\right)\beta_j + d_{li}^{n-1}\left(d_{li}^{n-1} + \sum_{j=1}^{n-1}{\alpha_j}^{-1}\delta_{li}^j\beta_j\right)\right]} \\ &= \frac{P_{A_{li}}(0) + P_{D_{li}}(0)}{\kappa\left(d_{li}^{n-1}\left(\left(P_{A_{li}}(0) + P_{D_{li}}(0)\right)/\kappa\right)\right)} = \frac{1}{d_{li}^{n-1}}. \end{aligned} \tag{A.2}$$

Considering assumptions of Case 2 and the same condition $a_{li}^{n-1} d_{li}^{n-1} > d_{li}^{n-2}$, it becomes

$$\tau_{\max}^{(li)} = \frac{P_{A_{li}}(0) + P_{D_{li}}(0)}{\kappa\left[2\left(a_{li}^{n-1} d_{li}^{n-1} - d_{li}^{n-2}\right) - \left(a_{li}^{n-1} d_{li}^{n-1} - d_{li}^{n-2}\right) + \sum_{j=1}^{n-1} \alpha_j{}^{-1} \psi_{li}\left(\alpha_j\right) \beta_j + 2\left(d_{li}^{n-1}\right)^2 - d_{li}^{n-1}\left(d_{li}^{n-1} + \sum_{j=1}^{n-1} \alpha_j{}^{-1} \delta_{li}^{j} \beta_j\right)\right]}$$
$$= \frac{P_{A_{li}}(0) + P_{D_{li}}(0)}{2\kappa\left(\left(a_{li}^{n-1} d_{li}^{n-1} - d_{li}^{n-2}\right) + \left(d_{li}^{n-1}\right)^2\right) - d_{li}^{n-1}\left(P_{A_{li}}(0) + P_{D_{li}}(0)\right)}. \quad \text{(A.3)}$$

The same steps will be followed for the other cases.

Conflicts of Interest

The authors declare that there are no conflicts of interest regarding the publication of this paper.

References

[1] D. Liberzon, *Switching in Cystems and Control*, Birkhäuser, Boston, Mass, USA, 2003.

[2] Z. Sun and S. S. Ge, *Switched Linear Systems-Control and Design*, Springer, 2005.

[3] K. Tanaka, M. Iwasaki, and H. O. Wang, "Switching control of an R/C hovercraft: Stabilization and smooth switching," *IEEE Transactions on Systems, Man, and Cybernetics, Part B: Cybernetics*, vol. 31, no. 6, pp. 853–863, 2001.

[4] R. Palm and D. Driankov, "Fuzzy switched hybrid systems-modeling and identification," in *Proceedings of the IEEE International Symposium on Intelligent Control*, pp. 130–135, September 1998.

[5] V. Ojleska, T. K. Gugulovska, and G. M. Dimirovski, "Superior performance of switched fuzzy control systems: an overview and simulation experiments," *International Journal of Simulation Systems, Science and Technology*, vol. 12, no. 2, pp. 19–29, 2011.

[6] J. Dong and G.-H. Yang, "State feedback control of continuous-time T-S fuzzy systems via switched fuzzy controllers," *Information Sciences. An International Journal*, vol. 178, no. 6, pp. 1680–1695, 2008.

[7] V. Ojleska and G. Stojanovski, "Switched fuzzy systems: overview and perspectives," in *Proceedings of the 9th International PhD Workshop on Systems and Control: Young Generation Viewpoint*, Izola, Slovenia, October 2008.

[8] K. Tanaka, M. Iwasaki, and H. O. Wang, "Stable switching fuzzy control and its application to a hovercraft type vehicle," in *Proceedings of the FUZZ-IEEE 2000: 9th IEEE International Conference on Fuzzy Systems*, vol. 2, pp. 804–809, May 2000.

[9] H. Yang, G. M. Dimirovski, and J. Zhao, "Switched fuzzy systems: Representation modelling, stability analysis, and control design," *IEEE Intelligent Systems*, pp. 306–311, 2006.

[10] J. P. Hespanha, D. Liberzon, and A. S. Morse, "Logic-based switching control of a nonholonomic system with parametric modeling uncertainty," *Systems & Control Letters*, vol. 38, no. 3, pp. 167–177, 1999.

[11] T. Takagi and M. Sugeno, "Fuzzy identification of systems and its applications to modeling and control," *IEEE Transactions on Systems, Man and Cybernetics*, vol. 15, no. 1, pp. 116–132, 1985.

[12] K. Tanaka and M. Sano, "A Robust Stabilization Problem of Fuzzy Control Systems and Its Application to Backing up Control of a Truck-Trailer," *IEEE Transactions on Fuzzy Systems*, vol. 2, no. 2, pp. 119–134, 1994.

[13] K. Tanaka, T. Ikeda, and H. O. Wang, "Robust stabilization of a class of uncertain nonlinear systems via fuzzy control: quadratic stabilizability, H^{∞} control theory, and linear matrix inequalities," *IEEE Transactions on Fuzzy Systems*, vol. 4, no. 1, pp. 1–13, 1996.

[14] G. Feng, "A survey on analysis and design of model-based fuzzy control systems," *IEEE Transactions on Fuzzy Systems*, vol. 14, no. 5, pp. 676–697, 2006.

[15] K. Tanaka and H. O. Wang, *Fuzzy Control Systems Design and Analysis: A LMI Approach*, John Wiley & Sons, Inc., New York, NY, USA, 2001.

[16] J.-P. Richard, "Time-delay systems: an overview of some recent advances and open problems," *Automatica. A Journal of IFAC, the International Federation of Automatic Control*, vol. 39, no. 10, pp. 1667–1694, 2003.

[17] Y. Cao and P. M. Frank, "Analysis and synthesis of nonlinear time-delay systems via fuzzy control approach," *IEEE Transactions on Fuzzy Systems*, vol. 8, no. 2, pp. 200–211, 2000.

[18] Y.-Y. Cao and P. M. Frank, "Stability analysis and synthesis of nonlinear time-delay systems via linear Takagi-Sugeno fuzzy models," *Fuzzy Sets and Systems. An International Journal in Information Science and Engineering*, vol. 124, no. 2, pp. 213–229, 2001.

[19] B. Chen and X. P. Liu, "Fuzzy guaranteed cost control for nonlinear systems with time-varying delay," *IEEE Transactions on Fuzzy Systems*, vol. 13, no. 2, pp. 238–249, 2005.

[20] M. Kermani and A. Sakly, "Delay-independent stability criteria under arbitrary switching of a class of switched nonlinear time-delay systems," *Advances in Difference Equations*, 2015:225, 20 pages, 2015.

[21] B. Chen and X. Liu, "Delay-dependent robust H_{∞} control for T-S fuzzy systems with time delay," *IEEE Transactions on Fuzzy Systems*, vol. 13, no. 4, pp. 544–556, 2005.

[22] L. Liu, Y. Yin, L. Wang, and R. Bai, "Stability analysis for switched positive T-S fuzzy systems," *Neurocomputing*, vol. 173, pp. 2009–2013, 2016.

[23] J.-S. Chiou, C.-J. Wang, C.-M. Cheng, and C.-C. Wang, "Analysis and synthesis of switched nonlinear systems using the T-S fuzzy model," *Applied Mathematical Modelling. Simulation and Computation for Engineering and Environmental Systems*, vol. 34, no. 6, pp. 1467–1481, 2010.

[24] K. Tanaka, M. Iwasaki, and H. O. Wang, "Stability and smoothness conditions for switching fuzzy systems," in *Proceedings of the American Control Conference (ACC '00)*, pp. 2474–2478, Chicago, Ill, USA, June 2000.

[25] L. Vu and D. Liberzon, "Common Lyapunov functions for families of commuting nonlinear systems," *Systems & Control Letters*, vol. 54, no. 5, pp. 405–416, 2005.

[26] D. Liberzon, J. P. Hespanha, and A. S. Morse, "Stability of switched systems: a Lie-algebraic condition," *Systems & Control Letters*, vol. 37, no. 3, pp. 117–122, 1999.

[27] H. Lin and P. J. Antsaklis, "Stability and stabilizability of switched linear systems: A short survey of recent results," in *Proceedings of the 20th IEEE International Symposium on Intelligent Control, ISIC '05 and the 13th Mediterranean Conference on Control and Automation, MED '05*, pp. 24–29, cyp, June 2005.

[28] D. Liberzon and A. S. Morse, "Basic problems in stability and design of switched systems," *IEEE Control Systems Magazine*, vol. 19, no. 5, pp. 59–70, 1999.

[29] J. L. Mancilla-Aguilar and R. A. García, "A converse Lyapunov theorem for nonlinear switched systems," *Systems & Control Letters*, vol. 41, no. 1, pp. 67–71, 2000.

[30] J. Zhao and G. M. Dimirovski, "Quadratic stability of a class of switched nonlinear systems," *IEEE Transactions on Automatic Control*, vol. 49, no. 4, pp. 574–578, 2004.

[31] R. N. Shorten and K. S. Narendra, "On the stability and existence of common Lyapunov functions for stable linear switching systems," in *Proceedings of the 37th IEEE Conference on Decision and Control*, pp. 3723-3724, December 1998.

[32] F. Ahmida and E. H. Tissir, "Exponential stability of uncertain T-S fuzzy switched systems with time delay," *International Journal of Automation and Computing*, vol. 10, no. 1, pp. 32–38, 2013.

[33] H. Gassara, A. El Hajjaji, and M. Chaabane, "Robust control of T-S fuzzy systems with time-varying delay using new approach," *International Journal of Robust and Nonlinear Control*, vol. 20, no. 14, pp. 1566–1578, 2010.

[34] G. Yu, Y. Mao, H. Zhang, and Y. Qin, "Robust stability analysis of uncertain switching fuzzy systems with time-varying delays," in *Proceedings of the 31st Chinese Control Conference (CCC '12)*, pp. 3419–3422, Hefei, China, July 2012.

[35] J. P. Hespanha and A. S. Morse, "Stability of switched systems with average dwell-time," in *Proceedings of the 38th IEEE Conference on Decision and Control (CDC '99)*, pp. 2655–2660, December 1999.

[36] M. Benrejeb, M. Gasmi, and P. Borne, "New stability conditions for TS fuzzy continuous nonlinear models," *Nonlinear Dynamics and Systems Theory—An International Journal of Research and Surveys*, vol. 5, no. 4, pp. 369–379, 2005.

[37] M. Benrejeb, D. Soudani, A. Sakly, and P. Borne, "New discrete Tanaka-Sugeno-Kang fuzzy systems characterization and stability domain," *International Journal of Computers, Communications & Control*, vol. 1, no. 4, pp. 9–19, 2006.

[38] M. Benrejeb, A. Sakly, K. B. Othman, and P. Borne, "Choice of conjunctive operator of TSK fuzzy systems and stability domain study," *Mathematics and Computers in Simulation*, vol. 76, no. 5-6, pp. 410–421, 2008.

[39] M. Benrejeb, P. Borne, and F. Laurent, "Sur une application de la représentation en flèche à l'analyse des processus," *Rairo Automatique/Systems Analysis and Control*, vol. 16, pp. 133–146, 1982.

[40] S. Elmadssia, K. Saadaoui, and M. Benrejeb, "New delay-dependent stability conditions for linear systems with delay," *Systems Science and Control Engineering: An Open Access Journal*, vol. 1, no. 1, pp. 2–11, 2013.

[41] L. T. Grujić, J. C. Gentina, and P. Borne, "General aggregation of large-scale systems by vector Lyapunov functions and vector norms," *International Journal of Control*, vol. 24, no. 4, pp. 529–550, 1976.

[42] F. Robert, "Recherche d'une M-matrice parmi les minorantes d'un opérateur linéaire," *Numerische Mathematik*, vol. 9, pp. 189–199, 1966.

[43] P. Borne, J. P. Richard, and N. E. Radhy, *Systèmes non linéaires, tome 2 : stabilité-stabilisation, chapitre 2*, Editions Masson, Paris, France, 1993.

[44] A. Sakly and M. Kermani, "Stability and stabilization studies for a class of switched nonlinear systems via vector norms approach," *ISA Transactions*, 2014.

[45] M. Kermani and A. Sakly, "Robust stability and stabilization studies for uncertain switched systems based on vector norms approach," *International Journal of Dynamics and Control*, vol. 4, no. 1, pp. 76–91, 2016.

[46] M. Kermani, A. Sakly, and F. M'Sahli, "Stability analysis and stabilization of switched linear systems based on vector norms approach," in *Proceedings of 2nd International Conference on Communications Computing and Control Applications, CCCA 2012*, fra, December 2012.

[47] M. Kermani, A. Sakly, and F. M'Sahli, "A new stability analysis and stabilization of uncertain switched linear systems based on vector norms approach," in *Proceedings of 2013 10th International Multi-Conference on Systems, Signals and Devices, SSD 2013*, tun, March 2013.

[48] M. Kermani and A. Sakly, "A new robust pole placement stabilization for a class of time-varying polytopic uncertain switched nonlinear systems under arbitrary switching," *Control Engineering and Applied Informatics*, vol. 17, no. 2, pp. 20–31, 2015.

[49] A. Jaballi, A. Sakly, and A. El Hajjaji, "Delay-independent stability criterion for switched T-S fuzzy systems with multiple delays," in *Proceedings of the 16th International Conference on Sciences and Techniques of Automatic Control and Computer Engineering (STA '15)*, pp. 870–875, Monastir, Tunisia, December 2015.

[50] A. Jaballi, A. Sakly, and A. E. Hajjaji, "M-matrix based robust stability and stabilization for uncertain discrete-time switched TS fuzzy systems with time-varying delays," *ISA Transactions*, vol. 63, pp. 60–68, 2016.

[51] M. Kermani and A. Sakly, "On stability analysis of discrete-time uncertain switched nonlinear time-delay systems," *Advances in Difference Equations*, 2014:233, 22 pages, 2014.

[52] M. Kermani and A. Sakly, "Stability analysis of switched nonlinear time-delay systems," *Systems Science & Control Engineering: An Open Access Journal*, vol. 2, no. 1, pp. 80–89, 2014.

[53] M. Kermani, A. Jaballi, and A. Sakly, "A new stability analysis for discrete-time switched time-delay systems," *International Journal of Control, Energy and Electrical Engineering*, vol. 1, pp. 68–74, 2014.

[54] D. M. Kotelyanski, "Some properties of matrices with positive elements," *Matematicheskii Sbornik*, vol. 31, pp. 497–505, 1952.

[55] P. Borne, "Nonlinear system stability: vector norm approach system and control," in *Encyclopedia*, vol. 5, pp. 3402–3406, 1987.